Deciphering the interplay of extracellular vesicles and neratinib-resistance in HER2-positive breast cancer: insights, biomarkers, and therapeutic implications

A thesis submitted to the University of Dublin, Trinity College

towards a degree of Doctor of Philosophy

May 2023

Sarai Martinez Pacheco

Based on research carried out under the supervision of
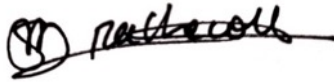
Prof. Lorraine O'Driscoll

School of Pharmacy & Pharmaceutical Sciences,

Trinity Biomedical Science Institute,

Trinity College Dublin.

Trinity College Dublin
Coláiste na Tríonóide, Baile Átha Cliath
The University of Dublin

Declaration

I declare that this thesis has not been submitted as an exercise for a degree at this or any other university and it is entirely my own work, unless where otherwise indicated. I agree to deposit this thesis in the University's open access institutional repository or allow the Library to do so on my behalf, subject to Irish Copyright Legislation and Trinity College Library conditioned of use and acknowledgement.

Signed: _____

Acknowledgements

To Jose, for being my life partner and following me wherever the waves take me, like buccaneers. Thank you for dealing with me in bad times (although in the good ones I am hilarious, you know it, and that is priceless), and certainly, thanks for the broccoli soup that has kept me alive this week. Because "when you hold me in your arms so tight, you let me know everything's alright". I love you.

Thanks to those who deserve it the most: my family. He tenido la suerte de no solo tener dos padres maravillosos, sino seis. Gracias a mis abuelos, por toda una vida de sacrificio para darnos un futuro mejor, por sus valores y por su amor incondicional. Esta tesis no hubiera sido posible sin vosotros. Todas mis victorias, siempre, irán dedicadas a vosotros. A mi abuela Pilar, por dedicar (y sacrificar) su vida por sus hijos y sus nietos. No hay vidas suficientes para que podamos devolverte todo lo que has hecho y sigues haciendo por nosotros; Te quiero. Gracias a mi abuelo Antonio, por enseñarme a ser cauta, a reflexionar y a ser paciente (para poder soportarle a veces). Eres un incomprendido, pero te quiero. A mi abuelo Andrés, por enseñarme la conciencia de clase, por transmitirme su pasión por la naturaleza y por calentarme el corazón desde el estómago con sus habichuelas. Te quiero y echo de menos las comidas de los sábados contigo en el campo. A mi abuela Mercedes, que sé que, aunque desde otro plano, me ha acompañado en esta etapa y siempre estará conmigo; te echo de menos. A mis padres, a los que admiro profundamente y siempre llevo en mi corazón. Soy el resultado de una mezcla explosiva que, parece ser, salió bien. Gracias a mi padre, por transmitirme, desde pequeña, la curiosidad por entender todo aquello que nos rodea y su pasión por la ciencia. Todavía recuerdo las noches mirando las estrellas y, aunque cambié un universo por las células, esta tesis se la dedico a ese adolescente que se quemó la cara haciendo experimentos de química en la cocina de su casa. Sin duda alguna, si me dedico a esto es gracias a ti. A mi madre, de la que he heredado la creatividad que tan necesaria es para ejercer esta profesión. Eres la única persona capaz de convencerme de que, al final, "todo saldrá bien". Os quiero y no puedo estar más orgullosa de teneros como padres. A mi hermano, Andrea, por alegrarme el corazón con su sonrisa. Sabes que siempre estaré ahí para ti porque "Mañana tengo examen, pero tú lo sabe', que si me llama', no estudio". Eres increíble y todavía no lo sabes, pero sé que harás historia. Te quiero. Al resto de mi familia, mis tías y mis primos. Os quiero.

Last but not least, I want to thank Bad Bunny for "Un Verano sin ti" playlist, my therapist Marta, and quoting Snoop Dogg, I want to thank me for believing in me, for doing all this hard work, for having no days off and for never quitting. You did it, girl!

Table of Contents

List of Figures

List of Tables

Summary

According to a World Health Organisation (WHO) report on 3rd March 2021, breast cancer is the most common form of cancer in the world and the leading cause of cancer death among females. In 2020, 2.26 million newly breast cancer patients were diagnosed (11.7% of all cancers) and approximately 685 000 died worldwide from this disease. The same year, 576,337 new breast cancers were diagnosed in WHO Europe countries with 157,111 predicted deaths in both sexes. In Ireland, there are 3,433 females diagnosed with breast cancer per year (23.8% of all invasive cancers) with 745 deaths per year (15.2% of all cancer deaths), making breast cancer the second most common cause of cancer deaths. Breast cancer cannot be considered as a single disease due to the high heterogeneity. This type of cancer includes distinct subtypes associated with different clinical outcomes. Understanding this heterogeneity is fundamental for the development of targeted personalised medicine and therapeutic intervention. Over-expression of human epidermal growth factor receptor 2 (HER2) occurs in ~ 20% of breast cancers and confers aggressive behaviour and poorer prognosis. Thankfully, several drugs such as trastuzumab, lapatinib, pertuzumab, and neratinib have been developed to target HER2, potentially providing substantial benefit for many patients. Despite the development of HER2-targeted therapies which have improved the survival outcomes for HER2- positive breast cancer patients, it is estimated that up to 70% of patients with HER2-overexpressing tumours do not gain benefit, because of innate-, acquired- and cross-resistance to HER2-targeted therapies; the main reason for which these drugs fail in the clinic. Further investigations and continued efforts are required to unravel the main effectors of resistance to predict the outcome of treatments and offer more therapeutic options to a wide range of patients. Extracellular vesicles (EVs) are a heterogenous group of cell-derived membranous structures present in biological fluids and involved in multiple physiological and pathological processes. Nowadays, EVs are considered an additional mechanism for intracellular communication, and it is essential to comprehend the cellular processes implicated in their biology to understand their physiological and pathological functions, as well as clinical applications involving their use and/or analysis. However, in this expanding field, much remains unknown regarding the origin, biogenesis, secretion, targeting, and future applications of these vesicles. Previous research performed by our group and others has shown that EVs are involved in transmitting resistance, and it demonstrated that EVs induced previously drug-sensitive cells to become drug-resistant. Specifically in cancer, EVs can act as intercellular mediators in tumorigenesis mechanisms including the transmission of resistance to anti- cancer drugs, angiogenesis, metastasis, and immunosuppression. Furthermore, there is evidence suggesting that EVs might bind drugs such as trastuzumab, reducing bioavailability of the drug to its receptor (HER2) on cancer cells. Due to that, EVs may be substantially inhibiting cancer patients gaining benefit from anti-cancer drugs.

This project aims to understand the transmission of resistance to anti-cancer drugs through EVs, investigate neratinib-resistance mechanisms in HER2+ breast cancer, and discover new pathways and biomarkers associated with neratinib resistance, ultimately benefiting cancer patients. The project involves various objectives such as comparing EVs separation methods, analysing proteome profiles of neratinib-sensitive and neratinib-resistant cells, EVs characterisation derived from neratinib-sensitive and neratinib-resistant breast cancer cell lines, studying hypoxia's influence, evaluating a 3D cell culture model, surveying *in vitro* models in cancer research, and examining the effect of tucatinib on EVs' release in breast cancer cell lines.

Thus, this project started by evaluating the importance of comparing EVs separation methods using multiple sources of conditioned medium (CM) to ensure accurate and generalisable results by comparing two different EVs separation methods: differential ultracentrifugation (dUC) and polyethylene glycol (PEG) precipitation followed by ultracentrifugation (PEG+UC). We found that different cell lines and separation methods resulted in variations in EVs characteristics, such as size, quantity, and protein content. Although both approaches showed to be reproducible methods for obtaining pure EVs, the inclusion of multiple CM sources is crucial for meaningful comparisons and generalisability of results across samples.

Additionally, we also aimed to explore the proteomic differences between HER2-positive breast cancer cell lines and their neratinib-resistant counterparts developed in our group previously. We discovered that neratinib-resistant cell lines HCC1943 NR and SKBR3 NR, which are HER2+ER-, exhibited significantly lower expression of AGR2 compared to their neratinib-sensitive counterparts. Conversely, the luminal B breast cancer cell lines (HER2+ER+) EFM192A and EFM192A NR did not show the same pattern of AGR2 expression. Notably, the overexpression of AGR2 in ER-positive breast cancer has been linked to a poor prognosis, particularly in hormone therapy-resistant tumours. Therefore, the next logical step was to investigate the role of AGR2 down-regulation in the aggressiveness of neratinib-resistant HER2+ breast cancer cell lines. For that, we performed functional assays after transfecting AGR2 into neratinib-resistant cells. The results showed that AGR2 transfection led to changes in cell migration, invasion, *anoikis*-resistance, and neratinib-resistance, as well as some alterations in the expression of EMT markers and HER2. We also evaluated in this project how neratinib-resistance can affect EVs' release and EVs' cargo in both normoxia and hypoxia conditions and by using different EVs separation approaches. We found that neratinib-resistant cell line variants release fewer EVs compared to their neratinib-sensitive counterparts in both normoxia and hypoxia. In addition, those EVs derived from neratinib-resistant cell lines carried less HER2 than their neratinib-sensitive counterparts. The results obtained under hypoxic conditions indicated that hypoxia modified the release and content of EVs in a manner specific to each cell type, which could potentially impact the invasiveness of breast cancer cells and their resistance to drugs. We also investigated the suitability of two different 3D-culture platforms to collect EVs and to include 3D cell culture in this comparison. We also performed the first worldwide survey about the existing pre-clinical *in vitro* models currently employed in cancer research. Finally, we investigated whether exposure to a low dose of tucatinib, taking into consideration limitations in achievable dosage of anti-HER2 therapies due to factors such as tumour size, location, and heterogeneity, could inadvertently lead to increased HER2 expression and/or release of EVs, potentially promoting tumour aggressiveness. We demonstrated that neratinib-resistance conferred cross-resistance to tucatinib in all three HER2+ breast cancer cell lines studied and that HCC1954 cells manifest innate resistance to tucatinib. The analysis of CM collected after tucatinib treatment showed a higher abundance of CD9+ and HER2+ events compared to their untreated counterparts, with significant differences observed in CM obtained from HCC1954 cells.

In conclusion, this research demonstrates that neratinib-resistant cell lines exhibit distinct proteomic profiles and altered EVs' release compared to their neratinib-sensitive counterparts in both normoxic and hypoxic conditions. Notably, an increased presence of E-cadherin, IL-6, IL-8, and HER2 was detected in EVs derived from HER2+ cancer cells under hypoxia. These changes in EVs' cargo composition have the potential to impact tumour progression and contribute to resistance against anti-HER2 therapies.

List of abbreviations

2D	Two-dimensional
3D	Three-dimensional
3Rs	Replacement, reduction, and refinement
ABC	Ammonium bicarbonate
ABCB1	Bone marrow-mesenchymal stem cells
ACN	Acetonitrile
AEs	Adverse events
AGAP2-AS1	Long non-coding ribonucleic acid AGAP2 antisense RNA 1
AGR2	Anterior gradient protein 2
AIs	Aromatase inhibitors
Akt	Protein kinase B
ALIX	Programmed cell death 6-interacting protein
APC	Allophycocyanin
ARNT	Aryl hydrocarbon receptor nuclear translocator
ATP	Adenosine triphosphate
BAX	Bcl-2-like protein 4
BC	Breast cancer
BCA	Bicinchoninic acid
BCL-2	B-cell leukaemia/lymphoma 2 protein
BM-MSCs	Bone marrow mesenchymal stem cells
BRCA1/BRCA2	Breast cancer gene 1 /2
BSA	Bovine serum albumin
cas-3	Caspase-3
cas-7	Caspase-7
CD63	Cluster of differentiation 63
CD9	Cluster of differentiation 9
cDNA	Complementary DNA
CL	Cell lysate
CM	Conditioned medium
COVID-19	Coronavirus disease 2019
CSC	Cancer stem cells
DEP	Differentially expressed proteins
dFBS	EVs- depleted FBS
DMSO	Dimethyl sulfoxide
DNA	Deoxyribonucleic acid
DPBS	Dulbecco's phosphate buffered saline
DTT	Dithiothreitol
dUC	Differential ultracentrifugation
E2F3	Insulin-like growth factor 1 receptor
ECM	Extracellular matrix

EDTA	General Data Protection Regulation
EGFP	Enhanced green fluorescent protein
EGFR	Epidermal growth factor receptor
EMA	European Medicines Agency
EMT	Epithelial-mesenchymal transition
ENO1	Enolase 1
EOC	Epithelial ovarian carcinoma
EPO	Erythropoietin
ER	Oestrogen receptor
ESCRT	Endosomal-sorting complex required for transport
EU	European Union
EVs	Extracellular vesicles
ExoSCOPE	Extracellular vesicle monitoring of small-molecule chemical occupancy and protein expression
ExteNET	Extended adjuvant treatment of breast cancer with neratinib
FACS	Fluorescence-activated cell sorting
FBS	Foetal bovine serum
FC	Flow Cytometry
FDA	Food and Drug Administration
FDR	False discovery rate
FGFRL1	Fibroblast growth factor receptor like 1
FITC	Fluorescein isothiocyanate
FLOT1	Flotillin-1
FOXO3A	Forkhead transcription factor FKHRL1
FSC	Forward scatter channel
GAPDH	Glyceraldehyde 3-phosphate dehydrogenase
GCO	Global Cancer Observatory
GDPR	Pearson correlation coefficient
GEC	Gastric or gastroesophageal junction adenocarcinoma
GFP	Green fluorescent protein
GLUT1	Glucose transporter 1
GLUT3	Glucose transporter 3
GNAS2	Guanine nucleotide binding protein, alpha stimulating
GPD1L	Glycerol-3-phosphate dehydrogenase 1
GPI	Glycosyl-phosphatidylinositol
GPR64	Orphan Adhesion G protein-coupled receptor
GRP94	Endoplasmin
GUC	Gradient ultracentrifugation
HER1/EGFR	Human epidermal growth factor receptor 1
HER2/ErbB2/neu	Human epidermal growth factor receptor 2
HER2+	HER2-positive
HER3	Human epidermal growth factor receptor 3

HER4	Human epidermal growth factor receptor 4
HES-1	Hairy and enhancer of split-1 transcription factor
HIF-1α	Hypoxia-inducible factor 1 alpha
HIF-1β	Hypoxia-inducible factor 1 beta
HIFs	Hypoxia-inducible factors
HOXA1	Homeobox A1 protein
HPLC	High-performance liquid chromatography
HR	Hormone receptor
HRE	Hypoxia response element
HS	High sensitivity
Hsp90	Heat shock protein 90
HUVECs	Human umbilical vein endothelial cells
IAA	Iodoacetamide
IC$_{10}$	Ten percent inhibitory concentration
IC$_{50}$	Half maximal inhibitory concentration
iDFS	Invasive disease-free survival
IFCM	Imaging flow cytometry
IGF	Insulin-like growth factors
IGF1R	Insulin-like growth factor 1 receptor
IHC	Immunohistochemical
IL-x	Interleukin
ILVs	Intraluminal vesicles
ISEV	International Society for Extracellular Vesicles
ISH	In situ hybridisation
ITB1	Integrin subunit beta 1
KEGG	Kyoto Encyclopaedia of Genes and Genomes
KITL	Ligand for the receptor-type protein-tyrosine kinase
LC-MS/MS	Liquid chromatography with tandem mass spectrometry
lEVs/bEVs	Large EVs
LFQ	Label-free quantification
LMD	Leptomeningeal Disease
LMO3	LIM domain only protein 3
lncRNAs	Long non-coding RNA
LOs	Large oncosomes
MAPK	Mitogen-activated protein kinase
MBC	Metastatic breast cancer
MEK/MAPK	Mitogen-activated protein kinase
MET	MET proto-oncogene, receptor tyrosine kinase
mEVs	Medium EVs
MFI	Mean fluorescence intensity
miRNA/miR	Micro-RNA
MISEV2018	Minimal information for studies of extracellular vesicles 2018

MS	Mass spectrometry
mTOR	Mammalian target of rapamycin
MVB	Multi-vesicular bodies
MVs	Microvesicles
MW	Molecular weight
NF-KB	Nuclear factor kappa B subunit 1
NMuMG	Murine mammary gland epithelial cells
NR	Neratinib-resistant
NTA	Nanoparticle tracking analysis
OD	Optical density
OS	Overall survival
P/S	Penicillin/streptomycin
p300/CBP	cAMP-response element binding protein
PAS	Helix-loop-helix proteins of the Per-ARNT-Sim family
PASEF	Parallel accumulation serial fragmentation
Pax-5	Pax-5 protein
PBS	Phosphate-buffered saline
PBS-T	Phosphate-buffered saline containing Tween
PCA	Principal component analysis
PCC	Pearson correlation coefficient
pCR	Pathologic complete response
PCR	Polymerase chain reaction
PD-L1	Programmed death-ligand 1
PDCD4	Programmed cell death 4
PE	Phycoerythrin
PE-Cy7	Phycoerythrin cyanine 7
PEG	Polyethylene glycol
PEG+UC	Polyethylene glycol-based method followed by ultracentrifugation step
PERP	53 Apoptosis effector related to PMP22
PET	Polyester
PFS	Progression-free survival
PHDs	Prolyl hydroxylase domain family proteins
PI3K	Phosphatidylinositol 3-kinase
PKD1	Polycystin 1, Transient receptor potential channel interacting
poly-HEMA	Poly (2-hydroxyethyl methacrylate)
PR	Progesterone receptor
Ps	Participants
PTEN	Phosphatidylinositol 3,4,5-trisphosphate 3-phosphatase
PVDF	Polyvinylidene fluoride
pVHL	von Hippel–Lindau tumour suppressor protein
RFS	Relapse free survival
RhoA	Ras Homolog Family Member A

RNA	Ribonucleic acid
ROCK1	Rho-associated coiled-coil-forming kinase I
ROS	Reactive oxygen species
RT	Room temperature
RT-PCR	Reverse-transcriptase polymerase chain reaction
RT-qPCR	Quantitative reverse transcription polymerase chain reaction
SDF	Stromal cell-derived factor
SEC	Size-exclusion chromatography
SEM	Standard error of mean
sEVs	Small EVs
SNAREs	Soluble N-ethylmaleimide-sensitive factor attachment protein receptors
SOCS1	Suppressor of cytokine signalling 1
SPV	Sulpho-phospho vanillin
SRS	Stereotactic radiosurgery
SSC	Side scatter channel
SSC	Side Scatter channel
STAT3	Signal transducer and activator of transcription 3
TCA	Tricarboxylic acid cycle
T-DM1	Trastuzumab-emtansine
T-Dxd	Trastuzumab deruxtecan
TEM	Transmission electron microscopy
TFA	Trifluoroacetic acid
TFF	Tangential flow filtration
TGF-β1	Transforming growth factor-beta 1
TGN	Trans-Golgi network
TIMP3	TIMP metallopeptidase inhibitor 3
TIMS	Trapped ion mobility spectrometry
TKIs	Tyrosine kinases inhibitors
TKs	Tyrosine kinases
TME	Tumour microenvironment
TNBC	Triple negative breast cancer
TP53	Tumour protein p53
TP53INP1	Tumour Protein P53 inducible nuclear protein 1
TPM1	Tropomyosin alpha-1 chain
TRF1	Telomeric repeat factor 1
Tsg101	Tumour susceptibility gene 101 protein
UHPnLC	Ultra-high pressure nanoflow chromatography system
VEGF	Vascular endothelial growth factor
Vps4	APTase vacuolar protein sorting 4
vsn	Variance stabilizing transformation
WHO	World Health Organisation
ZADH2	Zinc binding alcohol dehydrogenase domain containing 2

Chapter 1

Introduction

1.1 Breast cancer

Cancer comprises a range of distinct yet interconnected diseases with existing differences in the magnitude and profile of the diseases between different countries, being the leading cause of death worldwide, with nearly 10 million of deaths in 2020. According to GLOBOCAN estimates of cancer incidence and mortality produced by the International Agency for Research on Cancer, there are types of cancer that dominate globally and explain more than 30% of the cancer incidence and mortality worldwide: breast, lung, colon, and prostate cancers[1]. In 2020, the Global Cancer Observatory (GCO) established breast cancer as the most common form of cancer in the world, with 2.26 million new breast cancers diagnosed (11.7% all cancers) and approximately 685 000 deaths in both sexes. The same year, 576,337 new breast cancers were diagnosed in Europe countries with 157,111 predicted deaths from breast cancer in both sexes. In Ireland, there are 3,433 female breast cancer cases diagnosed per year (23.8% of all invasive cancers) with 745 deaths per year (15.2% of all cancer deaths), making breast cancer the second most common cause of cancer deaths[1,2]. Although mortality rates may be higher in less developed countries (with Fiji showing the highest mortality rates from breast cancer worldwide), in terms of incidence rates there is only a slight difference, being higher in high-income countries than less developed regions. Elevated incidence rates in developed countries are explained by the efficiency of breast cancer screening programs, early diagnosis, and a higher prevalence of the known risk factors.

It should be noted that coronavirus disease 2019 (COVID-19) has had an impact in cancer estimates as well as its repercussion causing delays in cancer diagnosis and treatment, health system closure, screening program suspension and reduce access to care. In concordance with these drawbacks, it is expected a short-term decline in cancer incidence followed by an increase of advance-stage diagnosed cases and cancer-related mortality in some locations[1,3].

Despite significant advances in cancer prevention medicine that has proven to be effective, breast cancer still being an important health problem not only in Ireland, but also worldwide and international efforts are necessary to resolved clinical and scientific problems remain[4].

1.1.1 Subtype classification

Breast cancer cannot be considered as a single disease due to the high heterogeneity. This type of cancer is composed of distinct subtypes associated with different clinical outcomes. Understanding this heterogeneity is fundamental for the development of targeted personalised medicine and therapeutic intervention[5]. First categorisations were based in traditional clinicopathological variables (tumour size, grade, and nodal involvement), together with the presence or absence of three cell surface receptors: oestrogen receptor (ER), progesterone receptor (PR) and over-expression of human epidermal growth factor receptor 2 (HER2, also called ErbB2/neu). Those that lack all three receptors are termed triple negative breast cancer (TNBC)[6].

In general terms, those cancer that express either ER, and/or HER2 are targetable with therapies directed against these receptors, whilst patients with TNBC do not benefit from these therapies and so chemotherapy alone is the standard systemic treatment for TNBC[7,8].

Currently, this classification has evolved because of Deoxyribonucleic acid (DNA) microarrays analysis performed in 2000, which enabled the comprehensive molecular classification of breast cancer based on its gene expression patterns. This technology categorised tumours into five distinct subtypes: luminal A, luminal B, HER2-enriched, basal-like, and normal-like. A summary of the main characteristics of the main breast cancer subtypes are collected in **Table 1.1**.

Tumours classified as luminal A are distinguished by the expression of ER and/or PR and the lack of HER2, representing 50-60% of all breast tumours. These tumours exhibit a low level of cell proliferation, as evidenced by the expression of the Ki-67 marker, compared to luminal B. Clinically, luminal A tumours have the best prognosis with less incidence of relapse and higher survival rate while luminal B represents 15-20% of breast cancers and are slightly more aggressive than luminal A cancers[9]. The higher expression of Ki-67 on this subtype contributes to the worse prognosis associated with luminal B tumours. In addition, luminal B tumours tend to have a higher percentage of lymph node involvement compared with luminal A[10]. Luminal breast cancers respond to endocrine therapies such as tamoxifen which inhibits the transcriptional activity of the ER[11].

HER2-enriched breast cancers represent 15-20% of all breast cancers and are represented by an amplification of the HER2 oncogene and overexpression of the HER2 receptor. This overexpression gives to this subtype a more aggressive clinical and biological behaviour compared to the other subtypes that do not present HER2 expressed[12].

Normal-like tumours, comprising 5-10% of cases, are not well understood and may be due to contamination of breast cancer cells with healthy tissue[12]. These tumours exhibit a poorer prognosis than luminal A tumours but with a similar expression profile to these tumours[8].

The classification schema for breast cancer has undergone further refinement through additional research. Another subtype was identified, claudin-low, which possesses distinct molecular characteristics and differs phenotypically from the original five subtypes. The claudin-low subtype is characterised by the absence of luminal differentiation markers and an elevated presence of EMT markers (i.e., vimentin and N-cadherin), immune response-related genes (i.e., *CD79b, CD14 and vav1*), and cancer stem cell (CSC) signatures. Typically, this subtype is associated with TNBC and a poor prognosis. Studies have shown that subtyping breast cancer can independently predict prognosis in different patient cohorts. Therefore, a more comprehensive classification schema has been developed to better anticipate clinical response[13–16].

In consonance with the above, in 2020 the "HER2-low" concept was introduced in breast cancer by some studies[17–21]. HER2-low breast cancer represents a heterogeneous group of breast cancer characterised by a low expression of HER2. Tarantino et al. (2020)[22] defined by first time this subtype, defining HER2-low breast cancer as tumours with an immunohistochemical (IHC) score of 1+ or score of 2+/in situ hybridisation (ISH) negative phenotype. This subtype is formed by a heterogeneous group of breast cancer, being the most of HER2-low tumours represented by luminal molecular subtypes, more common in hormone receptor (HR) - positive BCs (31-51%), showing a lower Ki-67 proliferation index and being less responsive to neoadjuvant chemotherapy. The clinical significance of HER2-low breast cancer is currently an area of active research, as it may represent a unique subset of breast cancer that could benefit from targeted therapies. Numerous therapeutic

agents are presently undergoing clinical development for the treatment of HER2-low breast cancer[23].

Table 1.1. Molecular subtypes of breast cancer.

Subtype	Molecular subtype	Molecular signature	Outcome
Luminal	Luminal A	[ER+|PR+] HER2- , Ki67-	Good
	Luminal B	[ER+|PR+] HER2- , Ki67+ [ER+|PR+] HER2+, Ki67+	Intermediate Poor
Normal-like	Normal-like	[ER+|PR+] HER2-, Ki67-	Intermediate
HER2+	HER2 over-expression	[ER-|PR-] HER2+	Poor
Triple negative	Basal-like*	[ER-|PR-] HER2-, basal marker+	Poor
	Claudin-low	[ER-|PR-] HER2-, EMT marker+, Stem-cell marker+, claudin-	Poor

*Breast cancer management still predominantly relies on immunohistochemistry (ICH) markers including ER, PR and HER2, being breast tumours grouped into four basic subgroups. *Basal-like is commonly classified as TNBC; EMT=Epithelial-Mesenchymal Transition.*

1.1.2 HER2 and HER2-overexpressing breast cancer

ErbB2/HER2 belongs to the epidermal growth factor receptor (EGFR) family of tyrosine kinases (TKs). EGFR-family is composed of EGFR/ErbB1, ErbB2/HER2, ErbB3/HER3 and ErbB4/HER4 and the activation of these kinases through ligand binding, receptor mutations, or their over-expression induce both homo- and heterodimerisation. However, each receptor has its specific characteristics, such as the fact that, unlike EGFR, ErbB-2 is a ligand-less receptor but the HER2 dimers are the most stable and favoured dimerisation partner[24]. Moreover, HER2, unlike the other EGFR receptors that are down-regulated by ligand-binding or constitutively, is resistant to this down-regulation, also inhibiting this process in the case of its heterodimerisation partner. The reasons why this takes place still further discussed[25]. As illustrated in **Figure 1.1**, once HER2 is phosphorylated and activated, it initiates signalling pathways downstream of these receptors such as PI3K/Akt and Ras/Raf/MEK/MAPK pathways, leading to cell survival, cell growth and tumour progression[26–29]. In approximately 20% of breast cancer cases, HER2 is amplified or over-expressed, being indicative of aggressive cancer cell, with high proliferation and metastatic potential. HER2 over-expression is also related to high tumour grade mitotic count and positive-lymph nodes [30].

Previous studies have indicated that there is a functional coupling between the oncogenic signalling and endosomal trafficking of many TK receptors[31–33]. Specifically, endosomal trafficking plays a critical role in regulating the strength and duration of signalling from receptors such as EGFR and MET[31,34]. However, in contrast to other receptor TKs, the mechanisms of HER2 trafficking are not

well understood and several studies showed discrepant results regarding this topic. Some studies have shown that HER2 present a resistance to its internalisation while others have proposed a rapid HER2 recycling process to the plasma membrane. In all the scenarios, HER2 is strictly restricted to the plasma membrane, being associated with proliferation and tumorigenesis-related pathways. Pietilä et al. (2019)[31] showed that different HER2-overexpressing breast cancer cell lines showed different patterns of localisation, reflecting the HER2 functions and the therapeutic efficiency of anti-HER2 therapies. In this study, lapatinib and trastuzumab resistant cell lines, including HCC1954 cells, displayed more intracellular HER2 compared to other therapy sensitive cell lines (BT474 and SKBR3, among others). The role of HER2 trafficking together with expression of trafficking proteins (i.e., cavelolin-1) are critical for the oncogenic activity of HER2 and the response to anti-HER2 therapies.

Despite the development of HER2-targeted therapies (such as trastuzumab, pertuzumab, lapatinib and neratinib) which have improved the survival outcomes for breast cancer patients with HER2-overexpressing tumours, the principal problem is that innate-, acquired- and cross-resistance to HER2-targeted therapies dominates as the main reason for which these drugs fail in the clinic[35,36]. In addition, the variations of HER2 play an important role in drug resistance such as Δ16HER-2 and p95HER-2, producing resistance to trastuzumab in patients who harbour any of them[37]. Further investigations and continued efforts are required to unravel the main mechanisms of resistance; to predict the outcome of treatments; and to offer more therapeutic options to a wide range of patients[38].
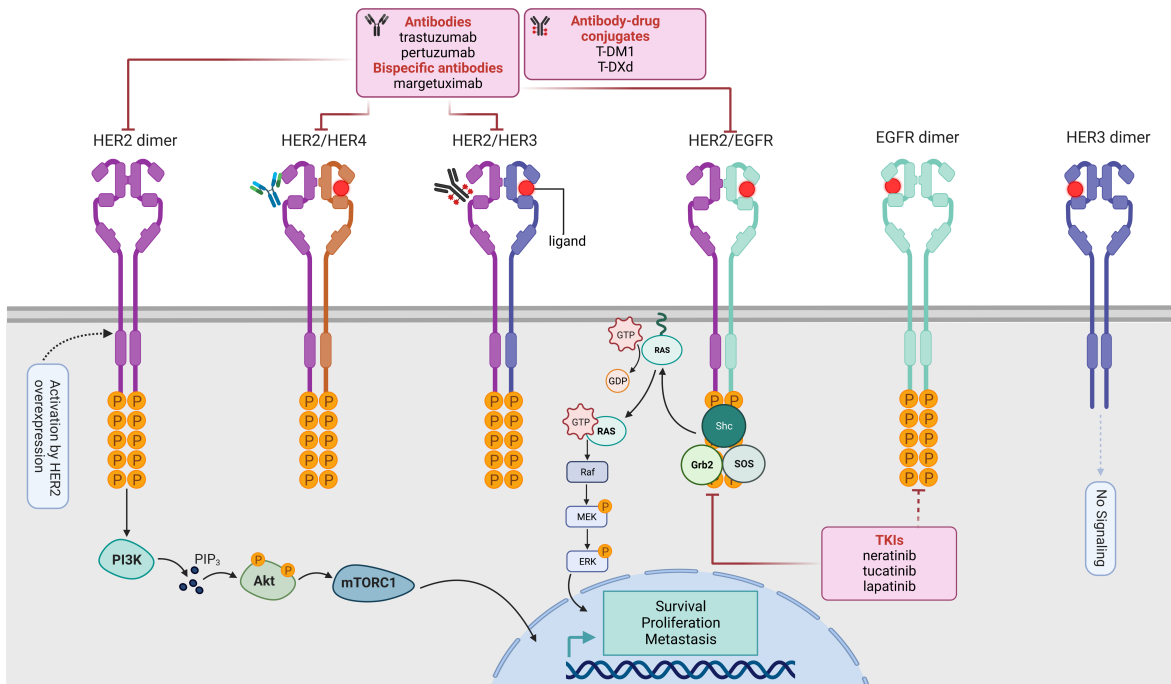
Figure 1.1. Schematic representation of HER2 signalling pathway and the mode of actions of current ErbB2 inhibitors and their interaction with receptors of the EGFR family.

The homo- and heterogeneity-dimerisation of HER2 with other EGFR family receptor results in cell signalling through the MAPK (Ras, Raf, MEK and ERK) pathway and PI3K/Akt pathway leading to cellular proliferation. Molecular approaches to HER2 targeted therapy appeared represented. While trastuzumab and trastuzumab-emtansine (T-DM1) binds domain IV of the extracellular component of the HER2 protein located close to the cell membrane, tyrosine kinase inhibitors (TKIs) such as lapatinib or neratinib, bind the intracellular adenosine triphosphate (ATP)-binding domain disrupting the phosphorylation of these domain and inhibiting of cell signalling[35,36,39]. Illustration created in *BioRender.com*.

1.2 Tyrosine kinase inhibitors for the treatment of HER2-positive breast cancer

In recent decades, many tyrosine kinase inhibitors (TKIs) have been approved for cancer treatment and several are currently being investigated. TKIs are specially designed to target TKs that are mutated or/and over-expressed in cancer. In these terms, several HER receptor inhibitors have been approved for the treatment of breast cancer treatment while others are in different stages of advanced clinical research. As illustrated in **Figure 1.1**, these small molecules typically block the binding of adenosine triphosphate (ATP) to the kinase domain of the receptor; irreversibly (e.g., neratinib) or reversibly (e.g., tucatinib) [36,38,40–43]. TKIs are characterised by different physico-chemical properties, particularly a considerably low molecular weight, allowing them a more efficacious penetration through the blood-brain barrier compared to monoclonal antibodies, relevant where brain metastases

have occurred. However, TKIs are associated with EGFR off-target toxicity that includes rash and diarrhoea.

1.2.1 Neratinib

Neratinib (HKI-272, Nerlynx®, Puma Biotechnology Inc.) is an oral, potent small-molecule irreversible pan-ErbB TKI of EGFR (HER1), ErbB2 (HER2/neu) and ErbB4 (HER4). The principal difference between neratinib and earlier compounds such as lapatinib is that the second one was designed as reversible inhibitor, competing with ATP for binding [43–45].

Neratinib was approved by Food and Drug Administration (FDA) in 2017, and by European Medicines Agency (EMA) in 2018, for extended adjuvant treatment of early stage HER2-positive (HER2+) breast cancer[46]. Neratinib is still undergoing clinical trials. A phase I/II study (NCT00398567) has been shown neratinib to be effective in HER2+ breast cancer with acquired and innate resistance to trastuzumab and its combination with trastuzumab was safe and well-tolerated, improving clinical outcomes in some subsets of patients[46]. A phase III trial (extended adjuvant treatment of breast cancer with neratinib (ExteNET), demonstrated a significantly improvement on 5-year invasive disease-free survival (iDFS) in early-stage breast cancer patients, after trastuzumab-based adjuvant therapy (NCT00878709)[47]. The SUMMIT trial (NCT01494662) is an open-label phase II monotherapy trial that evaluated the efficacy and safety of neratinib in combination with paclitaxel as a first-line treatment for patients with HER2+ metastatic breast cancer (MBC)[48]. When the safety of neratinib was evaluated in 1,408 patients the most common grade 3/4 adverse events (AEs) were diarrhoea (40%), vomiting (3%), nausea and abdominal pain (2% in both cases). Despite the concern about the diarrhoea, it was short-lived and can be manageable with the use of anti-diarrhoea agents. It was also reversible on discontinuation of neratinib[49].

Despite the benefit offered by neratinib to patients with HER2+ breast cancer, further investigation is needed to determine the best therapies combination and to better define patients who are most likely to benefit from therapies and the potential predictive biomarkers for response to these therapies, including HER2[49]. Neratinib is currently undergoing different clinical trials (key clinical trials summarised in **Table 1.2**).

Table 1.2. Key clinical trials of neratinib breast cancer patients.

ID	Drug(s)	Condition	Ps	Phase	Status	Ref.
NCT04366713	Neratinib Capecitabine Loperamide	HER2+BC	6	II	Completed	-
NCT00878709	Neratinib Placebo	Early Stage HER2+ BC	2840	III	Completed	[50]
NCT00741260	Neratinib Capecitabine	HER2+ MBC	105	I-II	Completed	[51]
NCT01111825	Temsirolimus Neratinib	HER2+ MBC or TNBC	99	I-II	Completed	-

NCT02236000	Neratinib T-DM1	HER2+ MBC	49	I-II	Completed	[52]
NCT00915018	Neratinib Trastuzumab Paclitaxel	HER2+ locally recurrent or MBC	479	II	Completed	[53]
NCT01808573	Neratinib Lapatinib Capecitabine	HER2+ MBC	621	III	Completed	[54]
NCT02400476	Neratinib Loperamide Colestipol Budenoside	Early Stage HER2+ BC	563	II	Completed	[55]
NCT00777101	Neratinib Lapatinib Capecitabine	HER2+ locally recurrent or MBC	233	II	Completed	[56]
NCT00706030	Neratinib Vinorelbine	HER2+ MBC	92	I-II	Completed	[57]
NCT01008150	Paclitaxel Trastuzumab Neratinib Doxorubicin Cyclophosphamide	HER2+ BC	141	II	Completed	[58,59]
NCT01670877	Neratinib Fulvestrant Trastuzumab	HER2 mutant BC	56	II	Completed	[60,61]
NCT00445458	Neratinib Paclitaxel	BC	110	I-II	Completed	[62]
NCT00398567	Neratinib Trastuzumab	Advanced HER2+ BC	45	I-II	Completed	[63]
NCT00300781	Neratinib	Advanced HER2+ BC	136	II	Completed	[63]
NCT00146172	Neratinib	Breast neoplasms	73	I	Completed	-

Key clinical trials that are currently completed. Information as on https://clinicaltrials.gov (information correct as of 8th May 2023). MBC =metastatic breast cancer; BC= breast cancer; T-DXd= Trastuzumab deruxtecan; Ps = participants.

1.2.1.1 Neratinib-resistance

Although neratinib has shown efficacy in blocking the signalling of EGFR family receptors, also may generate resistance as other TKIs. For that reason, further investigation to understand the mechanisms behind innate and acquired resistance is required[45]. Our group developed neratinib-resistant variants of HER2+ breast cancer cell lines, revealing a novel mechanism of neratinib resistance based on a rise of metabolism of neratinib in these cell variants due to increased CYP3A4

activity and HER2 expression was also down-regulated in the neratinib-resistant variants. Also, the resistance to neratinib conferred cross-resistance to other HER2-targeted therapies used for breast cancer such as trastuzumab, lapatinib and afatinib and resistant variants were more aggressive behaviour than their drug-sensitive counterparts[64].

As indicated in **Section 1.1.2**, the alteration of HER2 is a crucial mechanism of drug-resistance and neratinib could be an option for patients carrying a HER2-mutated protein. The analysis of data from high breast cancer genome sequencing projects identified 13 somatic HER2 mutations, seven of them were activating mutations that accelerate tumour growth. All these characterised mutations were sensitive to neratinib, including those that produce lapatinib resistance (such as HER2 L755S)[44,65,66].

In accordance with the above, the SUMMIT "basket" trial (NCT01953926) was performed to study therapeutic relevance of HER2 and HER3 mutations in tumours harbouring these mutations. For this, the patients were treated with 240 mg/day neratinib monotherapy or in combination with other therapies. Patients with missense mutations located in extracellular and kinases domains, as well as insertions in the kinase domain, responded to the treatment with neratinib. This showed that neratinib may have clinical benefit in patients with both HER2 amplification and mutation and it highlighted the necessity of clinical studies testing the efficacy of neratinib selectively in breast cancer patients whose tumours carry both amplification and mutation of HER2[65–71].

1.2.2 Tucatinib

Tucatinib (also known as Tukysa[TM], ONT-380, ARRY-380) is reversible small molecule that binds selectively to the kinase domain of HER2 and can cross the blood-brain barrier[72].

It was approved by the FDA on April 17, 2020, for use in combination with trastuzumab and capecitabine for the treatment of HER2+ MBC, including patients with brain metastases who has previously received one or more anti-HER2 treatments[73]. Moreover, tucatinib was approved in Switzerland, Australia, Canada and Singapore, and by EMA in 2021, expanding the treatment to patients with locally advanced or HER2+ MBC[74].

Tucatinib's approval by the FDA was based on the results of phase II HER2CLIMB trial (NCT02614794), where breast cancer patients with HER2-positive MBC (who had or did not have brain metastases) previously treated with trastuzumab, pertuzumab and trastuzumab-emtansine (T-DM1), received either tucatinib or placebo in combination with trastuzumab and capecitabine (tucatinib-combination or placebo-combination groups)[74]. The objective response was reached in 40.6% of patients receiving tucatinib versus 22.8% of those in the combination and placebo group of 511 patients. Amongst the 75 patients with active brain metastasis, intracranial objective response was improved (47.3% versus 20%, respectively), being consistent with the ability of tucatinib to penetrate the brain. The most common AEs registered in the tucatinib-combination group were diarrhoea, following by palmar-plantar erythrodysesthesia syndrome, fatigue, nausea, and vomiting. The HER2CLIMB-04 (NCT04539938)[75] open-label and single-arm trial is a phase 2 study that examines the safety and effectiveness of tucatinib and trastuzumab deruxtecan (T-DXd) in patients with HER2+ MBC who cannot undergo surgery and have undergone two or more prior HER2-based regimens in the metastatic setting. In comparison to treatment with tucatinib + capecitabine alone,

the combination of tucatinib + T-DXd + capecitabine produced statistically significant and clinically relevant improvements in progression-free survival (PFS), overall survival (OS), and PFS in patients with brain metastases. As a result, tucatinib in conjunction with T-DXd has been approved for use in patients with HER2+ MBC. The regulatory approval was based on data from the Destiny-Breast01 trial (NCT03248492), which was a single-arm study that confirmed a 61.4% confirmed objective response rate in patients with HER2+ MBC who had previously received T-DM1 treatment. Despite these advances, HER2+ MBC is still an incurable disease, and patients will eventually experience progression on existing treatments. Combining tucatinib and T-DXd may provide further improvements in efficacy compared to either agent used alone.

In addition, the I-SPY 2 trial (NCT01042379) represents a new generation Phase II neoadjuvant platform trial designed to rapidly identify new treatments and treatment combinations for high-risk, early-stage breast cancer. This ongoing multicentre trial is aimed at evaluating the efficacy of investigational treatment regimens against a shared control arm, which is the standard-of-care chemotherapy treatment. The primary endpoint of the trial is pathologic complete response (pCR), and the goal is to assess the activity of novel drugs in a priori defined biomarker subsets based on HR, HER2 expression, and MammaPrint status. Only patients with HR+HER2+ status and MammaPrint high or ultra-high-risk status are eligible for the trial[76–82]. Inside the I-SPY 2 trial, a ten-patient safety run-in to assess the safety and efficacy of tucatinib in combination with paclitaxel, pertuzumab, and trastuzumab was conducted. The objective of the run-in was to evaluate the safety of adding tucatinib to the existing combination therapy. Although the addition of tucatinib led to reversible liver function test elevations despite a reduction in tucatinib dosage, it resulted in a significant (>80%) reduction in tumour volume in 86% of the patients after 12 weeks. While tucatinib demonstrated a high level of activity when used with paclitaxel, trastuzumab, and pertuzumab, the combination was deemed unfeasible due to the observed safety concerns[83]. Furthermore, tucatinib is currently undergoing different clinical trials (Key clinical trials summarised in **Table 1.3**).

Table 1.3. Key clinical trials of tucatinib breast cancer patients.

ID	Drug(s)	Condition	Ps	Phase	Status	Ref.
NCT02892123	ZW25 (Zanidatamab) Capecitabine Vinorelbine Tucatinib	HER2-expressing cancers	279	I	Active, not recruiting	[84]
NCT05382364	Tucatinib	HER2+ MBC GEC Colorectal Cancer	25	I	Active, not recruiting	-
NCT02025192	Tucatinib Capecitabine Trastuzumab	HER2+ MBC	60	I	Completed	[74]
NCT01983501	Tucatinib T-DM1	HER2+ BC	57	I	Completed	[85]

NCT05553522	SRS Tucatinib Trastuzumab Capecitabine	Brain metastasis HER2+ BC	40	I	Not yet recruiting	-
NCT03054363	Tucatinib Palbociclib Letrozole	HER2+ BC	42	Ib-II	Active, not recruiting	-
NCT04538742	T-DM1 Durvalumab Paclitaxel Pertuzumab Tucatinib	HER2+ MBC	245	Ib-II	Recruiting	[86]
NCT04896320	Tucatinib	HER2+ MBC BC Stage IV	40	I-II	Recruiting	-
NCT05230810	Alpelisib Tucatinib Fulvestrant	PIK3CA-Mutant HER2+ MBC	40	Ib-II	Recruiting	-
NCT05319873	Carboplatin Docetaxel Fulvestrant Pertuzumab Ribociclib Trastuzumab Tucatinib	HER2+ MBC	18	Ib-II	Recruiting	-
NCT03501979	Tucatinib Trastuzumab Capecitabine	HER2+ MBC LMD	17	II	Active, not recruiting	-
NCT02614794	Tucatinib Capecitabine Trastuzumab Placebo	HER2+ BC	612	II	Completed	[74,87]
NCT04579380	Tucatinib Trastuzumab Fulvestrant	Locally advanced Unresectable or metastatic solid tumours driven by HER2 alterations	217	II	Active, not recruiting	-
NCT04721977	Tucatinib Trastuzumab Capecitabine	BC	56	II	Active, not recruiting	-
NCT04760431	Trastuzumab Taxanes Pertuzumab TKIs (Tucatinib)	Brain metastasis HER2+ BC	120	II	Not yet recruiting	-
NCT05748834	Tucatinib Doxil	HER2+ locally advanced or MBC	36	II	Not yet recruiting	-

NCT05800275	Tucatinib Capecitabine Trastuzumab	HER2+ MBC LMD	30	II	Not yet recruiting	-
NCT01042379	Tucatinib Trastuzumab Pertuzumab + Standard therapies	HER2+ BC HER2+ MBC Angiosarcoma TNBC HR+ tumour HR- tumour Early-stage BC Locally advanced BC	5000	II	Recruiting	[88–91]
NCT04539938	Tucatinib T-DM1	HER2+ BC	70	II	Recruiting	[92]
NCT05041842	Tucatinib Pertuzumab Trastuzumab Hormone therapy Pertuzumab/ Trastuzumab	HER2+ MBC with isolated brain progression	55	II	Recruiting	-
NCT04789096	Tucatinib Pembrolizumab Trastuzumab Capecitabine	HER2+ MBC	50	II	Recruiting	-
NCT05583110	Tucatinib Trastuzumab Vinorelbine	HER2+ MBC Locally advanced HER2+ BC	49	II	Recruiting	-
NCT05323955	Trastuzumab T-DM1 Pertuzumab Tucatinib	Brain metastases HER2+ BC Advanced BC	48	II	Recruiting	[87]
NCT05458674	Tucatinib Eribulin Trastuzumab	HER2+ MBC	30	II	Recruiting	-
NCT04457596	T-DM1 Placebo Tucatinib	HER2+ BC	1031	III	Recruiting	[93]
NCT05132582	Tucatinib Trastuzumab Pertuzumab Trastuzumab/Pertuzumab Placebo	HER2+ BC	650	III	Recruiting	-
NCT03975647	Tucatinib Placebo T-DM1	HER2+ BC	565	III	Recruiting	-

Current clinical trials that are complete, active, or recruiting. Information as on https://clinicaltrials.gov (information correct as of 8th May 2023). MBC =metastatic breast cancer; BC= breast cancer; T-DXd= Trastuzumab deruxtecan.; GEC = Gastric or Gastroesophageal Junction Adenocarcinoma; LMD = Leptomeningeal Disease; SRS = Stereotactic Radiosurgery; Ps = participants.

1.3 Extracellular vesicles

Extracellular vesicles (EVs), classically termed exosomes and microvesicles (MVs), are a heterogenous group of lipid bilayer bound vesicles secreted by cells and transported in the bloodstream and other body fluids[94–100]. Although the EVs field became popular in the last decades, the first concept of EVs had profiled more than 150 years ago when Charles Darwin already proposed the idea of cells secreting gemmules, minute size particles that contain molecules that serve to communicate the secreting cells to other cell types[101,102].

Building on the research performed in recent years, the current evidence indicates that these EVs mediated a wide range of physiological and pathological cell-to-cell communication activities, carrying bioactive material from their cells of origin. EVs are also considered as mini-maps of those cells, and interest in them has increased considerably due to their participation in numerous pathways including inflammation[103], tissue regeneration[104] and cancer, and due to their potential use as minimally invasive biomarkers and advanced drug delivery systems[97].

Substantial efforts are being invested in establishing guidelines to give support in EVs classifications, separation methods and establishment of EVs profiles in different biofluids. In 2018, the International Society for Extracellular Vesicles (ISEV) published the minimal information for studies of extracellular vesicles (MISEV2018) for the appropriate establishment of EVs separation methodologies and essential characterisation[105]. However, a lack of standards and consensus on the most optimal separation and purification method is still widespread[102,106].

EVs are frequently categorised based on their cellular origin, content, or physical properties such as size or density[107].

Based on their biogenesis, two subclasses of EVs exist; exosomes, formed by an endosomal pathway, derived from multi-vesicular bodies (MVB) and with a range in size from 30-150 nm, and MVs /ectosomes involving the endocytic route and being released directly from the cell membrane, with a higher range size vesicles (>150-1000 nm) (**Figure 1.2**).

Although the use of different terms has been reported (such as exomeres, ectosomes, large oncosomes (LOs), migrasomes, melanosomes, among others) to refer to EVs and/or apoptotic bodies it is difficult to determine whether EVs released outside the cell originated from the cell's endosomal region or directly from the cell membrane. Additionally, it is worth noting that there is no clear distinction between EVs sizes, and vesicles smaller than 150 nm can also bud from the cell membrane. Despite these challenges, it is crucial to understand the contribution of EVs, regardless of their size and origin, in diseases such as cancer.

Exosome's formation involves an endosomal route, involving the formation of early endosomes by inward budding of the cell membrane. Early endosomes' membranes invaginate to form intraluminal vesicles (ILVs), which are contained in MVBs. Those MVBs are then transported to the trans-Golgi network (TGN), a major secretory pathway sorting station. Here, these vesicles could follow different fates including endosome recycling, and the degradation of all their content by lysosomes, or their fusion with the cell membrane resulting in the release of exosomes to the extracellular space[107–110]. The endosomal-sorting complex required for transport (ESCRT) machinery is crucial for this process and involves four complexes (ESCRT-0, ESCRT-I, ESCRIT-II, and ESCRT-III) as well as associated

proteins including the APTase vacuolar protein sorting 4 (Vps4), the tumour susceptibility gene 101 protein (Tsg101) and the programmed cell death 6-interacting protein (ALIX).

ESCRT-0 orchestrate the recognition of ubiquitinated proteins and their sorting for ILVs integration. ESCRT-I and ESCRT-II are responsible of membrane deformation, creating membrane necks and recruitment of ESCRT-III and Vps4 produce vesicle neck fission and MVBs formation as well as ESCRT-III complex dissociation and recycling [98,111–115].

Recent studies established an ESCRT-independent pathway in exosome biogenesis involving lipids and associated protein including tetraspanin[116]. The cell membrane presents subdomains enriched in cholesterol, sphingolipids and glycosyl-phospathidylinositol (GPI)-anchored proteins known as lipid rafts and their presence stimulate the budding process and ILVs production[117].

In contrast to exosomes, MVs or ectosomes are release from the plasma membrane via budding or pinching. However, MVs can be generated through different mechanisms, some of them seems overlap with those involved in exosome biogenesis[118,119]. In addition, lipid rafts play an important role in budding and pinching of the cell membrane, and several studies shown that cholesterol is also essential to MVs release[107]. However, the precise mechanism underlying their formation and release is not well comprehended. An additional mechanism of MVs biogenesis is connected to non-apoptotic cell membrane blebs, frequently founded in aggressive cancer cells. These can be released as MVs via actin cytoskeleton reorganisations [119–124].

Apoptotic bodies (1000-5000 nm), released from apoptotic cells[125–127], are responsible for removing damaged cellular debris and are ultimately eliminated via phagocytosis[128]. The formation of apoptotic bodies is preceded by a sequence of distinctive events within dying cells, which ultimately result in the packaging of the cellular contents inside apoptotic bodies[129,130]. Among the critical alterations that occur are DNA fragmentation, externalisation of the plasma membrane, cell shrinkage, detachment from the extracellular matrix, and plasma membrane blebbing[131]. The formation of apoptotic bodies is vital for the survival of organisms as it prevents toxins and degrading enzymes from leaking into healthy cells[132,133]. Following the activation of caspase-mediated apoptotic pathways, the formation of apoptotic bodies is activated by Rho-associated coiled-coil-forming kinase I (ROCK1)[134]. Once the cellular content is packaged into apoptotic bodies, a sequence of events occurs, such as enucleation, expansion, and retraction, as described by Orlando et al. (2006)[135].
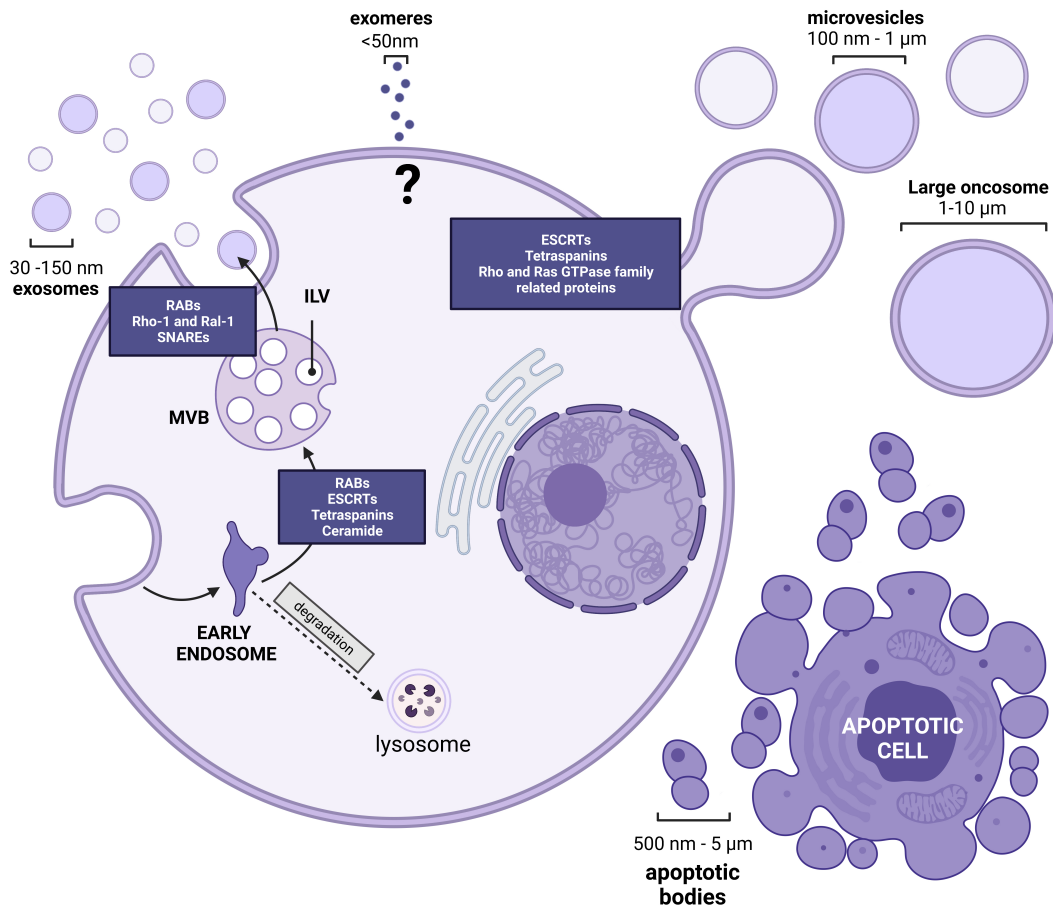
Figure 1.2. Extracellular vesicle biogenesis and secretion.

Schematic representation of the biogenesis and secretion of extracellular vesicles (EVs), specifically exosomes and microvesicles (MVs), by eukaryotic cells. Exosomes are generated from intraluminal vesicles (ILVs) that bud into early endosomes and multivesicular bodies (MVBs). The formation of ILVs involves various molecules, including lipids like ceramide and proteins such as tetraspanins (e.g., CD63, CD81, and CD9), as well as the endosomal sorting complex required for transport (ESCRT) machinery. The transportation of MVBs to the plasma membrane is facilitated by several Rab small guanosine triphosphatases (GTPases), and their fusion with the plasma membrane is aided by proteins like Rho-A, Ral-1, and soluble N-ethylmaleimide-sensitive factor attachment protein receptors (SNAREs). MVs, on the other hand, are generated by various proteins, including proteins associated with the Rho (ROCK) and the Ras GTPase family that control cytoskeleton rearrangements. Illustration created in *BioRender.com*.

In addition to the subtypes of EVs, there are other types that have been described in the literature. Exomeres, which are non-membranous nanoparticles with a size below 50 nm, were only recently discovered. It is possible that exomeres are aggregates of molecules, and further research is needed to elucidate their biogenesis and functional properties[136].

Migrasomes (500-3000 nm) were firstly described by Ma et al (2015)[137] and are generated by migrating cells. Their biogenesis ("migracytosis") depends on cell migration and actin polymerisation[138,139].

LOs (1000-10,000 nm) are exclusively release by cancer cells. LOs were firstly described in the scientific literature by Di Vizio et al. (2012)[140], although the term "oncosome" was originally conceived by Al-Nedawi et al. (2008)[141] to describe glioma-derived MVs containing a truncated oncogenic form of the EGFR, known as EGFRvIII. Additionally, previous studies have demonstrated that the detection of LOs can distinguish between healthy and cancer cells/tissues, especially in prostate cancer models[142]. However, further research is necessary to elucidate the role of LOs in other tumour models.

1.3.1 EVs sub-populations

As mentioned in previous section, EVs are defined based on different characteristics including biogenesis. However, taking into consideration the difficulty of assigning an EVs to a particular biogenesis pathway, the limitations of the terminology and the lack of consensus for specific EVs subtype markers, MISEV2018 suggested common definitions of EVs. MISEV2018 defined terms for EVs subtypes based on physical characteristics such as size or density, biochemical composition, and descriptions of conditions or cell of origin.

Regarding the size, MISEV2018 established three subcategories with ranges defined as small vesicles (sEVs) (<100 nm), or medium/large vesicles (m/lEVs) (>200 nm)[105]. One of the main methods of distinguishing different sub-populations of EVs is the use of immunoblotting to determine specific combination of protein markers often involved in their biogenesis. Distinct sets of proteins can determine the sub-population of EVs being studied. In keeping with this, MISEV guidelines also gave a clear overview of which proteins should be present on EVs and how to distinguish what sub-population is under investigation. **Table 1.4** lists some of the proteins that have been enriched in each subpopulation and includes protein markers that are used in this project. For general characterisation, MISEV 2018 guidelines recommended at least three positive protein markers for EVs, including at least one transmembrane/lipid-bound protein (Category 1) and cytosolic protein (Category 2), and at least one negative protein marker (Category 4).

Table 1.4. Protein markers for EVs sub-populations according to MISEV2018 guidelines.

EVs marker	MISEV Category	Large EVs	Medium EVs	Small EVs
CD9	1b	✓	✓	
CD63	1a	✓	✓	✓
CD81	1a	✓	✓	✓
Syntenin	2a	✓	✓	✓
Calnexin	4c	✓		
GRP94	4c	✓		

1.3.2 EVs in breast cancer

Several studies were performed on breast cancer to establish the relevance of EVs in numerous processes in cancer. This group[143] investigated the relevance of EVs in TNBC and demonstrated that EVs can confer phenotypic attributes of their cells of origin to other cells. In addition, Harris et al. (2015)[144] investigated the role of EVs in cancer progression using different breast cancer cell lines which possess different metastatic potential. This study showed that EVs promote cell migration and this stimulation directly depends on the metastatic potential of the cell of origin. Other studies in breast cancer also founded that EVs derived from breast cancer cells play a role in angiogenesis[145], immune response suppression and evasion, stimulate tumour growth [119,146] and also the transmission of resistance to anti-cancer drugs[147].

On the latter, EVs can mediate the transmission of drug resistance through different mechanisms including the suppression of immune cells[148–150], decreased the availability of the drug by sequestering and/or removing drug and thus decreasing the available drug concentration, and by transmitting the resistance from drug-resistant to drug-sensitive cells[151,152].

EVs can also affect not only to treatments based on small molecules but also monoclonal-antibody therapies. Research has shown that the up-regulation of miR-21 in sEVs is closely linked to trastuzumab resistance, both *in vitro* and *in vivo*[153–155]. Those sEVs not only contribute to resistance but also decrease the efficacy of trastuzumab. Ciravolo et al. (2012)[147] found that EVs from the HER2+ cell lines, SKBR3 and BT474, can bind trastuzumab, decreasing its bioavailability and so its effectiveness. EVs were also obtained from breast cancer patients' serum, and supporting the study performed *in vitro*, most of the EVs samples from breast cancer patients with HER2-overexpressing tumours had HER2-bearing EVs that bound to trastuzumab[146]. Consistent with these findings, sEVs derived from those breast cancer cells (BT474 and SKBR3) were found to decrease the trastuzumab-induced toxicity of peripheral blood mononuclear cells (PBMCs) to BT474 cells[156].

Moreover, a study performed previously in our group discovered that the resistance to anti-HER2 targeted drugs and anti-tumour immune response in HER2+ breast cancer is related to an increased level of transforming growth factor-beta 1 (TGF-β1) and programmed death-ligand 1 (PD-L1). These immunosuppressive molecules were carried by EVs from drug-resistant cells and were found in the serum of patients who got little benefit from treatments with HER-targeted drugs. This suggests their potential as predictive biomarkers companion diagnostics[146].

Analysing the downstream signalling pathways of sEVs' cargo molecules and the regulation of target genes expression can contribute to understand the drug resistance mechanism(s). It has been reported that anti-cancer drugs can significantly increase the secretion of sEVs from tumour cells, leading to chemoresistance and post-therapy relapse through the activation of signalling pathways and induction of inflammation[157]. Similarly, sEVs carrying the long non-coding ribonucleic acid (RNA) AGAP2 antisense RNA 1 (AGAP2-AS1) were found to enhance trastuzumab resistance in BT474 HER2+ breast cancer cells[158].

These advances in understanding the key role that EVs play in cancer only scratch the surface of their full implications and potential. Not only deciphering the different mechanisms by which they act, but also unravelling this drug-resistance communication may contribute to a therapeutic benefit for cancer patients, thus increasing their prognosis and survival.

1.4 Hypoxia signalling in breast cancer

Hypoxia refers to a physiological condition in which the oxygen supply to tissues is insufficient to maintain normal cellular function and homeostasis. This condition may arise from a variety of causes, including reduced oxygen supply due to decreased blood flow, low oxygen content in the blood (hypoxemia), or impaired oxygen utilisation by cells. The consequences of hypoxia can be severe and may include tissue damage, organ dysfunction, and even cell death[159]. In the context of cancer, hypoxia refers to a condition in which there is a low level of oxygen in the tumour microenvironment (TME) due to the demand for oxygen by the rapidly dividing cancer cells that exceeds the supply of oxygen from the blood vessels (frequently poorly formed and leaky) within the tumour. As a result, cancer cells undergo adaptations to survive and proliferate in this low oxygen environment, including the activation of specific pathways which leads to the production of proteins that promote cell survival and angiogenesis (the formation of new blood vessels) to provide a source of oxygen and nutrients to the tumour. Hypoxia-inducible factors (HIFs), which were initially discovered in the 1990s, are primarily responsible for regulating responses to hypoxia[160–162].

The hypoxia-inducible factor 1α (HIF-1α) is the key regulator that mediates the cellular response and survival to this condition[163–165]. HIFs are central players in cellular responses to low oxygen levels, composed of two basic helix-loop-helix proteins of the Per-ARNT-Sim (PAS) family: an oxygen-sensitive α-subunit and a constitutively expressed β-subunit[166]. Three HIF-α isoforms have been identified in mammals, with HIF-1α having a wide range of target genes, while HIF-2α exhibits more tissue-restricted expression, and less is known about HIF-3α[167]. The stability of HIF-α family proteins can be regulated by oxygen levels. In normoxic conditions, HIF-α subunits' hydroxylation within their oxygen-dependent degradation domain occurs at two critical proline residues by HIF prolyl hydroxylase domain family proteins (PHDs), using O_2, ferrous iron, and α-ketoglutarate as substrates. Mammals have three PHD subtypes, PHD1, PHD2, and PHD3, which regulate HIF-1α oxygen sensors' degradation. PHD2 is the main rate-limiting enzyme that keeps HIF-1α at a stable low level in an anoxic environment, and its activity is mainly controlled by the intracellular oxygen concentration. The von Hippel–Lindau tumour suppressor protein (pVHL) binds to HIF-α after hydroxylation and recruits an E3 ubiquitin ligase complex, leading to ubiquitination and proteasomal degradation of HIF-α. In the absence of oxygen, the hydroxylation process that inhibits HIF-α is decreased, causing HIF-α to become stable and translocate to the nucleus, where it pairs with HIF-β forming a dimer[168]. The HIF-α/β dimer interacts then with the transcriptional coactivator p300/CBP and hypoxia response element to activate the expression of HIF target genes located in the promoter region[169,170]. This mechanism is illustrated in **Figure 1.3**.
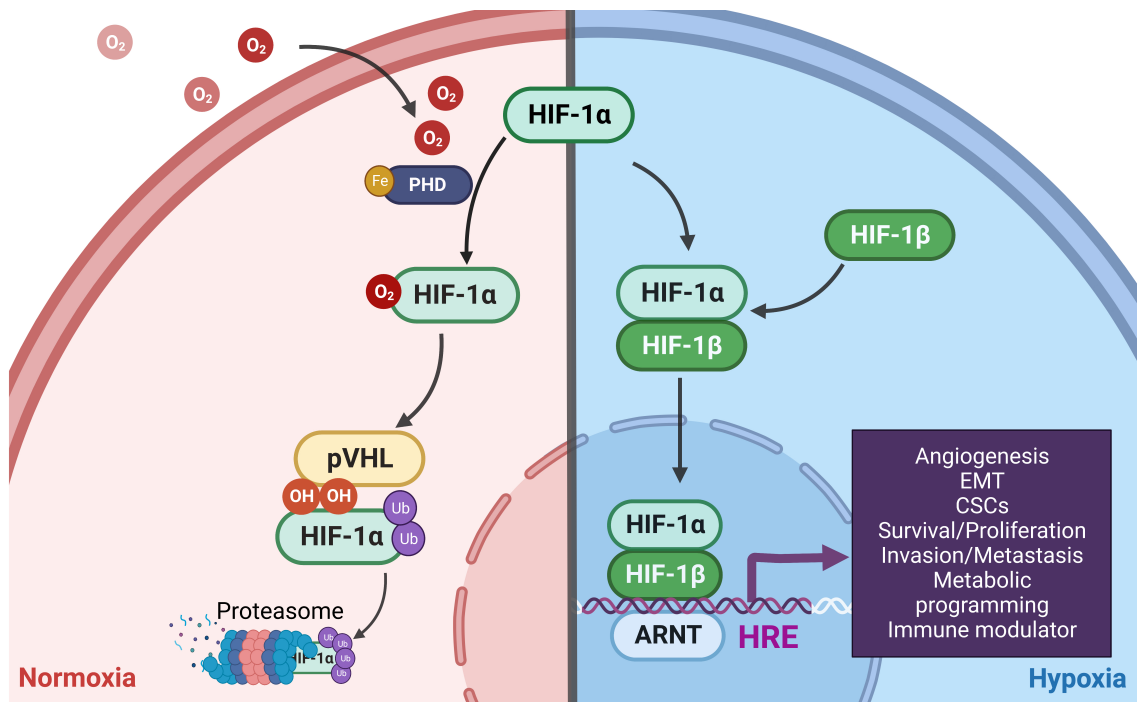
Figure 1.3. Overview of the HIF-1α pathway in normoxia and hypoxia.

Under normoxic conditions, HIF-1α subunit is hydroxylated by HIF prolyl hydroxylase domain family proteins (PHDs) and ubiquitinated by the von Hippel–Lindau tumour suppressor protein (pVHL) complex. These modifications indicate the degradation of the subunit by proteasome 26S. Under hypoxia, the HIF-1α subunit is stabilised and able to bind to the HIF-1β. The transcription factor is then translocated to the nucleus to bind the promotor region, resulting in the stimulation of the transcription of hypoxia related genes and the activation of cancer-related processes. *ARNT = Aryl hydrocarbon receptor nuclear translocator; HRE= Hypoxia response element*. Illustration created in *BioRender.com*.

Activation of the HIF pathway leads to the up-regulation of a variety of genes involved in the cellular response to hypoxia. These include genes encoding proteins involved in angiogenesis (i.e., VEGF, SDF1, KITL), glucose metabolism (i.e., GLUT1, GLUT3, PDK1, GAPDH, ENO1, and LDHA)[171], and erythropoiesis (i.e., EPO). The HIF pathway is also involved in the regulation of cell survival and apoptosis, as well as immune function and inflammation. Immunohistochemical analyses reveal that HIF-1α and HIF-2α are frequently overexpressed in human cancers and, besides intratumoural hypoxia, genetic alterations commonly observed in cancer can also modulate the expression of HIF-dependent target genes. Breast cancer is an example of this, where various signalling pathways, such as EGFR, AKT, PI3K, PTEN, mTOR, TP53, and HER2, can be altered to regulate HIF-dependent gene expression. For instance, Li et. al.[172] reported an interaction between the HIF and PI-3K/Akt pathways in HER2-overexpressing cancer cells. The findings of this study suggest that Akt-mediated HIF activation can be induced by HER2, suggesting that activation of the HER2/Akt pathway could promote angiogenesis in a hypoxia-independent manner. These results could have significant implications for the oncogenic effects of HER2 and Akt[160].

In recent years, there has been increased attention on HIF-1α and its relationship with drug resistance in various types of cancer cells. Different subtypes of breast cancer also showed different levels of HIF-1α expression[173]. In a study of 900 breast cancer patients, Bane et al. (2014) observed significant differences in HIF-1α expression between Luminal A tumours (46% positive), HER2-positive tumours (69% positive), and basal tumours (85% positive)[174]. As mentioned before, it has been found that HER2 signalling through the PI3K/AKT pathway increase HIF-1α activity[175]. However, PTEN, a protein that opposes HIF-1α, is present in approximately 60% of HER2-positive patients[176]. As a result, HER2+/PTEN- tumours may have elevated HIF-1α expression and increased drug resistance. Animal models and human studies have shown that hypoxic tumours exhibit an exacerbated drug resistance, which is linked to the overexpression of HIF-1α and HIF-2α. This resistance is associated with decreased OS rates[177]. Although the significance of HIF-1α-dependent drug resistance in breast cancer is well-established, the precise molecular mechanisms that result in reduced drug efficacy are yet to be fully understood. For instance, it has been shown that the activation of the STAT3/HIF-1α/Hes-1 signalling pathway leads to resistance to trastuzumab in SKBR3 HER2-overexpressing breast cancer cells. This resistance is mediated by the down-regulation of the tumour suppressor PTEN, suggesting that its targeting could be a potential strategy to overcome trastuzumab resistance in HER2-positive breast cancer[178].

1.5 Hypoxia and EVs' release in the context of cancer

Studies have shown that hypoxia has an impact on the production, size, and molecular composition of EVs in cancer. However, different observations have been reported using various cell models and hypoxic treatments[179–182].

Hypoxia can promote the biogenesis of ILVs and increase the secretion of EVs. The external microenvironment, including hypoxia, can regulate the selective loading of micro-RNAs (miRNAs; miRs) in the EVs. EVs biogenesis is a complex process that depends on the cargo and cell type. Hypoxia can regulate the expression of Rab proteins, including Rab7, Rab27a, and Rab22a, which promote the release of EVs in ovarian and breast cancer cells[180,183]. Rab5 has been shown to regulate EVs secretion in hypoxic prostate cancer cells by regulating the transport and fusion of early endosomes[184]. Hypoxia can also affect the rearrangement of the actin cytoskeleton through ROCK to influence EVs' release[185]. Hypoxia can also promote autophagy, which may affect the balance between the degradation of MVs and the release of exosomes[186]. Therefore, further investigation is needed to understand the complex mechanisms of EVs secretion in the hypoxic microenvironment. Hypoxia also have an impact in the EVs' cargo. Under hypoxia, miRNA levels in EVs are higher than under normoxia, and miRNA sorting may depend on HIF signalling[187]. Hypoxic EVs facilitate various cancer-related processes such as angiogenesis, proliferation, epithelial-mesenchymal transition (EMT), and metastasis through their cargo. Certain miRNAs, such as miR-210 and miR-135b, encapsulated within EVs, have been identified to play a crucial role in promoting angiogenesis and metastasis. These miRNAs could potentially serve as biomarker candidates or therapeutic targets for cancer treatment. miRNA-210 is one of the most stable and important miRNAs up-regulated in response to hypoxia. HIF-1α can directly bind to the hypoxia responsive element on the miR-210

promoter to regulate its expression[188]. In ovarian cancer, HIF induces the release of EVs enriched in various miRNAs, including miR-21-3p, miR-125b-5p, and miR-181d-5p[189]. However, the specific mechanisms of how hypoxia affects miRNA distribution in EVs still require further investigation. In breast cancer, miR-210 plays a role in the expression of vascular remodelling related genes, such as Ephrin A3 and PTP1B, which promote angiogenesis. Additionally, long non-coding RNA (lncRNAs) lncRNA SNHG1, enriched in hypoxic breast cancer cell-secreted exosomes, promotes angiogenesis, proliferation, and migration of Human umbilical vein endothelial cells (HUVECs). Studies indicate that hypoxic exosomes are preferentially taken up by hypoxic cancer cells, and GPR64, an autophagy-associated protein, is up-regulated in hypoxic exosomes derived from breast cancer-associated fibroblasts, stimulating the NF-κB pathway to enhance the invasiveness of recipient breast cancer cells. Besides, hypoxic exosomes also function in a paracrine manner in tumour development. Breast cancer cells encapsulate TGF-β into exosomes under hypoxia, which can be taken up by T cells, suppressing T cell proliferation and contributing to the immunosuppressive microenvironment in tumour progression[179,190,191].

Therefore, understanding the role of hypoxia in breast cancer and the special characteristics of hypoxic EVs could provide new insight into elaborating the role of hypoxia in the resistance to anti-HER2 therapies, and it is essential for the development of new therapeutic strategies that can overcome the challenges posed by hypoxia in breast cancer treatment.

1.6 *In vitro* preclinical models in cancer research

The use of *in vitro* and *in vivo* models has been and continues to be crucial in cancer research, enabling drug screening, the development of cancer therapies, drug screening, and a greater understanding of the molecular mechanisms of tumour growth and metastasis[192]. However, only 10% of potential anti-cancer drugs succeed during their clinical development, mainly due to a lack of efficacy or intolerable toxicity[193–195]. Animal models are usually too expensive, complicated, laborious to work with, and associated with ethical issues. It is noteworthy that some effects may appear which do not represent a specific human event and so limit their applicability. Moreover, the 3R strategy has been gaining presence in research and *in vitro* cell cultures have been used together with new methods developed in recent years to avoid large-scale and intensive animal testing[196,197]. Drug development, among other fields, requires *in vitro* models capable to produce reliable biomedical information through mimicking the cells' phenotype as it exists in the target tissue [198,199]. The simplest and most common approach for *in vitro* cancer studies is the monolayer culture of cancer cells in two-dimensional (2D) conditions. Nevertheless, its limitations have been increasingly recognised, mainly as an oversimplified version of tumour conditions *in vivo*, failing to address many of the more dominant pathological problems, such as the TME. Moreover, 2D cultures do not conserve the original shape and polarisation of cells[197,200]. To make real advances of precision medicine, new pre-clinical models that better represent *in vivo* biology and the microenvironmental factors, while also respecting the rights of animals, are urgently needed[192]. Since Mina Bissell studied (in 1980) the importance of the extracellular matrix (ECM) in cell behaviour, it is established that the three-dimensional (3D) cell culture models, in contrast to the 2D models, represents more

accurately the actual microenvironment and their behaviour is more reflective of *in vivo* cellular responses[201–203]. However, these models still have limitations to accurately represent the TME. Different approaches are being used to increase the complexity of the models. These start with the use of 2D co-cultures, including stromal cells, increasing stepwise with the use of 2.5D cultures, consisting of cells sandwiched between the surface and a layer of ECM, and finally 3D complex structures[202–204]. 3D cultures can be designed using different approaches including non-scaffold-based methods, scaffold-based technologies, specialised 3D culture platforms, as well as mathematical modelling[202]. The most common types of *in vitro* tumour models are summarised in **Figure 1.4**.
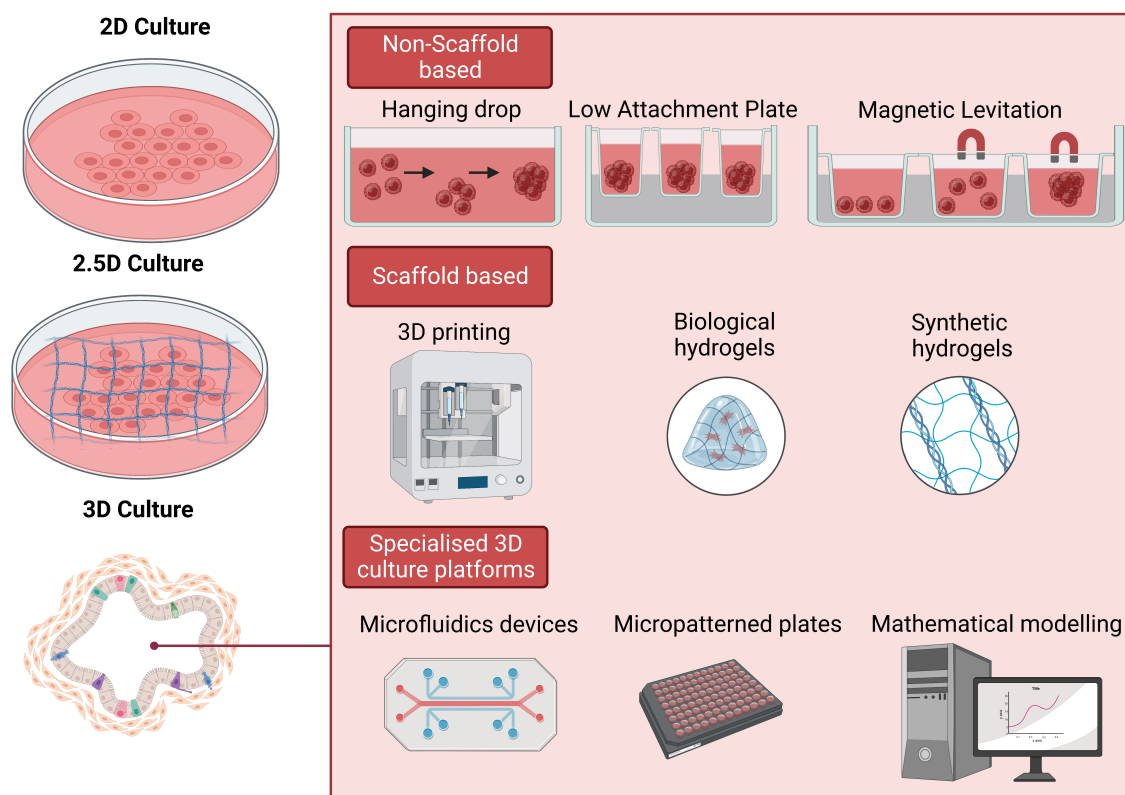
Figure 1.4. Most common *in vitro* models.

Illustrative scheme of the most common approaches for in vitro cell culture models. The most used techniques for 3D cell culture are collected in the red square: non-scaffold-based methodologies, scaffold-based methodologies, and specialised 3D culture platforms. Illustration created in *BioRender.com*.

Despite the strong recommendations to upgrade cell culture from 2D to 3D models, these approaches have not been extensively incorporated in research. Some of the issues preventing their regular use are the reproducibility, cost, time to set up, confusing terminology, as well as the necessity of a guidelines for techniques standardisation, among others[200,205].

1.7 Aims

This project focuses on the understanding of the transmission of resistance to anti-cancer drugs from cell-to-cell. Previous research initially performed by our group firstly and validated by others has shown that EVs are involved in transmitting resistance, causing previously drug-sensitive cells to become drug-resistant. Furthermore, we have evidence to suggest that EVs might bind drugs such as trastuzumab (Herceptin) and thus reduce it bioavailability to its receptor (HER2) on cancer cells. Collectively this means that EVs may be substantially inhibiting cancer patients gaining benefit from anti-cancer drugs. The <u>aim</u> of this project is to gain an in-depth understand of neratinib-resistance mechanism(s) in HER2+ breast cancer as well as further understand the involvement of EVs in those mechanism(s) and to investigate ways of exploiting this information present on the EVs. The major accomplishments of this project will be to discover new pathways and biomarkers involved in resistance to anti-cancer drugs, to better improve the general knowledge that we have on this field and future benefit for patients.

This aim included the accomplishment of the following objectives:

1. Perform an EVs separation methods comparison on conditioned media obtained from three different HER2+ breast cancer lines to compare the efficacy to enrich EVs from cell culture supernatants.
2. Compare proteome profiles of neratinib-sensitive and neratinib-resistant HER2+ cells to gain insights into the mechanisms of neratinib resistance in HER2+ breast cancer. Next, elucidate new mechanisms that may be responsible for neratinib resistance.
3. Fully characterise the EVs released from those neratinib-sensitive and neratinib-resistant cells and to investigate if those EVs reflect the HER2 status of their cells or origin, having potential as minimally invasive biomarkers.
4. Understand hypoxia's influence on EVs released by neratinib-sensitive and neratinib-resistant HER2+ breast cancer cell lines and their cargo.
5. Determine the suitability of a 3D cell culture model for EVs analysis of EVs released by HER2+ breast cancer cell lines cultured under normoxic and hypoxic conditions. Consequently, investigate the effect of hypoxia on the release of EVs under 3D conditions.
6. Perform the first global survey of current use of pre-clinical *in vitro* models in cancer research, to offer a snapshot of the different *in vitro* models used in cancer research and to help to identify the trends and practices in cancer research and for future standardisation.
7. Evaluate the effect of tucatinib in the release of EVs in breast cancer cell lines, to study the mechanism behind how cancer cells can promptly evade an anti-tumoral treatment.

Chapter 2

Evidence for the need to evaluate more than one source of EVs, rather than single or pooled samples only, when comparing EVs separation methods

Abstract

To study and exploit EVs for clinical benefit as biomarkers, therapeutics, or drug delivery vehicles in diseases such as cancer, typically we need to separate them from the biofluid into which they have been released by their cells of origin. For cultured cells, this fluid is conditioned medium (CM). Previous studies comparing EVs separation approaches have typically focused on CM from one cell line or pooled samples of other biofluids. We hypothesize that this is inadequate and that extrapolating from a single source of EVs may not be informative. Thus, in our study of methods not previously compared (i.e., the original differential ultracentrifugation (dUC) method and a PEG followed by ultracentrifugation (PEG+UC) method), we analysed CM from three different HER2-positive breast cancer cell lines (EFM192A, HCC1954, and SKBR3) that grow in the same culture medium type. CM from each was collected and equally divided between both protocols. The resulting isolates were compared on seven characteristics/parameters including particle size, concentration, structure/morphology, protein content, purity, detection of five EVs markers, and presence of HER2. Both dUC and PEG+UC generated reproducible data for any given breast cancer cell lines' CM. However, the seven characteristics of the EVs isolates were cell line- and method-dependent. This suggests the need to include more than one EVs source, rather than a single or pooled sample, when selecting an EVs separation method to be advanced for either research or clinical purposes.

2.1 Introduction

EVs are lipid-bilayer-enclosed nanoparticles released by most, if not all, cells. The EVs' cargo may include proteins, RNAs, DNA, and lipids, and they are often described as mini maps of their cells of origin. The EVs' bioactive cargo is instrumental in their role in cell-to-cell communication, mediating a broad range of physiological and pathological activities[94–98]. EVs have traditionally been categorised based on size and sub-cellular origin[107], with those derived from multi-vesicular bodies and having a size of approximately 30–150 nm termed exosomes, while those originating by budding/pinching from the cell membrane and typically have a size greater than 150 nm considered to be MVs[107,110]. EVs are detectable in a broad range of biofluids including cultured cells' conditioned medium (CM), blood plasma and serum, milk, urine, saliva, and cerebrospinal fluid[206,207]. These important sources of EVs are commonly studied, but we must accept that once in a biofluid, we cannot claim the EVs' exact origin and exit route(s) from their donor cells. Thus, the generally accepted collective term for exosomes and MVs is EVs.

Substantial effort has been invested by the EVs community in establishing guidelines on minimal information for studies of extracellular vesicles (MISEV2018) and on supporting transparent reporting and centralising knowledge in EVs research to achieve increasing rigor and reproducibility of the knowledge generated[105,208]. It is generally accepted that, in many studies, EVs are not always completely isolated as pure EVs from other materials that exist in their biofluid and so the preferred term by many is "EVs separation" or "EVs enrichment", rather than isolation; thus, these are the terms we will use here. Furthermore, as one EVs separation method does not fit all purposes, understandably, there is no consensus on the optimal EVs separation method. Interestingly, however, a survey performed in 2019 showed that although ultracentrifugation (UC)-based methods derived from the protocol described by Théry et al. (2006)[209] remain the most popular EVs separation methods[210], the comparison between the 2019 survey and a survey performed in 2016 showed a significant ($p < 0.05$) increase in the use of precipitation methods[210,211]. Many such precipitation methods are claimed to represent user-friendly approaches, but the substantial trade-offs may be the reduced purity of isolates (as most published studies of precipitation methods use commercial kits that simply precipitate almost all content from the biofluid of interest), the substantial costs of kits, and the lack of information on the exact make-up of the kits' precipitant, which would prevent the progress to utility that involves regulatory bodies. Bridging these issues, at least in part, a polyethylene glycol (PEG)-based method was developed that combines PEG-based precipitation and UC, resulting in EVs enriched samples that are suitable for downstream functional *in vivo* pre-clinical studies[212]. Thus, we were interested in directly comparing the more traditional differential UC (dUC) method with the PEG followed by UC (PEG+UC) method.

Although the EVs separation methods compared here have not previously been compared, many good publications have arisen from studies comparing other EVs separation techniques. However, typically, these comparison studies, whether they include CM[213,214] or other biofluids such as blood[106,215], involve using one pooled source of EVs. For our study, comparing PEG+UC to the traditional dUC method, we hypothesised that simply analysing one pooled sample may not be adequate for a fully informed comparison and that a range of similar, but different, sources of EVs

should be included. Thus, to test our hypothesis, we compared EVs isolates from CM of three different HER2+ breast cancer cell lines that grow in the same medium type. A graphical representation of both EVs separation methods and the subsequent characterisation methods used is summarised in **Figure 2.1.**
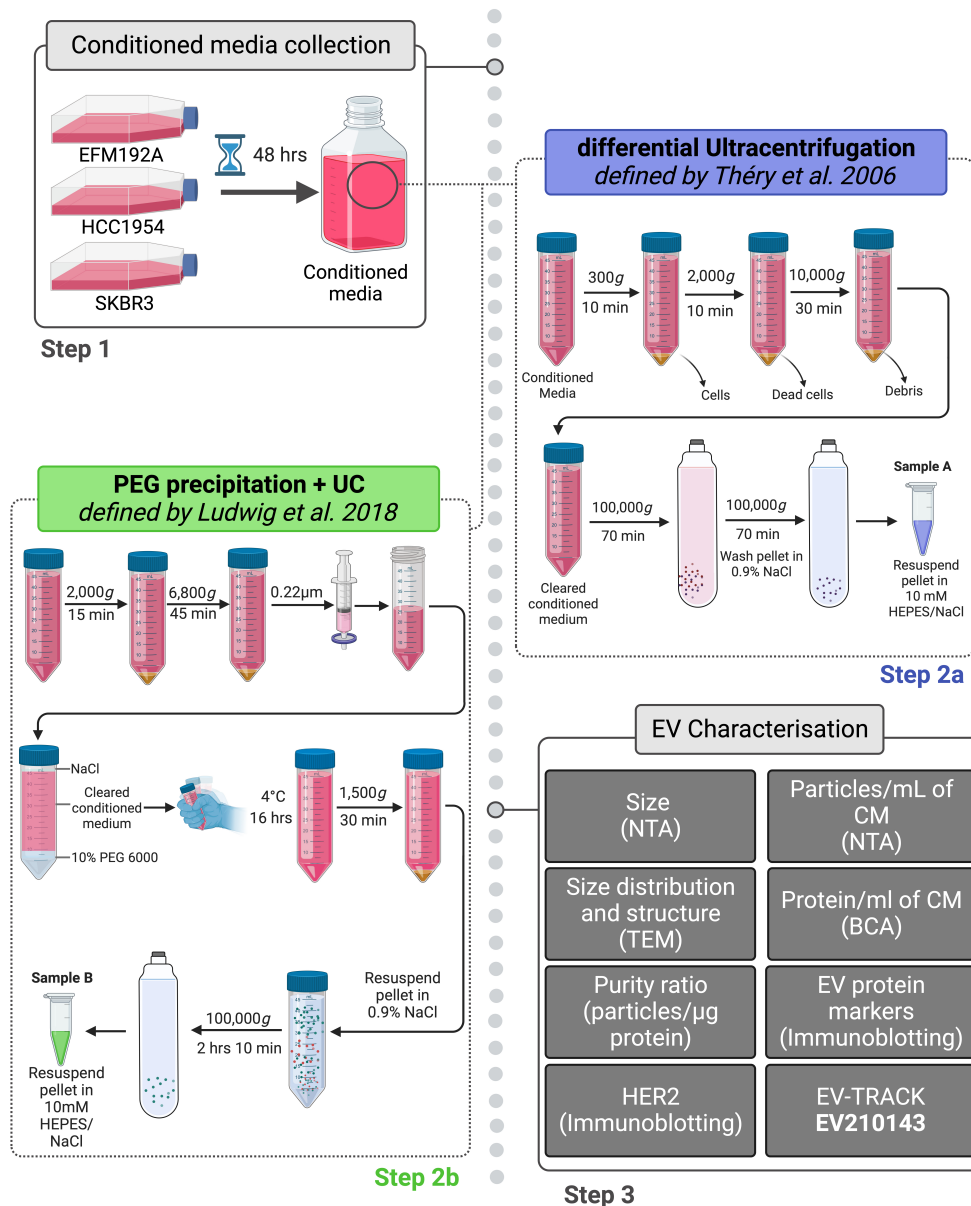
Figure 2.1. Flow diagram of methodology used.
(**1**) SKBR3, EFM192A, and HCC1954 cells were seeded in a complete medium and allowed to attach overnight. Complete medium was then replaced with medium containing EVs-depleted FBS (dFBS). After 48 hrs incubation, conditioned medium (CM) was collected and cells were counted. Each CM batch was divided into two equal volumes and used for EVs-enrichment method comparison (i.e., (**2a**) 312 ml of CM was used for EVs separation by differential ultracentrifugation (dUC); (**2b**) the other 312 ml were used for PEG-based method followed by ultracentrifugation (PEG+UC). The diagram shows the step-by-step of each approach used for EVs separation/enrichment and (**3**) the parameters evaluated during the subsequent characterisation of the isolates. The process was conducted a total of *n* = 3 times. Schematic representation was created with *BioRender.com*.

2.2 Aims of the study

The main aims of the study were to assess the adequacy of analysing a single pooled sample for making informed comparisons and to explore the necessity of including a range of similar but different sources of EVs. We hypothesised that relying solely on one pooled sample might not provide a comprehensive understanding of the suitability of the EVs separation method. To test this hypothesis, we compared EVs isolates obtained from the CM of three different HER2-positive breast cancer cell lines that were grown in the same medium type. By examining the EVs from these distinct sources, the study aimed to evaluate whether analysing multiple samples is essential for a more comprehensive and accurate comparison of EVs separation methods.

2.3 Materials and Methods

We submitted all relevant data of our experiments to the EV-TRACK knowledge base (EV-TRACK ID: EV210143)[208].

2.3.1 Cell culture

Three HER2-positive breast cancer cell lines (SKBR3, EFM192A and HCC1954) were routinely maintained in RPMI-1640 medium (Sigma-Aldrich, Cat. #: R0883) supplemented with 10% foetal bovine serum (FBS) (Thermo Fisher Scientific, Cat. #: 10270-106), and 2 mM L-Glutamine (Sigma-Aldrich, Cat. #: G7513) as complete medium. All cells were cultured at 37ºC with 5% CO_2 and routinely tested to ensure that they were free of *Mycoplasma* contamination by the reverse-transcriptase polymerase chain reaction (RT-PCR) (ATTC, Cat. #: 30-1212K).

2.3.2 EVs preparation from conditioned cell medium

Before CM collection, 26×T175 cm^2 flasks (Corning, Cat. #: 431080) for EFM192A (6×10^6 cells/flask), HCC1954, and SKBR3 (3×10^6 cells/flask) were seeded in complete RPMI-1640 medium. The medium was replaced the next day with RPMI-1640 medium containing 10% EVs-depleted- FBS (dFBS), 2mM L-Glutamine, and 1% penicillin/streptomycin (P/S) (Sigma-Aldrich, Cat. #: P4333). 1% P/S was only used for dFBS media for EVs separation. EVs-depleted FBS was collected after ultracentrifugation (18 hrs 30 min, 186,600 × *g*, 4ºC – Type 70Ti rotor, Optima XPN-100 ultracentrifuge, Beckman Coulter) and filtration through a 0.2 µm syringe filter (ThermoFisher, Cat. #: 723-2520). P/S was used for the EVs collection incubation period to prevent bacterial infections due to the increased handling involved in dFBS preparation.

After the cells conditioned the medium for 48 hrs, approximately 624 ml aliquots of CM were collected from each cell line and divided into equal volumes to progress through the two protocols illustrated in **Figure 2.1**. Cells were counted and their viability checked, showing all cultures to be ≥95% viable.

2.3.3 EVs separation by differential ultracentrifugation

For the dUC approach, separation of EVs was performed following the protocol described by Théry et al. (2006)[209]. Briefly, 312 ml freshly harvested CM was spun at 300× *g* for 10 min (5810R centrifuge, Eppendorf, Hamburg, Germany). The resulting supernatant was then centrifuged at 2,000× *g* for 10 min. After any dead cells were removed, the CM was further spun at 10,000× *g* for 30 min at 4ºC in a 5810R centrifuge. The supernatant was then transferred to 8 × 39 ml Quick-Seal® polypropylene centrifuge tubes (Beckman Coulter, Brea, CA, USA; Cat. #: 342414) and spun at 100,000× *g* for 70 min at 4ºC in an Optima XPN-100 Ultracentrifuge (Beckman Coulter) using a Type 70Ti fixed-angle rotor (Beckman Coulter, Cat. #: 337922). The resulting eight pellets with EVs were washed in a combined total of 39 ml of 0.9% NaCl (Sigma-Aldrich, Cat. #: 71376) and ultracentrifuged exactly as previously performed. The final EVs pellet was resuspended in 100 µl of 10 mM HEPES/NaCl (Thermo Fisher Scientific, Cat. #:15630049) and stored at −80ºC.

2.3.4 EVs precipitation by PEG+UC washing step

For the PEG + dUC approach, separation of EVs was performed following the protocol described by Ludwig et al. [212]. Briefly, 312 ml CM were spun at 2,000× g for 15 min and then 6,800× g for 45 min (5810R centrifuge, Eppendorf) and supernatants were filtered through a 0.2 µm syringe filter (ThermoFisher, Cat. #: 723-2520). A stock solution of PEG 6000 (50% (w/v)) (Sigma-Aldrich, Cat. #: 81260) was added to the supernatants for a final concentration of 10% PEG and 75 mM NaCl (Sigma-Aldrich, Cat. #: 71376). After inverting the tubes thrice to allow the samples to mix, the samples were stored at 4ºC for 16 hrs. Post 16 hrs incubation, samples were spun at 1,500× g for 30 min at 4ºC (5810R centrifuge, Eppendorf), and the supernatants were removed. To remove PEG residues, the pellets were combined and washed with 39 ml of 0.9% NaCl and transferred in 39 ml Quick-Seal® polypropylene centrifuge tubes (Beckman Coulter, Cat. #: 342414). Ultracentrifugation was performed using a Type 70Ti fixed-angle rotor (Beckman Coulter, Cat. #: 337922) in an Optima XPN-100 Ultracentrifuge (Beckman Coulter) at 110,000× g for 2 hrs 10 min at 4ºC. The final EVs pellet was resuspended in 100 µl of 10 mM HEPES/NaCl (Thermo Fisher Scientific, Cat. #:15630049) and stored at −80ºC.

2.3.5 Nanoparticle tracking analysis (NTA)

Average size distribution and particle concentration analyses of the EV-enriched isolates were performed using a NanoSight NS500 system (Malvern Instruments Ltd., Malvern). Brownian motion of the particles was captured at 30 frames/s speed. For this, EVs samples were diluted using filtered Dulbecco's Phosphate Buffered Saline (DPBS) (Sigma-Aldrich, Cat. #D8537), loaded onto the nanoparticle tracking analysis (NTA) using a NanoSight syringe pump, and videos of the particles were recorded and analysed using NTA version 3.3 software. Aliquots of the same filtered PBS were used as the control.

2.3.6 Collection of protein lysate and EVs lysate for immunoblotting analysis

Cells were seeded at densities detailed in **Section 2.3.2**. The following day, the medium was changed to 10% dFBS-containing RPMI-1640 medium as in **Section 2.3.2**. After 48 hrs of incubation, the medium was removed from the flask and the cells were washed twice with 4 ml of ice-cold PBS (Sigma-Aldrich, Cat. #: D8537). After washing, 1 ml of PBS was added to the flask and the cells were scraped by using a sterile cell scraper (Fisher Scientific, Cat. #: 08-100-241). Then, cells were placed in a 1.5 ml centrifuge tube (Eppendorf, Cat. #: 0030123328) and centrifuged at 10,000× g at 4°C for 5 min. After centrifugation step, supernatant was removed and the pellet was resuspended in 50 µl of cell lysis buffer (Invitrogen, Cat. #: FNN0011) and 1X protease inhibitor (Roche, Cat. #: 05892970001). The cell lysate was incubated for 30 min on ice, vortexed thrice (every 10 minutes, 10 sec). After 30 min incubation, the samples were centrifuged at 16,000× g at 4°C for 10 min and supernatant was transferred to a new 1.5 ml centrifuge tube and stored at -20°C until required. EVs

30

aliquots were lysed by using 1:1 ratio of EVs suspension (50 µl) and lysis buffer with protease inhibitor.

2.3.7 Protein content

The protein content of the EVs samples was determined using the Micro BCA™ Protein Assay Kit (Thermo Fisher Scientific, Cat. #23235). Protein analysis was performed according to the recommendations of the manufacturer using the 96-well plate procedure.

2.3.8 Immunoblotting

Cells and EVs isolates were lysed using cell lysis buffer (Thermo Fisher Scientific, Cat. #: FNN0011) supplemented with protease inhibitor cocktail (Roche, Basel, Switzerland; Cat. #: 04693116001). Ten µg of cell lysates and EVs lysates were loaded onto 7.5% Mini-PROTEAN TGX™ (Bio-Rad Laboratories, Cat. #: 4561023) or 10% Mini-PROTEAN TGX™ gels (Bio-Rad Laboratories, Cat. #: 4561034) accompanied by a molecular weight (MW) marker, SeeBlue Plus2 Pre-stained standard (Invitrogen, Cat. #: LC5925). Separated proteins were transferred to an Immun-Blot® polyvinylidene fluoride (PVDF) membrane (Bio-Rad Laboratories, Cat. #: 1620174) using Trans-Blot® Turbo™ Transfer System (Bio-Rad Laboratories, Cat. #: 1704150) and running MIXED MW (5-150 kDa; 7 min, 1.3 A constant, up to 25 V), or HIGH MW protocols (>150 kDa; 10 min, 1.3 A constant, up to 25 V). Following the transfer, the membranes were blocked with 5% (w/v) bovine serum albumin (BSA) in PBS containing 0.1% Tween-20 (PBS-T) and incubated overnight at 4ºC with the primary antibodies summarise **in Table 2.1.** After washing thrice with PBS-T, the membrane was incubated with anti-rabbit (1:1000; Cell Signaling Technology, Cat. #: 7074) or anti-mouse (1:1000, Cell Signaling; Cat. #: 7076) secondary antibodies in 5% BSA/PBS-T for 1 hr at room temperature (RT) and imaging was performed using an automated Chemidoc exposure system (Bio-Rad Laboratories) and using the SuperSignal West Femto Chemiluminescent Substrate Kit (Thermo Fisher Scientific, Cat. # 11859290) or SuperSignal West Femto Maximum Sensitivity Substrate (Thermo Fisher Scientific, Cat. #: 34096) for detection. Cell lysate (CL) from the individual cell line of origin was included in all gels as the control and densitometric analysis was performed using Fiji software[216].

Table 2.1. Antibody dilutions and conditions for immunoblotting.

Primary Antibody	Company, Cat. #	Dilution	Antibody condition	Secondary Antibody
Calnexin	Abcam, ab133615	1:1000	3% BSA/PBST	Anti-Rabbit IgG
CD9	Abcam, ab236630	1:1000	3% BSA/PBST	Anti-Rabbit IgG
CD63	Abcam, ab68418	1:500	3% BSA/PBST	Anti-Rabbit IgG
GRP94	Cell Signaling, 2104S	1:1000	3% BSA/PBST	Anti-Rabbit IgG
HER2	Calbiochem, OP15	1:1000	3% BSA/PBST	Anti-Mouse IgG
Syntenin	Abcam, ab133267	1:1000	3% BSA/PBST	Anti-Rabbit IgG

All secondary antibodies were diluted 1:1000 in 3% bovine serum albumin (BSA)/ PBS containing 0.1% Tween-20 (PBS-T)

2.3.9 Transmission Electron Microscopy

[TEM imaging of EVs was performed in the Advanced Microscopy Laboratory in Trinity Biomedical Sciences Institute by Mr. Neal Leddy as a paid service]

Samples were prepared from transmission electron microscopy (TEM) analysis following our published protocol[217,218] that was adapted from a previous publication[219]. Briefly, 10 µl of the sample was placed onto carbon-coated grids (Ted-Pella B 300 M, Mason Technology Ltd., Cat. #: 01813-F) and incubated for 10 min at RT. After incubation, samples were fixed with 4% glutaraldehyde and contrasted with 2% phospho-tungstic acid. The grids were examined at 100 kV using a JEOL JEM-2100 TEM (JOEL USA Inc.).

2.3.10 Statistical Analysis

All results presented were obtained from three independent experiments, starting each time with seeding a new batch of cells. Paired t-test analysis was performed using GraphPad Prism version 9.1.9 for macOS (GraphPad Software). Data are expressed as means ± standard error of the mean (SEM). *$p < 0.05$; ** $p < 0.01$; *** $p < 0.001$.

2.4 Results

2.4.1 Particle size and yield of EVs separated from CM differ based on the separation method and CM source

The average sizes and particle concentration of the products separated from CM by each method, dUC and PEG+UC, and analysed by NTA are shown in **Figure 2.2**. Isolates obtained from SKBR3 CM using the PEG+UC approach were significantly smaller than those obtained using the dUC method (**Figure 2.2A**). No significant differences in sizes were found for the HCC1954 and EFM192A isolates when comparing the two methods. Regarding the particle yield as determined by NTA, with CM from two of the three cell lines (i.e., EFM192A and SKBR3), significantly higher particle concentrations were obtained by the PEG+UC compared to the dUC method (**Figure 2.2B).** Specifically, the largest and most significant difference was found with the EFM192A samples (PEG+UC versus dUC: 6.9-fold; p = 0.0145), followed by the SKBR3 samples (2.75-fold; p = 0.0234). With the HCC1954 CM isolates, there was no significant difference whether they resulted from dUC or PEG+UC.

It is noteworthy, however, that the qualitative TEM approach showed that both methods produced a range of particle sizes from CM of each of the three cell lines (**Figure 2.3**). The NTA representative size distribution graphs with the mean and modal sizes are provided in the **Appendix I** (Figure I-1), with the average sizes and particle concentration of the samples detailed in the **Appendix I** (Table I-1).

A
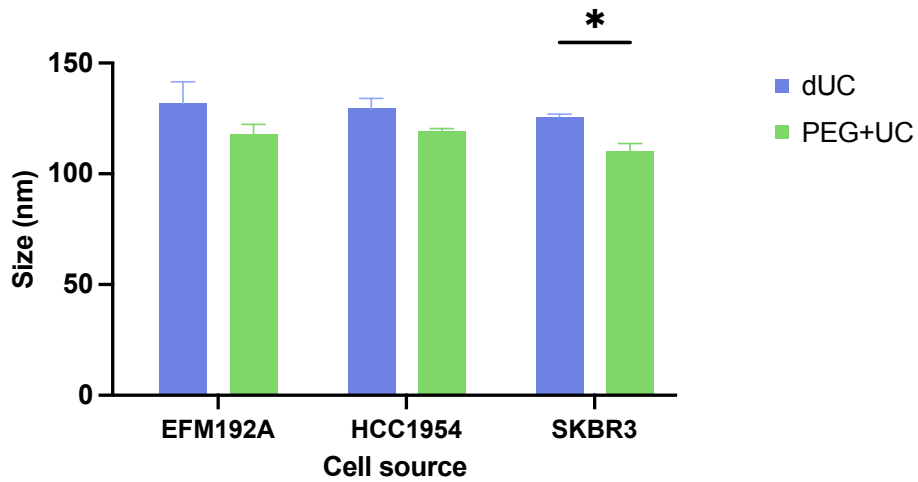
B
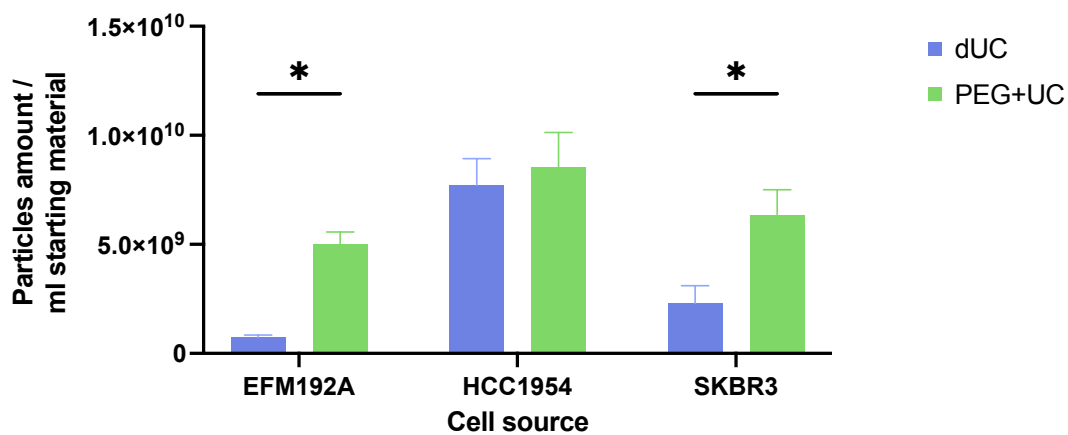
Figure 2.2. EVs characterisation by NTA.

Characterising particles/EVs, released by HER2-positive cell lines and harvested using differential ultracentrifugation (dUC) or polyethylene glycol-based precipitation followed by ultracentrifugation (PEG+UC), by NTA. (**A**) Particle size mode estimations. (**B**) Quantification of particle/EVs numbers and normalising to ml of CM. Results represent n = 3 isolates ± SEM, *$p < 0.05$.

EFM192A
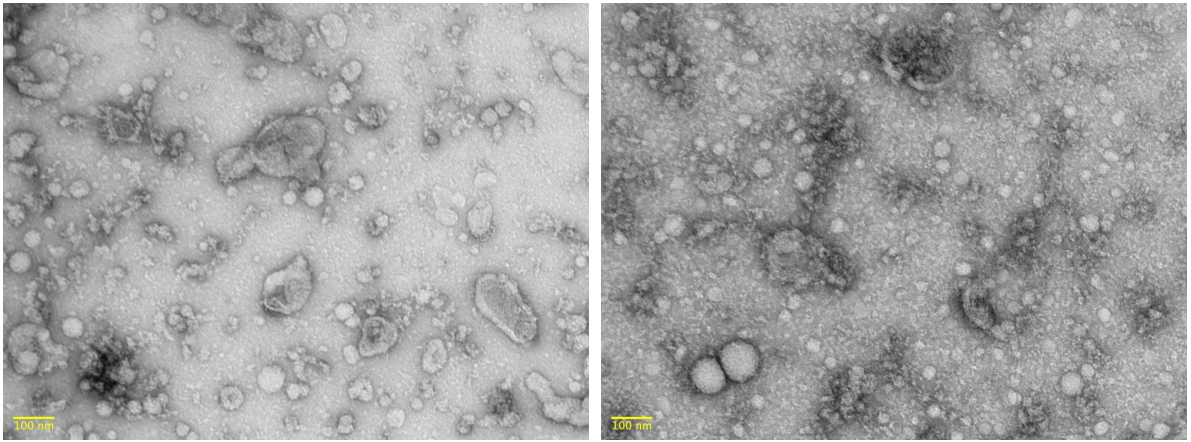
HCC1954
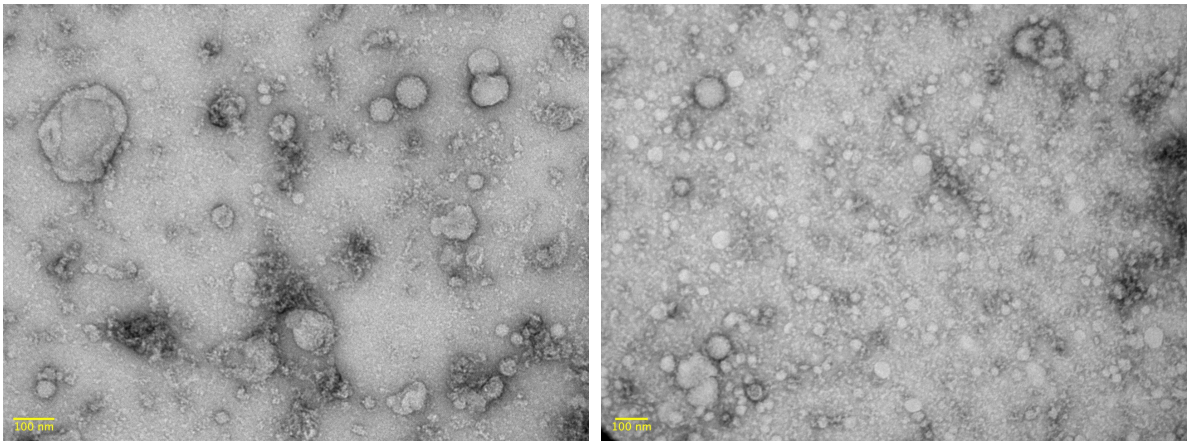
SKBR3
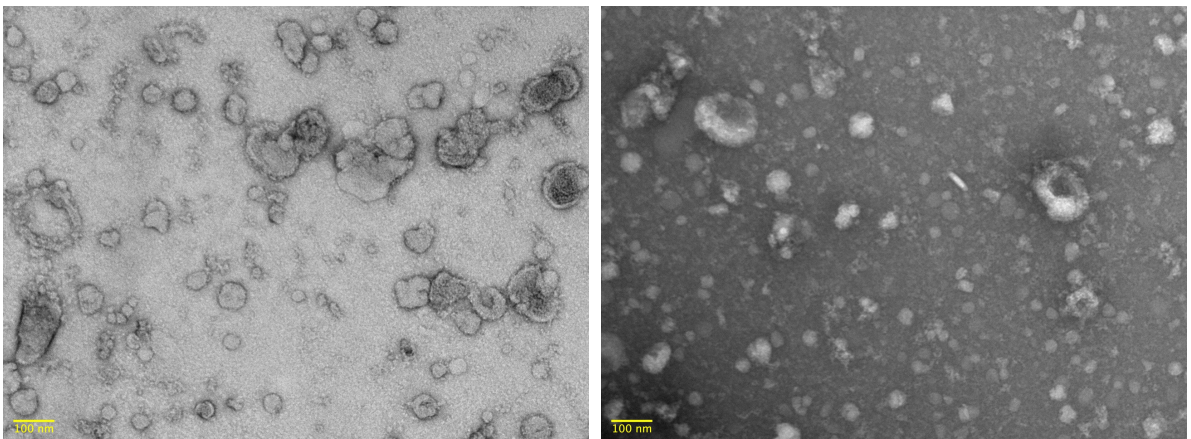
Figure 2.3. EVs characterisation by TEM.

Characterising particles/EVs released by HER2-positive cell lines and harvested using differential ultracentrifugation (dUC) or polyethylene glycol-based precipitation followed by ultracentrifugation (PEG+UC) by TEM. Scale bar = 100 nm.

2.4.2 Protein quantification present after EVs separation from CM and purity

As protein quantitates are sometimes analysed as a surrogate for EVs, here the relative amounts of protein (expressed as µg of protein/ml starting CM) present in each isolate was determined by the Micro BCA^{TM} Protein Assay Kit (**Figure 2.4**). These were found to differ significantly between the isolates of all three cell lines, always being highest in the samples obtained via the PEG+UC method. The means of protein amount for each condition are collected in the **Appendix I** (Table I-2).

The ratio of the particle counts to protein concentration (particle/protein ratio; P/µg) obtained using tools such as NTA and bicinchoninic acid (BCA) assay, respectively, have been proposed as straightforward method to estimate the purity of EVs[220]. That study established that ratios greater than $3×10^{10}$ P/µg are associated with high vesicular purity; ratios between $2×10^{10}$–$2×10^{9}$ P/µg are considered low purity; and ratios $<1.5×10^{9}$ P/µg are impure. As illustrated in **Figure 2.5**, all the samples analysed in this study—regardless of whether separated by dUC or PEG+UC—showed a ratio higher than $3×10^{10}$ P/µg and so would be of high purity. However, a relatively greater purity was achieved with dUC ($4.74×10^{11} ± 6.73×10^{10}$) compared to PEG+UC ($1.41×10^{11} ± 1.21 × 10^{10}$) for the HCC1954 samples. Conversely, the opposite was found with the SKBR3 samples ($4.45 × 10^{10} ± 8.40 × 10^{9}$ and $8.52 × 10^{10} ± 7.61 × 10^{9}$, respectively), where a higher purity ratio resulted in the samples obtained by the PEG+UC compared to the dUC approach, although statistical significance was not reached ($p = 0.054$).
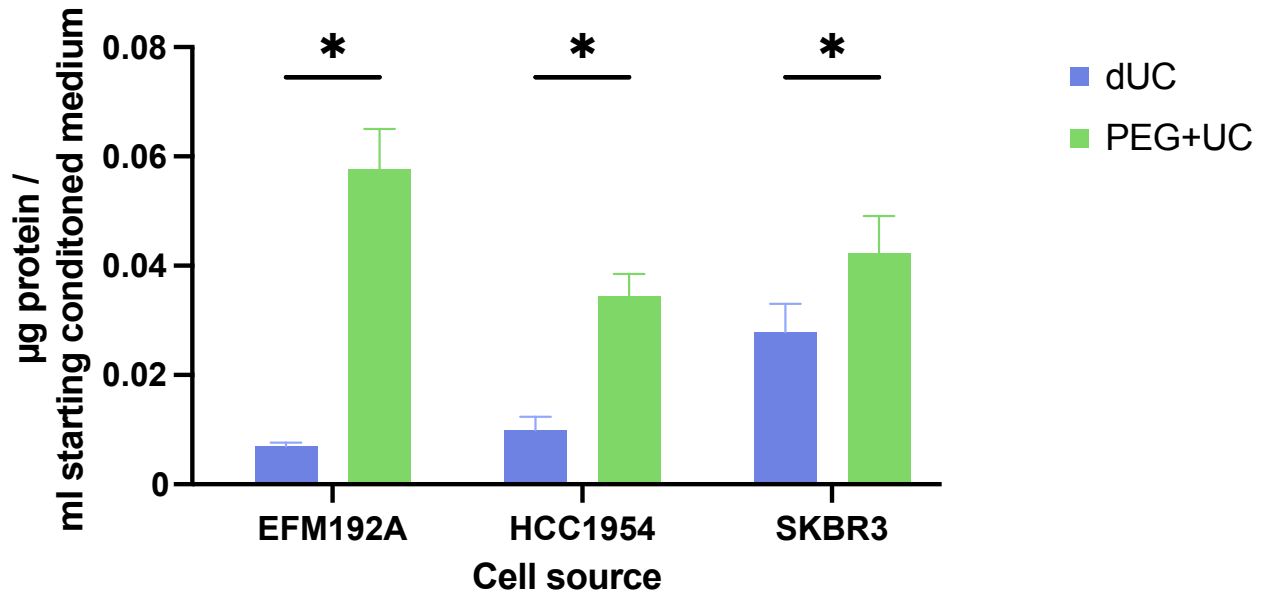
Figure 2.4. Protein quantification of EVs isolates.

Mean values of protein concentrations (µg of protein/ml of starting conditioned medium) of $n = 3$ isolates ± SEM are illustrated, *$p < 0.05$.
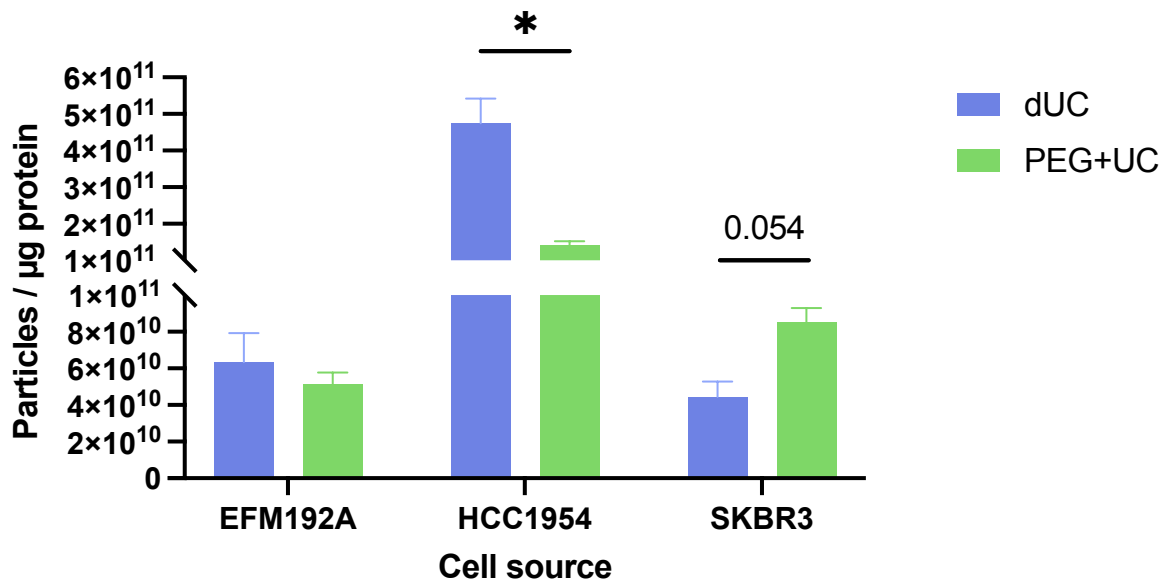
Figure 2.5. Particle to protein ratio to estimate EVs' purity.

Mean values of particles to protein ratios (particles/ µg of protein) of n = 3 isolates ± SEM are illustrated, *p < 0.05.

2.4.3 Presence of EVs specific markers and HER2 varied depending on the cells of origin and EVs separation method applied.

In keeping with MISEV2018 guidelines[105], immunoblotting analysis was performed on EVs lysates and cellular lysates for the EVs positive markers, CD63, syntenin, and CD9. Two proteins not considered to typically be enriched in EVs (i.e., GRP94 and calnexin) were also analysed. Regardless of the EVs separation method used, GRP94 and calnexin were not detected with any of the EVs samples analysed (**Figure 2.6A**). Both the dUC and PEG+UC generated samples were positive for all three EVs positive markers (**Figure 2.6A**, with densitometric analysis of n = 3 presented in **Figure 2.6B**). Although equal quantities of protein were loaded on the gels, the enrichment of EVs markers in isolates obtained was cell line- and EVs separation method-dependent. For SKBR3, there were no significant differences detected. CD63 was found to be enriched in PEG+UC versus dUC isolates obtained from EFM192A CM. However, its presence was lower in the HCC1954 samples using PEG+UC compared to dUC, albeit not significantly. With EFM192A and HCC1954, significantly more CD9 was detected following dUC compared to PEG+UC, while no significant difference was found with CD9 for SKBR3.
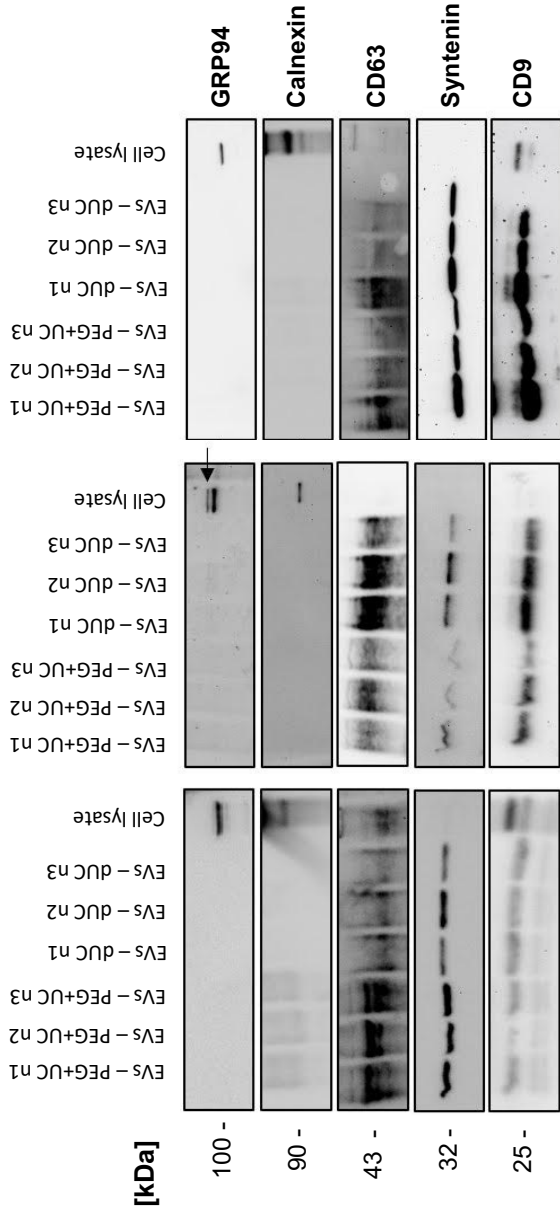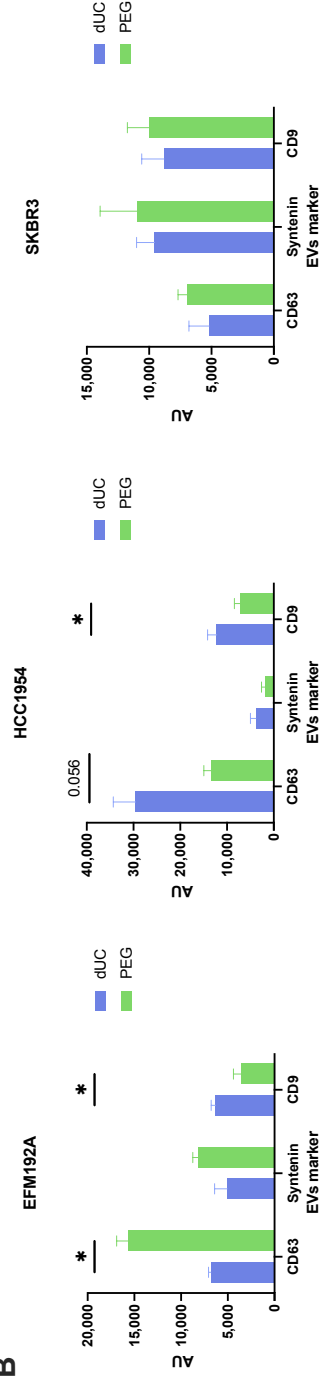
Figure 2.6. Immunoblots of EVs-positive and -negative markers present on the samples.

(**A**) Ten μg of protein lysates (EVs from PEG+UC or dUC, or corresponding donor cell line) was loaded per lane and analysed for GRP94, calnexin, CD63, syntenin, and CD9. Each blot represents three independent experiments and the densitometric analysis of these three are presented in (**B**) as the mean of $n = 3 \pm$ SEM, *$p < 0.05$.

As all three cell lines are HER2-positive, we investigated the presence of HER2 in these isolates (**Figure 2.7**). As for the EVs markers, although equal quantities of protein were loaded on the gels, the enrichment of HER2 in the isolates obtained was cell line-/EVs separation method-dependent. Specifically, for SKBR3, PEG+UC resulted in significantly more detectable HER2 compared to the isolates resulting from dUC. Conversely, for HCC1954, dUC compared to PEG+UC resulted in significantly more HER2.
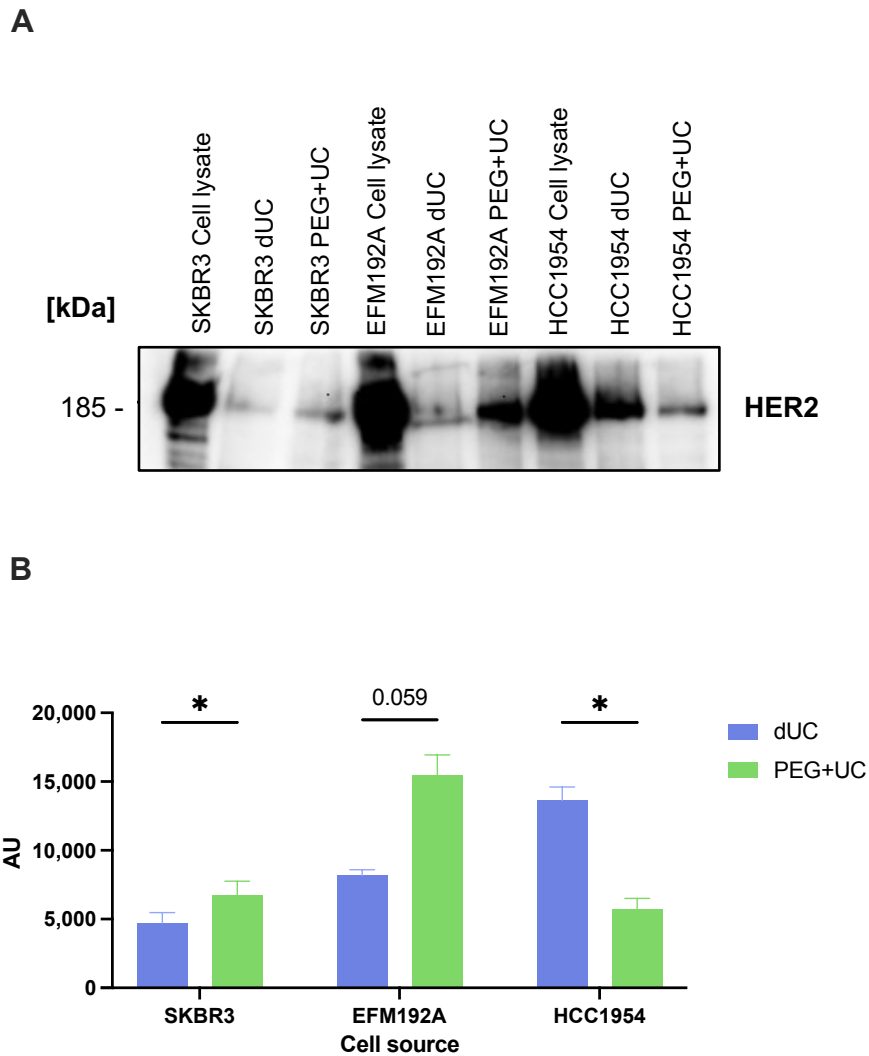
Figure 2.7. Immunoblots of HER2 markers present on the samples.

(**A**) Ten µg of protein lysates (EVs from PEG+UC or dUC, or corresponding donor cell line) was loaded per lane and analysed for HER2. This blot represents three independent experiments and the densitometric analysis of these three are presented in (**B**), with each bar representing the mean of the densities of the signals from $n = 3$ repeat experiments ± SEM, *$p < 0.05$.

2.4.4 Summary of findings

Table 2.2 brings together the main observations from this study.

Table 2.2. Summary of the comparison of dUC and PEG+UC separation of EVs from the CM of three cell lines.

Characteristics/ Parameters Evaluated (method)	Changes (statistically significant ↑ or ↓) with PEG+UC *versus* dUC		
	SKBR3 source	EFM192A source	HCC1954 source
Size (NTA)	↓ PEG+UC	ns	ns
Particles/ml of CM (NTA)	↑ PEG+UC	↑ PEG+UC	ns
Size distribution and structure (TEM)	Qualitative, so statistical analysis not possible	Qualitative, so statistical analysis not possible	Qualitative, so statistical analysis not possible
µg protein/ml of CM BCA)	↑ PEG+UC	↑ PEG+UC	↑ PEG+UC
Purity ratio (particles/µg protein as NTA/BCA)	ns	ns	↓ PEG+UC
EVs protein markers (immunoblots)	CD63: ns Syntenin: ns CD9: ns GRP94: Undetected Calnexin: Undetected	CD63: ↑ PEG+UC Syntenin: ns CD9: ↓ PEG+UC GRP94: Undetected Calnexin: Undetected	CD63: ns Syntenin: ns CD9: ↓ PEG+UC GRP94: Undetected Calnexin: Undetected
HER2 (immunoblots)	↑ PEG+UC	ns	↓ PEG+UC

ns = not significant

2.5 Discussion

EVs play an important role in normal and pathological mechanisms carrying functional molecules including proteins, lipids, and nucleic acids. Over recent years, interest in the EVs field has increased considerably and EVs have been associated with numerous pathological processes as well as physiological roles including inflammation[103], tissue regeneration[104], osteogenesis[221], and hypoxia[222]. In cancer, for example, our group was the first to show that EVs can transmit resistance to anti-cancer drugs[151,152]. The potential of EVs, for example, from mesenchymal stem cells (MSCs), as therapeutics and natural drug delivery systems is also of substantial interest[97,104]. Areas in this field that need further attention in our effort toward exploiting the therapeutic potential of EVs, especially those released from cultured mammalian cells, include the EVs separation/enrichment step[223,224].

As mentioned in the **Section 2.1**, indeed, a few EVs separation comparison studies have been reported; albeit not comparing the specific methods included here. The consensus from those studies is that the method of EVs separation used depends on the downstream application of the recovered EVs. While we are fully in agreement with this, we felt that it was important to take a further step back and establish whether information on the comparison of methods obtained from only one cell line's CM can be assumed to be correct for others and so extrapolated. As we have summarised in **Table 2.2**, considering CM from three similar, but different, cell lines (i.e., three independent HER2-positive cell lines, cultured in the same type of medium), had we only worked with one of these—rather than all 3—and extrapolated, we would have produced some misleading results. It is important to note that this is not due to a lack of reproducibility when working with dUC or PEG+UC on any of the cell lines' CM, as the results from all three independent repeat experiments were very reproducible for each of SKBR3, EFM192A, and HCC1954. Specifically, in relation to the EVs size recorded by NTA, PEG+UC resulted in smaller particles than those obtained by dUC for SKBR3, but not for EFM192A or HCC1954. In 2/3 cases (SKBR3 and EFM192A), PEG+UC resulted in a higher quantity of particles, but this was not so with HCC1954. One exception of the seven parameters considered (**Table 2.2**) was protein quantity, which possibly included protein "contaminants" and was significantly higher with PEG+UC vs. dUC. This was not unexpected, as the group who developed this protocol and applied it to CM from HEK293T cells[212] reported higher amounts of impurities/non-EVs associated molecules when comparing their method to sucrose density gradients (GUC). Conversely, however, the gain with PEG+UC was that the isolates maintained therapeutic activity (unlike those derived by GUC) and those therapeutic activities did not seem to be because of the impurities. Having said that, in relation to impurities, if we consider the method reported by Webber and Clayton[220] to estimate impurities, the isolates obtained from all three cell lines' CM using dUC or PEG+UC fell within the threshold of high vesicular purity, even if, within that range, the dUC isolates have a ratio value significantly higher than the PEG+UC isolates for one of the three cell lines (i.e., HCC1954).

Regardless of the CM source or method employed, all EVs samples were negative for GRP94 and calnexin, which are typically considered to be negative markers for EV; in keeping with the suggestion of—at most—minimal impurities being present. Conversely, all three proteins considered to be

positive markers of EVs (i.e., CD63, syntenin, and CD9) were detected to different extents in all isolates, supporting the presence of EVs. The only significant difference observed following densitometry analysis of all blots with PEG+UC compared to dUC was a significant decrease in CD9 for both EFM192A and HCC1954 and a significant increase in CD63 for EFM192A. Regarding HER2, although all three cell lines are HER2-positive and HER2 was detected on all EVs isolates (reflecting the status of their cancer cells of origin), the results obtained from the analysis of the products showed differences that were cell line-/method-dependent (i.e., comparing PEG+UC to dUC isolates). Specifically, for EFM192A, there was no significant difference in HER2 regardless of the method, while PEG+UC compared to dUC resulted in significantly more and significantly less HER2, respectively, for SKBR3 and HCC1954.

Altogether, our findings suggest that both dUC and PEG+UC have uses as reproducible methods for separating quite pure EVs, although PEG+UC tends to (but does not always) precipitate more particles and proteins that may not be of EVs origin. However, importantly, what our study also shows is that consideration must be given to the inclusion of more than one source of CM (and so potentially the same for other biofluids) when EVs separation techniques are being compared, rather than using a single or pooled sample that may not generate results that can be extrapolated to other samples.

2.6 Conclusions

Findings from the current study indicate that different EVs sources should be included into comparison studies of EVs separation methodologies to select the best methodology for a specific source of EVs.

Chapter 3

A potential role for AGR2 in neratinib-resistance in breast cancer

Abstract

HER2-overexpression occurs in ~20% of breast cancers and confers aggressive behaviour and poorer prognosis. Although several drugs such as neratinib have been developed to target HER2, it is estimated that up to 70% of patients with HER2-overexpressing breast cancer do not gain benefit, due to innate or acquired drug-resistance. This study investigated if differences in the proteome profile occurred between HER2-positive breast cancer cell lines (representing three patients' tumours) and their neratinib-resistant counterparts, to shed light on the neratinib resistance mechanism.

Mass spectrometry-based quantitative proteomics was used to analyse the protein expression profile of HER2-positive breast cancer cell lines (HCC1954, SKBR3 and EFM192A) and their neratinib-resistant (NR) counterparts developed in our laboratory (HCC1954 NR, SKBR3 NR and EFM192A NR). These experiments were repeated n = 3 times. The differential expression analysis of the three parental cell lines individually, versus their resistant counterparts was investigated. The workflow run in R was based on (DEP) package developed by Zhang et al. (2012)[225] and a total of 18 samples from HER2+ breast cancer cells were analysed. Gene Ontology and pathway analysis were performed by *enrichr* web tool. Principal component analysis (PCA) was also performed. Differentially expressed proteins were defined as false discovery rate (FDR) < 0.05 and |log2(fold change)|≥1.5.

A total of 105 differentially expressed proteins were found. Of those, 57 were differentially expressed between HCC1954 cell variants, 43 between SKBR3 cell variants and 7 between EFM192A cell variants. Notably, only AGR2 was down-regulated in two different cell line variant pairs (HCC1954 and SKBR3 variants) and no differentially expressed proteins were shared between the three different cell line pairs. Protein expression of AGR2 was assessed using immunoblotting analysis, and subsequent transfection of AGR2 in HCC1954 NR and SKBR3 NR cell line variants was performed to evaluate its role in the neratinib mechanism(s).

Successfully transfection of AGR2 into neratinib-resistant cell lines achieved a notable outcome by partially restoring their sensitivity to neratinib. Additionally, this transfection resulted in a decrease in the migratory and invasive abilities of the neratinib-resistant cell variants. Further analysis of AGR2 role in neratinib-resistant mechanisms is warranted.

3.1 Introduction

As mentioned in **Section 1.1**, the GCO identified breast cancer as the most common cancer form worldwide in 2020[1], with an estimated 15-20% of breast cancers over-expressing HER2[226]. The discovery of HER2 in the 1980s allowed the development of therapeutical strategies that have dramatically changed the natural history of HER2+ breast cancer, with significantly improved outcomes[227–229].

Despite the development of HER2-targeted therapies such as trastuzumab, lapatinib, pertuzumab, or neratinib, it is estimated that up to 70% of patients with HER2-overexpressing tumours do not gain benefit, because of innate-, acquired- and cross-resistance to HER2-targeted therapies; the main reason for which these drugs fail in the clinic. Further investigations and continued efforts are required to unravel the main effectors of resistance to predict the outcome of treatments and offer more therapeutic targets and thus options to a wider range of patients[230,231].

Neratinib was approved by FDA in 2017, and by EMA in 2018, for extended adjuvant treatment of early stage HER2+ BC. Neratinib is still undergoing clinical trials. A phase I/II study (NCT00398567) has been shown neratinib to be effective in HER2+ BC with acquired and innate resistance to trastuzumab and its combination with trastuzumab was safe and well-tolerated, improving clinical outcomes in some subsets of patients[46]. A phase III ExteNET trial demonstrated a significantly improvement on 5-year iDFS in early-stage BC patients, after trastuzumab-based adjuvant therapy (NCT00878709)[47]. An open-label phase II monotherapy trial is underway in HER2+ BC patients with brain metastasis (NCT01494662)[48]. Although neratinib has shown efficacy in blocking the signalling of EGFR family receptors, resistance to it may be acquired, as for anti-cancer drugs. For that reason, further investigation to understand the ability of cancer cells to acquire neratinib resistance and the associated effects on cell behaviour is required[45]. After developing novel neratinib-resistant cell variants of HER2+ breast cancer cell lines[64,232], our group revealed a novel mechanism of neratinib resistance based on a rise of metabolism of neratinib in these cell variants due to increased CYP3A4 activity. HER2 expression was also down-regulated in the neratinib resistant variants. Also, the resistance to neratinib conferred cross-resistance to other HER2-targeted therapies used for breast cancer including trastuzumab, lapatinib, and afatinib, and resistant variants had more aggressive behaviour (i.e., increased invasiveness) than their drug-sensitive counterparts[64]. However, no previous proteomic analysis has been performed before to compare the neratinib-sensitive cell lines with their neratinib-resistant counterparts.

3.2 Aims of the study

Here, in efforts to identify a mechanism(s) responsible for neratinib resistance, we apply a global proteomics approach to investigate the differences in proteome that occur between three HER2-positive breast cancer cell lines representing three patients' tumours and their neratinib counterparts. The subsequent overall objective was to validate those findings by immunoblot and to investigate if AGR2 expression was indicative of neratinib resistance by functional assays.

3.3 Materials and Methods

3.3.1 Proteomic profiling

Mass spectrometry (MS)-based quantitative proteomics was used to analyse the protein expression profile of the three pairs of cell line variants. These experiments were repeated n = 3 times. The differential expression analysis of the three parental cell lines individually, versus their resistant counterparts was investigated. The approach followed for the proteomic analysis is depicted in **Figure 3.1**.

3.3.1.1   Cell culture, protein extraction and processing

EFM192A and EFM192A NR (HER2+ER+) cells were seeded at 2×10^6 cells per T75 cm^2 flask (Corning, Cat. #: 431464U) and HCC1954, HCC1954 NR, SKBR3 and SKBR3 NR (HER2+ER-) were seeded at 1×10^6 cells in complete RPMI-1640 media and allowed to grow during 72 hrs until 80% confluence. Media was then removed, and cells were washed with cold PBS (Sigma-Aldrich, Cat. #: P8537) twice. One millilitre of PBS was then added to the flasks and the cells were scraped using a sterile cell scraper (Fisher Scientific, Cat. #: 08-100-241). Cell suspensions were centrifuged at 10,000× g at 4°C for 5 min and the pellet was resuspended in 6M urea (Sigma-Aldrich, Cat. #: U5378) and 50mM ammonium bicarbonate (ABC) (Honeywell, Cat. #: 1066- 33-7). Samples were vortexed and incubated for 30 min at RT and sonicated on ice 20 sec (pulse time 5 sec, pulse off time 5 sec). After sonication, samples were centrifuged at 16,000× g for 10 min. The protein concentration of all the samples were determined by the Bradford assay method[233]. Bio-Rad protein assay dye reagent (Bio-Rad, Cat. #: 500-0006). Briefly, 2 mg/ml BSA stock was prepared and diluted 1:10 to obtain a working concentration of 0.2 mg/ml. A standard curve was prepared using BSA standards of 0 – 50 µg/ml diluted in urea lysis buffer to calculate the protein content of the samples. 5 µl of each sample was mixed with 40 µl of Bio-Rad Dye concentrate reagent and MS grade H$_2$O for a final volume of 200 µl, mixing carefully. Absorbance was read at 595 nm after 20 min using a FLUOstar® OPTIMA microplate reader (BMG Labtech). After calculating the protein quantity of the samples from the standard curve, samples were prepared to contain 50 µg protein in 30 µl solution for their subsequent digestion.
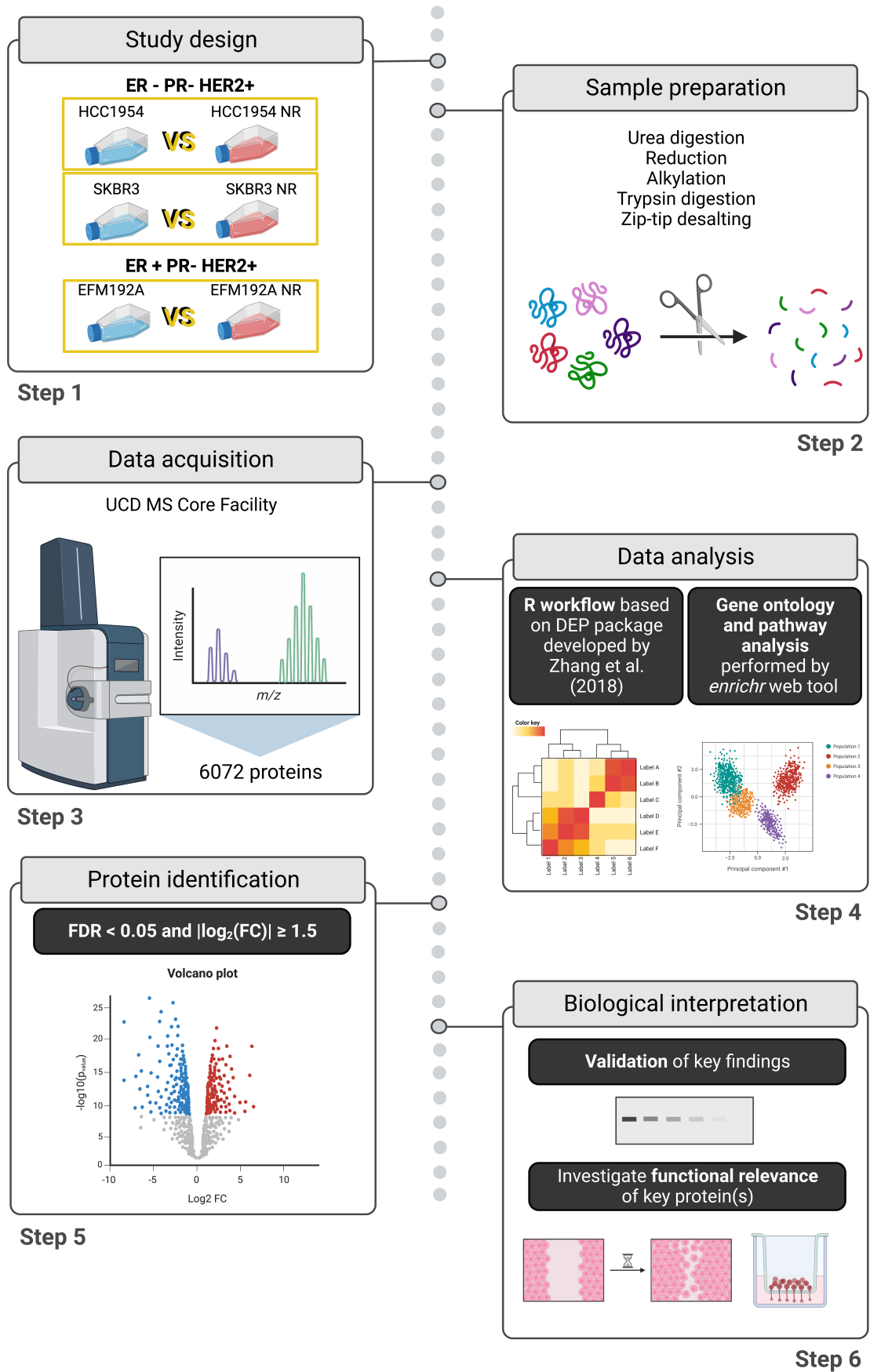
Figure 3.1. Workflow of proteomic profiling study.

Schematic representation was created with *BioRender.com*

3.3.1.2   Protein digestion by in-solution tryptic digestion

Freshly prepared 100 mM dithiothreitol (DTT) (Sigma-Aldrich, Cat. #: D0632-1G) was added to the cell lysate samples using a ratio of sample volume / 20 calculated for each sample to achieve a final concentration of 5mM. Tubes were vortexed and incubated at 60°C for 30 min to remove disulphide bonds in proteins. After incubation, samples were centrifuged to collect the protein samples down in the tube and 200mM of iodoacetamide solution (IAA) (Sigma-Aldrich, Cat. #: I1149-5G) was added using a ratio of total sample volume (including DTT)/20, calculated independently for each sample. Samples were then vortexed and incubated in the dark at RT for 30 min. Then samples were diluted sufficiently with 50mM ABC to reduce the concentration of urea to < 2M. A vial of trypsin singles (Sigma-Aldrich, Cat. #: T7575) was added to each reduced, alkylated sample. Followed the trypsin addition, samples were vortexed and incubated overnight at 37°C on a thermomixer (Eppendorf) at 350× rpm. Trypsin digestion was stopped by adding HPLC grade acetic acid (Fisher Scientific, Cat. #: A/0406/PB08), 1% of the final volume, and samples were prepared for peptide desalting step by centrifugation at 10,000× rpm for 5 min.

3.3.1.3   Quantitative LC-MS/MS analysis

[LC-MS/MS analysis was performed in the UCD Conway Proteomics Core - Mass Spectrometry Resource by Dr Eugène T. Dillon as a paid service]

Prior to Liquid Chromatography with tandem mass spectrometry (LC-MS/MS) analysis, the peptide samples were desalted using C18 ZipTip® pipette tips (Millipore, Cat. #: ZTC18S960) following the manufacturer's protocol. Briefly, 10 µl of wetting and elution solution [50% acetonitrile (ACN) in 0.1% trifluoroacetic acid (TFA) prepared in MS grade H_2O] was aspirated into the tip and dispensed to waste and repeated thrice. Once the tip was equilibrated, aspiration and dispensing cycles were performed 3-7 times (simple mixtures) up to 10 times (complex), consistently pipetting from just under the level of solution and not at the bottom of the tube to avoid insoluble aggregates that could clog the stage tip. After aspiration and dispensing sample cycles, equilibration and washing solution (0.1% TFA in MS grade H_2O) was aspirated and dispensed twice. After binding of the protein and washing step, 10 µl of elution solution was dispensed into a clean vial with a standard pipette tip and 3 aspiration and dispensing sample cycles were performed through the zip tip into the elution solution without introducing air. Following this, samples were subjected to an evaporation process for 10-15 min using the CentriVap concentrator and then resuspended in 25 µl of 0.5% acetic acid containing 2.5% ACN. Finally, samples were centrifuged at 15,000× rpm at 4°C for 5 min and 20 µl supernatant were transferred to the MS vial, leaving a small drop at bottom of the tube. To determine the peptide concentration of the samples, Pierce™ Quantitative Colorimetric Peptide Assay (Thermo Scientific, Cat. #: 23275) was used following the manufacturer's instructions. Briefly, eight standard concentrations were prepared in a range of 0-1000 µg/ml and 20 µl of standards or dilute samples were placed into a 96-well microplate. 180 µl of working reagent were added to each well and the plate was mixed using a plate shaker for 1 min. The plate was then covered and incubated at RT for 30 min and absorbance was read at 480 nm using a FLUOstar® OPTIMA microplate reader (BMG Labtech). Samples were diluted to a final concentration of 40 ng/µl for the identification and

quantification of the proteins using timsTOF Pro Mass Spectrometer (Bruker Daltonics, Bremen, Germany) coupled to a nanoElute (Bruker Daltonics, Bremen, Germany) ultra-high pressure nanoflow chromatography system (UHPnLC). The peptides were separated on a reversed-phase C18 Aurora column (25cm x 75 µm ID, C18, 1.6 µm; IonOpticks) at a constant flow rate of 250nL/min and an increasing acetonitrile gradient. Mobile phases were 0.1% (v/v) formic acid in water (phase A) and 0.1% (v/v) formic acid in acetonitrile (phase B). The peptides were separated by a gradient starting from 2% of mobile phase B and increased linearly to 32% for 60 min. This was stepped up to 95% of mobile phase B where it was maintained for 7 min. The injection volume was 5 µL, equivalent to a loading of 200 ng per sample.

The timsTOF Pro mass spectrometer was operated in positive ion polarity with TIMS (Trapped Ion Mobility Spectrometry), and PASEF (Parallel Accumulation Serial Fragmentation) modes enabled. The accumulation and ramp times for the TIMS were both set to 100 ms, with an ion mobility (1/k0) range from 0.62 to 1.46 Vs/cm. Spectra were recorded in the mass range from 100 to 1,700 m/z. The precursor MS Intensity Threshold was set to 2,500 and the precursor Target Intensity set to 20,000. Each PASEF cycle consisted of one MS ramp for precursor detection followed by 10 PASEF MS/MS ramps, with a total cycle time of 1.16 s.

3.3.1.4 Data mining and Bioinformatics analysis

[Bioinformatic analysis of proteomic data was performed by ESR Joaquin Jurado Maqueda under the supervision of Dr Carla Olivera, Bioinf2Bio, Porto, Portugal, as part of a TRAIN-EV MSCA-ITN collaboration]

The DEP package in R software version 1.4.1106 for Windows was used to analyse a total of 18 samples (*n* = 3 of six cell line variants) from HER2+ breast cancer cells[234]. Protein hits identified from the reversed database were removed and protein groups were filtered for q-value < 1%. Label-free quantification (LFQ) intensities extracted by MaxQuant were log2-transformed and normalised by variance stabilisation. Only those proteins with LFQ intensity > 0 and presented in more than one replicate of at least one cell line were considered. Missing values were replaced by imputation using random draws from a Gaussian distribution centered around a minimal value (*q*=0.01). Differential enrichment analysis was performed by applying empirical Bayes methods on protein-wise linear models using *limma* package[235]. False discovery rate (FDR) estimates were obtained by *fdrtool.* Differentially expressed proteins (DEP) were those with |log2(Fc)| > log2(1.5) and *q*-values (tail area-based FDR) < 0.05. Gene Ontology and pathway analysis were performed by *enrichr* web tool[236].

3.3.2 Immunoblotting

To validate differential expression of key proteins identified, immunoblot analysis was performed. A total of 30 µg protein per sample was resolved on a 10% Mini-PROTEAN TGX™ 10-well gel (Bio-Rad Laboratories; Cat. #: 4561034) as per **Section 2.3.8**. To evaluate the presence of AGR2 in the EVs' lysates, a total of 10 µg of protein was resolved as mentioned. All antibody conditions and

catalogue numbers used in this chapter are detailed in **Table 3.1.** Densitometric analysis was performed using Fiji software[216].

Table 3.1. Antibody dilutions and conditions for immunoblotting.

Primary Antibody	Company, Cat. #	Dilution	Antibody condition	Secondary Antibody
AGR2	Abcam, ab76473	1:1000	3% BSA/PBST	Anti-Rabbit IgG
β-Actin	Sigma-Aldrich, A1978	1:5000	3% BSA/PBST	Anti-Mouse IgG
E-cadherin	Abcam, ab40772	1:1000	3% BSA/PBST	Anti-Rabbit IgG
N-cadherin	Abcam, ab76011	1:1000	3% BSA/PBST	Anti-Rabbit IgG
Vinculin	Cell Signaling, 13901S	1:1000	3% BSA/PBST	Anti-Rabbit IgG
TGFβ-1	Abcam, ab179695	1:1000	3% BSA/PBST	Anti-Rabbit IgG
HER2	Calbiochem, OP15	1:1000	3% BSA/PBST	Anti-Mouse IgG

All secondary antibodies were diluted 1:1000 in 3% bovine serum albumin (BSA)/ PBS containing 0.1% Tween-20 (PBS-T)

3.3.3 VEGF ELISA

Vascular Endothelial Growth Factor (VEGF) concentration was quantified in the cell lysates (Human VEGF DuoSet ELISA, R&D Systems, Cat. #: DY2938-05) according to the manufacturer's instructions. In brief, the capture antibody (R&D Systems; Cat. #: 841495) was resuspended and diluted in PBS (R&D Systems, Cat. #: DY006), as recommended by the manufacturer. 100 µl/well of diluted capture antibody were placed in 96-well microplates (R&D Systems, Cat. #: DY990) and incubated overnight at RT. The following day, plates were washed thrice with diluted ELISA washing buffer (R&D Systems, Cat. #: WA126) and unspecific binding sites were blocked by adding 300 µl of diluted reagent diluent (R&D Systems; Cat. #: DY995) to each well during 1 hr at RT. After incubation time, wells were washed again thrice and 100 µl of samples (10 µg cell lysates) or standards in reagent diluent were added to the well and incubated at RT for 2 hrs. Then, plates were washed thrice and 100 µl of the detection antibody (R&D Systems, Cat. #: 840163) was added to each well and incubate during 2 hrs at RT. Then plates were washed thrice again and 100 µl of diluted streptavidin-HRP solution (R&D Systems, Cat. #: 893803; 40-fold) was added to each well. After 20 min of incubation in dark, wells were washed thrice and 100 µl of substrate solution (1:1 mixture of Color Reagent A and Color reagent B, R&D Systems, Cat. #: DY999) were added and incubated at RT in dark. The reaction was stopped by adding 50 µl of stop solution (R&D Systems, Cat. #: DY994) to each well and the optical density (OD) was determined immediately at 450 nm using a FLUOstar® OPTIMA microplate reader (BMG Labtech; Serial #: 08-100-241). Wavelength correction was performed by subtracting readings at 570 nm from the readings at 450 nm.

3.3.4 Generation of stable AGR2 transfectants

To perform cell transfection, HCC1954 NR and SKBR3 NR cells were seeded at 25×10^5 and 36×10^5 cells/well, respectively, into six-wells plates (Costar, Cat. #: 3516) and cultured for 24 hrs. Plasmids containing AGR2 cDNA (EX-I0122-M94), EGFP cDNA (EX-EGFP-M94) and empty vector (EX-NEG-M94) were purchased from Genecopoeia.

Two micrograms of plasmid were transfected using FuGENE 4K [Promega, Cat. #: E5911] according to manufacturer's protocol. Successful transfection was verified by fluorescence microscopy to detect expression of the integrated selection marker GFP. A day later, positive cells were selected in complete medium containing 2 µg/ml puromycin [Sigma-Aldrich; Cat. #: P4512]. These cells were expanded as pools of puromycin-resistant cells after 4 weeks under selection pressure. Un-transfected cells were used as negative controls. HCC1954 NR-pcAGR2, HCC1954 NR-pcEGFP, HCC1954 NR-pcEmpty, SKBR3 NR-pcAGR2, SKBR3 NR-pcEGFP, and SKBR3 NR-pcEmpty were established. The workflow followed is summarised in **Figure 3.2**.
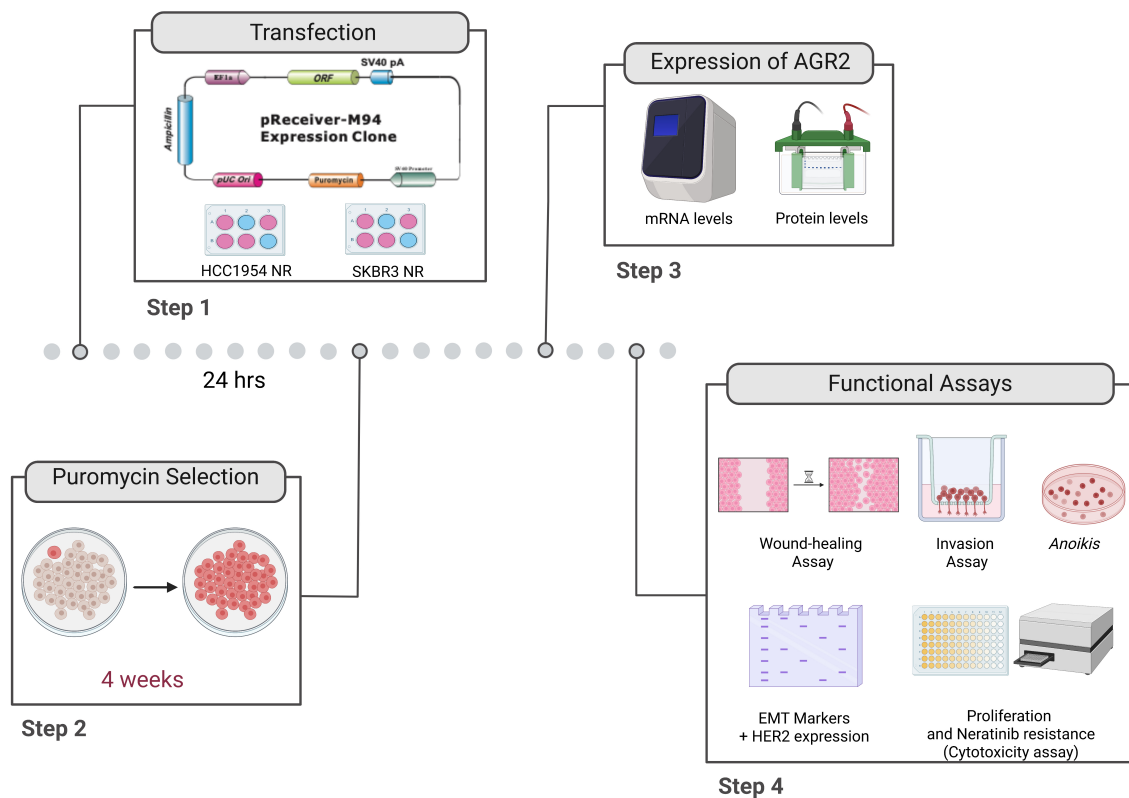
Figure 3.2. Pipeline for transfection protocol.

Schematic representation was created with *BioRender.com*

3.3.5 cDNA extraction and AGR2 expression study by RT-qPCR

cDNA from HCC1954, HCC1954 NR, HCC1954 NR-pcAGR2, HCC1954 NR-pcEMPTY, SKBR3, SKBR3 NR, SKBR3 NR-pcAGR2, and SKBR3 NR-pcEmpty was constructed using the SuperScript IV CellsDirect cDNA synthesis kit (Invitrogen, Cat. #: 11750150). Quantitative reverse transcription polymerase chain reaction (RT-qPCR) was performed using PowerUP™ SYBR™ Green Master Mix

(Invitrogren, Cat. #: A25741). Transfection efficiency was established by comparing levels of AGR2 amplification normalise to the housekeeping gene β-actin in each sample. Primers: AGR2 primer (GeneCopoeia, Cat. #: HQP090714); KiCqStart™ ACTB primers (Sigma-Aldrich, Cat. #: H_ACTB_1, NM_001101) were used. Amplification was performed in triplicate in a ViiA™ 7 Real-Time PCR System with 96-Well Block (Applied Biosystems™, Cat: # 4453534) according to the cycling protocol recommended by the Master Mix's manufacturer's recommendations (see **Table 3.2**) The specificity of the PCR products was confirmed by dissociation curve analysis.

Table 3.2. RT-qPCR reaction settings.

Step	Temperature	Time	Cycles
Hold Stage	50ºC	2 min	1
	95ºC	2 min	
PCR Stage	95ºC	1 sec	40
	60ºC	30 sec	
Melt Curve Stage	95ºC	15 sec	1
	60ºC	1 min	
	95ºC	15 sec	

3.3.6 Proliferation assay

HCC1954 and SKBR3 cell variants were seeded in 96-well plates (Costar, Cat. #: 3595) at a density of $3×10^3$/well and $5×10^3$/well, respectively. Cell proliferation was measured at 24, 48, 72 and 96 hrs after seeding using acid phosphatase assay method[237]. Briefly, the culture medium was removed, and cells were washed twice by adding 100 µl/well PBS. Then, fresh phosphatase substrate buffer was prepared by adding 0.27 g of 10mM p-nitrophenol phosphate (VWR chemicals, Cat. #: 27963.101) per 100 ml 1M sodium acetate buffer [500 ml dH2O, 4.1 g sodium acetate (Sigma-Aldrich, Cat. #: S5636), 500 µl Triton X (Sigma-Aldrich, Cat. #: T8787), pH to 5.5] and 100 µl was added to each well. The plates were kept in dark by wrapping them in aluminium foil and placed in an incubator at 37ºC (5% CO_2) for 1 hr 30 min. After the incubation period, 50 µl of 1M NaOH (Sigma Aldrich, Cat. # S5881) was added to each well to stop the reaction. The absorbance was read at 405 nm using the FLUOstar® OPTIMA microplate reader (Serial #: 08-100-241).

3.3.7 Cytotoxicity assay

The half-maximal inhibitory concentration (IC_{50}) values of HCC1954 and SKBR3 variants for neratinib was determined using in vitro cytotoxic proliferation assay. HCC1954 cell variants were seeded at $3×10^3$ cells/well while SKBR3 cell variants were seeded at $5×10^3$ cells/well in a 96-well plate (Costar, Cat. #: 3595). Twenty-four hours after seeding, cells were exposed to increasing concentrations of neratinib to obtain a final volume of 200 µl/well. Concentrations of neratinib were as follows: 0 – 100 nM for HCC1954 and SKBR3; 0 – 900 nM HCC1954 NR cell variants; 0 – 300 nM SKBR3 NR cell variants. After 5 days culture in the presence of neratinib, cell viability was measured using the acid phosphatase as described previously in **Section 3.3.6.**

3.3.8 *Anoikis*-resistance assay

Anoikis (Greek term that means "homeless wanderer) is a particular type of apoptosis that take place in the absence of ECM or upon cell adhesion to inappropriate location[238]. However, during metastatic colonisation, cancer cells need to be able to evade *anoikis*, becoming *anoikis*-resistant and survive in suspension[239].

Twenty-four-well plates were coated for *anoikis*-resistance assay by coating wells with 200 μl/well of poly (2-hydroxyethyl methacrylate) [poly-HEMA] (Sigma-Aldrich, Cat. #: P3932) solution (12 mg/ml poly-HEMA prepared in 95% ethanol). Poly-HEMA was allowed to completely evaporate by leaving in a biosafety cabinet overnight with the lid opened. The process was repeated the following day. As a control, wells were coated with 95% ethanol in place of the poly-HEMA. Cells were seeded at 2.5 x 10^4 cells/well in 400 μl of completed RPMI-1640 medium. After 72 hrs, 50 μl of AlamarBlue dye (Invitrogen, Cat. #: DAL1100) was added to each well and incubated at 37°C, 5% CO_2 for 3.5 hrs. Cell survival was determined by reading the plate at an absorbance of 570 nm using a FLUOstar® OPTIMA microplate reader.

3.3.9 Wound healing assay

HCC1954 and SKBR3 cell variants were seeded at 2.5×10^5 and 3×10^5 cells/well, respectively, in 24-well plates (6 wells were seeded for each cell variant) (Costar, Cat. #: 3524). Cells were allowed to attach overnight to form a monolayer. Medium was removed from wells and the monolayer of cells was scratched using a p200 tip. 1% FBS-supplemented RPMI medium was carefully placed in each well and the wound size was captured by phase contrast microscopy using ImageJ/Fiji® plugin Wound_healing_size_tool[240] at 0, 24 and 48 hrs. The wound area (%) calculated by the tool was used to calculate the percentage of wound closure, defined as the difference between the wound area at 0 hrs and the wound area at 24 or 48 hrs. The assay was repeated three times.

3.3.10 Transwell invasion assay

ECM (Sigma-Aldrich, Cat. #: E1270) diluted with serum-free RPMI medium at concentration of 1 mg/ml was thawed at 4°C overnight. Polyester (PET) membrane transwell inserts with a pore size of 8 μm (Falcon, Cat. #: 353097) were coated with the ECM by adding 200 μl to each insert placing them in a 24-well plate. The plate was incubated at 37°C, 5% CO_2 overnight. The following day, the ECM-coated inserts were washed twice with 200 μl serum-free RPMI media. HCC1954 and SKBR3 cell variants were seeded at 2.5×10^4 and 2.5×10^5 cells/well, respectively, in 400 μl 1% FBS-containing RPMI medium, respectively. 400 μl of complete 10% FBS supplemented RPMI-1640 was placed in the wells below the insert, to make a cell nutrient gradient to encourage cells to invade though the pores of the insert. Cells were allowed to invade through ECM and pores for 48 hrs. Following this, the inside of each insert was washed with a PBS-soaked Q-tip. Inserts were stained with 0.1% crystal violet (Sigma-Aldrich; Cat. #: C6158) for 10 mins while rocking. Following the staining, inserts were washed with PBS and images of the cells that had invaded were taken using a 10X objective lens using the Olympus IX81 inverted microscope. To estimate the percentage of

invading cells, inserts were placed in 200 μl of 33% acetic acid (Fisher Scientific; Cat. #: A/0406/PB08) for 10 mins to elute the crystal violet. After the 10 mins, 100 μl were placed in a 96-well plate and the absorbance was read at 595 nm using a FLUOstar® OPTIMA microplate reader.

3.3.11 Statistical Analysis

All statistical analyses were performed using GraphPad Prism version 9.1.9 for macOS (GraphPad Software). Data are presented as means ± SEM. 2-way *ANOVA* with Tukey post-test was performed to assess multiple comparison. For ELISA assay analysis, VEGF quantification was performed interpolating the absorbance values to the standard curve run alongside the samples. For RT-qPCR analysis, the mRNA fold changes were calculated according to the ΔΔCt value. The specificity of the PCR products was confirmed by dissociation curve analysis. One-way *ANOVA* or 2-way *ANOVA* with Tukey post-test were performed to assess statistical significance: *$p < 0.05$; ** $p < 0.01$; *** $p < 0.001$.

3.4 Results

3.4.1 Proteomic profiling

To identify common protein(s) differentially expressed in the neratinib-resistant cell variants versus their neratinib-sensitive counterparts that could be associated with conferring resistance to neratinib, we studied EFM192A, EFM192A NR, HCC1954, HCC1954 NR, SKBR3 and SKBR3 NR cell lysates. A principal component analysis (PCA) plot and a heatmap based on correlation between samples were performed. The conditions and replicates were clustered together accurately (**Figure 3.3**). One hundred and five significant differentially expressed proteins were identified. Of those, 7 were differentially expressed between EFM192A variants, 57 between HCC1954 cell variants and 43 between SKBR3 cell variants. Notably, only 1 differentially expressed protein was shared between the HCC1954 and SKBR3 cell variants (AGR2; anterior gradient protein 2), and 1 differentially expressed protein between EFM192A and SKBR3 cell variants (ZADH2; Zinc-Binding Alcohol Dehydrogenase Domain-Containing Protein 2). However, the final commonly differentially expressed protein was not taken into consideration due to the observed disparities in its regulation among distinct cell variants. ZADH2 demonstrated an up-regulation in SKBR3 NR cells compared to their neratinib-sensitive counterparts, whereas it exhibited down-regulation in the case of EFM192A NR cell line variants. Additional supplementary data regarding the proteomic profile is collected in the **Appendix II**.
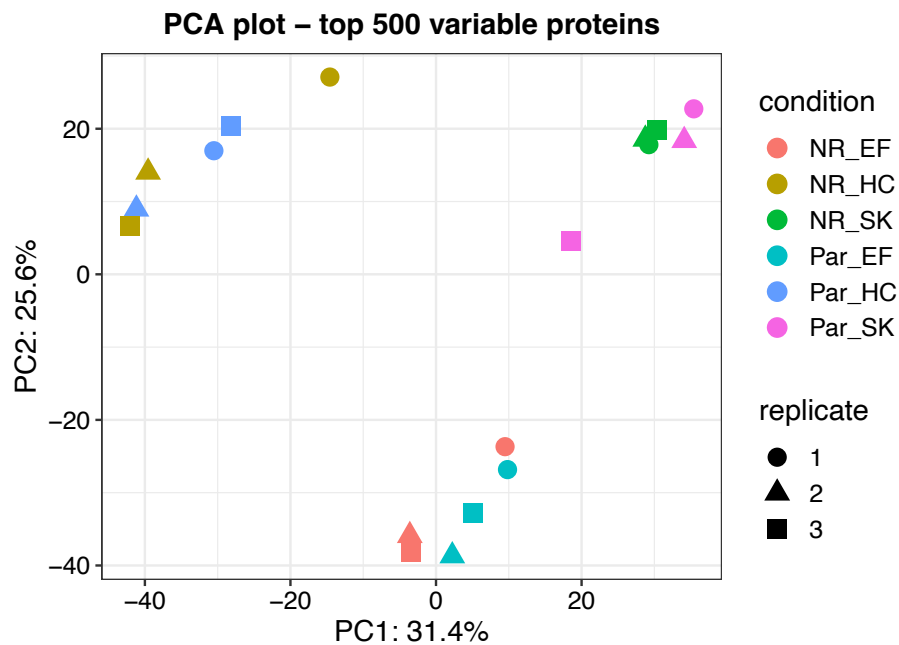
Figure 3.3. PCA performed for the top 500 most variable proteins.
NR_EF= EFM192A NR; NR_HC= HCC1954 NR; NR_SK= SKBR3 NR; Par_EF=EFM192A; Par_HC=HCC1954; Par_SK= SKBR3.

Specifically, AGR2 was downregulated in both HCC1954 NR and SKBR3 NR (HER2+ER-) cell variants with a fold-change of 37.79 ($p = 2.87 \times 10^{-9}$) and 4.96 ($p = 5.81 \times 10^{-5}$) compared with their respective neratinib-sensitive counterparts. Volcano plots for each comparison are available in the **Appendix II**.

To validate the data, immunoblotting analysis was performed. Immunoblotting results were entirely consistent with the mass spectrometry data (**Figure 3.4**). EFM192A and EFM192A NR showed an opposite trend to the other two pairs of cell variants. As luminal B cell variants, EFM192A NR showed a higher expression of AGR2 compared to EFM192A, although was not significant. Since these cell lines represent a different molecular subtype of breast cancer, they would not be used for the following functional assays.
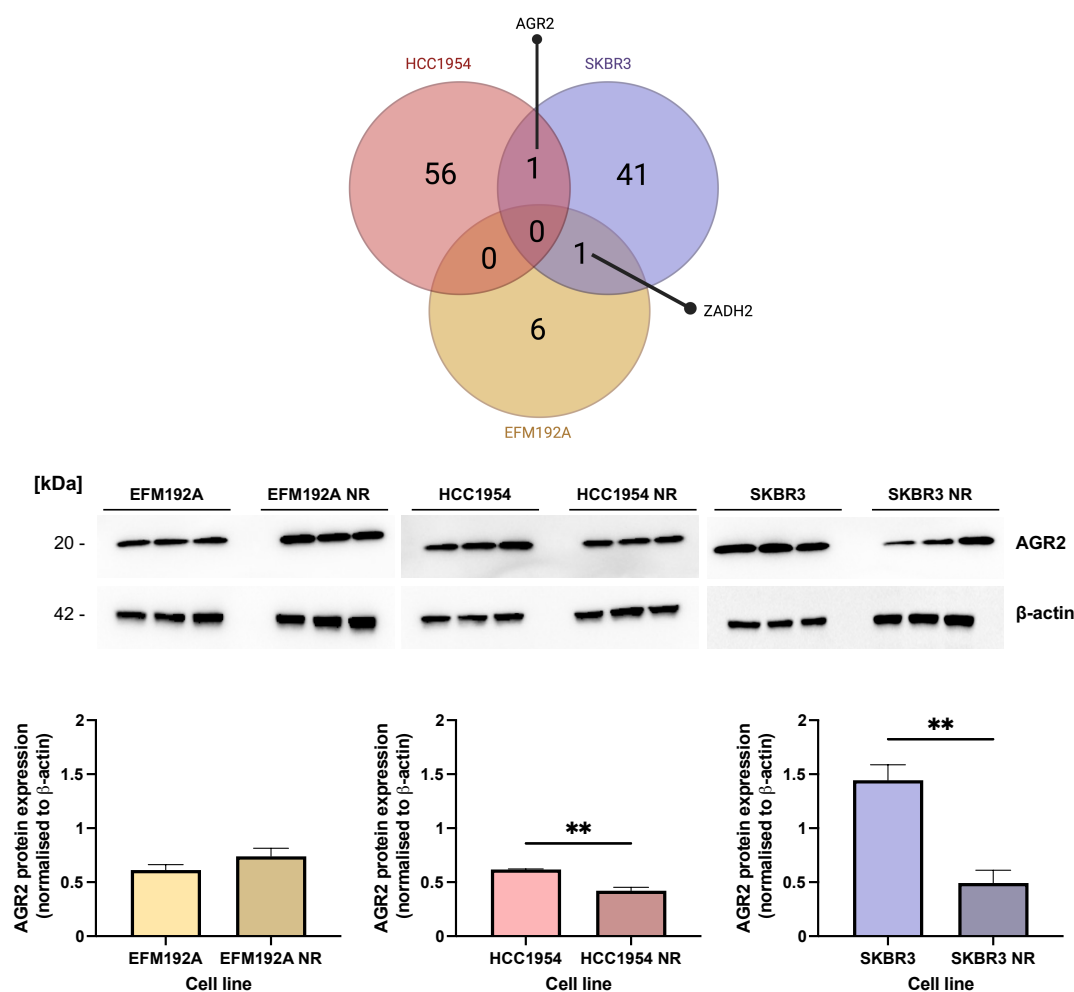
Figure 3.4. Identification of differentially expressed proteins in neratinib-resistance cells compare to their neratinib-sensitive counterparts.

(**Top**) Venn diagram showing the differentially expressed proteins (up-regulated and down-regulated) from comparative proteomic analysis and (**Bottom**) validation of those findings by immunoblotting. Thirty µg of cell lysates were loaded for their analysis. The relative intensity of the protein signal band was calculated using ImageJ software. β-actin was used as loading control and normalisation. Graphs shown are mean ± SEM ($n = 3$) **$p<0.01$.

3.4.2 Successful transfection of AGR2 in neratinib-resistant cell variants

Given that AGR2 was significantly decreased in two neratinib-resistant cells, we investigated if AGR2 represents a key component of neratinib-resistance mechanism. For that purpose, HCC1954 NR and SKBR3 NR cells were stably transfected with AGR2, EGFP (as marker of successful transfection), or EMPTY plasmid (as a control). The successful transfection was investigated by microscopy after puromycin selection (Additional images collected in the **Appendix II - Figure II-14**) as well by evaluating the AGR2 expression by RT-qPCR and immunoblotting. We found transfection with AGR2 plasmid significantly increased AGR2 expression in NR-transfected cells, achieving similar AGR2 levels as neratinib-sensitive counterparts (**Figure 3.5**).
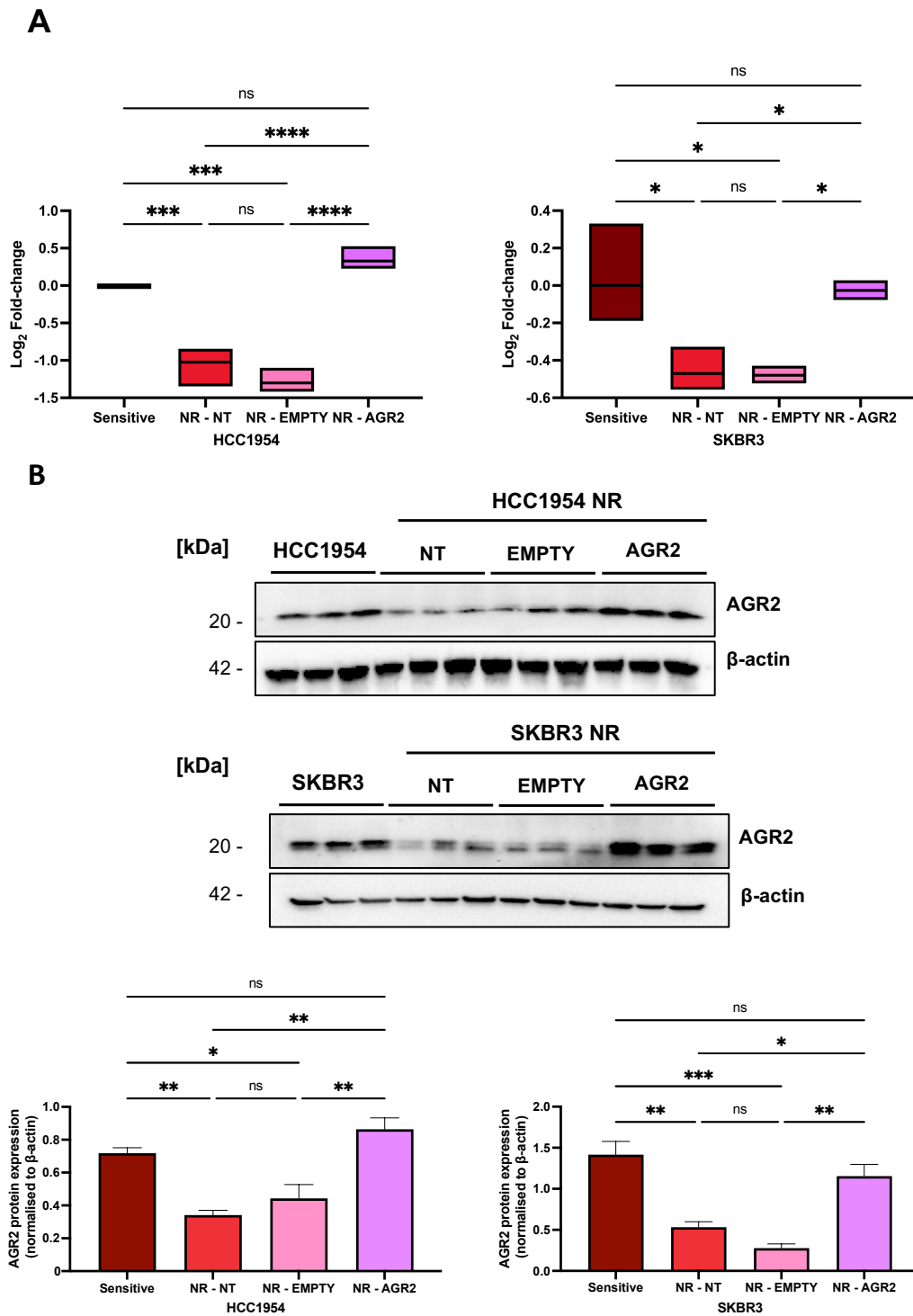
Figure 3.5. Successful transfection of AGR2 cDNA in neratinib-resistant cell variants.

(**A**) mRNA levels of AGR2 were analysed by RT-qPCR, ACTB mRNA served as an endogenous control for data normalisation. Data for RT-qPCR are the mean ± SEM obtained from three independent experiments. The increase of AGR2 mRNA level after AGR2 transfection (NR-AGR2) compared to non-transfected (NR-NT) and those transfected with an empty plasmid (NR-empty) were statistically significant (*p<0.05) for both cell lines. (**B**) immunoblotting analysis for detecting AGR2 in HCC1954 and SKBR3 cell line variants. The expression of AGR2 protein levels was normalised to *β*-actin. Data are represented as the mean ± SEM, *n* = 3. One-way *ANOVA* with Tukey post-test was performed for the multiple comparisons *p<0.05.

3.4.3 Up-regulation of AGR2 is associated with changes in EMT markers expression and HER2 expression

EMT is a biological process in which epithelial cells undergo a transformation into mesenchymal cells. EMT has been implicated in several physiological and pathological processes, including embryonic development, wound healing, fibrosis, and cancer metastasis. A study performed by Rajabi et al. (2014)[241] have reported that AGR2 can promote EMT in cancer cells and increased cell migration and invasion. On the other hand, there are also studies that suggest a role of AGR2 maintaining epithelial cell phenotype, inhibiting EMT induction, and enhancing the rate of adhesion to plastic substratum, thus playing a potential role in tumour development and progression[242,243]. Overall, the role of AGR2 in regulating EMT is still not fully understood, and the exact mechanisms by which AGR2 promotes or inhibits EMT may vary depending on the type of cancer and cellular context.

The molecular hallmarks of EMT encompass various changes in cell characteristics. These include the loss of cell polarity and epithelial markers like E-cadherin and ZO-1. Conversely, there is a gain in the expression of mesenchymal markers such as N-cadherin, vimentin, and fibronectin, signifying a shift towards a mesenchymal phenotype. Additionally, during EMT, cells undergo a significant cytoskeletal reorganization, transitioning from an epithelial, differentiated morphology to a fibroblast-like, motile, and invasive behaviour. Among the numerous growth factors that contribute to this process, TGF-β stands out as one of the most potent inducers of EMT. In addition, it has been reported that EMT enhances the tumorigenicity of murine mammary gland epithelial (NMuMG) cells through two key mechanisms. Firstly, EMT leads to the up-regulation of VEGF, promoting increased tumour angiogenesis. Secondly, the augmented tumour initiation capacity observed in breast cancer cells after undergoing EMT is dependent on the expression of VEGF[244].

To investigate the effect of AGR2 expression on EMT induction we evaluated the changes in the level of E-cadherin, N-cadherin, and TGF-β1 by immunoblotting and the expression of the VEGF by ELISA. We found N-cadherin expression was higher in HCC1954 NR and HCC1954 NR- pcEMPTY compared with HCC1954 cell line. HCC1954 NR cells transfected with pcAGR2 showed a down-regulation in N-cadherin expression, resulting in levels similar to the neratinib-sensitive counterparts. No significant differences were found for E-cadherin expression between different HCC1954 cell line variants and the three HCC1954 NR cell variant forms (transfected and non-transfected) presented a higher expression of TGF-β1 compared to HCC1954 cell line variant. Interestingly, HCC1954 NR-pcAGR2 showed a decrease in HER2 expression when compared with HCC1954 NR and HCC1954 (**Figure 3.6A**). No significant differences were found in the case of SKBR3 cell variants when those markers were investigated (**Figure 3.6B**).
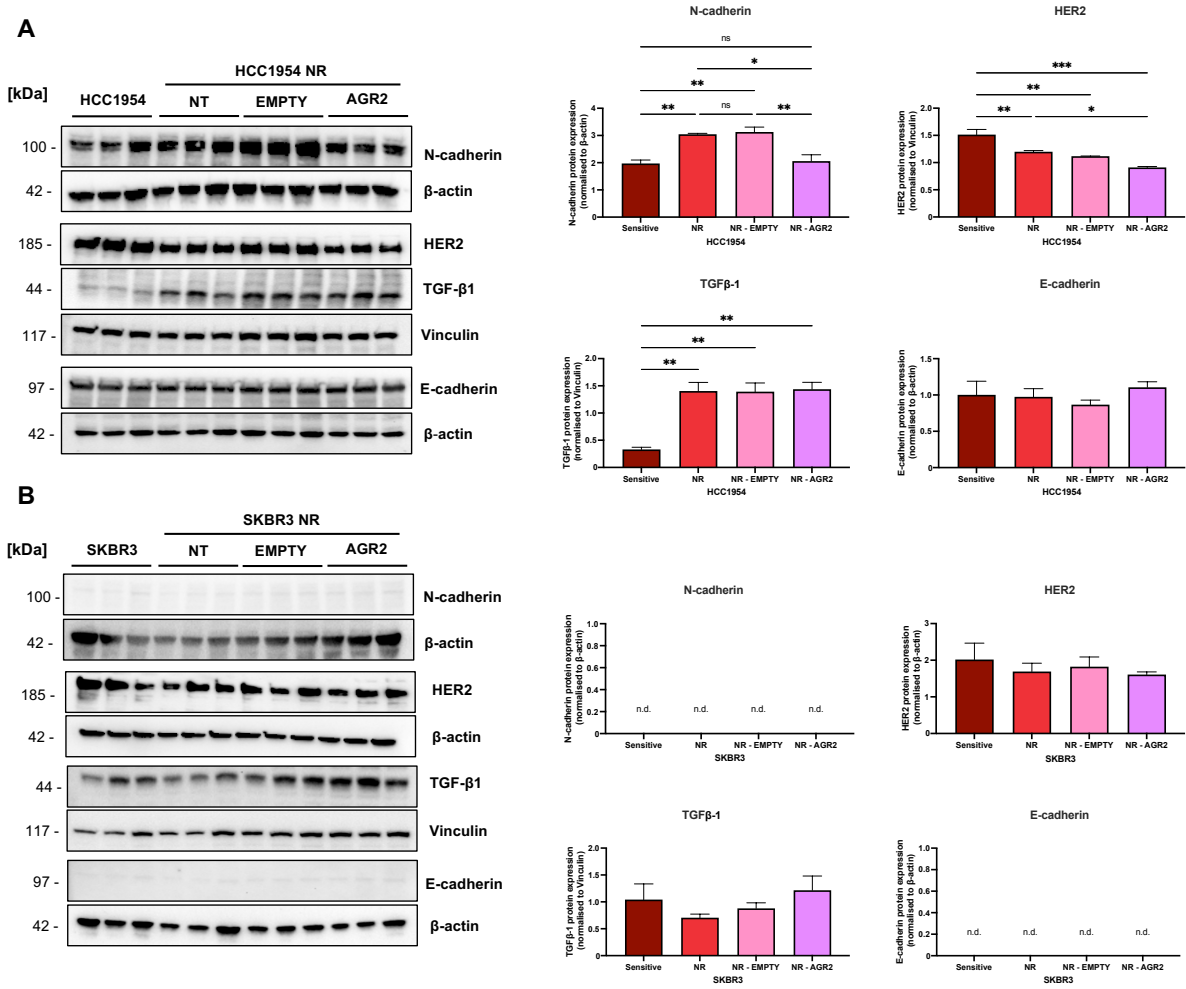
Figure 3.6. AGR2 transfection affects the expression of EMT markers and HER2.
N-cadherin, HER2, TGF-β1, and E-cadherin were detected by immunoblotting in (**A**) HCC1954 and
(**B**) SKBR3 cell variants. The expression of those proteins was normalised to β-actin/Vinculin. Data
are presented as the mean ± SEM, n = 3. One-way *ANOVA* with Tukey post-test was performed for
the multiple comparisons. *$p<0.05$, **$p<0.01$, ***$p<0.001$.

No significant differences were found for VEGF by ELISA assay for the different cell lines (**Figure
3.7**).
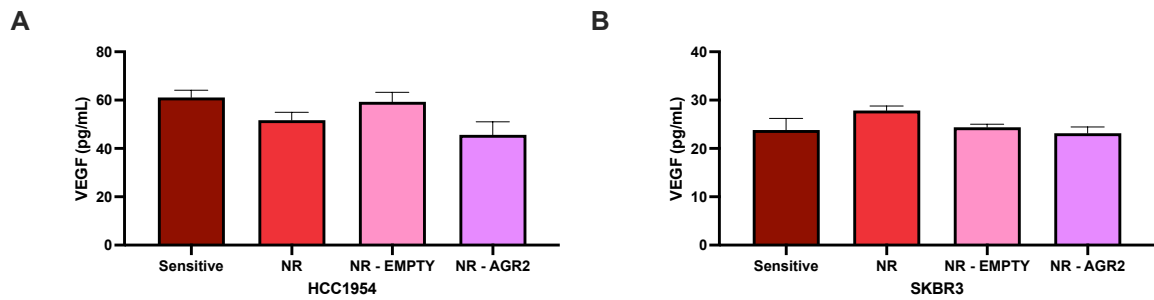
Figure 3.7. VEGF expression levels measured by ELISA.

VEGF expression in (**A**) HCC1954 and (**B**) SKBR3 cell variants. The data are expressed as the mean ± SEM obtained from three independent experiments.

3.4.4 Up-regulation of AGR2 could reduce the *anoikis*-resistance in neratinib-resistant cell variants

To assess for any resistance to *anoikis*, we compared the survival of SKBR3 and HCC1954 cell variants exposed to anchorage-independent conditions. We observed that there was no significant change in cell survival under anchorage-independent conditions. In the case of HCC1954 cell variants, no differences were found between HCC1954 and HCC1954 NR cell variants. However, the *anoikis*-resistance was significantly reduced in the case of HCC1954 NR-pcAGR2 when compared to HCC1954 NR and HCC1954 NR-pcEMPTY (**Figure 3.8A**). This reduction on the *anoikis* resistance can be translated to a less metastatic potential. No significant differences were found in *anoikis*-resistance between SKBR3 cell variants (**Figure 3.8B**). In fact, previously works showed that SKBR3 cells did not undergo *anoikis* when seeded in poly-HEMA[245], closely related with the lack of expression of known cadherins[246,247].
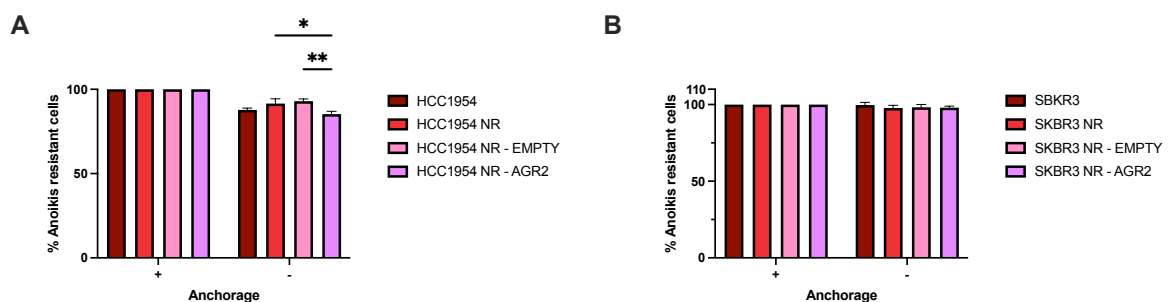
Figure 3.8. *Anoikis*-resistance analysis.

Resistance to *anoikis* was assessed by measuring the survival of (**A**) HCC1954 and (**B**) SKBR3 cell line variants under anchorage-independent conditions. Graphs represent % of cells resistant to *anoikis* under non-anchorage conditions when compared with the anchorage control. The data are expressed as the mean ± SEM obtained from three independent experiments. 2-way *ANOVA* with Tukey post-test was performed for the multiple comparisons: *$p<0.05$, **$p<0.01$.

3.4.5 Transfection of AGR2 in neratinib-resistant cells lead to reduced migration and invasion patterns similar to those of neratinib-sensitive cells

The migration of tumour cells is a crucial process for the invasion of the tumours ECM of nearby tissues and to enter blood vessels or lymphatic vessels, which allow them to spread to distant parts of the body and form metastases[237].

Using the wound healing assay to evaluate the migration, we found the transfection of pcAGR2 decreased the wound closure, showing no differences between neratinib-sensitive counterparts and neratinib-resistant cells transfected with pcAGR2 in both HCC1954 and SKBR3 cell lines at 24 hrs and 48 hrs (**Figure 3.9**). At the same time, HCC1954 NR and HCC1954 NR-pcEMPTY demonstrated an increased wound closure (i.e., migration) when compared to HCC1954 and HCC1954 NR-pcAGR2 at 24 hrs and 48 hrs. In the case of SKBR3 cell variants, SKBR3 NR and SKBR3 NR-pcEMPTY showed an increase on the wound closure when compared to SKBR3 and SKBR3 NR-pcAGR2 at 24 hrs and 48 hrs (**Figure 3.10**). Percentages of wound closure are collected in **Table 3.3.**

Figure 3.9. Up-regulation of AGR2 in HCC1954 NR cell variants reduced its migration.
(**Top**) Representative wound-healing images of HCC1954 cell line variants at 0, 24 and 48 hrs. Images were taken at 10x magnification. Scale bar 100 µm; (**Bottom**) % of wound closure at 24 and 48 hrs. Graph bars represent the means from three independent experiments, with error bars showing the SEM of the means. 2-way *ANOVA* with Tukey post-test was performed for the multiple comparisons (**$p<0.01$, ***$p<0.001$, ****$p<0.0001$).

Figure 3.10. Up-regulation of AGR2 in SKBR3 NR cell variants reduced its migration.

(**Top**) Representative wound-healing images of SKBR3 cell line variants at 0, 24 and 48 hrs. Images were taken at 10x magnification. Scale bar 100 μm; (**Bottom**) % of wound closure at 24 and 48 hrs. Graph bars represent the means from three independent experiments, with error bars showing the SEM of the means. 2-way *ANOVA* with Tukey post-test was performed for the multiple comparisons (****$p < 0.0001$).

Table 3.3. Percentages (%) of wound closure after 24 hrs and 48 hrs.

% Wound Closure - HCC1954			
Time	HCC1954	HCC1954 NR	HCC1954 NR - EMPTY	HCC1954 NR - AGR2
24 hrs	15.68 ± 1.88	30.98 ± 0.21	27.11 ± 1.43	19.65 ± 0.26
48 hrs	25.12 ± 1.38	42.56 ± 2.03	42.55 ± 1.86	26.14 ± 0.73
% Wound Closure - SKBR3			
Time	SKBR3	SKBR3 NR	SKBR3 NR - EMPTY	SKBR3 NR - AGR2
24 hrs	7.57 ± 1.59	19.22 ± 3.13	18.95 ± 2.22	9.02 ± 0.54
48 hrs	15.43 ± 0.61	31.71 ± 0.69	30.57 ± 2.57	16.03 ± 2.29

Wound closure (%) was calculate as the differences between the open area (%) at 0 hrs and the wound area at 24 or 48 hrs.

Invasion refers to the ability of cancer cells to penetrate and move through barriers, such as the extracellular matrix. This process requires the cancer cells to secrete enzymes that break down the ECM and other barriers, allowing them to move through and invade nearby tissues. HCC1954 NR and HCC1954 NR-pcEMPTY showed an increase of invasion compared to HCC1954. Interestingly, when HCC1954 NR cells were transfected with pcAGR2, invasion was reverted to HCC1954 levels, being non-significant differences between HCC1954 and HCC1954 NR-pcAGR2 (**Figure 3.10**). This decrease of the invasion percentage was significant between HCC1954 NR-pcAGR2 and both HCC1954 NR and HCC1954 NR-pcEMPTY cell variants.

When we investigated invasion in SKBR3 cell variants, we obtained a similar reduction in the invasiveness when we increased the expression on AGR2 level in SKBR3 NR cell variant (**Figure 3.11**). No significant differences in invasiveness were found between SKBR3 and SKBR3 NR-pcAGR2 while SKBR3 NR and SKBR3 NR-pcEMPTY showed to be more invasive compared to SKBR3 and SKBR3 NR-pcAGR2.

A
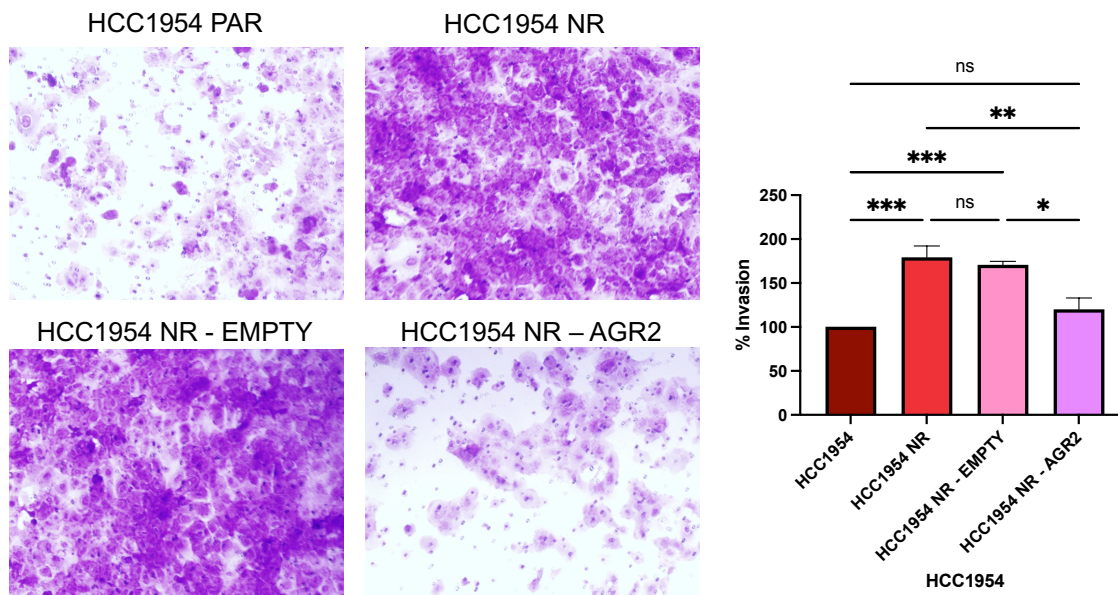
B
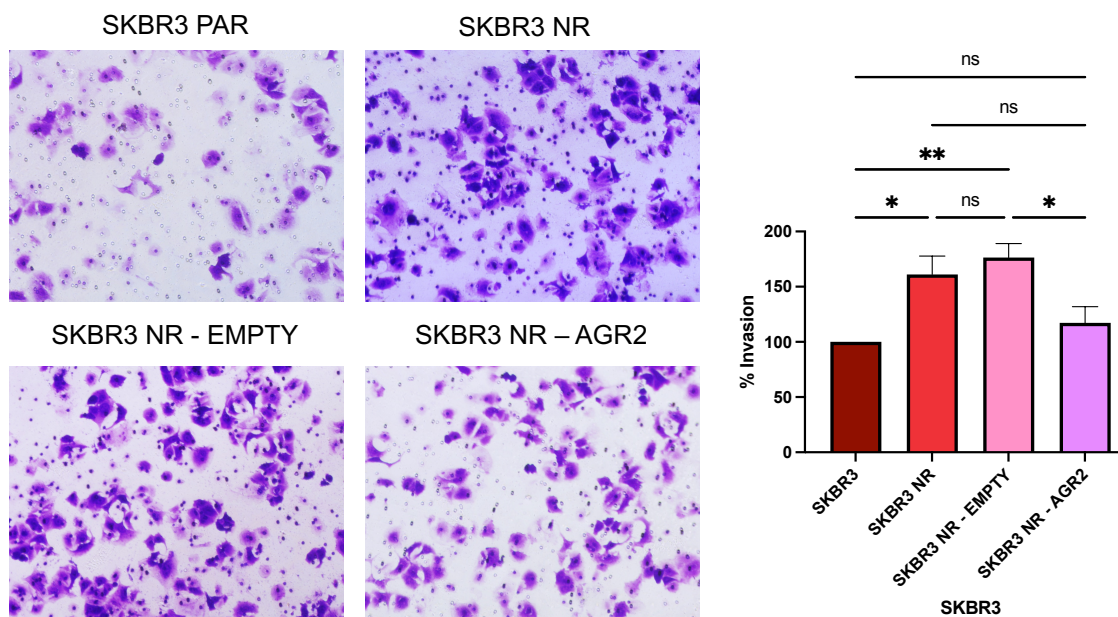
Figure 3.11. Increased levels of AGR2 in neratinib-resistant cell variants reduced the invasiveness of neratinib-resistant cell variants.

(**Left**) Representative images of (**A**) HCC1954 and (**B**) SKBR3 invasive cells after 48 hrs seeding. Images were taken at 10x magnification; (**Right**) % of invasion at 48 hrs. Graph bars represent the means for three independent experiments, with error bars showing the SEM of the means. One-way *ANOVA* with Tukey post-test was performed for the multiple comparisons: *$p < 0.05$, **$p < 0.01$, ***$p < 0.001$.

3.4.6 Up-regulation of AGR2 in neratinib-resistant cell variants does not affect proliferation rate, but it showed a decrease in resistance to neratinib

Proliferation plays an important role in cancer development and progression. We evaluate the effect of AGR2 expression on the cell growth at 24, 48, 72, and 96 hrs using acid phosphatase assay method. AGR2 seemed to have no noticeable proliferative effect in HCC1954 and SKBR3 cell variants (**Figure 3.12**).
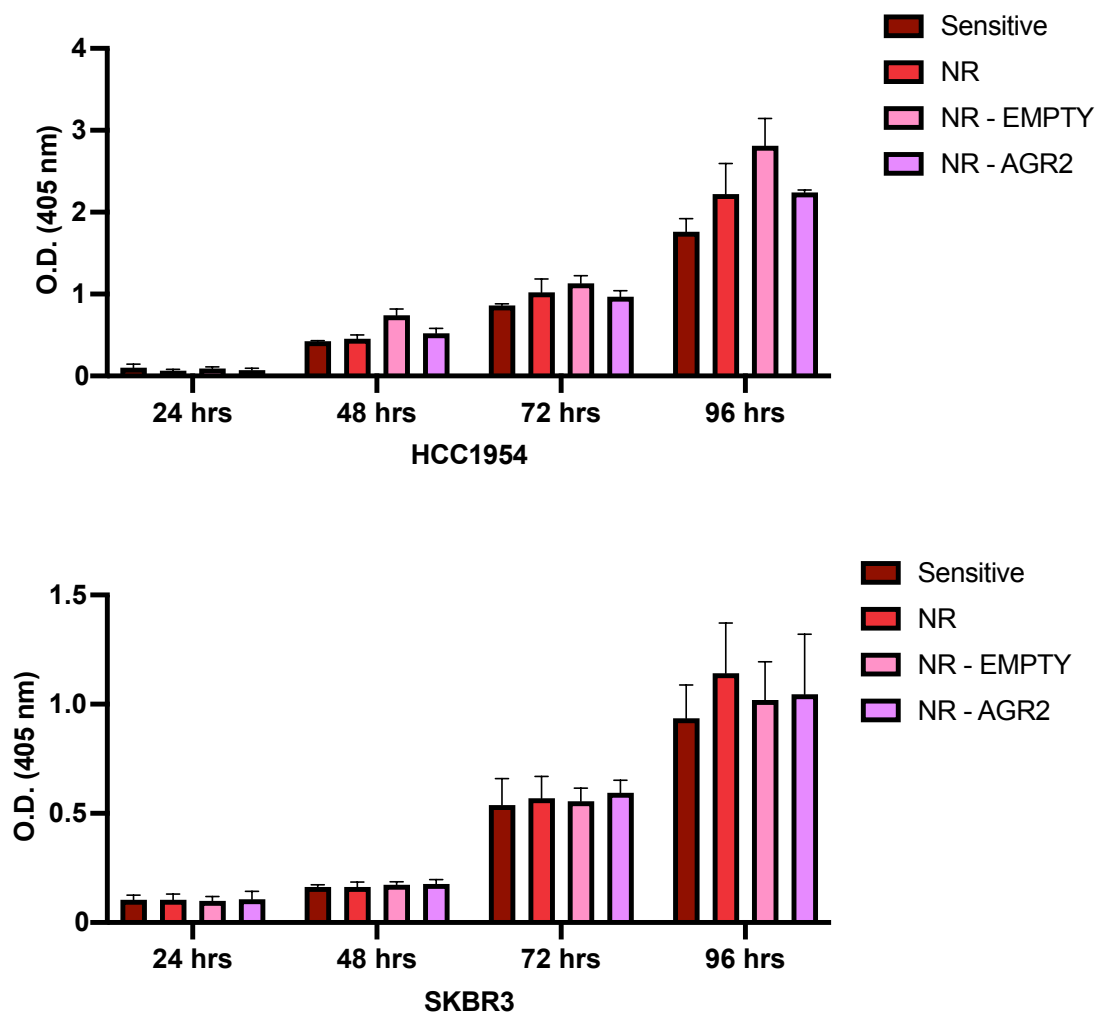
Figure 3.12. AGR2 seems not to affect cell proliferation in neratinib-resistant cell variants.
Acid phosphatase assay results at 24, 48, 72, and 96 hrs. The data represents the means from three independent experiments, with error bars showing the SEM of the means. OD_{405} = optical density at 405 nm.

In order to investigate the relation between AGR2 expression and resistance to neratinib, the *in vitro* cytotoxic proliferation assay was used to determine the IC_{50} values of neratinib for HCC1954 and SKBR3 variants (**Figure 3.13**). Although neratinib-resistant cell variants transfected with AGR2 still showed an increase in neratinib-resistance compared with the age-matched neratinib-sensitive control cells, a significant decrease in the IC_{50} on these cells was revealed when compared with the non-transfected and the NR-pcEMPTY transfected cell variants. As expected, no significant differences were found between NR and NR-pcEMPTY, demonstrating this reduction in the resistance to neratinib was mediated by the increase of AGR2 expression.
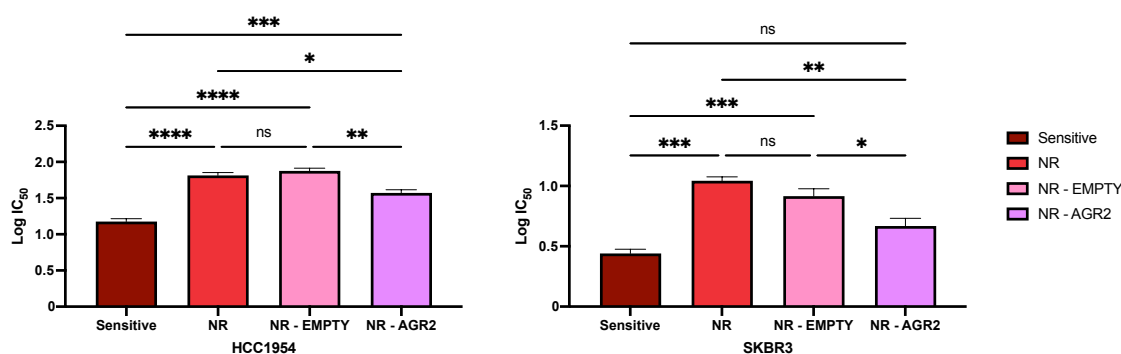
Figure 3.13. Transfection of AGR2 in neratinib-resistant cell variants partially restore sensitivity to neratinib compared with the non-transfected resistant variants.

The Log (IC_{50}) values for neratinib of (**left**) HCC1954 and (**right**) SKBR3 cell variants was determined using *in vitro* cytotoxic proliferation assay. After 4 days culture in the presence of neratinib, cell viability was measured at 405 nm. The data represent the means from three independent experiments, with error bars showing the SEM of the means. One-way *ANOVA* was performed for the multiple comparisons: *$p<0.05$, **$p<0.01$, ***$p<0.001$, ****$p<0.0001$.

The mean IC_{50} values for neratinib of HCC1954 and SKBR3 cell variants are collected in **Table 3.4**.

Table 3.4. The mean IC_{50} values obtained for neratinib.

IC_{50} (nM)			
HCC1954 cell variants			
Sensitive	**NR**	**NR-Empty**	**NR-AGR2**
14.96 ± 1.10	65 ± 1.09	74.99 ± 1.09	37.3 ± 1.1
SKBR3 cell variants			
Sensitive	**NR**	**NR-Empty**	**NR-AGR2**
2.76 ± 1.08	11.07 ± 1.08	9.77 ± 1.11	4.65 ± 1.16

The mean IC_{50} values (X ± SEM) for neratinib. IC = Inhibitory concentration.

3.4.7 Summary of findings

The main findings of the AGR2 transfection in neratinib-resistant cell lines are collected in **Table 3.5.**

Table 3.5. Summary of the main findings.

Assay		HCC1954 cell line variants	SKBR3 cell line variants
Immunoblots	HER2	NR vs sensitive (↓1.3-fold, p = 0.008) NR-EMPTY vs sensitive (↓1.4-fold, p = 0.002) NR-AGR2 vs sensitive (↓1.7-fold, p = 0.0001) NR vs NR-EMPTY (ns) NR-AGR2 vs NR (ns) NR-AGR2 vs NR-EMPTY (↓1.5-fold, p = 0.007)	(ns)
	N-cadherin	NR vs sensitive (↑1.5-fold, p = 0.006) NR-EMPTY vs sensitive (↑1.6-fold, p = 0.004) NR-AGR2 vs sensitive (ns) NR vs NR-EMPTY (ns) NR-AGR2 vs NR (↓1.5-fold, p = 0.01) NR-AGR2 vs NR-EMPTY (↓1.5-fold, p = 0.007)	N.D.
	E-cadherin	(ns)	N.D.
ELISA	TGF-β1	(ns)	(ns)
	VEGF	(ns)	(ns)
Proliferation	-	(ns)	(ns)
Anoikis-resistance	-	NR vs sensitive (ns) NR-EMPTY vs sensitive (ns) NR-AGR2 vs sensitive (ns) NR vs NR-EMPTY (ns) NR-AGR2 vs NR (↓, p = 0.02) NR-AGR2 vs NR-EMPTY (↓, p = 0.004)	(ns)
Migration	24 hrs	NR vs sensitive (↑2-fold, p<0.0001) NR-EMPTY vs sensitive (↑1.7-fold, p = 0.0002) NR-AGR2 vs sensitive (ns) NR vs NR-EMPTY (ns) NR-AGR2 vs NR (↓1.6-fold, p = 0.0002) NR-AGR2 vs NR-EMPTY (↓1.4-fold, p = 0.008)	NR vs sensitive (↑2.5-fold, p<0.0001) NR-EMPTY vs sensitive (↑2.5-fold, p<0.0001) NR-AGR2 vs sensitive (ns) NR vs NR-EMPTY (ns) NR-AGR2 vs NR (↓2.1-fold, p<0.0001) NR-AGR2 vs NR-EMPTY (↓2.1-fold, p<0.0001)
	48 hrs	NR vs sensitive (↑1.7-fold, p<0.0001) NR-EMPTY vs sensitive (↑1.7-fold, p<0.0001) NR-AGR2 vs sensitive (ns) NR vs NR-EMPTY (ns) NR-AGR2 vs NR (↓1.6-fold, p<0.0001) NR-AGR2 vs NR-EMPTY (↓1.6-fold, p<0.0001)	NR vs sensitive (↑2-fold, p<0.0001) NR-EMPTY vs sensitive (↑2-fold, p<0.0001) NR-AGR2 vs sensitive (ns) NR vs NR-EMPTY (ns) NR-AGR2 vs NR (↓2-fold, p<0.0001) NR-AGR2 vs NR-EMPTY (↓1.9-fold, p<0.0001)
Invasion	-	NR vs sensitive (↑1.8-fold, p = 0.0003) NR-EMPTY vs sensitive (↑1.7-fold, p = 0.0008) NR-AGR2 vs sensitive (ns) NR vs NR-EMPTY (ns) NR-AGR2 vs NR (↓1.5-fold, p = 0.003) NR-AGR2 vs NR-EMPTY (↓1.4-fold, p = 0.011)	NR vs sensitive (↑1.6-fold, p = 0.015) NR-EMPTY vs sensitive (↑1.8-fold, p = 0.002) NR-AGR2 vs sensitive (ns) NR vs NR-EMPTY (ns) NR-AGR2 vs NR (ns) NR-AGR2 vs NR-EMPTY (↓1.5-fold, p = 0.018)
Neratinib-resistance (IC_{50})	-	NR vs sensitive (↑, p <0.0001) NR-EMPTY vs sensitive (↑, p <0.0001) NR-AGR2 vs sensitive (↑, p = 0.0007) NR vs NR-EMPTY (ns) NR-AGR2 vs NR (↓, p = 0.02) NR-AGR2 vs NR-EMPTY (↓, p = 0.004)	NR vs sensitive (↑, p = 0.0001) NR-EMPTY vs sensitive (↑, p = 0.0007) NR-AGR2 vs sensitive (ns) NR vs NR-EMPTY (ns) NR-AGR2 vs NR (↓, p = 0.003) NR-AGR2 vs NR-EMPTY (↓, p = 0.033)

ns = not significant; N.D. = not detected.

3.5 Discussion

AGR2 was initially identified as a gene with increased expression in ER-positive breast cancer cell lines[248]. Further research has confirmed that AGR2 is upregulated in various adenocarcinomas, such as those affecting the breast, colon, oesophagus, lung, ovary, pancreas, and prostate. It is involved in various cellular processes, including protein folding and secretion[248]. Although some recent research has suggested that AGR2 may play a role in the development and progression of several types of cancer, the exact mechanisms by which AGR2 may promote cancer progression are still not fully understood. AGR2 has been shown to interact with several other proteins involved in cell signalling, proliferation, and survival, including EGFR, HER2, and Akt. These interactions may help to promote cancer cell survival and proliferation[249–251]. However, studies on AGR2 expression in breast cancer and other types of cancer have yielded mixed results, with some studies suggesting that higher expression levels are associated with poorer outcomes, while others have suggested a potential beneficial role. In addition, to the best of our knowledge, no prior studies have been conducted to explore the involvement of AGR2 in resistance using breast cancer cells resistant to anti-cancer drugs.

Here, we aimed to investigate the proteomic differences between HER2+ breast cancer cell lines (two cell lines, HER2+ER- and one luminal B) and their neratinib-resistant counterparts. The conditions and replicates were clustered together according to the PCA plot (**Figure 3.3**) and Pearson correlation's heatmap (**Figure II-2**). Gene ontologies and pathways of the differentially expressed proteins for the three different pairs of comparisons were performed by *enrichr* web tool (**Appendix II**). KEGG enrichment of differentially expressed proteins between EFM192A and EFM192A NR revealed that only pathways related with leukocyte trans-endothelial migration and vascular smooth muscle contraction were enriched. Although it seems these pathways are not related with cancer, similar KEGG enrichment has been found in lung cancer subtypes[252]. Cell migration through the vasculature is an important and complex mechanism that requires the presence and activity of several genes. This mechanism is crucial for immunosurveillance as well as for inflammatory responses. Vasculature's contraction is essential in controlling the blood flow and influx of oxygen and nutrients to tissues. This is important in the context of cancer, as tumours habitually have a higher microvessel density than normal tissues; however, these blood vessels are poorly formed, less elastic, and with different physiology than normal vessels. In the case of HCC1954 cell variants, drug metabolism-related pathways were the most enriched, and including other interesting pathways related with bladder cancer, ribosome, central carbon metabolism in cancer, HER2 signalling pathway and HIF-1 signalling pathway. HCC1954 NR cells showed cross-resistance to other anti-HER2 therapies, including afatinib and lapatinib[64], and could be linked with the KEGG enrichment results obtained in this research. In keeping with this, HCC1954 NR showed a decreased HER2 expression compared to their sensitive counterparts, explaining the dysregulation of HER2 signalling pathway.

KEGG pathways analysis for SKBR3 cell variants revealed that arginine and proline metabolism-related pathways were the most enriched, followed by pathways related with glycolysis/gluconeogenesis, caffein metabolism and insulin signalling pathway. The proline–glutamine–asparagine–arginine metabolic axis represents an important nodule of cancer metabolism[253]. These amino acids are also directly or indirectly link to the tricarboxylic acid (TCA) cycle, that metabolises glucose to generate ATP and reactive oxygen species (ROS) signalling, showing the importance of this axis/loop in cancer growth, proliferation, survival, and metastatic spread. Thus, several molecules involved in this pathway are potential targets for chemoprevention and targeted cancer therapy. Anomalous insulin-like growth factor (IGF) signalling has the potential to drive malignant transformations and promote tumour progression, making the targeting of the IGF axis a promising approach in cancer treatment[253–255]. Previously work performed by our group found that: (i) the expression of IGF1R was elevated in acquired lapatinib-resistant SKBR3 and HCC1954 cells (compared to their age-matched sensitive cells) and it was inversely correlated with decreased miR-630 expression in the same resistant cells; (ii) reduced miR-630 expression levels are associated with both innate- and acquired- resistance to anti-HER2 therapies, and (iii) the suppression of miR-630 -leading to an increased resistance and a metastatic phenotype in SKBR3 and HCC1954 cells- was correlated with elevated IGF1R expression in both cell lines[256]. In keeping with these previous results, our findings support this interaction between IGF1R and/or HER family receptors further investigation is warranted.

The list of the differentially expressed proteins for each pair of cells are collected in the **Appendix II**. We found that HER2+ER- cell lines HCC1943 NR and SKBR3 NR present a significant lower expression of AGR2 compared to their neratinib-sensitive counterparts while luminal B (HER2+ER+) breast cancer cell lines, EFM192A and EFM192A NR, showed the opposite trend. Interestingly, AGR2's overexpression in ER+ breast cancer is associated with poor prognosis, especially in tumours that are resistant to hormone therapies[257]. ER and PR positivity has been associated with AGR2 expression[258–260] in several breast cancer studies. On the other hand, the relationship between AGR2 and HER2 has never been investigated.

Low expression of AGR2 has been associated with poorer overall and relapse-free survival when considering all breast cancer patients. More specifically, low expression of AGR2 was associated with poor OS in luminal A and worst relapse free survival (RFS) in basal-like breast cancer. It has been reported that the reduction of AGR2 in patients aged $\leq$ 51 years, negativity of ER and PR, and nodal status[261].In another study, higher AGR2 expression was correlated with a longer OS time in breast cancer bone metastasis (p = 0.0044)[262]. A study performed by Alves et al. (2018)[263] in ovarian carcinoma showed that lower expression of AGR2 is a marker of poor prognosis in epithelial ovarian carcinoma (EOC) (p = 0.034). This study suggested that a higher AGR2 expression in the earlier stages of tumour could participate in the activation of proliferative mechanisms but the reduction in AGR2 could activate pathways involving invasion and metastasis by reducing adhesion molecules with tumour progression. Overall, the role of AGR2 as a prognostic marker in cancer

appears to be context-dependent, with its prognostic value varying depending on the type and subtype of cancer.

Through combined proteomic profiling and functional assays, we investigated how the AGR2 down-regulation may contribute to the aggressiveness of neratinib-resistant HER2+ breast cancer cell lines. After the successful transfection of AGR2 in neratinib-resistant cell variants, we evaluated the proliferation, migration, invasion, *anoikis*-resistance, and neratinib-resistance, as well as the status of EMT markers and HER2 expression. It was shown previously that the expression of AGR2 is connected to the expression of epithelial markers, and that the reduction in AGR2 induced by TGF-β1 conduce to obtain features of mesenchymal cells such as the loss of E- cadherin, and induction of N-cadherin, showing the importance of AGR2 in maintaining of epithelial phenotypes and suggesting a role of AGR2 in EMT[243]. N-cadherin has been extensively studied in various types of cancer, including breast cancer. It has been reported that N-cadherin promotes adhesion between invasive breast cancer cells and the stroma, essential for tumour growth and invasion[264]. Over-expression of N-cadherin in breast carcinoma has been shown to be associated with invasiveness and the resistance of breast cancer cells to chemotherapy and radiation therapy[265,266].

Here, we demonstrated that migration and invasion were altered, recovering migrative and invasive ratios of neratinib-sensitive cell line variants. Analysing the expression of some EMT markers such as E-cadherin, N-cadherin, and TGF-β1, we also demonstrated that N-cadherin was down-regulated in HCC1954 NR-pcAGR2 in comparison with non-transfected HCC1954 NR, showing a similar N-cadherin level that HCC1954, the neratinib-sensitive variant. No significant differences were found in the VEGF expression between the cell variants by ELISA. These results indicated that the EMT process may not be linked with VEGF expression under these conditions. We also found that in the case of HCC1954 cell variants, *anoikis* resistance was decreased after the transfection with AGR2 cDNA in comparison with HCC1954 NR-pcEMPTY and non-transfected HCC1954 NR cells. Drug resistance is a major challenge in cancer treatment, as it can limit the effectiveness of chemotherapy and targeted therapies. Drug resistance can result in treatment failure and disease progression, leading to poorer outcomes for patients. Therefore, understanding the mechanisms of drug resistance and developing strategies to overcome it is essential for improving cancer treatment. Recent studies have suggested that AGR2 can reduce resistance to chemotherapy in some cancers. For example, down-regulation of AGR2 was associated with tumour progression and chemotherapy resistance in EOC[263]. In addition, the Knock-down of AGR2 expression in PC3 prostate cancer cells resulted in docetaxel-resistance[267].

Finally, we also revealed that although no changes in proliferation rates were observed between drug-sensitive and neratinib-resistant cell variants, the resistance to neratinib was significantly decreased in neratinib-resistant cell variants after AGR2 transfection. Our concern is that the restoration of sensitivity to neratinib was only partial and the associated changes in EMT markers were only significant for N-cadherin. Further research is needed to fully understand how the reduction in AGR2 expression acts facilitating tumour progression.

3.6 Conclusion

The global proteomic profile revealed a consistent decrease in AGR2 protein expression in both the HCC1954 NR and SKBR3 NR cell variants compared to their neratinib-sensitive counterparts. The successful transfection of AGR2 in neratinib-resistant cell lines partially reinstated their sensitivity to neratinib. In summary, AGR2 appears to possess a multifaceted role in cancer progression and drug resistance, with preliminary evidence indicating its potential to mitigate chemotherapy resistance in specific cancer types. Further investigation is imperative to comprehensively comprehend the function of AGR2 in cancer and elucidate how the reduction of AGR2 may facilitate tumour progression.

Chapter 4

Characterisation of EVs released from neratinib-sensitive and neratinib-resistant cell line variants: considering 200K differential ultracentrifugation protocol and density gradient methodology for EVs collection

Abstract

Neratinib is an oral, irreversible TKI of HER1/EGFR, HER2 and HER4 approved by the FDA in 2017 and by the EMA in 2018 for adjuvant treatment of breast cancer patients. Since its approval, several studies have been investigating neratinib-resistance in breast cancer cell lines and patient specimens. These studies show that neratinib is both associated with innate and acquired resistance; the molecular mechanisms of resistance to this drug need to be elucidated to improve efficacy and treatment outcome for patients and to identify response-prediction biomarkers. Neratinib resistance cell lines were previously developed in this laboratory (EFM192A NR, HCC1954 NR, and SKBR3 NR) and we have shown that neratinib-resistant cell lines are cross-resistant to other HER2-targeted drugs such as lapatinib. The first aim of this project was to characterise the EVs released by neratinib-sensitive and neratinib-resistant cells. In addition, we inspected if those EVs reflect the HER2 and AGR2 status of their cells of origin and thus have potential as minimally invasive biomarkers.

EVs from three different HER2-positive breast cancer cell lines (EFM192A, HCC1954, and SKBR3) and their neratinib-resistant counterparts (EFM192A NR, HCC1954 NR, and SKBR3 NR) were collected after 48 hrs culture in RPMI-1640 media containing EVs-depleted FBS. EVs were then collected by using two different approaches 200K UC and GUC. Further characterisation of EVs was then performed by immunoblotting, protein content, NTA, IFCM, and TEM. The findings of this study suggest that the release of EVs is diminished in cell lines resistant to neratinib compared to their neratinib-sensitive counterparts. Similar results were observed using both 200K UC and GUC protocols. Furthermore, the presence of HER2 in EVs derived from neratinib-resistant cells was lower compared to those derived from neratinib-sensitive counterparts, consistent with the HER2 expression in their respective cells of origin. However, further investigation is necessary to comprehensively analyse the underlying mechanism behind this reduction and identify potential targets for elucidating the resistance mechanism.

4.1 Introduction

EVs are important mediators of cell-to-cell communication by facilitating bidirectional crosstalk between cancer cells and tumour microenvironments in several diseases, including breast cancer[152]. It has been reported that EVs can modify the tumorigenic properties of recipient cells by enhancing their ability to migrate, invade, and metastasize, as well as remodel the ECM and evade immune detection[268]. The aberrant cargo packaged in the EVs isolated from the cancer cells can directly alter the behaviour of recipient cells, leading to the development of bone disease, angiogenesis, immunosuppression, drug resistance, and ultimately promoting the progression of the disease[269].

Previous research performed initially by our group[151] and validated by others has shown that EVs are involved in transmitting resistance to anti-cancer drugs, causing previously drug-sensitive cells to become drug-resistant[96,146,152,270]. Specifically, our group demonstrated that EVs derived from DU145 and 22Rv1 docetaxel-resistant prostate cancer cells (DU145RD and 22RV1RD) transmitted docetaxel resistance via transfer of the multidrug resistance protein (MDR1/P-glycoprotein) to previously docetaxel-sensitive cell lines[151,271]. Our research team also demonstrated that exposing recipient cells to EVs derived from Hs578Ts(i)$_8$ – a highly aggressive variant of the TNBC cell line Hs578T – led to an increase in their proliferation, migration, and invasion, while the sensitivity to *anoikis* was increased, compared with the less aggressive Hs578T cell line variant (reflecting phenotypic characteristics of the EVs' cells of origin)[272].

The presence of some proteins on EVs' surfaces and their cargo has a large influence on the treatment effect of drugs having an impact in the treatment efficacy. Some studies have shown that EVs mediated the antibody-based drugs neutralisation, being involved in trastuzumab[147,273] resistance, response to anti-HER2 cancer therapies[146], and multidrug resistance[274], among others. Associated with trastuzumab resistance, Durcker et al. (2020)[275] performed a proteomic analysis of EVs derived from trastuzumab-sensitive (BT474 and MCF-7/HER2) and trastuzumab-resistant (BT474TR and HCC1419) HER2-positive BC cells after their treatment with trastuzumab. They found a set of proteins were up-regulated by trastuzumab treatment in trastuzumab-sensitive but not in trastuzumab-resistant cell lines (PERP, GNAS2, GNA13, RAB10, and ITB1). In addition, the increase in these proteins within EVs derived from blood appears to be associated with the positive outcomes experienced by a small group of breast cancer patients with HER2+ MBC who were treated with trastuzumab-based therapies. A study performed by Han et al. (2020)[273] found that miR-567, selected based on the differential expression between trastuzumab-resistant and -sensitive cells from GEO datasets and validated by RT-qPCR, is inhibited in trastuzumab- resistant cells. They also found that extracellular miR-567 could reverse trastuzumab resistance through incorporating it into EVs, suggesting a crucial role in trastuzumab resistance of breast cancer. Another study published by Hosseini et al. (2023)[276] showed that the blockade of exosome release by dihydrochloride hydrate (GW4869) in combination with trastuzumab treatment decreased the proliferation and induced apoptosis of HER2+ BC (SKBR3 and BT474) and HER2+ ovarian cancer cells (SK-OV3). Interestingly, exosome release inhibition could also have an effect in HER2 trafficking as this blockade decreased HER2 levels on the cell surface.

EVs can be used to improve trastuzumab treatment. Barok et al. (2018)[277] found that T-DM1 can bind to exosomes derived from HER2+ breast (SKBR3) and cancer gastric (SNU-216) while is not present in HER2- breast cancer line (MCF-7). Additionally, the treatment of recipient EFM192A breast cancer cells with T-DM1-exosomes derived from SKBR3 caused growth inhibition and activation of caspase activation (cas-3 and cas-7).

EVs can also be involved in the response to other anti-HER2 cancer therapies. Our group revealed a correlation between elevated levels of TGF-β1 and PD-L1 and resistance to HER2-targeted drugs[146]. This study demonstrated that EVs transfer these molecules, thereby inducing drug-sensitive cells to acquire the characteristics of the source cells. Our group further observed that EVs-associated TGF-β1 levels are linked to the response of HER2+ breast cancer patients to HER2-targeted therapy, implying that it could serve as a potential biomarker for therapeutic response.

Neratinib-resistant HER2+ breast cancer cells, developed by our group, display decreased HER2 expression compared to their drug-sensitive counterparts[64]. Additionally, as detailed in **Chapter 3**, proteomic profiling performed during this PhD project, identified a significant decrease in AGR2 expression by HCC1954 NR and SKBR3 NR cell lines compared to their neratinib-sensitive counterparts, indicating AGR2 to be associated with neratinib-resistance.

The recent study performed by Santamaria et al. (2021)[278] aimed to investigate the effects of neratinib treatment on endocytic trafficking and EVs' release in HER+ BC cells. The researchers used various imaging techniques, including immunofluorescence imaging and immunolabelling of the EVs, to track the movement of proteins and EVs within the cells. It has been found in this study that neratinib treatment altered the endocytic trafficking pathways in the cells, leading to an increase in the release of EVs in SKBR3 HER2+ BC cell line while decreased the HER2 content on the EVs. Overall, the findings suggest that neratinib treatment may have unintended consequences on EVs' release and protein trafficking in HER2+ breast cancer cells, which could have implications for disease progression and treatment resistance. Further research is needed to better understand the mechanisms underlying these effects and how they might be mitigated in clinical settings.

4.2 Aims of the study

This study aimed to perform the complete characterisation of EVs released from neratinib-sensitive and neratinib-resistant cells following MISEV2018 guidelines by using different EVs enrichment protocols. Next, we also aimed to investigate if EVs released from neratinib-sensitive and neratinib-resistant cells reflect the HER2 status of their cells of origin and thus have potential as minimally invasive biomarkers. Subsequently, we aimed to determine if EVs reflect the AGR2 status of their cells of origin, that we previously demonstrated to be associated with neratinib-resistant mechanism.

4.3 Materials and Methods

4.3.1 Cell lines and culture conditions

Six HER2-positive breast cancer cell line variants (EFM192A, HCC1954 and SKBR3 and their neratinib-resistant counterparts EFM192A NR, HCC1954 NR, and SKBR3 NR) were routinely maintained as explained in **Section 2.3.1**.

4.3.2 EVs separation by 200K ultracentrifugation protocol

For this step, only HCC1954, HCC1954 NR, SKBR3 and SKBR3 NR cell variants were used and seeded in 7×T175 cm^2 (Corning, Cat. #: 431080) at densities of 3×10^6 cells/flask in complete RPMI-1640 media. After 24 hrs seeding, complete RPMI-1640 media was replaced with 25 ml/flask of complete RPMI-1640 media supplemented with 10% dFBS and 1% P/S (see **Section 2.3.2**). After 48 hrs incubation with complete dFBS-RPMI-1640 media, CM was centrifuged at 300× g, for 10 min thrice to get rid of cells and cell debris. The supernatant was then centrifuged at 200,000× g for 6 hrs at 4°C to collect EVs. The resulting EVs pellet was washed in PBS, centrifuged as before, and the final samples were aliquoted and stored at -80°C (**Figure 4.1**).
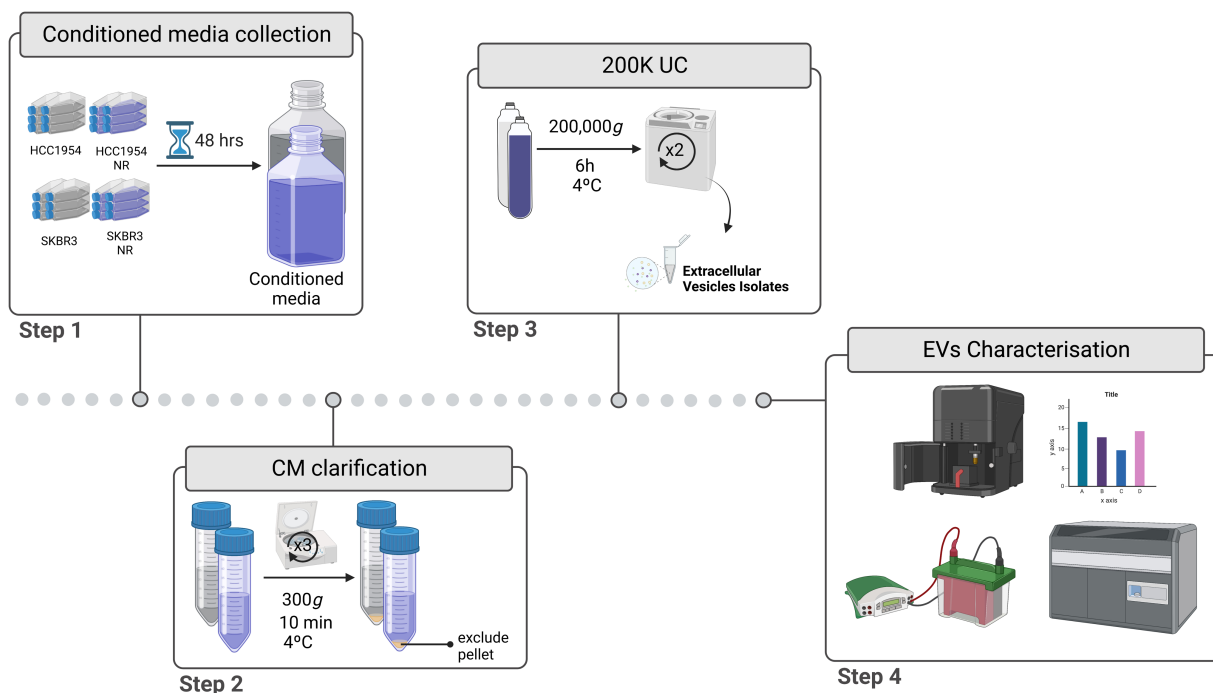
Figure 4.1. Workflow schematic of 200K protocol.
HER2-positive breast cancer cells and their neratinib-resistant counterparts were seeding at 3×10^6 million cells in 7×T175 cm^2 in presence of complete RPMI-1640 medium. After 24 hrs seeding, media was replaced with 25 ml of complete RPMI-1640 media containing EVs-depleted FBS (dFBS) and 1% penicillin/streptomycin (P/S). after 48 hrs incubation, supernatant was collected, and centrifuge as illustrated. The resulting EVs pellet was washed in PBS and the final aliquots were stored at -80ºC until further analysis. Schematic representation was created with *BioRender.com.*

4.3.3 EVs separation by GUC

[This EVs separation protocol was established by PhD student Mariadelva Catalano][279].

The six cell line variants EFM192A, EFM192A NR, HCC1954, HCC1954 NR, SKBR3, and SKBR3 NR were used in this part of the study. HCC1954, HCC1954, SKBR3, and SKBR3 NR were seeded in 6×T175cm^2 flasks (Corning, Cat. #: 431080) at 3×10^6 cells/flask while EFM192A and EFM192A NR cell variants were seeded at 6×10^6 cells/flask. The following day the medium was replaced with 25 ml of RPMI-1640 media supplemented with 10% dFBS and 1% P/S (see **Section 2.3.2**) and cultured for another 48 hrs. CM was then centrifuged at 300× *g* for 20 min to remove cellular debris. Approximately 150 ml of CM were then placed in new 50 ml Falcon tubes and concentrated to 1.5 ml using a tangential flow filtration (TFF)-based device (Hansabiomed; Cat. #: HBM-TFF/1). Next, the concentrated CM was loaded onto an OptiPrep^{TM} (Sigma, Cat. #: D1556) density gradient following the bottom-up approach, to separate EVs based on their density. Concentrated CM was diluted with 60% OptiPrep and with PBS to form the bottom layer of 40% (8 ml in total) and was placed in 17 ml Ultraclear UC tubes (Beckamann Coulter, Cat. #: 344061). Following this, Optiprep was loaded on top at concentrates of 30% (2.5 ml), 20% (2.5 ml), 10% (2.5 ml) and 5% (2 ml), forming subsequent layers. The formed density gradient was ultracentrifuged at 186,000× *g* for 18 hrs 30 min at 4°C in a SW 32.1 Ti swinging rotor (Beckman Coulter, Cat. #: 369651). Fractions of 1 ml were collected from top to bottom. The first two fractions were discarded (because of the lack of EVs presence) while fractions 3-9 were pooled (fractions 10-12 were discarded because of the presence of Calnexin)[279] and washed with PBS. Diluted fractions in PBS were placed in Quickseal 39 ml tubes (Beckman coulter, Cat. #: 342414) and ultracentrifuged using a Type 70Ti fixed-angle rotor (Beckman Coulter, Cat. #: 337922) in an Optima XPN-100 Ultracentrifuge (Beckman Coulter) at 120,000× *g* for 2 hrs. This washing step was repeated a second time and the final pellet was resuspended in 120 µl of sterile PBS or 120 µl lysis buffer for immunoblots. EVs were stored in Protein LoBind tubes (Eppendorf, Cat. #: 0030 108.116) at -80°C, while EVs lysates were stored at -20ºC (see **Figure 4.2** for workflow overview).
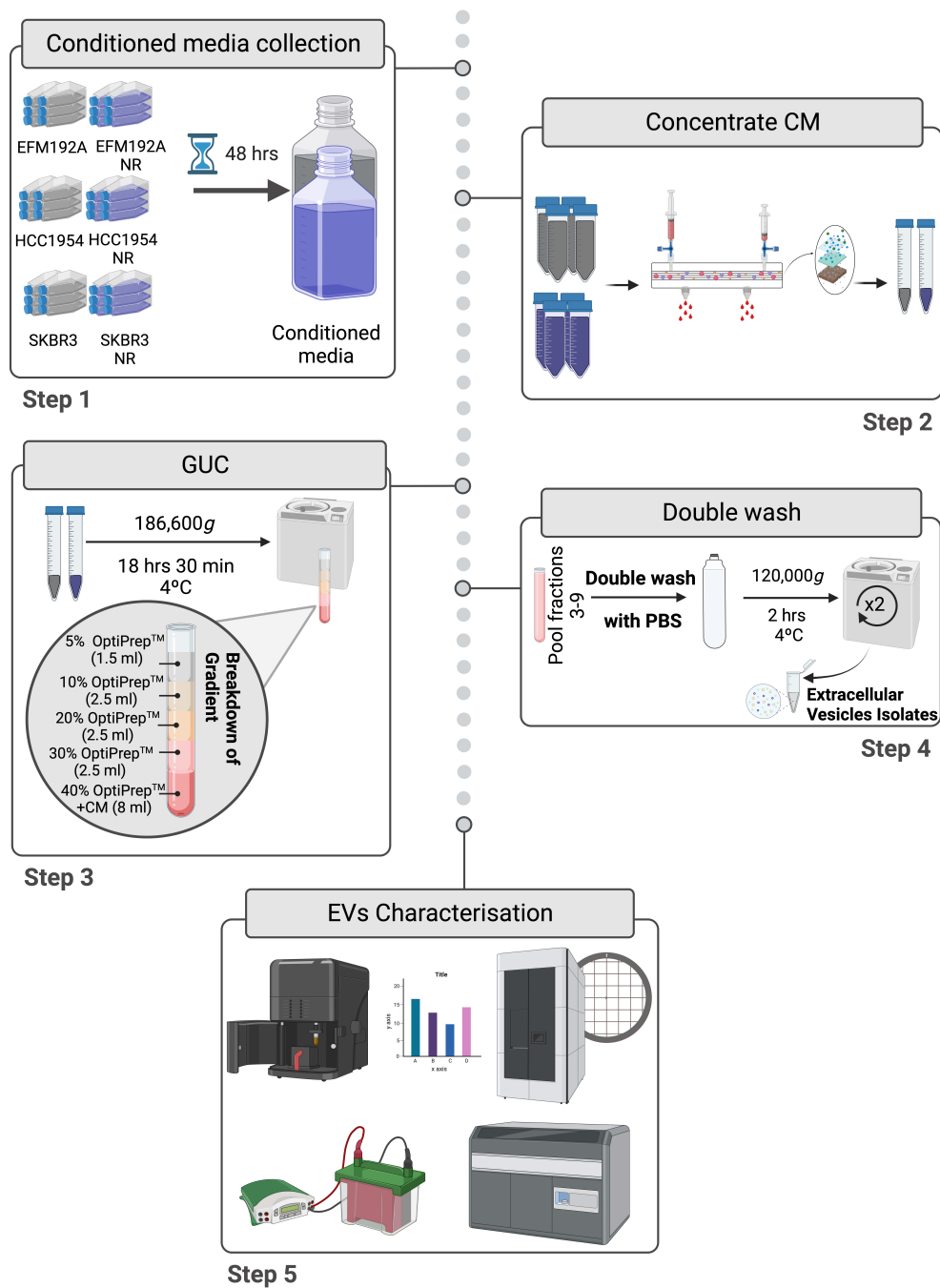
Figure 4.2. A flow diagram representation of density gradient ultracentrifugation approach for EVs separation.

HER2-positive breast cancer cells and their neratinib-resistant counterparts were seeding in 6×T175 cm^2 in presence of complete RPMI-1640 medium. After 24 hrs seeding, media was replaced with 25 ml of complete RPMI-1640 media containing EVs-depleted FBS (dFBS) and 1% penicillin/streptomycin (P/S). after 48 hrs incubation, supernatant was collected and concentrated to 1.5 ml by using a tangential flow filtration (TFF) based device. The concentrate CM was then loaded onto an OptiPrep™ density gradient and centrifuged as illustrated. Double wash step in PBS was performed and the final pellet was resuspended in 120 µl of sterile PBS or 120 µl lysis buffer for immunoblots. EVs were stored in Protein LoBind at -80°C while EVs lysates were stored at -20°C until further analysis. Schematic representation was created with *BioRender.com.*

4.3.4 Collection of protein lysate and EVs lysate for immunoblotting analysis

Cells were seeded at densities detailed in **Section 4.3.2**. The following day, the medium was changed to 10% dFBS-containing RPMI-1640 medium as in **Section 2.3.2**. After 48hrs of incubation, the medium was removed from the flasks and the cells were processed as previously describe in **Section 2.3.6**. The supernatant was transferred to a new tube and stored at -20ºC until required. 200K-EVs aliquots were lysed by using 1:1 ratio of EVs suspension (50 µl) and lysis buffer with protease inhibitor while EVs pellets obtained by GUC protocol were directly resuspended in 120 µl lysis buffer with protease inhibitor cocktail.

4.3.5 Protein quantification

Two methods of protein quantification were used during this study i.e., the standard bicinchoninic acid (BCA) assay (Bio-Rad, Cat. #: 500-0006) and the Micro BCA^{TM} assay kit (Thermo Scientific, Cat. #: 23235). The sensitivity of the Micro BCA^{TM} is greater and was used when the protein concentration was low (intact EVs' protein).

Protein lysates, EVs lysates were quantified as per **Section 3.3.1.1**. Protein of intact 200K isolates was measured using the Micro BCA^{TM} protein assay kit. Briefly, 10 µl of EVs suspensions were diluted with 140 µl of PBS (i.e., 1 in 15 dilution) and added to a 96-well plate (Corning, Cat. #: 3596). 150 µl of BSA standards (40-2 µg/ml) were also added and plate was mixed on a plate shaker for 30 secs. Then, the plate was sealed with its lid and incubated at 37°C for 2 hrs. Absorbance was read at 560 nm using a FLUOstar® OPTIMA microplate reader (Serial #: 08-100-241) and protein amounts were calculated from the BSA standard curve.

4.3.6 Immunoblotting of EVs-associated and other EVs cargo

For all immunoblotting performed in this chapter, total protein (30 µg for cell lysates' immunoblots or 10 µg for EVs' characterisation blots) was resolved as per **Section 2.3.8** on either 7.5% (Bio-Rad Laboratories, Cat. #: 4561023) or 10% Mini-PROTEAN TGX^{TM} 10-well gel (Bio-Rad Laboratories, Cat. #: 4561034) along with a MW marker, SeeBlue Plus 2 Pre-stained standard (Invitrogen, Cat. #: LC5925). All antibody conditions and catalogue numbers used in this chapter are detailed in **Table 4.1**. Cell lysate (CL) from the individual cell line of origin was included in all gels as the control and densitometric analysis was performed using Fiji software[216].

Table 4.1. Antibody dilutions and conditions for immunoblotting.

Primary Antibody	Company, Cat. #	Dilution	Antibody condition	Secondary Antibody
AGR2	Abcam, ab76473	1:1000	3% BSA/PBST	Anti-Rabbit IgG
β-Actin	Sigma-Aldrich, A1978	1:5000	3% BSA/PBST	Anti-Mouse IgG
Calnexin	Abcam, ab133615	1:1000	3% BSA/PBST	Anti-Rabbit IgG
CD9	Abcam, ab236630	1:1000	3% BSA/PBST	Anti-Rabbit IgG
CD63	Abcam, ab68418	1:500	3% BSA/PBST	Anti-Rabbit IgG
GRP94	Cell Signaling, 2104S	1:1000	3% BSA/PBST	Anti-Rabbit IgG
HER2	Calbiochem, OP15	1:1000	3% BSA/PBST	Anti-Mouse IgG
Syntenin	Abcam, ab133267	1:1000	3% BSA/PBST	Anti-Rabbit IgG

All secondary antibodies were diluted 1:1000 in 3% bovine serum albumin (BSA)/ PBS containing 0.1% Tween-20 (PBS-T)

4.3.7 200K-EVs isolates characterisation

4.3.7.1 NTA measurement with ZetaView®

[NTA measurements of EVs was performed in the Trinity Biomedical Science Institute, as a demonstration in our laboratory]

Particle numbers, as well as size distribution, of EVs were measured using the ZetaView® x30 (Particle Metrix). After an initial evaluation, all samples were diluted in PBS accordingly to ideal measurement concentrations (140–200 particles/frame). The manufacturer's default software settings for EVs (and liposomes or nanospheres) were selected. For each measurement, 11 cell positions were scanned and 60 frames per position were captured (video setting: high). After capture, the videos were analysed by the in-build ZetaView Software 8.05.11.

4.3.7.2 Imaging Flow Cytometry analysis of 200K-EVs isolates

[Imaging flow cytometry (IFCM) of EVs was performed by Postdoctoral Researcher Dr. Anindya Mukhopadhya]

Imaging flow cytometry (IFCM) analysis of EVs separated from HCC1954 and SKBR3 neratinib-sensitive and NR variants were performed following the approach previously published by Ricklefs et al. (2019)[280] and adapted by our group[218,281]. Briefly, antibodies diluted in 0.2 μm-filtered PBS containing 2% dFBS and supplemented with protease inhibitor and phosphatase inhibitor (IFCM buffer) were added to EVs samples. The specific antibodies used for this experiment are collected in **Table 4.2**. The EVs samples were incubated with the antibodies for 45 min at RT in the dark and washed using a 300kDa filter (Nanosep, Pall Biotech, Cat. #: 516-8531) and resuspended in 50 μl IFCM buffer. Data acquisition was performed within 2 hrs on the ImageStreamX Mk II imaging flow

cytometer (Amnis/Luminex, Seattle, USA) at 60x magnification and using low flow rate. Fluorescence was within detection linear range in the following channels: Brightfield in channel 1 and 9 (B/YG_435-480 and R/V_560-595 nm filter respectively), FITC was measured in channel 2 (B/YG_480–560 nm), PE in channel 3 (B/YG_560–595 nm filter), PE-Cy7 in channel 6 (B/ YG_745-780 nm filter), BV421 in channel 7 (R/V_435-480 nm filter), APC in channel 11 (R/V_642–745 nm, filter), and SSC in channel 12 (R/V_745-780 nm filter). Single-stained controls, fluorescence minus one (FMO) controls, unstained EVs, as well as only IFCM buffer were run in parallel. To certify that the observed positive events were indeed EVs, CM was incubated with 4% NP-40 (EMD Millipore, Cat. #: 492016) at a final concentration of 2% and samples were analysed using the same strategy. IDEAS software version 6.2 (Amnis/ Luminex, Seattle, USA) was used for data analysis.

Table 4.2. Antibodies specifications and dilutions for IFCM analysis on 200K-EVs isolates.

Anti-human antibody	Label	Company, Cat. #	Dilution
CD63	FITC	Biolegend, 353006	1:150
CD9	PE	Biolegend, 312106	1:1500
CD81	PE-Cy7	Biolegend, 349512	1:150
HER2	APC	Biolegend, 324407	1:150

4.3.8 EVs characterisation of EVs isolated by GUC protocol

4.3.8.1 NTA measurement

[NTA measurements of EVs was performed in the Laboratory for Biological Characterisation of Advanced Materials (LBCAM), Trinity Translational Medicine Institute, as a paid service]

Eighteen samples (*n* = 3 replicates for each of the EVs samples derived by the six cell variants) containing EVs were analysed via NTA using a NanoSight NS500 system (NanoSight, Malvern) equipped with a 405 nm laser. Particle size distribution and concentration can be estimated using NTA system which measures particles from 30 nm to 2 μm. Each sample was diluted manually in 0.2 μm-filtered PBS to obtain an optimum particle concentration suitable for NTA, with each dilution factor being recorded in the automatically generated reports. A total of four x 60 secs videos were recorded for each sample and the detection threshold during analysis was selected to ensure that only distinct nano-objects were analysed and ensuring artefacts were removed. The size and quantities of the particles were determined using the NTA Software (version 3.2).

4.3.8.2 TEM analysis of EVs isolates

[TEM imaging of EVs was performed in the Advanced Microscopy Laboratory in Trinity Biomedical Sciences Institute by Mr. Neal Leddy as a paid service]

Samples were prepared from TEM analysis as described in **Section 2.3.9**.

4.3.8.3 IFCM on GUC-derived EVs using CellMask protocol

The IFCM analysis EVs samples obtained from cells after 48 hrs incubation was performed following a protocol published previously with modifications[282]. Briefly, 10 μl of EVs samples were stained with 10 μl CellMask® Green plasma membrane stain (Thermo Fisher Scientific, Cat. #: C37608, 2X) for 30 min at 37ºC and 0.2 μm-filtered PBS was used as control. The stained samples were then incubated with a human APC-conjugated anti-HER2 antibody (BioLegend, Cat. #:324407; 1:10). After 1 hr incubation at RT, the samples were diluted up to 280 μl of 0.2 μm-filtered PBS and washed using a 300kDa filter (Nanosep, Pall Biotech, Ireland; Cat. #: 516-8531). After the first centrifugation step at 1,000× *g* for 1 min at 4ºC, 50 μl of 0.2 μm-filtered PBS was added to each filter, and they were centrifuge at the same condition repeatedly until reach a final volume of 100 μl was obtained. The samples were immediately analysed using an Amnis Image StreamX MKII flow cytometer (Luminex) at 60x magnification using the same settings as explained in **Section 4.3.7.2.** EVs were gated as SSC vs fluorescence and the gated EVs were confirmed in the IDEAS image Gallery (**Figure 4.3**).
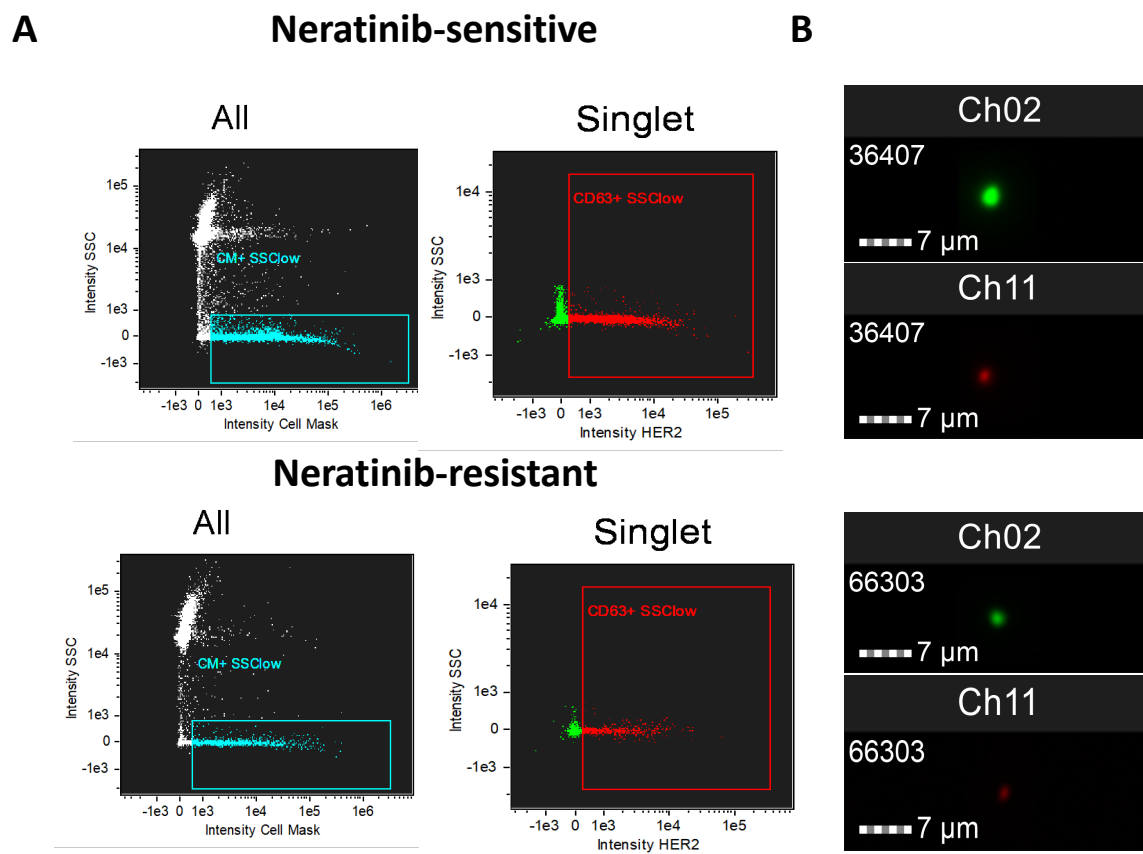
Figure 4.3. IFCM gating approach.

(**A**) Gating strategies used to establish EVs population from neratinib sensitive-derived isolates and neratinib resistant-derived isolates; (**B**) Representative images of EVs from IDEAS Image Gallery for CellMask+ events (Ch02) and HER2+ events (Ch11).

4.3.8.4   HER2-ELISA Assay

HER2 present in cell lysates, EVs lysates, and on intact EVs was quantified using the DuoSet ELISA kits (R&D Systems; Cat. #: DY1129B), following manufacturer's instruction and as explained per **Section 3.3.3**. Ten µg cell lysate for HCC1954, HCC1954 NR, EFM192A and EFM192A NR were used while 5 µg cell lysate for SKBR3 and SKBR3 cells. For EVs' analysis, 10 µl of intact EVs and 5 µg EVs lysates were used.

4.3.8.5   Data analysis and statistical testing

All statistical analyses were performed using GraphPad Prism version 9.1.9 for macOS (GraphPad Software). Regarding cell and EVs characterisation, values for arbitrary units (A.U.), EVs' number and EVs size are given as mean ± SEM (n = 3). Two-tailed unpaired t-test was applied (*p < 0.05 was considered as statistically significant).

For ELISA assay analysis, HER2 quantification was performed by interpolating the absorbance values to the standard curve run alongside the sample. Concentrations were represented as mean ± SEM (n = 3). Multiple unpaired t-test was applied: *p < 0.05.

4.4 Results

4.4.1 Neratinib-resistant cell variants evidently released fewer EVs than neratinib-sensitive counterparts when evaluating EVs collected using 200K protocol

4.4.1.1 Characterisation of 200K-EVs isolates from neratinib-sensitive and neratinib-resistant cells

4.4.1.2 Characterisation of 200K-EVs isolates by NTA

We were interested in investigating if resistance to neratinib could directly or indirectly affect the release of EVs by neratinib-resistant cell lines. For this, we used the 200K protocol to obtain the EVs. EVs size distribution and quantities were estimated using a ZetaView. The average size and particle numbers of the samples collected from CM by each cell variant are shown in **Table 4.3**.

Table 4.3. Comparative EVs size and quantities as evaluate by NTA using ZetaView.

	Size (nm)		
	Neratinib-sensitive	Neratinib-resistant	*p* value
HCC1954	157.2 ± 6.3	139.3 ± 5.3	0.097 (ns)
SKBR3	142.5 ± 2.3	142.9 ± 3.2	0.924 (ns)
Particle numbers (normalised by 10^6 cells)			
	Neratinib-sensitive	Neratinib-resistant	Fold change	*p* value
HCC1954	$1.51 \times 10^9 \pm 5.86 \times 10^8$	$3.51 \times 10^8 \pm 1.36 \times 10^8$	↓4.3	0.127 (ns)
SKBR3	$1.44 \times 10^9 \pm 3.75 \times 10^8$	$2.36 \times 10^8 \pm 4.59 \times 10^7$	↓6.1	0.033 (*)

Comparison of concentration of particles/10^6 cells (analysed by NTA) and average sizes from samples obtained from neratinib-sensitive cell variants and their neratinib-resistant counterparts by 200K protocol. Fold change is calculated as neratinib-resistant/neratinib-sensitive ratio.

NTA showed neratinib-resistant cell line variants released fewer EVs, when normalised per number of secreting cells, compared to their neratinib-sensitive counterparts (**Figure 4.4**). This difference was significant between EVs samples from SKBR3 and SKBR3 NR, but not for EVs from HCC1954 and HCC1954 NR. Non-significant differences were found in particle size (**Figure 4.4**).
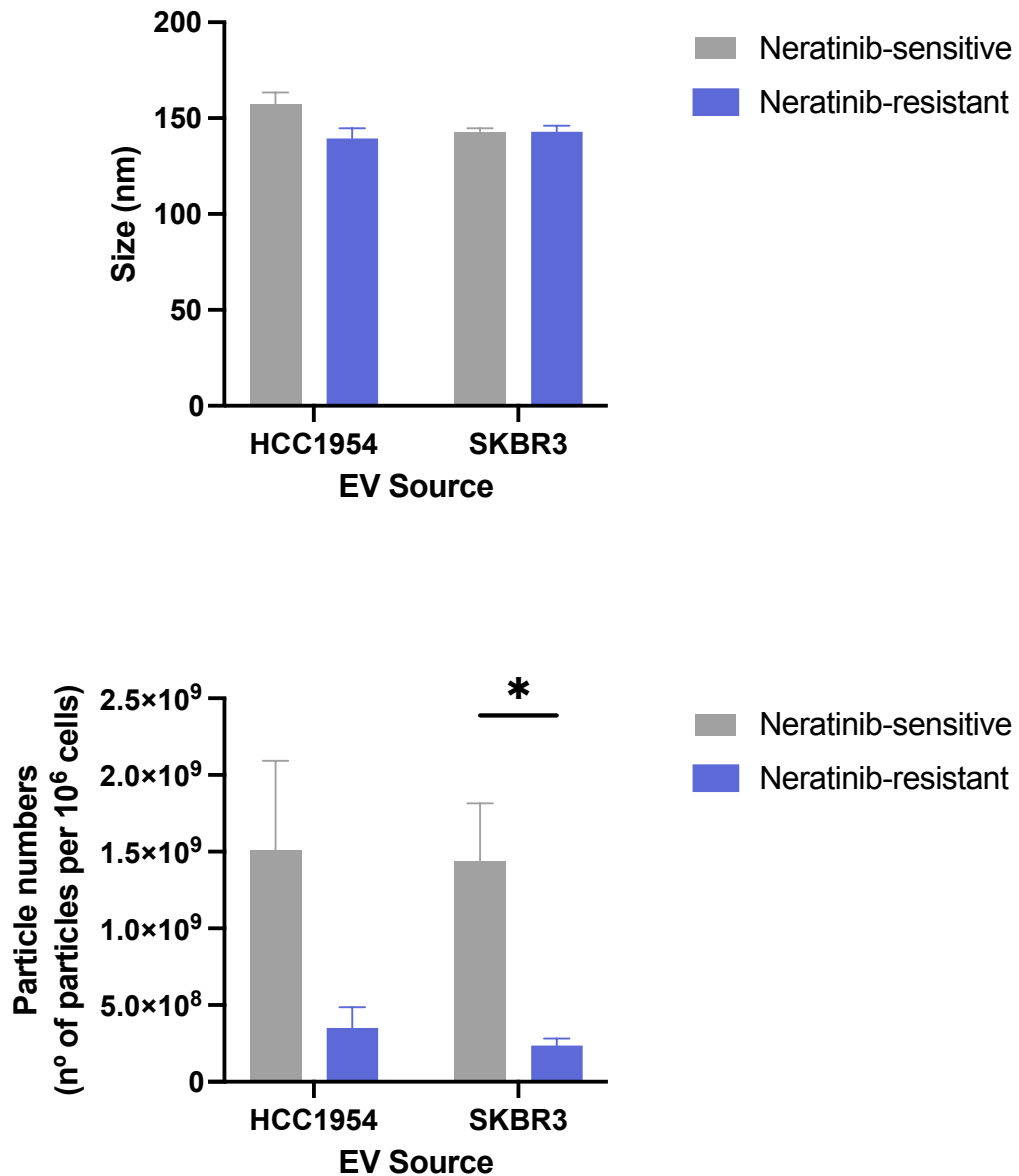
Figure 4.4. Particle quantities and sizes as evaluate by NTA.

EVs collected by 200K UC approach were analysed by Zetaview. (**Top**) Particle size measured by NTA. Representative of n = 3 experiments ± SEM. Unpaired t-test was used to calculate significance; (**Bottom**) NTA revealed a significantly decreased in EVs released from SKBR3 NR compared with their neratinib-sensitive counterparts. Representative of n = 3 experiments ± SEM. Unpaired t-test was used to calculate significance: *p<0.05.

4.4.1.3   Characterisation of 200K-EVs isolates by protein content

The relative amount of EVs protein (expressed as µg of protein/10^6 cells) in non-lysed EVs samples was determined by Micro BCA^{TM} Protein Assay Kit (**Figure 4.5**). No significant differences in terms of protein amount were found between neratinib-sensitive and neratinib-resistant cell lines' EVs isolates.
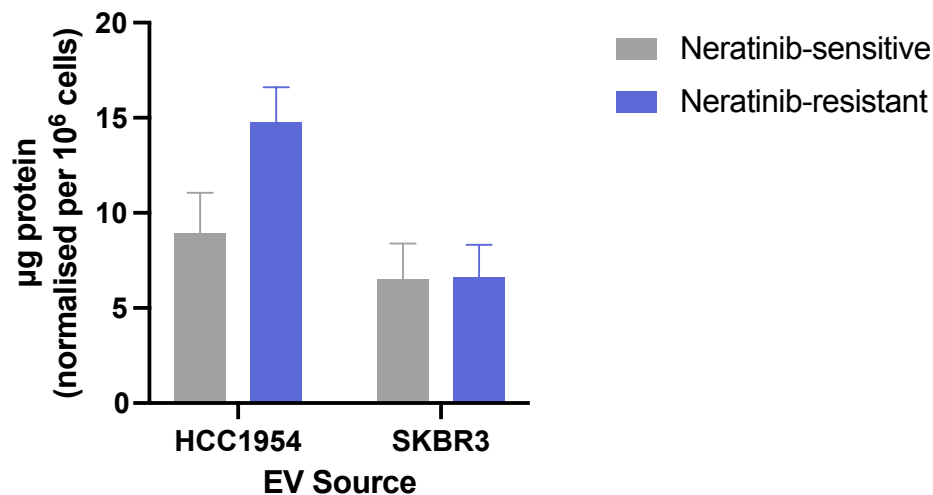
Figure 4.5. Protein quantification of EVs isolates.

Mean values of protein concentrations (μg of protein normalised by 10^6 cells) of n = 3 isolates ± SEM are illustrated. Unpaired t-test was used to calculate significance.

4.4.1.4 Characterisation of 200K-derived EVs by IFCM

IFCM was used to determine the presence of EVs markers based on the presence of widely accepted proteins by the EVs research community (CD9, CD63, and CD81) as indicative of EVs. When we analysed these EVs by IFCM we also observed fewer positive events for EVs positive markers for the EVs harvested from conditioned media on neratinib-resistant variants when we compare with their sensitive counterparts (**Figure 4.6**). Both neratinib-resistant variants released fewer positive events for CD9 and C63 than their counterparts, while for CD81-positive events this difference was only significant between SKBR3 cell line variants. Table 4.4 registers the positive events for each marker and the fold-change between the variants.
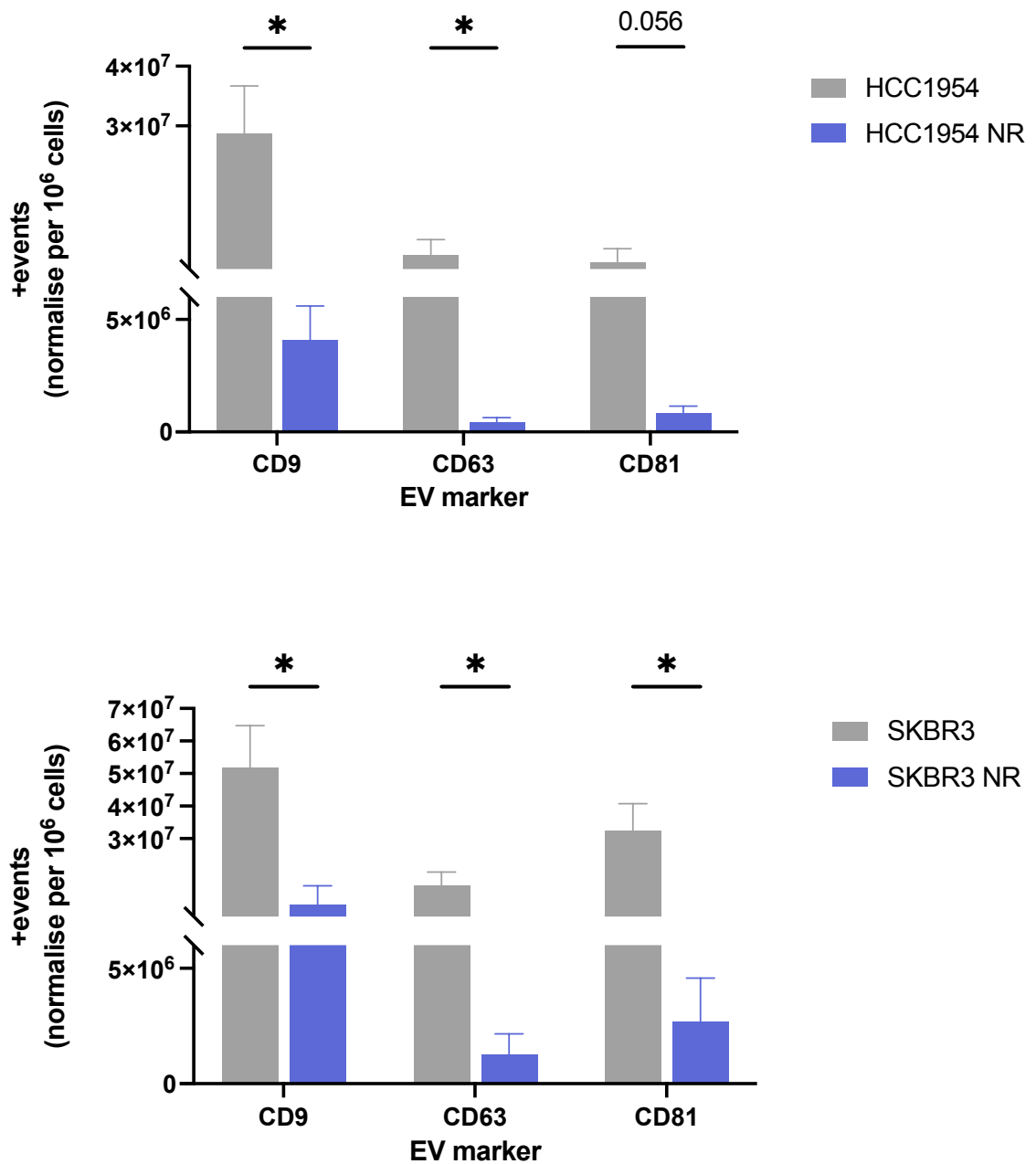
Figure 4.6. Imaging Flow Cytometry analysis of the surface of the EVs.

Amnis ImageStreamX was used to measure EVs positive markers on (**Top**) HCC1954 variants-derived isolates and (**Bottom**) SKBR3 variants-derived isolates. Neratinib-resistant (NR) cell variants released fewer CD9+, CD81+ and CD63+ particles compare to their neratinib-sensitive counterparts. Graphs are representative of n = 3 experiments ± SEM. Unpaired t test was used to calculate significance: *$p<0.05$.

Table 4.4. Positive events when analysing for EVs' markers by IFCM.

+Events/10^6 cells				
HCC1954				
Marker	Neratinib-sensitive	Neratinib-resistant	Fold change	*p* value
CD9	$2.88\times10^7 \pm 7.93\times10^6$	$4.08\times10^6 \pm 1.52\times10^6$	↓7.04	0.038 (*)
CD81	$7.10\times10^6 \pm 2.34\times10^6$	$8.22\times10^5 \pm 3.25\times10^5$	↓8.63	0.056 (ns)
CD63	$8.42\times10^6 \pm 2.54\times10^6$	$1.55\times10^7 \pm 4.14\times10^6$	↓19.28	0.035 (*)
SKBR3				
Marker	Neratinib-sensitive	Neratinib-resistant	Fold change	*p* value
CD9	$5.18\times10^7 \pm 1.29\times10^7$	$9.65\times10^6 \pm 5.84\times10^6$	↓5.37	0.041 (*)
CD81	$3.24\times10^7 \pm 8.36\times10^6$	$2.66\times10^6 \pm 1.92\times10^6$	↓12.2	0.026 (*)
CD63	$1.55\times10^7 \pm 4.15\times10^6$	$1.27\times10^6 \pm 8.96\times10^5$	↓12.25	0.028 (*)

Fold change is calculated as neratinib-resistant/neratinib-sensitive ratio.

4.4.1.5   Characterisation of 200K- EVs isolates by immunoblotting

Immunoblotting was also used to determine the presence of EVs markers based on the presence of proteins accepted by the EVs research community as indicative of EVs. CD63, syntenin and CD9 are widely accepted EVs markers, while the analysis of functional proteins, such as calnexin or GRP94, is required when claiming specific analysis of sEVs[105].EVs separated using 200,000× *g* ultracentrifugation positively carries EVs markers, syntenin, and/or tetraspanin CD63 and CD9, while GRP94 or calnexin were not detected in the samples (**Figure 4.7**). Interestingly, HCC1954 NR-derived EVs give rise to a weaker signal for CD63 (*p* = 0.052) and syntenin (*p* = 0.017*)* compared to the EVs recovered from neratinib-sensitive cell variant. In keeping with the results obtained for the EVs derived from HCC1954 cell variants, SKBR3 NR-derived EVs presented a decrease in tetraspanins presence (CD63 and CD9) compared with SKBR3-derived EVs while there was a complete lack of syntenin in the NR-derived EVs obtained by this protocol.
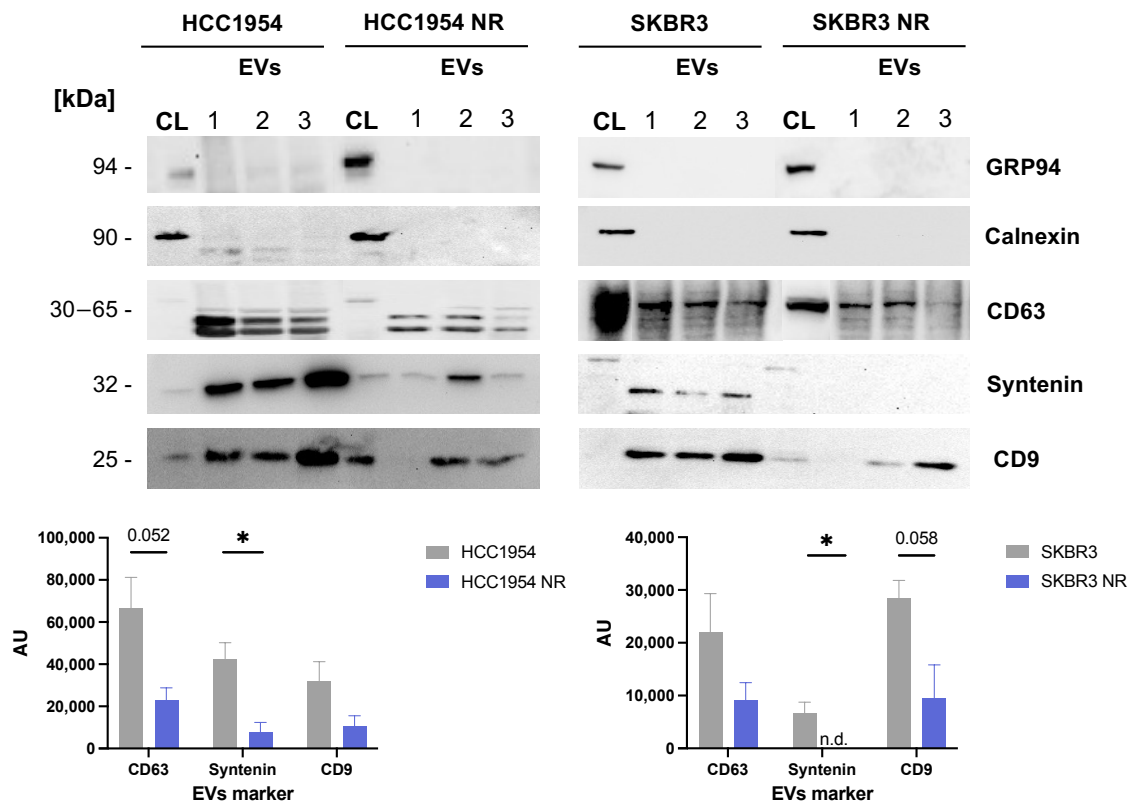
Figure 4.7. Immunoblots of EVs markers present on the EVs collected by 200K UC.
Cell conditioned media from HER2+ cell lines were subjected to 200,000× *g* UC protocol. (**Top**) Ten µg of EVs were loaded, together with ten µg of the corresponding cell lysate (CL) used as control. Samples were then analysed by immunoblotting for the presence of the following proteins: Calnexin and GRP94, proteins considered cell specific and are expected to be absent from sEVs; CD63 a tetraspanin used as general EVs marker; Syntenin-1, associated with sEVs population; and CD9 a tetraspanin associated with mEVs and lEVs. Each blot represents three independent experiments and the densitometric analysis of these three are presented in (**Bottom**) as the mean *n* = 3 ± SEM (*p<0.05).

4.4.1.6   HER2 status on the cells and their harvested 200K-EVs isolates

Once the EVs were fundamentally characterised, the next step was to investigate if EVs released from neratinib-sensitive and neratinib-resistant cells reflect the HER2 status of their cells of origin and, thus, have potential as minimally-invasive biomarkers. Immunoblot analysis of HER2 protein in three replicates of HCC1954, SKBR3, EFM192A, HCC1954 NR, SKBR3 NR and EFM192A NR cell lysates was performed.

Our group had previously published the HER2 status on the HCC1954 and EFM192A compared to their respective neratinib-resistant counterparts[232]. However, the comparison between SKBR3 and SKBR3 NR had not previously been analysed. In agreement with our previous publication for the HCC1954 and EFM192A cell variants, and established here for the SKBR3 variants, immunoblot analysis showed that NR cell line variants have significantly reduced HER2 protein expression compared to their respective neratinib-sensitive counterparts (**Figure 4.8A**). The presence of HER2 was also studied on the EVs harvested from SKBR3, SKBR3 NR, HCC1954 and HCC1954 NR by

immunoblotting (**Figure 4.8B**) as well as IFCM analysis (**Figure 4.9**). As EVs derived from EFM192A and EFM192A NR cell variants were not collected using 200K UC protocol, the presence of HER2 in those EVs were not analysed.

Results from both assays confirmed that EVs from neratinib-sensitive cells (SKBR3 and HCC1954) carried HER2, while those from NR cells (SKBR3 NR and HCC1954 NR) lacked HER2, reflecting the HER2 status of their cells of origin. When analysed by IFCM, we obtained a significant decrease of HER2+ events in the EVs isolates obtained from SKBR3 NR cells compared to their neratinib-sensitive counterparts (1.49-fold, p = 0.033) but it was not significant in the case of HCC1954 cell variants (1.2-fold, p = 0.065). We also analysed, by IFCM, the double positive events for the different EVs markers and HER2. In line with the results obtained, it was observed a reduction on the double positive events in NR-derived EVs when compared with their parental counterparts (**Appendix II; Figure III-1**).
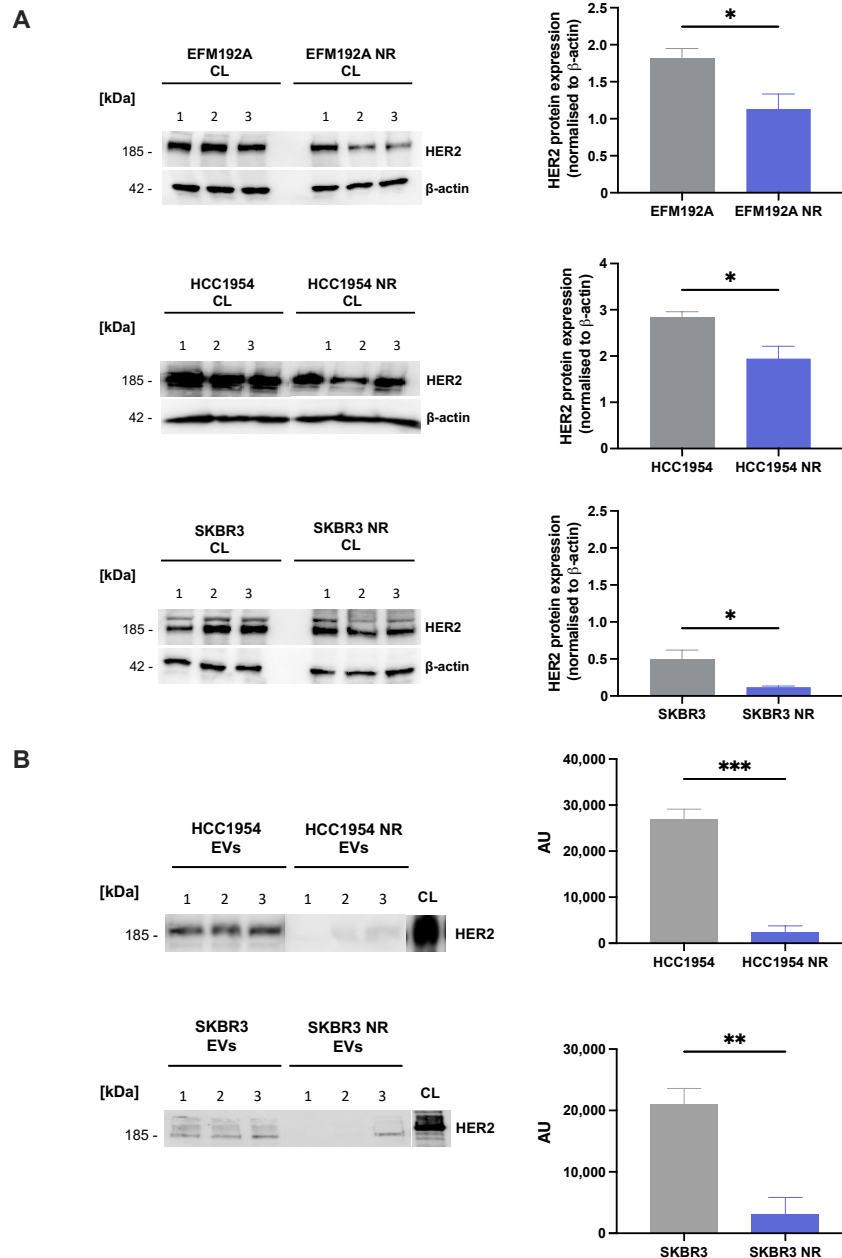
Figure 4.8. Evaluating the HER2 protein expression in neratinib-resistant and neratinib-sensitive cancer cells and its presence on their EVs, by immunoblotting.

(**A**) Immunoblots showing expression of HER2 in neratinib-sensitive and neratinib-resistant (Neratinib Resistant; NR) cancer cell lines. Thirty µg of HCC1954, HCC1954 NR, SKBR3, SKBR3 NR, EFM192A and EFM192A NR cell lysates (CL) were loaded for their analysis. The relative intensity (AU) of the protein signal band was calculated using ImageJ software. β-actin was used as loading control and normalisation. *$p<0.05$, $n = 3$ culture protein lysates (each replicate is numbered); (**B**) Representative immunoblots showing the presence of HER2 on EVs released by neratinib-sensitive and neratinib-resistant – derived EVs and CL. Ten µg of protein obtained from HCC1954, HCC1954 NR, SKBR3, and SKBR3 NR derived EVs were loaded for their analysis, together with CL used as control. Each line (1, 2, 3) represents three independent experiments and the densiometric analysis of these three are presented as the mean of $n = 3 \pm$ SEM (*$p<0.05$, **$p<0.01$, ***$p<0.001$).
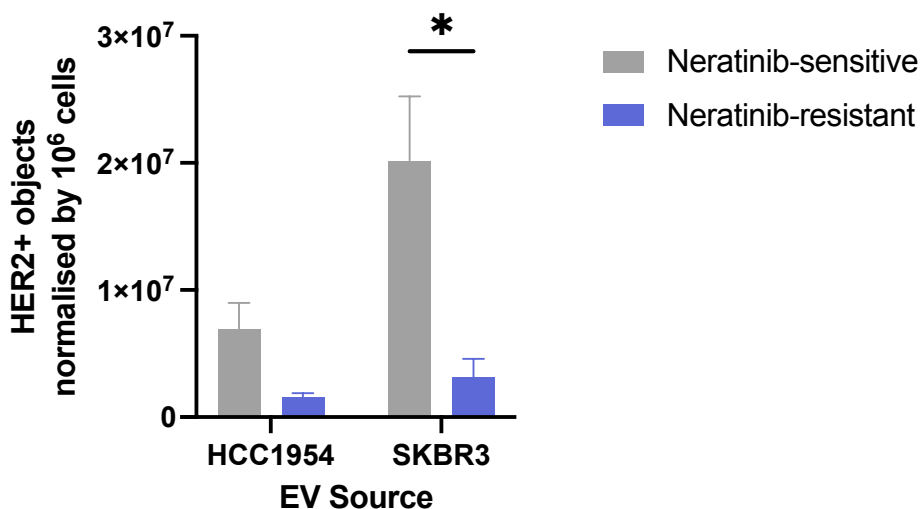
Figure 4.9. HER2 analysis on EVs surface, by IFCM.
Amnis Image Stream was used to measure HER2 on the surface of EVs. SKBR3 NR and HCC1954 NR released less HER2+ particles than their neratinib-sensitive counterparts. Graphs are representative of n = 3 experiments ± SEM. Unpaired t-test was used to calculate significance: *$p<0.05$.

4.4.2 Characterisation of GUC-EVs isolates from neratinib-sensitive and neratinib-resistant cells

Hence, before adding the other set of cell lines (EFM192A and EFM192A NR) to investigate the EVs cargo, we decided to take a step back and change to an EVs' collection protocol more accepted by the EVs community. GUC using Optiprep™ has become one of the most common protocols to achieve better EVs purity with less damage of EVs' surfaces, as it is cushioned. Then, we characterise EVs from neratinib-sensitive and neratinib-resistant cell lines using this protocol to confirm if the reduction in EVs' release is also evident with "purer" EVs isolates.

4.4.2.1 Characterisation of GUC-derived EVs by NTA (NanoSight)

The size and concentration of particles obtained by GUC protocol from the three neratinib sensitive/resistant pairs of HER2+ breast cancer cell lines are presented in **Table 4.5**. There were no statistically detected differences in terms of EVs size or EVs numbers between the EVs collected from neratinib-sensitive and neratinib-resistant cell variants in our study. The neratinib-sensitive cell lines EFM192A, HCC1954, and SKBR3 release EVs with an insignificantly lower mean dimension compared to their neratinib-resistant counterparts (**Figure 4.10**). No significant differences in particle quantities normalised per 10^6 cells were found between conditions, although particles released by neratinib cell lines seemed to be slightly decreased. However, the irreproducibility of results between replicates must be considered.

Table 4.5. EVs sizes and quantities as evaluate by NTA.

	Size (nm)		
	Neratinib-sensitive	Neratinib-resistant	*p* value
EFM192A	97.4 ± 6.8	101.1 ± 2.5	0.641 (ns)
HCC1954	99.3 ± 3.7	107.7 ± 7.1	0.355 (ns)
SKBR3	87.6 ± 7.1	99.9 ± 7.1	0.289 (ns)
	Particle numbers (normalised by 10^6 cells)		
	Parental	NR-resistant	Fold change	*p* value
EFM192A	$1.59 \times 10^9 \pm 7.87 \times 10^8$	$2.04 \times 10^9 \pm 7.36 \times 10^8$	↑1.28	0.697 (ns)
HCC1954	$7.45 \times 10^9 \pm 5.83 \times 10^9$	$6.75 \times 10^9 \pm 4.02 \times 10^9$	↓1.10	0.927 (ns)
SKBR3	$8.16 \times 10^{10} \pm 1.4 \times 10^{10}$	$6.06 \times 10^{10} \pm 2.35 \times 10^{10}$	↓1.35	0.486 (ns)
	Particle numbers 30-150 nm (normalised by 10^6 cells)		
	Parental	NR-resistant	Fold change	*p* value
EFM192A	$6.38 \times 10^9 \pm 5.11 \times 10^9$	$4.86 \times 10^9 \pm 2.78 \times 10^9$	↓1.75	0.806 (ns)
HCC1954	$5.47 \times 10^9 \pm 4.32 \times 10^9$	$4.52 \times 10^9 \pm 2.84 \times 10^9$	↓1.21	0.863 (ns)
SKBR3	$6.84 \times 10^9 \pm 5.33 \times 10^9$	$5.19 \times 10^9 \pm 3.16 \times 10^9$	↓1.32	0.803 (ns)

Comparison of number of particles/10^6 cells (analysed by NanoSight) from samples collected from neratinib-sensitive cell variants and their neratinib-resistant counterparts by GUC protocol. Fold change is calculated as neratinib-resistant/neratinib-sensitive ratio.
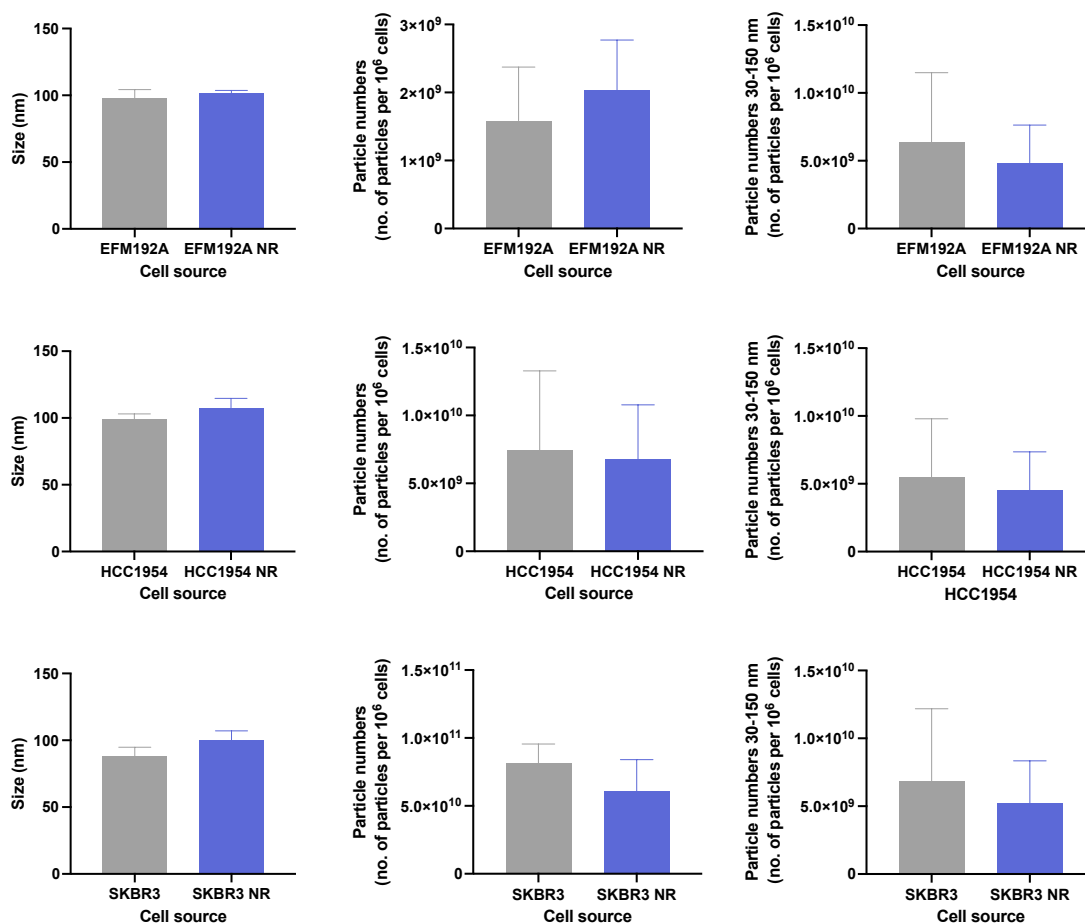
Figure 4.10. Mean EVs size and particles number as evaluate by NTA.
EVs separated by GUC approach were analysed by NanoSight; (**Left**) Size measured by NTA. (**Centre**) Total particle numbers normalise per 10^6 of secreting cells and (**Right**) particle numbers with a size between 30-150 nm normalised per 10^6 of secreting cells. Representative of *n* = 3 experiments ± SEM. Unpaired t-test was used to calculate significance. NR= neratinib-resistant.

4.4.2.2 Characterisation of GUC-derived EVs by protein content

The relative amount of protein (expressed as µg of protein/ 10^6 cells) present in lysed EVs samples was determined by bicinchoninic *acid* assay (**Figure 4.11**). No significant differences in terms of protein quantity were found between neratinib-sensitive and neratinib-resistant cell lines' EVs isolates.
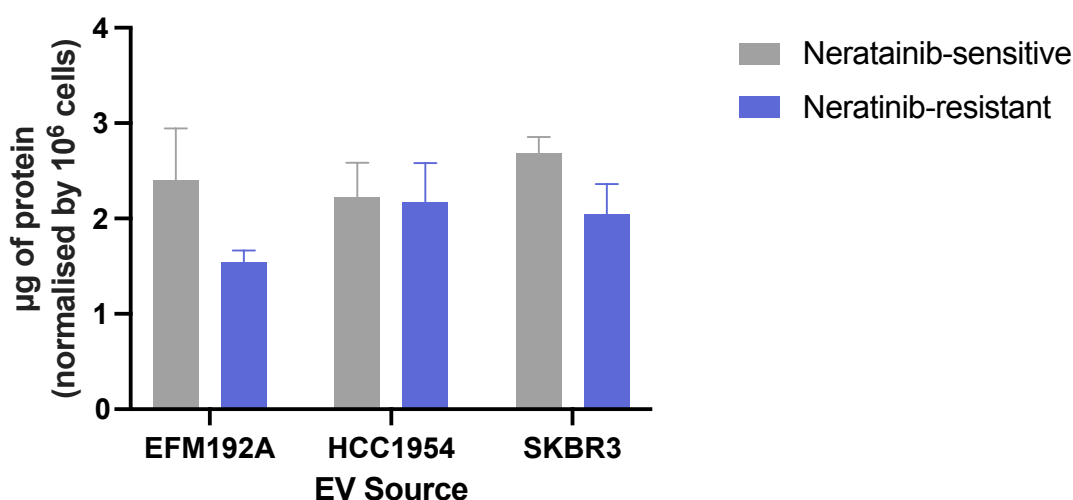
Figure 4.11. Protein quantification of EVs obtained by GUC approach.
Mean values of protein concentrations (μg of protein normalised by 10^6 cells) of n = 3 isolates ± SEM are illustrated. Unpaired t-test was used to calculate significance.

4.4.2.3 Characterisation of GUG-derived EVs by IFCM

Given that NTA is unreliable for evaluating EVs per se, to ensure that the resistance to neratinib was affecting EVs' release, the current efforts in the field are focusing to improve flow cytometry protocols for EVs characterisation. Particularly, we use a protocol staining the cell plasma membrane (staining "EVs" but also lipoproteins) and staining with HER2 antibody to assess the presence of HER2 on the EVs' surface, to try a better estimation on EVs' release. Results are presented in **Figure 4.12**.

IFCM assay using CellMask/HER2 staining revealed a significant decrease in the case of EFM192A NR-derived EVs samples (3-fold lower in CellMask+ events, p = 0.007; 3.5-fold lower in CellMask+/HER2+ events, p = 0.023) compared to the EVs derived from their neratinib-sensitive counterparts. When we examine the proportion of CellMask+/HER2+ events among all CellMask+ events, only a low percentage of those CellMask+ events were also positive for HER2, being EFM192A and EFM192A NR-derived EVs the ones with higher presence of double-positive events (50.8 vs 46.46%, respectively) compared with HCC1954 (32.15% vs 23.42%, p = 0.017) and SKBR3 variants (19.39% vs 28.69%).

As we were expecting more HER2+ events on EVs' surface, we decide to perform an HER2 ELISA assay with intact EVs and lysate EVs to determine if the presence of HER2 on those EVs was higher in the membrane or it has more important presence as EVs' cargo.
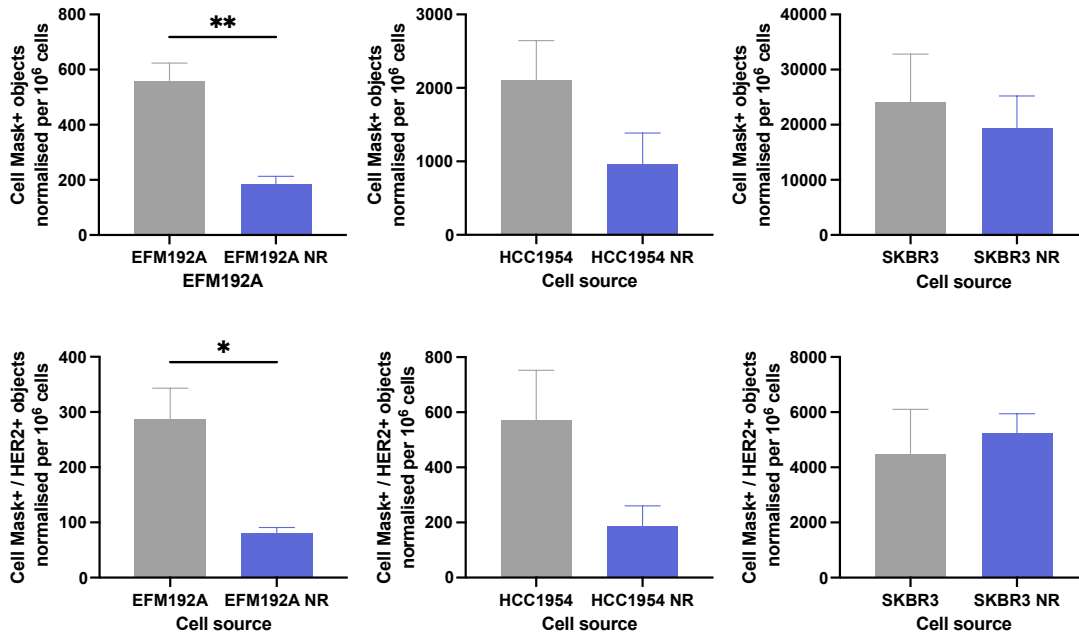
Figure 4.12. IFCM characterisation of EVs released by HER2+ cell lines.
Data were collected by measuring the CellMask cell plasma membrane stain signal (**Top**) and CellMask/HER2 signal (**Bottom**) on the EVs isolates obtained from (**Left**) EFM192A and EFM192A NR, (**Middle**) HCC1954 and HCC1954 NR, and (**Right**) SKBR3 and SKBR3 NR. Unpaired t-test was used as a statistical test. *p<0.05, **p<0.01 (n = 3 replicates).

4.4.2.4   Characterisation of GUG-derived EVs by immunoblotting

To evaluate EVs markers present on the different EVs isolates, immunoblotting was performed, and results presented in ¡Error! No se encuentra el origen de la referencia.. EVs were positive for all the markers used while calnexin (found in some types of EVs, but not enriched in the smaller EVs) was not detected. Only one EVs exclusion marker was used in this section. For this reason, GRP94 was not evaluated here.

Immunoblots performed on EVs lysates showed a decrease of CD63 and syntenin markers in EFM192A NR and SKBR3 NR isolates compared with their neratinib-sensitive derived-EVs counterparts, respectively. No substantial differences were found in the presence of CD9 on the isolates obtained from SKBR3 and EFM192A cell lines variants. The signal of syntenin band was decreased in HCC1954 NR-derived EVs compared to those released by HCC1954. No changes in the presence of CD63 or CD9 were detected between these two populations.
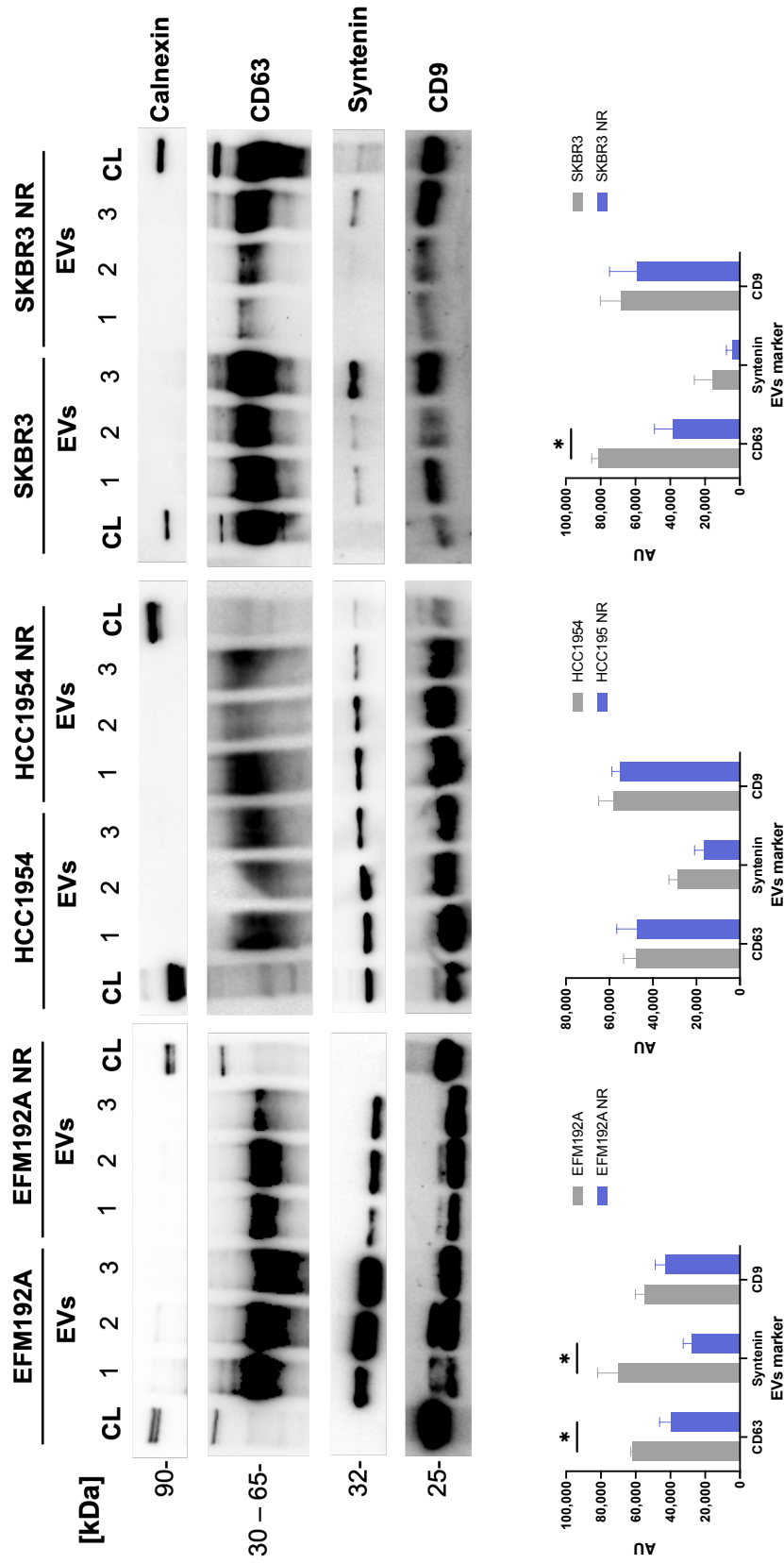
Figure 4.13. Evaluation of EVs markers by immunoblotting.

Four protein markers were evaluated: Calnexin, an endoplasmic reticulum-associated protein which is cell specific and is expected to be absent from small EVs; CD63 a tetraspanin used as general EVs marker; Syntenin-1, associated with sEVs population; and CD9 a tetraspanin associated with mEVs and lEVs. (**Top**)Ten µg of EFM192A, EFM192A NR, HCC1954, HCC1954 NR, SKBR3, and SKBR3 NR derived EVs or cell lysate (CL) as control were loaded for their analysis. Each blot represents three independent experiments and the densitometric analysis of these three are presented in (**Bottom**) as the mean $n = 3 \pm$ SEM (*$p < 0.05$).

4.4.2.5   Characterisation of GUC-derived EVs by TEM

Representative TEM pictures of EFM192A, EFM192A NR, HCC1954, HCC1954 NR, SKBR3 and SKBR3 NR -derived EVs are shown in **Figure 4.14**. Inspection of EVs revealed their integrity in most cases.

In line with the results obtained by NTA, we observed a representative size lower than 100 nm, with the presence also of both small (~50 nm) and medium EVs (≥100 nm) in all the EVs isolates. However, we can observe, in general, a reduction of particles in NR-derived isolates together with an increased presence of bigger particles.
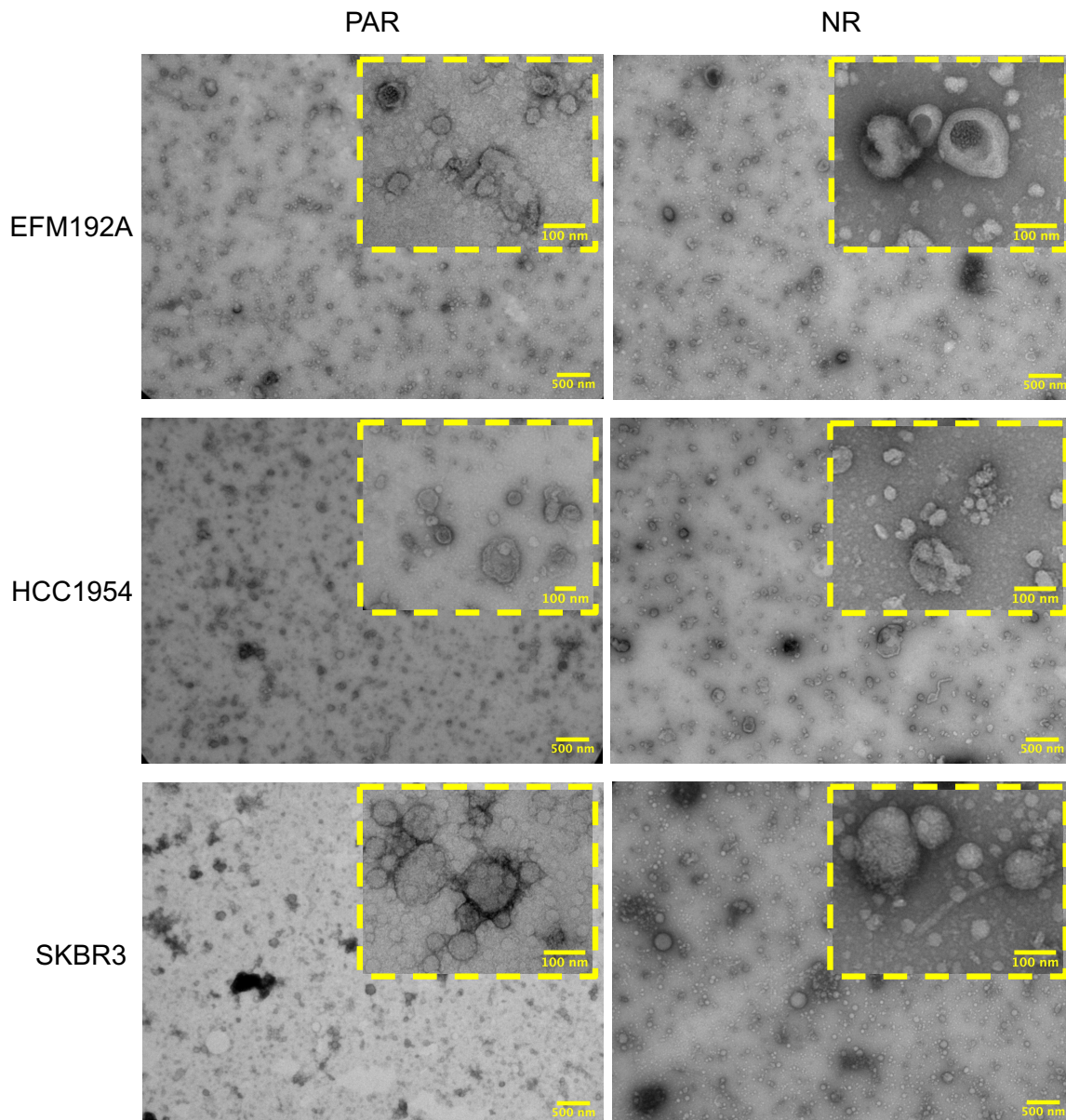
Figure 4.14. Representative TEM images of EVs isolates obtained by GUC method.

Representative transmission electron microscope (TEM) images of neratinib sensitive-derived and neratinib resistant-derived EVs. Big pictures represent a zoomed-out view (5000x; Scale bar = 500 nm), while the edged pictures depict a zoomed-in view (30000x; Scale bar = 100 nm) of the same spot.

4.4.2.6 Analysing HER2 cargo on the EVs released by neratinib-sensitive and neratinib-resistant cell lines

For the analysis of HER2 presence on the EVs surface and as EVs cargo, the protein content on lysate EVs and intact EVs was evaluated by ELISA assay (**Figure 4.15**).

While statistical significance was only achieved in non-lysate EFM192A-derived EVs samples, the data indicated a decrease in the HER2 content on NR-derived EVs' lysates compared with their neratinib-sensitive counterparts. Interestingly, although this reduction was also observed on the intact EVs samples derived from neratinib-resistant cell lines, it was less remarkable. These results suggest that NR-derived EVs carried less HER2, reflecting the reduction of HER2 expression observed in the neratinib-resistant cell lines.

Although we cannot directly compare the results obtained from lysate EVs (based on μg of protein) and intact EVs (based on volume), it seems the content of HER2 was higher on the lysate EVs than in the surface of those EVs. These results can indicate that those EVs probably originated in the endocytic pathway and the HER2 content could be part of the HER2 trafficking as suggested by others[276,278].
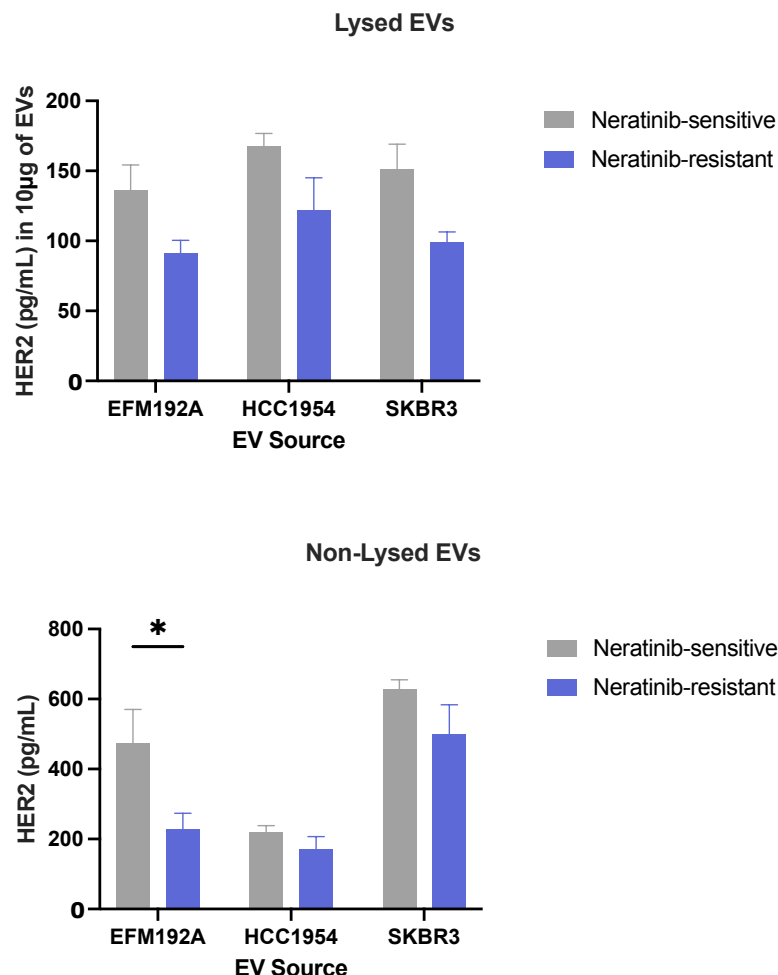
Figure 4.15. HER2 presence on the EVs isolates evaluated by ELISA assay.
EVs were isolated after 48 hrs incubation. After incubation time, EVs were separated from conditioned media, were lysed (**Top**) or not (**Bottom**) to evaluated HER2 levels. Graphs represent *n* = 3 biological repeats as mean ± SEM. Two-way *ANOVA* was used to calculate significance: *$p < 0.05$.

4.4.2.7 Analysing AGR2 cargo on the EVs released by neratinib-sensitive and neratinib-resistant cell lines.

We also investigated the presence of AGR2 on the EVs released by HER2+ breast cancer cell lines. Previously work performed and discussed in preceding Chapter 3, found that AGR2 was down-regulated in HC1954 NR and SKBR3 NR cell variants compared with their neratinib-sensitive counterparts. As a preliminary study, we analysed by immunoblotting the presence of AGR2 on those EVs lysates (**Figure 4.16**). Although we noticed the presence of AGR2 on the parental and NR-derived EVs, no significance differences existed.
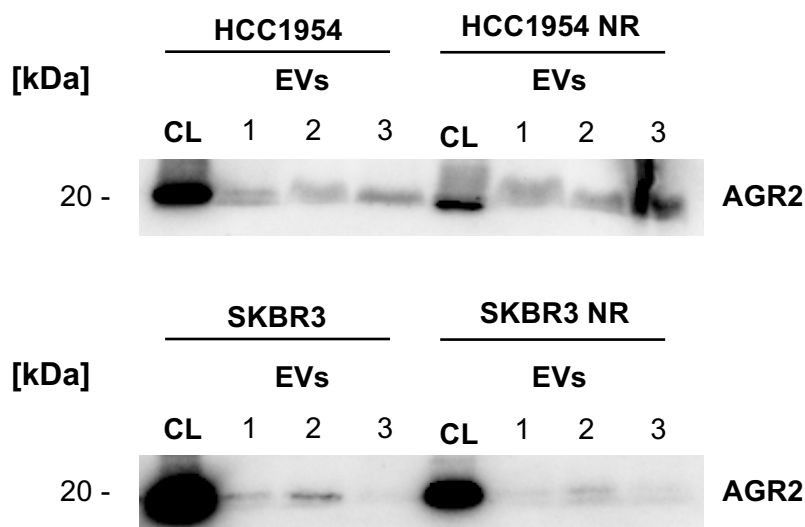
Figure 4.16. AGR2 content on the EVs evaluated by immunoblotting.

Ten µg of HCC1954, HCC1954 NR, SKBR3, and SKBR3 NR derived EVs or cell lysate (CL) used as control were loaded to evaluate the presence of AGR2. Images represent n = 3 experiments. NR=neratinib-resistant.

4.4.3 Summary of findings from EVs separation approaches

Table 4.6 summarise the findings obtained by using both different EVs separation approaches.

Table 4.6. Summary of all the substantial results obtained from the different EVs separation methodologies.

Assay	EFM192A (NR vs sensitive)	HCC1954 (NR vs sensitive)	SKBR3 (NR vs sensitive)
EVs collected by 200K UC protocol			
Protein amount	-	↑1.65-fold (*p* = 0.105)	n.d.
NTA: Particle amount	-	↓4.3-fold (*p* = 0.126)	↓6.1-fold (*p* = 0.033*)
NTA: Particle size	-	n.d.	n.d.
EVs markers (Immunoblotting)	-	↓CD63 (*p* = 0.052) ↓Syntenin (*p* = 0.017*)	↓Syntenin (*p* = 0.031*) ↓CD9 (*p* = 0.058)
HER2 (Immunoblotting)	-	↓HER2 (*p* = 0.0006***)	↓HER2 (*p* = 0.008**)
IFCM - EVs markers	-	↓CD9, 7.04-fold (*p* = 0.038*) ↓CD81, 8.63-fold (*p* = 0.056) ↓CD63, 19.28-fold (*p* = 0.035*)	↓CD9, 5.37-fold (*p* = 0.041*) ↓CD81, 12.2-fold (*p* = 0.026*) ↓CD63, 12.25-fold (*p* = 0.028*)
IFCM - HER2+	-	↓HER2, 4.43-fold (*p* = 0.0655)	↓HER2, 6.41-fold (*p* = 0.033*)
EVs collected by GUC protocol			
Protein amount	↓1.55-fold (*p* = 0.204)	n.d.	↓1.31-fold (*p* = 0.152)
NTA: Particle size	n.d.	n.d.	n.d.
NTA: Particle amount	↑1.28-fold (*p* = 0.697)	n.d.	↓1.35-fold (*p* = 0.486)
NTA: Particle amount 30-150 nm	↓1.75-fold (*p* = 0.806)	↓1.21-fold (*p* = 0.863)	↓1.32-fold (*p* = 0.803)
EVs markers (Immunoblotting)	↓CD63 (*p* = 0.028*) ↓Syntenin (*p* = 0.03*)	n.d.	↓CD63 (*p* = 0.02*) ↓Syntenin (*p* = 0.355)
AGR2 (Immunoblotting)	-	n.d.	n.d.
IFCM - Cell Mask+	↓3-fold (*p* = 0.007**)	↓2.2-fold (*p* = 0.174)	↓1.24-fold (*p* = 0.677)
IFCM - CellMask+HER2+	↓3.5-fold (*p* = 0.023*)	↓3.03-fold (*p* = 0.119)	n.d.
HER2 (ELISA) lysed EVs samples	↓2.18-fold (*p* = 0.095)	↓1.84-fold (*p* = 0.42)	↓2.74-fold (*p* = 0.155)
HER2 (ELISA) non lysed EVs samples	↓2.1-fold (*p* = 0.034*)	n.d.	↓1.44-fold (*p* = 0.67)

Findings with significant p values are highlighted. n.d. = no differences.

4.5 Discussion

EVs play a significant role in both physiological and pathophysiological conditions, primarily by promoting cell-to-cell communication and propagating signals throughout the body. In cancer, EVs released by cancer cells containing various proteins and nucleic acids can spread oncogenic signals to both nearby cancer and normal cells, promoting cancer progression. These signals activate processes such as increased cellular proliferation, resistance to chemotherapy, and migration, leading to the receiving cells becoming more aggressive, surviving, invading the extracellular matrix, accessing the bloodstream, and eventually metastasising to secondary areas of the body[283,284].

Previous research performed by our research group demonstrated that EVs from docetaxel-resistant cells partially promoted cell proliferation and increased docetaxel-resistance in receiving cells. This finding was supported by EVs collected from plasma of patients treated with docetaxel[151]. Collectively this means that EVs may be substantially inhibiting cancer patients gaining benefit from anti-cancer drugs. Thus, the aim of this project is to gain an in-depth understand of EVs in HER2+ breast cancer, including those released by neratinib-resistant HER2+ breast cancer cell lines. A study previously published by our group showed that HER2 expression in the HCC1954 NR and EFM192A NR was decreased, compared to their neratinib-sensitive counterparts [232]. However, the comparison between SKBR3 and SKBR3 NR had not previously been performed. We confirmed by immunoblot analysis that NR cell line variants have reduced HER2 protein expression compared to their respective neratinib-sensitive counterparts, including SKBR3 NR cell line.

We investigated if EVs reflect the HER2 status of their cells of origin, as well as the content of AGR2, a protein that we found to be down-regulated in neratinib-resistant cell variants that could play an important role in neratinib-resistant mechanism (see **Chapter 3**). To achieve this, we used different EVs separation protocols and different EVs characterisation techniques to shed light about the effect of NR phenotype on the EVs released and their properties.

The separation and purification of EVs from biological fluids is a critical step in EVs research, and several methods have been developed for this purpose. Among the most widely used methods are dUC, size exclusion chromatography, immunoprecipitation, microfluidics, ultrafiltration, and GUC. Each EVs separation method has its own advantages and limitations, and the choice of method will depend on the specific research question, the sample type, and the downstream application[97,285]. As we demonstrated previously (see **Chapter 2**), the use of multiple sources of cellular media is recommended while comparing EVs separation methods, as some results cannot be extrapolated to other samples, meaning that the efficiency of a methodology could be directly related with the CM source used.

We firstly use 200K UC protocol for EVs separation. However, before adding EFM192A and EFM192A NR cell lines to the comparison and investigate the EVs cargo, we decided to take a step back, switching to other protocol more accepted by the EVs community and more reproducible. GUC using Optiprep™ has become one of the most commonly protocols to achieve better EVs purity and more intact EVs[105,286]. Then, we characterise EVs from neratinib-sensitive and neratinib-neratinib cell lines using this protocol to confirm if a reduction in EVs' release was also evident with "purer" EVs isolates.

Here, we firstly separated EVs from HCC1954, HCC1954 NR, SKBR3, and SKBR3 NR conditioned media by 200K protocol. We evaluated and characterised the number and content of those EVs by NTA, immunoblotting and IFCM. It is well known that cancer cells produce EVs constitutively and abundantly[209,244]. However, NTA as well as IFCM showed a reduction in the EVs released by NR cell lines. The lack of significance in NTA results (**Section 4.4.1.2**) was very possibly due to high error bars with NTA. However, the lower presence of EVs markers (CD9, CD63, and CD81) analysed by IFCM in the EVs derived from NR cell variants compare with their neratinib-sensitive counterparts was significant in both HCC1954 and SKBR3 cell line variants. These results are in keeping with the results obtained by Dr Michelle Lowry in this group previously[232]. We also considered the possibility that the difference in EVs numbers derived from neratinib-sensitive and neratinib-resistant cell variants was due to significant differences in secreting cell numbers between cell variants. However, no significant differences in cell numbers were obtained between neratinib-sensitive and neratinib-resistant cell variants. These findings suggest that this decrease in EVs' release could be related with neratinib-resistance.

We also estimated the relative amount of EVs protein in EVs samples obtained by 200K UC protocol. Although no significant differences were found between neratinib-sensitive and neratinib-resistant – derived EVs, the results confirmed that protein is a very poor surrogate for EVs quantities. While IFCM and immunoblotting showed a substantial decrease of EVs markers in NR-derived EVs compared to their neratinib-sensitive counterparts, no significant differences were found in terms of amount of protein. Interestingly, higher amount of EVs protein was found in HCC1954 NR-derived EVs compared to their neratinib-sensitive counterparts.

We also evaluated the presence of HER2 protein on the EVs by immunoblotting and IFCM to settle if the 200K-EVs represent the HER2 status of their cells of origin. Immunoblotting analysis was performed for the CLs as well as EVs lysates. We founded that HER2 was not detected in 200K-EVs harvested from NR cell variants compared to the EVs released by their neratinib-sensitive counterparts. Interestingly, Ciravolo et al. (2012)[147] suggested that HER2+ EVs secretion could be exacerbated in advanced breast disease as compared to early stages, representing a mechanism of resistance.

In this point, we decide to introduce another pair of neratinib sensitive and neratinib resistant cell variants (EFM192A and EFM192A NR) to shed light to the neratinib mechanism and its involvement in EVs released and specifically, HER2+ EVs secretion. However, before including it, we needed to evaluate if this methodology used fit our purposes. The reason for switching from a 200K protocol to a GUC protocol for EVs separation is due to the limitations of the previous method. Although the UC is considered the gold standard method for EVs collection, it is a time-consuming and labour-intensive process that can lead to sample aggregation and loss of EVs during pelleting. In addition, we observed lot of variability between replicates by immunoblotting.

On the other hand, GUC methodology separates EVs based on their density and can be used to isolate specific EVs subpopulations. This method has the advantage of providing a higher yield of pure EVs with reduced contamination from other cellular components. Additionally, it requires a smaller sample volume although still being as labour-intensive as UC[287]. Therefore, we moved to a

GUC protocol for EVs separation as it offers a more efficient and reliable method for EVs collection that allows us to obtain high-quality EVs for downstream analysis.

A similar result, although not significant, were observed using EVs isolates obtained by GUC from EFM192A, HCC1954, and SKBR3 cell variants (neratinib-sensitive and neratinib-resistant). A general reduction was observed in the particle amount on the NR-derived EVs isolates as well as a decreased in EVs markers by immunoblotting. When we investigated the HER2 content on the non lysed and lysed EVs samples, we found a decrease as well on the NR-derived isolates when compared with the parental (neratinib-sensitive) counterparts. The study performed by Santamaria et al. (2021)[278] found that the treatment with neratinib increased the formation and release of EVs in HER2+ breast cancer cells. Neratinib also altered the endocytic trafficking of the cells, leading to the accumulation of vesicles inside the cells, suggesting that the increased release of EVs could play a role in the anti-tumour effects of neratinib. However, our findings suggest a decrease on EVs' release by neratinib-resistant cell variants, is not in line with these previous results performed in neratinib-sensitive cells, indicating that the development of neratinib-resistance could lead in changes of HER2 trafficking and EVs' release/biogenesis.

In keeping with this, the proteomic profiling of these six cell line variants discussed in **Chapter 3** and included in the **Appendix II**, showed that some of the differentially expressed proteins in HCC1954 NR and SKBR3 NR cell variants were related with EVs' release (i.e., RAB3A and flotillin-1, respectively), although were not shared between the different cell lines. No related proteins were found in the case of EFM192A NR with vesicle trafficking. More interestingly, those proteins related with EVs' release were differentially down-regulated in the neratinib-resistant cell variants. These results suggest that the release of EVs could vary between cancer cell lines with different levels of sensitivity or resistance to various treatments, and that the cargo of these EVs can also differ and potentially contribute to the development of resistance. Further analysis must be performed to discover the role of those proteins in the EVs' release in neratinib-resistant cell variants and to determine the biological reason under the EVs' release blockage in neratinib-resistant cell variants. Successively, we also analyse the presence of AGR2 on the HCC1954 and SKBR3-derived EVs in both neratinib-resistant and neratinib-sensitive cell variants. AGR2, as described in **Chapter 3**, is a common protein down-regulated in HCC1954 NR and SKBR3 NR that could play an important role in the neratinib-resistance mechanism. However, no significant differences were found by immunoblotting on the content of AGR2 between the neratinib sensitive and neratinib resistant-derived EVs. Quantitative analysis must be performed to determined differences in the content of this secreted protein on the EVs and its implication as secreted protein in the tumour microenvironment.

4.6 Conclusion

The results in this study indicate that EVs' release seems to be reduced in neratinib-resistant cell lines compared to their neratinib-sensitive counterparts. Similar results were obtained using both 200K UC and GUC protocols. In addition, HER2 presence in neratinib-resistant-derived EVs was lower than in those derived by neratinib-sensitive counterparts, as happened with the HER2 expression in their cells of origin. However, a deep analysis must be done to determine the possible mechanism behind this reduction and identify possible targets to elucidate the mechanism of resistance.

Chapter 5

Unravelling the effect of hypoxia on the cargo and release of EVs from neratinib-resistant and neratinib-sensitive HER2+ breast cancer

Abstract

Hypoxia, defined as low oxygen level, is considered a hallmark of solids tumours, and it is associated with cancer cell survival, EMT, metastasis, and drug resistance. Interestingly, previous research performed by our group and others has shown that EVs are involved in those mechanisms. Thus, this study aimed to understand hypoxia's influence on EVs' release by neratinib-resistant and neratinib-sensitive HER2+ breast cancer cell lines.

HER2-positive cell lines (HCC1954, EFM192A and SKBR3) and their neratinib-resistant counterparts (HCC1954-NR, EFM192A-NR, and SKBR3-NR) were seeded in complete medium and allowed to attach overnight. Before CM collection, media was switched to medium containing EVs-depleted FBS. Cells were then incubated in normoxic (21% O_2) or hypoxic conditions (1% O_2) for 48 hrs. 10K (10,000× g, 4ºC, 30min) and 120K (120,000× g, 4ºC, 1hr 15min) pellets were obtained from the CM by dUC. Particle numbers was measured by NTA. Protein concentration of EVs samples was determined by BCA assay. EVs and lysates of their cells of origin were characterised by immunoblots for EVs markers and hypoxia-related proteins. CellMask™ Plasma Membrane stain and HER2 were used to analyse EVs by IFCM. TEM images were taken to evaluate EVs' integrity. EVs' cargo was also evaluated by measuring the presence of E-cadherin, IL-6, IL-8, and HER2 by ELISA, as well as the presence of some miRs related with hypoxia and/or cancer progression (miR-21, miR-210, miR-155, and miR-630).

This study indicates that hypoxia has different cell-specific protein expression changes and modulates the release of EVs from cancer cells. Immunoblots performed on cell lysates showed a decrease of CD9 and CD63 tetraspanins considered positive markers for EVs, in hypoxia vs normoxia. However, no significant differences for those markers were found with the 10K and 120K EVs isolates. 120K and 10K pellets obtained under hypoxia showed an increase of µg of protein normalised by millions of donor cells compared with normoxia. NTA and IFCM showed disparities when EVs' number was evaluated. EVs under hypoxic conditions are influenced by the specific characteristics of the cells involved, as well as the impact on the cargo contained within these vesicles. Investigating the EVs' cargo, results indicated an increase in the levels of E-cadherin, IL-6, IL-8, and HER2 EVs derived from hypoxic HER2+ cancer cells. This increase in EVs carrying these specific molecules may contribute to tumour progression, aggressiveness, and the development of resistance to anti-HER2 drugs. Additionally, we have identified distinct populations of miRNAs enriched in these EVs, although it is important to consider the limitations of our methodology in this regard. These findings highlight a novel avenue for investigating EVs and their miRNA content. Understanding the role of EVs in the hypoxic TME is crucial for the advancement of effective cancer therapies.

5.1 Introduction

It is widely acknowledged that the presence of a hypoxic microenvironment can play a role in mutagenesis and the development of cancer. It is estimated that about 25 – 40% of invasive breast cancers exhibit hypoxic regions, with a clear association recognised between the existence of hypoxic areas in solid tumours and the processes of carcinogenesis, metastasis, treatment failure and patient mortality[288,289] . Studies have also established that hypoxia could affect the response of breast cancer cells to therapies such as chemotherapy and radiation. Hypoxic cells are known to be more resistant to these treatments, which can contribute to the lack of treatment response and disease progression[290]. A recent study in TNBC demonstrated that the up-regulation of HIF-1α under low oxygen conditions leads to increased expression of the anti-apoptotic protein survivin via miR-494, promoting resistance to docetaxel by inhibiting apoptosis and promoting cell survival[291]. Several studies have demonstrated an altered expression of miRNAs under hypoxic condition, with miR-210 being the most consistently and significantly induced miRNA reported in hypoxia. Together with miR-210, miR-21 is one of the most studied miRNAs involved in cancer progression. Due to its overexpression in several types of cancer, miR-21 is proposed as an authentic oncogene that enhances tumour growth and invasion[292]. The miRNAs involved in hypoxia investigated in this chapter and their major functions and roles are summarised in **Table 5.1**.

Previous work by our research group demonstrated that miR-630 negatively regulates the expression of insulin-like growth factor 1 receptor (IGF1R), a key protein in a signalling pathway involved in the development and progression of HER2 over-expressing breast cancer. Inhibition of miR-630 leads to increased expression of IGF1R, which in turn promotes cancer cell growth and resistance to HER-targeting drugs[256]. However, it is not established if hypoxia contributes to miR-630 inhibition, turning cancer cells more resistant to anti-HER2 therapies.

It has been shown that HIF-1α also promotes cap-dependent translation of specific messenger RNAs (mRNAs) by up-regulating the expression of the eukaryotic translation initiation factor 4E (eIF4E1) in hypoxic breast cancer cells[293]. In hypoxic cancer cells, HIF-1α-induced up-regulation of eIF4E1 enhances the cap-dependent translation of specific mRNAs that encode proteins crucial for the growth of breast cancer cells in tumourspheres. These findings provide novel insights into the mechanisms of protein synthesis in cancer cells under low oxygen levels.

EVs are important mediators of cell-to-cell communication that play an important role in the tumour microenvironment. EVs have been shown to transfer molecular cargo between cells, which can include miRNA, messenger RNA, DNA, and protein[100]. In the context of hypoxia, EVs released by hypoxic cancer cells can promote angiogenesis, cell survival, and invasion in recipient cells, thus contributing to the overall hypoxic response of the tumour[179,190,222,294–297]. It has been demonstrated that EVs released in hypoxic TME can also facilitated the suppression of immune cells and facilitating the tumour immune evasion[295,297].

Therefore, understanding the role of hypoxia in breast cancer and the special characteristics of EVs from cells cultured under hypoxic versus normoxic conditions could provide new insight into elaborating the role of hypoxia in resistance to anti-HER2 therapies; information that may be essential for the development of new therapeutic strategies to overcome the challenges posed by hypoxia in breast cancer treatment.

Table 5.1. An overview of miRNAs linked to hypoxia and investigated in this chapter.

miRNA	Expression in hypoxia	Cancer types	Main function and role associated with	Key target	Ref.
miR-210-3p	Up-regulated	Several types (including breast, glioblastoma, lung, pancreatic, or head and neck cancer)	Inhibits apoptosis and autophagy, increase cell survival, migration, and differentiation	E2F3 FGFRL1 GPD1L HIFs HOXA1 Pax-5	[298–300]
miR-21-5p	Up-regulated	Several types (including breast, lung, glioblastoma, thyroid, and prostate cancer)	Increases tumour angiogenesis, cell proliferation and drug resistance	Akt BAX BCL-2 PDCD4 TPM1 TIMP3 PDCD4 PTEN	[292,300,301]
miR-155-5p	Up-regulated	Several types (including breast, lung, colon, colorectal, gastric, and osteosarcoma)	Promotes cell survival, cell growth, chemoresistance, radioresistance, cell plasticity and EMT.	Caspase-3 FOXO3A RhoA SOCS1 TRF1 TP53INP1	[300,302,303]
miR-630	To be determined	Association with several tumours (including breast, lung, renal, colorectal, ovarian, and prostate cancer)	Cytokine signalling in immune system, migration, and invasion suppression	IGFR1 LMO3	[256,304–306]

EMT=Epithelial-Mesenchymal Transition

5.2 Aims of the study

The primary aim here was to investigate the effect of hypoxia on the HER2+ breast cancer cell lines by determining the expression of different markers as HIF-1α and HER2. In parallel, we also studied the effect of hypoxia on the release of EVs from neratinib-sensitive and neratinib-resistant HER2+ cell lines. Specifically, we aimed to quantify and characterise the EVs according to MISEV2018 guidelines. Subsequently we aimed to determine if the EVs' cargo differs between hypoxic and normoxic conditions.

5.3 Material and Methods

5.3.1 Cell lines and culture conditions

Six HER2-positive breast cancer cell line variants (EFM192A, HCC1954 and SKBR3 and their neratinib-resistant counterparts EFM192A NR, HCC1954 NR, and SKBR3 NR) were routinely maintained as explained in **Section 2.3.1**. A hypoxic atmosphere (1% O_2, 5%CO_2, 37ºC) was set in an InvivO$_2$ 400 Physoxia Workstation (Baker Ruskinn; Serial #: SP0287). After 24 hrs seeding, complete RPMI-1640 media was replaced with 25 ml/flask of complete RPMI-1640 media supplemented with 10% dFBS and 1% P/S (see **Section 2.3.2**) and cells were incubated under normoxic or hypoxic conditions during 48 hrs.

5.3.2 EVs separation by differential ultracentrifugation (dUC)

Before CM collection, 7×T175 cm^2 flasks of EFM192A and EFM192A NR at a density of 3×10^6 cells per flask and 7×T175 cm^2 flasks of HCC1954, HCC1954 NR, SKBR3, and SKBR3 NR at 2×10^6 cells per flask were seeded in complete RPMI-1640 medium. The medium was replaced the next day with RPMI-1640 medium containing 10% EVs-depleted-FBS (dFBS), 2mM L-Glutamine, and 1% penicillin/streptomycin (Sigma-Aldrich, Cat. #: P4333). After the cells conditioned the medium for 48 hrs, approximately 175 mL aliquots of CM were collected from each cell line and process through the workflow illustrated in **Figure 5.1**. Cells were counted and their viability checked using the LUNA-II™ automated cell counter (Logos biosystem, Cat. #: L40001) and 0.4% trypan blue stain (Logos biosystem, Cat. #: T13001), showing all cultures to be ≥95% viable.

CM was centrifuged at 300× g for 10 min as a pre-clearing step to remove cellular debris. Then, the CM was transferred to new 50 mL falcon tubes and centrifuged at 10,000× g for 30 min at 4ºC. The resulting pellets were then washed at the same speed with PBS to obtain the final 10K pellets. The CM was transferred to a Quickseal 39 mL tubes (Beckman Coulter, Cat. #: 342414) and centrifuged at 120,000× g for 75 min at 4ºC in an Optima XPN-100 Ultracentrifuge (Beckman Coulter) using a Type 70Ti fixed-angle rotor (Beckman Coulter, Cat. #: 337922). The obtained pellets (120K pellet) were washed with PBS and re-centrifuged at the same speed in a new Quickseal tubes. Finally, the 10K and 120K cleaned pellets were resuspended in 140 µl of PBS and stored in Protein LoBind tubes (Eppendorf, Cat. #: 0030 108.116) at -80ºC.
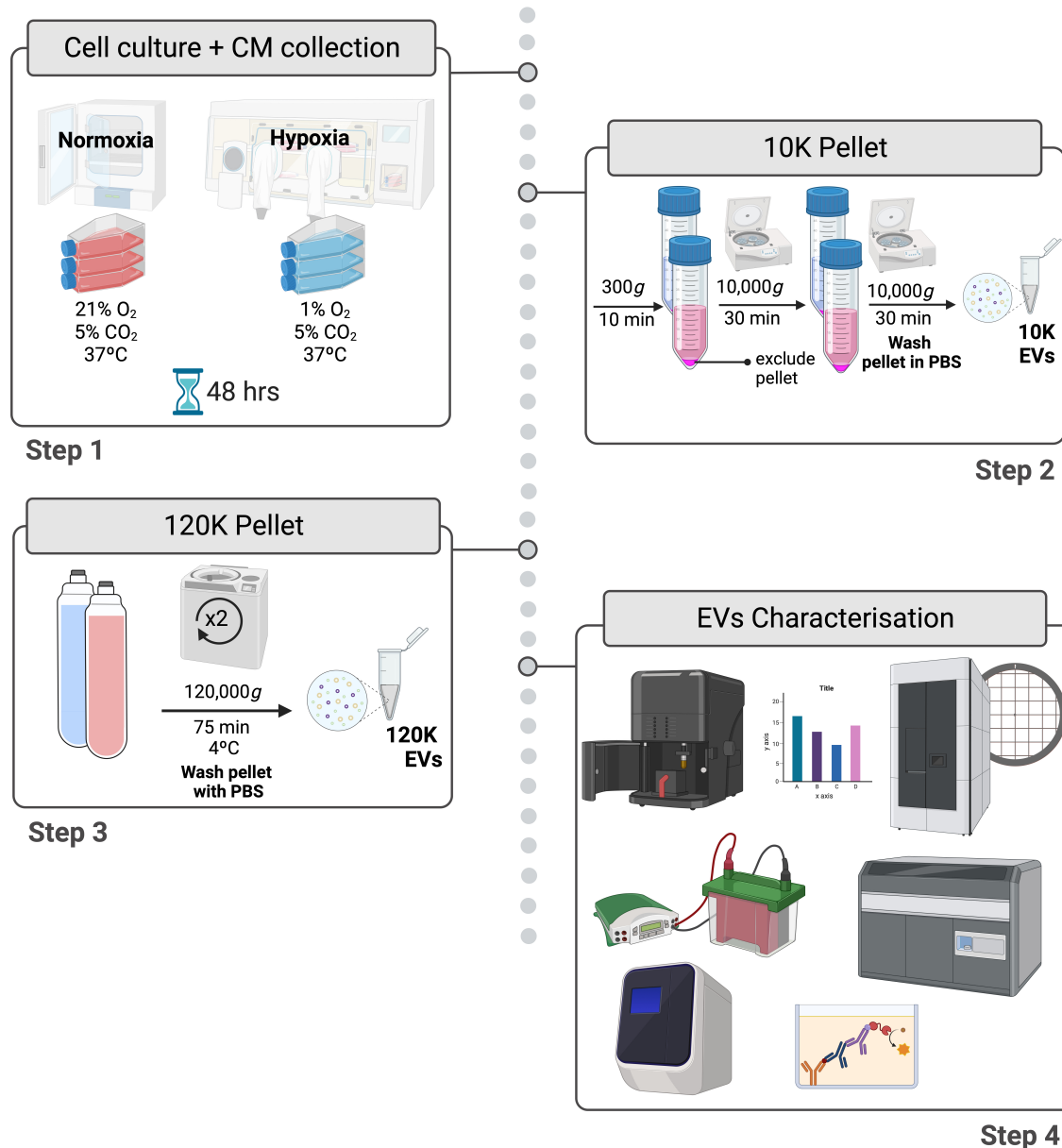
Figure 5.1. Workflow diagram of methodology used to assess the comparison between normoxic and hypoxic conditions and followed EVs characterisation.

(**1**) EFM192A, HCC1954, and SKBR3 neratinib-sensitive and neratinib-resistant cell variants were seeded in complete medium and allowed to attached overnight. Complete medium was then replaced with medium containing EVs-depleted FBS (dFBS). After 48 hrs incubation, conditioned medium (CM) was collected and cells were counted (**2-3**). The diagram displays the different steps for differential ultracentrifugation (dUC) for EVs separation/enrichment and (**4**) the parameters evaluated during the subsequent characterisation of the isolates. The process was conducted a minimum of n = 3 times. Schematic representation was created with *BioRender.com*.

5.3.3 Collection of protein lysate of normoxic and hypoxic cells and their EVs

EFM192A and EFM192A NR cells were seeded at 2×10^6 cells per T75 flask (Corning, Cat. #: 431464U) and HCC1954, HCC1954 NR, SKBR3 and SKBR3 NR were seeded at 1×10^6 cells. The following day the medium was changed to 10% EV-depleted FBS RPMI medium and placed in the incubator (21% O_2) or in the InvivO$_2$ 400 Physoxia Workstation (1% O_2). After 48 hrs of incubation, the medium was removed from the flasks and the cells were processed as previously describe in **Section 2.3.6**. The supernatant was transferred to a new tube and stored at -20ºC until required. EVs pellets were lysed by using 1:1 ratio of EVs suspension (50 µl) and lysis buffer containing protease inhibitor cocktail.

5.3.4 Protein quantification by BCA assay

Cell lysate and EVs lysate was quantified using the Bio-Rad protein assay Dye reagent (Bio-Rad, Cat. #: 500-0006) as previously described in **Section 3.3.1.1**.

5.3.5 Immunoblotting assays

For all immunoblotting performed in this chapter, total protein (30 µg for cell lysates' immunoblots or 10 µg for EVs' characterisation blots) was resolved as per **Section 2.3.8** on either 7.5% (Bio-Rad Laboratories, Cat. #: 4561023) or 10% Mini-PROTEAN TGX^{TM} 10-well gel (Bio-Rad Laboratories, Cat. #: 4561034) along with a MW marker, SeeBlue Plus 2 Pre-stained standard (Invitrogen, Cat. #: LC5925). All antibody conditions and catalogue numbers used in this chapter are detailed in **Table 5.2**. Densitometric analysis was performed using Fiji software[216].

Table 5.2. Antibody dilutions and conditions for immunoblotting.

Primary Antibody	Company, Cat. #	Dilution	Antibody condition	Secondary Antibody
β-Actin	Sigma-Aldrich, A1978	1:5000	3% BSA/PBST	Anti-Mouse IgG
β-Catenin	Abcam, ab32572	1:1000	3% BSA/PBST	Anti-Rabbit IgG
Calnexin	Abcam, ab133615	1:1000	3% BSA/PBST	Anti-Rabbit IgG
CD9	Abcam, ab236630	1:1000	3% BSA/PBST	Anti-Rabbit IgG
CD63	Abcam, ab68418	1:500	3% BSA/PBST	Anti-Rabbit IgG
eIF4E	Cell Signaling, 2067	1:1000	3% BSA/PBST	Anti-Rabbit IgG
HER2	Calbiochem, OP15	1:1000	3% BSA/PBST	Anti-Mouse IgG
HIF-1α	Abcam, ab179483	1:1000	3% BSA/PBST	Anti-Rabbit IgG
Syntenin	Abcam, ab133267	1:1000	3% BSA/PBST	Anti-Rabbit IgG
Vinculin	Cell Signaling, 7076	1:1000	3% BSA/PBST	Anti-Rabbit IgG

All secondary antibodies were diluted 1:1000 in 3% BSA/PBST

5.3.6 EVs characterisation

5.3.6.1 NTA on 120K EVs isolates

[NTA of EVs was performed in the Laboratory for Biological Characterisation of Advanced Materials (LBCAM), Trinity Translational Medicine Institute, as a paid service]

Sixty samples containing EVs were analysed via NTA using a NanoSight NS500 system as described previously in **Section 4.3.8.1**.

5.3.6.2 TEM analysis of 120K EVs isolates

[TEM imaging of EVs was performed in the Advanced Microscopy Laboratory in Trinity Biomedical Sciences Institute by Mr. Neal Leddy as a paid service]

Samples were prepared from TEM analysis as described in **Section 2.3.9**.

5.3.6.3 Imaging Flow Cytometry on 10K and 120K EVs isolates

The IFCM analysis of 10K and 120K pellets obtained from cells after 48 hrs in normoxic or hypoxic conditions was performed following the protocol described previously in **Section 4.3.8.3**.

5.3.7 Characterisation of EVs' cargo

5.3.7.1 ELISA assay

E-cadherin, HER2, IL-6 and IL-8 quantification was performed using the DuoSet ELISA kits (respectively R&D Systems, Cat. #: DY648, Cat. #: DY1129B, Cat. #: DY206-05 and Cat. #: DY208-05) and following manufacturer's instruction as explained in **Section 3.3.3**. Sample concentrations/volumes for each specific ELISA are summarised in **Table 5.3**.

Table 5.3. Type of sample and concentrations/volumes used for ELISA assays.

DuoSet® Elisa Kit	Type of EVs samples	Amount of EVs sample in 100 µl of reagent diluent	Amount of Cell lysate in 100 µl of reagent diluent
E-cadherin	Non-lysate EVs	4 µl	10 µg
HER2	Non-lysate EVs	10 µl	5-10 µg
IL-6	Lysate EVs	5 µg	20 µg
IL-8	Lysate EVs	5 µg	20 µg

5.3.7.2 Total EVs RNA extraction

For RNA extraction, 5×T175 cm^2 flasks of EFM192A, EFM192A NR, HCC1954, HCC1954 NR, SKBR3 and SKBR3 NR were seeded as described in **Section 5.3.2**. Differential ultracentrifugation was used to obtain the final 120K pellets as described in previous **Section 5.3.2** with minor

modifications. Briefly, final pellets were not resuspended in PBS and were instead directly lysate as described in the paragraph below.

Total RNA was isolated from EV-enriched or cell pellets using miRNeasy Tissue/Cells Advanced mini kit (Qiagen, Cat. #: 217604) and following manufacturer's instructions with slightly modifications. In brief, cell pellets and EVs pellets were resuspended in 450 µl of Buffer RPL and homogenise. Then 140 µl of Buffer AL was added and mix thoroughly. Additionally, 3 µl of exogenous miRNA (33 fmol) *cel-miR-39* (cel-miR-39 Spike-In Kit, Cat. #: # 59000, Norgen, Canada) were added to each sample then were left at RT (15–25°C) for 3 min.

After the 3 min incubation, lysates were placed in a gDNA eliminator spin column placed in a 2 ml collection tube and centrifuge for 30 sec at 8000× *g*. After this stage, the colourless supernatant was transferred to a new 2 ml reaction tube and mixed by pipetting with 1 volume of isopropanol (Sigma-Aldrich, Cat. #: I9516-500ML). The entire sample was then transfer to a RNeasy Mini column and a centrifuge step at 8,000× *g* for 15s was followed. This process was repeated twice to use the remainder of the sample. After this step, the flow-through were discarded and 700µl Buffer RWT were pipetted to the columns followed by centrifugation at 8,000× *g* for 15 sec. For next step the same procedure was applied, adding 500 µl Buffer RPE and discarding the flow-through after the centrifugation step. For the last step, where 500 µl of 80% ethanol was added to the columns, the centrifugation step was performed for 2 min and then the RNeasy Mini Spin columns were carefully removed from the collection tubes and placed in new 2 ml collection tubes. To dry the membrane, the columns were centrifuged a full speed for 1 min. Finally, 40 µl of RNase-free water was added directly to the centre of the spin column and incubate for 1 min. Sample were centrifuged for 1 min at full speed to elute the RNA. To maximise the RNA extraction, a second step was performed by adding 30 µl of RNase-free water with longer incubation time (10 min). As recommended by the manufacturer, then same procedure as before was applied. Finally, RNA samples were quantitate using the Qubit RNA High Sensitivity (HS) RNA kit (ThermoFisher, Cat. #: Q32852) with a Qubit 4.0 Fluorometer, following manufacturer's instructions.

5.3.7.3   cDNA synthesis of extracted RNA

For cDNA synthesis, 2 µl of sample eluent (< 5 ng/µl of extracted RNA) were required for TaqMan™ Advanced miRNA cDNA Synthesis Kit (Applied Biosystems™, Cat: # A28007) as recommended by manufacturer's instructions. Briefly, samples and cDNA synthesis reagents were thawed completely in ice and subsequently centrifuged to spin down the contents. Veriti 96-Well Thermal Cycler (Well thermocycler; Applied Biosystems™, Cat. #: 4375305) was used for the cDNA synthesis and the different steps were describe below.

5.3.7.3.1 Poly(A) tailing reaction

Table 5.4 collects the different reagents and volumes of reagents used in this step. Reaction mix and the sample were mixed in a 0.2 ml PCR tube (Fisher Scientific, Cat: # 951010006) and spin down. The reaction settings and standard cycling for this reaction are collected in **Table 5.5**. Once the reaction was done, the adaptor ligation reaction was immediately performed.

Table 5.4. Poly(A) tailing reaction preparation.

Component	Volume per sample (µl)
10X Poly(A) buffer	0.5
ATP	0.5
Poly(A) Enzyme	0.3
RNAase-free water	1.7
Total Poly(A) Reaction Mix Volume	**3.0**

Table 5.5. Poly(A) tailing reaction settings.

Step	Temperature	Time
Polyadenylation	37ºC	45 min
Stop reaction	65ºC	10 min
Hold	4ºC	Hold

5.3.7.3.2 Adaptor ligation reaction

Following poly(A) tailing reaction, 10 µl of the ligation reaction mix (volume and reagents used reported in **Table 5.6**) was added to each sample (final volume 15 µl), following by mixing and spin. The reaction settings and standard cycling for this reaction are collected in **Table 5.7**. Once the reaction was done, we proceeded immediately with the reverse transcription (RT) reaction.

Table 5.6. Adaptor ligation reaction preparation.

Component	Volume per sample (µl)
5X DNA Ligase Buffer	3
50% PEG 8000	4.5
25X Ligation Adaptor	0.6
RNA Ligase	1.5
RNAse free water	0.4
Total Ligation Reaction Mix	**10**

Table 5.7. Adaptor ligation reaction settings.

Step	Temperature	Time
Ligation	16ºC	60 min
Hold	4ºC	Hold

5.3.7.3.3 Reverse transcription (RT) reaction

After sample processing for ligation reaction, 15 µl RT reaction mix (details collected in **Table 5.8**) was added to each sample (to a final volume of 30 µl), following by mixing and spin down. The reaction settings and standard cycling for this reaction are collected in

Table 5.9. Once the reaction was done, we proceeded immediately with the final step. RT reaction products were stored at -80ºC.

Table 5.8. RT reaction preparation.

Component	Volume per sample (µl)
5X RT Buffer	6
dNTP Mix (25mM each)	1.2
20X Universal RT Primer	1.5
10X RT Enzyme Mix	3
RNAse free water	3.3
Total RT Reaction Mix volume	15

Table 5.9. RT reaction settings.

Step	Temperature	Time
Reverse transcription	42ºC	15 min
Stop reaction	85ºC	5 min
Hold	4ºC	Hold

5.3.7.3.4 miR-Amp reaction

For this step only 5 µl of the final RT product of each sample was required. Hence, reagents for miR-Amp reactions were prepared and related volume are reported in **Table 5.10.** Forty-five µl of the miR-Amp reagent mix was added to each sample (final volume 50 µl), following by mixing and spin down. The reaction settings and standard cycling for miR-Amp reaction are collected in **Table 5.11.** Undiluted miR-Amp products were stored at -80°C until the real-time PCR was performed.

Table 5.10. miR-Amp reaction preparation.

Component	Volume per sample (µL)
2X miR-Amp Master Mix	25
20X miR-Amp Primer Mix	2.5
RNAse free water	17.5
Total RT Reaction Mix volume	45

Table 5.11. miR-Amp reaction settings.

Step	Temperature	Time	Cycles
Enzyme activation	95ºC	5 min	1
Denature	95ºC	3 sec	14
Anneal/Extend	60ºC	30 sec	
Stop reaction	99ºC	10 min	1
Hold	4ºC	Hold	1

5.3.7.4   miRNA quantification by qPCR

The sequences of the mature miRNAs of interest were used as forward specific primers obtained from TaqMan® Advanced MicroRNA Assay (Applied Biosystem™, Cat. # A25576) (miRNA sequences reported in **Table 5.12)** while a universal primer, provided by the TaqMan™ Fast Advanced Master Mix (Applied Biosystem™, Cat. # 4444557), was used as a reverse primer. Five µl of cDNA template (1:10 dilution) were used in 20 µl reactions (volumes of each reagent are collected in

Table 5.13).

Table 5.12. qPCR preparation reagents.

Component	Volume per sample (µl)
TaqMan™ Fast Advanced Master Mix (2X)	10
TaqMan™ Advanced miRNA Assay (20X)	1
RNAse free water	4
Total RT Reaction Mix volume	**15**

Table 5.13. miRNA sequences used in this chapter.

miRNAs	Mature miRNA Sequence
hsa-miR-21-5p	UAGCUUAUCAGACUGAUGUUGA
hsa-miR-155-5p	UUAAUGCUAAUCGUGAUAGGGGUU
hsa-miR-210-3p	CUGUGCGUGUGACAGCGGCUGA
hsa-miR-630	AGUAUUCUGUACCAGGGAAGGU
Cel-miR-39-3p	UCACCGGGUGUAAAUCAGCUUG

Reactions were done in a MicroAmp™ Fast Optical 96-Well Reaction Plate with Barcode 0.1 ml (Applied Biosystems™, Cat: # 4346906). Therefore, 15 µl of PCR master mix was carefully added to each well followed by 5 µl of diluted cDNA samples, and plates were sealed using MicroAmp™ Optical Adhesive Film (Applied Biosystems™, Cat: # 4311971). qPCR was run using ViiA™ 7 Real-Time PCR System with 96-Well Block (Applied Biosystems™, Cat: # 4453534) according to the two-step cycling protocol summarised in **Table 5.14**.

Table 5.14. RT-qPCR reaction settings.

Step	Temperature	Time	Cycles
Enzyme activation	95ºC	20 sec	1
Denature	95ºC	1 sec	40
Anneal/Extend	60ºC	20 sec	

5.3.8 Data analysis and statistical testing

All statistical analyses were performed using GraphPad Prism version 9.1.9 for macOS (GraphPad Software). Regarding cell and EVs characterisation, values for arbitrary units (A.U.), EVs-numbers, and EVs-size are given as mean ± SEM (n = 3). Two-tailed paired t-test was applied (p < 0.05 was considered as statistically significant). For ELISA assay analysis, E-cadherin, HER2, IL-6 and IL-8 quantification was performed interpolating the absorbance values to the standard curve run alongside the sample.

For qPCR analysis, synthetic *Caenorhabditis elegans* miR-39 (cel-miR-39) was used to normalise the efficiency of the qPCR amplification and the relative expression of the specific miRNAs was evaluated in Log2x, based on the 2-ΔΔCt method. For each biological sample, miRNAs were analysed in triplicate and the mean value was obtained. All the data are expressed as mean ± SEM (n = 3). Two-tailed paired t-test and p value of less than 0.05 was considered statistically significant.

5.4 Results

5.4.1 Cell characterisation under hypoxic conditions in 2D culture

Hypoxia is a common characteristic of solid tumours. In response to hypoxia, cancer cells can undergo several changes that promote their survival and proliferation. We evaluated different parameters in order to establish which changes were happening on the cells under 48 hrs of hypoxic conditions before evaluating the EVs' release.

Compared to normoxia, both neratinib-sensitive and neratinib-resistant cell line variants showed a decrease in cell counts, that could be associated with a decrease of proliferation under hypoxic conditions (**Figure 5.2**). Only EFM192A cells showed a significant decrease on cell viability under hypoxic conditions compared to normoxia (98.2% in normoxia vs 96.6% in hypoxia, $p = 0.04$).
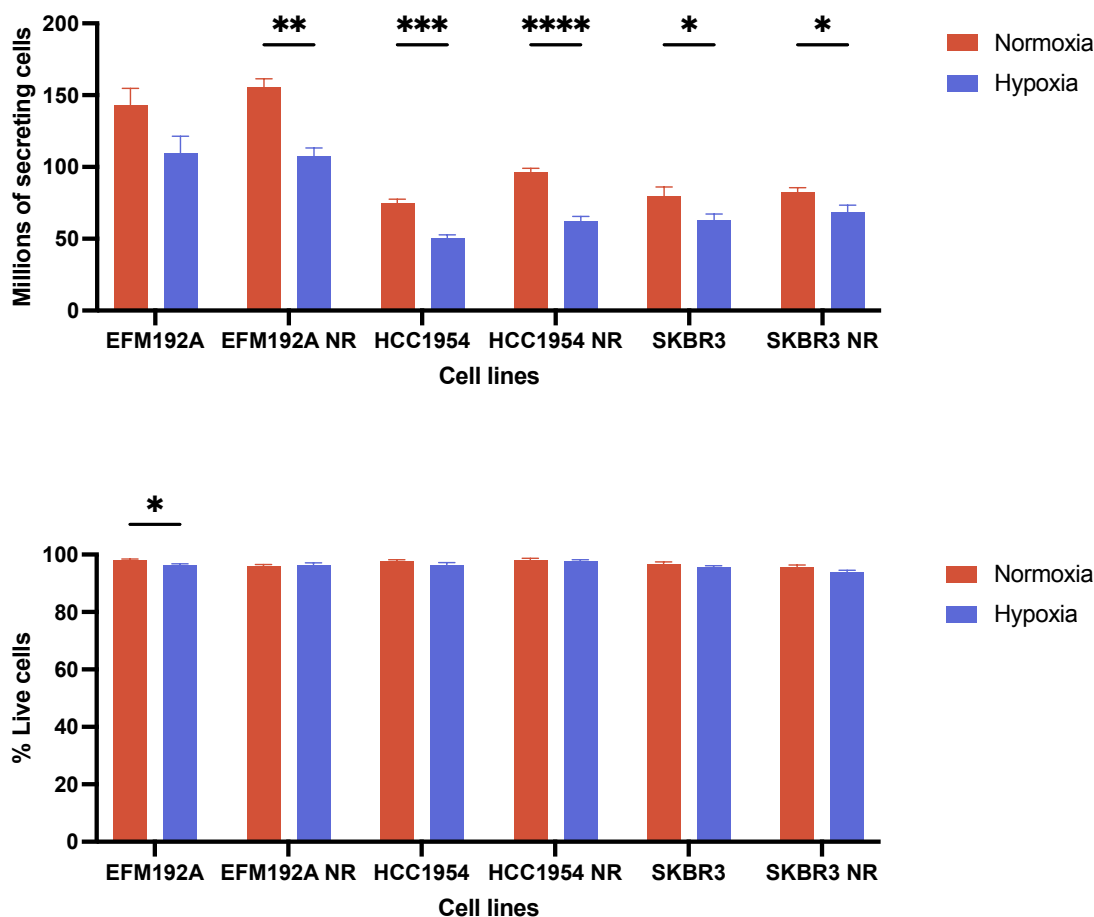
Figure 5.2. Cell count and cell viability.

(**Top**) Number of viable cells and (**Bottom**) percentage of cell viability was estimated by trypan blue exclusion assay. The number of viable cells was higher in normoxic conditions than their hypoxic counterparts in all the cases. Cell viability was always higher than 95% independently of oxygen level. Data shown are mean $\pm$ SEM ($n = 5$). $*p<0.05$, $**p<0.01$, $***p<0.001$, $****p<0.0001$.

We evaluated the expression of different markers as well. Firstly, the expression of HIF-1α and eIF4E were analysed, to evaluate the adaptation of these cells to the hypoxic conditions. We also evaluated the expression of HER2 to investigate the relation between HER2 and hypoxia. Finally, we explore the expression of tetraspanins, related with the release of EVs, as well as the expression of β-catenin, as it has been report to protect HBL-100 breast cancer cells from hypoxia effects[307].

All the six cell line variants showed a significant increase of HIF-1α under hypoxic conditions. (**Figures 5.3 – 5.5**). EFM192A cells showed a decrease of CD63 (1.8-fold, $p = 0.012$) and CD9 (1.3-fold, $p = 0.03$) markers under hypoxic conditions and an insignificant increase in HER2 expression. No significant differences were found in β-catenin and eIF4E markers. In contrast, we observed a decrease in HER2 (1.67-fold, $p = 0.053$) expression in EFM192A NR cell variant, as well a significant decrease in the levels of eIF4E (2.90-fold, $p = 0.021$). No significant differences were found in the expression of β-catenin or either tetraspanin CD9 and CD63 (**Figure 5.3**).
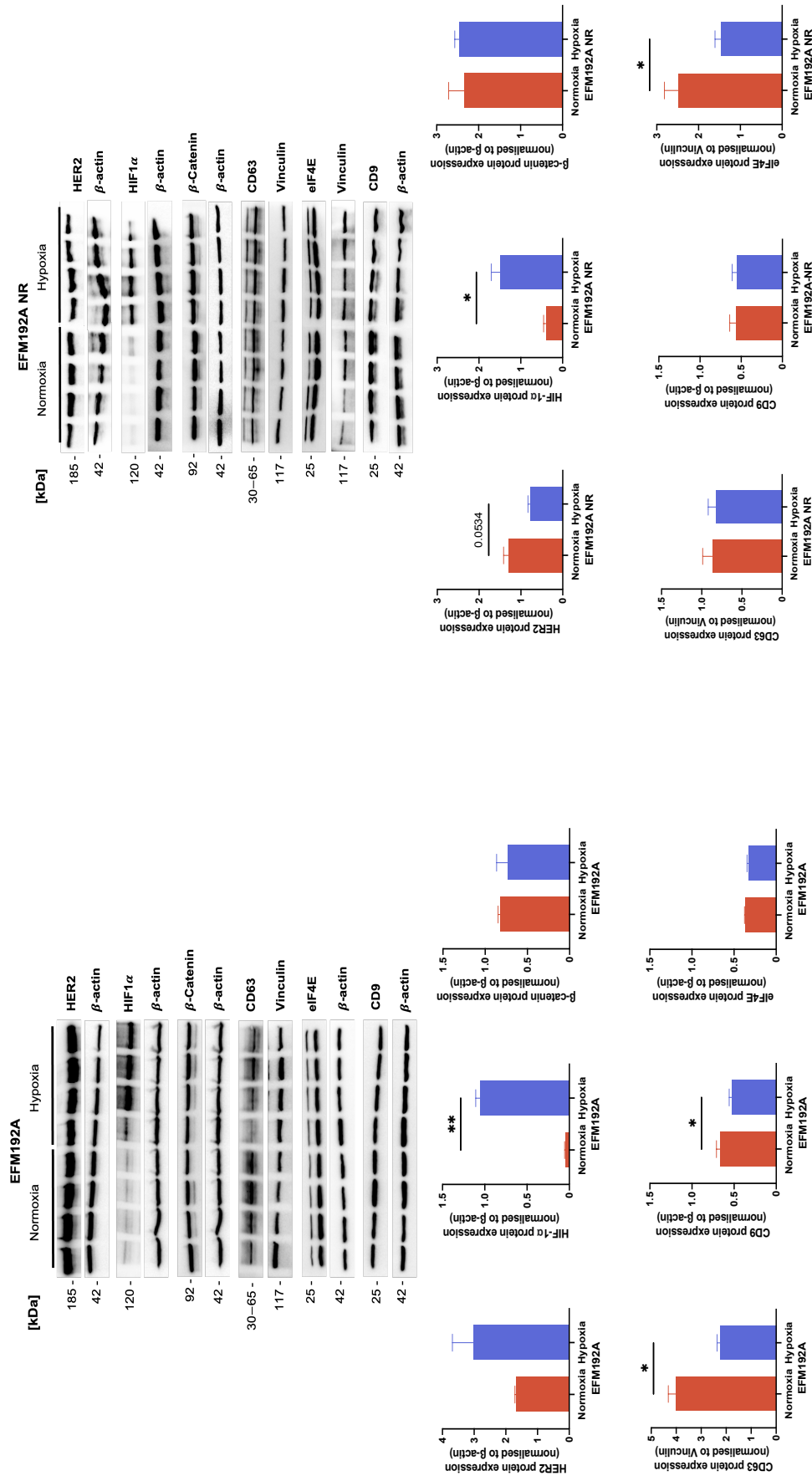
Figure 5.3. Characterisation of EFM192A and EFM192A NR under hypoxic conditions.

(**Top**) Immunoblots showing expression of HER2, HIF-1α, β-catenin, CD63, CD9, and EIF4E in neratinib-sensitive and neratinib-resistant (Neratinib Resistant; NR) EFM192A cancer cell variants. Thirty µg of EFM192A (**Left**) and EFM192A NR (**Right**) cell lysates were loaded for their analysis; (**Bottom**) The relative intensity (AU) of the protein signal band was calculated using ImageJ software. β-actin was used as loading control and Graphs shown are mean ± SEM ($n = 4$). * $p<0.05$, ** $p<0.01$.

The expression of β-catenin (1.7-fold, p = 0.016), CD63 (1.3-fold, p =0.048), and CD9 (1.85-fold, p = 0.0151) were also down-regulated in HCC1954 under hypoxic conditions compared to normoxia (**Figure 5.4**). In contrast, a slight increase of those markers were found under hypoxic conditions in the case of HCC1954 NR cell variant. In this last cell line, eIF4E was down-regulated in hypoxic conditions (1.6-fold, p =0.023).
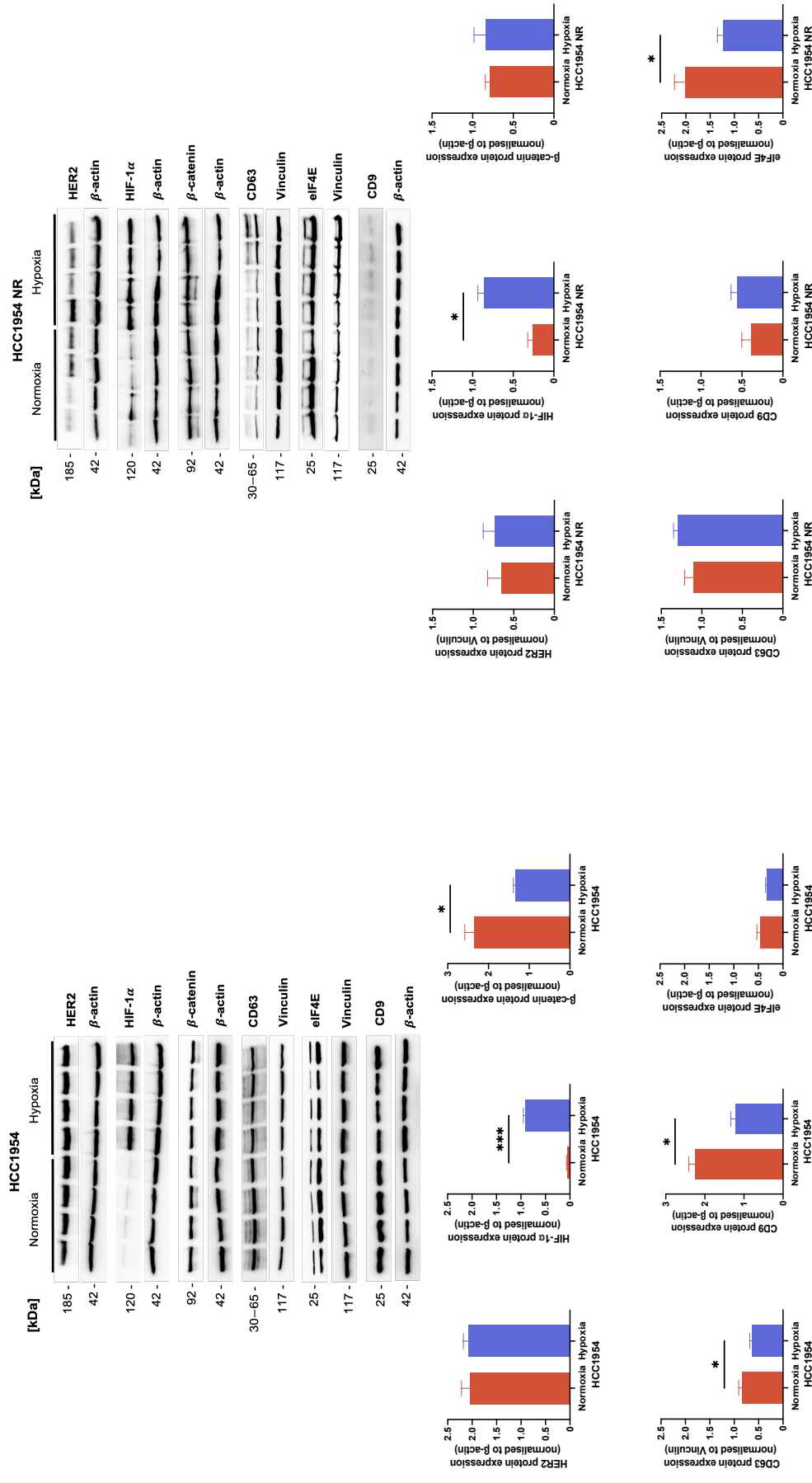
Figure 5.4. Characterisation of HCC1954 and HCC1954 NR under hypoxic conditions.

(**Top**) Immunoblots showing expression of HER2, HIF-1α, β-catenin, β-actin, CD63, CD9, and EIF4E in neratinib-sensitive and neratinib-resistant (Neratinib Resistant; NR) HCC1954 cancer cell variants. Thirty μg of (**Left**) HCC1954 and (**Right**) HCC1954 NR cell lysates were loaded for their analysis; (**Bottom**) The relative intensity (AU) of the protein signal band was calculated using ImageJ software. β-actin was used as loading control and normalisation. Graphs shown are mean ± SEM ($n = 4$). *$p<0.05$, ***$p<0.001$.

No significant differences were found in SKBR3 and SKBR3 NR for HER2, β-catenin, CD63, CD9 nor eIF4E (**Figure 5.5**). However, in both cases we could appreciate an increase in β-catenin levels and a slight decrease in eIF4E expression.
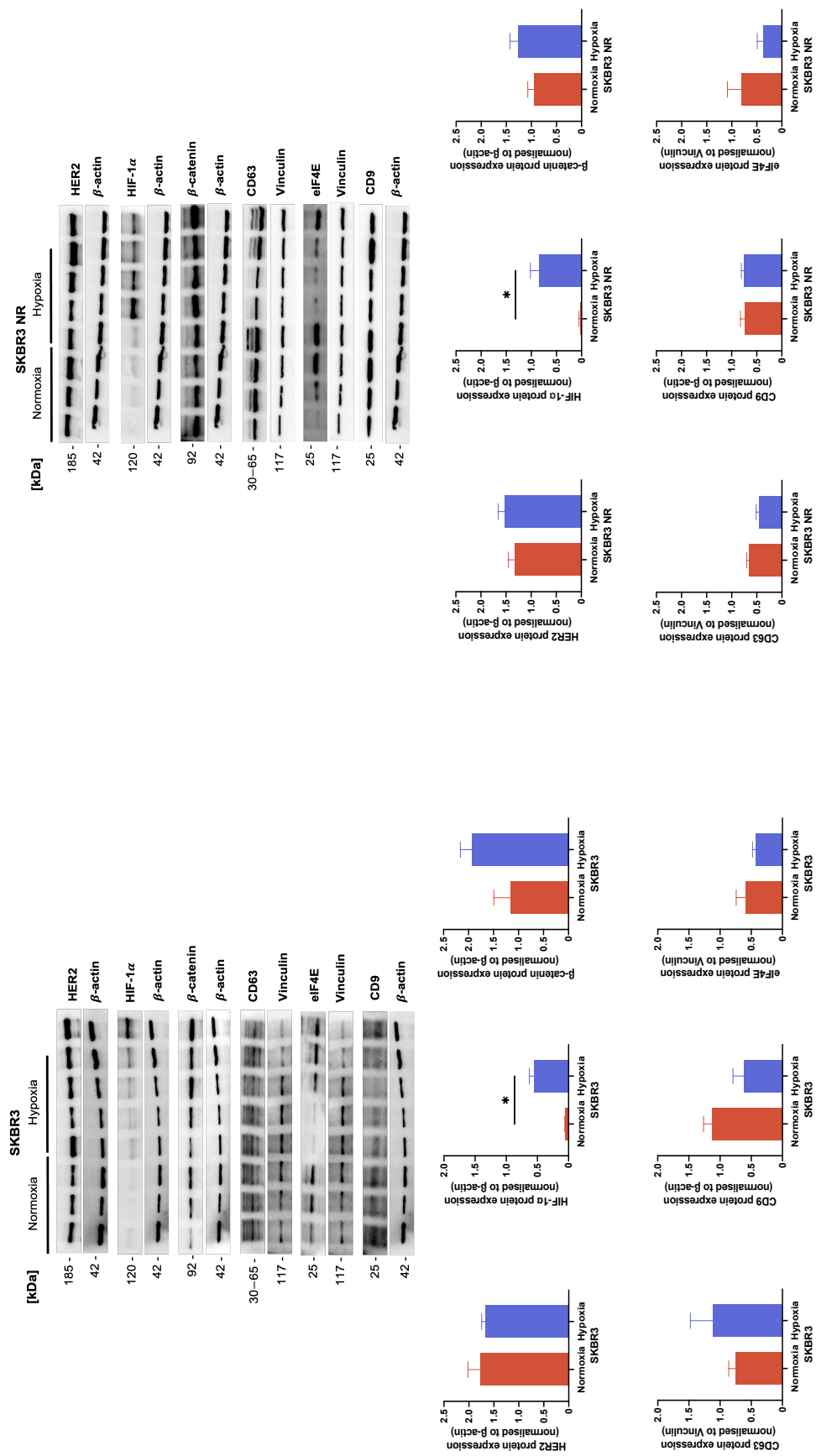
Figure 5.5. Characterisation of SKBR3 and SKBR3 NR under hypoxic conditions.

(**Top**) Immunoblots showing expression of HER2, HIF-1α, β-catenin, β-actin, CD63, CD9, and EIF4E in neratinib-sensitive and neratinib-resistant (Neratinib Resistant; NR) SKBR3 cancer cell variants. Thirty μg of (**Left**) SKBR3 and (**Right**) SKBR3 NR cell lysates were loaded for their analysis; (**Bottom**) The relative intensity (AU) of the protein signal band was calculated using ImageJ software. β-actin was used as loading control and normalisation. Graphs shown are mean ± SEM ($n = 4$) *$p<0.05$.

A summary of findings obtained for these three cell line pairs cultured under normoxic and hypoxic conditions is collected in **Table 5.15**.

Table 5.15. Summary of the cell characterisation findings.

	EFM192A	EFM192A NR	HCC1954	HCC1954 NR	SKBR3	SKBR3 NR
Cell count	↓1.3-fold (ns)	↓1.4-fold (**)	↓1.5-fold (***)	↓1.5-fold (****)	↓1.3-fold (*)	↓1.2-fold (*)
Cell viability	↓ (*)	n.d.	n.d.	n.d.	n.d.	n.d.
HER2	↑1.8-fold (ns)	↓1.7-fold ($p = 0.053$)	n.d.	n.d.	n.d.	n.d.
HIF-1α	↑24.8-fold (**)	↑3.9-fold (**)	↑15.2-fold (***)	↑3.2-fold (*)	↑10.5-fold (*)	↑24.4-fold (*)
β-catenin	n.d.	n.d.	↓1.7-fold (*)	n.d.	↑1.7-fold (ns)	↑1.3-fold (ns)
CD63	↓1.8-fold (*)	n.d.	↓1.3-fold (*)	↑1.2-fold (ns)	↑1.5-fold (ns)	1.5-fold (ns)
CD9	↓1.3-fold (*)	n.d.	↓1.8-fold (*)	↑1.4-fold (ns)	↓1.8-fold (ns)	n.d.
EIF4E	n.d.	↓1.7-fold (*)	↓1.5-fold (ns)	↓1.6-fold (*)	↓1.2-fold (ns)	↓2.2-fold (ns)

Summary of the cell viability and immunoblotting characterisation of the three cell line pairs comparing hypoxia and hypoxia. Fold change is calculated as hypoxia/normoxia ratio. n.d. = no differences. *p<0.05, **p<0.01, ***p<0.001, ****p<0.0001

5.4.2 Characterisation of EVs released by HER2+ breast cancer cell lines under hypoxic and normoxic conditions

We subsequently analysed the resultant EVs derived from those cells after 48 hrs incubation in EV-depleted FBS in normoxic or hypoxic conditions.

5.4.2.1 Protein quantification present in EVs samples

The relative amounts of protein (expressed as µg of protein/ml normalise by 10^6 harvested cells) present in each sample was determined by the BCA protein assay (**Figure 5.6**) in the 120K and 10K pellets. These were found to differ significantly between the normoxic and hypoxic isolates of all six cell line variants, always being highest in the EVs samples obtained from hypoxic conditions. Mean values of protein concentration are collected in **Table 5.16**.
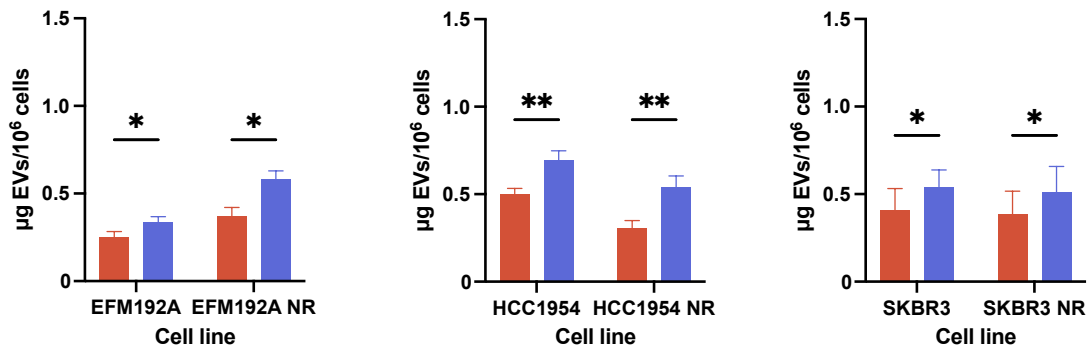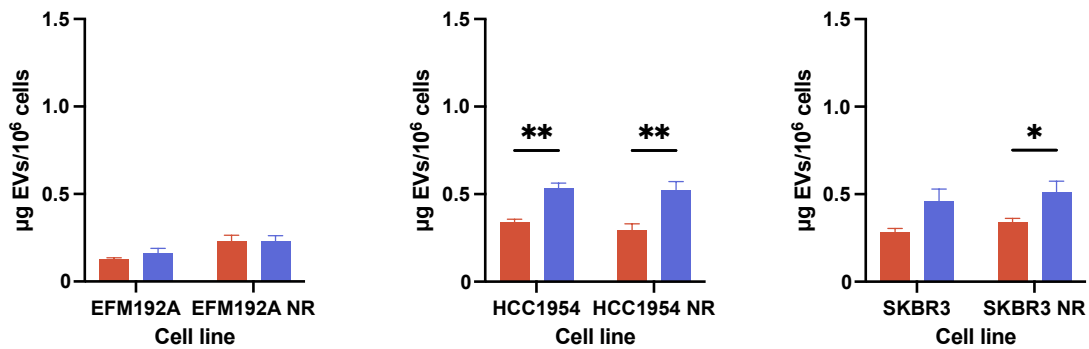
Figure 5.6. Protein content of 120K and 10K EVs isolates was measured by BCA.

The amount of protein was normalised to millions of cells (n = 3 ± SEM). Paired t-test used to calculate significance: *$p<0.05$, **$p<0.01$.

Table 5.16. Mean values ± of protein amounts for 120K and 10K EVs samples.

120K				
Cell line	Condition	µg EVs/10^6 cells	Fold change	*p* value
EFM192A	Normoxia	0.25 ± 0.03	1.4	0.014 (*)
	Hypoxia	0.34 ± 0.07		
EFM192A NR	Normoxia	0.37 ± 0.05	1.6	0.014 (*)
	Hypoxia	0.58 ± 0.05		
HCC1954	Normoxia	0.50 ± 0.03	1.4	0.007 (**)
	Hypoxia	0.69 ± 0.05		
HCC1954 NR	Normoxia	0.31 ± 0.04	1.8	0.003 (**)
	Hypoxia	0.54 ± 0.06		
SKBR3	Normoxia	0.41 ± 0.12	1.3	0.015 (*)
	Hypoxia	0.54 ± 0.1		
SKBR3 NR	Normoxia	0.38 ± 0.13	1.3	0.027 (*)
	Hypoxia	0.51 ± 0.15		
10K				
Cell line	Condition	µg EVs/10^6 cells	Fold change	*p* value
EFM192A	Normoxia	0.13 ± 0.01	1.3	0.283
	Hypoxia	0.16 ± 0.03		
EFM192A NR	Normoxia	0.23 ± 0.03	n.d.	0.994
	Hypoxia	0.23 ± 0.03		
HCC1954	Normoxia	0.34 ± 0.02	1.6	0.005 (**)
	Hypoxia	0.53 ± 0.03		
HCC1954 NR	Normoxia	0.29 ± 0.08	1.6	0.002 (**)
	Hypoxia	0.52 ± 0.05		
SKBR3	Normoxia	0.28 ± 0.02	2.	0.115
	Hypoxia	0.46 ± 0.07		
SKBR3 NR	Normoxia	0.34 ± 0.02	1.5	0.043 (*)
	Hypoxia	0.51 ± 0.06		

*Fold change is calculated as hypoxia/normoxia ratio (n=3). *p<0.05, **p<0.01.*

5.4.2.2 Presence of EVs specific markers and HIF-1α varied depending on the specific cell context

In keeping with MISEV2018 guidelines[105], immunoblotting analysis was performed on 120K and 10K EVs lysates and cellular lysates for the EVs positive markers, CD63, syntenin, and CD9. The purity of EVs, was determined by the presence or absence of an "exclusion marker"—endoplasmic reticulum protein calnexin—which is cell specific and is expected to be absent in EVs[308] (**Figure 5.7**). Regardless of the cell line of origin, Calnexin was not detected with any of the 120K EVs samples analysed. However, it was found in the 10K EVs samples. Although the 10K were also positive for some EVs markers and calnexin can be associated with some EVs (and may be detectable in an EVs preparation), we will focus our attention for some further analysis in the 120K

pellets that have the absence of this marker (Densitometric analysis of the 120K immunoblots are collected in **Appendix IV – Figure IV-2**). Although equal amount of protein was loaded on the gels, the enrichment of EVs markers in isolates obtained depended on the cell context and oxygen condition. CD9 was not detected in 120K pellets for EFM192A and EFM192A NR in both normoxia and hypoxia, when its enrichment was decreased significantly in 120K samples obtained from hypoxic SKBR3 NR cells compared to their normoxic counterparts. The presence of the tetraspanin CD63 was dependent on the cell of origin. For instance, CD63 presence in EFM192A-derived 120K samples under hypoxia was increased compared to normoxia, while SKBR3-derived 120K samples showed the opposite results. In summary, we obtained inconclusive results regarding the EVs markers enrichment depending on normoxic or hypoxic conditions. In the case of syntenin, no significant differences were found, with the exception of a significant decrease in its presence in the 120K samples obtained from hypoxic SKBR3 NR cells compared to their normoxic counterparts.
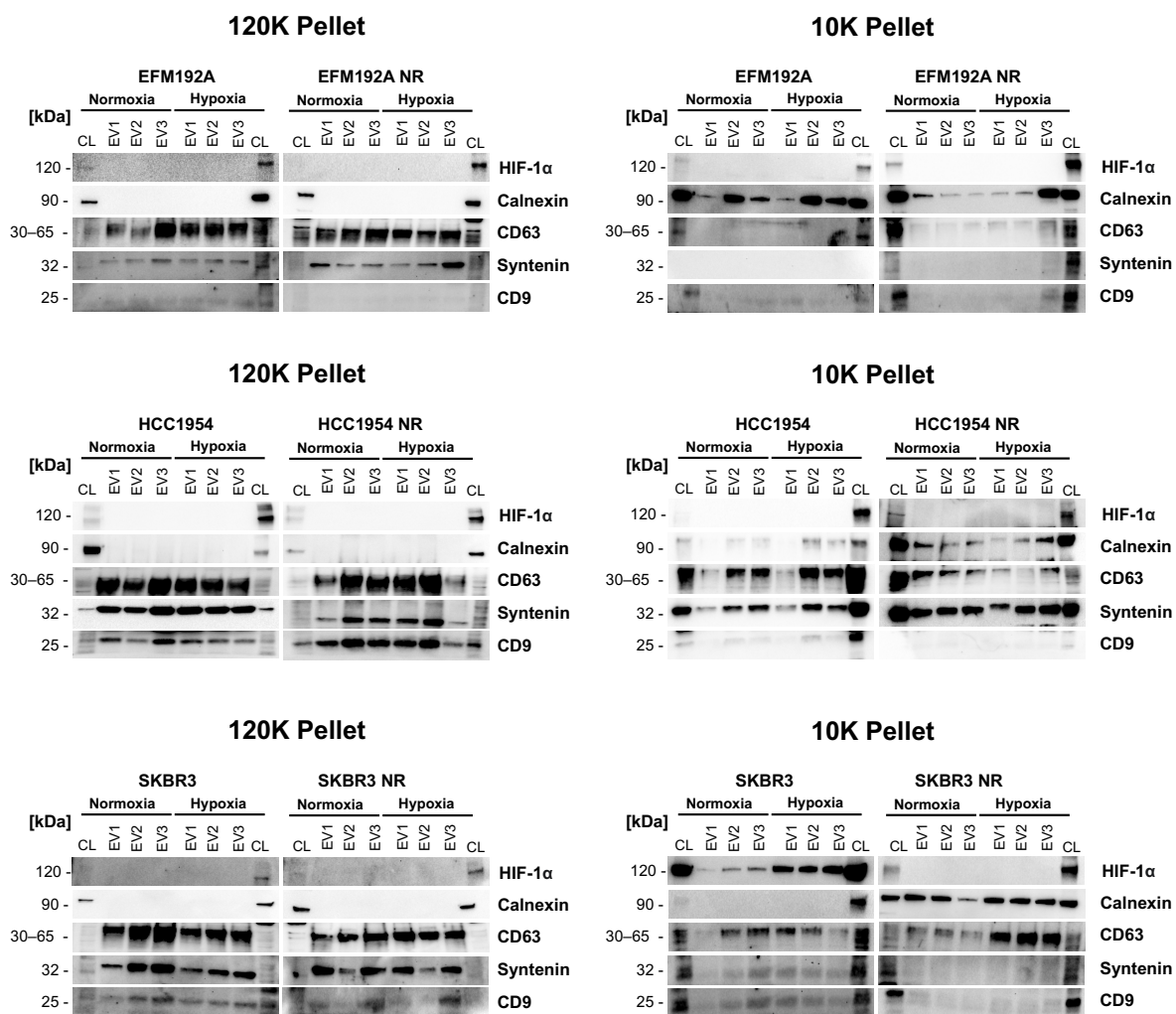
Figure 5.7. Immunoblots of EVs positive and negative markers present on the samples.
Enrichment of EVs positive and negative markers in EVs samples and cellular lysates (CL) analysed by immunoblotting in normoxic and hypoxic conditions. Ten µg of protein was equally loaded per lane and analysed for HIF-1α, Calnexin, CD63, Syntenin and CD9. Immunoblots images for three independent experiments. EV1, EV2, and EV3 refers to which replicate belongs each sample.

5.4.2.3 Particle size and yield of EVs separated from HER2+ breast cancer cells differ based on normoxic and hypoxic conditions

The average sizes and particle concentration of the 120K EVs isolates separated from CM by dUC and analysed by NTA are shown in **Figure 5.8**. In general terms, the particle size was higher in EVs samples obtained from hypoxic conditions when compared with normoxia samples (with the exception of HCC1954 NR-derived EVs), but those differences were only significant between EFM192A NR EVs isolates (*p*=0.006).
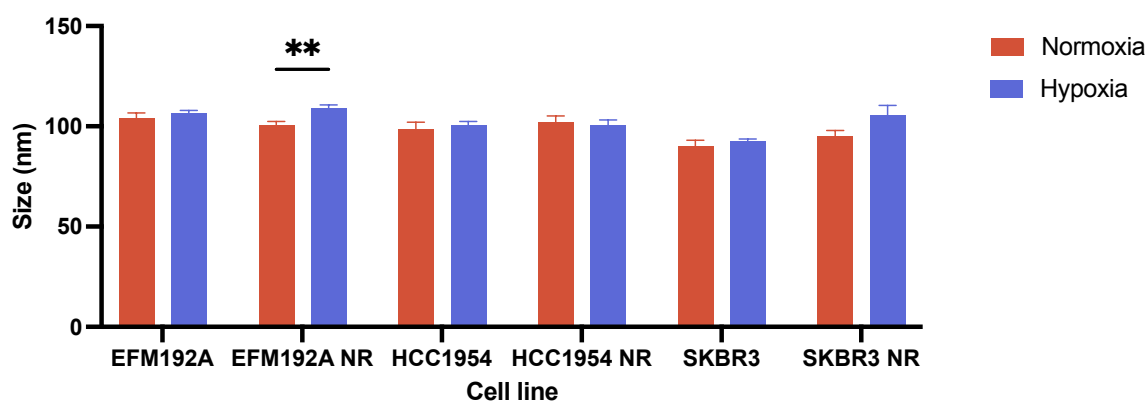
Figure 5.8. EVs' size measured by NTA.

Average sizes of the samples estimated by NTA of 120K EVs released under normoxic or hypoxic conditions. Error bars represent mean ± SEM (*n* = 5). Paired t-test used to calculate significance: **$p<0.01$.

Regarding the particle yield determined by NTA in the 120K EVs samples, significantly higher particle numbers between 30-150 nm were obtained in EVs isolates obtained from HCC1954 (2.47-fold; *p* = 0.029) and HCC1954 NR (1.85-fold, *p* = 0.032) under hypoxic conditions. No significant differences were found between normoxic and hypoxic conditions in the other four cell lines. It is noteworthy, however, that as it was found before using other EVs separation methods, the HCC1954 NR cell variant seemed to release fewer EVs than their neratinib-sensitive counterparts, in both normoxia and hypoxia conditions (3.2-fold in normoxia, *p* = 0.386; 3.6-fold in hypoxia, *p* = <0.0001) (**Figure 5.9**). The NTA representative size distribution graphs with the mean sizes are provided in the **Appendix IV** (**Figure IV-1**). The mean size and particle quantities of the EVs samples are detailed in **Table 5.17**.
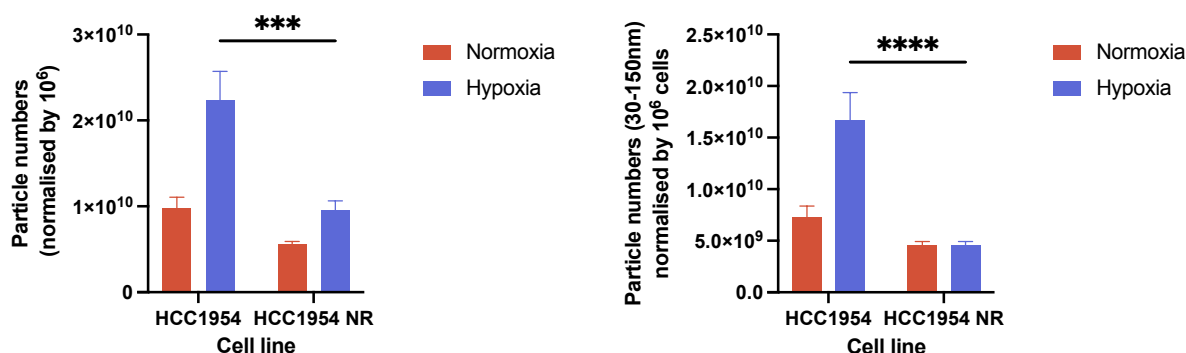
Figure 5.9. Particle numbers measured by NTA.

Quantification of EVs particle numbers estimated by NTA in HCC1954 and HCC1954 NR cell line variants. Particle amounts was significantly lower in the HCC1954 NR-derived isolates compared with their neratinib-sensitive counterparts in both normoxic and hypoxic conditions. Error bars represent SEM (n = 5). Two-way *ANOVA* was used to calculate the significance: ***p<0.001, ****p<0.0001.

Table 5.17. EVs sizes and quantities as evaluate by NTA.

	Size (nm)		
	Condition	Mean ± SEM	p value
EFM192A	Normoxia	104.12 ± 2.52	0.460 (ns)
	Hypoxia	106.62 ± 1.27	
EFM192A NR	Normoxia	100.52 ± 1.91	0.006 (**)
	Hypoxia	109.22 ± 1.48	
HCC1954	Normoxia	98.28 ± 3.73	0.386 (ns)
	Hypoxia	100.42 ± 2.05	
HCC1954 NR	Normoxia	101.88 ± 2.29	0.668 (ns)
	Hypoxia	100.34 ± 2.79	
SKBR3	Normoxia	90.18 ± 2.88	0.428 (ns)
	Hypoxia	92.58 ± 1.06	
SKBR3 NR	Normoxia	94.86 ± 3.03	0.144 (ns)
	Hypoxia	105.56 ± 4.88	
	Particle numbers (normalised by 10^6 cells)		
	Condition	Particle numbers normalised to 10^6 cells ± SEM	Fold change	p value
EFM192A	Normoxia	$1.65×10^{10} ± 5.75×10^9$	↑1.62	0.194 (ns)
	Hypoxia	$2.68×10^{10} ± 1.18×10^{10}$		
EFM192A NR	Normoxia	$7.21×10^9 ± 9.16×10^8$	↑1.3	0.125 (ns)
	Hypoxia	$9.18×10^9 ± 3.71×10^8$		
HCC1954	Normoxia	$9.72×10^9 ± 1.33×10^9$	↑2.29	0.01(**)
	Hypoxia	$2.23×10^{10} ± 3.18×10^9$		
HCC1954 NR	Normoxia	$5.58×10^9 ± 3.23×10^8$	↑1.7	0.012 (*)
	Hypoxia	$9.48×10^9 ±1.16×10^9$		

	Condition	Particle numbers normalised to 10^6 cells ± SEM	Fold change	p value
SKBR3	Normoxia	$6.61\times10^{10} \pm 1.03\times10^{10}$	n.d.	0.932 (ns)
	Hypoxia	$6.78\times10^{10} \pm 1.15\times10^{10}$		
SKBR3 NR	Normoxia	$5.72\times10^{10} \pm 5.17\times10^{9}$	n.d.	0.433 (ns)
	Hypoxia	$6.59\times10^{10} \pm 8.39\times10^{9}$		
Particle numbers 30-150 nm (normalised by 10^6 cells)				
	Condition	Particle numbers normalised to 10^6 cells ± SEM	Fold change	p value
EFM192A	Normoxia	$1.32\times10^{10} \pm 5.28\times10^{9}$	↑1.5	0.272 (ns)
	Hypoxia	$1.99\times10^{10} \pm 8.70\times10^{9}$		
EFM192A NR	Normoxia	$9.51\times10^{9} \pm 4.90\times10^{9}$	↑1.8	00.564 (ns)
	Hypoxia	$1.73\times10^{10} \pm 1.97\times10^{10}$		
HCC1954	Normoxia	$7.29\times10^{9} \pm 1.08\times10^{9}$	↑2.3	0.014 (*)
	Hypoxia	$1.66\times10^{10} \pm 2.73\times10^{9}$		
HCC1954 NR	Normoxia	$4.3\times10^{9} \pm 2.39\times10^{8}$	↑1.9	0.003 (**)
	Hypoxia	$7.69\times10^{9} \pm 6.29\times10^{8}$		
SKBR3	Normoxia	$4.98\times10^{10} \pm 7.51\times10^{9}$	n.d.	0.93 (ns)
	Hypoxia	$5.11\times10^{10} \pm 8.27\times10^{9}$		
SKBR3 NR	Normoxia	$4.48\times10^{10} \pm 5.27\times10^{9}$	↑1.3	0.718 (ns)
	Hypoxia	$4.83\times10^{10} \pm 6.61\times10^{9}$		

Comparison of number of particles/10^6 cells (analysed by NanoSight) from samples collected from neratinib-sensitive cell variants and their neratinib-resistant counterparts under hypoxic and normoxic conditions. Fold change is calculated as hypoxia/normoxia ratio (*p<0.05, **p<0.01). n.d. = no differences; ns = not significant.

5.4.2.4 Characterisation of EVs by TEM

Representative TEM pictures of EFM192A, EFM192A NR, HCC1954, HCC1954 NR, SKBR3 and SKBR3 NR -derived EVs are shown in **Figure 5.10**. Inspection of EVs revealed their integrity in most cases.

	Normoxia	Hypoxia
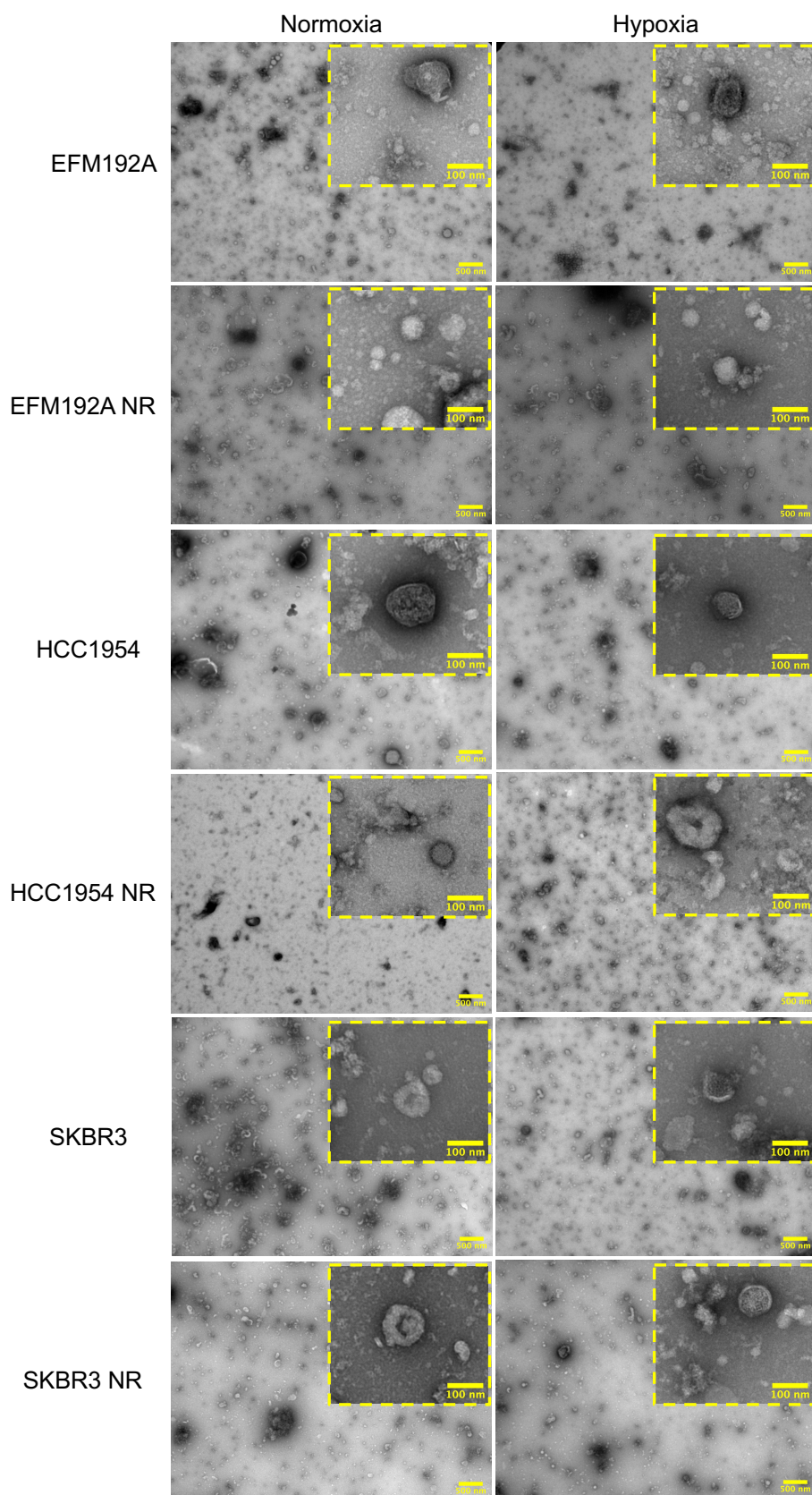
Figure 5.10. Representative images obtained by TEM.

EVs isolates enriched by using dUC protocol from three pairs of HER2+ breast cancer cell line variants under normoxic and hypoxic conditions. Big pictures represent a zoomed-out view (5000x; Scale bar = 500 nm), while the edged pictures depict a zoomed-in view (30000x; Scale bar = 100 nm) of the same spot.

5.4.2.5 Imaging flow cytometry

NTA can determine the size distribution and offer a rough estimate of the concentration of individual nanoparticles in a suspension, but it cannot be used to determine EVs' phenotype. On the other hand, TEM can capture images of particles smaller than 1 nm, but it is a time-consuming process. To assess these limitations, IFCM has emerged over the past few years as a technique that can effectively discriminate and analyse single EVs[309]. Several research groups have demonstrated IFCM's ability to detect submicron particles using fluorescent polystyrene beads or EVs derived from cell supernatants[310,311].

120K and 10K samples from normoxia and hypoxia were analysed by IFCM for CellMask® (plasma membrane marker) and HER2 (**Figures 5.11 – 5.13**). As happened with other characterisation methodologies, IFCM displayed different effects of hypoxia in the release of EVs depending on the cell line variant. While EFM192A and HCC1954 (p = 0.037) showed a decrease of CellMask+ events in hypoxia, EFM192A NR, SKBR3, and SKBR3 NR presented a slightly increase under hypoxia condition for those events. No differences were found for the samples obtained from HCC1954 NR cells between normoxia and hypoxia.

Double-positive events for CellMask and HER2 were also analysed. 120K EVs isolates derived under hypoxic conditions by EFM192A NR (p=0.037), SKBR3 (p = 0.026), and SKBR3 NR (p = 0.01537) exhibited an increase in those double-positive events. However, a significant decrease of double-positive events was found in the case of HCC1954-derived samples (p = 0.02) under hypoxia. In keeping with the obtained results for CellMask+ events in EFM192A and HCC1954 NR, no significant differences were found between conditions.

10K samples displayed an increase for CellMask+ events normalised by millions of cells for EVs derived from hypoxic cells compared to their paired-normoxic counterparts, being significant for the samples obtained from EFM192A (p = 0.030), HCC1954 (p = 0.037), and from SKBR3 NR (p = 0.003). Interestingly, EVs samples derived from hypoxic HCC1954 NR cells showed a significant decrease for CellMask events (p = 0.029). Regarding the CellMask+/HER2+ population, all the samples except for HCC1954 NR EVs isolates showed an increase in CellMask+/HER2+ events under hypoxic conditions. However, these differences were only significant in the case of EFM192A NR-derived EVs (p = 0.042).
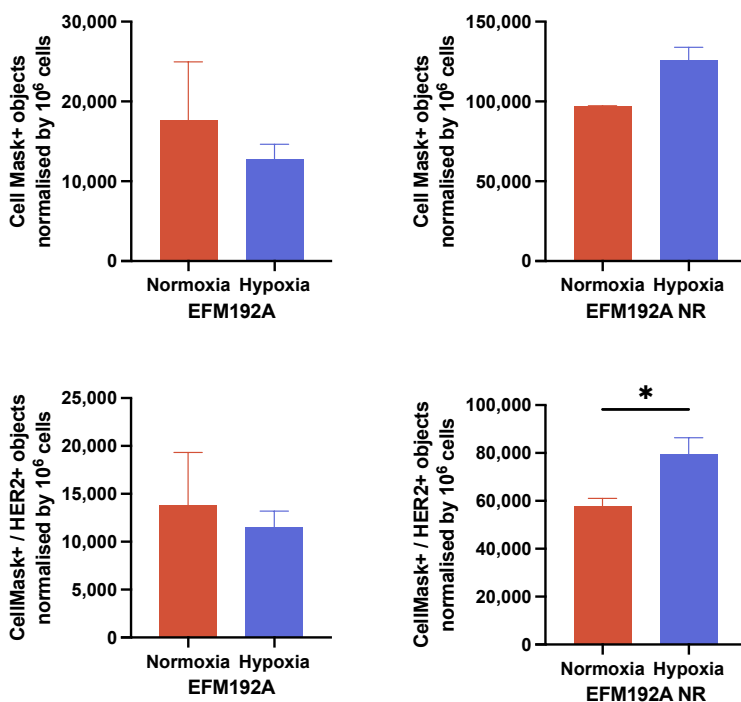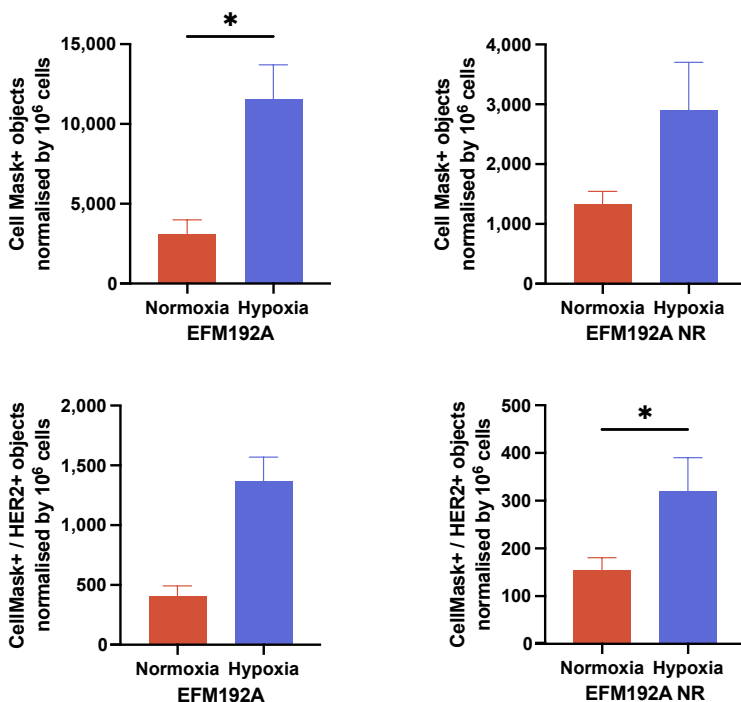
Figure 5.11. IFCM analysis of EFM192A-derived EVs.

Imaging flow cytometry (IFCM) analysis of 120K and 10K EVs samples obtained under normoxic and hypoxic conditions from EFM192A and EFM192A NR cell line variants. Data was collected by measuring the CellMask plasma membrane signal and HER2 signal separately on the 120K and 10K pellet samples obtained from EFM192A cell line variants under normoxic and hypoxic conditions. Paired t-test was used as a statistical test. *$p<0.05$ (n = 3 replicates).
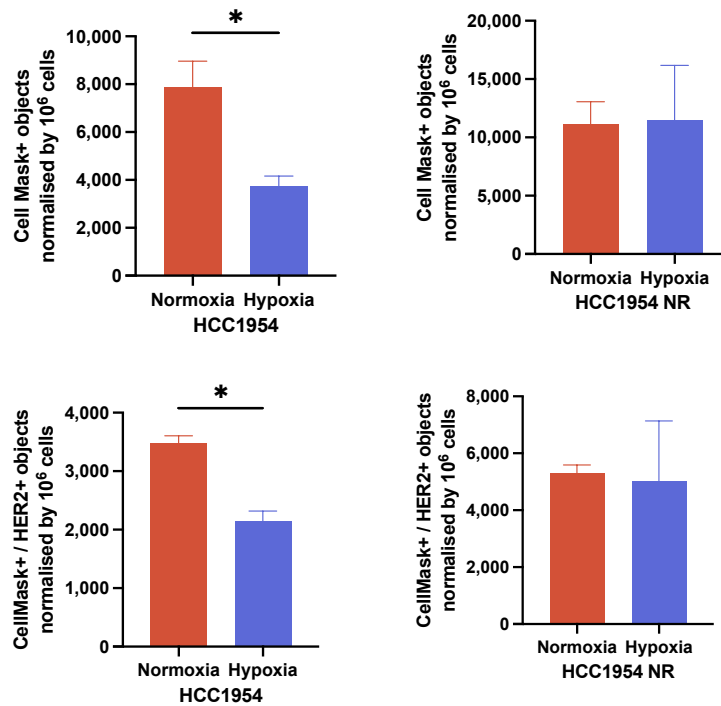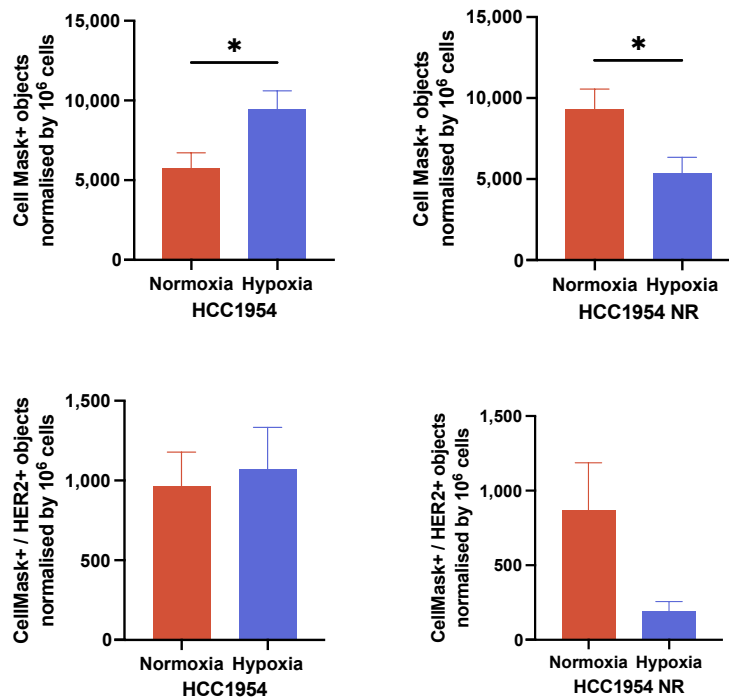
Figure 5.12. IFCM analysis of HCC1954-derived EVs.

Imaging flow cytometry (IFCM) analysis of 120K and 10K EVs samples obtained under normoxic and hypoxic conditions from HCC1954 and HCC1954 NR cell lines. Data was collected by measuring the CellMask plasma membrane signal and HER2 signal separately on the 120K and 10K pellet samples obtained from HCC1954 cell line variants under normoxic and hypoxic conditions. Paired t-test was used as a statistical test. *$p<0.05$ (n = 3 replicates).
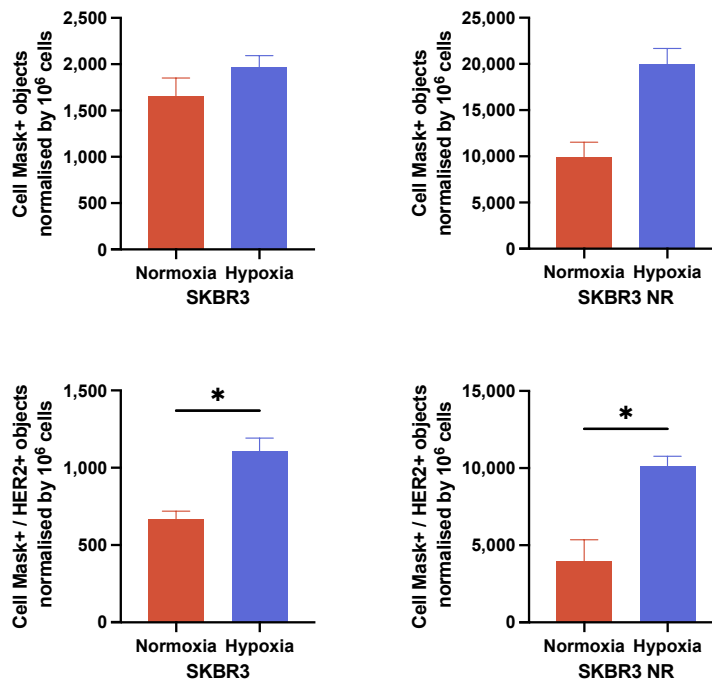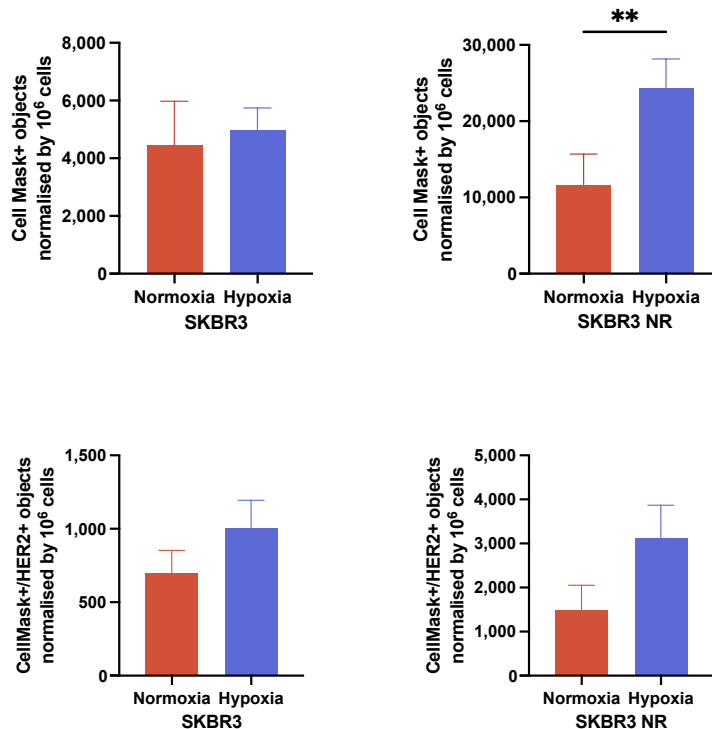
Figure 5.13. IFCM analysis of SKBR3-derived EVs.

Imaging flow cytometry (IFCM) analysis of 120K and 10K EVs samples obtained under normoxic and hypoxic conditions from SKBR3 and SKBR3 NR cell lines. Data was collected by measuring the CellMask plasma membrane signal and HER2 signal separately on the 120K and 10K pellet samples obtained from SKBR3 cell line variants under normoxic and hypoxic conditions. Paired t-test was used as a statistical test. *$p<0.05$, **$p<0.01$ ($n = 3$ replicates).

5.4.3 Investigating the EVs surface/cargo under hypoxic conditions

Different genes could be differentially expressed in response to low oxygen levels, or hypoxia. Hypoxia gene signatures have been identified in various cell types and tissues, including cancer cells and normal cells, and are typically used to assess the degree of hypoxia in each sample or to classify patients based on their hypoxic status[312,313].

In keeping with this, recent studies showed that the loss of E-cadherin, a cell adhesion molecule that plays an important role in cell-cell adhesion and maintaining tissue integrity, is associated with increased invasiveness and metastasis[314–316]. Hypoxia, or low oxygen levels, is known to promote EMT and the loss of E-cadherin in cancer cells, which contributes to their increased invasiveness and resistance to therapy[288,317]. We evaluated the expression of E-cadherin after exposing neratinib-sensitive and neratinib-resistant cell lines to 48 hrs hypoxia conditions as well as the presence of E-cadherin in the surface of the EVs released by those cells by ELISA (**Figure 5.14A**). Only significant differences were found on the cell lysate samples in SKBR3 cell variants. While SKBR3 showed a decreased of E-cadherin expression (1.60-fold, p = 0.036) after 48 hrs hypoxic conditions, SKBR3 NR showed an increase under this condition, being significantly higher the E-cadherin expression in NR cell variants than their counterparts in hypoxia (p = 0.012). Moreover, EVs released by all the cell line variants under hypoxic conditions, showed a higher presence of E-cadherin in their surface (**Figure 5.14B**). These differences were significant in both EFM192A neratinib-sensitive and neratinib-resistant cell variants, (p = 0.001 and p = 0.0004, respectively) and HCC1954 (p = 0.002) when compared with normoxic conditions. Noticeably, the levels of E-cadherin on EVs released under hypoxia were lower in HCC1954 NR-derived EVs compared to HCC1954-derived EVs (p = 0.0004).
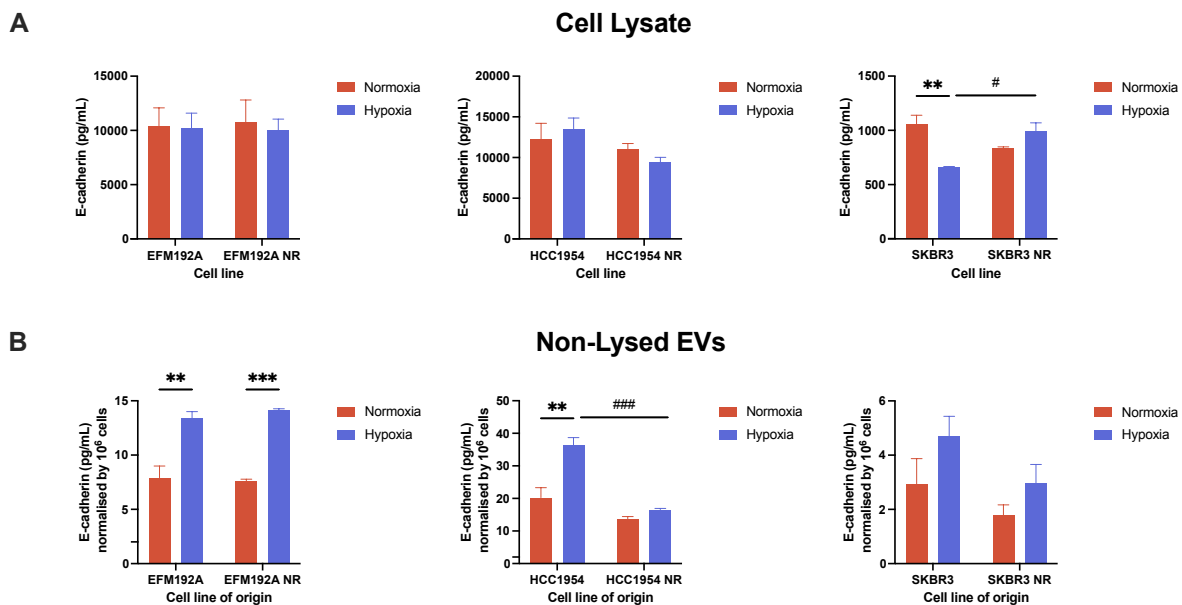
Figure 5.14. E-cadherin ELISA analysis.

Effect of hypoxia on (**A**) E-cadherin production and (**B**) its presence on 120K EVs isolates obtained by differential ultracentrifugation. Data are represented as mean ± SEM (n = 3). Paired t-test used to calculate significance between hypoxia and normoxia control (*p<0.05, **p<0.01, ***p<0.001), while 2-way *ANOVA* was used to calculate significance between neratinib-resistant and neratinib-sensitive control (#p<0.05, ###p<0.001).

On the other hand, we also evaluated the presence of pro-inflammatory cytokines (IL-6 and IL-8) in EVs released by those cells, as well as their expression in the cells of origin by ELISA. IL-6 is a pro-inflammatory cytokine that is involved in the regulation of immune responses, haematopoiesis, and cell proliferation while IL-8 is involved in the recruitment of neutrophils and other immune cells to sites of inflammation and cancer. It has been shown that both IL-6 and IL-8 are up-regulated in various types of cancer, including breast cancer, and they are associated with poor prognosis[318,319]. In addition, hypoxia has been shown to increase IL-6 and IL-8 expression through the activation of HIF-1α[320,321].

IL-6 was found to be up-regulated under hypoxic conditions in al the six cell lines, being significant in the case of EFM192A (p <0.0001), EFM192A NR (p = 0.0007), SKBR3 (p <0.0001), and SKBR3 NR (p = 0.0005) (**Figure 5.15**). No significant difference in the levels of IL-6 were found in the whole cell lysate from HCC1954 and HCC1954 NR. However, the increase in the presence of IL-6 on the EVs derived under hypoxia was significant in all samples, independently to the cell of origin. Noteworthy to mention that the levels of IL-6 on those EVs released by neratinib-sensitive cell lines seemed to be higher than the ones released by NR cell variants in both normoxia and hypoxia conditions, being those differences significant between EVs derived from hypoxic HCC1954 and HCC1954 NR cell variants (p = 0.004).
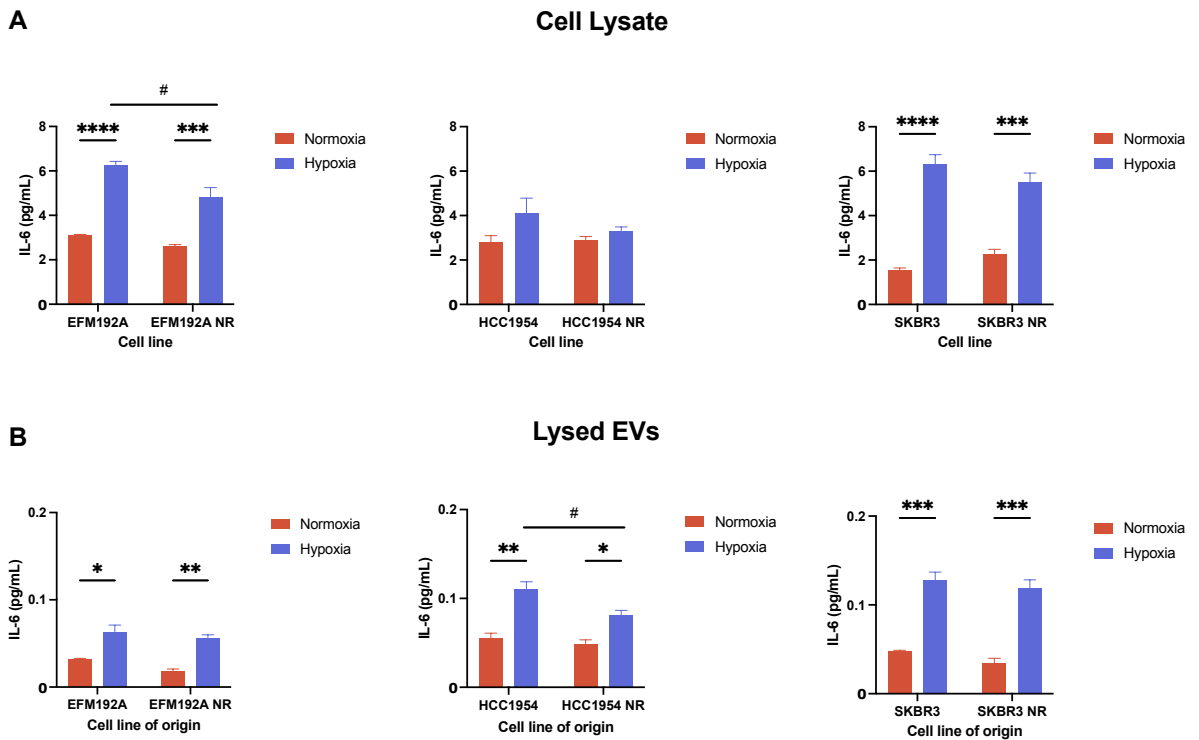
Figure 5.15. IL-6 ELISA analysis.

Effect of hypoxia on (**A**) cytokine IL-6 production and (**B**) its presence in EVs samples. Data are represented as mean ± SEM (n = 3). Paired t-test used to calculate significance between hypoxia and normoxia control (*$p<0.05$, **$p<0.01$, ***$p<0.001$, ****$p<0.0001$), while 2-way *ANOVA* was used to calculate significance between neratinib-resistant and neratinib-sensitive control (#$p<0.05$).

IL-8 was only detected in HCC1954 and HCC1954 NR samples (**Figure 5.16**). Although no differences were observed between normoxia and hypoxia in both cell lines, we appreciated a significant reduction in IL-8 expression in HCC1954 NR compared to HCC1954. Interestingly, the levels of IL-8 in both HCC1954 and HCC1954 NR-derived EVs were similar.
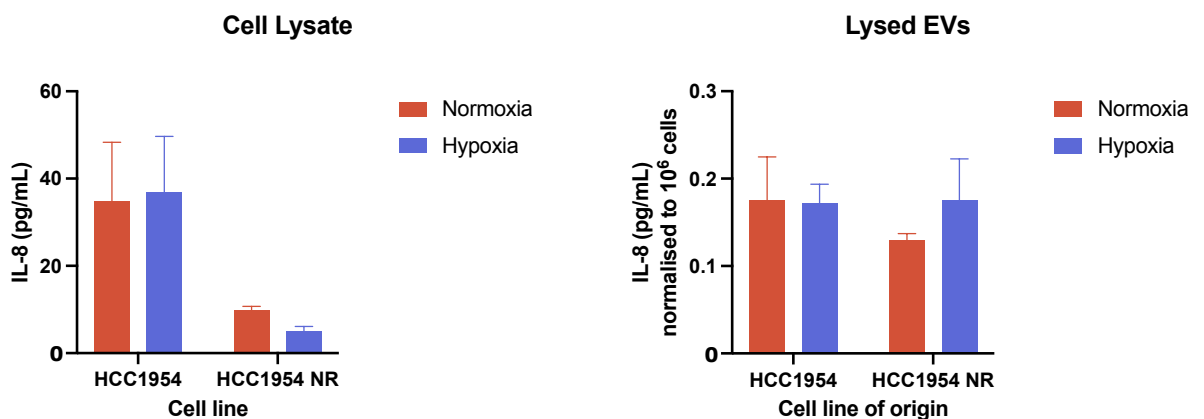
Figure 5.16. IL-8 ELISA analysis.

Effect of hypoxia on (**Left**) cytokine IL-8 production and (**Right**) its presence in EVs samples. IL-8 was not found in samples from EFM192A and SKBR3 cell variants. Data are represented as mean ± SEM (n = 3).

Finally, we investigated the presence of HER2 on the surface on those EVs and the harvested cells by ELISA, to investigate if they are representative of the HER2 status of their cells of origin and to shed a light on the HER2 pathway under hypoxic conditions and its relevance in neratinib-resistance. Although no significant differences were found in the level of HER2 between normoxia and hypoxia conditions on the cells, the presence of HER2 was higher on the surface of EVs released under hypoxia, being significant on those released by hypoxic EFM192A NR ($p = 0.005$), HCC1954 ($p = 0.003$), and HCC1954 NR ($p = 0.0003$) cells (**Figure 5.17**). In the case of EFM192A-derived EVs, this increase presence of HER2 under hypoxia was substantial ($p = 0.058$). We demonstrate here that under hypoxic conditions, EVs contained in their surface more HER2 receptor that those release under normal levels of oxygen.
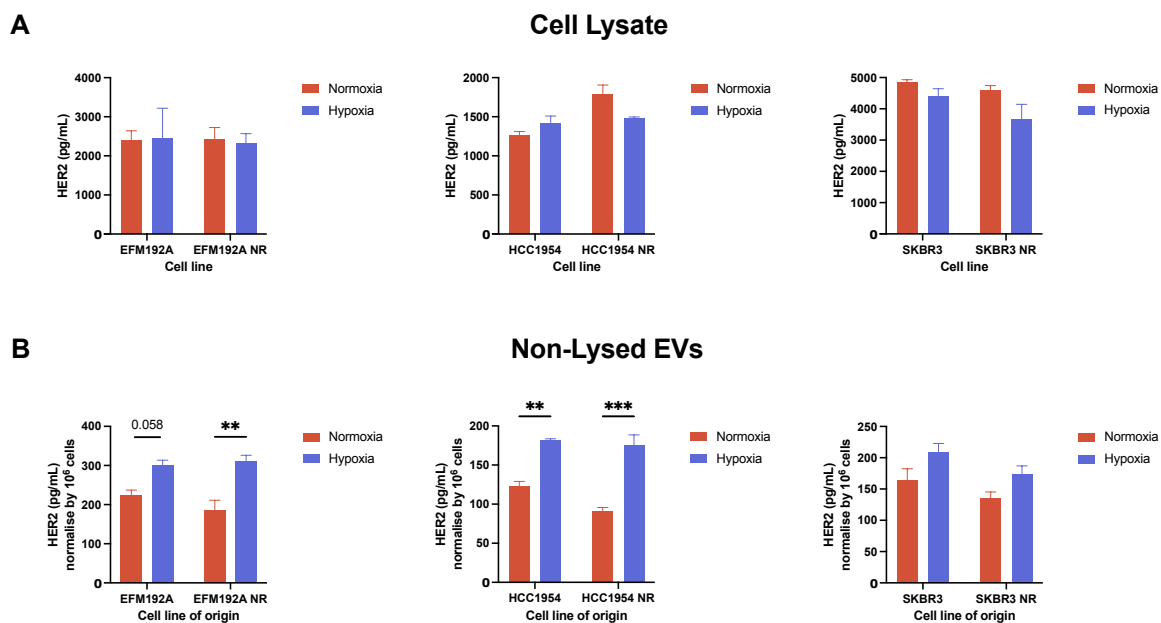
Figure 5.17. HER2 ELISA analysis.

Effect of hypoxia on (**A**) HER2 expression and (**B**) its presence on EVs samples. Data are represented as mean ± SEM ($n = 3$). Paired t-test used to calculate significance between hypoxia and normoxia control: *$p<0.05$, **$p<0.01$, ***$p<0.001$.

5.4.4 Evaluating the miR-content of EVs

As explained in **Section 5.1**, miRNAs are a class of small non-coding RNAs that play important roles in gene regulation. Dysregulation of miRNA expression has been implicated in the development and progression of various types of cancer. It has been demonstrated that hypoxia can induce changes in the expression of miRNAs, which can in turn impact the expression of target genes involved in cancer progression, such as angiogenesis, cell proliferation, and apoptosis[300].

The transfer of miRNAs via EVs represents a potential mechanism for cancer cells to modulate the behaviour of other cells in the TME and may represent a novel target for cancer therapy. By disrupting EVs-mediated transfer of miRNAs, it may be possible to inhibit the spread of pro-tumorigenic signals in the TME and limit cancer progression.

We investigated here the hypoxia-regulated miRNAs content of EVs released by the different neratinib-sensitive and neratinib-resistant cell lines to find any connection between resistance to neratinib and a higher expression of those miRNAs.

Pellets were directly lysed following the methodology explained previously in **Section 5.3.7.2**. Although no significant differences were found in the content of RNA between normoxia and hypoxia conditions, EVs from HCC1954, and SKBR3 NR seemed to have a higher RNA concentration than EFM192A-EVs in normoxic conditions. Under low levels of oxygen, EVs obtained from HCC1954, HCC1954 NR, SKBR3 and SKBR3 NR presented a higher RNA content than EFM192A and EFM192A NR. RNA yields (ng/µl normalised to million cells) and RNA purities (A260/A230; A260/280) for each sample are collected in the **Appendix IV** (**Table IV-1** and **Figure IV-3**).

The four mentioned miRNAs were chosen based on literature review for RT-qPCR analysis, along with one exogenous normalizer miRNAs (*cel-miR-39*) (**Figure 5.18**). All four miRNAs were detected by RT-qPCR in samples obtained from EFM192A, EFM192A NR, SKBR3 and SKBR3 NR. However, no amplification was detected for miR-630 for both HCC1954 and HCC1954 NR EVs samples and their respective cell controls. In EFM192A, EFM192A, SKBR3 and SKBR3 NR-derived EVs, miR-630 was found to be decreased in hypoxic condition with a 1.27-fold (p = 0.086), 1.95-fold (p = 0.072), 2.31-fold (p = 0.036) and 1.90-fold (p = 0.036) lower in EVs released under hypoxia, respectively. Interestingly, no significant differences were observed for miR-155-5p except for the HCC1954 NR-derived EVs, with a 3.3-fold (p = 0.037) higher in hypoxia. Higher or lower presence of miR-155-5p in hypoxia was dependent on the cell line, decreasing its presence exclusively on the EVs derived from hypoxic HCC1954 cells.

The most relevant was miR-210-3p, with a 10.4-fold (p = 0.003) and 8-fold (p = 0.036) higher in EVs derived from hypoxic SKBR3 and SKBR3 NR cells, respectively. EVs derived from hypoxic HCC1954 and HCC1954 NR showed a similar trend, with an increase of 3.3-fold (p = 0.03) and 4.3-fold (p = 0.002) compared to those released under normoxia conditions, respectively. Although its presence in EVs derived from hypoxic EFM192A cells was higher (7.614-fold), it was not significant due to variability between biological samples. Remarkably, miR-21 was found to be significant decreased in EVs derived exclusively from hypoxic HCC1954 (2.26-fold; p = 0.015) and EFM192A NR cells (1.25-fold; p = 0.124), while its relative expression was higher in EVs derived from hypoxic EFM192A (p = 0.924), HCC1954 NR (2.17-fold; p = 0.347), SKBR3 (2.86-fold; p = 0.012), and SKBR3 NR cells (1.7-fold; p = 0.462). Noticeably, the RT-qPCR results showed considerable biological variability between samples for the different hsa-miRNAs evaluated here. This variability is clear from the high standard error (SE) in many of the miRNAs examined via RT-qPCR.
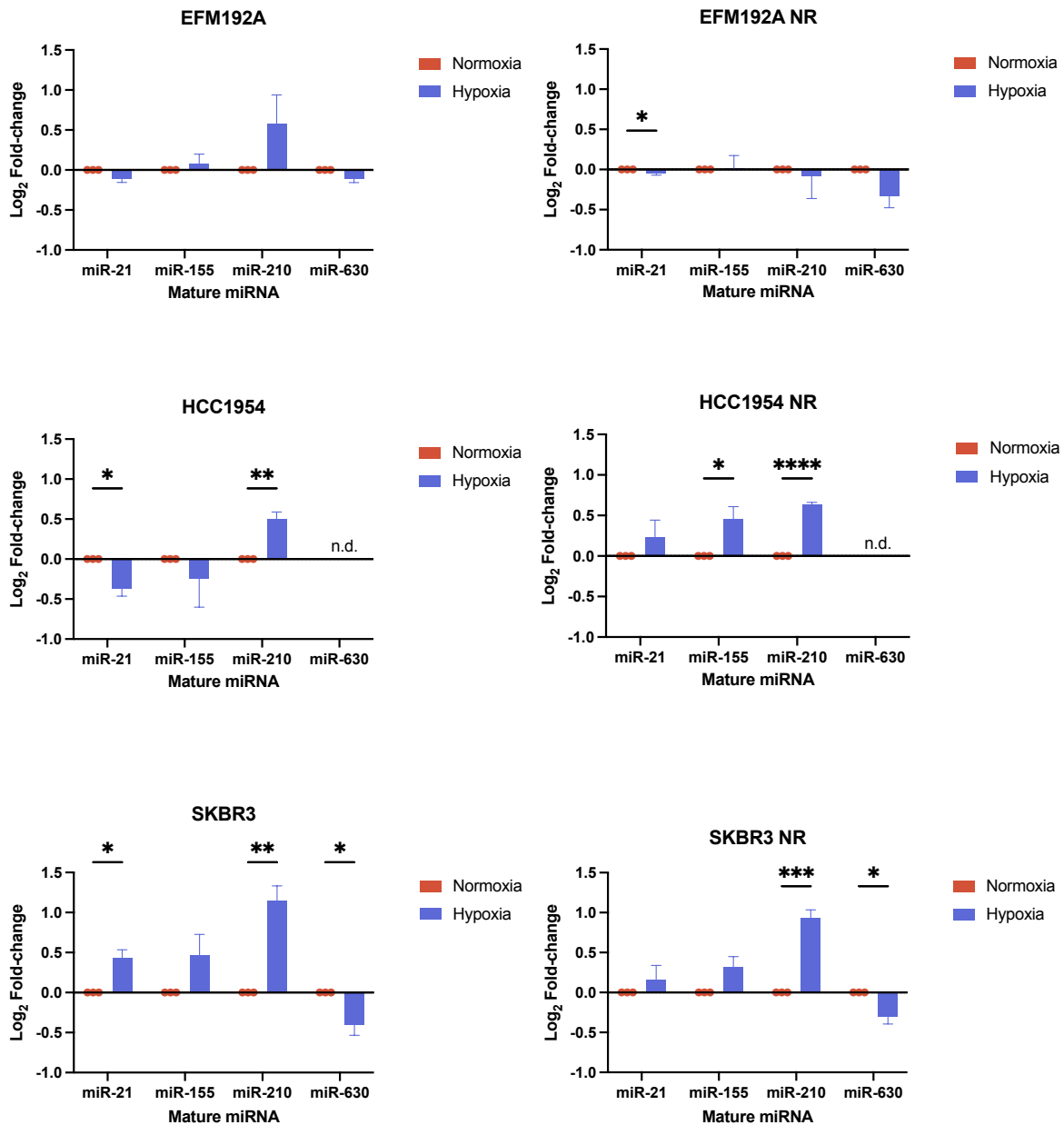
Figure 5.18. miRNA cargo levels in the EVs isolates.

Micro-RNA (miRNA) cargo levels of four miRNAs on EVs derived from different six cell line variants under normoxic and hypoxic conditions. *$p<0.05$, **$p<0.01$, ***$p<0.001$, ****$p<0.0001$; n.d.= not detected.

5.4.5 Summary of findings

Table 5.18 brings together the main observations in the EVs characterisation and analysis of its cargo under normoxic and hypoxic conditions.

Table 5.18. List of main observations from the EVs characterisation and the analysis of EVs' cargo.

120K						
Assay	EFM192A	EFM192A NR	HCC1954	HCC1954 NR	SKBR3	SKBR3 NR
Protein amount	↑ (*)	↑ (*)	↑ (**)	↑ (**)	↑ (*)	↑ (*)
EVs markers (Immunoblots)	n.d.	n.d.	n.d.	n.d.	↓CD9 (*)	↓Syntenin (*)
NTA: Particle size	n.d.	↑ (**)	n.d.	n.d.	n.d.	n.d.
NTA: Particle number	↑ (ns)	↑ (ns)	↑ (**)	↑ (*)	n.d.	n.d.
NTA: Particle number (30-150 nm)	↑ (ns)	↑ (ns)	↑ (*)	↑ (**)	n.d.	↑ (ns)
IFCM (CellMask+)	↓ (ns)	↑ (ns)	↓ (*)	n.d.	n.d.	↑ (ns)
IFCM (CellMask+/ HER2+)	n.d.	↑ (*)	↓ (*)	n.d.	↑ (*)	↑ (*)
E-cadherin	↑ (**)	↑ (***)	↑ (**)	n.d.	↑ (ns)	↑ (ns)
IL-6	↑ (*)	↑ (**)	↑ (**)	↑ (*)	↑ (***)	↑(***)
IL-8	ND	ND	n.d.	n.d.	ND	ND
HER2	↑ (ns)	↑ (**)	↑ (**)	↑ (***)	↑ (ns)	↑ (ns)
miR-21	↓ (ns)	↑ (*)	↓ (*)	↑ (*)	↑ (*)	↑ (ns)
miR-155	↑ (ns)	n.d.	↓ (ns)	↑ (*)	↑ (ns)	↑ (ns)
miR-210	↑ (ns)	n.d.	↑ (**)	↑ (****)	↑ (**)	↑ (***)
miR-630	↓ (ns)	↓ (ns)	ND	ND	↓ (*)	↓ (*)
10K						
Assay	EFM192A	EFM192A NR	HCC1954	HCC1954 NR	SKBR3	SKBR3 NR
Protein amount	↑ (ns)	n.d.	↑ (**)	↑ (**)	↑(ns)	↑ (*)
EVs markers (Immunoblots)	n.d.	n.d.	n.d.	n.d.	n.d.	↑CD63 (*)
IFCM (CellMask+)	↑ (*)	↑ (ns)	↑ (*)	↓ (*)	n.d.	↑ (**)
IFCM (CellMask+/ HER2+)	↑ (ns)	↑ (*)	n.d.	↓ (ns)	↑ (ns)	↑ (ns)

Arrows refers to the increase (↑) or decrease (↓) under hypoxia compared with normoxia for the different parameters. No differences (n.d.) was defined as a fold-change (hypoxia vs. normoxia) ~1; ns= not significant; ND= not detected; *p<0.05, **p<0.01, ***p<0.001, ****p<0.0001.

5.5 Discussion

Hypoxia is a common feature of solid tumours that has been associated with tumour progression, invasion, metastasis, and resistance to therapy. EVs have been shown to be involved in the adaptation of cancer cells to hypoxic conditions. In addition, EVs released by hypoxic cancer cells can transfer HIFs to recipient cells, which can activate genes involved in angiogenesis and cell survival. The study of EVs under hypoxic conditions is an active area of cancer research, and understanding their role in tumour progression and metastasis could lead to the development of new therapeutic strategies. In this context, our aim was to characterise firstly, three neratinib-sensitive cell lines and their three counterparts under hypoxic conditions, and secondly, the EVs isolates derived from these cells.

It is "established" that the EVs' release is increased under hypoxic conditions. However, prior to our experiments, we performed literature research to clarify this affirmation. We investigated EV-TRACK knowledgebase (evtrack.org)[208], an online toolset that combines seven features to guide researchers in using the EV-METRIC for reporting experimental parameters and centralising data on EVs characteristics and methods. The EV-METRIC is a percentage reflecting the transparency of reporting experimental parameters, with nine essential components. Researchers can improve their transparency by obtaining the EV-METRIC prior to peer review, and journal editors and reviewers can access the corresponding EV-TRACK data entry. EV-TRACK allows upload of experimental parameters of already published experiments and querying of publications for specific experimental parameters not easily searchable in biomedical literature databases. We used the keyword "hypoxia" and we selected only those experiments done in human samples. We found 134 entries associated with 46 publications, but only one of those reached the 78% of EV-METRIC, two presented 67% and four obtained a score higher that 50%. Investigating the top three papers we found that only one is related with cancer. The work performed by Samoylenko et al. (2021) showed an increase in the EVs' release by renal cell carcinoma (RCC) under hypoxic conditions, but it was dependent on the EVs separation method[322]. Noticeably, hypoxia induced the production of EVs by human renal adenocarcinoma-derived 786-O cells less than compared to mouse renal adenocarcinoma-derived Renca cells. However, these results were estimated without the normalisation by millions of cells, or at least it was not specified. Here, we investigated the release of EVs under hypoxic conditions in three HER2+ breast cancer cells sensitive to neratinib and their respective neratinib-resistant counterparts. We observed a significant decrease in cell count under hypoxic conditions. It is important to have this into consideration to normalise the EVs released by the number of secreting cells. We also characterised our cells for different markers, including HER2, HIF-1α, β-catenin, CD63, CD9 and eIF4E. As expected, HIF-1α was up-regulated under hypoxic conditions in all six cell lines. When we analyse HER2 expression by immunoblotting, we did not find any significant results, being up- or down-regulated depending on the cell line. When we analysed the expression of the tetraspanins CD63 and CD9, we found a decrease on CD63 expression in EFM192A (p = 0.012), HCC1954 (p = 0.048), and SKBR3 NR (p = 0.067). However, only SKBR3 NR-derived EVs showed a decrease in CD63 as their cells of origin. In the case of CD9, significant decrease was found in

EFM192A (p = 0.019) and HCC1954 (p = 0.016) cell lines. Interestingly, the presence of CD9 in EFM192A and HCC1954-derived isolates was not affected by this reduction either. It was also found that in both EFM192A NR and HCC1954 NR, EIF4E was down-regulated under hypoxic conditions. β-catenin and eIF4E were found to be as well dependent on the cell context. β-catenin was up-regulated in hypoxic SKBR3 and SKBR3 NR cells while it was significant down-regulated in HCC1954 cell line (p = 0.016). Wnt/ β-catenin pathway has been implicated in the development of pathological events including cancer. In this perspective, β-catenin is involved in cancer proliferation, metastasis, and drug resistance among others[323]. On the other side, eIF4E participates in the general stress response and it is involved in cap-dependent mRNA translation for protein synthesis[324], that it is usually down-regulated by hypoxia affecting cell proliferation and migration.

We collected the EVs isolates derived from the six different cell lines after 48 hrs under hypoxic conditions. When we analysed the protein concentration of those isolates, the results supported the main hypotheses about the increase of EVs released under hypoxic conditions mentioned above. We found a significantly increased protein concentration measured by BCA on 120K EVs isolates derived from hypoxic condition in all six conditions compared to normoxia. Most of the published papers that mentioned this increase used this type of measure. However, this measure is not totally accurate, as might be methodology-dependent. It is very important to include different characterisation methods to determine the EVs concentration and nature of the samples. We also characterised partly the 10K isolates, finding similar results as the mentioned for 120K. However, we found a high amount of calnexin by immunoblotting. Calnexin is considered a negative EVs marker, as is not enriched usually in small EVs. Thus, 10K EVs samples were not further analysed as done with 120K EVs samples.

We also evaluated the presence of HIF-1 α by immunoblotting in both 10K and 120K EVs isolates. HIF-1α was not detected on our EVs samples, although, as indicate above, it has been shown that EVs can transfer HIFs to recipient cells. Other HIFs (HIF-2α and HIF-3α) must be investigated, as well as include different methodologies to study the presence of HIFs on the EVs. Regarding EVs markers analysed by immunoblotting in 120K EVs isolates, no significant differences were found between normoxia and hypoxia in most of the cases. The most noticeable was a down-regulation of CD63 on EVs derived from SKBR3 NR hypoxic cells discussed above. The increase of protein concentration observed is not correlated with a higher presence of those EVs markers in hypoxic conditions. Syntenin is considered a marker enriched in sEVs, CD9 is enriched in lEVs and mEVs and CD63 in the three different populations. As there are other different EVs markers that were not analysed in this chapter, we could hypothesise that a different EVs population is being released under hypoxic conditions. NTA results followed the same trend, with no significant results except for HCC1954 and HCC1954 NR-derived isolates, that presented a significant increase in particle number under hypoxic conditions (p = 0.097 and p = 0.012, respectively). It is important to mention that although not significant, EFM192A NR-derived isolates showed a decrease in particle number in the case of hypoxia. The average sizes were similar in all the samples, with a significant increase

in the EVs derived from hypoxic EFM192A NR cells when compared with normoxia (109.2 nm vs 100.5 nm, p = 0.006). TEM analysis showed a range of particle sizes in both conditions.

We also characterised the EVs by IFCM using CellMask and HER2 staining. We found discrepancies with the results obtained by other methodologies. For instance, we found a significant increase in protein concentration and particle numbers by NTA in the case of HCC1954 120K pellets, while we found a significant decrease in CellMask+ events for the same samples (p = 0.037). When 10K isolates were analysed, it was found an increase under hypoxic conditions in EFM192A (p = 0.030), EFM192A NR (p = 0.077), HCC1954 (p = 0.037), and SKBR3 NR (p = 0.003) while CellMask+ events were decreased in HCC1954 NR-derived EVs by hypoxia (p = 0.03). The presence of double positive events for CellMask and HER2 was cell line-dependent in both 10K and 120K pellets. While hypoxia increased the occurrence of CellMask+/HER2+ events in 120K samples derived from EFM192A NR (p = 0.037), SKBR3 (p = 0.026) and SKBR3 NR (p = 0.015), the opposite tendency was found in HCC1954-derived isolates (p = 0.002). Interestingly, same tendency as observed in 120K isolates was spotted in 10K isolates, with a significant increase under hypoxia in EFM192A NR-derived EVs (p = 0.042). All these results give a partial picture of how necessary is to include different characterisation methodologies to assess the effect of hypoxia in EVs' release. As per our knowledge, we are the first investigating the EVs' release under hypoxic conditions in HER2+ neratinib resistant cell lines and their sensitive counterparts. Most of the results obtained here give us the idea that hypoxia is altering the EVs' release in a cell-dependent way, although the trend would be to increase the EVs release.

Moving on to the EVs cargo, we evaluated the presence of different proteins and miRNAs that are known to be part of the hypoxic response in cancer. Firstly, we evaluated the expression of E-cadherin in the cells, as well as its presence on the EVs released by those cells. It is known that hypoxia promotes EMT and the loss of E-cadherin in cancer cells, contributing to invasion and drug resistance. After 48 hrs under hypoxic conditions, E-cadherin was only decreased in hypoxic SKBR3 cells (p = 0.012). SKBR3 NR cells showed a lower E-cadherin expression than their neratinib-sensitive counterparts. However, under hypoxic conditions, the expression of this protein increased. It is also noticeable that E-cadherin expression was significant higher in NR cell variants than their counterparts in hypoxia (p = 0.012). SKBR3 cell variants are E-cadherin-defective, with levels of E-cadherin not detectable by immunoblotting. Hypoxia conditions make those cells even more deficient of E-cadherin, connected with tumour progression and metastasis. Surprisingly, when we analysed the non-lysed EVs samples, we found an increase of E-cadherin on the membrane of the EVs derived under hypoxia in all cases, being this rise significant in EFM192A (p = 0.001), EFM192A NR (p = 0.0004), and HCC1954 (p = 0.002). When we found similar levels of E-cadherin between EFM192A and EFM192A NR-derived EVs under hypoxia, we observed a significant decrease of E-cadherin presence on HCC1954 NR-derived EVs compared to HCC1954-derived EVs under hypoxia (p = 0.0004). There are different intracellular trafficking pathways to regulate the functions of E-cadherin, including exocytic and multiple endocytic pathways[325]. When intercellular adhesion is disrupted by the depletion of extracellular Ca^{2+} ions, E-cadherin is endocytosed into endosomal vesicles.

Researchers have observed that some of the E-cadherin molecules that are actively taken up by the cell are recycled back to the basolateral plasma membrane[326]. Additionally, Lock and Stow's study showed that both newly synthesised E-cadherin and the endocytosed E-cadherin pass through Rab11-positive recycling endosomes before they can reach the plasma membrane[327]. While the primary functions of E-cadherin occur at the plasma membrane of epithelial cells, there is increasing evidence that extracellular E-cadherin is present in human body fluids. This can occur through the shedding of E-cadherin from the plasma membrane via proteolytic cleavage, producing soluble E-cadherin[328], or through the recruitment of E-cadherin to the membrane of exosomes[329]. Recently, Tang et al. (2018)[330] demonstrated that EVs exhibiting E-cadherin can promote angiogenesis *in vitro* and *in vivo* by triggering a communication between the nuclear factor-κB (NFκB) and β-catenin signalling pathways. As a result, the formation of new blood vessels leads to the advancement and spreading of ovarian cancer. Nevertheless, the specific cellular constituents that play a role in bringing E-cadherin into EVs are still unknown[331]. Here, we found that hypoxic conditions are increasing the E-cadherin presence on the EVs' surface, which might affect breast cancer invasiveness.

Then, we evaluated the expression of IL-6 on those cells. IL-6, a key player in the inflammatory response, is a major contributor to the development of cancer. When cancer cells are exposed to IL-6 or secrete it as an autocrine factor, they display malignant characteristics, including intensified ability to infiltrate the ECM and enhanced resistance to drugs[332]. After 48 hrs hypoxic conditions, we found an increase of IL-6 in all six cell lines, being significant in EFM192A ($p<0.0001$), EFM192A NR ($p = 0.0007$), SKBR3 ($p<0.0001$) and SKBR3 NR ($p = 0.0005$). Remarkably, when comparing neratinib-sensitive and neratinib-resistant cells under hypoxia, we observed that neratinib-resistant cell lines revealed a lower expression of IL-6 than their neratinib-sensitive counterparts, being this difference significant for EFM192A cell variants ($p = 0.0108$). We observed the same trend on the EVs lysates obtained from those cells, being significant this increment in all six cases. Differences between hypoxic HCC1954 and HCC1954 NR-derived EVs were also significant ($p = 0.04$), being lower in neratinib resistant-derived isolates.

EVs are not only capable to deliver cytokines to distant target cells but also can improve the production of interleukins under cytotoxic stress conditions, facilitating tumour progression, and protect them from degradation by encapsulation[333,334]. The liberation of cytokines, whether in the form of EVs or freely circulating molecules, may signify an adjustment to specific physiological requirements. This is particularly relevant to determine whether these cytokines are required to function near the producing cell or at a distance.

In keeping with this, we also analysed the expression of IL-8, a CXC chemokine that induces angiogenesis, migration, cell proliferation and invasion. Its expression by tumour cells can influence their metastatic capacities. IL-8 was only detected in HCC1954 cell variants and their EVs. No significant differences were found between hypoxic and normoxic conditions. However, lower levels of IL-8 were found in HCC1954 NR samples. Nevertheless, it must be taken into account that the

non-detection of this interleukin on the surface of the EVs does not necessarily imply its absence as EVs' cargo.

We also analysed by ELISA the presence of HER2 on the EVs surface as well as the cell lysates of the cells of origin. No significant differences were found on cell lysates between normoxia and hypoxia. However, the trend was similar in all six cell lines, by reducing the HER2 expression under hypoxia. While it is known that HER2 can activate HIF-1α[175,335], there is limited evidence to suggest that HIF-1α can directly down-regulate HER2 expression[336]. According to a study conducted on clinical samples of breast cancer, it was found that HIF-2α levels were notably higher in samples that overexpressed HER2 receptors. This implies that the regulation of HIF-2α, rather than HIF-1α, may be influenced by HER2[337]. When we analysed the surface of the EVs derived from those cells, we found an increase of HER2 presence on the EVs derived under hypoxia compared with their normoxic counterparts. This increase on HER2-EVs surface may be related with HER2 trafficking. Research performed by Chandran et al. (2020) found that hypoxia can reduce the effectiveness of the breast cancer drug trastuzumab (Herceptin) by decreasing its uptake into cancer cells. They also found that hypoxia reduced the expression of HER2 on the surface of cancer cells, as well as the expression of P-glycoprotein and phosphorylated CAV-1 expression, which are associated with reduced trastuzumab uptake and HER2 signalling in breast cancer cells[338]. Other previous studies have demonstrated that CAV1 is involved in regulating downstream signalling of members of the HER family, as well as interfering with the activity of antibodies or ADCs targeting this family[339–343]. Pereira et al. (2018) observed in their study a direct impact of the inverse correlation between CAV1 and HER2 cellular expression on the stability and localisation of HER2 on the cell membrane, in consistency with previous reports that have shown CAV1's interaction with EGFR signalling[344]. In addition, HER2 localisation on the cell membrane is a dynamic process involving endocytosis, cytoplasmic recycling, and de novo synthesis. Additionally, HER2 membrane localisation can be heterogeneous within tumours. These findings suggest that hypoxia may contribute to the development of resistance to anti-HER2 therapies, and that strategies to overcome hypoxia in tumours may improve treatment outcomes.

Finally, we also investigated the presence of some hypoxia-related miRNAs on the EVs derived from these six HER2+ cell lines. It has been demonstrated previously that miRNAs miR-21, miR-210 and miR-155 are up-regulated under hypoxic conditions[345]. We also investigated the presence of miR-630 on those EVs as previously work performed in our group found that miR-630 down-regulation is involved with HER2-targeting drugs resistance through insulin like growth factor 1 (IGFR1) regulation[256]. Surprisingly, miR-21 was significantly down-regulated in EFM192A NR and HCC1954-derived EVs in hypoxia ($p = 0.034$ and $p = 0.015$, respectively), as well as EFM192A-derived EVs. HCC1954 NR, SKBR3 ($p = 0.012$), and SKBR3 NR-derived EVs showed an increase on miR-21 levels under hypoxic conditions. In contrast, miR-210, considered the master hypoxic-miRNA regulator, was up-regulated in all hypoxic EVs, apart from EFM192A NR-derived EVs. On the other hand, miR-155 was up-regulated in EFM192A, HCC1954 NR ($p = 0.0375$), SKBR3 and SKBR3, while it was found to be down-regulated in HCC1954-derived EVs. We also found that miR-630 was

reduced in hypoxic EVs derived by EFM192A, EFM192A NR, SKBR3 (p = 0.036), SKBR3 NR (p = 0.036) cells. Currently, there are some important limitations in general EVs miRNA research. For example, the different EVs separation methods, that can impact directly on downstream RNA profile[346,347]. Another important limitation is the lack of standardised normalisation strategies. Most studies employed endogenous reference gene sequences to standardise the abundance of miRNA and eliminate discrepancies arising from sample input or experimental variables. The key characteristic of an endogenous reference sequence is its consistent presence across the investigated conditions (including controls and cases unaffected by cancer grade or stage) to ensure precise abundance profiles. However, selecting appropriate references for miRNA studies continues to be challenging, with no consensus on the most appropriate miRNA controls in EVs. The specific encapsulation of miRNA into EVs implies that miRNA reference sequences commonly used for cell lines or tumour tissue cannot be presumed to be appropriate for use in EVs studies. Prior to application, within-sample validation is necessary[286]. For example, small nuclear RNA U6 (snU6) is broadly used as a miRNA reference sequence. However, we investigated the presence of U6 in our samples without success. A discussion is ongoing within the field concerning its presence in EVs samples, and other researchers before us declared snU6 as a not suitable endogenous control for miRNA's quantification[348]. Here, we use an alternative strategy, the use of exogenous spike-in. Spike-ins are non-human sequences that provide normalisation of technical factors. However, spike-ins are not taking in consideration pathological differences in starting miRNA concentration. The absence of standardised methods for quantifying miRNA abundance in EVs impacts reproducibility. To facilitate the clinical use of EVs miRNA biomarkers, quality normalisation techniques will be necessary. Establishing these methods during preclinical phases of research will enhance reproducibility and enable their application in clinical populations. The selection of a suitable normalisation approach is crucial, as the chosen methodology can influence the outcomes obtained[346].

5.6 Conclusions

In this Chapter, we demonstrated that EVs' release under hypoxic conditions is a cell-dependent process as well as the effect on their cargo. We found an increase of E-cadherin, IL-6, IL-8, and HER2 EVs derived from hypoxic HER2+ cancer cells that could lead to tumour progression, tumour aggressiveness, and anti-HER2 drug resistance. We also found different miRNA populations enriched on those EVs, with some methodology limitations. This points out a new possible approach for the evaluation of EVs-miRNAs. Understanding the role of EVs in hypoxic TME is critical for the development of effective cancer therapies.

Chapter 6

Evaluating the efficiency of an *in vitro* 3D cell culture model for EVs separation and the effect of hypoxic conditions on EVs' release under 3D culture conditions

Abstract

3D cell culture models offer a physiologically relevant environment for studying EVs in various diseases and physiological processes compared to traditional 2D cell culture systems. However, there are several challenges associated with establishing 3D cultures for EVs collection and characterisation. This study aims to address these challenges by investigating the suitability of different methodologies for spheroid formation and EVs isolation, focusing on HER2+ breast cancer cell lines and their neratinib-resistant counterparts. The selection of an appropriate 3D culture model, cell count determination at the collection time, and maintaining cell viability are critical factors in EVs isolation from 3D cultures. The heterogeneity of the EVs population poses additional challenges for isolation and characterisation, requiring careful consideration of EVs' isolation methods. Lack of standardisation in 3D cell culture techniques further complicates EVs isolation and characterisation.

To address these challenges, we evaluated the suitability of two different approaches for spheroid formation and EVs isolation. Ultimately, the 6-well Elplasia® plates were selected due to their ability to form rounded spheroids and accommodate larger sample volumes. However, spheroid disaggregation and cell count determination remained a major obstacle due to the lack of previous experience in 3D cell culture. Consequently, EVs counts were normalised to the protein content of the corresponding cell lysates obtained at the collection time to ensure reliable results.

Our findings revealed that hypoxic conditions led to reduced spheroid diameter and volume, accompanied by lower HER2 expression in most cell line variants. Hypoxia also resulted in anomalous expression of HIF-1α and down-regulation of β-catenin, which may impact various cellular processes, including proliferation and metastasis. Furthermore, EVs derived from 3D cultures showed an increase in EVs protein content in hypoxic conditions, particularly in HCC1954-derived EVs. Flow cytometry and ELISA analyses confirmed the presence of HER2 on EVs' surface, respectively, further supporting the hypothesis of enhanced HER2 trafficking under hypoxic conditions.

In conclusion, the Elplasia® plates proved to be a successful platform for EVs isolation, providing a substantial yield of EVs. However, refinement of the spheroid disaggregation step and accurate cell count determination are crucial for improving precision and reproducibility. Despite the challenges, this 3D cell culture-based EVs research offers promising opportunities for investigating disease mechanisms and developing therapeutic strategies.

6.1 Introduction

Over the decades, cell culture has been applied as a major strategy for cell biology studies, especially in the cancer field, and various 3D cell culture systems have emerged to better mimic *in vivo* conditions compared to traditional 2D cell cultures[198].

Previously in our group[349], it has been found that 3D cell cultures, which more closely mimic the *in vivo* microenvironment, provide a better platform for evaluating breast cancer drug sensitivity and resistance compared to traditional 2D monolayer cultures. In this study, a panel of HER2+ breast cancer cell lines (BT474, EFM192A, and HCC1954) were grown in 2D and "force floating" 3D cell culture conditions to compare drug response and resistance to two different anti-cancer therapies commonly used: neratinib and docetaxel. The results showed that the 3D cultures had a different drug sensitivity and resistance profile compared to the 2D cultures. Specifically, the cells cultured in 3D conditions were more resistant to neratinib and docetaxel, compared to cells cultured in 2D conditions. This difference was attributed to the up-regulation of several proteins involved in cell growth and survival (i.e. Akt, Erk and EGFR family), drug targets (EGFR and HER2), and drug efflux pump expression (PGP) contributing to multi-drug resistance in 3D cell culture[349]. Better representation of the heterogeneity of breast cancer tumours is a major challenge in cancer drug development. By incorporating 3D cell cultures into drug testing, researchers can better capture the complexity of tumours and improve the clinical relevance of preclinical drug development.

Yet, typically EVs research has been conducted with cells grown in a monolayer on a dish to facilitate the collection of EVs from the CM[350]. However, 2D cell cultures lack the impact of the ECM, which has been shown to dynamically affect multiple cellular processes such as proliferation, survival, and energy metabolism[351]. Furthermore, cell polarity may be lost, and diversity of phenotypes diminished, because of the cell morphology in the 2D cell culture[352], and the limited cell-cell and cell-matrix contacts do not promote formation of environmental niches[197]. In the 3D cell cultures, cells can become organised as in native tissues, and even form tissue-type features such as acinar structures of epithelium[353] or importantly, cancer spheroids[354].

3D culture has the potential to improve our understanding of EVs and their role in various biological processes and disease states. Some of the key advantages to consider are: (1) physiologically and pathologically relevant environment: as 3D cell culture can better mimic the *in vivo* conditions, this could lead to the production of EVs that better reflect the *in vivo* state of the cells and their microenvironment[355]; (2) complexity of cellular interactions: 3D cell culture can better replicate the cellular interactions and signalling pathways that occur *in vivo*, leading to a more complex and diverse EVs population. This can be particularly important for studying the role of EVs in intercellular communication and disease progression; (3) improved functionality of EVs: EVs isolated from 3D cultures have been shown to have improved functionality compared to those from 2D cultures. For example, Yan et al. (2020)[356] showed that EVs from umbilical MSC cultured in 3D have been shown to have greater osteochondral regenerative potential compared to that of 2D cell culture; (4) potential for high-throughput screening: 3D cell culture systems can be adapted for high-throughput screening of EVs, which can accelerate the discovery of new diagnostic or therapeutic targets[357].

Although in the past decade the use of 3D cell culture increased noticeably, their use to study EVs still being limited due to the lack of standards and reproducible methods for EVs analysis using these models. For instance, the choice of a proper EVs separation methodology can be more challenging for 3D cell cultures compared to 2D cultures. The use of some gel-like scaffold materials in 3D scaffold-based approaches can interfere with centrifugation steps involved in different separation methodologies, owing to the challenge of dissolving these materials[358].

Many 3D culture techniques can be used to create uniform-sized spheroids using a scaffold-free approach, including ultralow cell binding surfaces in individual U-bottom wells, the hanging drop method, and gyratory shaking[359]. Additionally, there are flasks or assay plates (i.e., Elplasia® plates) with arrays of microcavities that support the formation of individual spheroids per cavity, allowing the production of a considerable number of consistent-size spheroids [360].

Other scaffold-free methods use surface modification techniques to create micropatterns that alter cell adhesion and support spheroid formation (i.e., Nanoculture® Plates). However, this method tends to create heterogeneous clusters of cells with a broad size range, which may lead to differences in cell responsiveness to treatments among the population of 3D structures. T-flasks with a large ultralow binding surface can generate millions of spheroids, but heterogeneity in the size of structures remains an issue.

6.2 Aims of the study

The aim of this study was to determine the suitability of a 3D cell culture model using an Elplasia® dish for the comparison of EVs derived from six HER2+ breast cancer cell line variants (neratinib-sensitive and neratinib-resistant cell lines) cultured under hypoxic versus normoxic conditions. Subsequently, we also aimed to evaluate the presence of proteins related with hypoxia in the cells cultured in 3D, as well as to investigate the effect of hypoxia on the release of EVs in neratinib-sensitive and neratinib-resistant HER2+ cell lines cultured under 3D conditions.

6.3 Materials and Methods

6.3.1 Cell lines and culture conditions

Three HER2-positive breast cancer cell variants (EFM192A, HCC1954 and SKBR3, and their neratinib-resistant counterparts EFM192A NR, HCC1954 NR, and SKBR3 NR) were routinely maintained in complete RPMI-1640 medium as explained in **Section 2.3.1**.

In this chapter, cells referred to as 3D cultures were grown under "forced floating" conditions, where round-bottomed 96-well plates (Corning Costar, Cat. #: 3788) coated with poly (2-hydroxiethyl methacrylate) [poly-HEMA] (Sigma-Aldrich, Cat. #: P3932) or 6-well Elplasia® plates (Corning, Cat. #: 4440) were used. Poly-HEMA coated plates were prepared and used as previously by our group[349]; but here was adapted for EVs separation. In brief, 12 mg/ml stock of poly-HEMA was prepared (1.2 mg of poly-HEMA was dissolved in 100 ml 95% ethanol overnight on a rocker) and 50 μl of this solution was added to each well of the 96-well plate and allowed to dry overnight in a biosafety cabinet. This coating process was repeated once more, leaving to dry completely before addition of the cells. 6-well Elplasia® plates present an ultra-low attachment surface that promotes the formation of scaffold-free spheroids. Each well contains around 2885 microcavities, claimed to allow the development of the same number of spheroids/well. Elplasia® plates were pre-wet prior to seeding cells by adding 1.5 ml of supplemented RPMI-1640 media per well and centrifuging at 1,000× *g* for 1 min. This centrifugation step was repeated until all trapped air was removed.

Due to the possibility of disrupting the spheroids, cells were directly seeded in presence of RPMI media supplemented with 10% EVs-depleted FBS, 2mM L-Glutamine and 1% P/S. Densities used for each type of 3D culture are shown in **Table 6.1**. Cell density and volumes for the poly-HEMA coated 96-wells were established according Breslin et al. (2016)[349] while for the Elplasia® 6-well plates the manufacturer's recommendations were followed. Cells were then maintained in normoxia or directly placed in hypoxic (see details per **Section 5.3.1**) for 5 days after seeding.

Cells were counted and their viability checked by disaggregating the spheroids using 1X trypsin-EDTA solution (Sigma-Aldrich, Cat. #: T3924), 10x trypsin-EDTA solution (Sigma-Aldrich, Cat. #: T414-100ML) and/or Accumax - Cell Aggregate Dissociation Medium (Invitrogen, Cat. #: 00-4666-56) and incubating during 5–10 min at 37°C on a thermomixer (Eppendorf) at 350 rpm. The 3D cell culture screening workflow is illustrated in **Figure 6.1**.

Table 6.1. Seeding densities used for each 3D cell culture and the volumes of media used.

Cell lines	Plate type	Seeding density	Volume/well
EFM192A	Coated 96-well plate	8×10^3 cells/well	200 µl
EFM192A	6-well Elplasia® plate	700 cells/microcavity ($\sim 2 \times 10^6$ cells/well)	13 ml
EFM192A NR	Coated 96-well plate	8×10^3 cells/well	200 µl
EFM192A NR	6-well Elplasia® plate	700 cells/microcavity ($\sim 2 \times 10^6$ cells/well)	13 ml
HCC1954	Coated 96-well plate	3×10^3 cells/well	200 µl
HCC1954	6-well Elplasia® plate	500 cells/microcavity ($\sim 1.4 \times 10^6$ cells/well)	13 ml
HCC1954 NR	Coated 96-well plate	3×10^3 cells/well	200 µl
HCC1954 NR	6-well Elplasia® plate	500 cells/microcavity ($\sim 1.4 \times 10^6$ cells/well)	13 ml
SKBR3	Coated 96-well plate	5×10^3 cells/well	200 µl
SKBR3	6-well Elplasia® plate	500 cells/microcavity ($\sim 1.4 \times 10^6$ cells/well)	13 ml
SKBR3 NR	Coated 96-well plate	5×10^3 cells/well	200 µl
SKBR3 NR	6-well Elplasia® plate	500 cells/microcavity (1.4×10^6 cells/well)	13 ml
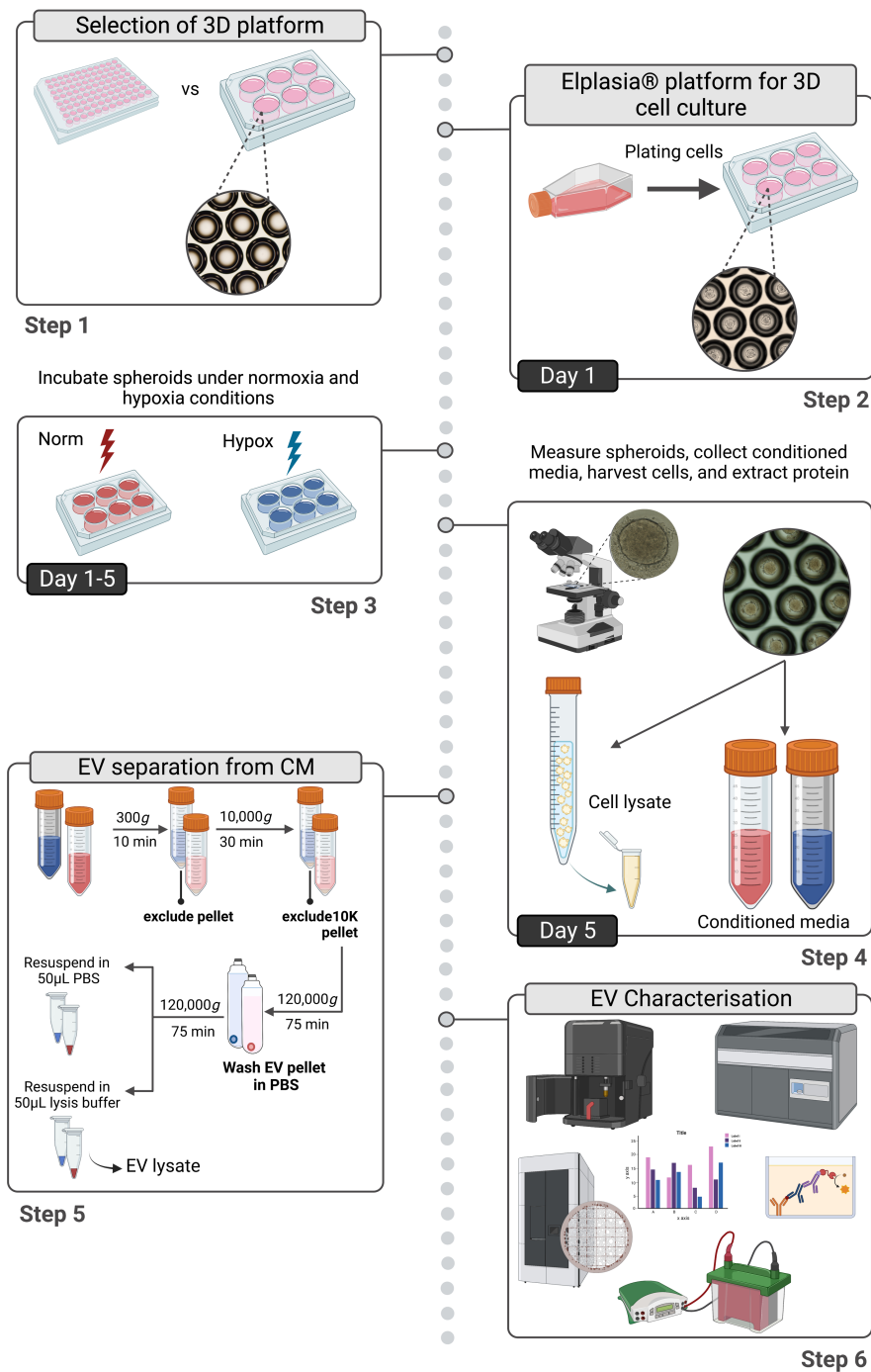
Figure 6.1. Schematic workflow diagram of our proposed method for EVs isolation from 3D cell culture cells.

(**Step 1**) Initially, two approaches were investigated for spheroid formation: poly-HEMA coated 96-well plates and 6-well Elplasia® plates; (**Step 2-3**) After the platform selection, cells were plated in 6-well Elplasia® wells and incubated under normoxia (21% O_2, 5% CO_2, 37ºC) or hypoxia (1% O_2, 5% CO_2, 37ºC) for 5 days; (**Step 4**) After 5 days incubation, spheroids were measured by estimating their diameter and volume and were harvested for cell lysate samples, as well as the collection of the conditioned media (CM); (**Step 5**) EVs were enriched from the CM by using dUC protocol. Resultant pellets were then resuspended in 50 µl of PBS or lysis buffer. (**Step 6**) EVs characterisation was performed on EVs samples by NTA, IFCM, TEM and immunoblotting analysis. Illustration created in *BioRender.com*.

6.3.2 EVs separation by differential ultracentrifugation (dUC)

After the cells conditioned the medium for 5 days, approximately 78 ml aliquots of CM were collected from EFM192A, EFM192A NR, HCC1954, and HCC1954 NR seeded in 6-well Elplasia® plates. CM was then centrifuged as explained previously in **Section 5.3.2** with some adaptations. In this case, 10K pellets were not analysed and thereby pellets were discarded. In addition, from the 78 ml aliquots, 39 ml of CM were processed as explained in **Section 5.3.2** and resuspended in 50 µl PBS and stored in Protein LoBind tubes (Eppendorf, Cat. #: 0030 108.116) at -80ºC, while the other 39 ml aliquot was processed and the final pellet was directly resuspended in 50 µl lysis buffer (Thermo Fisher Scientific, Cat. #: FNN0011) containing protease inhibitor cocktail (Roche, Basel, Switzerland; Cat. #: 04693116001) for further analysis.

6.3.3 Collection of protein lysate of cells cultured as 3D models under normoxic and hypoxic conditions, along with EVs collection

After 5 days of seeding, the CM was carefully removed from the plates and the cells were processed as previously described in **Section 2.3.6**, but with minor changes. Briefly, spheroids were resuspended in cold PBS and washed twice (by centrifuging 10,000× g at 4°C for 5 min and resuspending again in cold PBS) before being lysed. Cells were then centrifuged at 10,000× g at 4°C for 5 min. The pellet was then resuspended in 100 µl lysis buffer (Thermo Fisher Scientific, Cat. #: FNN0011) protease inhibitor cocktail (Roche, Basel, Switzerland; Cat. #: 04693116001), and samples were sonicated on ice 20 sec (pulse time 5 sec, pulse off time 5 sec). After sonication, samples were vortexed and incubated for 30 min at RT and finally centrifuged at 16,000× g for 10 min. The supernatant was transferred to a new 1.5 ml centrifge tube (Eppendorf, Cat. #: 0030123328) and stored at -20ºC until required. EVs lysates obtained from 39 ml aliquots were directly lysed as explained in **Section 2.3.6** by resuspending in 50 µl lysis buffer and protease inhibitor cocktail. The supernatant was stored at -20ºC until further analysis.

6.3.4 Optical Microscopy

The images of the spheroids were captured by phase contrast microscopy on an Olympus IX81 inverted microscope. The volume of a spheroid (V, µm^3) was calculated according to the equation: V = (a × b^2)/2, where a is the larger diameter (µm) and b is the smaller diameter (µm).

6.3.5 Protein quantification by Bicinchoninic acid (BCA) assay

Cell lysate and EVs lysate was quantified using the Bio-Rad protein assay Dye reagent (Bio-Rad, Cat. #: 500-0006) as previously described in **Section 3.3.1.1**. The amount of protein measured in the EVs isolates was normalised by seeding densities.

6.3.6 Immunoblotting

For all immunoblotting performed in this chapter, 30 µg total protein was resolved on either 7.5% Mini-PROTEAN TGX™ 15-well gel (Bio-Rad Laboratories; Cat. #: 4561026), or 10% Mini-PROTEAN TGX™ 15-well gel (Bio-Rad Laboratories; Cat. #: 4561026) for cell lysates and 10 µg total protein was resolved on 10% Mini-PROTEAN TGX™ 10-well gel (Bio-Rad Laboratories, Cat. #: 4561034) for EVs lysates, along with a MW marker, SeeBlue Plus 2 Pre-stained standards (Invitrogen, Cat. #: LC5925). Immunoblots were performed as described in **Section 2.3.8**. All antibody conditions and catalogue numbers used in this chapter are detailed in **Table 6.2**. Densitometric analysis was performed using Fiji software[216].

Table 6.2. Antibody dilutions and conditions for immunoblotting.

Primary Antibody	Company, Cat. #	Dilution	Antibody condition	Secondary Antibody
β-actin	Sigma-Aldrich, A1978	1:5000	3% BSA/PBST	Anti-Mouse IgG
Calnexin	Abcam, ab133615	1:1000	3% BSA/PBST	Anti-Rabbit IgG
CD9	Abcam, ab236630	1:1000	3% BSA/PBST	Anti-Rabbit IgG
CD63	Abcam, ab68418	1:500	3% BSA/PBST	Anti-Rabbit IgG
HER2	Calbiochem, OP15	1:1000	3% BSA/PBST	Anti-Mouse IgG
HIF-1α	Cell Signaling,	1:1000	3% BSA/PBST	Anti-Rabbit IgG
Syntenin	Abcam, ab133267	1:1000	3% BSA/PBST	Anti-Rabbit IgG

All secondary antibodies were diluted 1:1000 in 3% BSA/PBST

6.3.7 Characterisation of EVs pellets

6.3.7.1 NTA measurements on 120K pellets

[NTA of EVs was performed in the Laboratory for Biological Characterisation of Advanced Materials (LBCAM), Trinity Translational Medicine Institute, as a paid service]

Twenty-four samples containing EVs were analysed via NTA (Malvern UK) using a NanoSight NS500 system as described previously in **Section 4.3.8.1**.

6.3.7.2 TEM imaging of 120K pellets

[TEM imaging of EVs was performed in the Advanced Microscopy Laboratory in Trinity Biomedical Sciences Institute by Mr. Neal Leddy as a paid service]

Samples were prepared for TEM analysis as previously describe in **Section 2.3.9**.

6.3.7.3 Imaging Flow Cytometry on EVs isolates

The IFCM analysis on EVs obtained from 3D cells after 5 days in normoxic or hypoxic conditions was performed following the protocol described in **Section 4.3.8.3**.

6.3.8 HER2 analysis by ELISA

HER2 quantification was performed using the DuoSet ELISA kits (R&D Systems, Cat. #: DY1129B) and following manufacturer's instruction as explained in **Section 3.3.3**.

6.3.9 Data analysis and statistical testing

All statistical analyses were performed using GraphPad Prism version 9.1.9 for macOS (GraphPad Software). Regarding cell and EVs characterisation, values for arbitrary units (A.U.), spheroid diameters, spheroid volumes, EVs particle numbers, and EVs size are given as mean ± SEM (n=3). Two-tailed paired t-test was applied ($p < 0.05$ was considered as statistically significant) for comparison between normoxia and hypoxia, while two-way *ANOVA* was used for comparison between groups (neratinib-sensitive vs neratinib-resistant). For ELISA assay analysis, HER2 quantification was performed interpolating the absorbance values to the standard curve run alongside the samples.

6.4 Results

6.4.1 Evaluating the suitability of the methodologies for spheroid formation and cell characterisation

We firstly tested poly-HEMA coated 96-well plates for culturing cells for subsequent collection of EVs isolation, as used previously by our group. However, in that study only EVs quantity (estimated in µg/ml) was determined in EVs derived from cells cultured in 2D and 3D conditions. Here, our aim was to fully characterise those EVs isolates derived from 3D cell culture under normoxic and hypoxic conditions.

We observed that after 24 hrs incubation in poly-HEMA coated plates, SKBR3 cell variants were not able to form spheroids successfully while we obtained rounded and compact spheroids in the case of HCC1954 cell variants, and a less homogeneous 3D shape in the case of EFM192A cell variants (**Figure 6.2**). Noticeably, spheroids of those cell variants were less compact under hypoxic conditions, with some loose cells around the spheroid that was not observed when cultured under normoxic conditions.

It has been demonstrated that SKBR3 cells can only form compact aggregates under specific conditions (CellStar® Cell-Repellent Surface coated with 3.5% Matrigel), while in the other cases multiple small spheroids, loose aggregates, or single cell suspensions result[361,362]. We then decided to eliminate the SKBR3 cell variants for this technique, as they are not able to form the same structures as the HCC1954 and EFM192A variants.
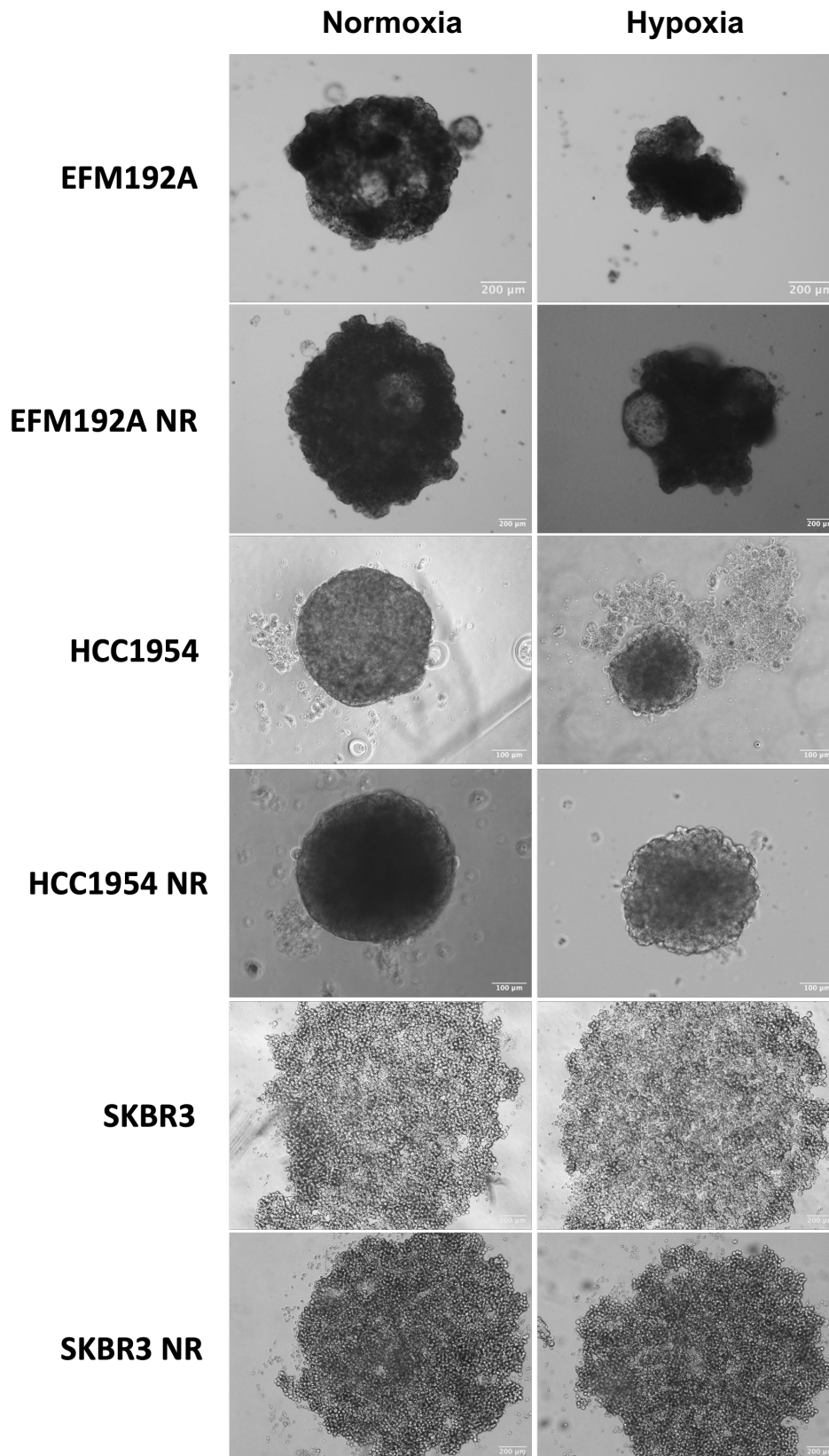
Figure 6.2. Bright-field microscope images of breast cancer spheroids.

Phase contrast images of 3D cell cultures in normoxia and hypoxia conditions using poly-HEMA coated 96-wells approach. Images of EFM192A, EFM192A NR, HCC1954, and HCC1954 NR were taken at 20x (scale bar = 100 μm) while SKBR3 and SKBR3 NR pictures were taking at 10x (scale bar = 200 μm).

At this initial phase of the research, our primary objective was to assess the effectiveness of poly-HEMA coated 96-well plates as a platform for separating EVs. To accomplish this proof-of-concept evaluation, we exclusively focus on analysing the HCC1954 and HCC1954 NR variants. These specific variants were chosen due to their consistent formation of uniform spheroids with a relatively smooth surface. The diameter and the volume of the HCC1954 and HCC1954 NR spheroids after 5 days of incubation in normoxic or hypoxic conditions was measured (**Figure 6.3**). HCC1954 NR cells were found to form bigger spheroids in diameter and volume than their neratinib-sensitive counterparts, whether cultured under normoxic or hypoxic conditions. In addition, hypoxia significantly decreased the diameter and the volume of spheroids in both HCC1954 and HCC1954 NR cell lines. The mean diameter and volume of the samples are detailed **Table 6.3**.
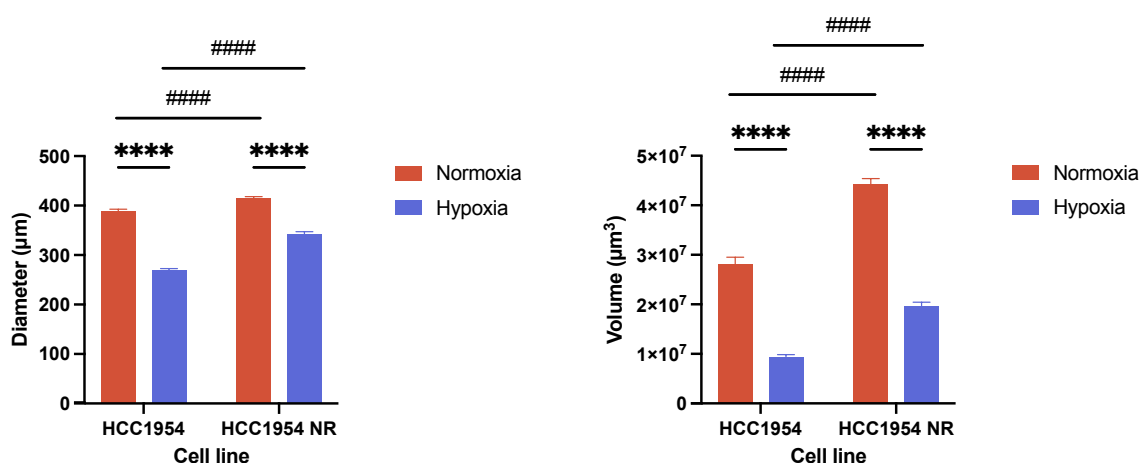
Figure 6.3. HER2+ breast cancer cell spheroid size.

(**A**) Spheroid diameter of cells 5 days post-seeding of 500-700 cells/microcavity. (**B**) Volume (*V*) of spheroids calculate by using the equation: $V = (a \times b^2)/2$, where *a* is the larger diameter and *b* is the smaller diameter. Error bars represent the SEM, n = 19-70. Multiple paired t-test was used to calculate the significance: ****p<0.0001 (hypoxia vs normoxia); ####p<0.0001 (neratinib-resistant vs neratinib-sensitive).

Table 6.3. Mean values of diameters and volume of the spheroids.

Diameter (µm)				
	Normoxia	Hypoxia	Fold change	*p* value
HCC1954	388.5 ± 4.3	269.0 ± 3.7	↓1.4	<0.0001(****)
HCC1954 NR	414.3 ± 3.9	342.7 ± 4.4	↓1.2	<0.0001(****)
Volume (µm³)				
	Normoxia	Hypoxia	Fold change	*p* value
HCC1954	$2.8\times10^7 \pm 1.3\times10^6$	$9.3\times10^6 \pm 5.3\times10^5$	↓3	<0.0001(****)
HCC1954 NR	$4.4\times10^7 \pm 1.2\times10^6$	$1.9\times10^7 \pm 8.8\times10^5$	↓2.3	<0.0001(****)

*Mean values of diameters and volume of the spheroids' growth in normoxia and hypoxia conditions using the poly-HEMA 96-well plates platform. Fold change is calculated as hypoxia/normoxia ratio (****p<0.0001).*

Once the capability of the cells to form spheroids in normoxic and hypoxic conditions was addressed, we studied the advantages and disadvantages compared to the Elplasia® plates. Those points are collected in **Table 6.4**. An important consideration for EVs separation is the CM volume required for the full characterisation of the EVs isolates. As we would like to compare with the 2D already performed in **Chapter 5**, dUC will be the methodology used for the EVs separation. To achieve this, several 96-well plates of CM would be required to obtain adequate CM volume. Conversely, from a 6-well Elplasia® plate x4 times more CM can be obtained compared to a 96-well plate. Another important consideration is the number of spheroids that would "conditioned" that media. While from a 96-well plate 14 ml of CM would be obtained, "conditioned" from approximately 96 spheroids compared to 78 ml of CM conditioned from a 6-well Elplasia® plate holding more than 17,000 spheroids.

The handling of the spheroids and the CM collection were also evaluated. Upon careful evaluation, it has been realised that to collect the CM from each well without disturbing/absorbing the spheroids from each 96-well plate was a time-consuming, arduous task and, considering the output generated, did not sufficiently justify the resources and effort expended. In addition to that, spheroids formed in 96-well plates were bigger and less reproducible to those formed in the 6-well Elplasia® microcavities. Taking everything into consideration, it was concluded that this approach was not suitable for our aims of CM collection and EVs characterisation.

Table 6.4. Advantages and disadvantages of each approach evaluated for EVs separation.

Plate	Volume CM/well	Spheroids /plate	Spheroid reproducibility	Handling	Time-demanding	Price
96-well plate coated with poly-HEMA	19 ml	96	+	+	+++	+
6-well Elplasia®	78 ml	17,310	+++	++	+	+++

Levels expressed as: + = low; +++ = high. Different levels were rated based on personal experience and data obtained during the development of this research.

The capability of the cell line variants to form spheroids in the Elplasia® plates was also evaluated. EFM192A and HCC1954 cell variants were equally capable of forming rounded spheroids. However, SKBR3 cell variants were not able to form the spheroids under these conditions either (**Figure 6.4**).

	Normoxia	**Hypoxia**
EFM192A		
EFM192A NR		
HCC1954		
HCC1954 NR		
SKBR3		
SKBR3 NR		
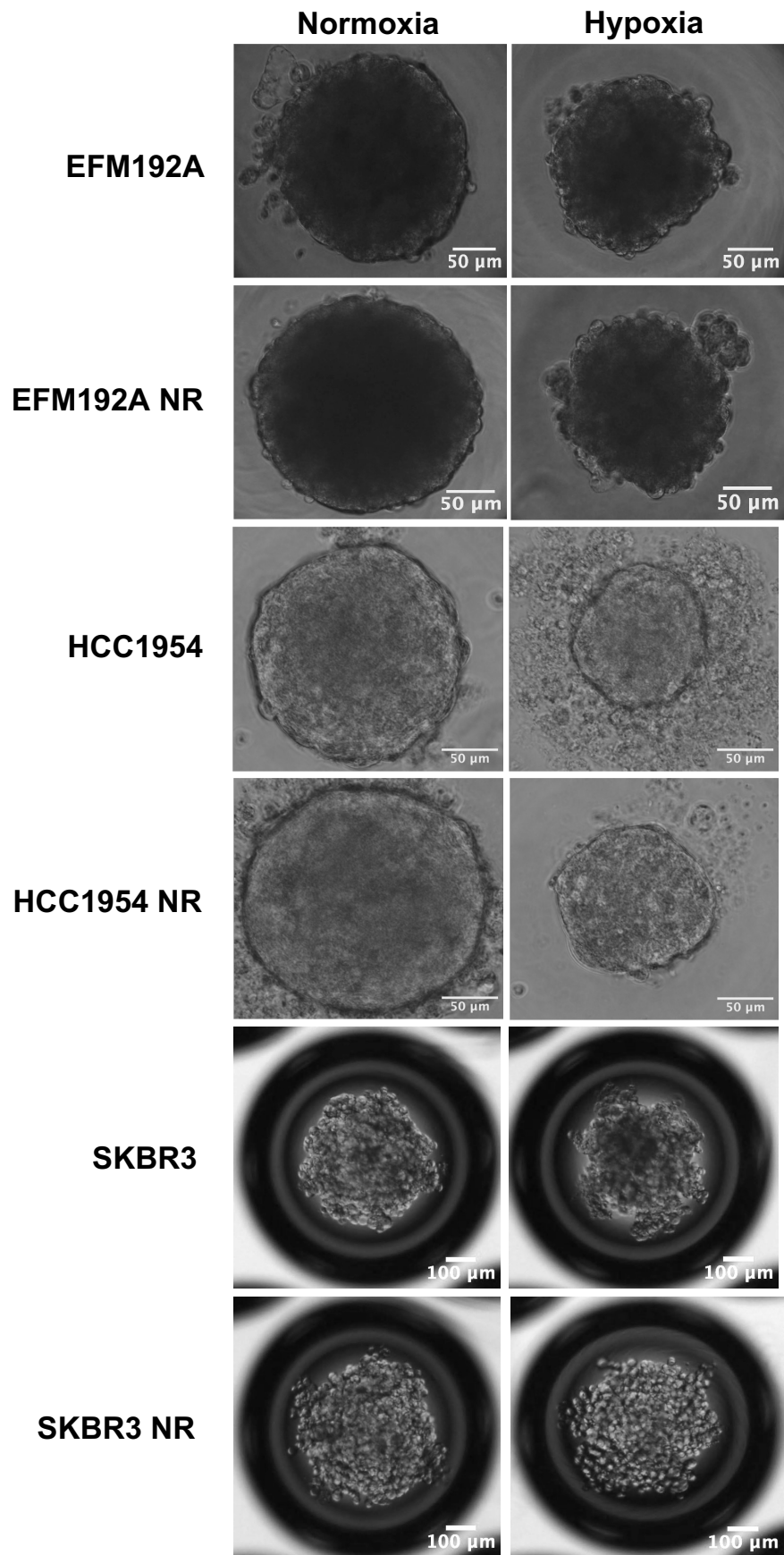
Figure 6.4. Representative microscope images of spheroids.

Representative images at Day 5 of the HER2+ breast cancer spheroids grown at the optimal seeding densities. Scale bars represent 50 µm (20x magnification) or 100 µm (10x magnification).

When seeded in 6-well Elplasia® plates, EFM192A, EFM192A NR, HCC1954, and HCC1954 NR cells formed smaller spheroids under hypoxia compared with normoxia, as previously observed in the 96-well plates (**Figure 6.5**). However, EFM192A NR cells seemed to form smaller spheroids than EFM192A in terms of diameter and volume. Although HCC1954 NR spheroids presented a bigger diameter compared with HCC1954 spheroids in both normoxic and hypoxic conditions, no significant differences in volume between those cells' lines were observed. The diameter and volume mean of the samples are detailed in **Table 6.5**.

A
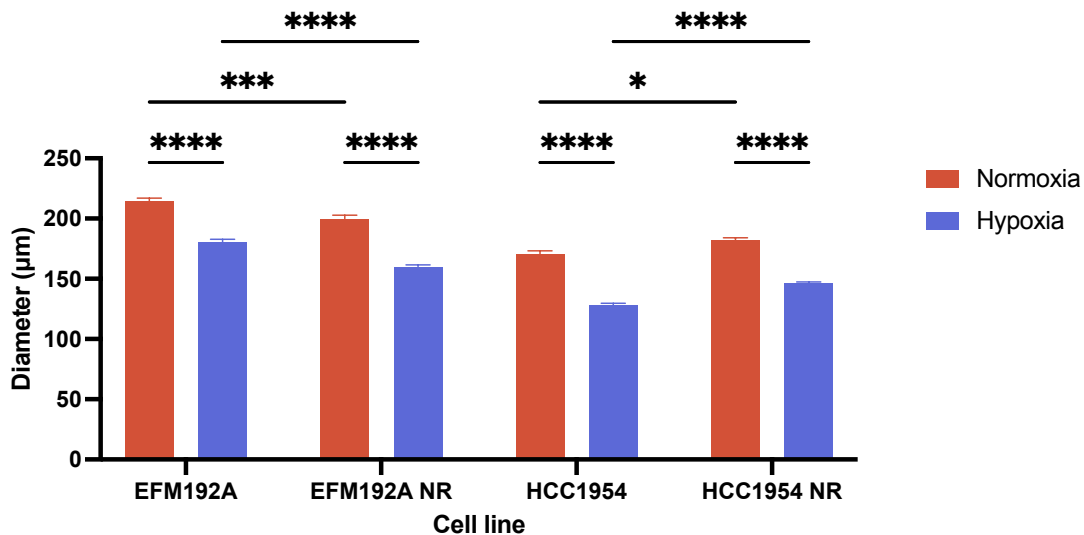
B
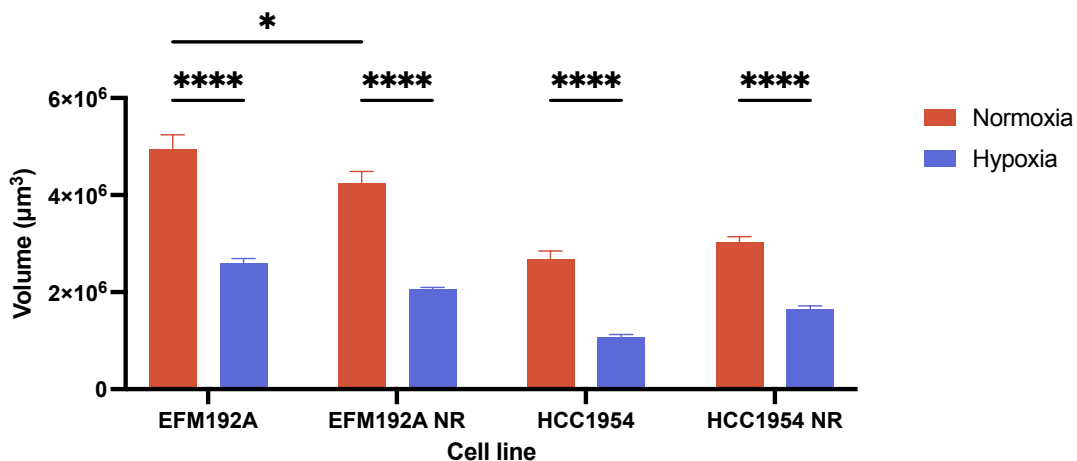
Figure 6.5. HER2+ breast cancer cell spheroid size and morphology.
(**A**) Spheroid diameter of cells 5 days post-seeding of 500-700 cells/microcavity; (**B**) Volume (*V*) of spheroids calculate by using the equation: $V = (a \times b^2)/2$, where *a* is the larger diameter and *b* is the smaller diameter. Error bars represent the SEM, *n* = 19-70. Two-way ANOVA was used to calculate the significance: *p<0.05, ***p<0.001, ****p<0.0001.

Table 6.5. Mean values of diameters and volume of the spheroids

Diameter (µm)			
	Normoxia	Hypoxia	Fold change	*p* value
EFM192A	214.2 ± 2.9	180.5 ± 2.4	1.2↓	<0.000001 (****)
EFM192A NR	199.9 ± 3.0	160.1 ± 1.5	1.3↓	<0.000001 (****)
HCC1954	170.8 ± 2.4	128.3 ± 1.5	1.3↓	<0.000001 (****)
HCC1954 NR	182.1 ± 2.0	146.1 ± 1.3	1.3↓	<0.000001 (****)
Volume (µm³)			
	Normoxia	Hypoxia	Fold Change	*p* value
EFM192A	$4.9 \times 10^6 \pm 2.9 \times 10^5$	$2.6 \times 10^6 \pm 1.1 \times 10^5$	1.9↓	<0.000001 (****)
EFM192A NR	$4.2 \times 10^6 \pm 2.5 \times 10^5$	$2 \times 10^6 \pm 5.2 \times 10^4$	2.1↓	<0.000001 (****)
HCC1954	$2.7 \times 10^6 \pm 1.7 \times 10^5$	$1.1 \times 10^6 \pm 4.9 \times 10^4$	2.5↓	<0.000001 (****)
HCC1954 NR	$3 \times 10^6 \pm 1.2 \times 10^5$	$1.6 \times 10^6 \pm 6.6 \times 10^4$	1.8↓	<0.000001 (****)

*Mean ± SEM values of diameters and volume of the spheroids' growth in normoxia and hypoxia conditions. Fold change is calculated as hypoxia/normoxia ratio. P values relates to differences between normoxic and hypoxic conditions, ****p<0.0001*

EVs count in 2D *in vitro* models are normalised based on the final cell concentration as a standard practice but in the case of 3D *in vitro* models this practice is not standardised. As the cell count at the time of conditioned media collection can be a challenge due to the need of a spheroid disaggregation, some studies normalise the EVs based on the seeding densities[355]. Here, as cells grow at different rates in normoxia and hypoxia conditions, we decide to compare the protein amounts we obtained from the cell lysates at the time of collection to evaluate if cell protein amount can be used to normalise the EVs analysis. We found that spheroids from HCC1954 and HCC1954 cell variants exposed higher amount of protein in normoxia compared to the hypoxic spheroids. No significant differences in terms of protein were found in spheroids from EFM192A and EFM192A NR cell variants (**Figure 6.6**).
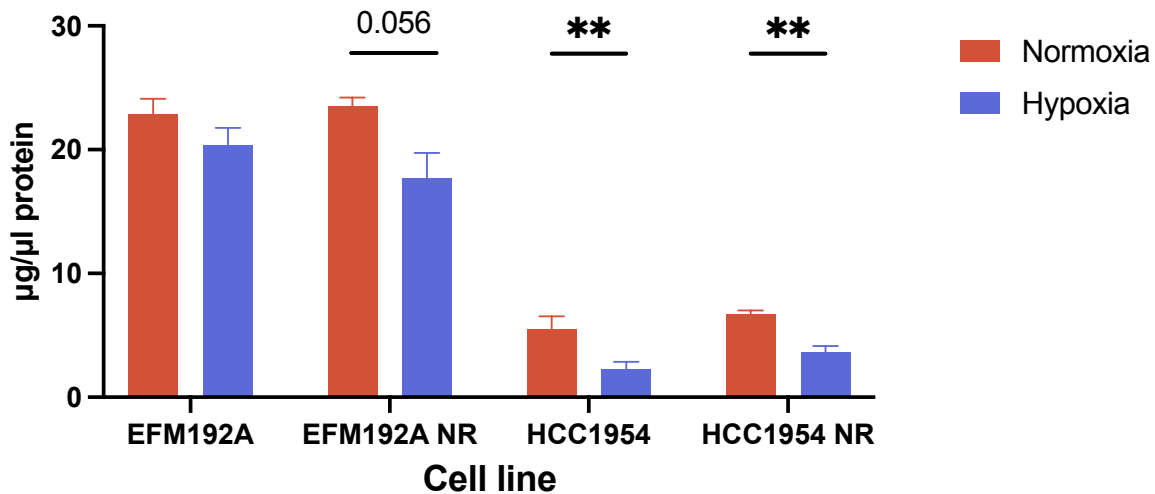
Figure 6.6. Spheroids' protein concentration.

Protein content of spheroids was measured by BCA. Paired t-test used to calculate significance: **$p<0.01$ ($n = 3 \pm$ SEM).

Once we evaluated the size of the spheroids formed in both conditions, we collected the protein cell lysates of those cells and performed immunoblot analysis of certain markers previously investigated in **Chapter 5** (see **Section 5.4.1**). We evaluated the expression of HER2, HIF-1α, β-catenin, and CD9 in EFM192A, EFM192A NR, HCC1954, and HCC1954 NR spheroids (**Figure 6.7** and **Figure 6.8**, respectively). As expected, an increase of HIF-1α expression under hypoxic conditions was found in both EFM192A and EFM192A NR spheroids (14.9-fold, $p = 0.0002$; 13.5-fold, $p = 0.005$, respectively). Interestingly, under hypoxic conditions, higher amount of HIF-1α expression was found in EFM192A spheroids compared with EFM192A NR (1.63-fold, $p = 0.044$). Similar expression levels of HER2 were observed in EFM192A and EFM192A NR spheroids.

With EFM192A and EFM192A NR spheroids, a down-regulation in β-catenin expression was observed in hypoxia, but only significant in the case of EFM192A (3.83-fold, $p = 0.013$;1.74-fold, $p = 0.170$, respectively). Similar amounts of β-catenin were observed between EFM192A and EFM192A NR in normoxic conditions. However, a higher amount of β-catenin was observed in EFM192A NR hypoxic spheroids compared to their neratinib-sensitive EFM192A counterparts.

The expression of CD9 was also evaluated in those spheroids. While in normoxic conditions EFM192A NR spheroids seem to have a higher expression of CD9 compared with EFM192A spheroids (1.49-fold, $p = 0.343$), a significant lower expression of CD9 was found in EFM192A NR hypoxic spheroids compared to their EFM192A counterparts (2.58-fold, $p = 0.023$). It was also noticeable that hypoxia slightly, but insignificantly increased the expression of CD9 in EFM192A spheroids (1.69-fold higher in hypoxia, $p = 0.134$) while showed the opposite effect on EFM192A NR spheroids (2.28-fold higher in normoxia, $p = 0.062$).
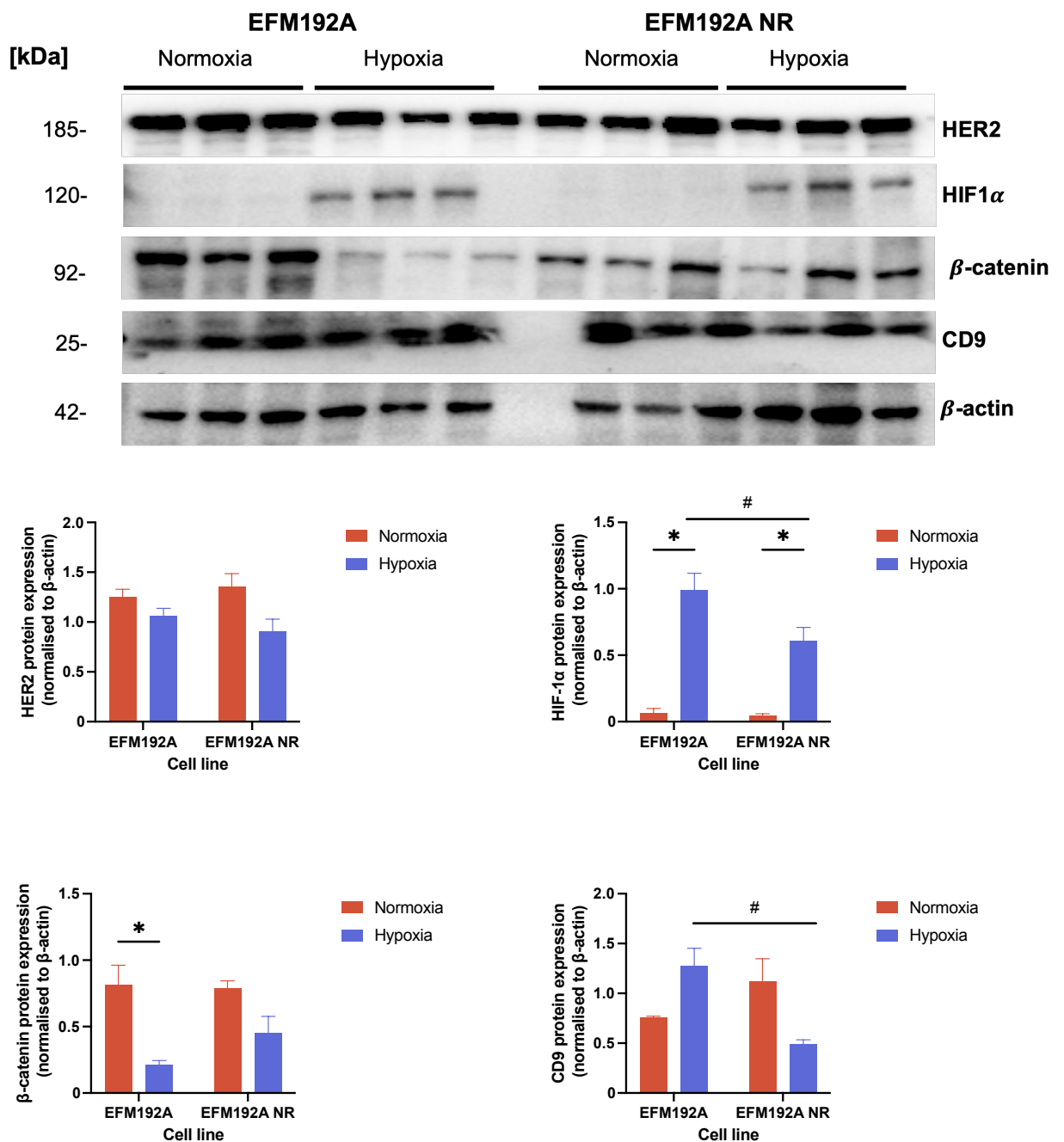
Figure 6.7. Characterisation of EFM192A and EFM192A NR spheroids under normoxic and hypoxic conditions.

(**Top**) Immunoblots showing expression of HER2, HIF-1α, β-catenin, β-actin, and CD9 in neratinib-sensitive and neratinib-resistant (neratinib-resistant; NR) EFM192A cancer cell variants. Thirty μg of EFM192A (**Left**) and EFM192A NR (**Right**) cell lysates were loaded for this analysis; (**Bottom**) The relative intensity (AU) of the protein signal band was calculated using ImageJ software. β-actin was used as loading control and normalisation. Multiple paired t-test was used to calculate the significance *$p<0.05$, $n = 3$ ± SEM culture protein lysates. #$p<0.05$ (neratinib-resistant vs neratinib-sensitive).

When we analyse these protein markers in HCC1954 cell variants (**Figure 6.8**), we observed a significant increase in HER2 expression under hypoxic conditions in HCC1954 NR spheroids (1.58-fold, $p = 0.0005$). Surprisingly, HCC1954 NR spheroids showed a higher HER2 expression than their neratinib-sensitive counterparts (1.37-fold, $p = 0.004$). It was also found that HCC1954 NR spheroids expressed similar amounts of HIF-1α in both normoxia and hypoxia. On the other hand, an increase in HIF-1α in the HCC1954 spheroids cultured under hypoxic conditions, this rise was not significant (2.73-fold, $p = 0.473$). In relation to CD9, similar results to those obtained for EFM192A cell variants were found in HCC1954 cell variants. An insignificant increase of CD9 was found in HCC1954 spheroids cultured under hypoxic conditions when compared to their normoxic counterparts (1.23-fold, $p = 0.759$), while HCC1954 NR spheroids showed a significant reduction of CD9 expression in hypoxia compared to normoxic conditions (3.17-fold, $p = 0.002$). Furthermore, CD9 protein was more abundantly expressed in normoxic HCC1954 NR spheroids than in HCC1954 spheroids (1.98-fold, $p = 0.014$).
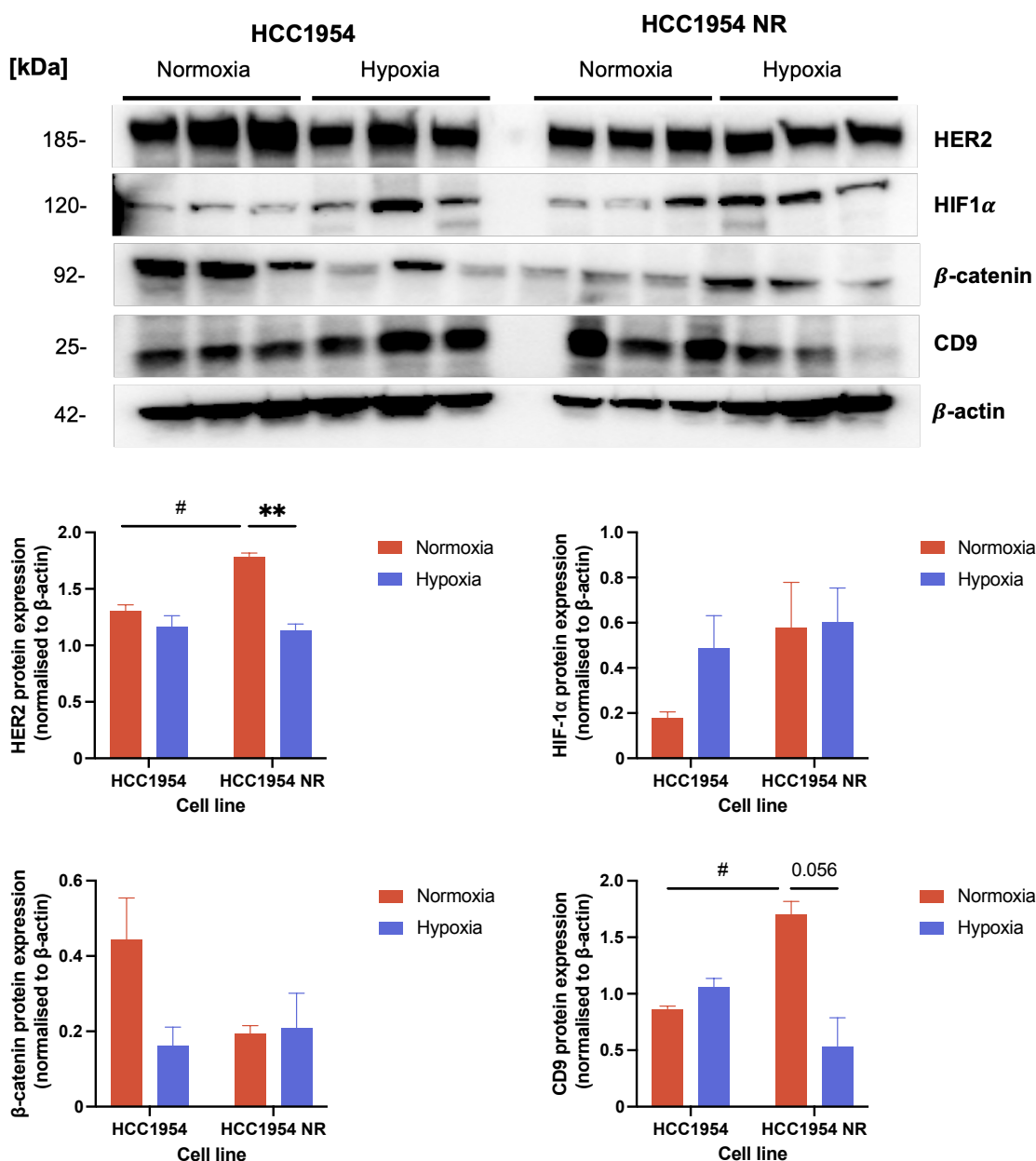
Figure 6.8. Characterisation of HCC1954 and HCC1954 NR spheroids under normoxic and hypoxic conditions.

(**Top**) Immunoblots showing expression of HER2, HIF-1α, β-catenin, β-actin, and CD9 in neratinib-sensitive and neratinib-resistant (neratinib-resistant; NR) HCC1954 cancer cell variants. Thirty μg of HCC1954 (**Left**) and HCC1954 NR (**Right**) cell lysates were loaded for this analysis; (**Bottom**) The relative intensity (AU) of the protein signal band was calculated using ImageJ software. β-actin was used as loading control and normalisation. Multiple paired t-test was used to calculate the significance: p**<0.01 (hypoxia vs normoxia) and #$p<0.05$ (neratinib-resistant vs neratinib-sensitive). $n = 3 \pm$ SEM culture protein lysates.

6.4.1.1 Summary of findings

An outline of the immunoblots results obtained for these two cell line pairs cultured in 2D and 3D under normoxic and hypoxic conditions is collected in **Table 6.6**. Although most of the analysed markers followed the same expression on the cells grown under 2D and 3D conditions, it was observed an opposite trend in the case of HER2 expression in EFM192A cells and differences in CD9 expression in EFM192A and HCC1954 NR cells depending on the cell culture used.

Table 6.6. Summary of cell characterisation in 2D and 3D under hypoxic conditions.

	EFM192A		EFM192A NR		HCC1954		HCC1954 NR	
Characteristic	2D	3D	2D	3D	2D	3D	2D	3D
HER2	↑	↓	↓	↓	n.d.	n.d.	n.d.	↓ (**)
HIF-1α	↑ (**)	↑ (*)	↑ (*)	↑ (*)	↑ (***)	↑	↑ (*)	n.d.
β-catenin	n.d.	↓ (*)	n.d.	↓	↓ (*)	↓	n.d.	n.d.
CD9	↓ (*)	↑	n.d.	↓	↓ (*)	n.d.	↑	↓

Summary of the characterisation of the two cell line pairs compared to their 2D-cultured counterparts under hypoxia. Arrows refers to the increase (↑) or decrease (↓) under hypoxia compared with normoxia for each cell culture technique. No differences (n.d.) was defined as a fold-change (hypoxia vs. normoxia) ~1. *p<0.05, **p<0.01, ***p<0.001.

6.4.2 Evaluating the suitability of the methodologies for EVs isolation

As the use of the 6-well Elplasia® plates was a simple way to form several spheroids with adequate production of CM, we decide to evaluate their suitability for EVs isolation and full characterisation of those EVs samples. Here, EVs results were normalised based on the protein amount of cell lysates obtained at the collection time. Normalisation based on the seeding density is also collected in the **Appendix V**.

6.4.2.1 Protein quantification present in EVs samples from normoxia and hypoxia conditions

The amounts of protein (expressed as µg of protein/µL) present in each sample was determined by the BCA protein assay and normalise by cell protein amount (**Figure 6.9**). Only a significant increase in protein content was found in EVs derived from HCC1954 cells under normoxic conditions compared to their normoxic pair (2.8-fold, $p = 0.009$). No other significant differences were found in relation to protein analysis of EVs samples whether derived from normoxic and hypoxic conditions or neratinib-sensitive or -resistant cells. Mean values of protein quantity are collected in **Table 6.7***.* Alternative normalisation using seeding density is collected in the **Appendix V** (**Figure V-1**).
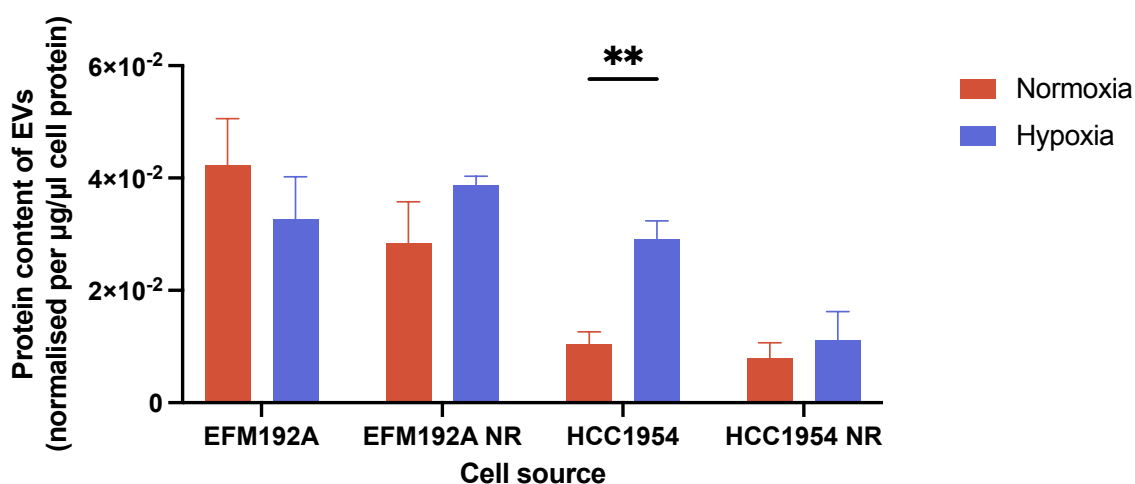
Figure 6.9. Protein content of EVs derived from 3D cultured cells was measured by BCA.
The amount of protein was normalised to amount of cell protein. Paired t-test used to calculate significance: **$p<0.01$ ($n = 3 \pm$ SEM).

Table 6.7. Mean values of protein amounts for EVs isolates.

EVs protein yield (Mean ± SEM)				
Cell line	Condition	µg EVs protein (Normalised by cell protein)	Fold-change	*p* value
EFM192A	Normoxia	0.042 ± 0.014	↓1.3	0.231 (ns)
	Hypoxia	0.033 ± 0.013		
EFM192A NR	Normoxia	0.028 ± 0.013	↑1.4	0.24 (ns)
	Hypoxia	0.039 ± 0.003		
HCC1954	Normoxia	0.010 ± 0.004	↑2.8	0.009 (**)
	Hypoxia	0.029 ± 0.005		
HCC1954 NR	Normoxia	0.008 ± 0.005	↑1.4	0.281 (ns)
	Hypoxia	0.011 ± 0.009		

*Mean values ± SEM obtained from 3D cultured cells under normoxia and hypoxia. Fold change is calculated as hypoxia/normoxia ratio (**p<0.01).*

6.4.2.2 Characterisation of EVs derived from 3D cultured cells by immunoblotting

Immunoblotting analysis was performed to evaluate the presence of EVs markers and HIF-1α for the different lysed EVs samples (**Figure 6.10**). Regardless of the cell line of origin, calnexin (used as "exclusion marker") was not detected with any of the EVs samples analysed.

All EVs were positive for all EVs markers proving the presence of different EVs population as indicated by the presence of CD63 (associated with all EVs populations), syntenin (mainly associated with smaller vesicles), and CD9 (mainly associated with medium/large EVs). However, all EVs were negative for HIF-1α.

Equal amounts (10 µg) of protein were loaded on the gels. However, the enrichment of EVs markers in the EVs isolates was dependent on the neratinib-resistant context and oxygen condition. For instance, it was observed an increase of CD63 in EVs derived from hypoxic EFM192A cells compared with the normoxic counterparts while no significant differences were observed in syntenin or CD9 presence between normoxic or hypoxic EFM192A-derived EVs. EFM192A NR-derived EVs seems to carry less CD63 than their neratinib-sensitive counterparts. Surprisingly, in the case of EFM192A NR-derived EVs, a decrease of CD63 was observed in the EVs released under hypoxic conditions compared with those released under normoxic conditions. No significant differences were found in the presence of syntenin or CD9 proteins. In the case of HCC1954-derived and HCC1954 NR-derived EVs, no significant differences were found in the presence of syntenin or CD63 between normoxic and hypoxic conditions while a significant decrease of CD9 was found on the HCC1954 NR-derived EVs under hypoxia (p = 0.024). Densitometric analysis of the EVs immunoblots are collected in **Appendix V – Figure V-2**.
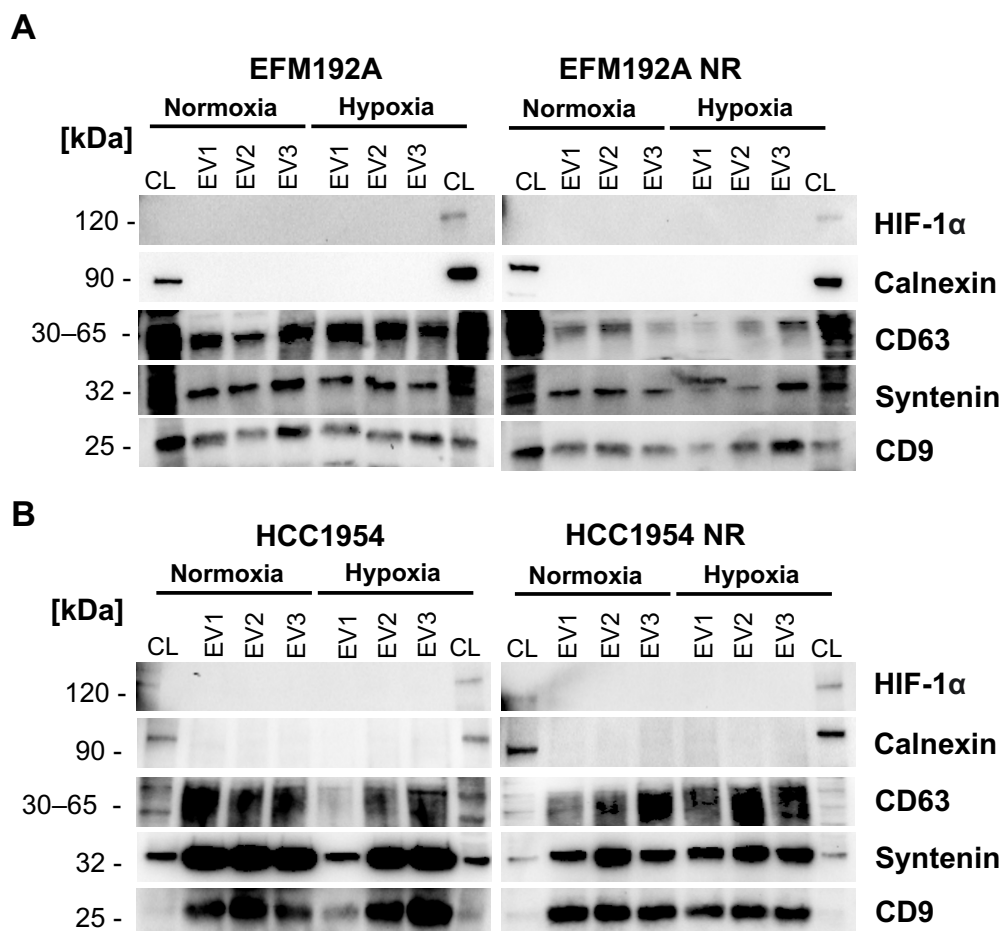
Figure 6.10. Immunoblotting analysis of EVs samples derived from 3D culture cells.
Enrichment of EVs positive and negative markers in EVs samples release from (**A**) EFM192A cell line variants and (**B**) HCC1954 cell line variants under normoxic and hypoxic conditions and their respective cellular lysate (CL) controls analysed by immunoblotting. Ten µg of protein was equally loaded per lane and analysed for HIF-1α, Calnexin, CD63, Syntenin and CD9. Immunoblots images for n = 3 independent experiments.

6.4.2.3   Characterisation of EVs by NTA

As mentioned before in *Section 6.4.1*, the main problem we faced during the optimisation of this study was the cell count and the viability calculation, as it proved impossible to break the spheroids down to intact single cells. MISEV 2018 guidelines established that it is especially important for EVs characterisation from conditioned media to establish the percent of dead cells at the time of EVs harvest, as well as establish the density/confluency at harvest. In 2D cultured cells experiments we typically normalise by number of harvesting cells, as best effort to standardise growth and harvesting (e.g., hypoxia decreased the final number of cells compared with normoxia). Nevertheless, here, we use the cell protein amount at collection time. This decision stems from existing challenges in developing a viable method for fully disaggregating the spheroids and conducting cell counts without compromising cell viability. Alternative normalisation using seeding density is collected in the **Appendix V** (**Figure V-3**). We subsequently analysed the resultant EVs derived from the spheroids. In **Table 6.8**, the results obtained from the NTA are presented. We did not observe any significant difference in the diameter of the vesicles between the conditions.

Table 6.8. Mean size and particles yield analysed by NTA.

Mean size (nm)			
	Normoxia	Hypoxia	*p* value
EFM192A	109.3 ± 7.2	114.3 ± 1.6	0.5575 (ns)
EFM192A NR	115.5 ± 4.0	117.6 ± 3.2	0.7993 (ns)
HCC1954	110.4 ± 4.0	127.4 ± 6.7	0.0608 (ns)
HCC1954 NR	117.7 ± 4.5	127.6± 1.4	0.0885 (ns)
Particle numbers				
	Normoxia	Hypoxia	FC	*p* value
EFM192A	$1.32\times10^{10} \pm 1.55\times10^{8}$	$1.49\times10^{9} \pm 3.23\times10^{8}$	n.d.	0.680 (ns)
EFM192A NR	$7.16\times10^{8} \pm 1.29\times10^{8}$	$7.33\times10^{8} \pm 3.37\times10^{8}$	n.d.	0.940 (ns)
HCC1954	$1.22\times10^{9} \pm 4.21\times10^{8}$	$1.90\times10^{9} \pm 8.76\times10^{8}$	↑1.6	0.497 (ns)
HCC1954 NR	$3.87\times10^{8} \pm 1.42\times10^{8}$	$1.41\times10^{9} \pm 4.58\times10^{8}$	↑3.7	0.419 (ns)
Particle numbers (30-150 nm)				
	Normoxia	Hypoxia	FC	*p* value
EFM192A	$8.7\times10^{8} \pm 1.21\times10^{8}$	$9.27\times10^{8} \pm 1.70\times10^{8}$	n.d.	0.744 (ns)
EFM192A NR	$4.58\times10^{8} \pm 7.34\times10^{7}$	$4.60\times10^{8} \pm 2.22\times10^{8}$	n.d.	0.988 (ns)
HCC1954	$6.89\times10^{8} \pm 2.62\times10^{8}$	$1.02\times10^{9} \pm 4.47\times10^{8}$	↑1.5	0.553 (ns)
HCC1954 NR	$4.30\times10^{8} \pm 2.12\times10^{8}$	$7.04\times10^{8} \pm 1.69\times10^{8}$	↑1.6	0.486 (ns)

Mean size and particles yield (normalised to cell protein ± SEM), as analysed by NTA. Fold change (FC) is calculated as hypoxia/normoxia ratio. ns = not significant; n.d. = no differences

6.4.2.4 Characterisation of EVs by IFCM

As explained in **Section 4.4.2.3**, NTA can estimate the size distribution and number of individual nanoparticles in a suspension, but it cannot be used to determine phenotype. In order to obtain a better estimation of the EVs quantities, we also analysed these samples by imaging flow cytometry. EVs samples derived from 3D cell culture under normoxia and hypoxia were analysed by IFCM using CellMask® (plasma membrane marker) and anti-HER2 antibody (**Figure 6.11**). As happened with other characterisation methodologies and in keeping with the results obtained from the EVs isolates derived from 2D culture, IFCM displayed different effects of hypoxia in the release of EVs that seemed to relate to cell context (resistance to neratinib). While HCC1954-derived EVs collected from hypoxic cells showed a significant increase of CellMask+ events (3.1-fold, $p = 0.024$) compared to those released from normoxic HCC1954 cells, EFM192A NR (1.7-fold, $p = 0.571$) and HCC1954 NR (2.7-fold, $p = 0.255$) -derived EVs samples also presented an insignificant increase for CellMask+ events when cells were cultured in hypoxic conditions. On the other hand, EFM192A showed no significant differences of CellMask+ events in hypoxia compared to normoxia.

It is also important to note that EFM192A NR spheroids seemed to release fewer CellMask+ events compared to their neratinib sensitive counterparts in normoxic conditions, while under hypoxia similar CellMask+ events were found in EFM192A NR-derived EVs isolates compared with EFM192A-derived EVs. In the case of HCC1954 cell lines, spheroids formed by HCC1954 NR seemed to release fewer CellMask+ events compared to HCC1954 spheroids in both normoxic and hypoxic conditions, being significant in the latest (3.6-fold, $p = 0.012$).

Double-positive events for CellMask and HER2 were also analysed. EVs samples obtained from HCC1954 spheroids cultured under hypoxic conditions exhibited an increase in those double-positive compared to those EVs samples release under normoxia (2.2-fold, $p = 0.028$). In keeping with the obtained results for CellMask+ events in HCC1954 cell variants, a significant decrease in CellMask+/HER2+ events was found in HCC1954 NR-derived EVs compared to HCC1954-derived EVs in hypoxia (5.6-fold, $p = 0.003$). Alternative normalisation using seeding density is collected in the **Appendix V** (**Figure V-4**).
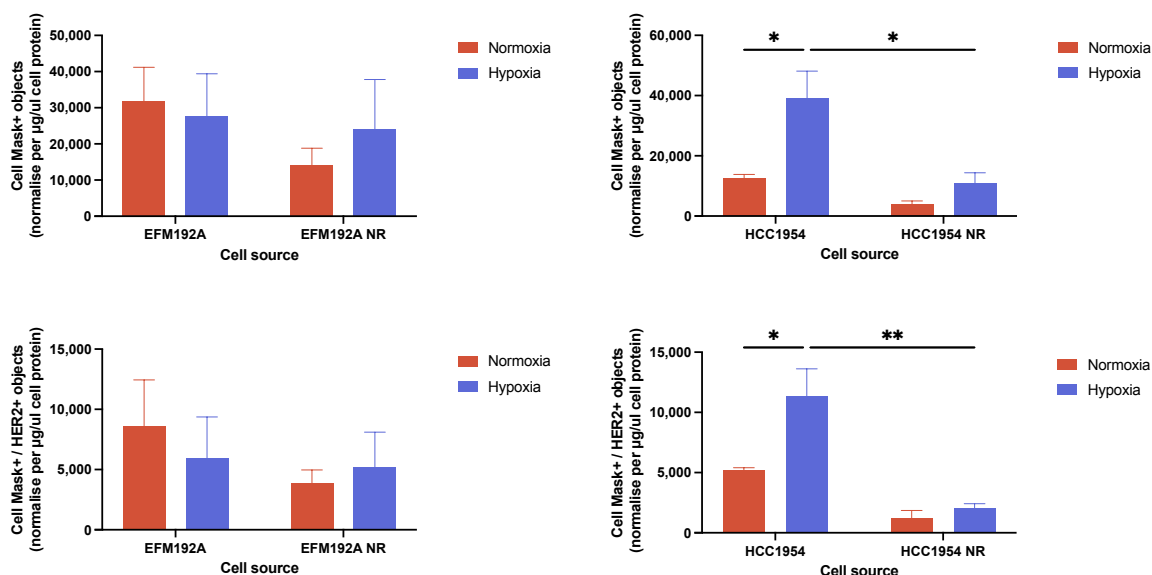
Figure 6.11. IFCM analysis of EVs derived from 3D cell cultured cells.

Imaging flow cytometry (IFCM) analysis of EVs samples obtained from 3D cultured cells under normoxic and hypoxic conditions. Data was collected by measuring the CellMask cell membrane signal (**Top**) and CellMask together with HER2 signal (**Bottom**) on the EVs samples obtained from two HER2+ cell lines and their neratinib-resistant counterparts. Two-way *ANOVA* was used to calculate significance: *$p<0.05$, **$p<0.01$ (n = 3 ± SEM).

6.4.2.5   Characterisation of EVs by TEM

We also analysed the EVs samples by TEM, to evaluate their integrity and appearance. **Figure 6.12** illustrates representative images of EVs derived from EFM192A, EFM192A NR, HCC1954, and HCC1954 NR spheroids. The qualitative TEM approach showed that both conditions produced a range of particle sizes on the isolates derived from those spheroids.
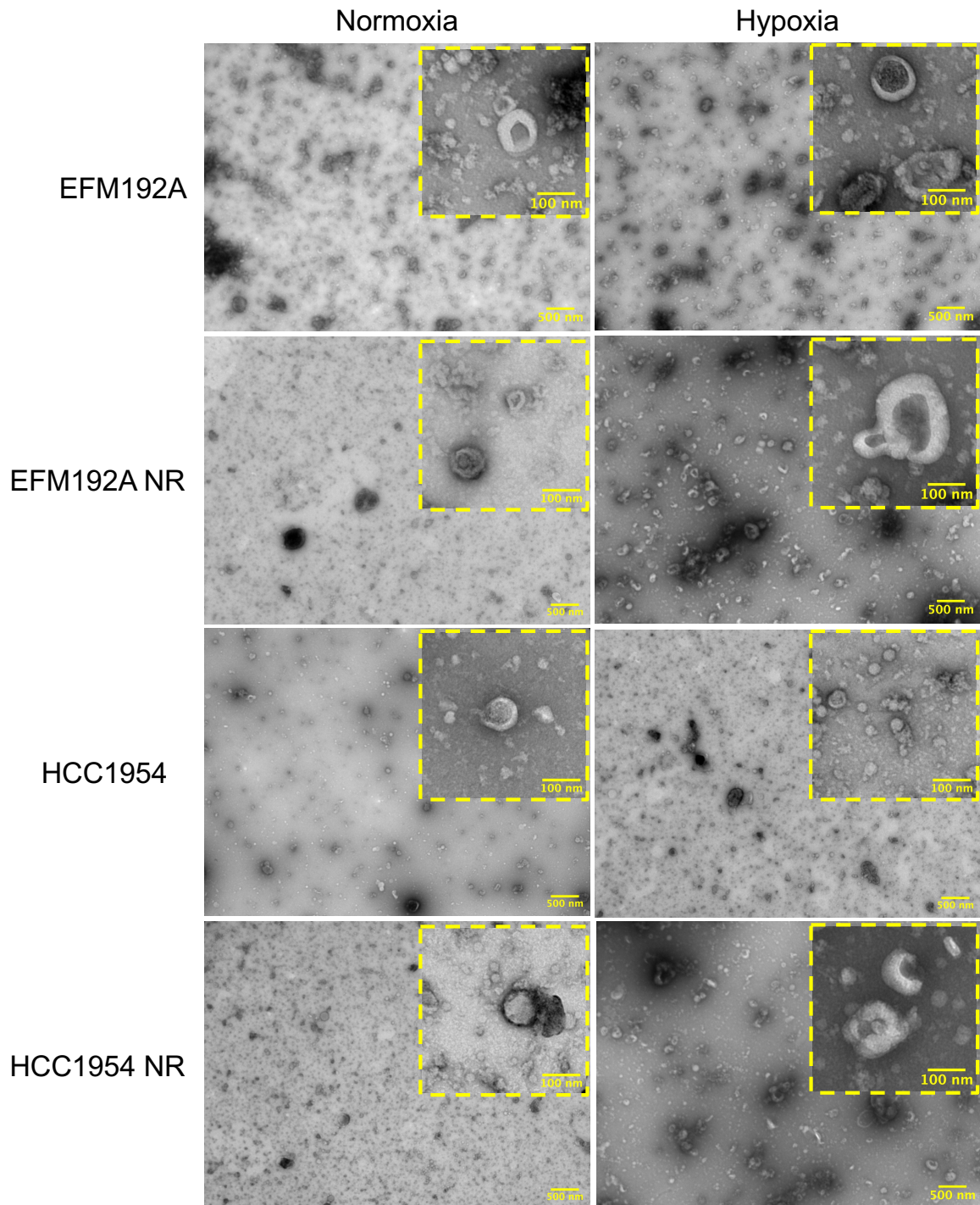
Figure 6.12. Representative images obtained by TEM.

EVs isolates derived from 3D spheroids were enriched by using dUC protocol from two pairs of HER2+ breast cancer cell line variants under normoxic and hypoxic conditions. Big pictures represent a zoomed-out view (5000x; Scale bar = 500 nm), while the edged pictures depict a zoomed-in view (30000x; Scale bar = 100 nm) of the same spot.

6.4.2.6 Investigating the HER2 presence on the EVs surface

As previously investigated in **Chapter 5** (see **Section 5.4.3**), we investigated here the presence of HER2 on the surface of non-lysed EVs samples derived from 3D culture cells and the corresponding harvested spheroids by ELISA, to investigate if they are representative of the HER2 status of their cells of origin (**Figure 6.13**). As obtained by immunoblotting, EFM192A and EFM192A NR spheroids presented a slightly lower HER2 expression under hypoxia compared to normoxia. However, no significant differences were found in HER2 expression between HCC1954 and HCC1954 NR spheroids by ELISA. When we analysed the presence of HER2 on the EVs surface, we found an increase on the EVs released under hypoxic conditions from EFM192A NR (1.8-fold, $p = 0.034$), HCC1954 (2.7-fold, $p = 0.202$), and HCC1954 NR (2.1-fold, $p = 0.015$) cells. No significant differences were found in the case of the EVs derived from EFM192A cells between hypoxic and normoxic conditions. Alternative normalisation using seeding density is collected in the **Appendix V** (**Figure V-5**).
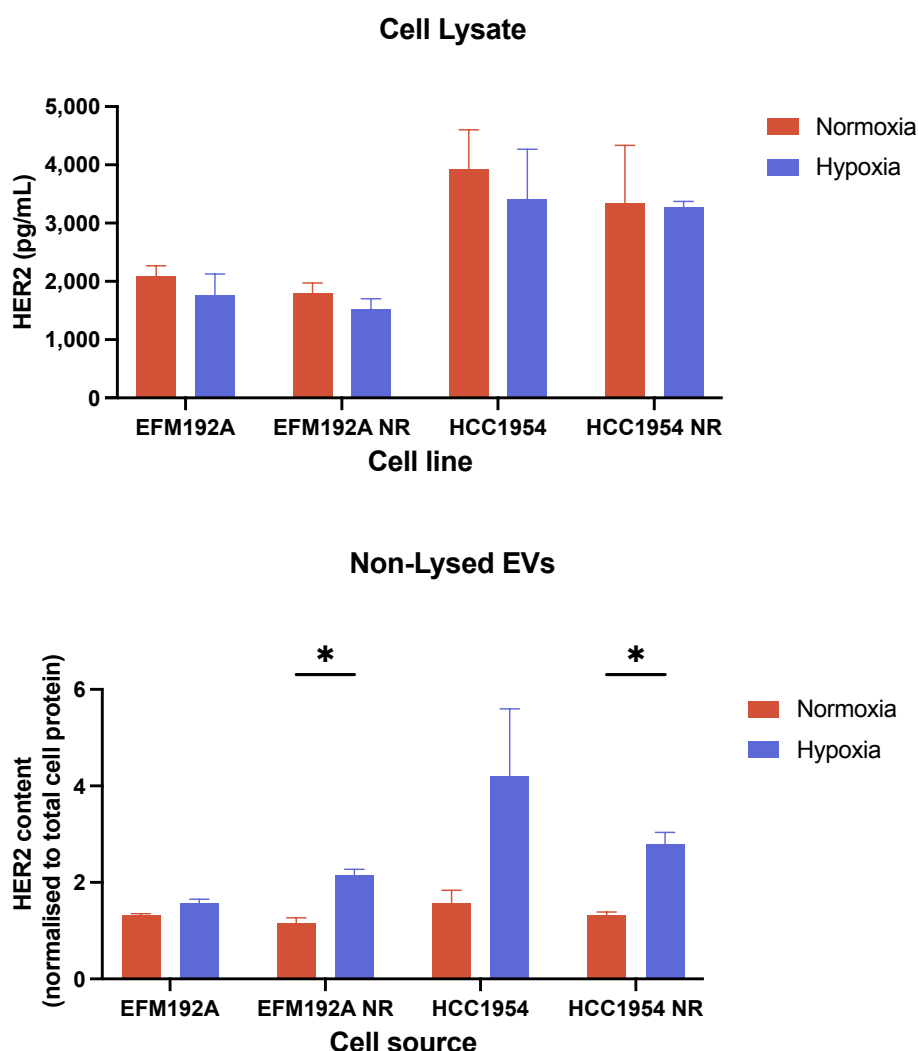
Figure 6.13. HER2 ELISA analysis.

Investigating the HER2 expression on HER2+ breast cancer spheroids (**Top**) and its presence on non-lysed EVs isolates under normoxic and hypoxic conditions (**Bottom**). Data are represented as mean ± SEM ($n = 3$). Multiple paired t-test was used to calculate the significance: *$p<0.05$.

6.4.2.7 Summary of findings for the EVs characterisation

An overview of the results obtained for the characterisation of EVs released by 3D cultured breast cancer cells under normoxic and hypoxic conditions is collected in **Table 6.9**.

Table 6.9. Review of main findings.

EVs derived from 3D cultured cells				
Assay	EFM192A	EFM192A NR	HCC1954	HCC1954 NR
Protein amount	↓1.3-fold (p = 0.231)	↑1.4-fold (p = 0.239)	↑2.8-fold (_p = 0.009_**)	↑1.4-fold (p = 0.281)
NTA: Particle size	n.d.	n.d.	n.d.	n.d.
NTA: Particle amount	n.d.	n.d.	↑1.6-fold (p = 0.497)	↑3.7 -fold (p = 0.419)
NTA: Particle amount 30-150 nm	n.d.	n.d.	↑1.5-fold (p = 0.553)	↑1.6-fold (p = 0.486)
EVs markers (Immunoblotting)	↑CD63 (p = 0.196)	n.d.	↓CD63 (p = 0.27)	↓CD9 (_p = 0.024_*)
IFCM - Cell Mask+	n.d.	↑1.7-fold (p = 0.571)	↑3.1-fold (_p = 0.024_*)	↑2.7-fold (p = 0.255)
IFCM - CellMask+HER2+	n.d.	n.d.	↑2.2-fold (_p = 0.028_*)	↑1.7-fold (p = 0.089)
HER2 (ELISA) non lysed EVs samples	n.d.	↑1.8-fold (_p = 0.034_*)	↑2.7-fold (p = 0.202)	↑2.1-fold (_p = 0.015_*)

*Summary of all the substantial results obtained from the different EVs samples derived from 3D cell culture under normoxia and hypoxia. Fold change is calculated as hypoxia/normoxia ratio. Findings with significant p values are highlighted (*p<0.05, **p<0.01); n.d. = no differences.*

6.5 Discussion

In general, 3D cell culture can provide a more physiologically relevant environment for studying EVs compared to traditional 2D cell culture, and it can be used to investigate the role of EVs in various diseases and physiological processes. However, there are limitations to establishing 3D cultures for EVs collection and characterisation. For instance, the selection of the 3D culture model, the cell count at the collection time, and the cell viability (the existence of a necrotic core in cancer spheroids could increase the presence of apoptotic bodies in EVs samples compared to 2D cell culture)[363].This complexity can make it more difficult to isolate and characterise EVs, as there may be more heterogeneity in the EVs population. The choice of EVs isolation method is another factor to consider, as EVs separation can be more challenging for 3D cell cultures compared to 2D cultures. For instance, dUC, which is a common method for isolating EVs, may not work as well for 3D cultures due to the presence of scaffold materials or other factors that can interfere with the centrifugation process. Other consideration is that the release of EVs from cells in 3D culture can be more variable compared to 2D culture, depending on factors such as the type of culture method used and the specific cell type. These factors can make more challenging the standardisation and analysis of EVs derived from 3D cultures. Finally, 3D cultures may require larger sample volumes compared to 2D cultures to obtain enough EVs for analysis.

Due to the lack of standardisation in the 3D cell culture[364] and for the separation of the EVs harvested from these structures, our first investigation involved the selection of the best methodology for spheroid formation and the EVs separation from those spheroids. As it would be part of the future work to compare EVs derived from 2D and 3D cell culture from normoxic and hypoxic conditions, the EVs separation method would be dUC. However, as explained in **Section 6.1**, the use of some scaffolds/medium factors could interfere with the centrifuge steps. We then decided to assess the suitability of a methodology previously employed in this lab to form spheroids[349] based on poly-HEMA coated 96-well plates. However, the volume was the main limitation together with the handling of several individual wells to collect the CM without disrupting or absorbing the spheroids. After considering different platforms for spheroid formation and comparing different parameters including volume of CM, number of spheroids, and price, we decide to assess the fitness of the 6-well Elplasia® plates to our aims. Elplasia® plate contains an estimated number of 2,887 microcavities in each well that allows to form approximately 2,887 spheroids/well. In addition, around 13 mL of media can be held per well, allowing an increase in the volume of CM that can be obtained per plate as well as a large-scale spheroid formation.

The main issue we found in obtaining reproducible results was a problem not directly related with the Elplasia® platform, rather our lack of previous experience in the use of 3D cell culture. This main problem was the spheroid disaggregation step together with the subsequent cell count and cell viability calculations. Despite adhering to various published protocols that claim an efficient disaggregation of the spheroids[365,366], none of these approaches were effective without affecting the cell viability. Some spheroids were intact, while other cells were completely in the single cell suspension. In 2D *in vitro* models, the quantification of EVs is commonly normalised according to the final cell concentration, which is considered a standard practice[355]. However, when it comes to 3D

in vitro models, the normalisation of EVs is not standardised[367–369]. This is primarily due to the challenge of determining the cell count at the time of conditioned media collection, which requires the disaggregation of spheroids. Consequently, some studies opt to normalise EVs based on the seeding densities or ml of starting material. However, we faced problems to establish a successful way to completely disaggregate the spheroids and count the cells without affecting the viability of the cells. In addition to this, previous results obtained in 2D cell culture (see **Section 5.4.1**) showed a significant decrease in cell counts under hypoxia conditions compare with normoxia. Because of this, we decided to normalise EVs counts to the protein amount of the corresponding cell lysates obtained at the collection time in an effort to achieve the most reliable results.

It has been shown that the ability to form rounded 3D structures is not an innate characteristic of all breast cancer cell lines, as SKBR3 and SKBR3 NR showed. SKBR3 cells have been shown to be able to form only a compact aggregate under specific conditions, while the usual structure formed was a loosely bound, flat aggregates, or a single cell suspension[361,362,370]. Consequently, these cells were not considered for assessing the efficiency of the methodology for EVs isolation.

EFM192A, EFM192A NR, HCC1954 and HCC1954 NR were found to be able to form compact and rounded spheroids in the 6-well Elplasia® plates. However, hypoxia seemed to affect the roundness, smoothness and compactness showed by the spheroids. Both the spheroids diameter and the volume were significantly decreased under hypoxic conditions in all the cell line variants.

When we analysed protein from those spheroids by immunoblotting, we found that HER2 expression was lower in hypoxia compared to normoxia in all the cell line variants; being significantly so in HCC1954 NR cells. These results differ with those obtained in 2D cell culture (**Chapter 5**) for EFM192A and EFM192A NR cell variants. Surprisingly, HCC1954 NR spheroids demonstrated a higher expression of HER2 compared to their neratinib-sensitive counterparts. This result appears to be in contrast between our previous findings in 2D cell culture, where we found a significant HER2 down-regulation in neratinib-resistant cell lines compared with their neratinib-sensitive counterparts (see **Section 5.4.1**), suggesting that the HER2 expression differs in 2D compared to 3D culture. Previously work performed by our group showed a significant increase of HER2, HER3 and EGFR in BT474, HCC1954 and EFM192A breast cancer cells cultured in 3D compared with their 2D cultured counterparts[349]. However, the comparison between neratinib-sensitive and neratinib-resistant in 2D and 3D cell culture was not addressed.

In keeping with this, previous work found that SKBR3 breast cancer cells and SKOV-3 ovarian cancer cells cultured in 3D exposed higher levels of HER2 activation, as well as increased expression of genes involved in cell growth and survival pathways[371]. This overexpression of HER2 in 3D models could be due to a more physiologically relevant environment obtained by 3D cell culture compared with the traditional 2D cell culture.

It was also found that HCC1954 NR spheroids expressed similar amounts of HIF-1α in both normoxia and hypoxia. In the monolayer-cultured HCC1954 NR cells, HIF-1α protein expression was also detected under normal culture conditions, although its expression was higher under hypoxic conditions. This abnormal expression of HIF-1α could be related with the resistance to neratinib, as HIF-1α together with HIF-2 α have been found to be a significant regulator of adaptive processes that could promote tumour cell malignant phenotypes, including proliferation, invasiveness, and

metastasis[372,373]. In addition, KEGG pathways analysis of the differentially expressed proteins between HCC1954 and HCC1954 NR cell variants showed HIF-1 signalling pathway as one of the top 10 enriched KEGG pathways (see **Appendix II**).

It has been shown that β-catenin could protect breast cancer cells from hypoxia effects[307]. In addition, Wnt/β-catenin pathway has been associated with the progression of various pathological conditions, including cancer. In this context, β-catenin plays a significant role in promoting cancer development, including aspects such as cell proliferation, metastasis, and resistance to treatment, among other factors[323]. β-catenin was found to be down-regulated under hypoxic conditions in EFM192A and HCC1954 spheroids, while no differences in its expression were found in the case of EFM192A NR and HCC1954 NR spheroids. The down-regulation of β-catenin in hypoxia may have implications for various cellular processes, such as cell proliferation, migration, and apoptosis. Previously work performed by Cai et al. (2014)[374] demonstrated that β-catenin down-regulation promotes a decrease of epithelial E-cadherin expression together with an increase mesenchymal vimentin expression, suggesting the promotion of EMT.

The expression of CD9 seemed to correlate with the level of resistance to neratinib. While EFM192A and HCC1954 showed an increase of CD9 under hypoxic conditions, EFM192A NR and HCC1954 NR spheroids showed a significant reduction of CD9 expression in hypoxia compared to normoxic conditions. Furthermore, CD9 protein was more abundantly expressed in EFM192A NR and HCC1954 NR spheroids cultured in normoxia conditions than their neratinib-sensitive counterparts. However, under low levels of oxygen, the expression of CD9 was higher on EFM192A and HCC1954 than their neratinib-resistant counterparts. In addition to its location at the cell membrane and EVs (converting CD9 a classical marker for EVs characterisation), CD9 is implicated in various diseases and pathological conditions, including cancer and inflammation.

For example, the transfection of miR-518F-5p in the TNBC cell line MDA-MB-231 caused a decrease in CD9 expression leading an increase in cell migration[375]. In addition, several studies associated the lower expression of CD9 with poor prognosis and recurrence in breast cancer patients[376–378].

We thus characterised the suitability of this methodology for EVs isolation and the effect of hypoxia condition on EVs release by EFM192A, EFM192A NR, HCC1954 and HCC1954 NR cultured in 3D culture. As per our knowledge, this is the first time that EVs isolates from HER2+ breast cancer cell lines and their neratinib-resistant counterparts growing in 3D culture are fully characterised. We collected the EVs isolates derived from the different four cell variants after 5 days under normoxic/hypoxic conditions.

An increase of EVs protein content was observed in EVs derived from EFM192A NR, HCC1954, and HCC1954 NR under hypoxic conditions compare to their normoxic counterparts, being significant in the case of the HCC1954-derived EVs (p = 0.009). In addition to this, EVs markers investigated by immunoblotting showed their enrichment in the 3D-derived isolates were cell line specific and dependent of the oxygen level. For instance, only substantial differences on the presence of CD63 were found. EFM192A-derived EVs isolates under hypoxic conditions presented a higher presence of CD63 compared with their normoxic counterparts. EVs released in normal conditions by EFM192A NR spheroids showed a higher enrichment of CD63 compared to the EVs harvested in hypoxia. EFM192A NR-derived EVs also seems to carry less CD63 than their neratinib-sensitive counterparts.

When those samples were analysed by NTA, no differences were found in terms of particle size and particle numbers (normalised to total cell protein). However, when analysed by IFCM, HCC1954 showed a significant increase of CellMask+ events in hypoxia (p = 0.024) whereas no significant differences were found between EVs samples derived from the other cell lines under hypoxia and normoxia. It is also important to note that EFM192A NR and HCC1954 NR spheroids seemed to release fewer CellMask+ events compared to their neratinib sensitive counterparts. Those results matched with the previous obtained by monolayer-culture of the cells, where we obtained a decrease on EVs released by neratinib-resistant cell lines. Double-positive events for CellMask and HER2 were higher in EVs derived from HCC1954 cultured in hypoxia compared to normoxic conditions (p = 0.028), together with a significant decrease on those events in HCC1954 NR-derived isolates compared to their HCC1954-derived counterparts in both conditions. These results are consistent with the ones obtained from the HCC1954 cells cultured in 2D in previous chapter (see **Section 5.4.2.5**).

Previous studies have demonstrated that 3D cultures exhibit a greater release of EVs compared to 2D cultures. Additionally, it has been observed that oxygen deprivation can contribute to an increase in the release of EVs[379,380]. However, here the comparative between 2D and 3D culture under hypoxic and normoxic conditions was not yet addressed. In order to perform this comparison between 2D and 3D cell culture, a suitable normalisation process and equally standardised conditions have to be applied for both cell culture methodologies.

We also investigated the HER2 expression of those cells and the presence of HER2 on the surface on the non-lysed EVs by ELISA. No significant differences were found on HER2 protein level between cells cultured in hypoxia and normoxia. However, higher presence of HER2 on the EVs' surface was found on the EVs samples obtained from hypoxic EFM192A NR, HCC1954, and HCC1954 NR cells (p = 0.033, p = 0.020, and p = 0.015, respectively). These findings together with the decrease of HER2 expression demonstrated by immunoblotting on the hypoxic cells provide strong support for the hypothesis of a higher HER2 trafficking under hypoxic condition, as the observed results are consistent with the previously obtained by 2D cell culture (see **Section 5.4.3**).

Considering all the advantages and challenges addressed in this chapter, the use of Elplasia® plates as a 3D platform for EVs isolation proved to be a successful strategy, as it yielded a substantial amount of EVs. This indicates that the 3D platform is well-suited for the isolation of EVs and can be a reliable method for EVs research, particularly for applications where a high yield of EVs is desired. Although the approach shows potential, there are specific areas that still require further optimisation. Notably, the spheroid disaggregation step and subsequent cell count and viability determination need to be refined to improve accuracy and precision. Addressing these aspects of the methodology will be critical in ensuring the reliability and reproducibility of the results.

6.6 Conclusion

Over the past few decades, substantial advancements have been made in the development of representative 3D tumour models, which have enabled more accurate drug screening by creating tumour structures that closely mimic the natural microenvironments of tumour growth. Our attempt in the use of Elplasia® plates to obtain EVs released by spheroids in an optimum concentration for their characterisation showed that this system could precisely hold larger number of spheroids than other 3D platforms and that it was suitable in obtaining an appropriate EVs yield to investigate the differences between normoxia and hypoxia culture conditions. While the methodology shows promise, further optimisation is necessary to enhance its efficacy and reliability.

Chapter 7

Pre-clinical *in vitro* models used in cancer research: results of a worldwide survey

Abstract

To develop and subsequently get cancer researchers to use organotypic 3D models that can recapitulate the complexity of human *in vivo* tumours in an *in vitro* setting, it is important to establish what *in vitro* model(s) researchers are currently using and the reasons why. Thus, we developed a survey on this topic, obtained ethics approval, and circulated it throughout the world. The survey was completed by 101 researchers, across all career stages, in academia, clinical or industry settings. It included 40 questions, many with multiple options. Respondents reported on their field of cancer research; type of cancers studied; use of 2D/monolayer, 2.5D and/or 3D cultures; if using co-cultures, the cell types(s) they co-culture; if using 3D cultures, whether these involve culturing the cells in a particular way to generate spheroids, or if they use additional supports/scaffolds; techniques used to analyse the 2D/2.5D/3D; and their downstream applications. Most researchers (>66%) only use 2D cultures, mainly due to lack of experience and costs. Despite most cancer researchers currently not using the 3D format, >80% recognise their importance and would like to progress to using 3D models. This suggests an urgent need to standardise reliable, robust, reproducible methods for establishing cost-effective 3D cell culture models and their subsequent characterisation.

7.1 Introduction

Cancer research requires *in vitro* models capable to produce reliable biomedical information through mimicking the cells' phenotype as it exists in the target tissue [198]. Thus, the use of pre-clinical *in vitro* models, as well as *in vivo* models, continues to be crucial in cancer research. These models are necessary for deciphering molecular mechanisms of key events such as tumour growth, metastasis, drug resistance, and aspects of immune evasion. They are also necessary for anti-cancer drug screening and development[192]. However, as only 10% of potential anti-cancer drugs succeed during their clinical development, mainly due to a lack of efficacy or intolerable toxicity[193–195], this puts into question the relevance of the models used.

Before any cancer research progresses to clinical utility, it typically involves studies in animal models. However, for many reasons, including ethics and the 3Rs (replacement, reduction, and refinement of the inclusion of animals in research), costs, complicated and laborious techniques requiring research specialists, appropriate *in vitro* models should always be used first to their maximum potential[196,197].

The simplest approach for *in vitro* cancer studies is the monolayer culture of cancer cells in 2D conditions. A 2D culture is straightforward with and low-cost maintenance, which might be considered one of their main advantages[381].

Nevertheless, its limitations have been increasingly recognised, proven its inadequacy as a fully reliable pre-clinical tumour model, mainly as an over-simplified version of tumour conditions *in vivo*, often failing to address many of the more dominant pathological problems, such as the TME. Moreover, it is reported that 2D cultures do not conserve the original shape and polarisation of cells[197,200], which could affect other properties such as their functions, organelles' organisation, and cell signalling[381].

From the 1980s when Mina Bissell highlighted the importance of the ECM in cell behaviour[382–385], it is generally accepted that 3D cell culture models (if developed appropriately) should more accurately represent the tumour and its microenvironment and that their behaviour should be more reflective of *in vivo* cellular responses when compared to the 2D models[198,201,202,204].

To make real advances in developing precision medicine for cancer, pre-clinical models that represent *in vivo* biology and the microenvironmental factors, while also respecting the rights of animals, are necessary[192]. Indeed, several approaches are being used to increase the complexity of the models. These include 2D co-cultures of, i.e., cancer cells with stromal cells; 2.5D cultures, which consist of cells growing on top of a layer of ECM proteins; and 3D cultures which are more complex structures[202,203,386]. Three-dimensional cultures can be designed using different approaches and divided into: (i) non-scaffold-based cultures or spheroids; (ii) scaffold-based cultures; (iii) specialised 3D culture platforms, including microfluidic cell culture platforms and *organ-on-chip* systems that allows the control of different conditions (i.e., the creation of chemical gradients by the fluid flow)[387], and (iv) hybrid systems that integrate spheroids into a scaffold structure[388], providing improved tumour models for screening anti-cancer drugs.

Using the bibliometric tool Scopus to identify growth metrics of the terms "*in vitro* tumor models" and "3D *in vitro* tumor models", a substantial increase in publication numbers was observed (**Figure 7.1**), year on year, indicating increasing interest in this field.
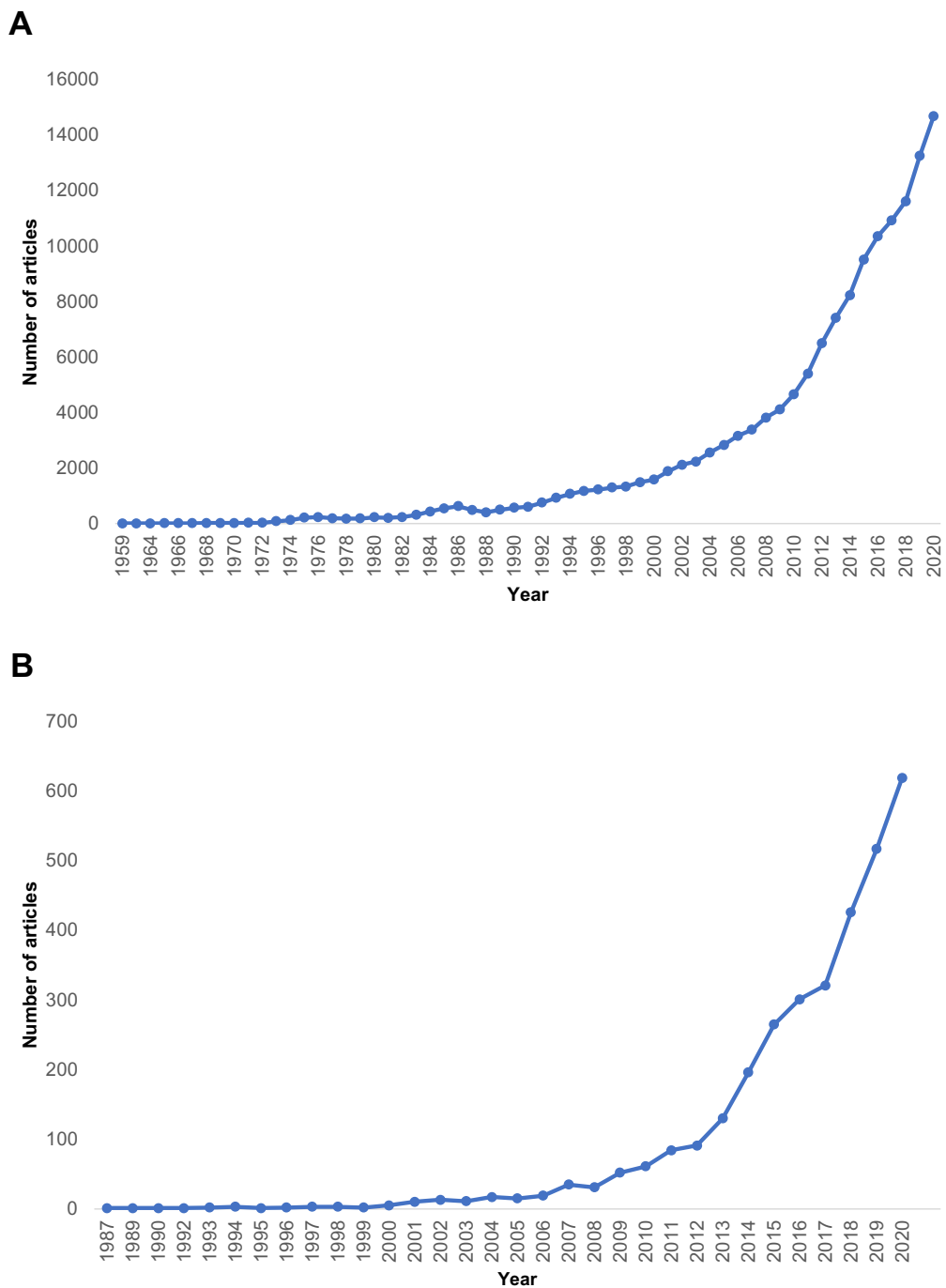
Figure 7.1. Number of articles per year.

Expansion in the numbers of peer-reviewed published articles with the term (**A**) "*in vitro* tumor models" or (**B**) "3D *in vitro* tumor models"; (*source: Scopus; Accessed over time, most recently 17 November 2021*).

Despite the general agreement in the cancer research community that *in vitro* 3D models can be more representative of tumours in the body than 2D models, these approaches have not been extensively incorporated in research[200,205]. Reviewing the published literature gives us information on what *in vitro* models were used in research that was published. However, it gives us no indication on why such models were chosen—or, indeed, what models are being used in unpublished cancer research and why.

7.2 Aims of the study

Thus, this study aimed to perform the first global survey of currently used pre-clinical *in vitro* models for cancer research, the reasons for the choices made, and the considered strengths and limitations of these models.

7.3 Materials and Methods

7.3.1 Survey Design

Survey questions (n = 40) were generated by using Typeform (Barcelona, Spain; *http://typeform.com*) and were designed with logic jumps, meaning that respondents were only brought to certain sections based on their previous answers. The survey design is shown in the **Appendix IV.**

After obtaining ethics approval including General Data Protection Regulation (GDPR) considerations from the School of Pharmacy and Pharmaceutical Sciences Research Ethics Committee of Trinity College Dublin (No. 2020-04-01), the survey was circulated extensively to cancer research centres by email and by sharing on social media channels. The survey was opened on 28 May 2020 and closed in December 2020. A total of 101 full submissions were collected to an Excel file and consequently analysed.

7.3.2 Statistical Analysis

Analysis was performed using IBM SPSS 28. Nominal data are presented as percentages. The existence of correlation between variables was assessed using the Pearson correlation coefficient (PCC).

7.4 Results

The extensive reach of the survey was clear by the fact that the respondents were from 19 countries spanning four continents (**Figure 7.2A**). No relatively strong correlations (PCC>0.4) or strong negative correlations (PCC<−0.4) were found between continent and cancer type or field. Of the respondents, 96% belonged to academia, 3% from clinical settings, and 1% from industry. Principal investigators (39.6%), post-doctoral researchers (17.8%) and senior researchers (8.9%) represented more than 66% of the responses, reflecting a strong level of interest in the topic at the senior level. Respondents also included PhD students (26.7%), clinical researchers (2%), as well as associate researchers (1%), laboratory technicians (1%) and research assistants (1%).

Regarding the fields of cancer research performed by the respondents, the most reported was fundamental cancer biology, followed by cancer biomarkers and cancer drug sensitivity/resistance (**Figure 7.2B**). No relatively strong correlations (Pearson's R > 0.4) or relatively negative correlations (PCC < −0.4) were found between field and cancer type studied. In this relatively new and specialised field of research, EVs research in cancer was reported to be the interest of almost 17% of respondents. The cancer types represented by the *in vitro* models varied widely. The most common cancer types being studied were breast, colorectal, lung and prostate cancer. Cervical cancers were the most under-studied based on the responses (see **Figure 7.2C**).
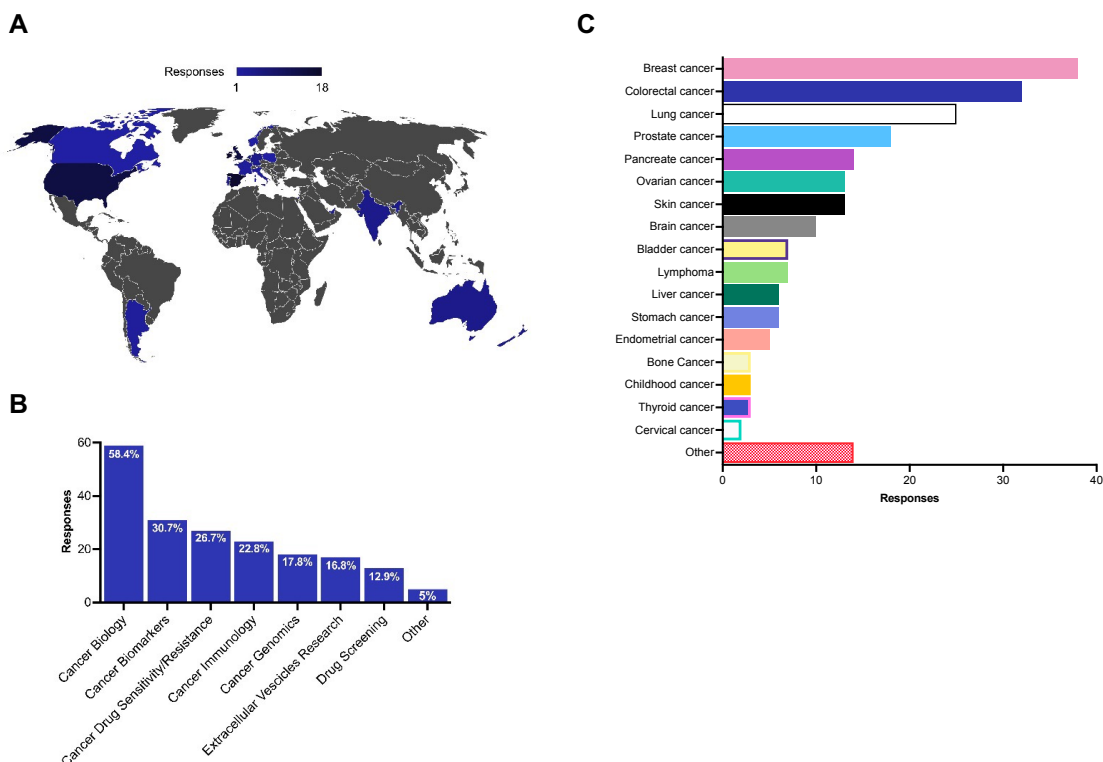
Figure 7.2. General profile of the respondents.
(**A**) Number of respondents categorised by the country of work. The graph was obtained from 101 responses; (**B**) Field of cancer research performed; (**C**) Cancer type studied by the respondents. *Note: some respondents indicated that they are involved in more than one field of research and/or work on more than one cancer type.*

7.4.1 Principal characteristics of *in vitro* models

A key component of any *in vitro* tumour model is the source of cancer cells. Commercially available cell lines were the most widely chosen option, accounting for 81.2% of the responses; with primary cells accounting for 38.6%, and other undeclared sources making up the remaining approximately 5%.

The vast majority of the respondents indicated that cancer cells are the principal cell type for their *in vitro* models (91.1%) whilst the second most used were immune cells (20.8%), followed by stem cells (7.9%) and stromal cells (6.9%). Of those who reported working with cancer cells, 93.8% indicate that these were of primary tumour origin; 21.9% reported that their studies involved working with cells from the pre-metastatic niche; 25%, from the non-tumour cell part of the metastatic niche; and only 18.8% were secondary tumour cells.

Co-culture is an approach in which two or more different types of cells (rather than just cancer cells alone) are cultured together to better represent a tumour and the TME[389]. However, only 40.6% of the researchers reported that they use any co-culture model, in any form of *in vitro* model (**Figure 7.3A**). When we asked what type of cells were co-cultured with their main cell source, the researchers indicated cancer cells (56.1%), immune cells (46.3%), stromal cells (39%) and stem cells (7.3%) (see **Figure 7.3B**).
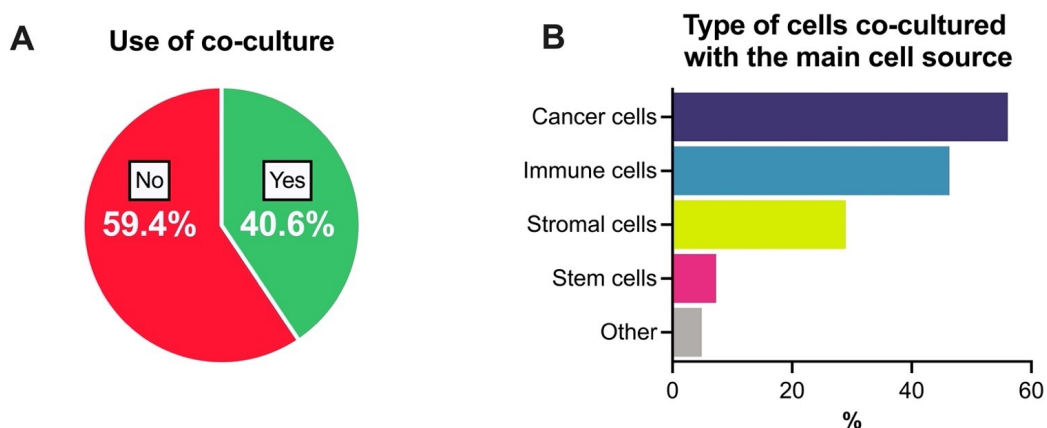
Figure 7.3. Co-culture use in preclinical *in vitro* tumour models.
(**A**) Use of co-culture models and (**B**) types of cells used in these co-culture models together with the main cell source. Results represented as percentages (%). *Note: Figure 7.3B represents a question with multiple choice. Some respondents indicate that their co-culture models involved more than one type of cells.*

7.4.2 3D models and types used in cancer research

The development of *in vitro* tumour models, with increased complexity, has been aided by our improving understanding of tumour biology, tissue engineering, as well as advanced in the development of biomaterials and microfluidics[192]. However, despite such progress the use of 2D culture models exclusively is still being the most preferred option; followed the use of more than one

in vitro model but using of 2D culture in all cases, and the use of 3D culture exclusively was the third chosen option (**Figure 7.4A**).

When the correlations between the cell types used and the culture types were analysed, it was found relative strongly negative correlations between the use of stem cells in 2D Culture (PCC = −0.459; *p* = <0.001) and the use of cells obtained from the metastatic niche in 3D Culture (PCC = −0.419; *p* = <0.001). Regarding the positive correlations, a relative strongly correlation was found between the use of primary cells in 3D Culture (PCC = 0.442; *p* = <0.001).

We also asked about the use of co-culture when using 3D models specifically. Fewer than 26% of studies used co-cultures, while 74.2% of 3D constructs were monocultures (**Figure 7.4B**). In the cases was used, stromal cells (75%) and immune cells (62.5%) were the most used type of cells in combination with cancer cells. Only 12.5% of respondents indicated the use of other cancer cells in a co-culture (**Figure 7.4C**).
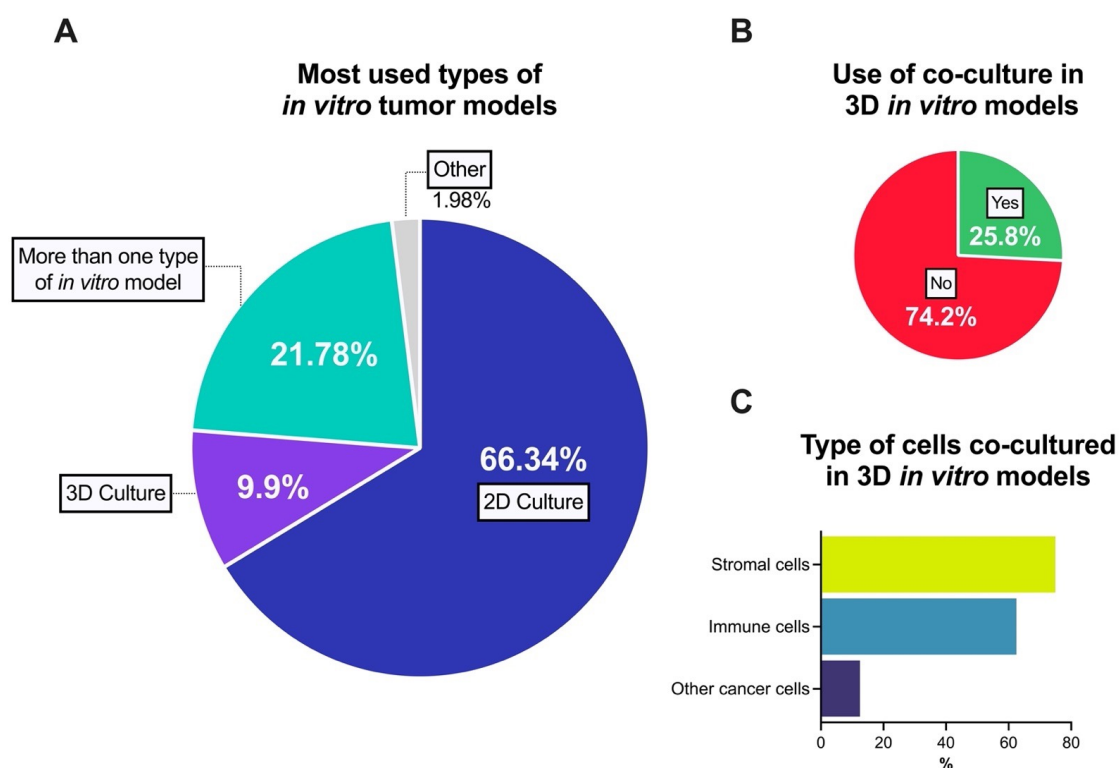
Figure 7.4. Use of 3D *in vitro* models in preclinical cancer research.

(**A**) Main *in vitro* tumour models; (**B**) Use of co-cultured approach related to 3D *in vitro* tumour models; (**C**) Most used cell types to co-culture with cancer cells in 3D *in vitro* tumour models. *Note: Figure 7.4C represents a question with multiple choice. Some respondents indicate that their co-culture models involved more than one type of cells.*

The survey also included questions related to the characteristics of the principal 3D model used (see **Figure 7.5**). For those using 3D models at all, it was found that the most extended approach used was scaffold-based models (51.6%), followed by scaffold-free culture (38.7%) (**Figure 7.5A**). No one reporting using a hybrid system. A natural scaffold was the preferred option for those who used scaffold-based models (81.25% of the respondents), followed by synthetic (43.8%), and then semi-

synthetic (12.5%) materials (**Figure 7.5B**). A list of materials that might be used was included in the questions for the three categories (see **Appendix VI**; **Q15**). Only two synthetics [Polyethylene glycol, PEG (31.2%); Polyhydroxy ethyl methacrylate, poly-HEMA (6.2%)] and two semi-synthetic materials (PEGylated protein scaffolds, 23.1%; HyStemTM, 7.7%) were reported to be used by any of the respondents. Natural materials were widely used (**Figure 7.5C**). We also queried the functionalisation of the materials used. Most (62.5%) of the respondents indicated that the material that they used in their 3D models was not functionalised, while 25% were (the remaining 12.5% indicated that the functionalisation was not applicable). Another approach used in 3D culture are multicellular tumour spheroids, dense tri-dimensional aggregates of cancer cells alone or combined with other cell types in suspension culture and where scaffold are not used[196,390]. Various techniques can be used to produce such spheroids. When we asked about the procedures used for spheroid formation, researchers indicated that the main three approaches used were low attachment plate (51.6%), matrix-embedded (45.2%) and hanging drop (12.9%), among others (**Figure 7.5D**).
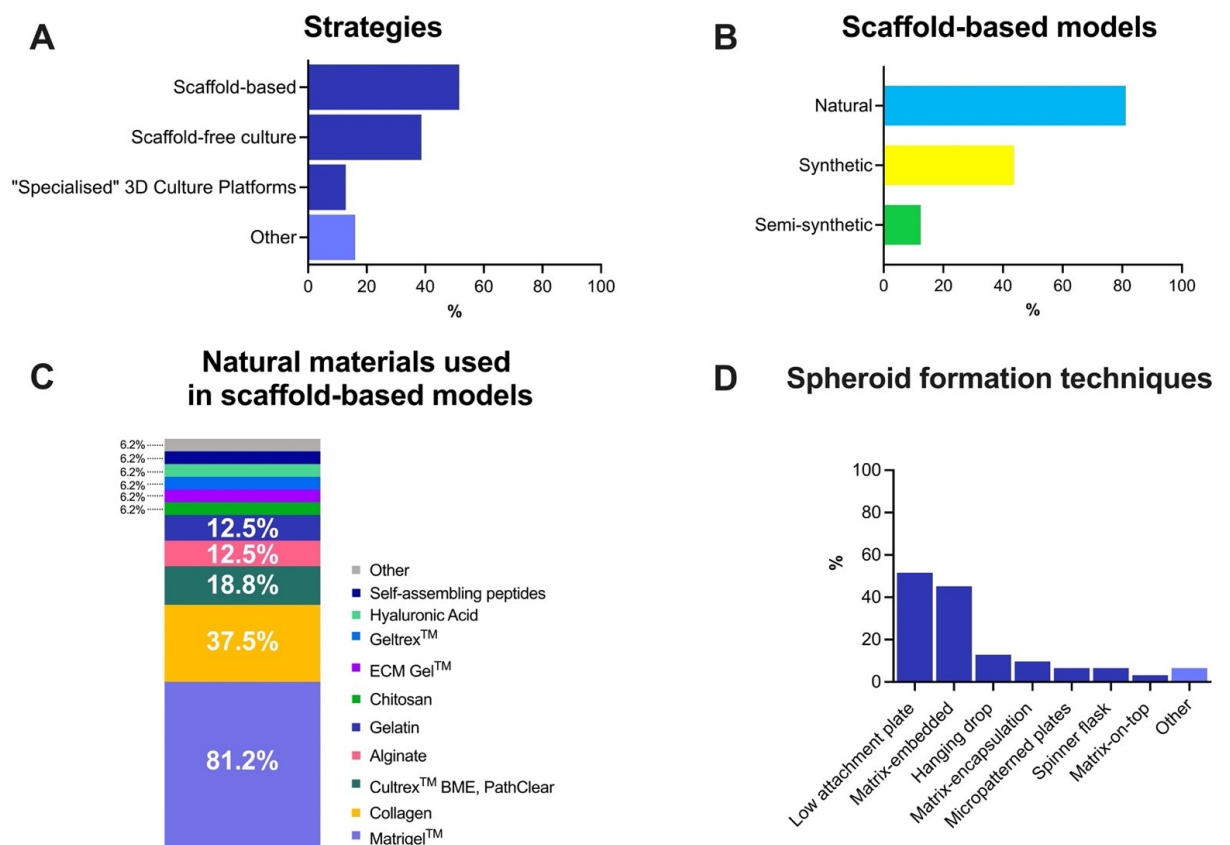
Figure 7.5. Overview of 3D culture models in cancer research.

 (**A**) Main strategies used for 3D models; (**B**) Types of scaffold-based models used in cancer research; (**C**) The most used natural materials in scaffold-based models; (**D**) Procedures used for spheroid formation. Results represented as percentages (%). *Note: some respondents indicated that they used more than one strategy, scaffold-based model type and/or spheroid formation technique.*

Regarding the numbers of different 3D model types used by any given researcher, 64.5% of respondents using 3D culture indicated they use just one model, whilst the remaining 35.5% used

more than one 3D culture. The characteristics of these additional 3D models are collected in the **Appendix VI** (**Figure VI-1**).

7.4.3 Characterisation of the models and downstream applications

Analysing the techniques used to characterize the cells of the different types of models, we observed that cell viability assays were the most used method to analyse the cells in 2D, 2.5D and 3D culture. This was followed, in popularity, by flow cytometry and optical microscopy. Another trend we can observe in the case of other models, where the most used techniques were quantitative reverse transcription PCR (RT-qPCR), immunoblotting and flow cytometry (see **Figure 7.6A**).

The intended downstream application may influence the choice of cell culture models for cancer research. Here, we asked researchers what model(s) they used for some of the most common assays used in cancer research: i.e., proliferation/migration/invasion assays, drug screening assays, angiogenesis assay, cellular uptake/release assays, immune cell response assays, EVs' *in vitro* function assays, and gene manipulation. Unsurprisingly, 2D culture was the most used method for all the downstream applications (see **Figure 7.6B**).
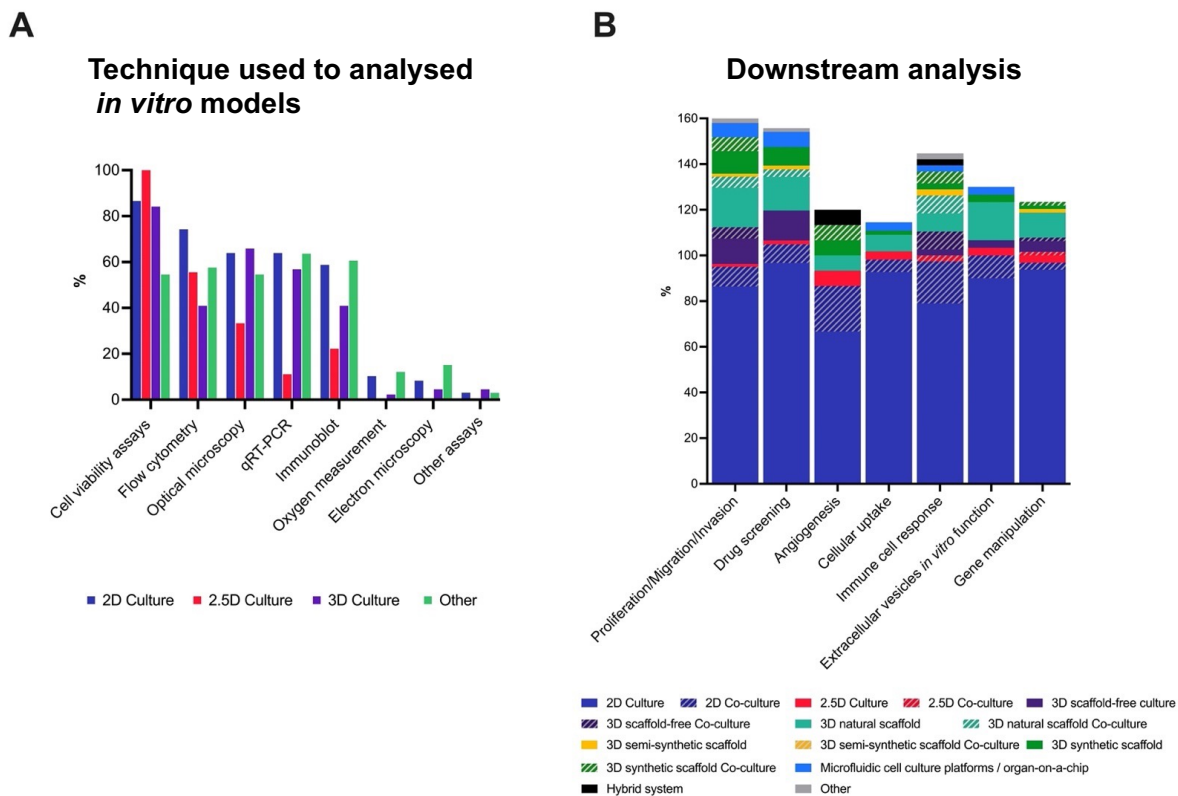
Figure 7.6. Analysis of pre-clinical in vitro model and their main applications.
 (**A**) Most used techniques to analyse *in vitro* models.; (**B**) Choice of cell culture models for application in various downstream application. Most used *in vitro* models used for proliferation/migration/invasion assays, drug screening analysis, angiogenesis assay, cellular uptake/release assays, immune cell response assays, extracellular vesicles *in vitro* functional assay and gene manipulation assays. Bars represents the percentage for each option, with respondents being able to choose more than one option as appropriate. Percentages were calculated based on the reported used of each technique.

Correlations between the techniques used to analyse the different *in vitro* models and the downstream analysis were evaluated and those PCC values above 0.4 (considered relatively strong) were summarised in **Table 7.1**. No strongly negative correlations were found between the use of any technique to analyse *in vitro* models and the downstream analysis.

Table 7.1. Significant correlations between techniques used to analyse *in vitro* models and downstream analysis.

	Technique to analyse the model	Downstream analysis	PCC	*p*-value
2D models	Cell viability assays	Proliferation	0.448	<0.001 (**)
	RT-qPCR	Gene manipulation	0.412	<0.001 (**)
2.5D models	Flow Cytometry	Immune cell response (2.5D Co-culture model)	0.492	<0.001 (**)
	Optical Microscopy	Immune cell response (2.5D Co-culture)	0.704	<0.001 (**)
	Flow Cytometry	Gene manipulation (2.5D Co-culture model)	0.492	<0.001 (**)
	Optical Microscopy	Gene manipulation (2.5D Co-culture model)	0.704	<0.001 (**)
3D models	Immunoblot	Proliferation (Scaffold-free model)	0.49	<0.001 (**)
	Flow cytometry	Proliferation (Natural scaffold-based model)	0.459	<0.001 (**)
	Optical microscopy	Proliferation (Natural scaffold-based model)	0.489	<0.001 (**)
	RT-qPCR	Proliferation (Natural scaffold-based model)	0.411	<0.001 (**)
	Immunoblot	Proliferation (Natural scaffold-based model)	0.439	<0.001 (**)
	Flow cytometry	Drug screening (Natural scaffold-based model)	0.417	<0.001 (**)
	Optical microscopy	Drug screening (Natural scaffold-based model)	0.505	<0.001 (**)
	Cryosectioning	Drug screening (Natural scaffold-based co-culture model)	0.454	<0.001 (**)
	Electron microscopy	Drug screening (Natural scaffold-based co-culture model)	0.49	<0.001 (**)
	Electron microscopy	Gene manipulation (Scaffold-free co-culture model)	0.704	<0.001 (**)
	Flow cytometry	Gene manipulation (Natural scaffold-based model)	0.502	<0.001 (**)
	Other	Angiogenesis 3D (Synthetic scaffold-based model)	0.704	<0.001 (**)
Other models	Oxygen measurement	Immune cell response	0.492	<0.001 (**)

*Pearson correlation coefficient (PCC > 0.4). **Correlation is significant at the 0.01 level (two-tailed).*

7.5 Benefits and limitations of *in vitro* models in cancer research

Although the interest and the use of 3D models has increased over the last decade, these models are still used by the minority of cancer researchers who perform *in vitro* studies.

We asked those who indicated not using 3D culture models at all about the main reasons why this was so. The principal reasons given were lack of experience (25%) and the additional cost when compared to 2D cultures (18%). However, 4% of the respondents indicated an intent to develop a 3D culture in the next step their research (**Figure 7.7**).

25%	Lack of experience
18%	Additional cost
13%	Lack of availability/access
11%	Complexity
9%	Lower throughput
8%	Time-limitation
5%	Lack of infrastructure
4%	Next step in the research
4%	Other reasons
3%	Not required/relevant for the study
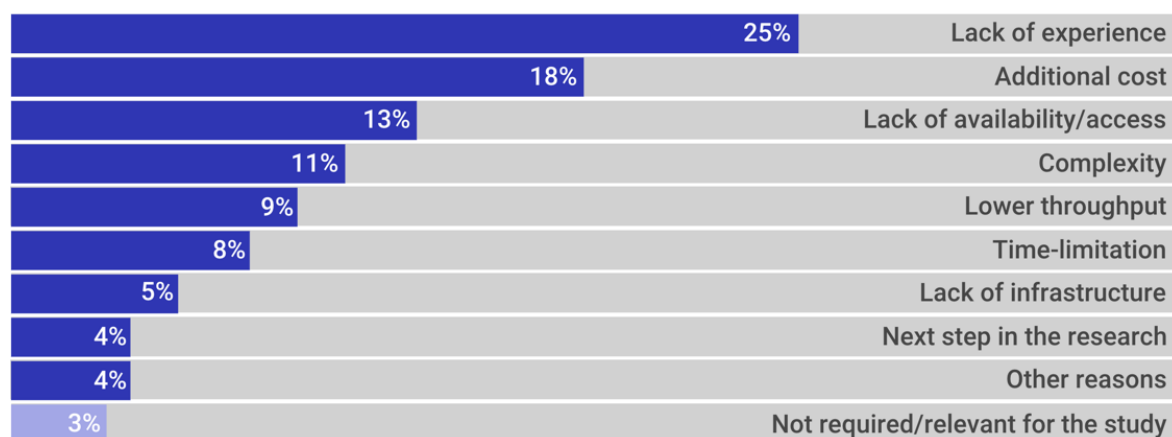
Figure 7.7. Principal reasons for not using 3D models (%).

Note: Multiple-answer question. Some respondents indicated more than one reason for not using 3D models.

The time required for the establishment of model de novo was reported to be on average 6 weeks. It was also asked about the time needed not only to establish a model de novo but also the time required to routinely apply the model. Similarly, the time required to be able to use a model was reported as, on average, 6 weeks. Obviously, the time required for the development depends on the complexity of the model and would be a principal reason why the times could vary between different models.

Researchers were also asked to give their opinion on the benefits and limitations of using 3D models. In relation to the advantages, as predicted, some respondents reported that these models are more realistic and better represent the tumour physiopathology and microenvironment when compared with 2D models. Other answers included: better-represented tumour growth, better-replicated metabolism, or considering the cell–cell interactions. Three-dimensional models were considered less time-consuming and less expensive than *in vivo* models and the importance of reducing the use of animals was highlighted. When researchers were asked about their interest in using 3D culture models, 81.3% expressed interest, 11.9% remained neutral, and only 7% of the respondents indicated no/low interest. However, only 33.7% agreed with the proposal that 2D cell culture models should be completely replaced by 3D cell culture models, 23.8% remained neutral, and 42.7% disagreed with this suggestion.

Regarding limitations, respondents predominantly reported the limitations as lack of reproducibility and reliability, combined with variability in results, due, at least in part, to an absence of standardised protocols for establishing 3D models. These issues include those with assays developed for 2D systems that are not directly translatable to 3D models. In fact, approximately 57% of those surveyed indicated their main concern with the utilisation of 3D culture models is that many routine assays used with 2D cultures are not translatable to 3D. It is noteworthy that only 28.7% of the respondents indicated that they have developed and published a protocol for a novel *in vitro* model that they developed themselves. Issues were also raised about the necessity of additional expertise, time, and consumables required to develop, maintain, and optimize 3D models compared to classic 2D models. The point was also made that, in some circumstances, 3D models have no additional benefits compared to 2D models; for example, when trying to mimic the immune response in cancer. So, adding this additional step between 2D and necessary pre-clinical *in vivo* studies was considered by some as not relevant to their research.

Considering the use of *in vivo* models, 56.4% of the respondents reported that—in addition to *in vitro* models—they also use *in vivo* models in their laboratory, but only 40.4% of those based on their research predominantly perform *in vivo* studies. The principal reasons given for not using *in vivo* models were lack of availability (30%), lack of resources (26.7%) and the 3Rs (18.3%). Only 11.7% of the researchers simply indicate that the choice to not include *in vivo* models was a personal choice. Most of the respondents agreed that it is still not feasible to completely replace *in vivo* animal models with 2D/2.5D/3D *in vitro* models (83.3%). However, if both *in vitro* models and *in vivo* models could achieve the same benefits for cancer research, they would prefer to use an *in vitro* approach.

Concerning the advantages and limitations of this survey, an advantage of the approach used for this worldwide survey includes the fact that it was open to anyone in the world who wished to partake. The survey was widely advertised via social media and via email to reach as many interested parties as possible. The fact that time and appropriate steps were invested in getting ethics approval to complete the survey and to ensure that no personal data were collected meant that respondents could be confident of the integrity of the research; that they could answer completely honestly with no concern that their name would be associated with any response; and that their contact details would not be used for any other purpose. Another advantage was the fact that it was not mandatory for respondents to answer all questions if they wished to avoid some, and they could complete as much of the survey as they wished. The design of the survey (logic jumps) meant that respondents were only brought to certain sections, based on their previous answers. This meant that respondents did not have to spend time reading through questions that were not relevant to them, based on their answer to a previously presented question. The main limitation of the survey—as with any such survey—is that there are people working with preclinical *in vitro* models in cancer research who the survey may not have reached or who were not interested in completing the survey. Thus, the responses achieved are, of course, only from those who were interested in taking the time to complete the survey.

7.6 Discussion

Although 3D *in vitro* models are increasingly used and there are increasing numbers of support structure and/or co-culture options for this, the use of 2D models only is still most typical among cancer researchers. It is generally accepted that, although 2.5D and 3D cultures/co-cultures are a stepping-stone between 2D cultures and animal models when trying to answer many questions in cancer research, they are more expensive, more time-consuming, and require a higher level of expertise; and yet none of them is complex and sophisticated enough to substitute animal models. Therefore, although the use of 2D/2.5D/3D pre-clinical *in vitro* models can reduce the need for animals in some areas of cancer research, they still cannot mimic in full the heterogeneity of tumours and their microenvironment as they exist *in vivo*. The inclusion of organoids offers a lot of promise Furthermore, the inclusion of mathematical models/in silico procedures could help to reduce wet-laboratory experiments, complementing *in vitro* models[391] and helping to advance to achieving personalised medicine[392].

However, the relatively limited availability of these to many academic and industry cancer researchers means that other options will continue to be needed. Concerted efforts are now needed to bring academia and industry together to develop the most sophisticated 3D models possible, to develop guidelines and standard operating procedures for the establishment of the same in the interest of rigor, reproducibility, standardisation, and best practice. These need to be as cost-effective as possible. In parallel, rather than trying to apply downstream analyses optimised for 2D models, there is an urgent need to develop compatible downstream analyses for 3D cancer models.

As things stand in cancer research, animal models are still needed following all currently available *in vitro* models. However, *in vivo* approaches have inherent limitations including the prohibitive costs in large animal studies and differences in cancer development between species and ethical concerns[393].

Two-dimensional *in vitro* models were shown not to fully represent the architecture, heterogeneity and complexity of human tumours and more representative models are needed to better reflect key aspects of tumour biology. Thus, there is an urgent need for standardised methods and the establishment of guidelines[394] and/or a transparent knowledge base for the development and characterisation of more sophisticated 3D cell culture/co-culture models. Additionally, these improvements should be beneficial in pre-clinical studies, advancing on current approaches and even substituting any current methods that are not ideal. This clearly indicates that additional research in this field is needed to improve preclinical *in vitro* models that replicate the key elements of tumour complexity and heterogeneity and find reliable alternative strategies to animal models.

7.7 Conclusion

While 2D cell culture models remain the predominant choice in cancer research, they are limited in their ability to replicate the complexity and heterogeneity of human tumours. Although 3D models, including 2.5D and 3D cultures/co-cultures, offer a closer approximation to *in vivo* conditions, they are more costly, time-consuming, and require specialised expertise. Furthermore, none of these models can fully substitute animal models, which also have their inherent limitations. The inclusion of organoids and the integration of mathematical models and in silico procedures hold promise for improving the representation of tumour biology and advancing personalised medicine. Collaborative efforts between academia and industry are necessary to develop sophisticated and cost-effective 3D models, establish guidelines and standard operating procedures, and develop compatible downstream analyses. While animal models are still needed, there is a pressing need for improved *in vitro* models that better capture the complexities of tumours and explore alternative strategies to reduce reliance on animal models in cancer research.

Chapter 8

Effect of tucatinib on the release of EVs from breast cancer cell lines

Abstract

HER2 is frequently amplified and/or overexpressed in breast cancer and so tucatinib, a HER-targeted TKI, is approved for HER2-overexpressing breast cancer. Unfortunately, resistance often limits the benefit of such drugs. Previously our group discovered that EVs released from cancer cells are associated with transmitting drug resistance. Here, we aimed to investigate if exposure to low levels of tucatinib -which may be all that is achieved depending on the tumour size, location, heterogeneity, etc.- might stimulate HER2 expression and/or EVs' release and so inadvertently and unintentionally contribute to tumour aggressiveness.

Tucatinib's IC_{50} and IC_{10} for three HER2-positive breast cancer cell lines, HCC1954, SKBR3 and EFM192A, and their neratinib-resistant counterparts were established using acid phosphatase miniaturised assay. Effects of cell exposure to this low level of tucatinib, for 48 hrs, was evaluated by analysing cellular HER2 by both immunoblotting and flow cytometry analysis. To get an indication of any changes in EVs' release, the corresponding CM was centrifuged and analysed for the presence of both HER2 and the EV's tetraspanin marker CD9, using imaging flow cytometry (IFCM).

HCC1954 cells were found to be innate resistant to tucatinib, in comparison to SKBR3 and EFM192A cells. In addition, the three cell line variants resistant to neratinib exhibited a higher IC_{50} for tucatinib compared to their neratinib-sensitive counterparts, indicating that the development of neratinib resistance also conferred cross-resistance to tucatinib in all three HER2+ breast cancer cell variants. Immunoblotting of lysed cells following tucatinib treatment showed significantly increased HER2 levels only in HCC1954 cells, although flow cytometry analysis of the HER2 on the surface of intact cells indicated that tucatinib significantly increased its expression in both HCC1954 and SKBR3 cells. Regarding analysis of CD9+ and HER2+ events in corresponding CM, IFCM showed an upward trend of CD9+ and HER2+ events in all cases following tucatinib treatment.

Interestingly, the most consistent and substantial effects of low level tucatinib were manifest on the cancer cells which are already innately resistant to tucatinib. While further studies, including comprehensive analysis of collected EVs and the functional relevance of the increased HER2, are warranted -and including more cell lines and tumour samples- this suggest that sub-optimal treatment of tumours that are innately drug-resistant may actually increase their aggressiveness. Given that tucatinib is indicated for breast cancer where at least two prior anti-HER2 treatment regimens have been used and subsequently failed, this may have important implications when choosing optimal treatment regimes.

8.1 Introduction

Trastuzumab, the first approved therapy targeting HER2 for the treatment of breast cancer, received approval in the late 1990s[395]. Since then, additional HER2-targeted therapies have been approved, including pertuzumab, another HER2-directed monoclonal antibody, as well as ado-trastuzumab emtansine and fam-trastuzumab deruxtecan, which are antibody-drug conjugates. Recently, margetuximab, a HER2-directed antibody designed to modify Fc-receptor affinity to CD16 and induce CD16-mediated cytotoxicity, has also been approved[396].

In the realm of HER2+ breast cancer, small molecule TKIs offer another treatment option for patients at both early and advanced stages. Afatinib, an irreversible inhibitor of EGFR, HER2, and HER4, initially gained approval for the treatment of lung cancer with EGFR mutations[397]. Although afatinib demonstrated promising results in phase I-II breast cancer studies, it failed to exhibit efficacy in phase 3 trials[398]. On the other hand, lapatinib, neratinib, pyrotinib, and tucatinib, all small molecule TKIs, have shown positive outcomes in phase 3 trials for HER2+ breast cancer patients[54,399,400]. Unlike dual inhibitors such as lapatinib and neratinib, which target both EGFR and HER2, tucatinib specifically and reversibly inhibits the TK activity of HER2, with minimal inhibition of EGFR[401].

These TKIs have proven effective in combination with chemotherapy and other HER2-directed agents, both in early-stage and metastatic settings[395]. Studies indicate that patients who experience progression while on trastuzumab may benefit from HER2-directed TKIs, either with or without trastuzumab. This efficacy may be attributed to the distinct mechanisms of action and targets within the HER2 receptor, which enable TKIs to overcome mechanisms of resistance to trastuzumab. However, various intrinsic and acquired mechanisms of resistance to HER2 TKIs agents have been extensively studied and documented[402,403]. The reactivation of HER2 or signalling pathways downstream from the HER2 receptor (i.e., activation of the PI3K pathway was associated with trastuzumab resistance in breast cancer[404]) together with HER2 mutations (i.e., L755S, the most frequent acquired activating mutation of HER2 in MBC, has been associated with resistance to lapatinib and neratinib and cross resistance to tucatinib has been reported *in vitro*[405]) have been recognised as well-known factors contributing to both intrinsic and acquired resistance to HER2-targeted therapies.

Although some advances have been done to elucidate these mechanisms, current efforts are still required to unravel all the key factors. It is also important, from a clinical viewpoint, to investigate the mechanism of how the cancer cells can evade promptly an anti-tumoral treatment.

While the role of EVs secreted by tumour cells in facilitating communication between tumours and the host is well-established, the influence of anti-cancer therapies on EVs secretion and function remains relatively understudied. It has been observed that the administration of chemotherapeutic drugs to cancer cells significantly enhances the secretion of EVs and may alter their composition[157,406,407]. For instance, a study performed by Kreger et al. (2016)[408] revealed that MDA-MB-231 breast cancer cells exposed to paclitaxel exhibit an increased secretion of exosomes enriched with the protein survivin. These exosomes carrying survivin promoted cell survival to NIH3T3 fibroblasts and enhance resistance to paclitaxel chemotherapy in SKBR3 cells. This research sheds light on the mechanisms by which exosomes contribute to chemoresistance in breast

cancer, highlighting the potential significance of survivin-targeted interventions in overcoming this resistance[408].

Another study performed by Wang et al. (2019)[409] investigated the effects of low-dose chemotherapeutic agents (doxorubicin and rhodamine 123) on the release and recycling of EVs in resistant human oral epidermoid carcinoma KBv200 cells. They found that EVs' release from drug-resistant cells was significantly increased by the presence of chemotherapeutic agents as well as the EVs uptake by recipient cells. These processes were induced by Rab8B and Rab5 dysregulation.

8.2 Aims of the study

Here, we aimed to investigate if exposure to low levels of tucatinib -which may be all that is achieved depending on the tumour size, location, heterogeneity, etc.- might actually stimulate HER2 expression and/or EVs' release and so inadvertently and unintentionally contribute to tumour aggressiveness. For that purpose, the IC_{50} was determined to investigate the existence of cross-resistance in NR cell variants or innate resistance in neratinib-sensitive cell variants while IC_{10} was determined to investigate the effect of the treatment of tucatinib on the EVs' release after 48 hrs treatment.

8.3 Materials & Methods

8.3.1 Cell culture

Three HER2-positive breast cancer cell variants (EFM192A, HCC1954 and SKBR3) and their neratinib-resistant counterparts (EFM192A NR, HCC1954 NR, and SKBR3 NR) were routinely maintained in complete RPMI-1640 medium as explained in **Section 2.3.1**.

8.3.2 Toxicity assay

The IC_{50} values of EFM192A, EFM192A NR, HCC1954, HCC1954 NR, SKBR3, and SKBR3 NR for tucatinib were determined using *in vitro* cytotoxic proliferation assay. Tucatinib was solubilised following the suggested protocol by the supplier, to obtain a 5mM solution (Selleckchem, Cat. #: S8362) in dimethyl sulfoxide (DMSO) (Sigma, Cat. #: D2650). EFM192A and EFM192A NR were seeded at 8×10^3 cells/well, HCC1954 and HCC1954 NR cells were seeded at 3×10^3 cells/well, and SKBR3 and SKBR3 NR cells were seeded at 5×10^3 cells/well in a 96-well plate (Sigma-Aldrich, Cat. #3595). 24 hrs after seeding, cells were exposed to increasing concentrations of tucatinib to obtain a final volume of 200µl/well. Concentrations of tucatinib used for paired cell lines were as follows: 0 – 10 µM EFM192A, EF192A NR, SKBR3, and SKBR3 NR; 0 – 50 µM for HCC1954 and HCC1954 NR. After 120 hrs (5 days) of growth in the presence of tucatinib, the acid phosphatase assay method was performed to measure cell viability as explained in **Section 3.3.6**.

To evaluate the IC_{10} values (defined as the concentration that is capable to kill 10% of the cells) to be used to study the changes on EVs' release without being toxic to the cells, another set of cytotoxicity assays werw performed. EFM192A, HCC1954, and SKBR3 cells were seeded (16×10^3 cells/well, 1×10^4 cells/well and 8×10^3 cells/well, respectively) and allowed to attach overnight. The following day, the medium was replaced with RPMI medium supplemented with 10% EVs-depleted FBS (dFBS) and cells were treated with increasing concentration as follows: 1 nM – 50 µM for HCC1954 cells; 1 nM – 10 µM for SKBR3 and EFM192A cells. After 2 days post-treatment, an acid phosphatase assay was performed to measure cell viability as mentioned above.

8.3.3 Evaluation of 48 hrs tucatinib treatment effect

To extensively evaluate the effect of EVs' release after 48 hrs treatment on HER2+ cell lines and investigate the HER2 status on the cells and the EVs released on conditioned media (CM), flow cytometry was performed. EFM192A cells were seeded at 6×10^5 cells/well while HCC1954 and SKBR3 cells were seeded at 3×10^5 cells/well plate in a 6-well plate (Corning, Cat. #: 3516) and allowed to attach overnight. 24 hrs after seeding, the medium was replaced with RPMI medium supplemented with 10% dFBS in presence (treated) or absence (untreated) of tucatinib. Treated wells contained IC_{10} concentration of tucatinib for each cell line at a final volume of 1.5 ml/well. After 2 days of incubation, CM was collected for flow cytometry analysis and centrifuged thrice at 300× *g* for 5 min to exclude debris and dead cells and stored at -80°C for future analysis; cells were counted and divided for flow analysis and cell lysate was prepared as explained in **Section 2.3.6** and its

protein content was measured as explained in **Section 3.3.1.1**. A representative diagram of the experimental design is presented in **Figure 8.1**.
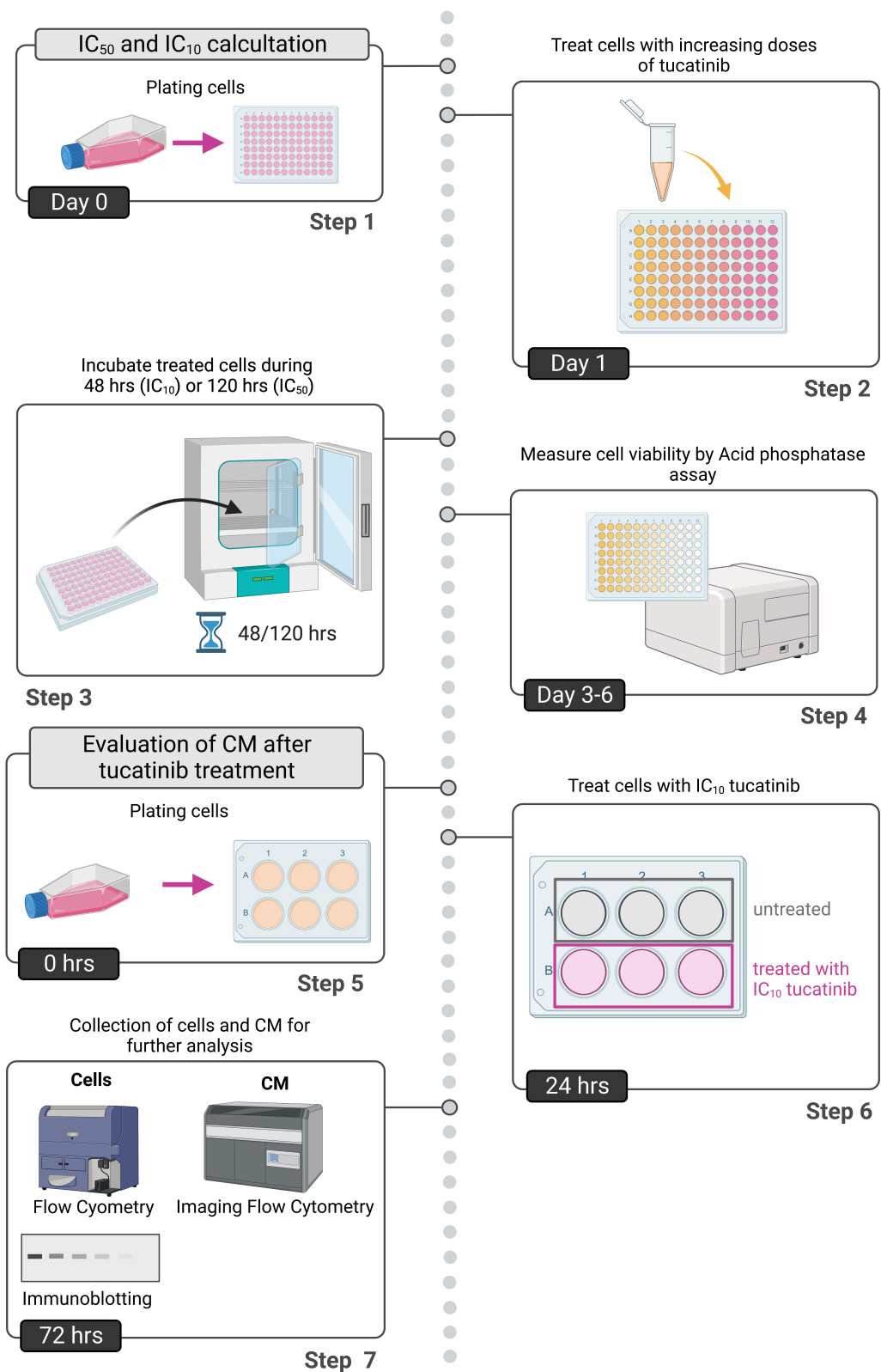
Figure 8.1. Schematic diagram of experimental workflow.

Overview of the approach used in this study to investigate tucatinib effect on HER2+ breast cancer cells. CM = conditioned media. Illustration created in *BioRender.com*.

8.3.3.1 Flow cytometry cell preparation

Following the generation of single cells suspension, explained in the previous section (see **Section 8.3.3**), cells were divided for different staining at a concentration of 2×10^5 cells/condition. **Table 8.1** presents the antibody/stain dilutions and lasers used for this experiment. Unstained control, single-HER2 stained control and Live/Dead stained control was used.

Table 8.1. Antibody dilutions and conditions for immunoblotting.

Specificity	Purpose	Fluorochrome	Company, Cat. #	Dilution	Laser (nm)	Filter/ Bandpass
HER2	HER2+ cells gating	APC	Biolegend, 324407	1:100	633	660/20
Dead cells	Dead cell exclusion	Zombie NIR™ Fixable Viability Kit	Biolegend, 423105	1:250	746	780/60

Dead cells were generated by heating 50% of the sample at 65°C for 5 min and then incubating at 4°C for another 5 min. Following this, the dead cells were mixed 1:1 with live cells for the rest of the steps. Cells were washed once with PBS and spun at 400× g for 3 min. The pellet was resuspended in 50 µl of diluted viability stain in PBS and incubated for 30 min at 4°C. After incubation, 200 µl PBS was added to the samples and centrifuged at 400× g for 3 min. Cell samples were then resuspended in 20 µl fluorescence-activated cell sorting (FACS) buffer [2%FBS, 1mM ethylenediaminetetraacetic acid (EDTA) (Invitrogen, Cat. #: 15575-038) and 0.1% Sodium Azide (Sigma, Cat. #: 71289-5G)] containing diluted 1:10 Fc Receptor blocking solution (Human TruStain FcX™, Biolegend, Cat. #: 422301) and incubated for 10 min at 4°C. After 10 min of incubation, the antibody master mix was added directly to the samples at a final volume of 100 µl. Cell samples, in presence of a single antibody, were incubated for 30 min at 4°C. Cells were sequentially washed adding 500 µl FACS buffer and centrifuged for 3 min at 400× g and finally resuspended in 500 µl FACS buffer and immediately analysed using the BD FACSCanto™ Cell Analyzer (BD Biosciences) and the unstained and single-stained controls were used for compensation using Compensation Wizard tool. 5,000 positive events were registered for compensation controls while 10,000 positive events were registered into live cells gate and subsequently analysed using FlowJo™ Software version 10.7 for Windows (**Figure 8.2**).
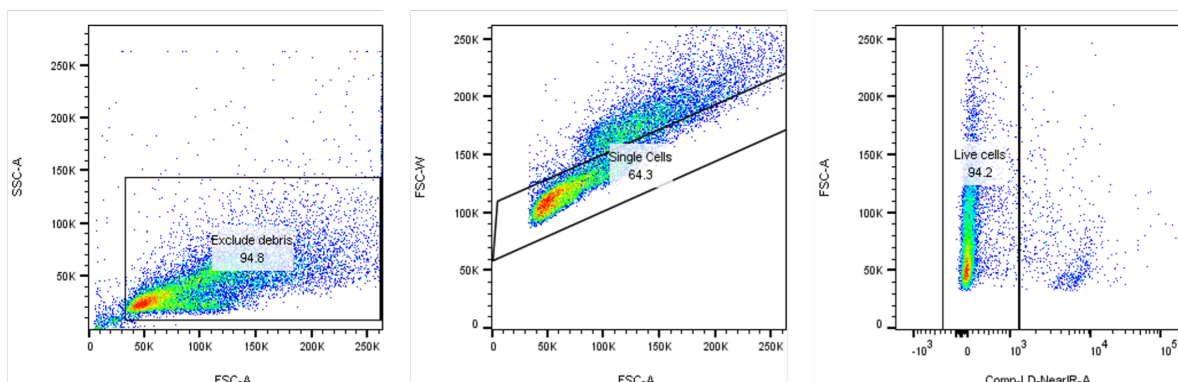
Figure 8.2. Gating strategies used to establish live cells population.

8.3.3.2 Imaging Flow cytometry analysis of CM

The IFCM analysis of CM obtained from cells after 48 hrs treatment with tucatinib was performed using the single-staining protocol. CM was centrifuged thrice at 300× *g* for 5 min prior to the assay. 25 µl of diluted single stain preparations in 0.2 µm-filtered PBS for APC conjugated with anti-human HER2 (1:25, BioLegend, Cat. #324407) or PE conjugated with anti-human CD9 (1:25, exbio, Cat. #: 1P-208-T100) antibodies were prepared. Antibodies were centrifuged at 16,000× *g* at 4 ºC for 5 min and added to the 25 µl of CM samples. The CM samples with the antibodies were incubated for 2 hrs at RT in the dark, and washed using a 300 kDa filter (Nanosep, Pall Biotech, Cat. #: 516-8531) and resuspended in PBS. The data acquisition was performed within 2 hrs on the ImageStreamX Mk II imaging flow cytometer (Amnis/ Luminex) at 60x magnification and using low flow rate, as previously defined[280]. Each sample was run for 5 min. Unstained and only media controls were run in parallel. Fluorescence was within detection linear range in the following channels: Brightfield in channel 1 and 9 (B/YG_435-480 and R/V_560-595 nm filter respectively), PE in channel 3 (B/YG_560–595 nm filter), Side Scatter Channel (SSC) in channel 6 (R/V_745-780 nm filter) and APC in channel 11 (R/V_642–745 nm, filter). To certify that the observed positive events were indeed EVs, CM was incubated with 4% NP-40 at a final concentration of 2% and samples were analysed using the same strategy. IDEAS software version 6.2 (Amnis/ Luminex) was used for data analysis. EVs were gated as SSC *vs* fluorescence and the gated EVs were confirmed in the IDEAS Image Gallery (**Figure 8.3**).
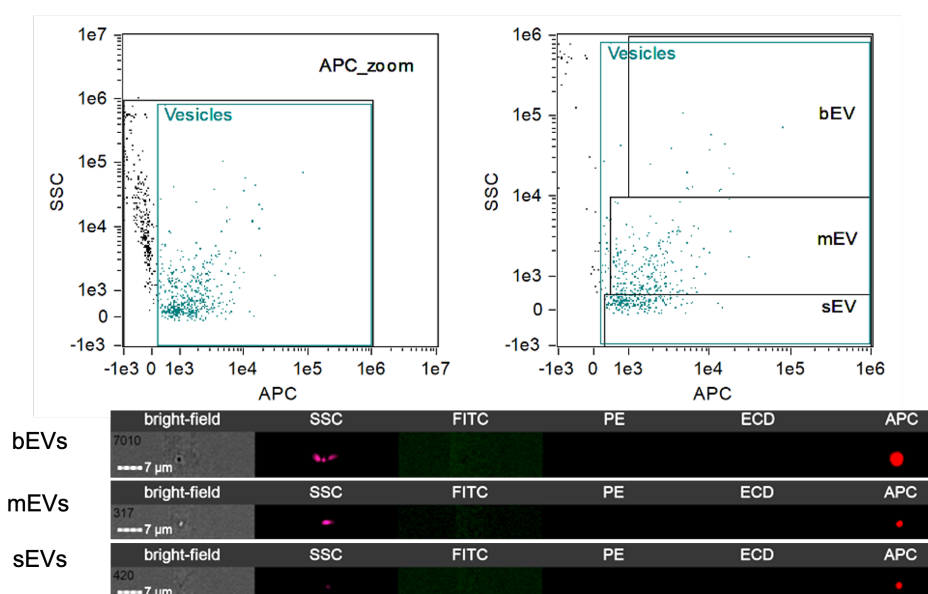
Figure 8.3. Gating strategies used to establish different EVs sub-populations.
(**Top**) EVs gates used to establish the specific numbers for EVs sub-populations: small EVs (sEVs), medium EVs (mEVs), and large EVs (bEVs); (**Bottom**) Representative image of EVs from IDEAS Image Gallery. EVs were acquired at 60x magnification, slow flow rate on the Amnis ImageStreamX Mk II imaging flow cytometer. EVs were gated as per top figure and positive for HER2 (APC) channel.

8.3.4 Immunoblotting

For immunoblotting performed in this chapter, 30 µg total cell protein was resolved on 7.5% Mini-PROTEAN TGX™ 10-well gel (Bio-Rad Laboratories; Cat. #: 4561023) along with a MW marker, SeeBlue Plus 2 Pre-stained standards (Invitrogen, Cat. #: LC5925). Immunoblots were performed as described in **Section 2.3.8**. All antibody conditions and catalogue numbers used in this chapter are detailed in **Table 8.2**.

Table 8.2. Antibody dilutions and conditions for immunoblotting.

Primary Antibody	Company, Cat. #	Dilution	Antibody condition	Secondary Antibody
β-actin	Sigma-Aldrich, A1978	1:5000	3% BSA/PBST	Anti-Mouse IgG
HER2	Calbiochem, OP15	1:1000	3% BSA/PBST	Anti-Mouse IgG

All secondary antibodies were diluted 1:1000 in 3% BSA/PBST

8.3.5 Data analysis and statistical testing

All statistical analyses were performed using GraphPad Prism version 9.1.9 for macOS (GraphPad Software). Regarding toxicity assays, IC_{50} and IC_{10} values were calculated using the nonlinear regression in GraphPad Prism version 9.1.9 for macOS (GraphPad Software). The percent viability was calculated using the DMSO (vehicle) treated cells as representative for 100% viability. Unpaired t-test was applied in all the analysis performed in this chapter (*$p < 0.05$) and results are given as mean ± SEM ($n = 3$).

8.4 Results

8.4.1 Establishing of tucatinib IC_{50} and IC_{10} concentrations

To determine the appropriate tucatinib concentration to be used for each cell line, cytotoxicity assay was performed to evaluate the cellular viability on EFM192A, HCC1954, SKBR3, and their NR counterparts (see *Section 2.5*). Cell viability was monitored after 48 hrs and 120 hrs of incubation by acid phosphatase assay: 48 hrs to establish the IC_{10} on the neratinib-sensitive cells, as this is the time that cells are seeded for EVs recovering, while 120 hrs incubation was used to determine the IC_{50} of each cell line for tucatinib treatment.

After 120 hrs incubation with tucatinib, NR cell variants showed a higher IC_{50} in comparison with their counterparts, demonstrating that neratinib-resistance conferred cross-resistance to tucatinib in all three neratinib-resistant HER2+ breast cancer cell variants. HCC1954 cells showed an innate resistance to tucatinib in comparison with EFM192A and SKBR3 cell lines (**Table 8.3**). Finally, EFM192A NR cell line showed the highest IC_{50} fold change in comparison with their neratinib-sensitive counterpart (23.4-fold, $p = 0.038$).

Table 8.3. IC_{50} values for tucatinib and fold-change values.

IC_{50} values				
	neratinib-sensitive	neratinib-resistant	Fold change	P value
HCC1954	1.6 ± 0.7 µM	2.7 ± 0.6 µM	↑1.8	ns
SKBR3	36.2 ± 9 nM	104.2 ± 22.4 nM	↑2.9	0.048 (*)
EFM192A	43.2 ± 8.5 nM	1.0 ± 0.3 µM	↑23.4	0.038 (*)

IC_{50} and fold change values between variants were obtained after 120 hrs incubation with tucatinib. Fold change is calculated as neratinib-resistant/neratinib-sensitive ratio.

IC_{10} was established for neratinib-sensitive cell lines to investigate the effect of low doses of tucatinib on the EVs' release. Again, the highest IC_{10} was determined for HCC1954 samples (**Table 8.4**).

Table 8.4. IC_{10} values obtained for 48 hrs treatment.

IC_{10} values		
	Tucatinib	R square
HCC1954	747.4 nM	0.91
SKBR3	1.19 nM	0.94
EFM192A	2.62 nM	0.96

IC_{10} values and R square of the curves between variants obtained after 48 hrs incubation with tucatinib.

8.4.2 Flow cytometry analysis of cells treated with IC$_{10}$ concentration of tucatinib

To make sure cells treated with the selected concentration of tucatinib were alive during the incubation period, flow cytometry (FC) was performed using the viability stain Zombie NIR^{TM} to assess live versus dead status of the cells in combination with the antibody of interest. Zombie NIR™ is a polar water-soluble amine reactive fluorescent dye that is permeable to the cells with compromised membranes while is non-permeable to live cells. The events were gated to have 10,000 events for live cells according to the negative stain of Zombie NIR in the Near IR channel (see **Section 8.4.2**).

After gating for live cells, HER2 mean fluorescence intensity (MFI) was estimated. A representative flow cytometry graph showing HER2 histograms for the three cell lines are given in **Figure 8.4A**. Tucatinib seemed to enhance the presence of HER2 on the surface after 48 hrs treatment in HCC1954 and SKBR3 cells while was decreased in EFM192A cells (**Figure 8.4B**).
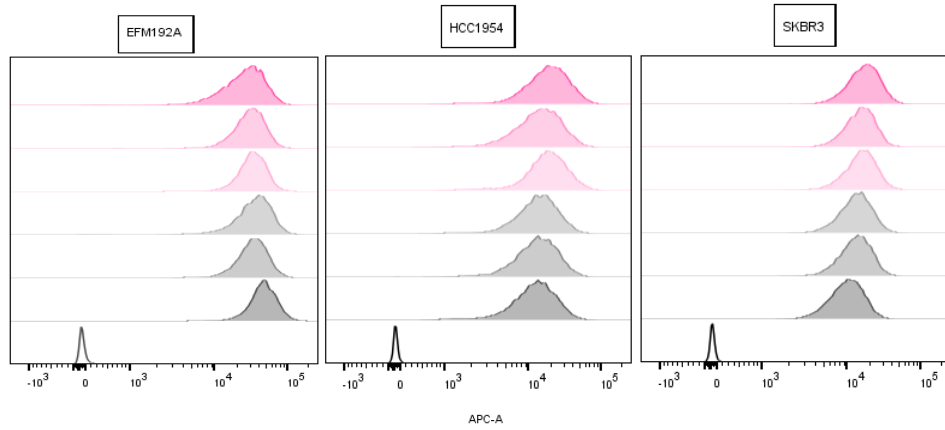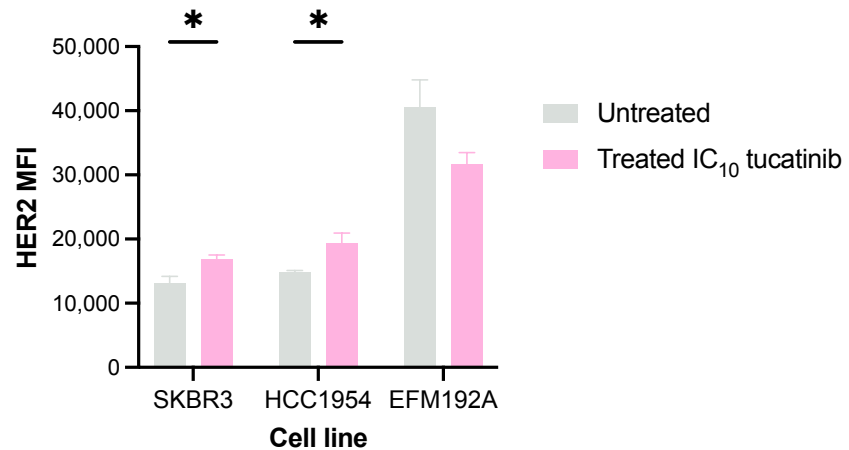
Figure 8.4. Flow cytometry histograms of signal intensity of HER2.

(**A**) Staining of surface expression of HER2 after 48 hrs treatment with tucatinib on EFM192A (**Left**), HCC1954 (**Centre**), and SKBR3 (**Right**) cells show surface expression of HER2 after 48 hrs treatment with tucatinib. 2×10^4 cells were analysed per experiment (**B**) Representative graph of mean fluorescence intensities (MFI). Each bar represents the mean of the MFI ± SEM of n = 3 experiments. Unpaired t-test was used to calculate significance: *$p < 0.05$.

8.4.3 Immunoblotting analysis of cell lysates

In parallel with flow cytometry analysis, immunoblotting analysis was performed to analyse HER2 expression after tucatinib treatment in comparison with the untreated control. (**Figure 8.5**). In harmony with the results obtained by flow cytometry, the treatment with tucatinib for 48 hrs has a slightly effect on the presence of HER2 in HCC1954. SKBR3 and EFM192A cells also showed an increase in HER2 protein expression but was not significant.
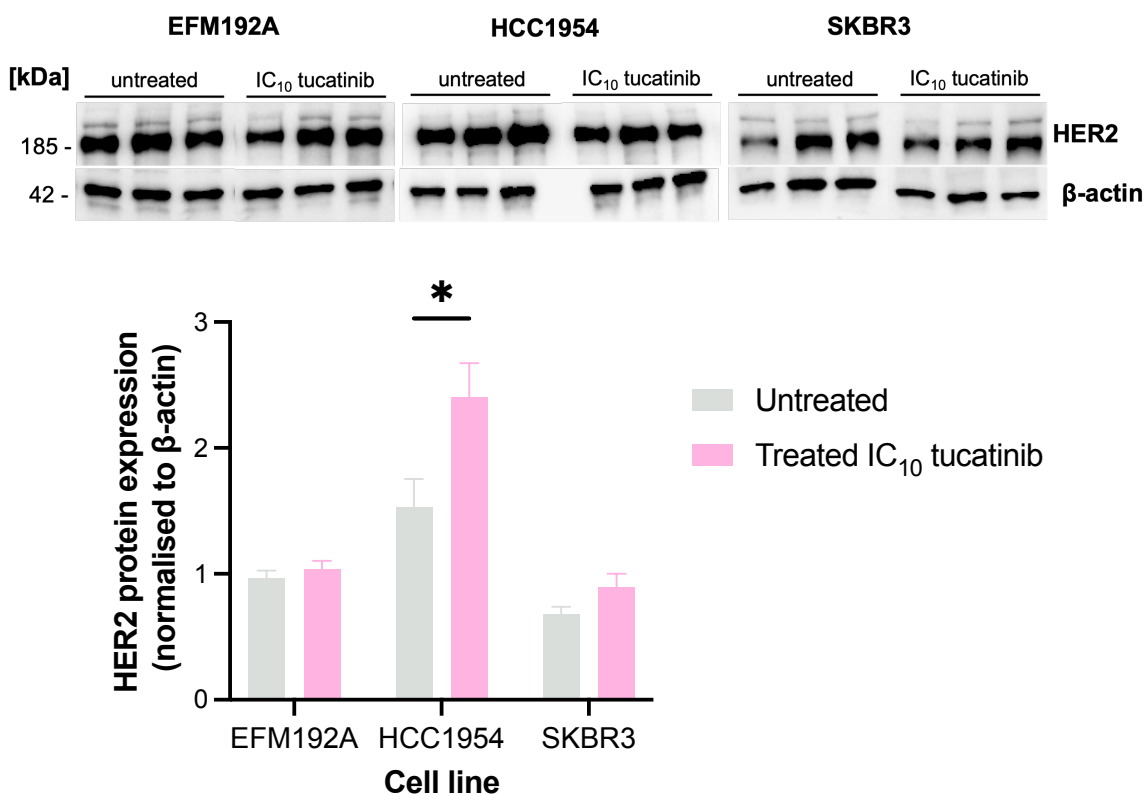
Figure 8.5. Qualitative immunoblot analysis of HER2 in cell lysates after 48h treatment with IC10 concentration of tucatinib.

Equal amount of protein (30 µg) was loaded per lane and analysed for HER2. (**Top**) Immunoblots for control and treated cell samples and densitometry analysis is presented in (**Bottom**). Each bar represents the mean of the densities normalised to β-actin protein ± SEM of n = 3 experiments. Unpaired t-test was used to calculate significance *$p<0.05$.

8.4.4 Analysis of CM (without separating EVs) by IFCM

CM obtained from EFM192A, HCC1954 and SKBR3 after 48 hrs incubation in presence of IC_{10} of tucatinib was collected and cleared by 300× g centrifugation. CM from untreated cells was used as control for the effect of tucatinib. Unstained control as well as media and NP-40 controls were run as controls for the assay. A representative image of each condition depicted in the **Appendix VII**

.

A significant increase of CD9+ events was found in CM samples obtained from EFM192A treated cells compared with CM derived from EFM192A untreated cells in sEVs (2.1-fold, p = 0.022) and

mEVs populations (2.3-fold, p = 0.023) while it was not significant in the case of the lEVs population (1.8-fold, p = 0.063). No significant differences were found between untreated and treated CM samples derived from the other cell lines for CD9+ events. However, an upward trend was observed in sEVs, mEVs and lEVs populations when we treated HCC1954, and SKBRR3 with their respective IC$_{10}$. (**Figure 8.6**).

When HER2+ events were analysed after the treatment with tucatinib, EFM192A CM obtained from EFM192A treated cells showed a higher number of HER2+ events in sEVs and mEVs, although this increment was not significant. It was observed a significant increase of HER2+ events in sEVs (2.6-fold, p = 0.034) and mEVs (1.9-fold, p = 0.04) populations resulted when HCC1954 cells were treated with IC$_{10}$ tucatinib for 48 hrs in comparison with the untreated control (**Figure 8.6**). CM obtained from SKBR3 cells treated with IC$_{10}$ tucatinib showed a higher population of HER2+ mEVs, but this increase was not significant. In all cases the smallest population for CD9+ or HER2+ was represented by lEVs.
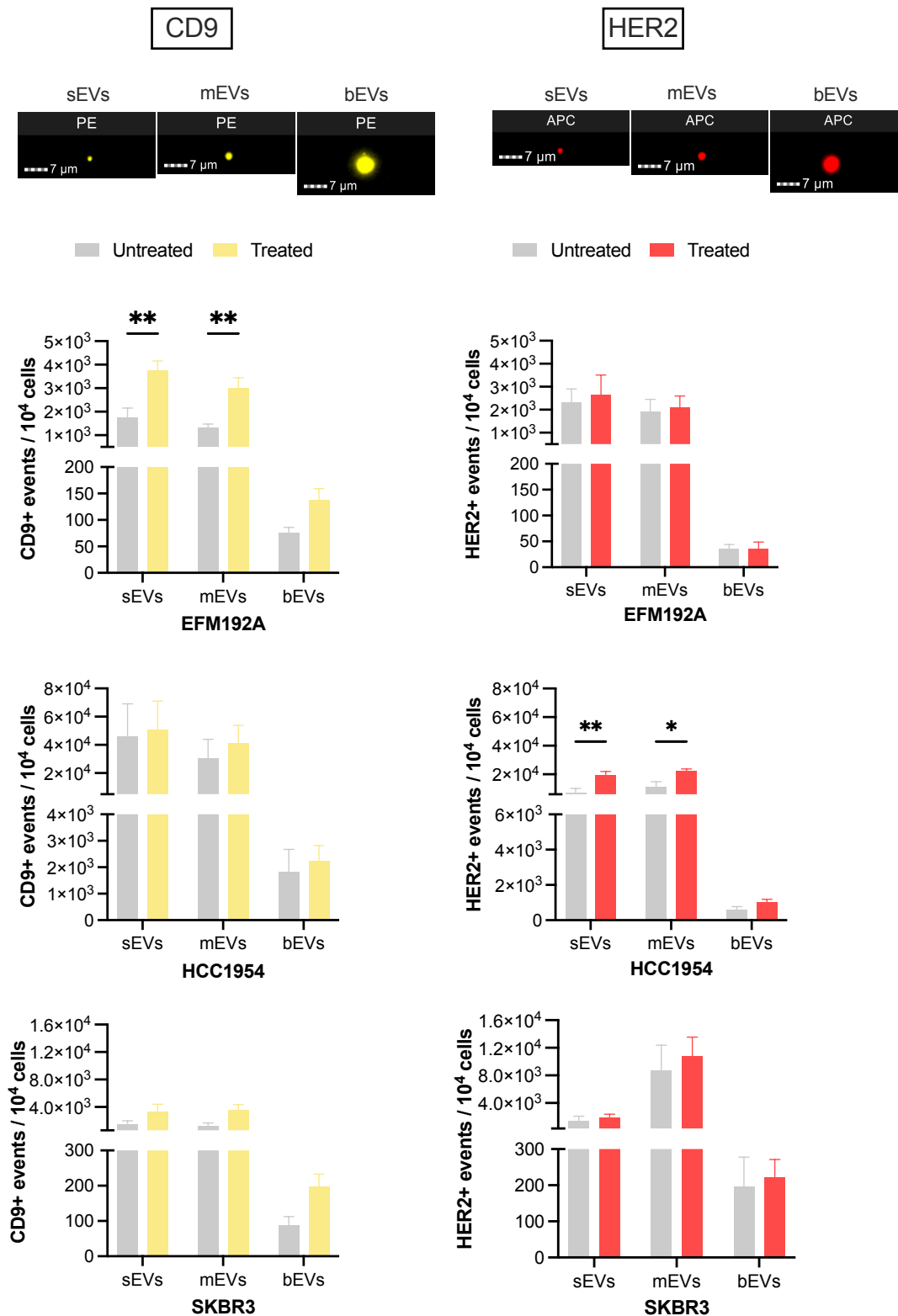
Figure 8.6. Analysis of the presence of CD9 and HER2 on CM by IFCM.

Amnis ImageStreamX was used to measure CD9+ events (**Left**) or HER2+ events (**Right**) on CM. After 48 hrs treatment with tucatinib, EFM192A and HCC1954 seemed to release more CD9+ and HER2+ particles compare to their untreated pairs. Representative images of positive events for each EVs subpopulation are showed on the top. Graphs are representative of n = 3 experiments ± SEM. Multiple unpaired t-test was used to calculate significance: *p<0.05, **p<0.01. sEVs = small EVs; mEVs= medium EVs; bEVs= large EVs.

8.4.5 Summary of findings

The following **Table 8.5** presents a summary of the key findings from this chapter.

Table 8.5 List of main observations from the treatment with tucatinib on the cells and the obtained conditioned media.

Cells						
Assay	**EFM192A**	**EFM192A NR**	**HCC1954**	**HCC1954 NR**	**SKBR3**	**SKBR3 NR**
Resistance to tucatinib (IC_{50})	Sensitive	Cross-resistant	Innate resistant	Innate/cross-resistant	Sensitive	Cross-resistant
HER2 expression by FC (IC_{10} treatment)	↓ (ns)	-	↑ (*)	-	↑ (*)	-
HER2 expression by immunoblotting (IC_{10} treatment)	N.D.	-	↑ (*)	-	↑(ns)	-
Conditioned media screening (IC_{10} treatment)						
Assay	**EFM192A**	**EFM192A NR**	**HCC1954**	**HCC1954 NR**	**SKBR3**	**SKBR3 NR**
IFCM (CD9+ events)	↑ (**) sEVs ↑ (*) mEVs	-	N.D.	-	N.D.	-
IFCM (HER2+ events)	N.D.	-	↑ (**) sEVs ↑ (*) mEVs	-	N.D.	-

*Arrows refers to the increase (↑) or decrease (↓) under treated compared with untreated control for the different parameters. ND= not detected; ns= not significant. *$p<0.05$, **$p<0.01$.*

8.5 Discussion

For several years, researchers have been focused on investigating how cancer cells are able to express intrinsic resistance or are capable to acquire a long-term resistance to anti-tumour therapies. Although some advances have been done to elucidate these mechanisms, current efforts are still required to unravel all the key factors. It is also important, from a clinical viewpoint, to investigate the mechanism of how the cancer cells can evade promptly an anti-tumoral treatment.

Numerous studies have demonstrated the adverse effects of chemotherapy treatment on the release of EVs and their implications in cancer progression. Following the administration of chemotherapeutic agents, there is an observed increase in EVs' release, which has been associated with enhanced chemoresistance, tumour metastasis, and altered EVs cargo composition. For instance, vincristine-resistant human oral epidermoid carcinoma cells, KB, treated with vincristine exhibited elevated EVs' release accompanied by increased levels of ABCB1 protein on the EVs' surface[409]. These EVs were capable of transferring ABCB1 to recipient sensitive cells, resulting in the spread of chemoresistance to doxorubicin, a substrate of ABCB1. Additionally, EVs released by cisplatin-treated ovarian cancer spheroids were found to promote a pro-tumorigenic profile in bone marrow-mesenchymal stem cells (BM-MSCs). These EVs increased BM-MSC migration, secretion of IL-6 and VEGF, angiogenesis induction, and invasion of the low-metastatic ovarian cancer cell line, Ovcar3[410]. These findings highlight the complex interplay between chemotherapy, EVs' release, and cancer progression, emphasising the need for further investigation into the mechanisms underlying these processes. However, no specific publications investigating the impact of low-dose anti-HER2 therapies on the release of EVs were found.

Here, our aim was to investigate in first place if neratinib-resistant cell variants show cross-resistance to tucatinib treatment or if neratinib-sensitive cancer cells have innate resistance. To achieve this, we determined the IC_{50} values for each cell line and their neratinib-resistant variant. Neratinib-resistant cell variants were found to have a higher IC_{50} in comparison with their neratinib-sensitive counterparts, demonstrating that neratinib-resistance conferred cross-resistance to tucatinib in all three HER2+ breast cancer cell variants. Interestingly, HCC1954 cells manifest innate resistance to tucatinib in comparison with EFM192A and SKBR3 cell lines. HCC1954 cells were found previously to be innately resistant to trastuzumab, but not to lapatinib[411]. This study discovered the increase of activation of the PI3K/AKT pathway due to the loss of PTEN or the presence of activating mutations in PI3K, was correlated with trastuzumab resistance. Further analysis must be performed to unravel the innate resistance to tucatinib and investigate the implication of PI3K/AKT pathway in tucatinib resistance, as could have a clinical relevance for patients' treatment.

Secondly, we investigated if neratinib-sensitive breast cancer cells also show an increased EVs' release after the treatment with low-dosage anti-HER2 therapies to understand how sensitive cancer cells acquire an urgent resistance against the treatment under the exposure of low-dose anti-HER2 agents. We used the IFCM assay on the CM as a small-scale screening assay to identify alterations

in EVs' release from HER2+ cell lines in vitro. In this way, it can be determined whether an inhibitor or drug may have an impact on the release of EVs from cancer cells, without the need for long, laborious separation of EVs.

Once we established the IC_{10} and IC_{50} of each cell line for tucatinib, CM was collected after 48 hrs and analysed by IFCM. CM from cells treated with IC_{10} tucatinib showed higher amounts of CD9+ and HER2+ events than their untreated matched counterparts. Interestingly, these differences were notable in sEVs and mEVs populations, but only the increment of HER2+ events in the CM derived from the innate tucatinib-resistant HCC1954 cells was significant. These results highlighted the potential of EVs as a means of monitoring therapy response and as liquid biopsies. These EVs could assist in categorising individuals with varying tumour types into specific treatment groups tailored to their needs. For instance, HCC1954 cells represent a patient's tumour and would not gain the benefit of tucatinib treatment, with an increase of EVs released carrying HER2 from tumour cells thus debilitating the effects of the drug.

However, this screening of CM by IFCM has limitations. For instance, only CD9 was used as EVs marker in this assay to compare the CM obtained from untreated and treated cells. CD9 was not present in all the EVs subpopulations, and it may be a missing part of the big picture about the effects of tucatinib treatment in EVs' release. Further validation with more EVs markers is therefore needed, including markers as CD63 and CD81. In addition, investigating the effect of EVs' release after tucatinib treatment in neratinib-resistant cell variants can also provide new and interesting insights in acquire and cross-resistance mechanisms.

There is an increasing emphasis on providing personalised therapy that considers the specific characteristics of each patient and their disease. The compelling evidence suggests that EVs offer an ideal platform for personalised medicine, not only because they can provide useful information to molecularly subtype a patient's tumour to determine the most effective treatment approach, but also because they can assess the impact of a specific drug on EV's release response. The term "liquid biopsy," a non-invasive alternative to traditional biopsies, has been long-awaited across various medical fields due to its potential for minimally-invasive screening, assessment, monitoring, and diagnosis[412–414]. EVs, found abundantly in all bodily fluids and considered a mini-maps of their cells or origin, play a vital role in liquid biopsies[414]. Their utilisation in this context can be particularly advantageous for diseases that are challenging to diagnose in their early asymptomatic stages, such as pancreatic cancer[412,413,415]. Furthermore, the identification of EVs-specific biomarkers that contribute to disease could present opportunities for early intervention and treatment[415].

Existing technologies for assessing drug-target interactions require intricate processing and invasive tissue biopsies, which restrict their clinical applicability in monitoring cancer treatment. Recent research has developed different analytical platforms that exploit circulating EVs to enable activity-based evaluation of tum our-specific drug-target interactions in patient blood samples. For instance, Pan et al. (2023)[416] developed a technology (extracellular vesicle monitoring of small-molecule

chemical occupancy and protein expression; ExoSCOPE) that employs bio-orthogonal probe amplification and spatial patterning of molecular reactions within matched plasmonic nanoring resonators. It detects changes in the presence of the drug and protein's profile in molecular subpopulations of EVs. This platform was used to monitor various targeted therapies, revealing EVs signatures that closely reflected cellular treatment efficacy. ExoSCOPE was also able to accurately classify disease status and targeted treatment outcomes 24 hrs after the start of treatment. In addition, Wang et al. (2020)[417] showed the viability of monitoring patient treatment responses by analysing the EVs' phenotype changes using a novel multiplex EVs' phenotype analyser chip. This platform incorporates cutting-edge technologies, including the nanomixing-enhanced microchip and the multiplex surface-enhanced Raman scattering nanotag system, which allow direct EVs phenotyping without the need for EVs enrichment. By using this platform, cancer-specific EVs phenotypes from the plasma of melanoma patients were successfully identified, revealing specific EVs' profiles associated with the development of drug resistance and demonstrating the potential of EVs phenotyping as a valuable tool for monitoring treatment responses.

It is important to have into consideration that EVs play dual roles in normal homeostatic processes, both safeguarding against cancer and promoting cancer and this duality must be considered to comprehend the context of EVs' communication as biomarkers or therapeutic agents[415]. Further analysis of these EVs released by cells after treatment must be done to decipher new mechanism behind the quick response of HER2+ breast cancer cells to the anti-HER2 treatments and to discover a potential way to improve small-drug therapies effectiveness (i.e., by inhibiting or enhancing targets related with this acquire response).

8.6 Conclusion

Several studies have confirmed that the release of EVs from tumour cells following treatment can exert detrimental effects on tumour clearance and facilitate the growth of cancer cells. This occurs through the development of resistance to chemotherapy, promoting metastasis, and initiating the formation of pre-metastatic niches. Moreover, chemotherapy can induce alterations in the cargo of EVs released by cancer cells, allowing the transfer of these changes to neighbouring cancer cells. This sets in motion a vicious cycle that adversely impacts treatment outcomes.

To assess the impact of tucatinib, an anti-HER2 therapy, on EVs' release, we performed a screening assay in the CM by IFCM. An increase of CD9+ and HER2+ events was found in the CM obtained from tucatinib-treated cells, HCC1954. Those cells were also found to be innate resistant to tucatinib. However, additional validation is necessary, which includes conducting a comprehensive EVs separation process. This step will help determine if the screening results accurately reflect the actual effect on EVs' release.

Chapter 9

Discussion, conclusion, and future work

9.1 Discussion

As discussed in **Chapter 1**, HER2-overexpression occurs in ~20% of breast cancers and confers aggressive behaviour and poorer prognosis. Although several drugs such as neratinib have been developed to target HER2, it is estimated that up to 70% of patients with HER2-overexpressing breast cancer do not gain benefit, due to innate or acquired drug-resistance.

A primary objective of our project was to gain a comprehensive understanding of the mechanisms underlying neratinib resistance in HER2+ breast cancer. Additionally, we aimed to explore the involvement of EVs in these mechanisms and investigate potential strategies for exploiting information carried by EVs. To achieve these aims, we used three HER2+ breast cancer cell variants and their neratinib-resistant counterparts previously developed in our group[64,232].

The EVs' field is rapidly expanding, with increasing interest in their potential therapeutic applications. However, one of the major challenges in this field is the separation and enrichment of EVs from complex biological fluids. In **Chapter 2**, we aimed to compare two commonly used methods for EVs separation, dUC and PEG+UC, using CM from the three different HER2-positive cell lines. Our results in **Chapter 2** show that both dUC and PEG+UC can be used as reproducible methods for separating quite pure EVs. However, PEG+UC tended to precipitate more particles and proteins that may not be of EVs origin [220].

Interestingly, our study also showed that the method of EVs separation used can have an impact on the characteristics of the recovered EVs. This is consistent with previous studies that have reported different outcomes depending on the method of EVs isolation used[105,308]. Therefore, it is important to carefully consider the downstream application of the EVs when selecting the method of EVs collection. Another important finding of our study is that consideration must be given to the inclusion of more than one source of CM (obtained from a single cell line) when EVs separation techniques are being compared, rather than using a single or pooled sample that may not generate results that can be extrapolated to other samples. This is because our results showed that information on the comparison of methods obtained from only one cell line's CM cannot be assumed to be correct for others and so extrapolated.

In order to investigate neratinib resistance mechanism(s) in HER2+ breast cancer and the involvement of EVs in this resistance, in **Chapter 3** we investigated the changes in proteome occurring between HER2-positive breast cancer cell lines and their neratinib-resistant counterparts. Proteomic profiling revealed that only one protein was significantly differentially expressed in two neratinib-resistant variants compared to the neratinib-sensitive counterparts. Specifically, this protein, AGR2, was down-regulated in both HCC1954 NR and SKBR3 NR cell variants compared to their neratinib-sensitive counterparts. Although some studies suggested that AGR2 may be involved in the development and progression of various cancer types, it is important to note that there is conflicting evidence and further research is needed to establish a clear understanding of its role. The available evidence regarding AGR2's involvement in cancer has been inconsistent and inconclusive.

While it exists evidence of association of AGR2 expression and poor prognosis in patients with ER+ or PR+ breast cancer[257,258], the relationship between AGR2 and HER2 has never been investigated. In addition, there are no studies regarding its association with HER2-overexpressing breast cancer or resistance to anti-HER2 therapies.

In this project and, as per our knowledge, for the first time, we investigated the relationship between AGR2 down-regulation and the resistance to neratinib. To study the AGR2's contribution to neratinib-resistance, we transfected AGR2 in NR cell variants and performed functional assays to show if the restoration of AGR2 expression to neratinib-sensitive levels have an effect in the aggressiveness of neratinib-resistance cell variants. When NR cell variants were transfected with AGR2 cDNA (producing HCC1954 NR-pcAGR2 and SKBR3 NR-pcAGR2 cells) and the protein was expressed at amounts comparable to that in neratinib-resistant counterparts, migration and invasion were reduced to levels similar to that of neratinib-sensitive HCC1954 cells. In addition, N-cadherin, an EMT marker, was down-regulated in HCC1954 NR-pcAGR2 compared with HCC1954 NR cells, to a similar level as showed by the HCC1954 cells. More interestingly, although no changes in proliferation rates were observed between transfected NR cell variants and non-transfected cells, resistance to neratinib was significantly decreased in both HCC1954 NR and SKBR3 NR cell variants after AGR2 transfection. Restoration of sensitivity to neratinib, at least partly, suggests that AGR2 could potentially have therapeutic potential as a means of adding value to neratinib. A more detailed investigation is now warranted to better understand the relevance of AGR2 in neratinib-resistance; its possible involvement in resistance to other HER2-targeted drugs such as trastuzumab, pertuzumab, T-DM1, and lapatinib, and its potential use as a biomarker of such resistance.

The proteomic profiling of these six cell line variants discussed in **Chapter 3** and included in the **Appendix II**, also showed the down-regulation of RAB3A and flotillin-1 in HCC1954 NR and SKBR3 NR cell variants, respectively. These proteins are related with EVs' release mechanisms. Research for this thesis then progressed on to performing the complete characterisation of EVs released from these neratinib-sensitive and neratinib-resistant cells following MISEV2018 guidelines and investigating if EVs released from neratinib-sensitive and neratinib-resistant cells reflect the HER2 and AGR2 status of their cells of origin.

Chapter 4, thus, aimed to compare the EVs released by neratinib-resistant and neratinib-sensitive cell lines using different EVs separation protocols and characterisation techniques. Initially, EVs from HCC1954 and SKBR3 cell line variants were separated using a 200K dUC protocol. However, due to limitations and variability observed in the results, we moved to a GUC protocol for better EVs purity, intactness, and in efforts to maintain functionality of membrane-associated proteins. EVs from the three pairs of HER2+ breast cancer cell lines were evaluated and characterised using NTA, immunoblotting, TEM, and IFCM. We found a reduction in the number of EVs released by neratinib-resistant cell lines compared to their sensitive counterparts, collected by both 200K dUC and GUC protocols. The decrease in EVs' release was not due to differences in cell numbers between the variants. The presence of HER2 protein on EVs was decreased in the neratinib-resistant isolates

compared to the sensitive counterparts as occurred in the cells of origin. This suggests a decrease in HER2+ EVs secretion in neratinib-resistant cells and could indicate changes in HER2 trafficking and EVs' release/biogenesis in neratinib-resistant cells. Of note, these results contrast with a previous study suggesting increased HER2+ EVs secretion in advanced breast disease[278]. It has been demonstrated that chemotherapeutic agents also stimulate the secretion and recycling EVs and assisting sensitive cancer cells to develop an urgent resistant phenotype[157]. However, as per our knowledge, this is the first time to completely characterise EVs derived from neratinib-resistant cell variants, which may involve different EVs' release mechanisms to those related to the urgent response to chemotherapeutic agents.

As mentioned, proteomic profiling of the cell variants performed in **Chapter 3** revealed differentially expressed proteins related to EVs' release, which were down-regulated in some of the neratinib-resistant cell line variants. This suggests that EVs' release may vary between cancer cell lines with different sensitivities or resistance to treatments, and that the cargo of EVs can contribute to resistance development to neratinib. We also examined the presence of AGR2 in the EVs derived from HCC1954 and SKBR3 cell lines by immunoblotting. However, no conclusive results were obtained in the content of AGR2 between neratinib-sensitive and neratinib-resistant-derived EVs. Further analysis is needed to determine differences in AGR2 content and its role as a secreted protein in the tumour microenvironment.

In addition to evaluating the EVs' release from neratinib-sensitive and neratinib-resistant HER2+ breast cancer cell lines, the microenvironment's effect of hypoxia on the release of EVs from neratinib-sensitive and neratinib-resistant HER2+ cell lines was also investigated (**Chapter 5**). Although previous research established the release of EVs is exacerbated under hypoxic conditions, most of these publications did not address the completed characterisation of those EVs or did not follow MISEV2018 guidelines. Protein quantities measurements, as a crude surrogate for EVs quantities, supported the established hypothesis of increased EVs' release under hypoxic conditions. However, characterisation of EVs using immunoblotting and NTA showed variable results (i.e., while IFCM showed an increase of positive events, we observed a decrease in some EVs markers for SKBR3-derived 120K isolates). IFCM analysis using CellMask® staining and anti-HER2 antibody binding revealed discrepancies with other methodologies (i.e., with NTA, showing opposite trends). This chapter also examined the presence of E-cadherin, IL-6, IL-8, and HER2 in the cells and their derived EVs. E-cadherin expression decreased in hypoxic SKBR3 cells and was found to be enriched in the EVs derived under hypoxia. IL-6 expression increased in all cell lines under hypoxia, and it was also enriched in the EVs derived from hypoxic cells. IL-8 was only detected in HCC1954 cells and their EVs, but not in EFM192A and SKBR3 cell line variants and their derived EVs. HER2 expression showed a decrease in cell lysates under hypoxia but was enriched on the surface of EVs derived from hypoxic conditions. The increase of these proteins as EVs' cargo may lead in tumour progression, aggressiveness, and resistance to anti-HER2 therapies, as showed by others[334]. We also explored the presence of specific miRNAs (miR-21, miR-210, miR-155, and miR-630) in the EVs derived from the six HER2+ cell line variants. These miRNAs were selected because they are known

to be associated with hypoxic conditions and drug resistance in HER2-targeting therapies. Surprisingly, miR-21 was down-regulated in EVs released by hypoxic EFM192A and HCC1954 cells, while miR-210 was up-regulated in all EVs released under hypoxic conditions except those derived from hypoxic EFM192A NR cells. miR-155 showed mixed results, and miR-630 was not detected in EVs derived from hypoxic HCC1954 cell line variants. These findings suggest that hypoxia can alter the release and cargo of EVs in a cell-dependent manner, potentially influencing breast cancer invasiveness and drug resistance. However, due to the current limitations in EVs miRNA research (lack of standardised normalisation strategies, impact of EVs separation methodology on the downstream RNA profile, lack of consensus on appropriate mRNA controls in EVs, etc.) these results must be interpreted with caution.

Advancing further in this research vein, we decided to assess whether the observed effects of hypoxia on neratinib-sensitive and neratinib-resistant HER2+ breast cancer cell lines and EVs' release could also be observed when the cells were cultured in a 3D environment. Generally, utilising 3D cell culture offers a more biologically relevant setting for studying EVs compared to conventional 2D cell culture. It allows for exploring the involvement of EVs in diverse diseases and physiological processes. Nonetheless, challenges exist in establishing 3D cultures, specifically for the collection and characterisation of EVs where large numbers of cells and their conditioned media are typically required. The first aim of **Chapter 6** was to determine the suitability of a 3D cell culture model using an Elplasia® plate for EVs collection, together with a previously methodology for spheroid formation based on poly-HEMA coated 96-well plates which was previously used by our group[349]. Here, we encountered limitations in the poly-HEMA coated 96-well methodology related to volume limitations and the collection of CM without disrupting or absorbing the spheroids. Elplasia®, conversely, offered a high number of microcavities per well, allowing for the formation of numerous spheroids, and it could accommodate a larger volume of CM, facilitating larger-scale spheroid formation. One substantial challenge we faced was the disaggregation of the spheroidsand subsequent cell count and viability calculations. In 2D cell culture models, EVs quantification is commonly normalised based on the final cell numbers (i.e., numbers of cells that have produced the EVs), which is considered as standard practice. However, in 3D models, normalisation of EVs is not standardised, and some studies opt for normalisation based on seeding densities or the volume of starting material. However, taking into consideration the significant decrease in cell counts under hypoxic conditions compared to normoxia, we normalised EVs counts to the protein content of the corresponding cell lysates obtained at the time of EVs collection.

Once the suitability of Elplasia® plates for EVs collection from 3D cultured cells was addressed, EFM192A, EFM192A, HCC1954, and HCC1954 NR were cultured in 3D conditions under normoxia and hypoxia and the EVs were collected. We found that hypoxia affected the roundness, smoothness, and compactness of the spheroids, leading to a significant decrease in their diameter and volume across all cell line variants. We observed an increase in EVs protein content in EVs derived from EFM192A NR, HCC1954, and HCC1954 NR under hypoxic conditions compared to normoxia, with significant differences observed in HCC1954-derived EVs. Immunoblotting and flow

cytometry analysis revealed cell line-specific differences and oxygen-dependent changes in EVs markers. The comparative analysis between 2D and 3D culture under hypoxic and normoxic conditions was not yet addressed, but previous studies have demonstrated that 3D cultures exhibit a greater release of EVs compared to 2D cultures, and oxygen deprivation can contribute to increased EVs' release[418]. We also investigated HER2 expression in cells and the presence of HER2 on the surface of non-lysed EVs. While no significant differences were found in HER2 protein levels between spheroids cultured in hypoxia and normoxia, a higher presence of HER2 on the EVs' surface was observed in the EVs samples derived from hypoxic EFM192A NR, HCC1954, and HCC1954 NR spheroids. Previously research performed in our group established that BT474, EFM192A, and HCC1954 cells grown in 3D show a degree of resistance to neratinib and docetaxel compared to 2D cell cultures. In addition, some proteins involved in cell growth and survival (Akt, pAkt, Erk, and EGFR family of receptors), common drug targets (EGFR and HER2), and a drug-transporter that confers multiple-drug resistance (PGP) were all increased in those cells grown in 3D, contributing to the increase in innate resistance to neratinib and docetaxel[349]. However, this comparison was not addressed in their neratinib-resistant counterparts and/or under hypoxic conditions. To expand the comparisons not only between 2D and 3D culture but also between conditions (hypoxia *vs* normoxia; neratinib-resistant *vs* neratinib-sensitive), refinement of the spheroid disaggregation step and cell count/viability determination is necessary for improved accuracy and reproducibility of the results.

In keeping with the 3D culture and the lack of standardised practices, we decide to develop the first global survey of currently used pre-clinical *in vitro* models for cancer research. The survey provides an overview of the current trend in the use of different pre-clinical *in vitro* tumour models. Despite its limitations, 2D *in vitro* models are still the most used mode, as this is the most straightforward cell culture model, less time-consuming and least expensive. Currently, there is an urgent need for the establishment of a standard methodology for the cell culture models and their characterisation, as that would simplify the improvement of current *in vitro* models that may be beneficial in pre-clinical studies, considering that those may complement or even substitute current methods that are not ideal. Additional research to improve pre-clinical *in vitro* models in cancer research that capture elements of tumour complexity and heterogeneity is a must.

Finally, we explored the possibility that the exposure to a low dose of tucatinib (considering that factors such as tumour size, location, heterogeneity, and other variables may limit the achievable dosage of anti-HER2 therapies) can inadvertently enhance HER2 expression and/or EVs' release, potentially promoting tumour aggressiveness. We first investigated if neratinib-resistant cell variants show cross-resistance to tucatinib treatment or if neratinib-sensitive cancer cells have innate resistance. Thus, we determined IC_{50} values for tucatinib for each cell line and their neratinib-resistant variant. Neratinib-resistant cell variants showed a higher IC_{50} when compared with their sensitive counterparts, demonstrating that neratinib-resistance conferred cross-resistance to tucatinib in all three HER2+ breast cancer cell lines studied. Interestingly, HCC1954 cells manifest innate resistance to tucatinib compared to EFM192A and SKBR3 cell lines. Moreover, we

investigated if neratinib-sensitive breast cancer cells also show an increased EVs' release after the treatment with low-dosage of tucatinib to understand how sensitive cancer cells acquire an urgent resistance against the treatment under the exposure of low-dose anti-HER2 agents. Once we established the IC_{10} for tucatinib in each cell line, CM was collected after 48 hrs of treatment and analysed by IFCM. CM from cells treated with IC_{10} tucatinib showed an increase of CD9+ and HER2+ events than their untreated matched counterparts. These differences were notable in both sEVs and mEVs populations, but only significant in HCC1954 cells. Further analysis of these EVs released by cells after treatment is a must to decipher new mechanism behind the quick response of HER2+ breast cancer cells to the anti-HER2 treatments and to discover a potential way to improve small-drug therapies effectiveness (i.e., by inhibiting or enhancing targets related with this acquired response).

9.2 Conclusion

The research presented here indicates that neratinib-resistant cell lines display differences in proteome profile and EVs' release compared to their neratinib-sensitive counterparts. Furthermore, the resistance to neratinib has been found to be associated with cross-resistance to tucatinib. We found that neratinib-resistance is mediated, at least in part, by decreased AGR2 in HCC1954 NR and SKBR3 NR cell variants. We also demonstrated that EVs quantities were altered in neratinib-resistant cell variants compared with their neratinib-sensitive counterparts.

We also demonstrated that EVs' release is affected under hypoxic conditions as well their cargo. The increase of E-cadherin, IL-6, IL-8 and HER2 in/on EVs derived from HER2+ cancer cells under hypoxia may have an effect in tumour progression and resistance to anti-HER2 therapies. We also evaluated the suitability of the Elplasia® plates to obtain EVs released by spheroids cultured under normoxia and hypoxia conditions in an optimum concentration for their characterisation. Finally, we also performed the first global survey about the use of preclinical *in vitro* models in cancer research to implement their use and improve the reproducibility and standardisation of the models.

9.3 Future work

The work presented in this thesis provides a basis for future investigations, suggesting several possibilities for further exploration. The following examples outline potential areas for further investigation based on the work presented.

9.3.1 Deeper insight on the role of AGR2 in neratinib-resistance

We demonstrated *in vitro* that the transfection of AGR2 in neratinib-resistant cell lines restored partially the sensitivity to neratinib in those cells. However, more research can be performed to shed light in the role of AGR2 in neratinib-resistance. For instance, a blockage of AGR2 in neratinib-sensitive cells can be performed to evaluate if their resistance to neratinib it is increased after blockade. Once the *in vitro* experiments are done, the next step would be to determinate the effect of AGR2 *in vivo.* For that, the effect of the AGR2 transfection with respect to tumour growth and metastasis formation must be addressed. Mouse xenograft models could be used for that purpose, by injecting neratinib-sensitive cells, non-transfected neratinib-resistant cells, or transfected neratinib-resistant cells.

Although there are studies analysing the association between AGR2 and tumour prognosis in breast cancer, the stratified analysis did not consider the differences between HER2, ER, and PR status without a clear differentiation between them. In addition, no clinical study relating AGR2 and resistance to anti-HER2 therapies was found, including neratinib. Accessing samples from patients who have developed resistance to various anti-HER2 therapies to assess the AGR2 status could contribute to the enhancement of our comprehension of the relationship between AGR2 and the development of resistance, having potential in the clinic as a predictive biomarker for patient response to therapy.

9.3.2 Presence of AGR2 in the EVs released from neratinib-sensitive and neratinib-resistant cell lines

So far, only an immunoblotting assay was performed in order to evaluate the presence of AGR2 in the EVs release from neratinib-sensitive and neratinib-resistance cell line variants. To better quantify the presence of AGR2 in those EVs samples, an AGR2 ELISA will be performed.

9.3.3 Expand cell characterisation under hypoxia conditions

In order to better understand the effect of hypoxia on neratinib-sensitive and neratinib-resistant cancer cell line variants, the expression of other proteins related with hypoxia may be performed. For instance, include in the comparison proteins such as HIF-2α, multidrug resistance protein 1 (MRP1), as well as the expression of immunosuppressive cytokines IL-10 and TGF-β1. DNA barcoding to evaluate differences between normoxia and hypoxia conditions can be also useful in these terms.

9.3.4 Perform a proper 2D and 3D culture comparison

After demonstrating the suitability of Elplasia® plates to collect EVs derived from spheroids, a comparison between 2D and 3D culture could be performed to establish if there are differences in terms of EVs' numbers or the presence of different EVs subpopulations enriched by differences in the cell culture methodology used. In addition, investigate the miRNA content in the EVs derived from 3D cell cultured cells under normoxia and hypoxia as was performed for those derived from 2D cell culture.

9.3.5 Better characterisation of EVs released from neratinib-sensitive and neratinib-resistant cell lines and their cargo

Characterisation of these EVs can be improved by adding more EVs markers by IFCM, as well as including new image techniques (i.e., super-resolution microscopy).
In order to evaluate not only the EVs number but also their cargo, a proteomic/metabolomic profile of the EVs could be performed comparing normoxia vs hypoxia, as well as 2D vs 3D to evaluate the changes in the EVs cargo under different conditions.

9.3.6 Functional assays with EVs derived from hypoxic conditions from 2D and 3D culture

Once the EVs from breast cancer cells cultured by normoxia and hypoxia would be collected and characterised, functional assays to evaluate how those EVs affect the proliferation, migration, invasion, and *anoikis*-resistance can be evaluated. The purpose would be to investigate if the EVs release by hypoxic cells are able to transfer more aggressive behaviours to receiving cells compared to those released by normoxic cells.

9.3.7 Evaluate the mitochondrial activity under hypoxic conditions

Another line of research that may be interesting is to evaluate the mitochondrial activity under normoxia and hypoxia conditions in neratinib-sensitive and neratinib-resistant cell line variants. During periods of hypoxia, mitochondria divide and present themselves as individual organelles, potentially facilitating mitophagy. This process aids in maintaining a low level of reactive oxygen species (ROS) production within the physiological range while preserving the integrity of the mitochondria through a reduction in respiratory activity. Evaluating if there is a differential adaptation to hypoxia conditions between neratinib-sensitive and neratinib-resistant cells can facilitate the discovery of new biomarkers.

9.3.8 Investigate the connection between AGR2 and hypoxia

A study performed by Hong et al. (2013)[419] claimed that AGR2 expression is regulated by HIF-1α in glioblastoma, while a study performed by Li et al. (2015)[420] reported that AGR2 is an essential

regulator in hypoxia-induced doxorubicin resistance through the binding and stabilization of HIF-1α in MCF-7 cells. Exploring the expression of AGR2 in the six different cell line variants may help to elucidate if AGR2 status change under the presence of low oxygen level (transfected neratinib-cell variants could be included in this comparative as well).

9.3.9 Complete characterisation of EVs released by HER2-positive breast cancer cells after tucatinib treatment

Here we only investigated the presence of EVs in the clarified CM collected from neratinib-sensitive cells after 48 hrs treatment with tucatinib. As some interesting results were found in terms of HER2+ and CD9+ events by IFCM, the characterisation of the separated EVs collected from neratinib-sensitive and neratinib-resistant may help to elucidated if the EVs' release is affected by tucatinib treatment as well as evaluate changes in the EVs' cargo.

References

1. Sung, H., Ferlay, J., Siegel, R. L., Laversanne, M., Soerjomataram, I., Jemal, A., & Bray, F. (2021). Global Cancer Statistics 2020: GLOBOCAN Estimates of Incidence and Mortality Worldwide for 36 Cancers in 185 Countries. CA: A Cancer Journal for Clinicians, 71(3), 209–249. https://doi.org/10.3322/caac.21660

2. Cancer (IARC), T. I. A. for R. on. (n.d.). Global Cancer Observatory. Retrieved 9 May 2023, from https://gco.iarc.fr/

3. Kutikov, A., Weinberg, D. S., Edelman, M. J., Horwitz, E. M., Uzzo, R. G., & Fisher, R. I. (2020). A War on Two Fronts: Cancer Care in the Time of COVID-19. Annals of Internal Medicine, 172(11), 756–758. https://doi.org/10.7326/M20-1133

4. Serrano, D., Bonanni, B., & Brown, K. (2019). Therapeutic cancer prevention: Achievements and ongoing challenges – a focus on breast and colorectal cancer. Molecular Oncology, 13(3), 579–590. https://doi.org/10.1002/1878-0261.12461

5. Polyak, K. (2007). Breast cancer: Origins and evolution. The Journal of Clinical Investigation, 117(11), 3155–3163. https://doi.org/10.1172/JCI33295

6. Dai, X., Xiang, L., Li, T., & Bai, Z. (2016). Cancer Hallmarks, Biomarkers and Breast Cancer Molecular Subtypes. Journal of Cancer, 7(10), 1281–1294. https://doi.org/10.7150/jca.13141

7. Yao, H., He, G., Yan, S., Chen, C., Song, L., Rosol, T. J., & Deng, X. (2017). Triple-negative breast cancer: Is there a treatment on the horizon? Oncotarget, 8(1), 1913–1924. https://doi.org/10.18632/oncotarget.12284

8. Dai, X., Li, T., Bai, Z., Yang, Y., Liu, X., Zhan, J., & Shi, B. (2015). Breast cancer intrinsic subtype classification, clinical use and future trends. American Journal of Cancer Research, 5(10), 2929–2943.

9. Creighton, C. J. (2012). The molecular profile of luminal B breast cancer. Biologics : Targets & Therapy, 6, 289–297. https://doi.org/10.2147/BTT.S29923

10. Inic, Z., Zegarac, M., Inic, M., Markovic, I., Kozomara, Z., Djurisic, I., Inic, I., Pupic, G., & Jancic, S. (2014). Difference between Luminal A and Luminal B Subtypes According to Ki-67, Tumor Size, and Progesterone Receptor Negativity Providing Prognostic Information. Clinical Medicine Insights. Oncology, 8, 107–111. https://doi.org/10.4137/CMO.S18006

11. Abdel-Hafiz, H. A. (2017). Epigenetic Mechanisms of Tamoxifen Resistance in Luminal Breast Cancer. Diseases, 5(3), 16. https://doi.org/10.3390/diseases5030016

12. Yersal, O., & Barutca, S. (2014). Biological subtypes of breast cancer: Prognostic and therapeutic implications. World Journal of Clinical Oncology, 5(3), 412–424. https://doi.org/10.5306/wjco.v5.i3.41

13. Herschkowitz, J. I., Simin, K., Weigman, V. J., Mikaelian, I., Usary, J., Hu, Z., Rasmussen, K. E., Jones, L. P., Assefnia, S., Chandrasekharan, S., Backlund, M. G., Yin, Y., Khramtsov, A. I., Bastein, R., Quackenbush, J., Glazer, R. I., Brown, P. H., Green, J. E., Kopelovich, L., … Perou, C. M. (2007). Identification of conserved gene expression features between murine mammary carcinoma models and human breast tumors. Genome Biology, 8(5), R76. https://doi.org/10.1186/gb-2007-8-5-r76

14. Prat, A., Parker, J. S., Karginova, O., Fan, C., Livasy, C., Herschkowitz, J. I., He, X., & Perou, C. M. (2010). Phenotypic and molecular characterization of the claudin-low intrinsic subtype of breast cancer. Breast Cancer Research, 12(5), R68. https://doi.org/10.1186/bcr2635

15. Turner, K. M., Yeo, S. K., Holm, T. M., Shaughnessy, E., & Guan, J.-L. (2021). Heterogeneity within molecular subtypes of breast cancer. American Journal of Physiology - Cell Physiology, 321(2), C343–C354. https://doi.org/10.1152/ajpcell.00109.2021

16. Orrantia-Borunda, E., Anchondo-Nuñez, P., Acuña-Aguilar, L. E., Gómez-Valles, F. O., & Ramírez-Valdespino, C. A. (2022). Subtypes of Breast Cancer. In Breast Cancer [Internet]. Exon Publications. https://doi.org/10.36255/exon-publications-breast-cancer-subtypes

17. Corti, C., Giugliano, F., Nicolò, E., Tarantino, P., Criscitiello, C., & Curigliano, G. (2023). HER2-Low Breast Cancer: A New Subtype? Current Treatment Options in Oncology, 24(5), 468–478. https://doi.org/10.1007/s11864-023-01068-1

18. van den Ende, N. S., Smid, M., Timmermans, A., van Brakel, J. B., Hansum, T., Foekens, R., Trapman, A. M. A. C., Heemskerk-Gerritsen, B. A. M., Jager, A., Martens, J. W. M., & van Deurzen, C. H. M. (2022). HER2-low breast cancer shows a lower immune response compared to HER2-negative cases. Scientific Reports, 12(1), 12974. https://doi.org/10.1038/s41598-022-16898-6

19. Giugliano, F., Curigliano, G., & Tarantino, P. (2023). HER2-low expression in breast oncology: Treatment implications in the smart chemotherapy era. European Journal of Cancer Prevention: The Official Journal of the European Cancer Prevention Organisation (ECP), 32(2), 149–154. https://doi.org/10.1097/CEJ.0000000000000781

20. Molinelli, C., Jacobs, F., Marchiò, C., Pitto, F., Cosso, M., Spinaci, S., de Azambuja, E., Schettini, F., Agostinetto, E., & Lambertini, M. (2022). HER2-Low Breast Cancer: Where Are We? Breast Care (Basel, Switzerland), 17(6), 533–545. https://doi.org/10.1159/000527391

21. Di Cosimo, S., La Rocca, E., Ljevar, S., De Santis, M. C., Bini, M., Cappelletti, V., Valenti, M., Baili, P., de Braud, F. G., Folli, S., Scaperrotta, G., Volpi, C., Vingiani, A., Vernieri, C., Verderio, P., Miceli, R., & Pruneri, G. (2022). Moving HER2-low breast cancer predictive and prognostic data from clinical trials into the real world. Frontiers in Molecular Biosciences, 9, 996434. https://doi.org/10.3389/fmolb.2022.996434

22. Tarantino, P., Hamilton, E., Tolaney, S. M., Cortes, J., Morganti, S., Ferraro, E., Marra, A., Viale, G., Trapani, D., Cardoso, F., Penault-Llorca, F., Viale, G., Andrè, F., & Curigliano, G. (2020). HER2-Low Breast Cancer: Pathological and Clinical Landscape. Journal of Clinical Oncology: Official Journal of the American Society of Clinical Oncology, 38(17), 1951–1962. https://doi.org/10.1200/JCO.19.02488

23. Prat, A., Bardia, A., Curigliano, G., Hammond, M. E. H., Loibl, S., Tolaney, S. M., & Viale, G. (2022). An Overview of Clinical Development of Agents for Metastatic or Advanced Breast Cancer Without ERBB2 Amplification (HER2-Low). JAMA Oncology. https://doi.org/10.1001/jamaoncol.2022.4175

24. Citri, A., Skaria, K. B., & Yarden, Y. (2003). The deaf and the dumb: The biology of ErbB-2 and ErbB-3. Experimental Cell Research, 284(1), 54–65. https://doi.org/10.1016/s0014-4827(02)00101-5

25. Bertelsen, V., & Stang, E. (2014). The Mysterious Ways of ErbB2/HER2 Trafficking. Membranes, 4(3), 424–446. https://doi.org/10.3390/membranes4030424

26. Higgins, M. J., & Baselga, J. (2011). Targeted therapies for breast cancer. The Journal of Clinical Investigation, 121(10), 3797–3803. https://doi.org/10.1172/JCI57152

27. Sirkisoon, S. R., Carpenter, R. L., Rimkus, T., Miller, L., Metheny-Barlow, L., & Lo, H.-W. (2016). EGFR and HER2 signaling in breast cancer brain metastasis. Frontiers in Bioscience (Elite Edition), 8, 245–263.

28. Giordano, S. H., Temin, S., Chandarlapaty, S., Crews, J. R., Esteva, F. J., Kirshner, J. J., Krop, I. E., Levinson, J., Lin, N. U., Modi, S., Patt, D. A., Perlmutter, J., Ramakrishna, N., Winer, E. P., & Davidson, N. E. (2018). Systemic Therapy for Patients With Advanced Human Epidermal Growth Factor Receptor 2-Positive Breast Cancer: ASCO Clinical Practice Guideline Update. Journal of Clinical Oncology: Official Journal of the American Society of Clinical Oncology, 36(26), 2736–2740. https://doi.org/10.1200/JCO.2018.79.2697

29. Owens, M. A., Horten, B. C., & Silva, M. M. D. (2004). HER2 Amplification Ratios by Fluorescence In Situ Hybridization and Correlation with Immunohistochemistry in a Cohort of 6556 Breast Cancer Tissues. Clinical Breast Cancer, 5(1), 63–69. https://doi.org/10.3816/CBC.2004.n.011

30. Ross, J. S., Slodkowska, E. A., Symmans, W. F., Pusztai, L., Ravdin, P. M., & Hortobagyi, G. N. (2009). The HER-2 receptor and breast cancer: Ten years of targeted anti-HER-2 therapy and personalized medicine. The Oncologist, 14(4), 320–368. https://doi.org/10.1634/theoncologist.2008-0230

31. Pietilä, M., Sahgal, P., Peuhu, E., Jäntti, N. Z., Paatero, I., Närvä, E., Al-Akhrass, H., Lilja, J., Georgiadou, M., Andersen, O. M., Padzik, A., Sihto, H., Joensuu, H., Blomqvist, M., Saarinen, I., Boström, P. J., Taimen, P., & Ivaska, J. (2019). SORLA regulates endosomal trafficking and oncogenic fitness of HER2. Nature Communications, 10(1), Article 1. https://doi.org/10.1038/s41467-019-10275-0

32. Wang, Y., Pennock, S., Chen, X., & Wang, Z. (2002). Endosomal Signaling of Epidermal Growth Factor Receptor Stimulates Signal Transduction Pathways Leading to Cell Survival. Molecular and Cellular Biology, 22(20), 7279–7290. https://doi.org/10.1128/MCB.22.20.7279-7290.2002

33. Muharram, G., Sahgal, P., Korpela, T., De Franceschi, N., Kaukonen, R., Clark, K., Tulasne, D., Carpén, O., & Ivaska, J. (2014). Tensin-4-Dependent MET Stabilization Is Essential for Survival and Proliferation in Carcinoma Cells. Developmental Cell, 29(5), 629–630. https://doi.org/10.1016/j.devcel.2014.05.018

34. Hammond, D. E., Carter, S., McCullough, J., Urbé, S., Vande Woude, G., & Clague, M. J. (2003). Endosomal Dynamics of Met Determine Signaling Output. Molecular Biology of the Cell, 14(4), 1346–1354. https://doi.org/10.1091/mbc.e02-09-0578

35. Wong, D. J. L., & Hurvitz, S. A. (2014). Recent advances in the development of anti-HER2 antibodies and antibody-drug conjugates. Annals of Translational Medicine, 2(12), 122. https://doi.org/10.3978/j.issn.2305-5839.2014.08.13

36. Viale, G., Morganti, S., Ferraro, E., Zagami, P., Marra, A., & Curigliano, G. (2019). What therapies are on the horizon for HER2 positive breast cancer? Expert Review of Anticancer Therapy, 19(9), 811–822. https://doi.org/10.1080/14737140.2019.1660164

37. Sun, Z., Shi, Y., Shen, Y., Cao, L., Zhang, W., & Guan, X. (2015). Analysis of different HER-2 mutations in breast cancer progression and drug resistance. Journal of Cellular and Molecular Medicine, 19(12), 2691–2701. https://doi.org/10.1111/jcmm.12662

38. Ferrando-Díez, A., Felip, E., Pous, A., Bergamino Sirven, M., & Margelí, M. (2022). Targeted Therapeutic Options and Future Perspectives for HER2-Positive Breast Cancer. Cancers, 14(14), 3305. https://doi.org/10.3390/cancers14143305

39. Bredin, P., Walshe, J. M., & Denduluri, N. (2020). Systemic therapy for metastatic HER2-positive breast cancer. Seminars in Oncology, 47(5), 259–269. https://doi.org/10.1053/j.seminoncol.2020.07.008

40. Meric-Bernstam, F., Johnson, A. M., Dumbrava, E. E. I., Raghav, K., Balaji, K., Bhatt, M., Murthy, R. K., Rodon, J., & Piha-Paul, S. A. (2019). Advances in HER2-Targeted Therapy: Novel Agents and Opportunities Beyond Breast and Gastric Cancer. Clinical Cancer Research: An Official Journal of the American Association for Cancer Research, 25(7), 2033–2041. https://doi.org/10.1158/1078-0432.CCR-18-2275

41. Erp, N. P. van, Gelderblom, H., & Guchelaar, H.-J. (2009). Clinical pharmacokinetics of tyrosine kinase inhibitors. Cancer Treatment Reviews, 35(8), 692–706. https://doi.org/10.1016/j.ctrv.2009.08.004

42. Lin, N. U., & Winer, E. P. (2004). New targets for therapy in breast cancer: Small molecule tyrosine kinase inhibitors. Breast Cancer Research: BCR, 6(5), 204–210. https://doi.org/10.1186/bcr919

43. Landi, L., & Cappuzzo, F. (2013). Irreversible EGFR-TKIs: Dreaming perfection. Translational Lung Cancer Research, 2(1), 40–49. https://doi.org/10.3978/j.issn.2218-6751.2012.12.05

44. Feldinger, K., & Kong, A. (2015). Profile of neratinib and its potential in the treatment of breast cancer. Breast Cancer (Dove Medical Press), 7, 147–162. https://doi.org/10.2147/BCTT.S54414

45. Collins, D. M., Conlon, N. T., Kannan, S., Verma, C. S., Eli, L. D., Lalani, A. S., & Crown, J. (2019). Preclinical Characteristics of the Irreversible Pan-HER Kinase Inhibitor Neratinib Compared with Lapatinib: Implications for the Treatment of HER2-Positive and HER2-Mutated Breast Cancer. Cancers, 11(6), 737. https://doi.org/10.3390/cancers11060737

46. Blackwell, K. L., Zaman, K., Qin, S., Tkaczuk, K. H. R., Campone, M., Hunt, D., Bryce, R., & Goldstein, L. J. (2019). Neratinib in Combination With Trastuzumab for the Treatment of Patients With Advanced HER2-positive Breast Cancer: A Phase I/II Study. Clinical Breast Cancer, 19(2), 97-104.e4. https://doi.org/10.1016/j.clbc.2018.12.011

47. Delaloge, S., Cella, D., Ye, Y., Buyse, M., Chan, A., Barrios, C. H., Holmes, F. A., Mansi, J., Iwata, H., Ejlertsen, B., Moy, B., Chia, S. K. L., Gnant, M., Smichkoska, S., Ciceniene, A., Martinez, N., Filipović, S., Ben-Baruch, N. E., Joy, A. A., … Martin, M. (2019). Effects of neratinib on health-related quality of life in women with HER2-positive early-stage breast cancer: Longitudinal analyses from the randomized phase III ExteNET trial. Annals of Oncology: Official Journal of the European Society for Medical Oncology, 30(4), 567–574. https://doi.org/10.1093/annonc/mdz016

48. Freedman, R. A., Gelman, R. S., Agar, N. Y. R., Santagata, S., Randall, E. C., Gimenez-Cassina Lopez, B., Connolly, R. M., Dunn, I. F., Van Poznak, C. H., Anders, C. K., Melisko, M. E., Silvestri, K., Cotter, C. M., Componeschi, K. P., Marte, J. M., Moy, B., Blackwell, K. L., Puhalla, S. L., Ibrahim, N., … Translational Breast Cancer Research Consortium (TBCRC). (2020). Pre- and Postoperative Neratinib for HER2-Positive Breast Cancer Brain Metastases: Translational Breast Cancer Research Consortium 022. Clinical Breast Cancer, 20(2), 145-151.e2. https://doi.org/10.1016/j.clbc.2019.07.011

49. Singh, H., Walker, A. J., Amiri-Kordestani, L., Cheng, J., Tang, S., Balcazar, P., Barnett-Ringgold, K., Palmby, T. R., Cao, X., Zheng, N., Liu, Q., Yu, J., Pierce, W. F., Daniels, S. R., Sridhara, R., Ibrahim, A., Kluetz, P. G., Blumenthal, G. M., Beaver, J. A., & Pazdur, R. (2018). U.S. Food and Drug Administration Approval: Neratinib for the Extended Adjuvant Treatment of Early-Stage HER2-Positive Breast Cancer. Clinical Cancer Research: An Official Journal of the American Association for Cancer Research, 24(15), 3486–3491. https://doi.org/10.1158/1078-0432.CCR-17-3628

50. Holmes, F. A., Moy, B., Delaloge, S., Chia, S. K. L., Ejlertsen, B., Mansi, J., Iwata, H., Gnant, M., Buyse, M., Barrios, C. H., Silovski, T., Šeparović, R., Bashford, A., Zotano, A. G., Denduluri, N., Patt, D., Gokmen, E., Gore, I., Smith, J. W., … ExteNET Study Group. (2023). Overall survival with neratinib after trastuzumab-based adjuvant therapy in HER2-positive breast cancer (ExteNET): A randomised, double-blind, placebo-controlled, phase 3 trial. European Journal of Cancer (Oxford, England: 1990), 184, 48–59. https://doi.org/10.1016/j.ejca.2023.02.002

51. Saura, C., Garcia-Saenz, J. A., Xu, B., Harb, W., Moroose, R., Pluard, T., Cortés, J., Kiger, C., Germa, C., Wang, K., Martin, M., Baselga, J., & Kim, S.-B. (2014). Safety and efficacy of neratinib in combination with capecitabine in patients with metastatic human epidermal growth factor receptor 2-positive breast cancer. Journal of Clinical Oncology: Official Journal of the American Society of Clinical Oncology, 32(32), 3626–3633. https://doi.org/10.1200/JCO.2014.56.3809

52. Abraham, J., Montero, A. J., Jankowitz, R. C., Salkeni, M. A., Beumer, J. H., Kiesel, B. F., Piette, F., Adamson, L. M., Nagy, R. J., Lanman, R. B., Sperinde, J., Huang, W., Allegra, C. J., Srinivasan, A., Wang, Y., Pogue-Geile, K. L., Lucas, P. C., & Jacobs, S. A. (2019). Safety and Efficacy of T-DM1 Plus Neratinib in Patients With Metastatic HER2-Positive Breast Cancer: NSABP Foundation Trial FB-10. Journal of Clinical Oncology: Official Journal of the American Society of Clinical Oncology, 37(29), 2601–2609. https://doi.org/10.1200/JCO.19.00858

53. Awada, A., Colomer, R., Inoue, K., Bondarenko, I., Badwe, R. A., Demetriou, G., Lee, S.-C., Mehta, A. O., Kim, S.-B., Bachelot, T., Goswami, C., Deo, S., Bose, R., Wong, A., Xu, F., Yao, B., Bryce, R., & Carey, L. A. (2016). Neratinib Plus Paclitaxel vs Trastuzumab Plus Paclitaxel in Previously Untreated Metastatic ERBB2-Positive Breast Cancer: The NEfERT-T Randomized Clinical Trial. JAMA Oncology, 2(12), 1557–1564. https://doi.org/10.1001/jamaoncol.2016.0237

54. Saura, C., Oliveira, M., Feng, Y.-H., Dai, M.-S., Chen, S.-W., Hurvitz, S. A., Kim, S.-B., Moy, B., Delaloge, S., Gradishar, W., Masuda, N., Palacova, M., Trudeau, M. E., Mattson, J., Yap, Y. S., Hou, M.-F., De Laurentiis, M., Yeh, Y.-M., Chang, H.-T., … NALA Investigators. (2020). Neratinib Plus Capecitabine Versus Lapatinib Plus Capecitabine in HER2-Positive Metastatic Breast Cancer Previously Treated With ≥ 2 HER2-Directed Regimens: Phase III NALA Trial. Journal of Clinical Oncology: Official Journal of the American Society of Clinical Oncology, 38(27), 3138–3149. https://doi.org/10.1200/JCO.20.00147

55. Barcenas, C. H., Hurvitz, S. A., Di Palma, J. A., Bose, R., Chien, A. J., Iannotti, N., Marx, G., Brufsky, A., Litvak, A., Ibrahim, E., Alvarez, R. H., Ruiz-Borrego, M., Chan, N., Manalo, Y., Kellum, A., Trudeau, M., Thirlwell, M., Garcia Saenz, J., Hunt, D., … CONTROL Study Investigators. (2020). Improved tolerability of neratinib in patients with HER2-positive early-stage breast cancer: The CONTROL trial. Annals of Oncology: Official Journal of the European Society for Medical Oncology, 31(9), 1223–1230. https://doi.org/10.1016/j.annonc.2020.05.012

56. Martin, M., Bonneterre, J., Geyer, C. E., Ito, Y., Ro, J., Lang, I., Kim, S.-B., Germa, C., Vermette, J., Wang, K., Wang, K., & Awada, A. (2013). A phase two randomised trial of neratinib monotherapy versus lapatinib plus capecitabine combination therapy in patients with HER2+ advanced breast cancer. European Journal of Cancer (Oxford, England: 1990), 49(18), 3763–3772. https://doi.org/10.1016/j.ejca.2013.07.142

57. Awada, A., Dirix, L., Manso Sanchez, L., Xu, B., Luu, T., Diéras, V., Hershman, D. L., Agrapart, V., Ananthakrishnan, R., & Staroslawska, E. (2013). Safety and efficacy of neratinib (HKI-272) plus vinorelbine in the treatment of patients with ErbB2-positive metastatic breast cancer pretreated with anti-HER2 therapy. Annals of Oncology: Official Journal of the European Society for Medical Oncology, 24(1), 109–116. https://doi.org/10.1093/annonc/mds284

58. Jankowitz, R. C., Abraham, J., Tan, A. R., Limentani, S. A., Tierno, M. B., Adamson, L. M., Buyse, M., Wolmark, N., & Jacobs, S. A. (2013). Safety and efficacy of neratinib in combination with weekly paclitaxel and trastuzumab in women with metastatic HER2-positive breast cancer: An NSABP Foundation Research Program phase I study. Cancer Chemotherapy and Pharmacology, 72(6), 1205–1212. https://doi.org/10.1007/s00280-013-2262-2

59. Jacobs, S. A., Robidoux, A., Abraham, J., Pérez-Garcia, J. M., La Verde, N., Orcutt, J. M., Cazzaniga, M. E., Piette, F., Antolín, S., Aguirre, E., Cortes, J., Llombart-Cussac, A., Di Cosimo, S., Kim, R. S., Feng, H., Lipchik, C., Lucas, P. C., Srinivasan, A., Wang, Y., … Pogue-Geile, K. L. (2019). NSABP FB-7: A phase II randomized neoadjuvant trial with paclitaxel + trastuzumab and/or neratinib followed by chemotherapy and postoperative trastuzumab in HER2+ breast cancer. Breast Cancer Research: BCR, 21(1), 133. https://doi.org/10.1186/s13058-019-1196-y

60. Exman, P., Garrido-Castro, A. C., Hughes, M. E., Freedman, R. A., Li, T., Trippa, L., Bychkovsky, B. L., Barroso-Sousa, R., Di Lascio, S., Mackichan, C., Lloyd, M. R., Krevalin, M., Cerami, E., Merrill, M. S., Santiago, R., Crowley, L., Kuhnly, N., Files, J., Lindeman, N. I., … Lin, N. U. (2019). Identifying ERBB2

Activating Mutations in HER2-Negative Breast Cancer: Clinical Impact of Institute-Wide Genomic Testing and Enrollment in Matched Therapy Trials. JCO Precision Oncology, 3, PO.19.00087. https://doi.org/10.1200/PO.19.00087

61. Ma, C. X., Bose, R., Gao, F., Freedman, R. A., Pegram, M. D., Blackwell, K., Bedard, P. L., Hayes, D. F., Goetz, M. P., Niravath, P. A., Russell, C. A., Tripathy, D., Cobleigh, M. A., Forero, A., Pluard, T. J., Anders, C. K., Bumb, C., Naughton, M., Al-Kateb, H., & Ellis, M. J. (2016). Phase II trial of neratinib for HER2 mutated, non-amplified metastatic breast cancer (HER2mut MBC). Journal of Clinical Oncology, 34(15_suppl), 516–516. https://doi.org/10.1200/JCO.2016.34.15_suppl.516

62. Chow, L. W.-C., Xu, B., Gupta, S., Freyman, A., Zhao, Y., Abbas, R., Vo Van, M.-L., & Bondarenko, I. (2013). Combination neratinib (HKI-272) and paclitaxel therapy in patients with HER2-positive metastatic breast cancer. British Journal of Cancer, 108(10), 1985–1993. https://doi.org/10.1038/bjc.2013.178

63. Xu, B., Kim, S.-B., Inoue, K., Lee, J., Zhang, B., Bryce, R., & Chow, L. W.-C. (2019). Neratinib-based therapy in patients with metastatic HER2-positive breast cancer from Asia. Future Oncology, 15(28), 3243–3253. https://doi.org/10.2217/fon-2019-0222

64. Breslin, S., Lowry, M. C., & O'Driscoll, L. (2017). Neratinib resistance and cross-resistance to other HER2-targeted drugs due to increased activity of metabolism enzyme cytochrome P4503A4. British Journal of Cancer, 116(5), 620–625. https://doi.org/10.1038/bjc.2016.445

65. Bose, R., Kavuri, S. M., Searleman, A. C., Shen, W., Shen, D., Koboldt, D. C., Monsey, J., Goel, N., Aronson, A. B., Li, S., Ma, C. X., Ding, L., Mardis, E. R., & Ellis, M. J. (2013). Activating HER2 mutations in HER2 gene amplification negative breast cancer. Cancer Discovery, 3(2), 224–237. https://doi.org/10.1158/2159-8290.CD-12-0349

66. Cocco, E., Javier Carmona, F., Razavi, P., Won, H. H., Cai, Y., Rossi, V., Chan, C., Cownie, J., Soong, J., Toska, E., Shifman, S. G., Sarotto, I., Savas, P., Wick, M. J., Papadopoulos, K. P., Moriarty, A., Cutler, R. E., Avogadri-Connors, F., Lalani, A. S., … Scaltriti, M. (2018). Neratinib is effective in breast tumors bearing both amplification and mutation of ERBB2 (HER2). Science Signaling, 11(551), eaat9773. https://doi.org/10.1126/scisignal.aat9773

67. Hyman, D. M., Piha-Paul, S. A., Won, H., Rodon, J., Saura, C., Shapiro, G. I., Juric, D., Quinn, D. I., Moreno, V., Doger, B., Mayer, I. A., Boni, V., Calvo, E., Loi, S., Lockhart, A. C., Erinjeri, J. P., Scaltriti, M., Ulaner, G. A., Patel, J., …

Solit, D. B. (2018). HER kinase inhibition in patients with HER2- and HER3-mutant cancers. Nature, 554(7691), 189–194. https://doi.org/10.1038/nature25475

68. Smyth, L. M., Piha-Paul, S. A., Won, H. H., Schram, A. M., Saura, C., Loi, S., Lu, J., Shapiro, G. I., Juric, D., Mayer, I. A., Arteaga, C. L., de la Fuente, M. I., Brufksy, A. M., Spanggaard, I., Mau-Sørensen, M., Arnedos, M., Moreno, V., Boni, V., Sohn, J., … Hyman, D. M. (2020). Efficacy and Determinants of Response to HER Kinase Inhibition in HER2-Mutant Metastatic Breast Cancer. Cancer Discovery, 10(2), 198–213. https://doi.org/10.1158/2159-8290.CD-19-0966

69. Oaknin, A., Friedman, C. F., Roman, L. D., D'Souza, A., Brana, I., Bidard, F.-C., Goldman, J., Alvarez, E. A., Boni, V., ElNaggar, A. C., Passalacqua, R., Do, K. T. M., Santin, A. D., Keyvanjah, K., Xu, F., Eli, L. D., Lalani, A. S., Bryce, R. P., Hyman, D. M., … Monk, B. J. (2020). Neratinib in patients with HER2-mutant, metastatic cervical cancer: Findings from the phase 2 SUMMIT basket trial. Gynecologic Oncology, 159(1), 150–156. https://doi.org/10.1016/j.ygyno.2020.07.025

70. Ulaner, G. A., Saura, C., Piha-Paul, S. A., Mayer, I., Quinn, D., Jhaveri, K., Stone, B., Shahin, S., Mann, G., Dujka, M., Bryce, R., Meric-Bernstam, F., Solit, D. B., & Hyman, D. M. (2019). Impact of FDG PET Imaging for Expanding Patient Eligibility and Measuring Treatment Response in a Genome-Driven Basket Trial of the Pan-HER Kinase Inhibitor, Neratinib. Clinical Cancer Research: An Official Journal of the American Association for Cancer Research, 25(24), 7381–7387. https://doi.org/10.1158/1078-0432.CCR-19-1658

71. Hanker, A. B., Brewer, M. R., Sheehan, J. H., Koch, J. P., Sliwoski, G. R., Nagy, R., Lanman, R., Berger, M. F., Hyman, D. M., Solit, D. B., He, J., Miller, V., Cutler, R. E., Lalani, A. S., Cross, D., Lovly, C. M., Meiler, J., & Arteaga, C. L. (2017). An Acquired HER2T798I Gatekeeper Mutation Induces Resistance to Neratinib in a Patient with HER2 Mutant-Driven Breast Cancer. Cancer Discovery, 7(6), 575–585. https://doi.org/10.1158/2159-8290.CD-16-1431

72. Dinkel, V., Anderson, D., Winski, S., Winkler, J., Koch, K., & Lee, P. A. (2012). Abstract 852: ARRY-380, a potent, small molecule inhibitor of ErbB2, increases survival in intracranial ErbB2+ xenograft models in mice. Cancer Research, 72(8_Supplement), 852. https://doi.org/10.1158/1538-7445.AM2012-852

73. Murthy, R., Borges, V. F., Conlin, A., Chaves, J., Chamberlain, M., Gray, T., Vo, A., & Hamilton, E. (2018). Tucatinib with capecitabine and trastuzumab in

advanced HER2-positive metastatic breast cancer with and without brain metastases: A non-randomised, open-label, phase 1b study. The Lancet. Oncology, 19(7), 880–888. https://doi.org/10.1016/S1470-2045(18)30256-0

74. Corti, C., & Criscitiello, C. (2021). Tucatinib approval by EMA expands options for HER2-positive locally advanced or metastatic breast cancer. ESMO Open, 6(2), 100063. https://doi.org/10.1016/j.esmoop.2021.100063

75. Krop, I. E., Carey, L. A., Ramos, J., Chen, Y., & Hamilton, E. P. (2022). Phase 2 trial of tucatinib plus trastuzumab deruxtecan in patients with HER2+ locally advanced or metastatic breast cancer with and without brain metastases (HER2CLIMB-04, trial in progress). Journal of Clinical Oncology, 40(16_suppl), TPS1111–TPS1111. https://doi.org/10.1200/JCO.2022.40.16_suppl.TPS1111

76. Wolf, D. M., Yau, C., Wulfkuhle, J., Brown-Swigart, L., Gallagher, R. I., Lee, P. R. E., Zhu, Z., Magbanua, M. J., Sayaman, R., O'Grady, N., Basu, A., Delson, A., Coppé, J. P., Lu, R., Braun, J., Asare, S. M., Sit, L., Matthews, J. B., Perlmutter, J., … Veer, L. J. van 't. (2022). Redefining breast cancer subtypes to guide treatment prioritization and maximize response: Predictive biomarkers across 10 cancer therapies. Cancer Cell, 40(6), 609-623.e6. https://doi.org/10.1016/j.ccell.2022.05.005

77. Spring, L. M., Fell, G., Arfe, A., Sharma, C., Greenup, R., Reynolds, K. L., Smith, B. L., Alexander, B., Moy, B., Isakoff, S. J., Parmigiani, G., Trippa, L., & Bardia, A. (2020). Pathologic Complete Response after Neoadjuvant Chemotherapy and Impact on Breast Cancer Recurrence and Survival: A Comprehensive Meta-analysis. Clinical Cancer Research: An Official Journal of the American Association for Cancer Research, 26(12), 2838–2848. https://doi.org/10.1158/1078-0432.CCR-19-3492

78. Chien, A. J., Tripathy, D., Albain, K. S., Symmans, W. F., Rugo, H. S., Melisko, M. E., Wallace, A. M., Schwab, R., Helsten, T., Forero-Torres, A., Stringer-Reasor, E., Ellis, E. D., Kaplan, H. G., Nanda, R., Jaskowiak, N., Murthy, R., Godellas, C., Boughey, J. C., Elias, A. D., … I-SPY 2 Consortium. (2020). MK-2206 and Standard Neoadjuvant Chemotherapy Improves Response in Patients With Human Epidermal Growth Factor Receptor 2-Positive and/or Hormone Receptor-Negative Breast Cancers in the I-SPY 2 Trial. Journal of Clinical Oncology: Official Journal of the American Society of Clinical Oncology, 38(10), 1059–1069. https://doi.org/10.1200/JCO.19.01027

79. Nanda, R., Liu, M. C., Yau, C., Shatsky, R., Pusztai, L., Wallace, A., Chien, A. J., Forero-Torres, A., Ellis, E., Han, H., Clark, A., Albain, K., Boughey, J. C., Jaskowiak, N. T., Elias, A., Isaacs, C., Kemmer, K., Helsten, T., Majure, M., … Esserman, L. J. (2020). Effect of Pembrolizumab Plus Neoadjuvant

Chemotherapy on Pathologic Complete Response in Women With Early-Stage Breast Cancer: An Analysis of the Ongoing Phase 2 Adaptively Randomized I-SPY2 Trial. JAMA Oncology, 6(5), 676–684. https://doi.org/10.1001/jamaoncol.2019.6650

80. Rugo, H. S., Rumble, R. B., Macrae, E., Barton, D. L., Connolly, H. K., Dickler, M. N., Fallowfield, L., Fowble, B., Ingle, J. N., Jahanzeb, M., Johnston, S. R. D., Korde, L. A., Khatcheressian, J. L., Mehta, R. S., Muss, H. B., & Burstein, H. J. (2016). Endocrine Therapy for Hormone Receptor-Positive Metastatic Breast Cancer: American Society of Clinical Oncology Guideline. Journal of Clinical Oncology: Official Journal of the American Society of Clinical Oncology, 34(25), 3069–3103. https://doi.org/10.1200/JCO.2016.67.1487

81. Wang, H., & Yee, D. (2019). I-SPY 2: A Neoadjuvant Adaptive Clinical Trial Designed to Improve Outcomes in High-Risk Breast Cancer. Current Breast Cancer Reports, 11(4), 303–310. https://doi.org/10.1007/s12609-019-00334-2

82. Park, J. W., Liu, M. C., Yee, D., Yau, C., van 't Veer, L. J., Symmans, W. F., Paoloni, M., Perlmutter, J., Hylton, N. M., Hogarth, M., DeMichele, A., Buxton, M. B., Chien, A. J., Wallace, A. M., Boughey, J. C., Haddad, T. C., Chui, S. Y., Kemmer, K. A., Kaplan, H. G., … I-SPY 2 Investigators. (2016). Adaptive Randomization of Neratinib in Early Breast Cancer. The New England Journal of Medicine, 375(1), 11–22. https://doi.org/10.1056/NEJMoa1513750

83. Potter, D. A., Roesch, E., Yau, C., Lu, R., Wolf, D., Samson, S., Stafford, D., Albain, K. S., Isaacs, C., Trivedi, M., Yee, D., Boughey, J., Thomas, A., Chien, A. J., Hylton, N., Li, W., DeMichele, A., Perlmutter, J., Symmans, W. F., … Esserman, L. J. (2022). Abstract PD8-07: Evaluation of Tucatinib + (Paclitaxel + Pertuzumab + Trastuzumab) followed by AC in high-risk HER2 positive (HER2+) stage II/III breast cancer: Results from the I-SPY 2 TRIAL. Cancer Research, 82(4_Supplement), PD8-07. https://doi.org/10.1158/1538-7445.SABCS21-PD8-07

84. Meric-Bernstam, F., Beeram, M., Hamilton, E., Oh, D.-Y., Hanna, D. L., Kang, Y.-K., Elimova, E., Chaves, J., Goodwin, R., Lee, J., Nabell, L., Rha, S. Y., Mayordomo, J., El-Khoueiry, A., Pant, S., Raghav, K., Kim, J. W., Patnaik, A., Gray, T., … Lee, K.-W. (2022). Zanidatamab, a novel bispecific antibody, for the treatment of locally advanced or metastatic HER2-expressing or HER2-amplified cancers: A phase 1, dose-escalation and expansion study. The Lancet. Oncology, 23(12), 1558–1570. https://doi.org/10.1016/S1470-2045(22)00621-0

85. Borges, V. F., Ferrario, C., Aucoin, N., Falkson, C., Khan, Q., Krop, I., Welch, S., Conlin, A., Chaves, J., Bedard, P. L., Chamberlain, M., Gray, T., Vo,

A., & Hamilton, E. (2018). Tucatinib Combined With Ado-Trastuzumab Emtansine in Advanced ERBB2/HER2-Positive Metastatic Breast Cancer: A Phase 1b Clinical Trial. JAMA Oncology, 4(9), 1214–1220. https://doi.org/10.1001/jamaoncol.2018.1812

86. Pérez-García, J. M., Vaz Batista, M., Cortez, P., Ruiz-Borrego, M., Cejalvo, J. M., de la Haba-Rodriguez, J., Garrigós, L., Racca, F., Servitja, S., Blanch, S., Gion, M., Nave, M., Fernández-Abad, M., Martinez-Bueno, A., Llombart-Cussac, A., Sampayo-Cordero, M., Malfettone, A., Cortés, J., & Braga, S. (2022). Trastuzumab deruxtecan in patients with central nervous system involvement from HER2-positive breast cancer: The DEBBRAH trial. Neuro-Oncology, 25(1), 157–166. https://doi.org/10.1093/neuonc/noac144

87. Lin, N. U., Borges, V., Anders, C., Murthy, R. K., Paplomata, E., Hamilton, E., Hurvitz, S., Loi, S., Okines, A., Abramson, V., Bedard, P. L., Oliveira, M., Mueller, V., Zelnak, A., DiGiovanna, M. P., Bachelot, T., Chien, A. J., O'Regan, R., Wardley, A., … Winer, E. P. (2020). Intracranial Efficacy and Survival With Tucatinib Plus Trastuzumab and Capecitabine for Previously Treated HER2-Positive Breast Cancer With Brain Metastases in the HER2CLIMB Trial. Journal of Clinical Oncology: Official Journal of the American Society of Clinical Oncology, 38(23), 2610–2619. https://doi.org/10.1200/JCO.20.00775

88. Esserman, L. J., Berry, D. A., DeMichele, A., Carey, L., Davis, S. E., Buxton, M., Hudis, C., Gray, J. W., Perou, C., Yau, C., Livasy, C., Krontiras, H., Montgomery, L., Tripathy, D., Lehman, C., Liu, M. C., Olopade, O. I., Rugo, H. S., Carpenter, J. T., … Hylton, N. (2012). Pathologic complete response predicts recurrence-free survival more effectively by cancer subset: Results from the I-SPY 1 TRIAL--CALGB 150007/150012, ACRIN 6657. Journal of Clinical Oncology: Official Journal of the American Society of Clinical Oncology, 30(26), 3242–3249. https://doi.org/10.1200/JCO.2011.39.2779

89. Hylton, N. M., Blume, J. D., Bernreuter, W. K., Pisano, E. D., Rosen, M. A., Morris, E. A., Weatherall, P. T., Lehman, C. D., Newstead, G. M., Polin, S., Marques, H. S., Esserman, L. J., Schnall, M. D., & ACRIN 6657 Trial Team and I-SPY 1 TRIAL Investigators. (2012). Locally advanced breast cancer: MR imaging for prediction of response to neoadjuvant chemotherapy--results from ACRIN 6657/I-SPY TRIAL. Radiology, 263(3), 663–672. https://doi.org/10.1148/radiol.12110748

90. Lin, C., Buxton, M. B., Moore, D., Krontiras, H., Carey, L., DeMichele, A., Montgomery, L., Tripathy, D., Lehman, C., Liu, M., Olapade, O., Yau, C., Berry, D., Esserman, L. J., & I-SPY TRIAL Investigators. (2012). Locally advanced breast cancers are more likely to present as Interval Cancers: Results from the

I-SPY 1 TRIAL (CALGB 150007/150012, ACRIN 6657, InterSPORE Trial). Breast Cancer Research and Treatment, 132(3), 871–879. https://doi.org/10.1007/s10549-011-1670-4

91. Esserman, L. J., Berry, D. A., Cheang, M. C. U., Yau, C., Perou, C. M., Carey, L., DeMichele, A., Gray, J. W., Conway-Dorsey, K., Lenburg, M. E., Buxton, M. B., Davis, S. E., van't Veer, L. J., Hudis, C., Chin, K., Wolf, D., Krontiras, H., Montgomery, L., Tripathy, D., … I-SPY 1 TRIAL Investigators. (2012). Chemotherapy response and recurrence-free survival in neoadjuvant breast cancer depends on biomarker profiles: Results from the I-SPY 1 TRIAL (CALGB 150007/150012; ACRIN 6657). Breast Cancer Research and Treatment, 132(3), 1049–1062. https://doi.org/10.1007/s10549-011-1895-2

92. Krop, I. E., Ramos, J., Zhang, C., & Hamilton, E. P. (2021). HER2CLIMB-04: Phase 2 open label trial of tucatinib plus trastuzumab deruxtecan in patients with HER2+ unresectable locally advanced or metastatic breast cancer with and without brain metastases (trial in progress). Journal of Clinical Oncology, 39(15_suppl), TPS1097–TPS1097. https://doi.org/10.1200/JCO.2021.39.15_suppl.TPS1097

93. O'Sullivan, C. C., Ballman, K. V., McCall, L., Kommalapati, A., Zemla, T., Weiss, A., Mitchell, M., Blinder, V., Tung, N. M., Irvin, W. J., Lee, M., Goetz, M. P., Symmans, W. F., Borges, V. F., Krop, I., Carey, L. A., & Partridge, A. H. (2021). Alliance A011801 (compassHER2 RD): Postneoadjuvant T-DM1 + tucatinib/placebo in patients with residual HER2-positive invasive breast cancer. Future Oncology (London, England), 17(34), 4665–4676. https://doi.org/10.2217/fon-2021-0753

94. Yáñez-Mó, M., Siljander, P. R.-M., Andreu, Z., Zavec, A. B., Borràs, F. E., Buzas, E. I., Buzas, K., Casal, E., Cappello, F., Carvalho, J., Colás, E., Cordeiro-da Silva, A., Fais, S., Falcon-Perez, J. M., Ghobrial, I. M., Giebel, B., Gimona, M., Graner, M., Gursel, I., … De Wever, O. (2015). Biological properties of extracellular vesicles and their physiological functions. Journal of Extracellular Vesicles, 4, 27066. https://doi.org/10.3402/jev.v4.27066

95. Soekmadji, C., Li, B., Huang, Y., Wang, H., An, T., Liu, C., Pan, W., Chen, J., Cheung, L., Falcon-Perez, J. M., Gho, Y. S., Holthofer, H. B., Le, M. T. N., Marcilla, A., O'Driscoll, L., Shekari, F., Shen, T. L., Torrecilhas, A. C., Yan, X., … Zheng, L. (n.d.). The future of Extracellular Vesicles as Theranostics – an ISEV meeting report. Journal of Extracellular Vesicles, 9(1), 1809766. https://doi.org/10.1080/20013078.2020.1809766

96. Rankin-Turner, S., Vader, P., O'Driscoll, L., Giebel, B., Heaney, L. M., & Davies, O. G. (2021). A call for the standardised reporting of factors affecting

the exogenous loading of extracellular vesicles with therapeutic cargos. Advanced Drug Delivery Reviews, 173, 479–491. https://doi.org/10.1016/j.addr.2021.04.012

97. Daly, R., & O'Driscoll, L. (2021). Extracellular vesicles in blood: Are they viable as diagnostic and predictive tools in breast cancer? Drug Discovery Today, 26(3), 778–785. https://doi.org/10.1016/j.drudis.2020.11.001

98. Colombo, M., Raposo, G., & Théry, C. (2014). Biogenesis, secretion, and intercellular interactions of exosomes and other extracellular vesicles. Annual Review of Cell and Developmental Biology, 30, 255–289. https://doi.org/10.1146/annurev-cellbio-101512-122326

99. Doyle, L. M., & Wang, M. Z. (2019). Overview of Extracellular Vesicles, Their Origin, Composition, Purpose, and Methods for Exosome Isolation and Analysis. Cells, 8(7), 727. https://doi.org/10.3390/cells8070727

100. Zaborowski, M. P., Balaj, L., Breakefield, X. O., & Lai, C. P. (2015). Extracellular Vesicles: Composition, Biological Relevance, and Methods of Study. BioScience, 65(8), 783–797. https://doi.org/10.1093/biosci/biv084

101. Liu, Y., & Chen, Q. (2018). 150 years of Darwin's theory of intercellular flow of hereditary information. Nature Reviews. Molecular Cell Biology, 19(12), 749–750. https://doi.org/10.1038/s41580-018-0072-4

102. Margolis, L., & Sadovsky, Y. (2019). The biology of extracellular vesicles: The known unknowns. PLoS Biology, 17(7), e3000363. https://doi.org/10.1371/journal.pbio.3000363

103. van Niel, G., Raposo, G., Candalh, C., Boussac, M., Hershberg, R., Cerf-Bensussan, N., & Heyman, M. (2001). Intestinal epithelial cells secrete exosome-like vesicles. Gastroenterology, 121(2), 337–349. https://doi.org/10.1053/gast.2001.26263

104. Tsiapalis, D., & O'Driscoll, L. (2020). Mesenchymal Stem Cell Derived Extracellular Vesicles for Tissue Engineering and Regenerative Medicine Applications. Cells, 9(4), 991. https://doi.org/10.3390/cells9040991

105. Théry, C., Witwer, K. W., Aikawa, E., Alcaraz, M. J., Anderson, J. D., Andriantsitohaina, R., Antoniou, A., Arab, T., Archer, F., Atkin-Smith, G. K., Ayre, D. C., Bach, J.-M., Bachurski, D., Baharvand, H., Balaj, L., Baldacchino, S., Bauer, N. N., Baxter, A. A., Bebawy, M., … Zuba-Surma, E. K. (2018). Minimal information for studies of extracellular vesicles 2018 (MISEV2018): A position statement of the International Society for Extracellular Vesicles and

update of the MISEV2014 guidelines. Journal of Extracellular Vesicles, 7(1), 1535750. https://doi.org/10.1080/20013078.2018.1535750

106. García-Romero, N., Madurga, R., Rackov, G., Palacín-Aliana, I., Núñez-Torres, R., Asensi-Puig, A., Carrión-Navarro, J., Esteban-Rubio, S., Peinado, H., González-Neira, A., González-Rumayor, V., Belda-Iniesta, C., & Ayuso-Sacido, A. (2019). Polyethylene glycol improves current methods for circulating extracellular vesicle-derived DNA isolation. Journal of Translational Medicine, 17(1), 75. https://doi.org/10.1186/s12967-019-1825-3

107. Catalano, M., & O'Driscoll, L. (2020). Inhibiting extracellular vesicles formation and release: A review of EV inhibitors. Journal of Extracellular Vesicles, 9(1), 1703244. https://doi.org/10.1080/20013078.2019.1703244

108. Gu, F., Crump, C. M., & Thomas, G. (2001). Trans-Golgi network sorting. Cellular and Molecular Life Sciences: CMLS, 58(8), 1067–1084. https://doi.org/10.1007/PL00000922

109. Yue, B., Yang, H., Wang, J., Ru, W., Wu, J., Huang, Y., Lan, X., Lei, C., & Chen, H. (2020). Exosome biogenesis, secretion and function of exosomal miRNAs in skeletal muscle myogenesis. Cell Proliferation, 53(7), e12857. https://doi.org/10.1111/cpr.12857

110. Raposo, G., & Stoorvogel, W. (2013). Extracellular vesicles: Exosomes, microvesicles, and friends. The Journal of Cell Biology, 200(4), 373–383. https://doi.org/10.1083/jcb.201211138

111. Raiborg, C., & Stenmark, H. (2009). The ESCRT machinery in endosomal sorting of ubiquitylated membrane proteins. Nature, 458(7237), 445–452. https://doi.org/10.1038/nature07961

112. Piper, R. C., & Katzmann, D. J. (2007). Biogenesis and function of multivesicular bodies. Annual Review of Cell and Developmental Biology, 23, 519–547. https://doi.org/10.1146/annurev.cellbio.23.090506.123319

113. Wollert, T., & Hurley, J. H. (2010). Molecular mechanism of multivesicular body biogenesis by ESCRT complexes. Nature, 464(7290), 864–869. https://doi.org/10.1038/nature08849

114. Kalluri, R., & LeBleu, V. S. (2020). The biology, function, and biomedical applications of exosomes. Science (New York, N.Y.), 367(6478), eaau6977. https://doi.org/10.1126/science.aau6977

115. Juan, T., & Fürthauer, M. (2018). Biogenesis and function of ESCRT-dependent extracellular vesicles. Seminars in Cell & Developmental Biology, 74, 66–77. https://doi.org/10.1016/j.semcdb.2017.08.022

116. Tschuschke, M., Kocherova, I., Bryja, A., Mozdziak, P., Angelova Volponi, A., Janowicz, K., Sibiak, R., Piotrowska-Kempisty, H., Iżycki, D., Bukowska, D., Antosik, P., Shibli, J. A., Dyszkiewicz-Konwińska, M., & Kempisty, B. (2020). Inclusion Biogenesis, Methods of Isolation and Clinical Application of Human Cellular Exosomes. Journal of Clinical Medicine, 9(2), Article 2. https://doi.org/10.3390/jcm9020436

117. Phuyal, S., Hessvik, N. P., Skotland, T., Sandvig, K., & Llorente, A. (2014). Regulation of exosome release by glycosphingolipids and flotillins. The FEBS Journal, 281(9), 2214–2227. https://doi.org/10.1111/febs.12775

118. Nabhan, J. F., Hu, R., Oh, R. S., Cohen, S. N., & Lu, Q. (2012). Formation and release of arrestin domain-containing protein 1-mediated microvesicles (ARMMs) at plasma membrane by recruitment of TSG101 protein. Proceedings of the National Academy of Sciences of the United States of America, 109(11), 4146–4151. https://doi.org/10.1073/pnas.1200448109

119. Bebelman, M. P., Smit, M. J., Pegtel, D. M., & Baglio, S. R. (2018). Biogenesis and function of extracellular vesicles in cancer. Pharmacology & Therapeutics, 188, 1–11. https://doi.org/10.1016/j.pharmthera.2018.02.013

120. Fackler, O. T., & Grosse, R. (2008). Cell motility through plasma membrane blebbing. The Journal of Cell Biology, 181(6), 879–884. https://doi.org/10.1083/jcb.200802081

121. Li, B., Antonyak, M. A., Zhang, J., & Cerione, R. A. (2012). RhoA triggers a specific signaling pathway that generates transforming microvesicles in cancer cells. Oncogene, 31(45), 4740–4749. https://doi.org/10.1038/onc.2011.636

122. Muralidharan-Chari, V., Clancy, J., Plou, C., Romao, M., Chavrier, P., Raposo, G., & D'Souza-Schorey, C. (2009). ARF6-regulated shedding of tumor cell-derived plasma membrane microvesicles. Current Biology: CB, 19(22), 1875–1885. https://doi.org/10.1016/j.cub.2009.09.059

123. Schlienger, S., Campbell, S., & Claing, A. (2014). ARF1 regulates the Rho/MLC pathway to control EGF-dependent breast cancer cell invasion. Molecular Biology of the Cell, 25(1), 17–29. https://doi.org/10.1091/mbc.E13-06-0335

124. Sedgwick, A. E., Clancy, J. W., Olivia Balmert, M., & D'Souza-Schorey, C. (2015). Extracellular microvesicles and invadopodia mediate non-overlapping modes of tumor cell invasion. Scientific Reports, 5, 14748. https://doi.org/10.1038/srep14748

125. Mathivanan, S., Ji, H., & Simpson, R. J. (2010). Exosomes: Extracellular organelles important in intercellular communication. Journal of Proteomics, 73(10), 1907–1920. https://doi.org/10.1016/j.jprot.2010.06.006

126. Kalra, H., Drummen, G. P. C., & Mathivanan, S. (2016). Focus on Extracellular Vesicles: Introducing the Next Small Big Thing. International Journal of Molecular Sciences, 17(2), 170. https://doi.org/10.3390/ijms17020170

127. Santavanond, J. P., Rutter, S. F., Atkin-Smith, G. K., & Poon, I. K. H. (2021). Apoptotic Bodies: Mechanism of Formation, Isolation and Functional Relevance. In S. Mathivanan, P. Fonseka, C. Nedeva, & I. Atukorala (Eds.), New Frontiers: Extracellular Vesicles (pp. 61–88). Springer International Publishing. https://doi.org/10.1007/978-3-030-67171-6_4

128. Poon, I. K. H., Lucas, C. D., Rossi, A. G., & Ravichandran, K. S. (2014). Apoptotic cell clearance: Basic biology and therapeutic potential. Nature Reviews. Immunology, 14(3), 166–180. https://doi.org/10.1038/nri3607

129. Jiang, L., Paone, S., Caruso, S., Atkin-Smith, G. K., Phan, T. K., Hulett, M. D., & Poon, I. K. H. (2017). Determining the contents and cell origins of apoptotic bodies by flow cytometry. Scientific Reports, 7(1), 14444. https://doi.org/10.1038/s41598-017-14305-z

130. Caruso, S., & Poon, I. K. H. (2018). Apoptotic Cell-Derived Extracellular Vesicles: More Than Just Debris. Frontiers in Immunology, 9, 1486. https://doi.org/10.3389/fimmu.2018.01486

131. Atkin-Smith, G. K., Tixeira, R., Paone, S., Mathivanan, S., Collins, C., Liem, M., Goodall, K. J., Ravichandran, K. S., Hulett, M. D., & Poon, I. K. H. (2015). A novel mechanism of generating extracellular vesicles during apoptosis via a beads-on-a-string membrane structure. Nature Communications, 6, 7439. https://doi.org/10.1038/ncomms8439

132. Liu, D., Kou, X., Chen, C., Liu, S., Liu, Y., Yu, W., Yu, T., Yang, R., Wang, R., Zhou, Y., & Shi, S. (2018). Circulating apoptotic bodies maintain mesenchymal stem cell homeostasis and ameliorate osteopenia via transferring multiple cellular factors. Cell Research, 28(9), 918–933. https://doi.org/10.1038/s41422-018-0070-2

133. Gavrilescu, L. C., & Denkers, E. Y. (2003). Apoptosis and the balance of homeostatic and pathologic responses to protozoan infection. Infection and Immunity, 71(11), 6109–6115. https://doi.org/10.1128/IAI.71.11.6109-6115.2003

134. Shi, J., & Wei, L. (2007). Rho kinase in the regulation of cell death and survival. Archivum Immunologiae Et Therapiae Experimentalis, 55(2), 61–75. https://doi.org/10.1007/s00005-007-0009-7

135. Orlando, K. A., Stone, N. L., & Pittman, R. N. (2006). Rho kinase regulates fragmentation and phagocytosis of apoptotic cells. Experimental Cell Research, 312(1), 5–15. https://doi.org/10.1016/j.yexcr.2005.09.012

136. Zijlstra, A., & Di Vizio, D. (2018). Size matters in nanoscale communication. Nature Cell Biology, 20(3), 228–230. https://doi.org/10.1038/s41556-018-0049-8

137. Ma, L., Li, Y., Peng, J., Wu, D., Zhao, X., Cui, Y., Chen, L., Yan, X., Du, Y., & Yu, L. (2015). Discovery of the migrasome, an organelle mediating release of cytoplasmic contents during cell migration. Cell Research, 25(1), 24–38. https://doi.org/10.1038/cr.2014.135

138. da Rocha-Azevedo, B., & Schmid, S. L. (2015). Migrasomes: A new organelle of migrating cells. Cell Research, 25(1), 1–2. https://doi.org/10.1038/cr.2014.146

139. Tavano, S., & Heisenberg, C.-P. (2019). Migrasomes take center stage. Nature Cell Biology, 21(8), 918–920. https://doi.org/10.1038/s41556-019-0369-3

140. Di Vizio, D., Morello, M., Dudley, A. C., Schow, P. W., Adam, R. M., Morley, S., Mulholland, D., Rotinen, M., Hager, M. H., Insabato, L., Moses, M. A., Demichelis, F., Lisanti, M. P., Wu, H., Klagsbrun, M., Bhowmick, N. A., Rubin, M. A., D'Souza-Schorey, C., & Freeman, M. R. (2012). Large oncosomes in human prostate cancer tissues and in the circulation of mice with metastatic disease. The American Journal of Pathology, 181(5), 1573–1584. https://doi.org/10.1016/j.ajpath.2012.07.030

141. Al-Nedawi, K., Meehan, B., Micallef, J., Lhotak, V., May, L., Guha, A., & Rak, J. (2008). Intercellular transfer of the oncogenic receptor EGFRvIII by microvesicles derived from tumour cells. Nature Cell Biology, 10(5), 619–624. https://doi.org/10.1038/ncb1725

142. Ciardiello, C., Migliorino, R., Leone, A., & Budillon, A. (2020). Large extracellular vesicles: Size matters in tumor progression. Cytokine & Growth Factor Reviews, 51, 69–74. https://doi.org/10.1016/j.cytogfr.2019.12.007

143. O'Brien, K., Rani, S., Corcoran, C., Wallace, R., Hughes, L., Friel, A. M., McDonnell, S., Crown, J., Radomski, M. W., & O'Driscoll, L. (2013). Exosomes from triple-negative breast cancer cells can transfer phenotypic traits

representing their cells of origin to secondary cells. European Journal of Cancer, 49(8), 1845–1859. https://doi.org/10.1016/j.ejca.2013.01.017

144. Harris, D. A., Patel, S. H., Gucek, M., Hendrix, A., Westbroek, W., & Taraska, J. W. (2015). Exosomes Released from Breast Cancer Carcinomas Stimulate Cell Movement. PLoS ONE, 10(3), e0117495. https://doi.org/10.1371/journal.pone.0117495

145. Singh, R., Pochampally, R., Watabe, K., Lu, Z., & Mo, Y.-Y. (2014). Exosome-mediated transfer of miR-10b promotes cell invasion in breast cancer. Molecular Cancer, 13, 256. https://doi.org/10.1186/1476-4598-13-256

146. Martinez, V. G., O'Neill, S., Salimu, J., Breslin, S., Clayton, A., Crown, J., & O'Driscoll, L. (2017). Resistance to HER2-targeted anti-cancer drugs is associated with immune evasion in cancer cells and their derived extracellular vesicles. Oncoimmunology, 6(12), e1362530. https://doi.org/10.1080/2162402X.2017.1362530

147. Ciravolo, V., Huber, V., Ghedini, G. C., Venturelli, E., Bianchi, F., Campiglio, M., Morelli, D., Villa, A., Della Mina, P., Menard, S., Filipazzi, P., Rivoltini, L., Tagliabue, E., & Pupa, S. M. (2012). Potential role of HER2-overexpressing exosomes in countering trastuzumab-based therapy. Journal of Cellular Physiology, 227(2), 658–667. https://doi.org/10.1002/jcp.22773

148. Wolfers, J., Lozier, A., Raposo, G., Regnault, A., Théry, C., Masurier, C., Flament, C., Pouzieux, S., Faure, F., Tursz, T., Angevin, E., Amigorena, S., & Zitvogel, L. (2001). Tumor-derived exosomes are a source of shared tumor rejection antigens for CTL cross-priming. Nature Medicine, 7(3), 297–303. https://doi.org/10.1038/85438

149. Marton, A., Vizler, C., Kusz, E., Temesfoi, V., Szathmary, Z., Nagy, K., Szegletes, Z., Varo, G., Siklos, L., Katona, R. L., Tubak, V., Howard, O. M. Z., Duda, E., Minarovits, J., Nagy, K., & Buzas, K. (2012). Melanoma cell-derived exosomes alter macrophage and dendritic cell functions in vitro. Immunology Letters, 148(1), 34–38. https://doi.org/10.1016/j.imlet.2012.07.006

150. Ye, S.-B., Li, Z.-L., Luo, D.-H., Huang, B.-J., Chen, Y.-S., Zhang, X.-S., Cui, J., Zeng, Y.-X., & Li, J. (2014). Tumor-derived exosomes promote tumor progression and T-cell dysfunction through the regulation of enriched exosomal microRNAs in human nasopharyngeal carcinoma. Oncotarget, 5(14), 5439–5452. https://doi.org/10.18632/oncotarget.2118

151. Corcoran, C., Rani, S., O'Brien, K., O'Neill, A., Prencipe, M., Sheikh, R., Webb, G., McDermott, R., Watson, W., Crown, J., & O'Driscoll, L. (2012). Docetaxel-resistance in prostate cancer: Evaluating associated phenotypic

changes and potential for resistance transfer via exosomes. PloS One, 7(12), e50999. https://doi.org/10.1371/journal.pone.0050999

152. Namee, N. M., & O'Driscoll, L. (2018). Extracellular vesicles and anti-cancer drug resistance. Biochimica et Biophysica Acta (BBA) - Reviews on Cancer, 1870(2), 123–136. https://doi.org/10.1016/j.bbcan.2018.07.003

153. Yi, X., Huang, D., Li, Z., Wang, X., Yang, T., Zhao, M., Wu, J., & Zhong, T. (2022). The role and application of small extracellular vesicles in breast cancer. Frontiers in Oncology, 12, 980404. https://doi.org/10.3389/fonc.2022.980404

154. De Mattos-Arruda, L., Bottai, G., Nuciforo, P. G., Di Tommaso, L., Giovannetti, E., Peg, V., Losurdo, A., Pérez-Garcia, J., Masci, G., Corsi, F., Cortés, J., Seoane, J., Calin, G. A., & Santarpia, L. (2015). MicroRNA-21 links epithelial-to-mesenchymal transition and inflammatory signals to confer resistance to neoadjuvant trastuzumab and chemotherapy in HER2-positive breast cancer patients. Oncotarget, 6(35), 37269–37280.

155. Gong, C., Yao, Y., Wang, Y., Liu, B., Wu, W., Chen, J., Su, F., Yao, H., & Song, E. (2011). Up-regulation of miR-21 Mediates Resistance to Trastuzumab Therapy for Breast Cancer. The Journal of Biological Chemistry, 286(21), 19127–19137. https://doi.org/10.1074/jbc.M110.216887

156. Battke, C., Ruiss, R., Welsch, U., Wimberger, P., Lang, S., Jochum, S., & Zeidler, R. (2011). Tumour exosomes inhibit binding of tumour-reactive antibodies to tumour cells and reduce ADCC. Cancer Immunology, Immunotherapy, 60(5), 639–648. https://doi.org/10.1007/s00262-011-0979-5

157. Bandari, S. K., Purushothaman, A., Ramani, V. C., Brinkley, G. J., Chandrashekar, D. S., Varambally, S., Mobley, J. A., Zhang, Y., Brown, E. E., Vlodavsky, I., & Sanderson, R. D. (2018). Chemotherapy induces secretion of exosomes loaded with heparanase that degrades extracellular matrix and impacts tumor and host cell behavior. Matrix Biology: Journal of the International Society for Matrix Biology, 65, 104–118. https://doi.org/10.1016/j.matbio.2017.09.001

158. Zheng, Z., Chen, M., Xing, P., Yan, X., & Xie, B. (2019). Increased Expression of Exosomal AGAP2-AS1 (AGAP2 Antisense RNA 1) In Breast Cancer Cells Inhibits Trastuzumab-Induced Cell Cytotoxicity. Medical Science Monitor: International Medical Journal of Experimental and Clinical Research, 25, 2211–2220. https://doi.org/10.12659/MSM.915419

159. Bhutta, B. S., Alghoula, F., & Berim, I. (2022). Hypoxia. In StatPearls [Internet]. StatPearls Publishing. https://www.ncbi.nlm.nih.gov/books/NBK482316/

160. Shi, R., Liao, C., & Zhang, Q. (2021). Hypoxia-Driven Effects in Cancer: Characterization, Mechanisms, and Therapeutic Implications. Cells, 10(3), 678. https://doi.org/10.3390/cells10030678

161. Wang, G. L., & Semenza, G. L. (1995). Purification and characterization of hypoxia-inducible factor 1. The Journal of Biological Chemistry, 270(3), 1230–1237. https://doi.org/10.1074/jbc.270.3.1230

162. Wang, G. L., Jiang, B. H., Rue, E. A., & Semenza, G. L. (1995). Hypoxia-inducible factor 1 is a basic-helix-loop-helix-PAS heterodimer regulated by cellular O2 tension. Proceedings of the National Academy of Sciences of the United States of America, 92(12), 5510–5514. https://doi.org/10.1073/pnas.92.12.5510

163. Jing, X., Yang, F., Shao, C., Wei, K., Xie, M., Shen, H., & Shu, Y. (2019). Role of hypoxia in cancer therapy by regulating the tumor microenvironment. Molecular Cancer, 18, 157. https://doi.org/10.1186/s12943-019-1089-9

164. Huang, Y., Lin, D., & Taniguchi, C. M. (2017). Hypoxia inducible factor (HIF) in the tumor microenvironment: Friend or foe? Science China. Life Sciences, 60(10), 1114–1124. https://doi.org/10.1007/s11427-017-9178-y

165. McKeown, S. R. (2014). Defining normoxia, physoxia and hypoxia in tumours—Implications for treatment response. The British Journal of Radiology, 87(1035), 20130676. https://doi.org/10.1259/bjr.20130676

166. Semenza, G. L. (2003). Targeting HIF-1 for cancer therapy. Nature Reviews. Cancer, 3(10), 721–732. https://doi.org/10.1038/nrc1187

167. Wiesener, M. S., Jürgensen, J. S., Rosenberger, C., Scholze, C. K., Hörstrup, J. H., Warnecke, C., Mandriota, S., Bechmann, I., Frei, U. A., Pugh, C. W., Ratcliffe, P. J., Bachmann, S., Maxwell, P. H., & Eckardt, K.-U. (2003). Widespread hypoxia-inducible expression of HIF-2alpha in distinct cell populations of different organs. FASEB Journal: Official Publication of the Federation of American Societies for Experimental Biology, 17(2), 271–273. https://doi.org/10.1096/fj.02-0445fje

168. Semenza, G. L. (2010). Defining the Role of Hypoxia-Inducible Factor 1 in Cancer Biology and Therapeutics. Oncogene, 29(5), 625–634. https://doi.org/10.1038/onc.2009.441

169. Majmundar, A. J., Wong, W. J., & Simon, M. C. (2010). Hypoxia-Inducible Factors and the Response to Hypoxic Stress. Molecular Cell, 40(2), 294–309. https://doi.org/10.1016/j.molcel.2010.09.022

170. Semenza, G. L. (2014). Oxygen sensing, hypoxia-inducible factors, and disease pathophysiology. Annual Review of Pathology, 9, 47–71. https://doi.org/10.1146/annurev-pathol-012513-104720

171. McIntyre, A., & Harris, A. L. (2015). Metabolic and hypoxic adaptation to anti-angiogenic therapy: A target for induced essentiality. EMBO Molecular Medicine, 7(4), 368–379. https://doi.org/10.15252/emmm.201404271

172. Li, D., Qu, Y., Mao, M., Zhang, X., Li, J., Ferriero, D., & Mu, D. (2009). Involvement of the PTEN-AKT-FOXO3a pathway in neuronal apoptosis in developing rat brain after hypoxia-ischemia. Journal of Cerebral Blood Flow and Metabolism: Official Journal of the International Society of Cerebral Blood Flow and Metabolism, 29(12), 1903–1913. https://doi.org/10.1038/jcbfm.2009.102

173. McAleese, C. E., Choudhury, C., Butcher, N. J., & Minchin, R. F. (2021). Hypoxia-mediated drug resistance in breast cancers. Cancer Letters, 502, 189–199. https://doi.org/10.1016/j.canlet.2020.11.045

174. Bane, A. L., Whelan, T. J., Pond, G. R., Parpia, S., Gohla, G., Fyles, A. W., Pignol, J.-P., Pritchard, K. I., Chambers, S., & Levine, M. N. (2014). Tumor factors predictive of response to hypofractionated radiotherapy in a randomized trial following breast conserving therapy. Annals of Oncology, 25(5), 992–998. https://doi.org/10.1093/annonc/mdu090

175. Laughner, E., Taghavi, P., Chiles, K., Mahon, P. C., & Semenza, G. L. (2001). HER2 (neu) Signaling Increases the Rate of Hypoxia-Inducible Factor 1α (HIF-1α) Synthesis: Novel Mechanism for HIF-1-Mediated Vascular Endothelial Growth Factor Expression. Molecular and Cellular Biology, 21(12), 3995–4004. https://doi.org/10.1128/MCB.21.12.3995-4004.2001

176. Gschwantler-Kaulich, D., Tan, Y. Y., Fuchs, E.-M., Hudelist, G., Köstler, W. J., Reiner, A., Leser, C., Salama, M., Attems, J., Deutschmann, C., Zielinski, C. C., & Singer, C. F. (2017). PTEN expression as a predictor for the response to trastuzumab-based therapy in Her-2 overexpressing metastatic breast cancer. PLOS ONE, 12(3), e0172911. https://doi.org/10.1371/journal.pone.0172911

177. Campbell, E. J., Dachs, G. U., Morrin, H. R., Davey, V. C., Robinson, B. A., & Vissers, M. C. M. (2019). Activation of the hypoxia pathway in breast cancer tissue and patient survival are inversely associated with tumor ascorbate levels. BMC Cancer, 19(1), 307. https://doi.org/10.1186/s12885-019-5503-x

178. Aghazadeh, S., & Yazdanparast, R. (2017). Activation of STAT3/HIF-1α/Hes-1 axis promotes trastuzumab resistance in HER2-overexpressing breast cancer cells via down-regulation of PTEN. Biochimica et Biophysica Acta (BBA) - General Subjects, 1861(8), 1970–1980. https://doi.org/10.1016/j.bbagen.2017.05.009

179. Venturella, M., Criscuoli, M., Carraro, F., Naldini, A., & Zocco, D. (2021). Interplay between Hypoxia and Extracellular Vesicles in Cancer and Inflammation. Biology, 10(7), 606. https://doi.org/10.3390/biology10070606

180. Wang, T., Gilkes, D. M., Takano, N., Xiang, L., Luo, W., Bishop, C. J., Chaturvedi, P., Green, J. J., & Semenza, G. L. (2014). Hypoxia-inducible factors and RAB22A mediate formation of microvesicles that stimulate breast cancer invasion and metastasis. Proceedings of the National Academy of Sciences of the United States of America, 111(31), E3234-3242. https://doi.org/10.1073/pnas.1410041111

181. Park, J. E., Dutta, B., Tse, S. W., Gupta, N., Tan, C. F., Low, J. K., Yeoh, K. W., Kon, O. L., Tam, J. P., & Sze, S. K. (2019). Hypoxia-induced tumor exosomes promote M2-like macrophage polarization of infiltrating myeloid cells and microRNA-mediated metabolic shift. Oncogene, 38(26), 5158–5173. https://doi.org/10.1038/s41388-019-0782-x

182. Ramteke, A., Ting, H., Agarwal, C., Mateen, S., Somasagara, R., Hussain, A., Graner, M., Frederick, B., Agarwal, R., & Deep, G. (2015). Exosomes Secreted under Hypoxia Enhance Invasiveness and Stemness of Prostate Cancer Cells by Targeting Adherens Junction Molecules. Molecular Carcinogenesis, 54(7), 554–565. https://doi.org/10.1002/mc.22124

183. Dorayappan, K. D. P., Wanner, R., Wallbillich, J. J., Saini, U., Zingarelli, R., Suarez, A. A., Cohn, D. E., & Selvendiran, K. (2018). Hypoxia-induced exosomes contribute to a more aggressive and chemoresistant ovarian cancer phenotype: A novel mechanism linking STAT3/Rab proteins. Oncogene, 37(28), 3806–3821. https://doi.org/10.1038/s41388-018-0189-0

184. Panigrahi, G. K., Praharaj, P. P., Peak, T. C., Long, J., Singh, R., Rhim, J. S., Abd Elmageed, Z. Y., & Deep, G. (2018). Hypoxia-induced exosome secretion promotes survival of African-American and Caucasian prostate cancer cells. Scientific Reports, 8(1), 3853. https://doi.org/10.1038/s41598-018-22068-4

185. Wang, Z., Jin, N., Ganguli, S., Swartz, D. R., Li, L., & Rhoades, R. A. (2001). Rho-kinase activation is involved in hypoxia-induced pulmonary

vasoconstriction. American Journal of Respiratory Cell and Molecular Biology, 25(5), 628–635. https://doi.org/10.1165/ajrcmb.25.5.4461

186. Zheng, J., Tan, J., Miao, Y.-Y., & Zhang, Q. (2019). Extracellular vesicles degradation pathway based autophagy lysosome pathway. American Journal of Translational Research, 11(3), 1170–1183.

187. King, H. W., Michael, M. Z., & Gleadle, J. M. (2012). Hypoxic enhancement of exosome release by breast cancer cells. BMC Cancer, 12, 421. https://doi.org/10.1186/1471-2407-12-421

188. Jung, K. O., Youn, H., Lee, C.-H., Kang, K. W., & Chung, J.-K. (2017). Visualization of exosome-mediated miR-210 transfer from hypoxic tumor cells. Oncotarget, 8(6), 9899–9910. https://doi.org/10.18632/oncotarget.14247

189. Chen, X., Zhou, J., Li, X., Wang, X., Lin, Y., & Wang, X. (2018). Exosomes derived from hypoxic epithelial ovarian cancer cells deliver microRNAs to macrophages and elicit a tumor-promoted phenotype. Cancer Letters, 435, 80–91. https://doi.org/10.1016/j.canlet.2018.08.001

190. Jiang, H., Zhao, H., Zhang, M., He, Y., Li, X., Xu, Y., & Liu, X. (2022). Hypoxia Induced Changes of Exosome Cargo and Subsequent Biological Effects. Frontiers in Immunology, 13. https://www.frontiersin.org/articles/10.3389/fimmu.2022.824188

191. Qian, D., Xie, Y., Huang, M., & Gu, J. (2022). Tumor-derived exosomes in hypoxic microenvironment: Release mechanism, biological function and clinical application. Journal of Cancer, 13(5), 1685–1694. https://doi.org/10.7150/jca.69278

192. Katt, M. E., Placone, A. L., Wong, A. D., Xu, Z. S., & Searson, P. C. (2016). In Vitro Tumor Models: Advantages, Disadvantages, Variables, and Selecting the Right Platform. Frontiers in Bioengineering and Biotechnology, 4, 12. https://doi.org/10.3389/fbioe.2016.00012

193. Hait, W. N. (2010). Anticancer drug development: The grand challenges. Nature Reviews. Drug Discovery, 9(4), 253–254. https://doi.org/10.1038/nrd3144

194. Hopkins, A. L. (2008). Network pharmacology: The next paradigm in drug discovery. Nature Chemical Biology, 4(11), 682–690. https://doi.org/10.1038/nchembio.118

195. Kola, I. (2008). The state of innovation in drug development. Clinical Pharmacology and Therapeutics, 83(2), 227–230. https://doi.org/10.1038/sj.clpt.6100479

196. Rodrigues, J., Heinrich, M. A., Teixeira, L. M., & Prakash, J. (2021). 3D In Vitro Model (R)evolution: Unveiling Tumor-Stroma Interactions. Trends in Cancer, 7(3), 249–264. https://doi.org/10.1016/j.trecan.2020.10.009

197. Edmondson, R., Broglie, J. J., Adcock, A. F., & Yang, L. (2014). Three-dimensional cell culture systems and their applications in drug discovery and cell-based biosensors. Assay and Drug Development Technologies, 12(4), 207–218. https://doi.org/10.1089/adt.2014.573

198. Breslin, S., & O'Driscoll, L. (2013). Three-dimensional cell culture: The missing link in drug discovery. Drug Discovery Today, 18(5–6), 240–249. https://doi.org/10.1016/j.drudis.2012.10.003

199. Habanjar, O., Diab-Assaf, M., Caldefie-Chezet, F., & Delort, L. (2021). 3D Cell Culture Systems: Tumor Application, Advantages, and Disadvantages. International Journal of Molecular Sciences, 22(22), 12200. https://doi.org/10.3390/ijms222212200

200. Datta, P., Dey, M., Ataie, Z., Unutmaz, D., & Ozbolat, I. T. (2020). 3D bioprinting for reconstituting the cancer microenvironment. NPJ Precision Oncology, 4, 18. https://doi.org/10.1038/s41698-020-0121-2

201. Pampaloni, F., Reynaud, E. G., & Stelzer, E. H. K. (2007). The third dimension bridges the gap between cell culture and live tissue. Nature Reviews. Molecular Cell Biology, 8(10), 839–845. https://doi.org/10.1038/nrm2236

202. Langhans, S. A. (2018). Three-Dimensional in Vitro Cell Culture Models in Drug Discovery and Drug Repositioning. Frontiers in Pharmacology, 9, 6. https://doi.org/10.3389/fphar.2018.00006

203. Pebworth, M.-P., Cismas, S., & Asuri, P. (2014). A Novel 2.5D Culture Platform to Investigate the Role of Stiffness Gradients on Adhesion-Independent Cell Migration. PloS One, 9, e110453. https://doi.org/10.1371/journal.pone.0110453

204. Ravi, M., Paramesh, V., Kaviya, S. R., Anuradha, E., & Solomon, F. D. P. (2015). 3D cell culture systems: Advantages and applications. Journal of Cellular Physiology, 230(1), 16–26. https://doi.org/10.1002/jcp.24683

205. Stock, K., Estrada, M. F., Vidic, S., Gjerde, K., Rudisch, A., Santo, V. E., Barbier, M., Blom, S., Arundkar, S. C., Selvam, I., Osswald, A., Stein, Y., Gruenewald, S., Brito, C., van Weerden, W., Rotter, V., Boghaert, E., Oren, M., Sommergruber, W., … Graeser, R. (2016). Capturing tumor complexity in vitro:

Comparative analysis of 2D and 3D tumor models for drug discovery. Scientific Reports, 6, 28951. https://doi.org/10.1038/srep28951

206. Fernández-Lázaro, D., García Hernández, J. L., Caballero García, A., Caballero del Castillo, A., Villaverde Hueso, M., & Cruz-Hernández, J. J. (2020). Clinical Perspective and Translational Oncology of Liquid Biopsy. Diagnostics, 10(7), Article 7. https://doi.org/10.3390/diagnostics10070443

207. Lozano-Ramos, I., Bancu, I., Oliveira-Tercero, A., Armengol, M. P., Menezes-Neto, A., Del Portillo, H. A., Lauzurica-Valdemoros, R., & Borràs, F. E. (2015). Size-exclusion chromatography-based enrichment of extracellular vesicles from urine samples. Journal of Extracellular Vesicles, 4, 27369. https://doi.org/10.3402/jev.v4.27369

208. Van Deun, J., Mestdagh, P., Agostinis, P., Akay, Ö., Anand, S., Anckaert, J., Martinez, Z. A., Baetens, T., Beghein, E., Bertier, L., Berx, G., Boere, J., Boukouris, S., Bremer, M., Buschmann, D., Byrd, J. B., Casert, C., Cheng, L., Cmoch, A., … Hendrix, A. (2017). EV-TRACK: Transparent reporting and centralizing knowledge in extracellular vesicle research. Nature Methods, 14(3), Article 3. https://doi.org/10.1038/nmeth.4185

209. Théry, C., Amigorena, S., Raposo, G., & Clayton, A. (2006). Isolation and characterization of exosomes from cell culture supernatants and biological fluids. Current Protocols in Cell Biology, Chapter 3, Unit 3.22. https://doi.org/10.1002/0471143030.cb0322s30

210. Royo, F., Théry, C., Falcón-Pérez, J. M., Nieuwland, R., & Witwer, K. W. (2020). Methods for Separation and Characterization of Extracellular Vesicles: Results of a Worldwide Survey Performed by the ISEV Rigor and Standardization Subcommittee. Cells, 9(9), Article 9. https://doi.org/10.3390/cells9091955

211. Gardiner, C., Vizio, D. D., Sahoo, S., Théry, C., Witwer, K. W., Wauben, M., & Hill, A. F. (2016). Techniques used for the isolation and characterization of extracellular vesicles: Results of a worldwide survey. Journal of Extracellular Vesicles, 5(1), 32945. https://doi.org/10.3402/jev.v5.32945

212. Ludwig, A.-K., De Miroschedji, K., Doeppner, T. R., Börger, V., Ruesing, J., Rebmann, V., Durst, S., Jansen, S., Bremer, M., Behrmann, E., Singer, B. B., Jastrow, H., Kuhlmann, J. D., El Magraoui, F., Meyer, H. E., Hermann, D. M., Opalka, B., Raunser, S., Epple, M., … Giebel, B. (2018). Precipitation with polyethylene glycol followed by washing and pelleting by ultracentrifugation enriches extracellular vesicles from tissue culture supernatants in small and

large scales. Journal of Extracellular Vesicles, 7(1), 1528109. https://doi.org/10.1080/20013078.2018.1528109

213. Van Deun, J., Mestdagh, P., Sormunen, R., Cocquyt, V., Vermaelen, K., Vandesompele, J., Bracke, M., De Wever, O., & Hendrix, A. (2014). The impact of disparate isolation methods for extracellular vesicles on downstream RNA profiling. Journal of Extracellular Vesicles, 3. https://doi.org/10.3402/jev.v3.24858

214. Duong, P., Chung, A., Bouchareychas, L., & Raffai, R. L. (2020). Correction: Cushioned-Density Gradient Ultracentrifugation (C-DGUC) improves the isolation efficiency of extracellular vesicles. PloS One, 15(7), e0236914. https://doi.org/10.1371/journal.pone.0236914

215. Karimi, N., Cvjetkovic, A., Jang, S. C., Crescitelli, R., Hosseinpour Feizi, M. A., Nieuwland, R., Lötvall, J., & Lässer, C. (2018). Detailed analysis of the plasma extracellular vesicle proteome after separation from lipoproteins. Cellular and Molecular Life Sciences: CMLS, 75(15), 2873–2886. https://doi.org/10.1007/s00018-018-2773-4

216. Schindelin, J., Arganda-Carreras, I., Frise, E., Kaynig, V., Longair, M., Pietzsch, T., Preibisch, S., Rueden, C., Saalfeld, S., Schmid, B., Tinevez, J.-Y., White, D. J., Hartenstein, V., Eliceiri, K., Tomancak, P., & Cardona, A. (2012). Fiji: An open-source platform for biological-image analysis. Nature Methods, 9(7), 676–682. https://doi.org/10.1038/nmeth.2019

217. Useckaite, Z., Mukhopadhya, A., Moran, B., & O'Driscoll, L. (2020). Extracellular vesicles report on the MET status of their cells of origin regardless of the method used for their isolation. Scientific Reports, 10(1), 19020. https://doi.org/10.1038/s41598-020-75817-9

218. Mukhopadhya, A., Santoro, J., Moran, B., Useckaite, Z., & O'Driscoll, L. (2021). Optimisation and comparison of orthogonal methods for separation and characterisation of extracellular vesicles to investigate how representative infant milk formula is of milk. Food Chemistry, 353, 129309. https://doi.org/10.1016/j.foodchem.2021.129309

219. Visnovitz, T., Osteikoetxea, X., Sódar, B. W., Mihály, J., Lőrincz, P., Vukman, K. V., Tóth, E. Á., Koncz, A., Székács, I., Horváth, R., Varga, Z., & Buzás, E. I. (2019). An improved 96 well plate format lipid quantification assay for standardisation of experiments with extracellular vesicles. Journal of Extracellular Vesicles, 8(1), 1565263. https://doi.org/10.1080/20013078.2019.1565263

220. Webber, J., & Clayton, A. (2013). How pure are your vesicles? Journal of Extracellular Vesicles, 2. https://doi.org/10.3402/jev.v2i0.19861

221. Eichholz, K. F., Woods, I., Riffault, M., Johnson, G. P., Corrigan, M., Lowry, M. C., Shen, N., Labour, M.-N., Wynne, K., O'Driscoll, L., & Hoey, D. A. (2020). Human bone marrow stem/stromal cell osteogenesis is regulated via mechanically activated osteocyte-derived extracellular vesicles. Stem Cells Translational Medicine, 9(11), 1431–1447. https://doi.org/10.1002/sctm.19-0405

222. Lowry, M. C., & O'Driscoll, L. (2018). Can hi-jacking hypoxia inhibit extracellular vesicles in cancer? Drug Discovery Today, 23(6), 1267–1273. https://doi.org/10.1016/j.drudis.2018.03.006

223. Mentkowski, K. I., Snitzer, J. D., Rusnak, S., & Lang, J. K. (2018). Therapeutic Potential of Engineered Extracellular Vesicles. The AAPS Journal, 20(3), 50. https://doi.org/10.1208/s12248-018-0211-z

224. Elsharkasy, O. M., Nordin, J. Z., Hagey, D. W., de Jong, O. G., Schiffelers, R. M., Andaloussi, S. E., & Vader, P. (2020). Extracellular vesicles as drug delivery systems: Why and how? Advanced Drug Delivery Reviews, 159, 332–343. https://doi.org/10.1016/j.addr.2020.04.004

225. Zhang, P.-F., Zeng, G.-Q., Hu, R., Li, C., Yi, H., Li, M.-Y., Li, X.-H., Qu, J.-Q., Wan, X.-X., He, Q.-Y., Li, J.-H., Chen, Y., Ye, X., Li, J.-Y., Wang, Y.-Y., Feng, X.-P., & Xiao, Z.-Q. (2012). Identification of flotillin-1 as a novel biomarker for lymph node metastasis and prognosis of lung adenocarcinoma by quantitative plasma membrane proteome analysis. Journal of Proteomics, 77, 202–214. https://doi.org/10.1016/j.jprot.2012.08.021

226. Furrer, D., Paquet, C., Jacob, S., & Diorio, C. (2018). The Human Epidermal Growth Factor Receptor 2 (HER2) as a Prognostic and Predictive Biomarker: Molecular Insights into HER2 Activation and Diagnostic Implications. In G.-J. Lemamy (Ed.), Cancer Prognosis. IntechOpen. https://doi.org/10.5772/intechopen.78271

227. Coussens, L., Yang-Feng, T. L., Liao, Y.-C., Chen, E., Gray, A., McGrath, J., Seeburg, P. H., Libermann, T. A., Schlessinger, J., Francke, U., Levinson, A., & Ullrich, A. (1985). Tyrosine Kinase Receptor with Extensive Homology to EGF Receptor Shares Chromosomal Location with neu Oncogene. Science, 230(4730), 1132–1139. https://doi.org/10.1126/science.2999974

228. Slamon, D. J., Leyland-Jones, B., Shak, S., Fuchs, H., Paton, V., Bajamonde, A., Fleming, T., Eiermann, W., Wolter, J., Pegram, M., Baselga, J., & Norton, L. (2001). Use of Chemotherapy plus a Monoclonal Antibody against

HER2 for Metastatic Breast Cancer That Overexpresses HER2. New England Journal of Medicine, 344(11), 783–792. https://doi.org/10.1056/NEJM200103153441101

229. Venetis, K., Crimini, E., Sajjadi, E., Corti, C., Guerini-Rocco, E., Viale, G., Curigliano, G., Criscitiello, C., & Fusco, N. (2022). HER2 Low, Ultra-low, and Novel Complementary Biomarkers: Expanding the Spectrum of HER2 Positivity in Breast Cancer. Frontiers in Molecular Biosciences, 9, 834651. https://doi.org/10.3389/fmolb.2022.834651

230. Wang, J., & Xu, B. (2019). Targeted therapeutic options and future perspectives for HER2-positive breast cancer. Signal Transduction and Targeted Therapy, 4, 34. https://doi.org/10.1038/s41392-019-0069-2

231. Goutsouliak, K., Veeraraghavan, J., Sethunath, V., De Angelis, C., Osborne, C. K., Rimawi, M. F., & Schiff, R. (2020). Towards personalized treatment for early stage HER2-positive breast cancer. Nature Reviews Clinical Oncology, 17(4), 233–250. https://doi.org/10.1038/s41571-019-0299-9

232. Lowry, M. (2019). Investigating mechanisms of anti-cancer drug resistance in breast cancer cells and extracellular vesicles [Thesis, Trinity College Dublin. School of Pharmacy & Pharma. Sciences. Discipline of Pharmacy]. http://www.tara.tcd.ie/handle/2262/86081

233. Bradford, M. M. (1976). A rapid and sensitive method for the quantitation of microgram quantities of protein utilizing the principle of protein-dye binding. Analytical Biochemistry, 72(1–2), 248–254. https://doi.org/10.1016/0003-2697(76)90527-3

234. Zhang, X., Smits, A. H., van Tilburg, G. B., Ovaa, H., Huber, W., & Vermeulen, M. (2018). Proteome-wide identification of ubiquitin interactions using UbIA-MS. Nature Protocols, 13(3), 530–550. https://doi.org/10.1038/nprot.2017.147

235. Ritchie, M. E., Phipson, B., Wu, D., Hu, Y., Law, C. W., Shi, W., & Smyth, G. K. (2015). Limma powers differential expression analyses for RNA-sequencing and microarray studies. Nucleic Acids Research, 43(7), e47–e47. https://doi.org/10.1093/nar/gkv007

236. Kuleshov, M. V., Jones, M. R., Rouillard, A. D., Fernandez, N. F., Duan, Q., Wang, Z., Koplev, S., Jenkins, S. L., Jagodnik, K. M., Lachmann, A., McDermott, M. G., Monteiro, C. D., Gundersen, G. W., & Ma'ayan, A. (2016). Enrichr: A comprehensive gene set enrichment analysis web server 2016 update. Nucleic Acids Research, 44(W1), W90–W97. https://doi.org/10.1093/nar/gkw377

237. Polacheck, W. J., Zervantonakis, I. K., & Kamm, R. D. (2013). Tumor cell migration in complex microenvironments. Cellular and Molecular Life Sciences, 70(8), 1335–1356. https://doi.org/10.1007/s00018-012-1115-1

238. McNamee, N., & O'Driscoll, L. (2021). Miniaturized In Vitro Assays to Study Cellular Phenotypic Characteristics: Proliferation, Migration, Invasion, and Anoikis-Resistance. Methods in Molecular Biology (Clifton, N.J.), 2283, 225–232. https://doi.org/10.1007/978-1-0716-1302-3_19

239. Pedanou, V. E., Gobeil, S., Tabariès, S., Simone, T. M., Zhu, L. J., Siegel, P. M., & Green, M. R. (2016). The histone H3K9 demethylase KDM3A promotes anoikis by transcriptionally activating pro-apoptotic genes BNIP3 and BNIP3L. ELife, 5, e16844. https://doi.org/10.7554/eLife.16844

240. Suarez-Arnedo, A., Torres Figueroa, F., Clavijo, C., Arbeláez, P., Cruz, J. C., & Muñoz-Camargo, C. (2020). An image J plugin for the high throughput image analysis of in vitro scratch wound healing assays. PLOS ONE, 15(7), e0232565. https://doi.org/10.1371/journal.pone.0232565

241. Rajabi, H., Alam, M., Takahashi, H., Kharbanda, A., Guha, M., Ahmad, R., & Kufe, D. (2014). MUC1-C oncoprotein activates the ZEB1/miR-200c regulatory loop and epithelial–mesenchymal transition. Oncogene, 33(13), 1680–1689. https://doi.org/10.1038/onc.2013.114

242. Liu, D., Rudland, P. S., Sibson, D. R., Platt-Higgins, A., & Barraclough, R. (2005). Human Homologue of Cement Gland Protein, a Novel Metastasis Inducer Associated with Breast Carcinomas. Cancer Research, 65(9), 3796–3805. https://doi.org/10.1158/0008-5472.CAN-04-3823

243. Sommerova, L., Ondrouskova, E., Martisova, A., Zoumpourlis, V., Galtsidis, S., & Hrstka, R. (2020). ZEB1/miR-200c/AGR2: A New Regulatory Loop Modulating the Epithelial-Mesenchymal Transition in Lung Adenocarcinomas. Cancers, 12(6), 1614. https://doi.org/10.3390/cancers12061614

244. Al-Nedawi, K., Meehan, B., Kerbel, R. S., Allison, A. C., & Rak, J. (2009). Endothelial expression of autocrine VEGF upon the uptake of tumor-derived microvesicles containing oncogenic EGFR. Proceedings of the National Academy of Sciences of the United States of America, 106(10), 3794–3799. https://doi.org/10.1073/pnas.0804543106

245. Gupta, P., Gupta, N., Fofaria, N. M., Ranjan, A., & Srivastava, S. K. (2019). HER2-mediated GLI2 stabilization promotes anoikis resistance and metastasis of breast cancer cells. Cancer Letters, 442, 68–81. https://doi.org/10.1016/j.canlet.2018.10.021

246. Lecuit, T., & Yap, A. S. (2015). E-cadherin junctions as active mechanical integrators in tissue dynamics. Nature Cell Biology, 17(5), 533–539. https://doi.org/10.1038/ncb3136

247. Feltes, C. M., Kudo, A., Blaschuk, O., & Byers, S. W. (2002). An alternatively spliced cadherin-11 enhances human breast cancer cell invasion. Cancer Research, 62(22), 6688–6697.

248. Salmans, M. L., Zhao, F., & Andersen, B. (2013). The estrogen-regulated anterior gradient 2 (AGR2) protein in breast cancer: A potential drug target and biomarker. Breast Cancer Research, 15(2), 204. https://doi.org/10.1186/bcr3408

249. Brix, D. M., Bundgaard Clemmensen, K. K., & Kallunki, T. (2014). When Good Turns Bad: Regulation of Invasion and Metastasis by ErbB2 Receptor Tyrosine Kinase. Cells, 3(1), 53–78. https://doi.org/10.3390/cells3010053

250. Wodziak, D., Dong, A., Basin, M. F., & Lowe, A. W. (2016). Anterior Gradient 2 (AGR2) Induced Epidermal Growth Factor Receptor (EGFR) Signaling Is Essential for Murine Pancreatitis-Associated Tissue Regeneration. PloS One, 11(10), e0164968. https://doi.org/10.1371/journal.pone.0164968

251. Liu, Q.-G., Li, Y.-J., & Yao, L. (2018). Knockdown of AGR2 induces cell apoptosis and reduces chemotherapy resistance of pancreatic cancer cells with the involvement of ERK/AKT axis. Pancreatology: Official Journal of the International Association of Pancreatology (IAP) ... [et Al.], 18(6), 678–688. https://doi.org/10.1016/j.pan.2018.07.003

252. Kerkentzes, K., Lagani, V., Tsamardinos, I., Vyberg, M., & Røe, O. D. (2014). Hidden treasures in 'ancient' microarrays: Gene-expression portrays biology and potential resistance pathways of major lung cancer subtypes and normal tissue. Frontiers in Oncology, 4, 251. https://doi.org/10.3389/fonc.2014.00251

253. Kuo, M. T., Chen, H. H. W., Feun, L. G., & Savaraj, N. (2021). Targeting the Proline–Glutamine–Asparagine–Arginine Metabolic Axis in Amino Acid Starvation Cancer Therapy. Pharmaceuticals, 14(1), 72. https://doi.org/10.3390/ph14010072

254. Du, T., & Han, J. (2021). Arginine Metabolism and Its Potential in Treatment of Colorectal Cancer. Frontiers in Cell and Developmental Biology, 9, 658861. https://doi.org/10.3389/fcell.2021.658861

255. Burke, L., Guterman, I., Palacios Gallego, R., Britton, R. G., Burschowsky, D., Tufarelli, C., & Rufini, A. (2020). The Janus-like role of proline metabolism in

cancer. Cell Death Discovery, 6, 104. https://doi.org/10.1038/s41420-020-00341-8

256. Corcoran, C., Rani, S., Breslin, S., Gogarty, M., Ghobrial, I. M., Crown, J., & O'Driscoll, L. (2014). MiR-630 targets IGF1R to regulate response to HER-targeting drugs and overall cancer cell progression in HER2 over-expressing breast cancer. Molecular Cancer, 13, 71. https://doi.org/10.1186/1476-4598-13-71

257. Hrstka, R., Nenutil, R., Fourtouna, A., Maslon, M. M., Naughton, C., Langdon, S., Murray, E., Larionov, A., Petrakova, K., Muller, P., Dixon, M. J., Hupp, T. R., & Vojtesek, B. (2010). The pro-metastatic protein anterior gradient-2 predicts poor prognosis in tamoxifen-treated breast cancers. Oncogene, 29(34), Article 34. https://doi.org/10.1038/onc.2010.228

258. Lacambra, M. D., Tsang, J. Y. S., Ni, Y.-B., Chan, S.-K., Tan, P. H., & Tse, G. M. (2015). Anterior Gradient 2 is a Poor Outcome Indicator in Luminal Breast Cancer. Annals of Surgical Oncology, 22(11), 3489–3496. https://doi.org/10.1245/s10434-015-4420-8

259. Fritzsche, F. R., Dahl, E., Pahl, S., Burkhardt, M., Luo, J., Mayordomo, E., Gansukh, T., Dankof, A., Knuechel, R., Denkert, C., Winzer, K.-J., Dietel, M., & Kristiansen, G. (2006). Prognostic relevance of AGR2 expression in breast cancer. Clinical Cancer Research: An Official Journal of the American Association for Cancer Research, 12(6), 1728–1734. https://doi.org/10.1158/1078-0432.CCR-05-2057

260. Barraclough, D. L., Platt-Higgins, A., de Silva Rudland, S., Barraclough, R., Winstanley, J., West, C. R., & Rudland, P. S. (2009). The metastasis-associated anterior gradient 2 protein is correlated with poor survival of breast cancer patients. The American Journal of Pathology, 175(5), 1848–1857. https://doi.org/10.2353/ajpath.2009.090246

261. de Moraes, C. L., Cruz e Melo, N., Valoyes, M. A. V., & Naves do Amaral, W. (2022). AGR2 and AGR3 play an important role in the clinical characterization and prognosis of basal like breast cancer. Clinical Breast Cancer, 22(2), e242–e252. https://doi.org/10.1016/j.clbc.2021.07.008

262. Li, J.-J., Wang, S., Guan, Z.-N., Zhang, J.-X., Zhan, R.-X., & Zhu, J.-L. (2022). Anterior Gradient 2 is a Significant Prognostic Biomarker in Bone Metastasis of Breast Cancer. Pathology and Oncology Research, 28, 1610538. https://doi.org/10.3389/pore.2022.1610538

263. Alves, M. R., e Melo, N. C., Barros-Filho, M. C., do Amaral, N. S., Silva, F. I. de B., Baiocchi Neto, G., Soares, F. A., de Brot Andrade, L., & Rocha, R. M.

(2018). Downregulation of AGR2, p21, and cyclin D and alterations in p53 function were associated with tumor progression and chemotherapy resistance in epithelial ovarian carcinoma. Cancer Medicine, 7(7), 3188–3199. https://doi.org/10.1002/cam4.1530

264. Hazan, R. B., Qiao, R., Keren, R., Badano, I., & Suyama, K. (2004). Cadherin switch in tumor progression. Annals of the New York Academy of Sciences, 1014, 155–163. https://doi.org/10.1196/annals.1294.016

265. Jeanes, A., Gottardi, C. J., & Yap, A. S. (2008). Cadherins and cancer: How does cadherin dysfunction promote tumor progression? Oncogene, 27(55), 6920–6929. https://doi.org/10.1038/onc.2008.343

266. Wheelock, M. J., Shintani, Y., Maeda, M., Fukumoto, Y., & Johnson, K. R. (2008). Cadherin switching. Journal of Cell Science, 121(Pt 6), 727–735. https://doi.org/10.1242/jcs.000455

267. Zhao, L., Lee, B. Y., Brown, D. A., Molloy, M. P., Marx, G. M., Pavlakis, N., Boyer, M. J., Stockler, M. R., Kaplan, W., Breit, S. N., Sutherland, R. L., Henshall, S. M., & Horvath, L. G. (2009). Identification of candidate biomarkers of therapeutic response to docetaxel by proteomic profiling. Cancer Research, 69(19), 7696–7703. https://doi.org/10.1158/0008-5472.CAN-08-4901

268. Becker, A., Thakur, B. K., Weiss, J. M., Kim, H. S., Peinado, H., & Lyden, D. (2016). Extracellular vesicles in cancer: Cell-to-cell mediators of metastasis. Cancer Cell, 30(6), 836–848. https://doi.org/10.1016/j.ccell.2016.10.009

269. Chang, W.-H., Cerione, R. A., & Antonyak, M. A. (2021). Extracellular Vesicles and Their Roles in Cancer Progression. Methods in Molecular Biology (Clifton, N.J.), 2174, 143–170. https://doi.org/10.1007/978-1-0716-0759-6_10

270. van Dommelen, S. M., van der Meel, R., van Solinge, W. W., Coimbra, M., Vader, P., & Schiffelers, R. M. (2016). Cetuximab treatment alters the content of extracellular vesicles released from tumor cells. Nanomedicine (London, England), 11(8), 881–890. https://doi.org/10.2217/nnm-2015-0009

271. Corcoran, C., Rani, S., & O'Driscoll, L. (2014). MiR-34a is an intracellular and exosomal predictive biomarker for response to docetaxel with clinical relevance to prostate cancer progression. The Prostate, 74(13), 1320–1334. https://doi.org/10.1002/pros.22848

272. Exosomes from triple-negative breast cancer cells can transfer phenotypic traits representing their cells of origin to secondary cells—European Journal of Cancer. (n.d.). Retrieved 20 April 2023, from https://www.ejcancer.com/article/S0959-8049(13)00079-8/fulltext

273. Han, M., Hu, J., Lu, P., Cao, H., Yu, C., Li, X., Qian, X., Yang, X., Yang, Y., Han, N., Dou, D., Zhang, F., Ye, M., Yang, C., Gu, Y., & Dong, H. (2020). Exosome-transmitted miR-567 reverses trastuzumab resistance by inhibiting ATG5 in breast cancer. Cell Death & Disease, 11(1), 43. https://doi.org/10.1038/s41419-020-2250-5

274. Gong, J., Jaiswal, R., Mathys, J.-M., Combes, V., Grau, G. E. R., & Bebawy, M. (2012). Microparticles and their emerging role in cancer multidrug resistance. Cancer Treatment Reviews, 38(3), 226–234. https://doi.org/10.1016/j.ctrv.2011.06.005

275. Durcker, A., Yoo, B. H., Khan, I. A., Choi, D., Montermini, L., Liu, X., Jovanovic, S., Younis, T., & Rosen, K. V. (2020). Trastuzumab-induced upregulation of a protein set in extracellular vesicles emitted by ErbB2-positive breast cancer cells correlates with their trastuzumab sensitivity. Breast Cancer Research : BCR, 22, 105. https://doi.org/10.1186/s13058-020-01342-2

276. Hosseini, R., Asef-Kabiri, L., Sarvnaz, H., Ghanavatinejad, A., Rezayat, F., Eskandari, N., & Akbari, M. E. (2023). Blockade of exosome release alters HER2 trafficking to the plasma membrane and gives a boost to Trastuzumab. Clinical & Translational Oncology: Official Publication of the Federation of Spanish Oncology Societies and of the National Cancer Institute of Mexico, 25(1), 185–198. https://doi.org/10.1007/s12094-022-02925-5

277. Barok, M., Puhka, M., Vereb, G., Szollosi, J., Isola, J., & Joensuu, H. (2018). Cancer-derived exosomes from HER2-positive cancer cells carry trastuzumab-emtansine into cancer cells leading to growth inhibition and caspase activation. BMC Cancer, 18, 504. https://doi.org/10.1186/s12885-018-4418-2

278. Santamaria, S., Gagliani, M. C., Bellese, G., Marconi, S., Lechiara, A., Dameri, M., Aiello, C., Tagliatti, E., Castagnola, P., & Cortese, K. (2021). Imaging of Endocytic Trafficking and Extracellular Vesicles Released Under Neratinib Treatment in ERBB2+ Breast Cancer Cells. Journal of Histochemistry and Cytochemistry, 69(7), 461–473. https://doi.org/10.1369/00221554211026297

279. Catalano, M. (2022). Tumour microenvironment, extracellular vesicles and their effect on prostate cancer progression and docetaxel resistance [Thesis, Trinity College Dublin. School of Pharmacy & Pharma. Sciences. Discipline of Pharmacy]. http://www.tara.tcd.ie/handle/2262/98604

280. Ricklefs, F. L., Maire, C. L., Reimer, R., Dührsen, L., Kolbe, K., Holz, M., Schneider, E., Rissiek, A., Babayan, A., Hille, C., Pantel, K., Krasemann, S.,

Glatzel, M., Heiland, D. H., Flitsch, J., Martens, T., Schmidt, N. O., Peine, S., Breakefield, X. O., … Lamszus, K. (2019). Imaging flow cytometry facilitates multiparametric characterization of extracellular vesicles in malignant brain tumours. Journal of Extracellular Vesicles, 8(1), 1588555. https://doi.org/10.1080/20013078.2019.1588555

281. Mukhopadhya, A., Tsiapalis, D., McNamee, N., Talbot, B., & O'Driscoll, L. (2023). Doxorubicin Loading into Milk and Mesenchymal Stem Cells' Extracellular Vesicles as Drug Delivery Vehicles. Pharmaceutics, 15(3), Article 3. https://doi.org/10.3390/pharmaceutics15030718

282. Ma, S., Mangala, L. S., Hu, W., Bayaktar, E., Yokoi, A., Hu, W., Pradeep, S., Lee, S., Piehowski, P. D., Villar-Prados, A., Wu, S. Y., McGuire, M. H., Lara, O. D., Rodriguez-Aguayo, C., LaFargue, C. J., Jennings, N. B., Rodland, K. D., Liu, T., Kundra, V., … Sood, A. K. (2021). CD63-mediated cloaking of VEGF in small extracellular vesicles contributes to anti-VEGF therapy resistance. Cell Reports, 36(7), 109549. https://doi.org/10.1016/j.celrep.2021.109549

283. Clancy, J., & D'Souza-Schorey, C. (2018). Extracellular Vesicles in Cancer: Purpose and Promise. Cancer Journal (Sudbury, Mass.), 24(2), 65–69. https://doi.org/10.1097/PPO.0000000000000306

284. Berumen Sánchez, G., Bunn, K. E., Pua, H. H., & Rafat, M. (2021). Extracellular vesicles: Mediators of intercellular communication in tissue injury and disease. Cell Communication and Signaling, 19(1), 104. https://doi.org/10.1186/s12964-021-00787-y

285. Konoshenko, M. Yu., Lekchnov, E. A., Vlassov, A. V., & Laktionov, P. P. (2018). Isolation of Extracellular Vesicles: General Methodologies and Latest Trends. BioMed Research International, 2018, 8545347. https://doi.org/10.1155/2018/8545347

286. Mateescu, B., Kowal, E. J. K., van Balkom, B. W. M., Bartel, S., Bhattacharyya, S. N., Buzás, E. I., Buck, A. H., de Candia, P., Chow, F. W. N., Das, S., Driedonks, T. A. P., Fernández-Messina, L., Haderk, F., Hill, A. F., Jones, J. C., Van Keuren-Jensen, K. R., Lai, C. P., Lässer, C., di Liegro, I., … Nolte-'t Hoen, E. N. M. (2017). Obstacles and opportunities in the functional analysis of extracellular vesicle RNA – an ISEV position paper. Journal of Extracellular Vesicles, 6(1), 1286095. https://doi.org/10.1080/20013078.2017.1286095

287. Clos-Sansalvador, M., Monguió-Tortajada, M., Roura, S., Franquesa, M., & Borràs, F. E. (2022). Commonly used methods for extracellular vesicles'

enrichment: Implications in downstream analyses and use. European Journal of Cell Biology, 101(3), 151227. https://doi.org/10.1016/j.ejcb.2022.151227

288. Muz, B., de la Puente, P., Azab, F., & Azab, A. K. (2015). The role of hypoxia in cancer progression, angiogenesis, metastasis, and resistance to therapy. Hypoxia, 3, 83–92. https://doi.org/10.2147/HP.S93413

289. Zhang, Y., Zhang, H., Wang, M., Schmid, T., Xin, Z., Kozhuharova, L., Yu, W.-K., Huang, Y., Cai, F., & Biskup, E. (2021). Hypoxia in Breast Cancer— Scientific Translation to Therapeutic and Diagnostic Clinical Applications. Frontiers in Oncology, 11, 652266. https://doi.org/10.3389/fonc.2021.652266

290. Vaupel, P., Mayer, A., Briest, S., & Höckel, M. (2005). Hypoxia in breast cancer: Role of blood flow, oxygen diffusion distances, and anemia in the development of oxygen depletion. Advances in Experimental Medicine and Biology, 566, 333–342. https://doi.org/10.1007/0-387-26206-7_44

291. Li, H., Sun, X., Li, J., Liu, W., Pan, G., Mao, A., Liu, J., Zhang, Q., Rao, L., Xie, X., & Sheng, X. (2022). Hypoxia induces docetaxel resistance in triple-negative breast cancer via the HIF-1α/miR-494/Survivin signaling pathway. Neoplasia, 32, 100821. https://doi.org/10.1016/j.neo.2022.100821

292. Najjary, S., Mohammadzadeh, R., Mokhtarzadeh, A., Mohammadi, A., Kojabad, A. B., & Baradaran, B. (2020). Role of miR-21 as an authentic oncogene in mediating drug resistance in breast cancer. Gene, 738, 144453. https://doi.org/10.1016/j.gene.2020.144453

293. Yi, T., Papadopoulos, E., Hagner, P. R., & Wagner, G. (2013). Hypoxia-inducible Factor-1α (HIF-1α) Promotes Cap-dependent Translation of Selective mRNAs through Up-regulating Initiation Factor eIF4E1 in Breast Cancer Cells under Hypoxia Conditions. The Journal of Biological Chemistry, 288(26), 18732–18742. https://doi.org/10.1074/jbc.M113.471466

294. Mortezaee, K., & Majidpoor, J. (2023). The impact of hypoxia on extracellular vesicle secretome profile of cancer. Medical Oncology (Northwood, London, England), 40(5), 128. https://doi.org/10.1007/s12032-023-01995-x

295. Ren, W., Hou, J., Yang, C., Wang, H., Wu, S., Wu, Y., Zhao, X., & Lu, C. (2019). Extracellular vesicles secreted by hypoxia pre-challenged mesenchymal stem cells promote non-small cell lung cancer cell growth and mobility as well as macrophage M2 polarization via miR-21-5p delivery. Journal of Experimental & Clinical Cancer Research, 38(1), 62. https://doi.org/10.1186/s13046-019-1027-0

296. He, G., Peng, X., Wei, S., Yang, S., Li, X., Huang, M., Tang, S., Jin, H., Liu, J., Zhang, S., Zheng, H., Fan, Q., Liu, J., Yang, L., & Li, H. (2022). Exosomes in the hypoxic TME: From release, uptake and biofunctions to clinical applications. Molecular Cancer, 21(1), 19. https://doi.org/10.1186/s12943-021-01440-5

297. Shao, X., Hua, S., Feng, T., Ocansey, D. K. W., & Yin, L. (2022). Hypoxia-Regulated Tumor-Derived Exosomes and Tumor Progression: A Focus on Immune Evasion. International Journal of Molecular Sciences, 23(19), Article 19. https://doi.org/10.3390/ijms231911789

298. Chan, Y. C., Banerjee, J., Choi, S. Y., & Sen, C. K. (2012). miR-210: The master hypoxamir. Microcirculation (New York, N.Y. : 1994), 19(3), 215–223. https://doi.org/10.1111/j.1549-8719.2011.00154.x

299. Wang, J., Zhao, J., Shi, M., Ding, Y., Sun, H., Yuan, F., & Zou, Z. (2014). Elevated Expression of miR-210 Predicts Poor Survival of Cancer Patients: A Systematic Review and Meta-Analysis. PLOS ONE, 9(2), e89223. https://doi.org/10.1371/journal.pone.0089223

300. Yang, M., Zhang, Y., Li, M., Liu, X., & Darvishi, M. (2023). The various role of microRNAs in breast cancer angiogenesis, with a special focus on novel miRNA-based delivery strategies. Cancer Cell International, 23(1), 24. https://doi.org/10.1186/s12935-022-02837-y

301. Liu, L.-Z., Li, C., Chen, Q., Jing, Y., Carpenter, R., Jiang, Y., Kung, H.-F., Lai, L., & Jiang, B.-H. (2011). MiR-21 Induced Angiogenesis through AKT and ERK Activation and HIF-1α Expression. PLOS ONE, 6(4), e19139. https://doi.org/10.1371/journal.pone.0019139

302. Babar, I. A., Czochor, J., Steinmetz, A., Weidhaas, J. B., Glazer, P. M., & Slack, F. J. (2011). Inhibition of hypoxia-induced miR-155 radiosensitizes hypoxic lung cancer cells. Cancer Biology & Therapy, 12(10), 908–914. https://doi.org/10.4161/cbt.12.10.17681

303. Mattiske, S., Suetani, R. J., Neilsen, P. M., & Callen, D. F. (2012). The Oncogenic Role of miR-155 in Breast Cancer. Cancer Epidemiology, Biomarkers & Prevention, 21(8), 1236–1243. https://doi.org/10.1158/1055-9965.EPI-12-0173

304. Kadkhoda, S., & Ghafouri-Fard, S. (2022). The importance of miRNA-630 in human diseases with an especial focus on cancers. Cancer Cell International, 22(1), 105. https://doi.org/10.1186/s12935-022-02531-z

305. Song, Y.-F., Hong, J.-F., Liu, D.-L., Lin, Q.-A., Lan, X.-P., & Lai, G.-X. (2015). MiR-630 targets LMO3 to regulate cell growth and metastasis in lung cancer. American Journal of Translational Research, 7(7), 1271–1279.

306. Zhou, C.-X., Wang, C.-L., Yu, A.-L., Wang, Q.-Y., Zhan, M.-N., Tang, J., Gong, X.-F., Yin, Q.-Q., He, M., He, J.-R., Chen, G.-Q., & Zhao, Q. (2015). MiR-630 suppresses breast cancer progression by targeting metadherin. Oncotarget, 7(2), 1288–1299.

307. Scherbakov, A. M., Stefanova, L. B., Sorokin, D. V., Semina, S. E., Berstein, L. M., & Krasil'nikov, M. A. (2013). Snail/beta-catenin signaling protects breast cancer cells from hypoxia attack. Experimental Cell Research, 319(20), 3150–3159. https://doi.org/10.1016/j.yexcr.2013.08.019

308. Lobb, R. J., Becker, M., Wen Wen, S., Wong, C. S. F., Wiegmans, A. P., Leimgruber, A., & Möller, A. (2015). Optimized exosome isolation protocol for cell culture supernatant and human plasma. Journal of Extracellular Vesicles, 4(1), 27031. https://doi.org/10.3402/jev.v4.27031

309. Woud, W. W., van der Pol, E., Mul, E., Hoogduijn, M. J., Baan, C. C., Boer, K., & Merino, A. (2022). An imaging flow cytometry-based methodology for the analysis of single extracellular vesicles in unprocessed human plasma. Communications Biology, 5(1), Article 1. https://doi.org/10.1038/s42003-022-03569-5

310. Görgens, A., Bremer, M., Ferrer-Tur, R., Murke, F., Tertel, T., Horn, P. A., Thalmann, S., Welsh, J. A., Probst, C., Guerin, C., Boulanger, C. M., Jones, J. C., Hanenberg, H., Erdbrügger, U., Lannigan, J., Ricklefs, F. L., El-Andaloussi, S., & Giebel, B. (2019). Optimisation of imaging flow cytometry for the analysis of single extracellular vesicles by using fluorescence-tagged vesicles as biological reference material. Journal of Extracellular Vesicles, 8(1), 1587567. https://doi.org/10.1080/20013078.2019.1587567

311. Headland, S. E., Jones, H. R., D'Sa, A. S. V., Perretti, M., & Norling, L. V. (2014). Cutting-Edge Analysis of Extracellular Microparticles using ImageStreamX Imaging Flow Cytometry. Scientific Reports, 4(1), Article 1. https://doi.org/10.1038/srep05237

312. Giaccia, A. J., Simon, M. C., & Johnson, R. (2004). The biology of hypoxia: The role of oxygen sensing in development, normal function, and disease. Genes & Development, 18(18), 2183–2194. https://doi.org/10.1101/gad.1243304

313. Chi, J.-T., Wang, Z., Nuyten, D. S. A., Rodriguez, E. H., Schaner, M. E., Salim, A., Wang, Y., Kristensen, G. B., Helland, A., Børresen-Dale, A.-L.,

Giaccia, A., Longaker, M. T., Hastie, T., Yang, G. P., van de Vijver, M. J., & Brown, P. O. (2006). Gene expression programs in response to hypoxia: Cell type specificity and prognostic significance in human cancers. PLoS Medicine, 3(3), e47. https://doi.org/10.1371/journal.pmed.0030047

314. Kaszak, I., Witkowska-Piłaszewicz, O., Niewiadomska, Z., Dworecka-Kaszak, B., Ngosa Toka, F., & Jurka, P. (2020). Role of Cadherins in Cancer—A Review. International Journal of Molecular Sciences, 21(20), 7624. https://doi.org/10.3390/ijms21207624

315. Serrano-Gomez, S. J., Maziveyi, M., & Alahari, S. K. (2016). Regulation of epithelial-mesenchymal transition through epigenetic and post-translational modifications. Molecular Cancer, 15, 18. https://doi.org/10.1186/s12943-016-0502-x

316. Bruner, H. C., & Derksen, P. W. B. (2018). Loss of E-Cadherin-Dependent Cell-Cell Adhesion and the Development and Progression of Cancer. Cold Spring Harbor Perspectives in Biology, 10(3), a029330. https://doi.org/10.1101/cshperspect.a029330

317. Theys, J., Jutten, B., Habets, R., Paesmans, K., Groot, A. J., Lambin, P., Wouters, B. G., Lammering, G., & Vooijs, M. (2011). E-Cadherin loss associated with EMT promotes radioresistance in human tumor cells. Radiotherapy and Oncology: Journal of the European Society for Therapeutic Radiology and Oncology, 99(3), 392–397. https://doi.org/10.1016/j.radonc.2011.05.044

318. Chen, J., Wei, Y., Yang, W., Huang, Q., Chen, Y., Zeng, K., & Chen, J. (2022). IL-6: The Link Between Inflammation, Immunity and Breast Cancer. Frontiers in Oncology, 12, 903800. https://doi.org/10.3389/fonc.2022.903800

319. Todorović-Raković, N., & Milovanović, J. (2013). Interleukin-8 in Breast Cancer Progression. Journal of Interferon & Cytokine Research, 33(10), 563–570. https://doi.org/10.1089/jir.2013.0023

320. Xu, L., Xie, K., Mukaida, N., Matsushima, K., & Fidler, I. J. (1999). Hypoxia-induced Elevation in Interleukin-8 Expression by Human Ovarian Carcinoma Cells1. Cancer Research, 59(22), 5822–5829.

321. Malkov, M. I., Lee, C. T., & Taylor, C. T. (2021). Regulation of the Hypoxia-Inducible Factor (HIF) by Pro-Inflammatory Cytokines. Cells, 10(9), Article 9. https://doi.org/10.3390/cells10092340

322. Samoylenko, A., Kögler, M., Zhyvolozhnyi, A., Makieieva, O., Bart, G., Andoh, S. S., Roussey, M., Vainio, S. J., & Hiltunen, J. (2021). Time-gated

Raman spectroscopy and proteomics analyses of hypoxic and normoxic renal carcinoma extracellular vesicles. Scientific Reports, 11, 19594. https://doi.org/10.1038/s41598-021-99004-6

323. Liu, H.-L., Liu, D., Ding, G.-R., Liao, P.-F., & Zhang, J.-W. (2015). Hypoxia-inducible factor-1α and Wnt/β-catenin signaling pathways promote the invasion of hypoxic gastric cancer cells. Molecular Medicine Reports, 12(3), 3365–3373. https://doi.org/10.3892/mmr.2015.3812

324. Pola, C., Formenti, S. C., & Schneider, R. J. (2013). Vitronectin–αvβ3 Integrin Engagement Directs Hypoxia-Resistant mTOR Activity and Sustained Protein Synthesis Linked to Invasion by Breast Cancer Cells. Cancer Research, 73(14), 4571–4578. https://doi.org/10.1158/0008-5472.CAN-13-0218

325. Bryant, D. M., & Stow, J. L. (2004). The ins and outs of E-cadherin trafficking. Trends in Cell Biology, 14(8), 427–434. https://doi.org/10.1016/j.tcb.2004.07.007

326. Kartenbeck, J., Schmelz, M., Franke, W. W., & Geiger, B. (1991). Endocytosis of junctional cadherins in bovine kidney epithelial (MDBK) cells cultured in low Ca2+ ion medium. The Journal of Cell Biology, 113(4), 881–892.

327. Lock, J. G., & Stow, J. L. (2005). Rab11 in Recycling Endosomes Regulates the Sorting and Basolateral Transport of E-Cadherin. Molecular Biology of the Cell, 16(4), 1744–1755. https://doi.org/10.1091/mbc.e04-10-0867

328. Grabowska, M. M., & Day, M. L. (2012). Soluble E-cadherin: More than a symptom of disease. Frontiers in Bioscience (Landmark Edition), 17(5), 1948–1964. https://doi.org/10.2741/4031

329. Zhang, Y., Liu, Z., Li, S., Wang, M., Dai, D., Jing, H., & Liu, L. (2020). Upregulation of E-cadherin in bronchoalveolar lavage fluid-derived exosomes in patients with lung cancer. Thoracic Cancer, 11(1), 41–47. https://doi.org/10.1111/1759-7714.13220

330. Tang, M. K. S., Yue, P. Y. K., Ip, P. P., Huang, R.-L., Lai, H.-C., Cheung, A. N. Y., Tse, K. Y., Ngan, H. Y. S., & Wong, A. S. T. (2018). Soluble E-cadherin promotes tumor angiogenesis and localizes to exosome surface. Nature Communications, 9(1), 2270. https://doi.org/10.1038/s41467-018-04695-7

331. Bänfer, S., Kutscher, S., Fleck, F., Dienst, M., Preußer, C., Pogge von Strandmann, E., & Jacob, R. (2022). Late domain dependent E-cadherin recruitment into extracellular vesicles. Frontiers in Cell and Developmental Biology, 10, 878620. https://doi.org/10.3389/fcell.2022.878620

332. Sanguinetti, A., Santini, D., Bonafè, M., Taffurelli, M., & Avenia, N. (2015). Interleukin-6 and pro inflammatory status in the breast tumor microenvironment. World Journal of Surgical Oncology, 13(1), 129. https://doi.org/10.1186/s12957-015-0529-2

333. Fitzgerald, W., Freeman, M. L., Lederman, M. M., Vasilieva, E., Romero, R., & Margolis, L. (2018). A System of Cytokines Encapsulated in ExtraCellular Vesicles. Scientific Reports, 8(1), Article 1. https://doi.org/10.1038/s41598-018-27190-x

334. Aiello, A., Giannessi, F., Percario, Z. A., & Affabris, E. (2020). An emerging interplay between extracellular vesicles and cytokines. Cytokine & Growth Factor Reviews, 51, 49–60. https://doi.org/10.1016/j.cytogfr.2019.12.003

335. Li, Y. M., Zhou, B. P., Deng, J., Pan, Y., Hay, N., & Hung, M.-C. (2005). A hypoxia-independent hypoxia-inducible factor-1 activation pathway induced by phosphatidylinositol-3 kinase/Akt in HER2 overexpressing cells. Cancer Research, 65(8), 3257–3263. https://doi.org/10.1158/0008-5472.CAN-04-1284

336. Tasharrofi, B., Soudyab, M., Nikpayam, E., Iranpour, M., Mirfakhraie, R., Sarrafzadeh, S., Geranpayeh, L., Azargashb, E., Sayad, A., & Ghafouri-Fard, S. (2016). Comparative expression analysis of hypoxia-inducible factor-alpha and its natural occurring antisense in breast cancer tissues and adjacent noncancerous tissues. Cell Biochemistry and Function, 34(8), 572–578. https://doi.org/10.1002/cbf.3230

337. Jarman, E. J., Ward, C., Turnbull, A. K., Martinez-Perez, C., Meehan, J., Xintaropoulou, C., Sims, A. H., & Langdon, S. P. (2019). HER2 regulates HIF-2α and drives an increased hypoxic response in breast cancer. Breast Cancer Research, 21(1), 10. https://doi.org/10.1186/s13058-019-1097-0

338. Indira Chandran, V., Månsson, A.-S., Barbachowska, M., Cerezo-Magaña, M., Nodin, B., Joshi, B., Koppada, N., Saad, O. M., Gluz, O., Isaksson, K., Borgquist, S., Jirström, K., Nabi, I. R., Jernström, H., & Belting, M. (2020). Hypoxia Attenuates Trastuzumab Uptake and Trastuzumab-Emtansine (T-DM1) Cytotoxicity through Redistribution of Phosphorylated Caveolin-1. Molecular Cancer Research, 18(4), 644–656. https://doi.org/10.1158/1541-7786.MCR-19-0856

339. Pereira, P. M. R., Sharma, S. K., Carter, L. M., Edwards, K. J., Pourat, J., Ragupathi, A., Janjigian, Y. Y., Durack, J. C., & Lewis, J. S. (2018). Caveolin-1 mediates cellular distribution of HER2 and affects trastuzumab binding and

therapeutic efficacy. Nature Communications, 9, 5137.
https://doi.org/10.1038/s41467-018-07608-w

340. Mosesson, Y., Mills, G. B., & Yarden, Y. (2008). Derailed endocytosis: An emerging feature of cancer. Nature Reviews. Cancer, 8(11), 835–850. https://doi.org/10.1038/nrc2521

341. Sorkin, A., & Goh, L. K. (2009). Endocytosis and intracellular trafficking of ErbBs. Experimental Cell Research, 315(4), 683–696. https://doi.org/10.1016/j.yexcr.2008.07.029

342. Austin, C. D., De Mazière, A. M., Pisacane, P. I., van Dijk, S. M., Eigenbrot, C., Sliwkowski, M. X., Klumperman, J., & Scheller, R. H. (2004). Endocytosis and Sorting of ErbB2 and the Site of Action of Cancer Therapeutics Trastuzumab and Geldanamycin. Molecular Biology of the Cell, 15(12), 5268–5282. https://doi.org/10.1091/mbc.e04-07-0591

343. Chung, Y.-C., Kuo, J.-F., Wei, W.-C., Chang, K.-J., & Chao, W.-T. (2015). Caveolin-1 Dependent Endocytosis Enhances the Chemosensitivity of HER-2 Positive Breast Cancer Cells to Trastuzumab Emtansine (T-DM1). PLoS ONE, 10(7), e0133072. https://doi.org/10.1371/journal.pone.0133072

344. Abulrob, A., Giuseppin, S., Andrade, M. F., McDermid, A., Moreno, M., & Stanimirovic, D. (2004). Interactions of EGFR and caveolin-1 in human glioblastoma cells: Evidence that tyrosine phosphorylation regulates EGFR association with caveolae. Oncogene, 23(41), Article 41. https://doi.org/10.1038/sj.onc.1207911

345. Ivan, M., Harris, A. L., Martelli, F., & Kulshreshtha, R. (2008). Hypoxia response and microRNAs: No longer two separate worlds. Journal of Cellular and Molecular Medicine, 12(5a), 1426–1431. https://doi.org/10.1111/j.1582-4934.2008.00398.x

346. Paterson, E., Blenkiron, C., Danielson, K., & Henry, C. (2022). Recommendations for extracellular vesicle miRNA biomarker research in the endometrial cancer context. Translational Oncology, 23, 101478. https://doi.org/10.1016/j.tranon.2022.101478

347. Buschmann, D., Kirchner, B., Hermann, S., Märte, M., Wurmser, C., Brandes, F., Kotschote, S., Bonin, M., Steinlein, O. K., Pfaffl, M. W., Schelling, G., & Reithmair, M. (2018). Evaluation of serum extracellular vesicle isolation methods for profiling miRNAs by next-generation sequencing. Journal of Extracellular Vesicles, 7(1), 1481321. https://doi.org/10.1080/20013078.2018.1481321

348. Xiang, M., Zeng, Y., Yang, R., Xu, H., Chen, Z., Zhong, J., Xie, H., Xu, Y., & Zeng, X. (2014). U6 is not a suitable endogenous control for the quantification of circulating microRNAs. Biochemical and Biophysical Research Communications, 454(1), 210–214. https://doi.org/10.1016/j.bbrc.2014.10.064

349. Breslin, S., & O'Driscoll, L. (2016). The relevance of using 3D cell cultures, in addition to 2D monolayer cultures, when evaluating breast cancer drug sensitivity and resistance. Oncotarget, 7(29), 45745–45756. https://doi.org/10.18632/oncotarget.9935

350. Gudbergsson, J. M., Johnsen, K. B., Skov, M. N., & Duroux, M. (2016). Systematic review of factors influencing extracellular vesicle yield from cell cultures. Cytotechnology, 68(4), 579–592. https://doi.org/10.1007/s10616-015-9913-6

351. Jensen, C., & Teng, Y. (2020). Is It Time to Start Transitioning From 2D to 3D Cell Culture? Frontiers in Molecular Biosciences, 7, 33. https://doi.org/10.3389/fmolb.2020.00033

352. Duval, K., Grover, H., Han, L.-H., Mou, Y., Pegoraro, A. F., Fredberg, J., & Chen, Z. (2017). Modeling Physiological Events in 2D vs. 3D Cell Culture. Physiology (Bethesda, Md.), 32(4), 266–277. https://doi.org/10.1152/physiol.00036.2016

353. Vidi, P.-A., Bissell, M. J., & Lelièvre, S. A. (2013). Three-dimensional culture of human breast epithelial cells: The how and the why. Methods in Molecular Biology (Clifton, N.J.), 945, 193–219. https://doi.org/10.1007/978-1-62703-125-7_13

354. Nath, S., & Devi, G. R. (2016). Three-dimensional culture systems in cancer research: Focus on tumor spheroid model. Pharmacology & Therapeutics, 163, 94–108. https://doi.org/10.1016/j.pharmthera.2016.03.013

355. Abdollahi, S. (2021). Extracellular vesicles from organoids and 3D culture systems. Biotechnology and Bioengineering, 118(3), 1029–1049. https://doi.org/10.1002/bit.27606

356. Yan, L., & Wu, X. (2020). Exosomes produced from 3D cultures of umbilical cord mesenchymal stem cells in a hollow-fiber bioreactor show improved osteochondral regeneration activity. Cell Biology and Toxicology, 36(2), 165–178. https://doi.org/10.1007/s10565-019-09504-5

357. Farhat, J., Pandey, I., & AlWahsh, M. (2021). Transcending toward Advanced 3D-Cell Culture Modalities: A Review about an Emerging Paradigm

in Translational Oncology. Cells, 10(7), Article 7. https://doi.org/10.3390/cells10071657

358. Kyykallio, H., Faria, A. V. S., Hartmann, R., Capra, J., Rilla, K., & Siljander, P. R.-M. (2022). A quick pipeline for the isolation of 3D cell culture-derived extracellular vesicles. Journal of Extracellular Vesicles, 11(10), 12273. https://doi.org/10.1002/jev2.12273

359. Riss, T., & Trask, O. J. (2021). Factors to consider when interrogating 3D culture models with plate readers or automated microscopes. In Vitro Cellular & Developmental Biology. Animal, 57(2), 238–256. https://doi.org/10.1007/s11626-020-00537-3

360. Limraksasin, P., Okawa, H., Zhang, M., Kondo, T., Osathanon, T., Pavasant, P., & Egusa, H. (2020). Size-Optimized Microspace Culture Facilitates Differentiation of Mouse Induced Pluripotent Stem Cells into Osteoid-Rich Bone Constructs. Stem Cells International, 2020, 7082679. https://doi.org/10.1155/2020/7082679

361. Froehlich, K., Haeger, J.-D., Heger, J., Pastuschek, J., Photini, S. M., Yan, Y., Lupp, A., Pfarrer, C., Mrowka, R., Schleußner, E., Markert, U. R., & Schmidt, A. (2016). Generation of Multicellular Breast Cancer Tumor Spheroids: Comparison of Different Protocols. Journal of Mammary Gland Biology and Neoplasia, 21(3–4), 89–98. https://doi.org/10.1007/s10911-016-9359-2

362. Flörkemeier, I., Steinhauer, T. N., Hedemann, N., Weimer, J. P., Rogmans, C., van Mackelenbergh, M. T., Maass, N., Clement, B., & Bauerschlag, D. O. (2022). High Antitumor Activity of the Dual Topoisomerase Inhibitor P8-D6 in Breast Cancer. Cancers, 14(1), Article 1. https://doi.org/10.3390/cancers14010002

363. Wang, A., Madden, L. A., & Paunov, V. N. (2020). Advanced biomedical applications based on emerging 3D cell culturing platforms. Journal of Materials Chemistry B, 8(46), 10487–10501. https://doi.org/10.1039/D0TB01658F

364. Temple, J., Velliou, E., Shehata, M., Lévy, R., & Gupta, P. (2022). Current strategies with implementation of three-dimensional cell culture: The challenge of quantification. Interface Focus, 12(5), 20220019. https://doi.org/10.1098/rsfs.2022.0019

365. Metzger, W., Rösch, B., Sossong, D., Bubel, M., & Pohlemann, T. (2021). Flow cytometric quantification of apoptotic and proliferating cells applying an improved method for dissociation of spheroids. Cell Biology International, 45(8), 1633–1643. https://doi.org/10.1002/cbin.11618

366. Paniushkina, L., Grueso-Navarro, E., Cheng, X., & Nazarenko, I. (2020). Chapter Twelve—Three-dimensional cell models for extracellular vesicles production, isolation, and characterization. In S. Spada & L. Galluzzi (Eds.), Methods in Enzymology (Vol. 645, pp. 209–230). Academic Press. https://doi.org/10.1016/bs.mie.2020.09.005

367. Patel, D. B., Gray, K. M., Santharam, Y., Lamichhane, T. N., Stroka, K. M., & Jay, S. M. (2017). Impact of cell culture parameters on production and vascularization bioactivity of mesenchymal stem cell-derived extracellular vesicles. Bioengineering & Translational Medicine, 2(2), 170–179. https://doi.org/10.1002/btm2.10065

368. Rocha, S., Carvalho, J., Oliveira, P., Voglstaetter, M., Schvartz, D., Thomsen, A. R., Walter, N., Khanduri, R., Sanchez, J.-C., Keller, A., Oliveira, C., & Nazarenko, I. (2019). 3D Cellular Architecture Affects MicroRNA and Protein Cargo of Extracellular Vesicles. Advanced Science (Weinheim, Baden-Wurttemberg, Germany), 6(4), 1800948. https://doi.org/10.1002/advs.201800948

369. Villasante, A., Marturano-Kruik, A., Ambati, S. R., Liu, Z., Godier-Furnemont, A., Parsa, H., Lee, B. W., Moore, M. A. S., & Vunjak-Novakovic, G. (2016). Recapitulating the Size and Cargo of Tumor Exosomes in a Tissue-Engineered Model. Theranostics, 6(8), 1119–1130. https://doi.org/10.7150/thno.13944

370. Ivascu, A., & Kubbies, M. (2006). Rapid Generation of Single-Tumor Spheroids for High-Throughput Cell Function and Toxicity Analysis. Journal of Biomolecular Screening, 11(8), 922–932. https://doi.org/10.1177/1087057106292763

371. Pickl, M., & Ries, C. H. (2009). Comparison of 3D and 2D tumor models reveals enhanced HER2 activation in 3D associated with an increased response to trastuzumab. Oncogene, 28(3), Article 3. https://doi.org/10.1038/onc.2008.394

372. Tian, X., Wang, W., Zhang, Q., Zhao, L., Wei, J., Xing, H., Song, Y., Wang, S., Ma, D., Meng, L., & Chen, G. (2010). Hypoxia-inducible factor-1α enhances the malignant phenotype of multicellular spheroid HeLa cells in vitro. Oncology Letters, 1(5), 893–897. https://doi.org/10.3892/ol_00000159

373. Ebright, R. Y., Zachariah, M. A., Micalizzi, D. S., Wittner, B. S., Niederhoffer, K. L., Nieman, L. T., Chirn, B., Wiley, D. F., Wesley, B., Shaw, B., Nieblas-Bedolla, E., Atlas, L., Szabolcs, A., Iafrate, A. J., Toner, M., Ting, D. T., Brastianos, P. K., Haber, D. A., & Maheswaran, S. (2020). HIF1A signaling

selectively supports proliferation of breast cancer in the brain. Nature Communications, 11(1), Article 1. https://doi.org/10.1038/s41467-020-20144-w

374. Cai, K., Jiang, L., Wang, J., Zhang, H., Wang, X., Cheng, D., & Dou, J. (2014). Downregulation of β-catenin decreases the tumorigenicity, but promotes epithelial-mesenchymal transition in breast cancer cells. Journal of Cancer Research and Therapeutics, 10(4), 1063–1070. https://doi.org/10.4103/0973-1482.139378

375. Lorico, A., Lorico-Rappa, M., Karbanová, J., Corbeil, D., & Pizzorno, G. (2021). CD9, a tetraspanin target for cancer therapy? Experimental Biology and Medicine, 246(9), 1121–1138. https://doi.org/10.1177/1535370220981855

376. Miyake, M., Nakano, K., Itoi, S. I., Koh, T., & Taki, T. (1996). Motility-related protein-1 (MRP-1/CD9) reduction as a factor of poor prognosis in breast cancer. Cancer Research, 56(6), 1244–1249.

377. Mimori, K., Kataoka, A., Yoshinaga, K., Ohta, M., Sagara, Y., Yoshikawa, Y., Ohno, S., Barnard, G. F., & Mori, M. (2005). Identification of molecular markers for metastasis-related genes in primary breast cancer cells. Clinical & Experimental Metastasis, 22(1), 59–67. https://doi.org/10.1007/s10585-005-4417-y

378. Huang, C. I., Kohno, N., Ogawa, E., Adachi, M., Taki, T., & Miyake, M. (1998). Correlation of reduction in MRP-1/CD9 and KAI1/CD82 expression with recurrences in breast cancer patients. The American Journal of Pathology, 153(3), 973–983. https://doi.org/10.1016/s0002-9440(10)65639-8

379. Bhattacharya, S., Calar, K., Evans, C., Petrasko, M., & de la Puente, P. (2020). Bioengineering the Oxygen-Deprived Tumor Microenvironment Within a Three-Dimensional Platform for Studying Tumor-Immune Interactions. Frontiers in Bioengineering and Biotechnology, 8, 1040. https://doi.org/10.3389/fbioe.2020.01040

380. Szvicsek, Z., Oszvald, Á., Szabó, L., Sándor, G. O., Kelemen, A., Soós, A. Á., Pálóczi, K., Harsányi, L., Tölgyes, T., Dede, K., Bursics, A., Buzás, E. I., Zeöld, A., & Wiener, Z. (2019). Extracellular vesicle release from intestinal organoids is modulated by Apc mutation and other colorectal cancer progression factors. Cellular and Molecular Life Sciences: CMLS, 76(12), 2463–2476. https://doi.org/10.1007/s00018-019-03052-1

381. Kapałczyńska, M., Kolenda, T., Przybyła, W., Zajączkowska, M., Teresiak, A., Filas, V., Ibbs, M., Bliźniak, R., Łuczewski, Ł., & Lamperska, K. (2016). 2D and 3D cell cultures – a comparison of different types of cancer cell cultures. Archives of Medical Science. https://doi.org/10.5114/aoms.2016.63743

382. Bissell, M. J., Kenny, P. A., & Radisky, D. C. (2005). Microenvironmental regulators of tissue structure and function also regulate tumor induction and progression: The role of extracellular matrix and its degrading enzymes. Cold Spring Harbor Symposia on Quantitative Biology, 70, 343–356. https://doi.org/10.1101/sqb.2005.70.013

383. Nelson, C. M., & Bissell, M. J. (2006). Of extracellular matrix, scaffolds, and signaling: Tissue architecture regulates development, homeostasis, and cancer. Annual Review of Cell and Developmental Biology, 22, 287–309. https://doi.org/10.1146/annurev.cellbio.22.010305.104315

384. Bissell, M. J. (2007). Architecture Is the Message: The role of extracellular matrix and 3-D structure in tissue-specific gene expression and breast cancer. The Pezcoller Foundation Journal: News from the Pezcoller Foundation World, 16(29), 2–17.

385. Spencer, V. A., Xu, R., & Bissell, M. J. (2007). Extracellular Matrix, Nuclear and Chromatin Structure, and Gene Expression in Normal Tissues and Malignant Tumors: A Work in Progress. Advances in Cancer Research, 97, 275–294. https://doi.org/10.1016/S0065-230X(06)97012-2

386. Sugawa-Shimada, A. (2020). Emerging "2.5-dimensional" Culture: Character-oriented Cultural Practices and "Community of Preferences" as a New Fandom in Japan and Beyond. Mechademia, 12(2), 124–139.

387. Halldorsson, S., Lucumi, E., Gómez-Sjöberg, R., & Fleming, R. M. T. (2015). Advantages and challenges of microfluidic cell culture in polydimethylsiloxane devices. Biosensors and Bioelectronics, 63, 218–231. https://doi.org/10.1016/j.bios.2014.07.029

388. Ho, W. J., Pham, E. A., Kim, J. W., Ng, C. W., Kim, J. H., Kamei, D. T., & Wu, B. M. (2010). Incorporation of multicellular spheroids into 3-D polymeric scaffolds provides an improved tumor model for screening anticancer drugs. Cancer Science, 101(12), 2637–2643. https://doi.org/10.1111/j.1349-7006.2010.01723.x

389. Miki, Y., Ono, K., Hata, S., Suzuki, T., Kumamoto, H., & Sasano, H. (2012). The advantages of co-culture over mono cell culture in simulating in vivo environment. The Journal of Steroid Biochemistry and Molecular Biology, 131(3–5), 68–75. https://doi.org/10.1016/j.jsbmb.2011.12.004

390. Kunz-Schughart, L. A., Freyer, J. P., Hofstaedter, F., & Ebner, R. (2004). The use of 3-D cultures for high-throughput screening: The multicellular spheroid model. Journal of Biomolecular Screening, 9(4), 273–285. https://doi.org/10.1177/1087057104265040

391. Jean-Quartier, C., Jeanquartier, F., Jurisica, I., & Holzinger, A. (2018). In silico cancer research towards 3R. BMC Cancer, 18(1), 408. https://doi.org/10.1186/s12885-018-4302-0

392. Karolak, A., Markov, D. A., McCawley, L. J., & Rejniak, K. A. (2018). Towards personalized computational oncology: From spatial models of tumour spheroids, to organoids, to tissues. Journal of The Royal Society Interface, 15(138), 20170703. https://doi.org/10.1098/rsif.2017.0703

393. Mak, I. W., Evaniew, N., & Ghert, M. (2014). Lost in translation: Animal models and clinical trials in cancer treatment. American Journal of Translational Research, 6(2), 114–118.

394. Ekert, J. E., Deakyne, J., Pribul-Allen, P., Terry, R., Schofield, C., Jeong, C. G., Storey, J., Mohamet, L., Francis, J., Naidoo, A., Amador, A., Klein, J.-L., & Rowan, W. (2020). Recommended Guidelines for Developing, Qualifying, and Implementing Complex In Vitro Models (CIVMs) for Drug Discovery. SLAS DISCOVERY: Advancing the Science of Drug Discovery, 25(10), 1174–1190. https://doi.org/10.1177/2472555220923332

395. Schlam, I., & Swain, S. M. (2021). HER2-positive breast cancer and tyrosine kinase inhibitors: The time is now. NPJ Breast Cancer, 7, 56. https://doi.org/10.1038/s41523-021-00265-1

396. Rugo, H. S., Im, S.-A., Cardoso, F., Cortés, J., Curigliano, G., Musolino, A., Pegram, M. D., Wright, G. S., Saura, C., Escrivá-de-Romaní, S., De Laurentiis, M., Levy, C., Brown-Glaberman, U., Ferrero, J.-M., de Boer, M., Kim, S.-B., Petráková, K., Yardley, D. A., Freedman, O., … SOPHIA Study Group. (2021). Efficacy of Margetuximab vs Trastuzumab in Patients With Pretreated ERBB2-Positive Advanced Breast Cancer: A Phase 3 Randomized Clinical Trial. JAMA Oncology, 7(4), 573–584. https://doi.org/10.1001/jamaoncol.2020.7932

397. Dungo, R. T., & Keating, G. M. (2013). Afatinib: First global approval. Drugs, 73(13), 1503–1515. https://doi.org/10.1007/s40265-013-0111-6

398. Wu, Z., Wang, J., You, F., Li, X., & Xiao, C. (2023). The role of irreversible pan-HER tyrosine kinase inhibitors in the treatment of HER2-Positive metastatic breast cancer. Frontiers in Pharmacology, 14. https://www.frontiersin.org/articles/10.3389/fphar.2023.1142087

399. Xu, B., Yan, M., Ma, F., Hu, X., Feng, J., Ouyang, Q., Tong, Z., Li, H., Zhang, Q., Sun, T., Wang, X., Yin, Y., Cheng, Y., Li, W., Gu, Y., Chen, Q., Liu, J., Cheng, J., Geng, C., … PHOEBE Investigators. (2021). Pyrotinib plus capecitabine versus lapatinib plus capecitabine for the treatment of HER2-

positive metastatic breast cancer (PHOEBE): A multicentre, open-label, randomised, controlled, phase 3 trial. The Lancet. Oncology, 22(3), 351–360. https://doi.org/10.1016/S1470-2045(20)30702-6

400. Curigliano, G., Mueller, V., Borges, V., Hamilton, E., Hurvitz, S., Loi, S., Murthy, R., Okines, A., Paplomata, E., Cameron, D., Carey, L. A., Gelmon, K., Hortobagyi, G. N., Krop, I., Loibl, S., Pegram, M., Slamon, D., Ramos, J., Feng, W., & Winer, E. (2022). Tucatinib versus placebo added to trastuzumab and capecitabine for patients with pretreated HER2+ metastatic breast cancer with and without brain metastases (HER2CLIMB): Final overall survival analysis. Annals of Oncology: Official Journal of the European Society for Medical Oncology, 33(3), 321–329. https://doi.org/10.1016/j.annonc.2021.12.005

401. Sirhan, Z., Thyagarajan, A., & Sahu, R. P. (2022). The efficacy of tucatinib-based therapeutic approaches for HER2-positive breast cancer. Military Medical Research, 9, 39. https://doi.org/10.1186/s40779-022-00401-3

402. Wu, X., Yang, H., Yu, X., & Qin, J.-J. (2022). Drug-resistant HER2-positive breast cancer: Molecular mechanisms and overcoming strategies. Frontiers in Pharmacology, 13. https://www.frontiersin.org/articles/10.3389/fphar.2022.1012552

403. de Melo Gagliato, D., Leonardo Fontes Jardim, D., Marchesi, M. S. P., & Hortobagyi, G. N. (2016). Mechanisms of resistance and sensitivity to anti-HER2 therapies in HER2+ breast cancer. Oncotarget, 7(39), 64431–64446. https://doi.org/10.18632/oncotarget.7043

404. Berns, K., Horlings, H. M., Hennessy, B. T., Madiredjo, M., Hijmans, E. M., Beelen, K., Linn, S. C., Gonzalez-Angulo, A. M., Stemke-Hale, K., Hauptmann, M., Beijersbergen, R. L., Mills, G. B., van de Vijver, M. J., & Bernards, R. (2007). A functional genetic approach identifies the PI3K pathway as a major determinant of trastuzumab resistance in breast cancer. Cancer Cell, 12(4), 395–402. https://doi.org/10.1016/j.ccr.2007.08.030

405. Veeraraghavan, J., Mistry, R., Nanda, S., Sethunath, V., Shea, M., Mitchell, T., Anurag, M., Mancini, M. A., Stossi, F., Osborne, C. K., Rimawi, M. F., & Schiff, R. (2020). Abstract 1911: HER2 L755S mutation is associated with acquired resistance to lapatinib and neratinib, and confers cross-resistance to tucatinib in HER2-positive breast cancer models. Cancer Research, 80(16_Supplement), 1911. https://doi.org/10.1158/1538-7445.AM2020-1911

406. Bandari, S. K., Tripathi, K., Rangarajan, S., & Sanderson, R. D. (2020). Therapy-induced chemoexosomes: Sinister small extracellular vesicles that

support tumor survival and progression. Cancer Letters, 493, 113–119.
https://doi.org/10.1016/j.canlet.2020.08.022

407. Lv, L.-H., Wan, Y.-L., Lin, Y., Zhang, W., Yang, M., Li, G.-L., Lin, H.-M.,
Shang, C.-Z., Chen, Y.-J., & Min, J. (2012). Anticancer Drugs Cause Release of
Exosomes with Heat Shock Proteins from Human Hepatocellular Carcinoma
Cells That Elicit Effective Natural Killer Cell Antitumor Responses in Vitro. The
Journal of Biological Chemistry, 287(19), 15874–15885.
https://doi.org/10.1074/jbc.M112.340588

408. Kreger, B. T., Johansen, E. R., Cerione, R. A., & Antonyak, M. A. (2016).
The Enrichment of Survivin in Exosomes from Breast Cancer Cells Treated with
Paclitaxel Promotes Cell Survival and Chemoresistance. Cancers, 8(12), 111.
https://doi.org/10.3390/cancers8120111

409. Wang, X., Qiao, D., Chen, L., Xu, M., Chen, S., Huang, L., Wang, F.,
Chen, Z., Cai, J., & Fu, L. (2019). Chemotherapeutic drugs stimulate the
release and recycling of extracellular vesicles to assist cancer cells in
developing an urgent chemoresistance. Molecular Cancer, 18(1), 182.
https://doi.org/10.1186/s12943-019-1114-z

410. Vera, N., Acuña-Gallardo, S., Grünenwald, F., Caceres-Verschae, A.,
Realini, O., Acuña, R., Lladser, A., Illanes, S. E., & Varas-Godoy, M. (2019).
Small Extracellular Vesicles Released from Ovarian Cancer Spheroids in
Response to Cisplatin Promote the Pro-Tumorigenic Activity of Mesenchymal
Stem Cells. International Journal of Molecular Sciences, 20(20), 4972.
https://doi.org/10.3390/ijms20204972

411. O'Brien, N. A., Browne, B. C., Chow, L., Wang, Y., Ginther, C., Arboleda,
J., Duffy, M. J., Crown, J., O'Donovan, N., & Slamon, D. J. (2010). Activated
Phosphoinositide 3-Kinase/AKT Signaling Confers Resistance to Trastuzumab
but not Lapatinib. Molecular Cancer Therapeutics, 9(6), 1489–1502.
https://doi.org/10.1158/1535-7163.MCT-09-1171

412. Beetler, D. J., Di Florio, D. N., Bruno, K. A., Ikezu, T., March, K. L.,
Cooper, L. T., Wolfram, J., & Fairweather, D. (2023). Extracellular vesicles as
personalized medicine. Molecular Aspects of Medicine, 91, 101155.
https://doi.org/10.1016/j.mam.2022.101155

413. Lone, S. N., Nisar, S., Masoodi, T., Singh, M., Rizwan, A., Hashem, S., El-
Rifai, W., Bedognetti, D., Batra, S. K., Haris, M., Bhat, A. A., & Macha, M. A.
(2022). Liquid biopsy: A step closer to transform diagnosis, prognosis and
future of cancer treatments. Molecular Cancer, 21(1), 79.
https://doi.org/10.1186/s12943-022-01543-7

414. Shang, M., Ji, J. S., Song, C., Gao, B. J., Jin, J. G., Kuo, W. P., & Kang, H. (2017). Extracellular Vesicles: A Brief Overview and Its Role in Precision Medicine. In W. P. Kuo & S. Jia (Eds.), Extracellular Vesicles: Methods and Protocols (pp. 1–14). Springer. https://doi.org/10.1007/978-1-4939-7253-1_1

415. Yates, A. G., Pink, R. C., Erdbrügger, U., Siljander, P. R.-M., Dellar, E. R., Pantazi, P., Akbar, N., Cooke, W. R., Vatish, M., Dias-Neto, E., Anthony, D. C., & Couch, Y. (2022). In sickness and in health: The functional role of extracellular vesicles in physiology and pathology in vivo: Part I: Health and Normal Physiology: Part I: Health and Normal Physiology. Journal of Extracellular Vesicles, 11(1), e12151. https://doi.org/10.1002/jev2.12151

416. Pan, S., Zhang, Y., Natalia, A., Lim, C. Z. J., Ho, N. R. Y., Chowbay, B., Loh, T. P., Tam, J. K. C., & Shao, H. (2021). Extracellular vesicle drug occupancy enables real-time monitoring of targeted cancer therapy. Nature Nanotechnology, 16(6), 734–742. https://doi.org/10.1038/s41565-021-00872-w

417. Wang, J., Wuethrich, A., Sina, A. A. I., Lane, R. E., Lin, L. L., Wang, Y., Cebon, J., Behren, A., & Trau, M. (2020). Tracking extracellular vesicle phenotypic changes enables treatment monitoring in melanoma. Science Advances, 6(9), eaax3223. https://doi.org/10.1126/sciadv.aax3223

418. Bister, N., Pistono, C., Huremagic, B., Jolkkonen, J., Giugno, R., & Malm, T. (2020). Hypoxia and extracellular vesicles: A review on methods, vesicular cargo and functions. Journal of Extracellular Vesicles, 10(1), e12002. https://doi.org/10.1002/jev2.12002

419. Hong, X.-Y., Wang, J., & Li, Z. (2013). AGR2 expression is regulated by HIF-1 and contributes to growth and angiogenesis of glioblastoma. Cell Biochemistry and Biophysics, 67(3), 1487–1495. https://doi.org/10.1007/s12013-013-9650-4

420. Li, Z., Zhu, Q., Hu, L., Chen, H., Wu, Z., & Li, D. (2015). Anterior gradient 2 is a binding stabilizer of hypoxia inducible factor-1α that enhances CoCl2-induced doxorubicin resistance in breast cancer cells. Cancer Science, 106(8), 1041–1049. https://doi.org/10.1111/cas.12714

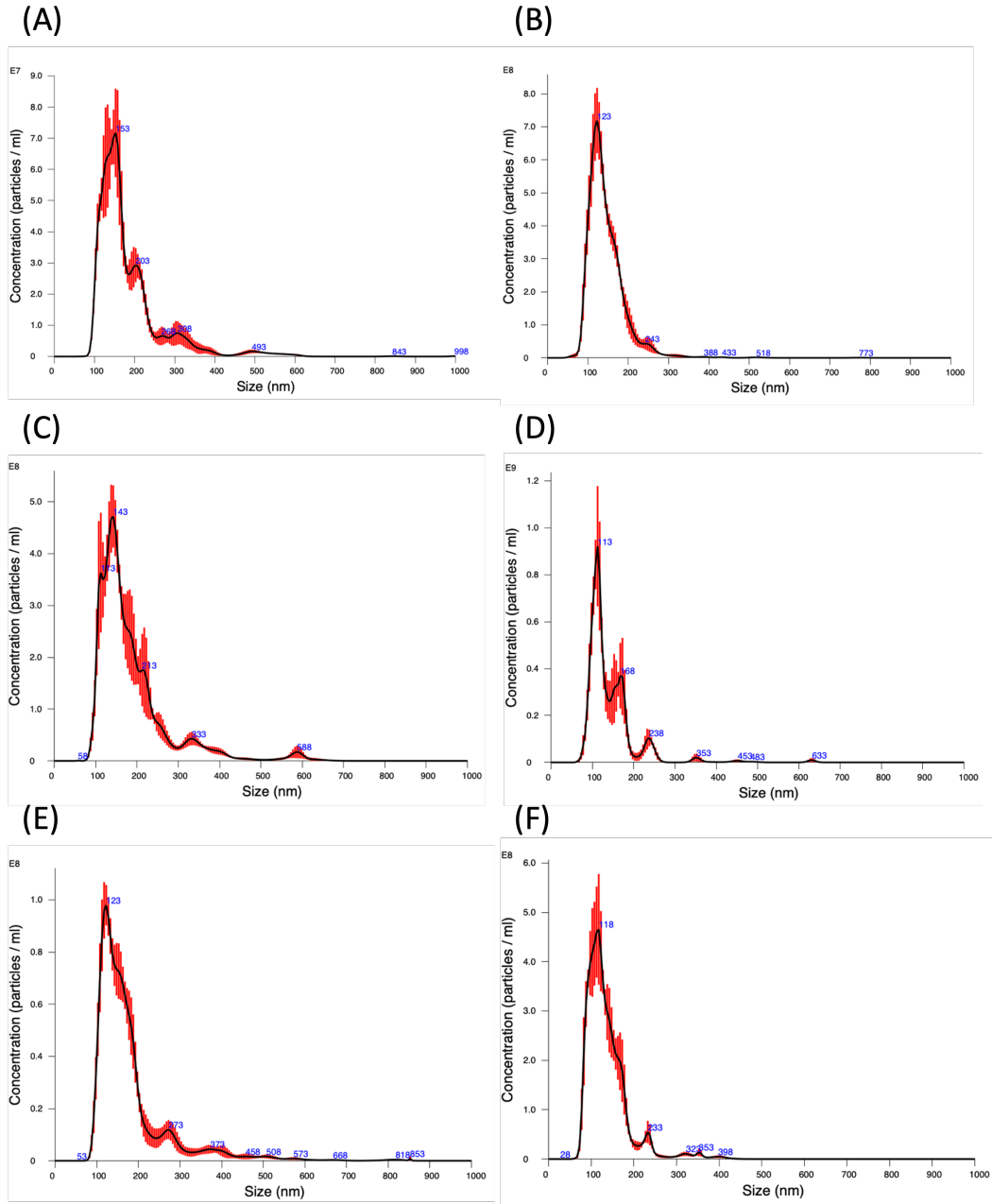# Appendix I

Chapter 2 – NTA Supplementary Data

Figure I-1. Representative nanoparticle tracking analysis (NTA) images.

EFM192A isolates obtained by (**A**) dUC and (**B**) PEG+UC; HCC1954 isolates obtained by (**C**) dUC and (**D**) PEG+UC; SKBR3 isolates obtained by (**E**) dUC and (**F**) PEG+UC.

Table I-1. Sizes and particles yield, as analysed by NTA.

	Size (nm)		
	dUC	PEG+UC	P value
EFM192A	131.7 ± 17.2	117.7 ± 7.9	ns
HCC1954	129.4 ± 8.0	119.3 ± 1.8	ns
SKBR3	125.7 ± 2.0	110.2 ± 6.0	0.04 (*)
	Particle concentration/ml starting CM		
	dUC	PEG+UC	Fold change	P value
EFM192A	$4.20 \times 10^8 \pm 6.37 \times 10^7$	$2.99 \times 10^9 \pm 3.20 \times 10^8$	6.9	0.014 (*)
HCC1954	$4.45 \times 10^9 \pm 7.08 \times 10^8$	$4.92 \times 10^9 \pm 9.30 \times 10^8$	1.11	ns
SKBR3	$1.33 \times 10^9 \pm 4.66 \times 10^8$	$3.65 \times 10^9 \pm 6.9 \times 10^8$	2.75	0.023 (*)

Data are shown as mean ± SEM of n = 3 and compared with paired t-test (*p<0.05.)

Table I-2. Comparison of relative amount of protein normalised to ml of starting conditioned medium (CM) on samples obtained by dUC versus PEG+UC.

	Relative amount of protein (µg of protein/ml starting CM)			
	dUC	PEG+UC	Fold change	P value
EFM192A	0.007 ± 0.0007	0.06 ± 0.007	8.3	0.017 (*)
HCC1954	0.010 ± 0.002	0.034 ± 0.004	3.5	0.014 (*)
SKBR3	0.028 ± 0.005	0.042 ± 0.007	1.5	0.013 (*)

Data are shown as mean ± SEM of n = 3 and compared with paired t-test (*p<0.05).

Chapter 3 – Elucidating mechanisms of resistance to neratinib in HER2+ breast cancer by proteomic profiling.

Proteins per sample
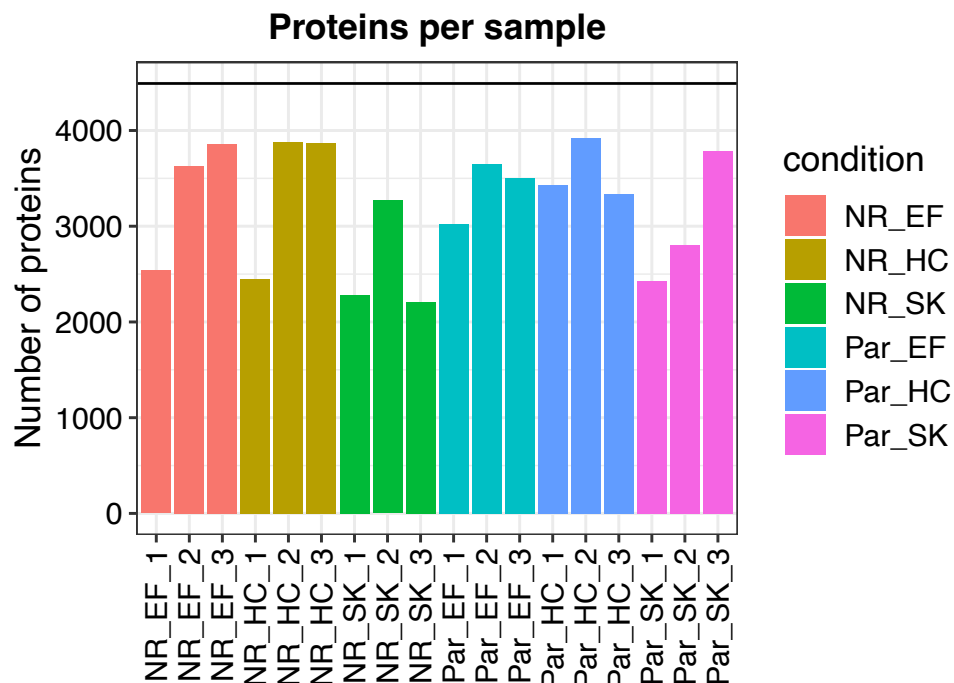
Figure II-1. Number of proteins identified per sample.

After filtering, the number of identified proteins per sample was plotted as a bar plot. NR_EF= EFM192A NR; NR_HC= HCC1954 NR; NR_SK= SKBR3 NR; Par_EF= EFM192A; Par_HC= HCC1954; Par_SK= SKBR3. Numbers (1-3) refer to each replicate.
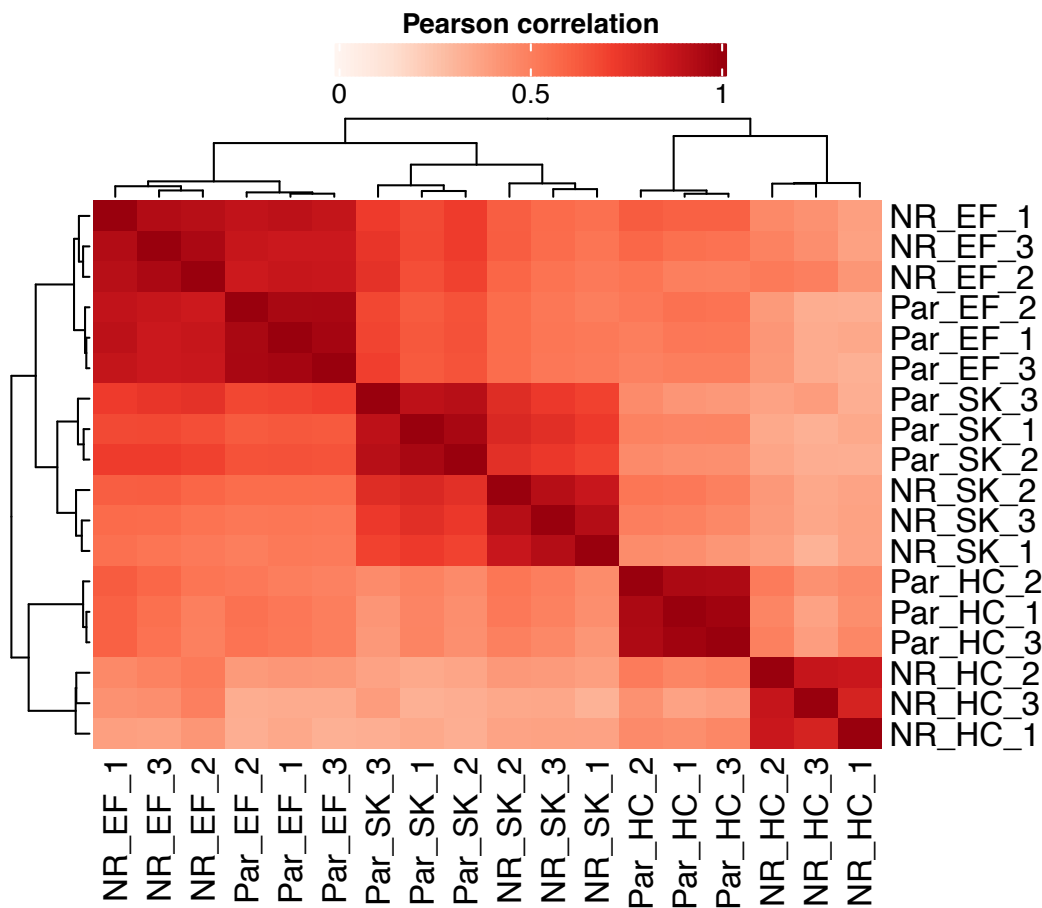
Figure II-2. Pearson correlation's heatmap.

Heatmap depicting Pearson correlations between samples, based on protein intensities. NR_EF= EFM192A NR; NR_HC= HCC1954 NR; NR_SK= SKBR3 NR; Par_EF= EFM192A; Par_HC= HCC1954; Par_SK= SKBR3. Numbers (1-3) refer to each replicate.

The heatmap representation gives an overview of all significant proteins (rows) in all samples (columns). This allows to see general trends, for instance, if one sample or replicate is different compared to the others. Additionally, the clustering of samples (columns) can indicate closer related samples and clustering of proteins (rows) indicates similarly behaving proteins. The proteins can be clustered by k-means clustering and the number of clusters can be defined by argument *k*.
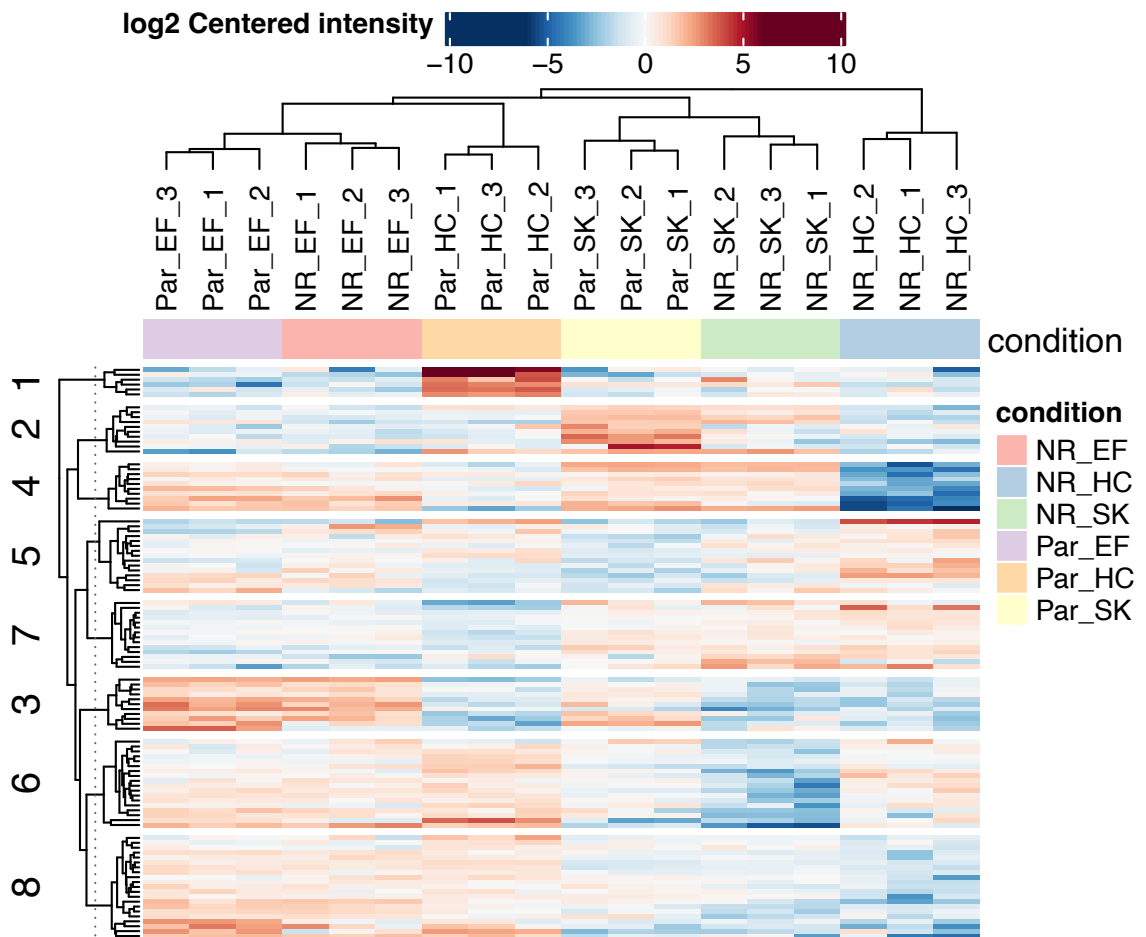
Figure II-3. Heatmap of log2 mean-centered intensity of 105 differentially expressed proteins. Proteins were clustered by *k*-means with *k*=8. Hierarchical clustering was applied for the samples. NR_EF= EFM192A NR; NR_HC= HCC1954 NR; NR_SK= SKBR3 NR; Par_EF= EFM192A; Par_HC= HCC1954; Par_SK= SKBR3. Numbers (1-3) refer to each replicate.

Alternatively, a heatmap can be plotted using the contrasts, i.e., the direct sample comparisons, as columns. **Figure II-4** emphasises the fact that HCC1954 cell line variants have many biological differences with the other 2 pairs of cell lines.

v
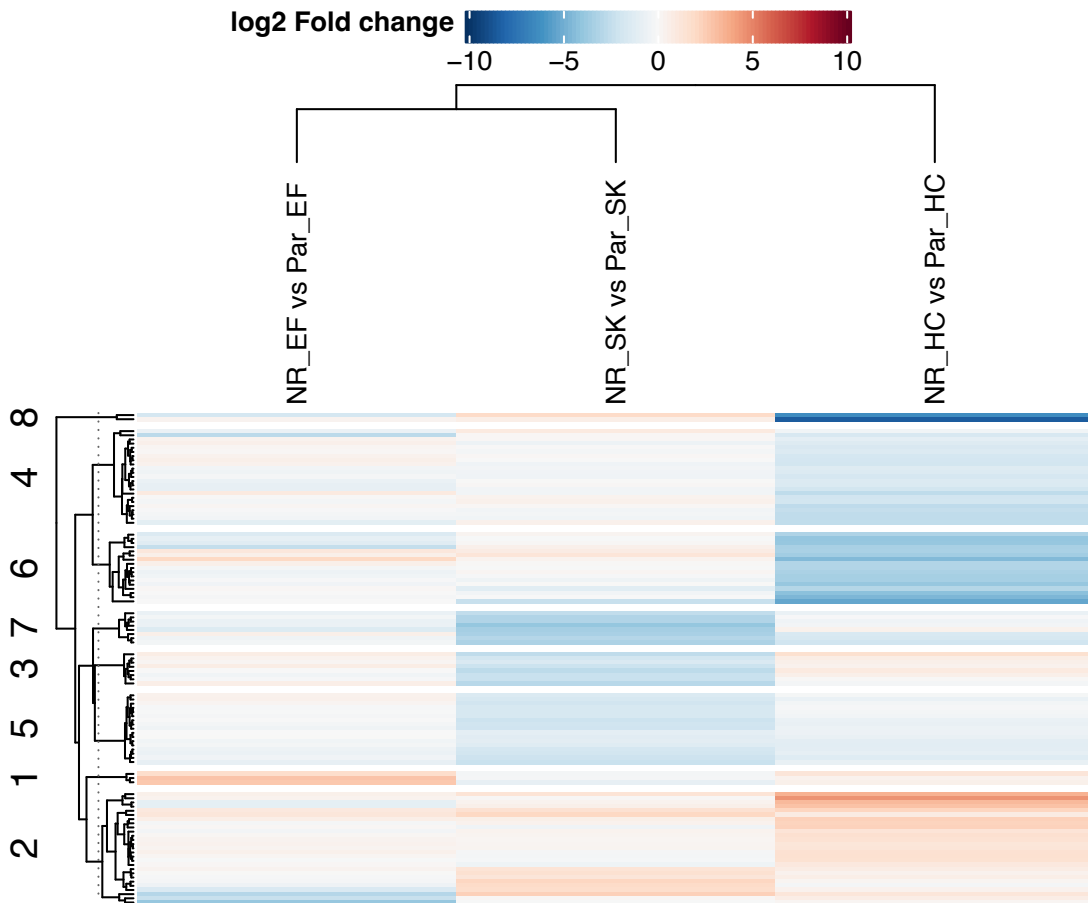
Figure II-4. Heatmap of log2 fold-change of 105 differentially expressed proteins in each condition comparison.

Proteins were clustered by *k*-means with *k*=8. Hierarchical clustering was applied for the 3 comparisons. NR_EF= EFM192A NR; NR_HC= HCC1954 NR; NR_SK= SKBR3 NR; Par_EF= EFM192A; Par_HC= HCC1954; Par_SK= SKBR3.

Figure II-5. Volcano plot for EFM192A cell line variants.

Differentially expressed proteins are highlighted in black. Dashed lines indicated fold-change cutoff. Par_EFM= EFM192A; NR_EF= EFM192A NR.

Figure II-6. Log2 centred intensity heatmap.

Heatmap depicting log2 centred intensity for each differentially expressed proteins in EFM192A cell line variants. Par_EF= EFM192A; NR_EF= EFM192A NR. Numbers refer to each replicate.

Table II-1. Differentially expressed proteins in EFM192A NR cell variant compared to EFM192A neratinib-sensitive counterpart.

Down-regulated in EFM192A NR	Up-regulated in EFM192A NR
MYL9	TRMT6
ZADH2	DNTTIP1
TTC19	
WIPF2	MPHOSPH8

Biological process

- regulation of DNA methylation (GO:0044030)
- mRNA methylation (GO:0080009)
- mitochondrial respiratory chain complex III assembly (GO:0034551)
- regulation of muscle system process (GO:0090257)
- respiratory chain complex III assembly (GO:0017062)
- mitochondrial respiratory chain complex III biogenesis (GO:0097033)
- positive regulation of actin nucleation (GO:0051127)
- mRNA modification (GO:0016556)
- regulation of actin nucleation (GO:0051125)
- cortical actin cytoskeleton organization (GO:0030866)

Cellular component

- endocytic patch (GO:0061645)
- actin cortical patch (GO:0030479)
- nuclear nucleosome (GO:0000788)
- nuclear heterochromatin (GO:0005720)
- heterochromatin (GO:0000792)
- cortical actin cytoskeleton (GO:0030864)
- actin filament (GO:0005884)
- nucleolus (GO:0005730)
- microbody (GO:0042579)
- peroxisome (GO:0005777)

Molecular function

- methylation–dependent protein binding (GO:0140034)
- methylated histone binding (GO:0035064)
- oxidoreductase activity, acting on the CH–OH group of donors, NAD or NADP as acceptor (GO:0016616)
- actin filament binding (GO:0051015)
- actin binding (GO:0003779)
- ubiquitin protein ligase binding (GO:0031625)
- ubiquitin–like protein ligase binding (GO:0044389)
- ubiquitin–protein transferase activity (GO:0004842)
- protein homodimerization activity (GO:0042803)
- DNA binding (GO:0003677)

KEGG pathways

- Leukocyte transendothelial migration
- Vascular smooth muscle contraction
- Oxytocin signaling pathway
- cGMP–PKG signaling pathway
- Tight junction
- Axon guidance
- Focal adhesion
- cAMP signaling pathway
- Regulation of actin cytoskeleton
- Endocytosis

Figure II-7. Gene ontologies and pathways analyses of the differentially expressed proteins in EFM192A NR compared to their neratinib-sensitive counterpart ordered by *p*-value ranking.
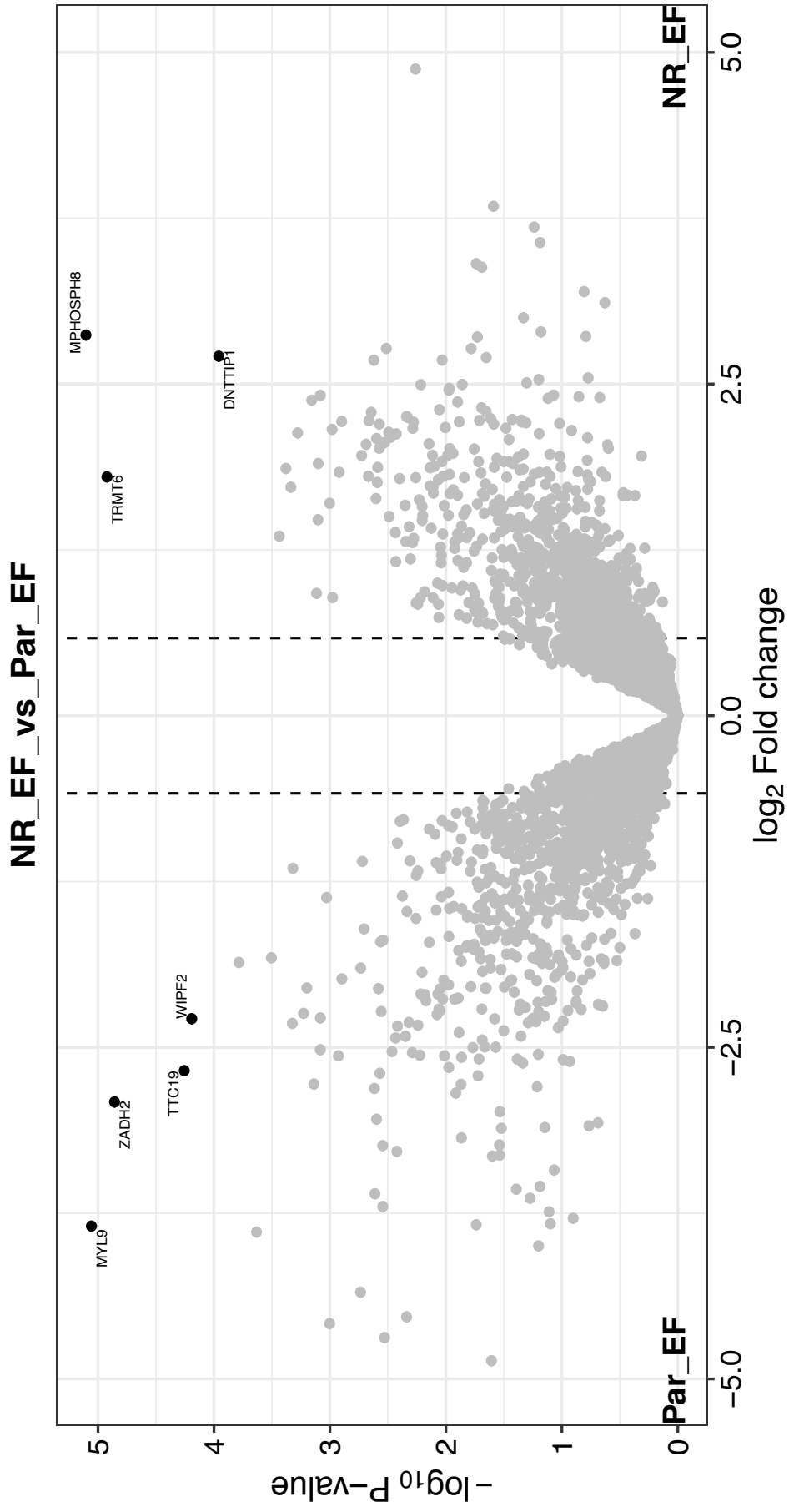
Figure II-8. Volcano plot for HCC1954 cell line variants.

Differentially expressed proteins are highlighted in black. Dashed lines indicated fold-change cutoff. Par_HC= HCC1954; NR_HC= HCC1954 NR.
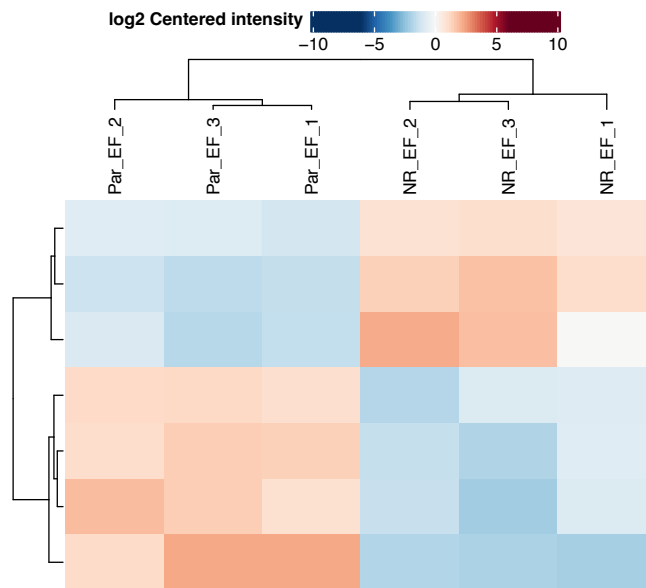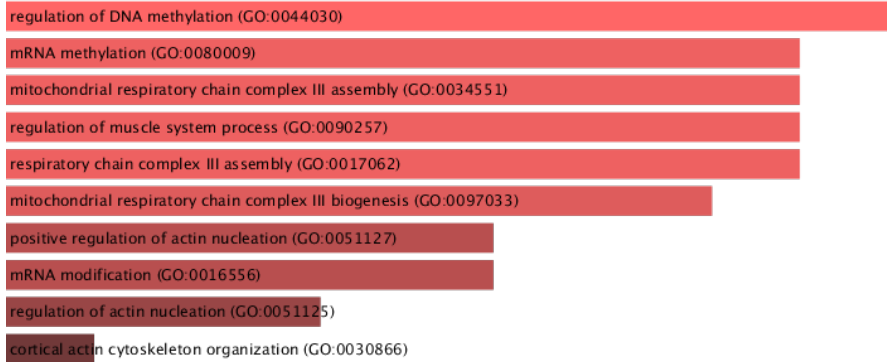
Figure II-9. Log2 centred intensity heatmap.

Heatmap depicting log2 centred intensity for each differentially expressed proteins in HCC1954 cell variants. Par_HC= HCC1954; NR_HC= HCC1954 NR. Numbers refer to each replicate.
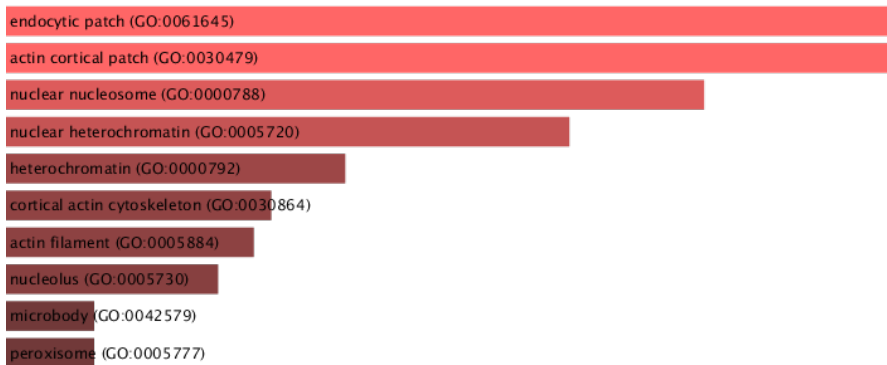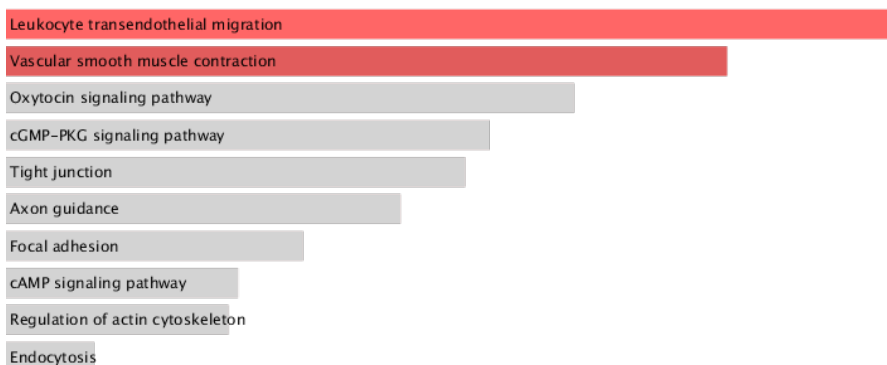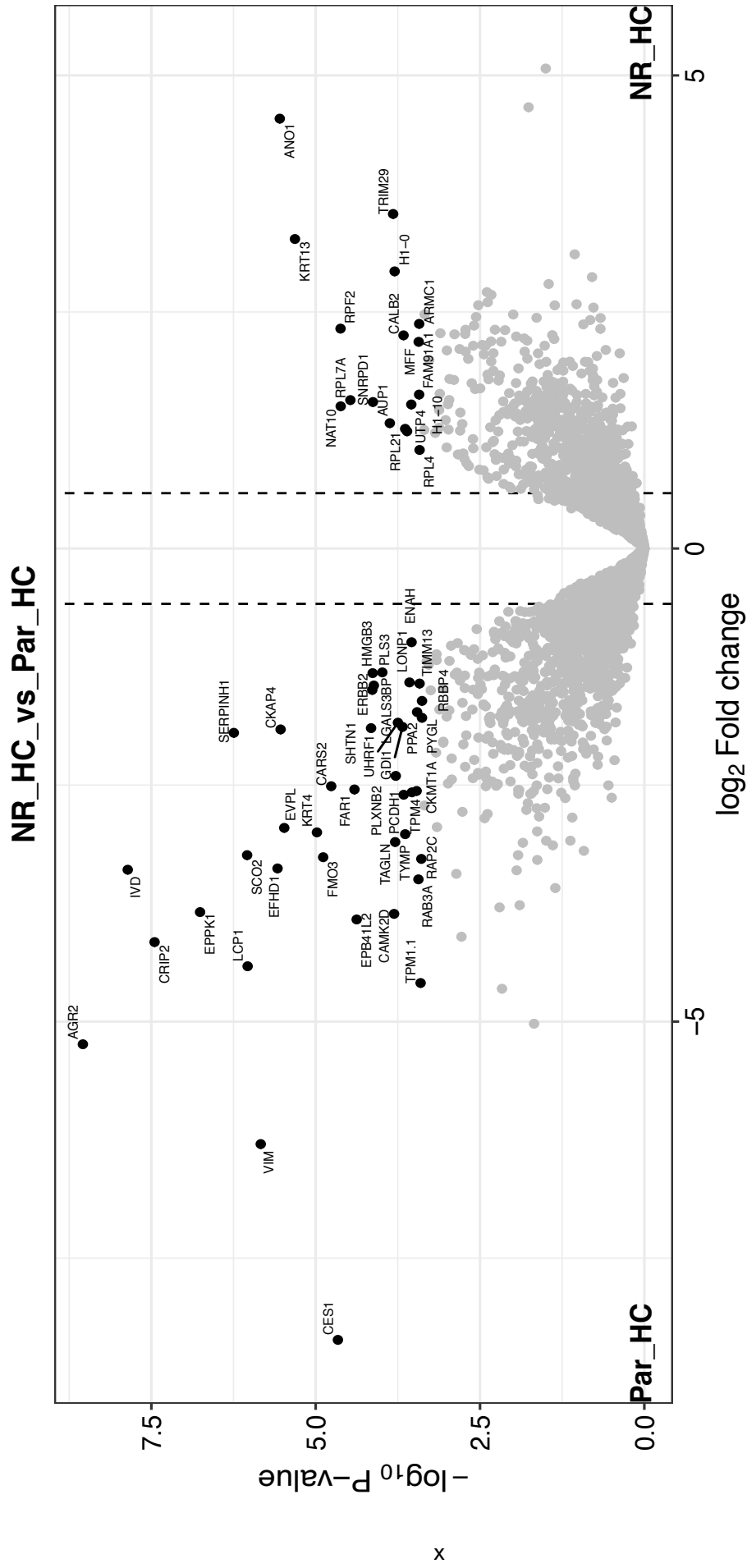
Table II-2. Differentially expressed proteins in HCC1954 NR cell variant compared to HCC1954 neratinib-sensitive counterpart.

Down-regulated in HCC1954 NR		Up-regulated in HCC1954 NR
CES1	TPM4	RPL4
VIM	CKMT1A	UTP4
AGR2	FAR1	RPL21
TPM1.1	CARS2	AUP1
LCP1	PLXNB2	NAT10
CRIP2	SERPINH1	H1-10
EPB41L2	CKAP4	SNRPD1
CAMK2D	SHTN1	RPL7A
EPPK1	GDI1	FAM91A1
RAB3A	UHRF	MFF
IVD	PYGL	CALB2
EFHD1	PPA2	RPF2
RAP2C	RBBP4	ARMC1
FMO3	ERBB2	H1-0
SCO2	LGALS3BP	KRT13
TAGLN	TIMM13	TRIM29
TYMP	LONP1	ANO1
KRT4	HMGB3	
EVPL	PLS3	
PCDH1	ENAH	

xi

Biological process

regulation of protein targeting to membrane (GO:0090313)

actin filament network formation (GO:0051639)

rRNA processing (GO:0006364)

actin crosslink formation (GO:0051764)

ribosome biogenesis (GO:0042254)

mitochondrial genome maintenance (GO:0000002)

regulation of epithelial cell proliferation (GO:0050678)

mitochondrion organization (GO:0007005)

regulation of neuron migration (GO:2001222)

maturation of LSU–rRNA (GO:0000470)

Cellular component

intermediate filament (GO:0005882)

keratin filament (GO:0045095)

cytoskeleton (GO:0005856)

intermediate filament cytoskeleton (GO:0045111)

focal adhesion (GO:0005925)

polymeric cytoskeletal fiber (GO:0099513)

actin filament (GO:0005884)

cytosolic large ribosomal subunit (GO:0022625)

large ribosomal subunit (GO:0015934)

peroxisome (GO:0005777)

Molecular function

RNA binding (GO:0003723)

phosphorylase activity (GO:0004645)

intermediate filament binding (GO:0019215)

actin filament binding (GO:0051015)

DNA polymerase binding (GO:0070182)

actin binding (GO:0003779)

protein homodimerization activity (GO:0042803)

cadherin binding (GO:0045296)

RNA polymerase I core binding (GO:0001042)

sodium channel inhibitor activity (GO:0019871)

KEGG pathways

Drug metabolism

Bladder cancer

Ribosome

Central carbon metabolism in cancer

Axon guidance

ErbB signaling pathway

Insulin secretion

HIF–1 signaling pathway

Ribosome biogenesis in eukaryotes

Glucagon signaling pathway

Figure II-10. Gene ontologies and pathways analyses of the differentially expressed proteins in HCC1954 NR compared to their neratinib-sensitive counterpart ordered by *p*-value ranking.

Figure II-11. Volcano plot for SKBR3 cell line variants.

Differentially expressed proteins are highlighted in black. Dashed lines indicated fold-change cutoff. Par_SK= SKBR3; NR_SK= SKBR3 NR.
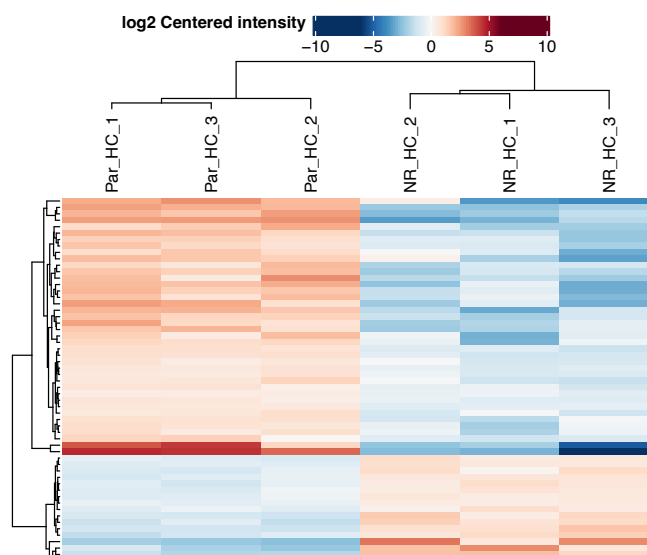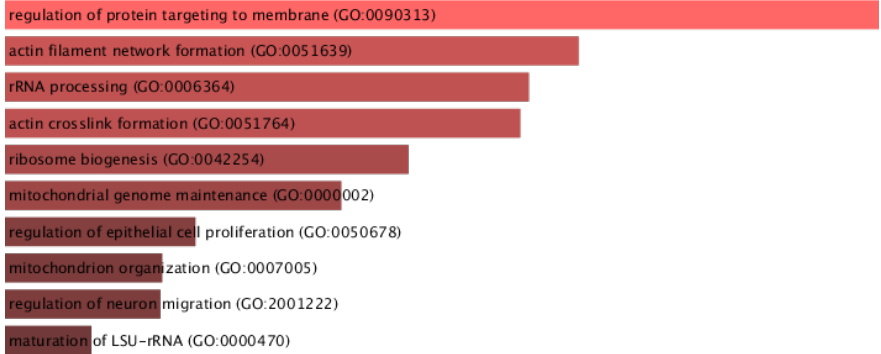
Figure II-12. Log2 centred intensity heatmap.

Heatmap depicting log2 centred intensity for each differentially expressed proteins in SKBR3 cell variants. Par_SK= SKBR3; NR_SK= SKBR3 NR. Numbers refer to each replicate.
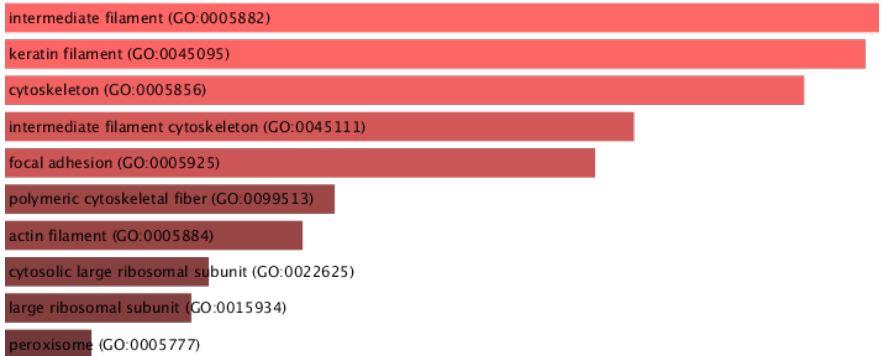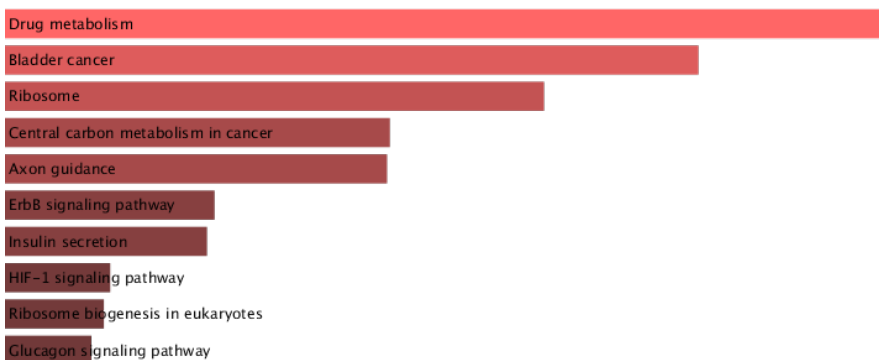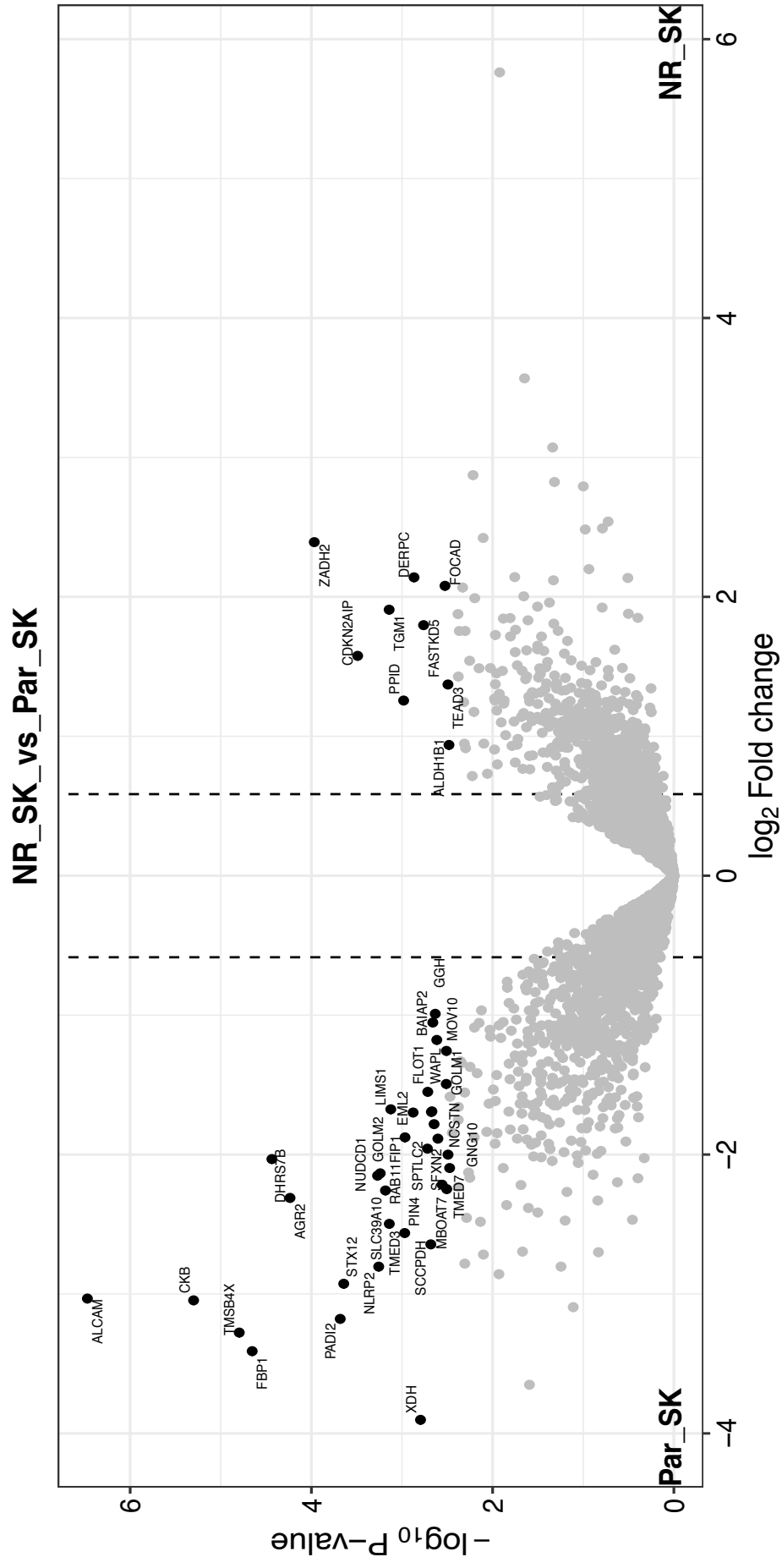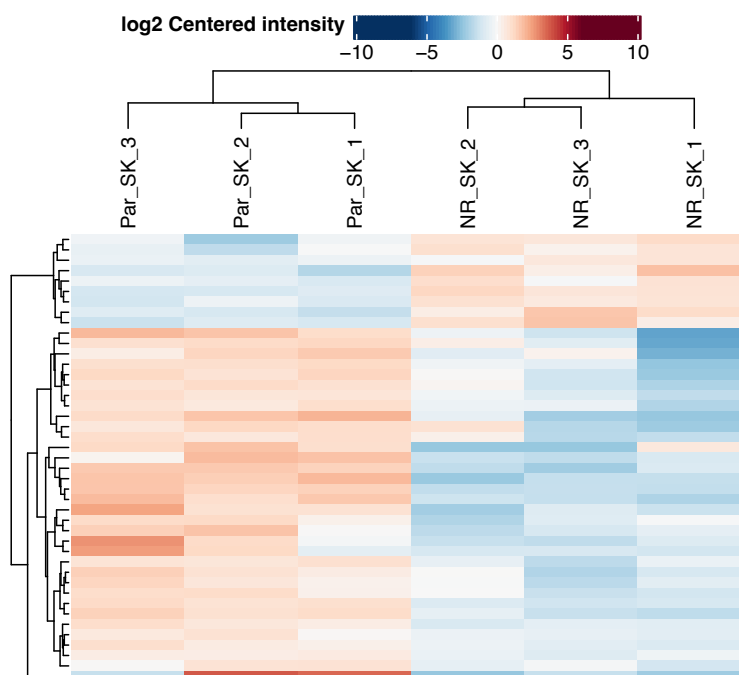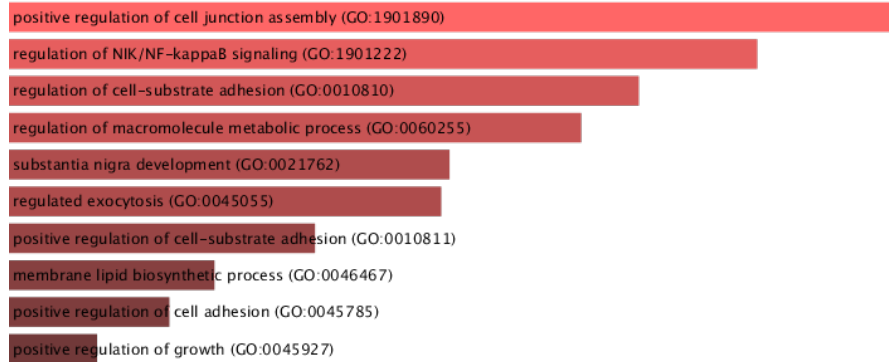
Table II-3. Differentially expressed proteins in SKBR3 NR cell variant compared to SKBR3 neratinib-sensitive counterpart.

Down-regulated in SKBR3 NR		Up-regulated in SKBR3 NR
XDH	GNG10	ALDH1B1
FBP1	DHRS7B	PPID
TMSB4X	NCSTN	TEAD3
PADI2	SPTLC2	CDKN2AIP
CKB	SFXN2	FASTKD5
ALCAM	RAB11FIP1	TGM1
STX12	MUC1	FOCAD
NLRP2	EML2	DERPC
SCCPDH	CLMN	ZADH2
PIN4	EIF4A2	
TMED2	LIMS1	
AGR2	FLOT1	
SLC39A10	WAPL	
TMED7	GOLM1	
MBOAT7	MOV10	
NUDCD1	BAIAP2	
GOLM2	GGH	

Biological process

positive regulation of cell junction assembly (GO:1901890)

regulation of NIK/NF-kappaB signaling (GO:1901222)

regulation of cell-substrate adhesion (GO:0010810)

regulation of macromolecule metabolic process (GO:0060255)

substantia nigra development (GO:0021762)

regulated exocytosis (GO:0045055)

positive regulation of cell-substrate adhesion (GO:0010811)

membrane lipid biosynthetic process (GO:0046467)

positive regulation of cell adhesion (GO:0045785)

positive regulation of growth (GO:0045927)

Cellular component

COPI vesicle coat (GO:0030126)

COPI-coated vesicle membrane (GO:0030663)

focal adhesion (GO:0005925)

vesicle coat (GO:0030120)

azurophil granule (GO:0042582)

endoplasmic reticulum-Golgi intermediate compartment membrane (GO:0033116)

secretory granule lumen (GO:0034774)

Golgi-associated vesicle (GO:0005798)

platelet alpha granule lumen (GO:0031093)

coated vesicle (GO:0030135)

Molecular function

estrogen receptor binding (GO:0030331)

steroid hormone receptor binding (GO:0035258)

protein-glutamine gamma-glutamyltransferase activity (GO:0003810)

omega peptidase activity (GO:0008242)

2-acylglycerol-3-phosphate O-acyltransferase activity (GO:0047144)

hydrolase activity, acting on carbon-nitrogen (but not peptide) bonds, in linear amidines (GO:0016813)

2 iron, 2 sulfur cluster binding (GO:0051537)

aldehyde dehydrogenase (NAD) activity (GO:0004029)

transferase activity, transferring amino-acyl groups (GO:0016755)

1-acylglycerol-3-phosphate O-acyltransferase activity (GO:0003841)

KEGG pathways

Arginine and proline metabolism

Glycolysis / Gluconeogenesis

Caffeine metabolism

Insulin signaling pathway

Histidine metabolism

Folate biosynthesis

Ascorbate and aldarate metabolism

Pentose phosphate pathway

beta-Alanine metabolism

Fructose and mannose metabolism

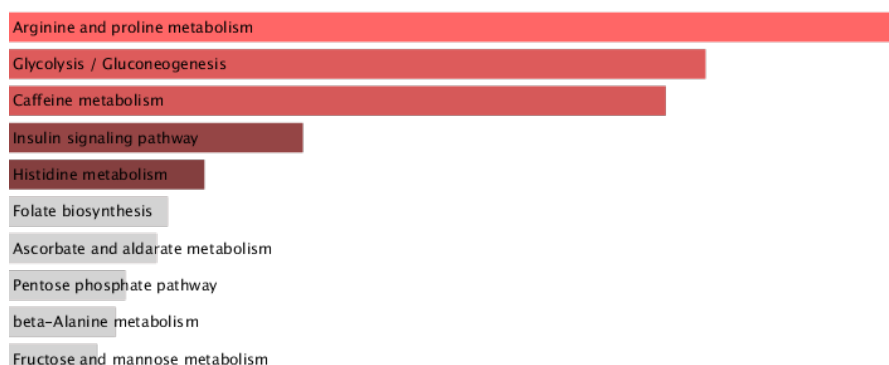**Figure II-13. Gene ontologies and pathways analyses of the differentially expressed proteins in SKBR3 NR compared to their neratinib-sensitive counterpart ordered by *p*-value ranking.**
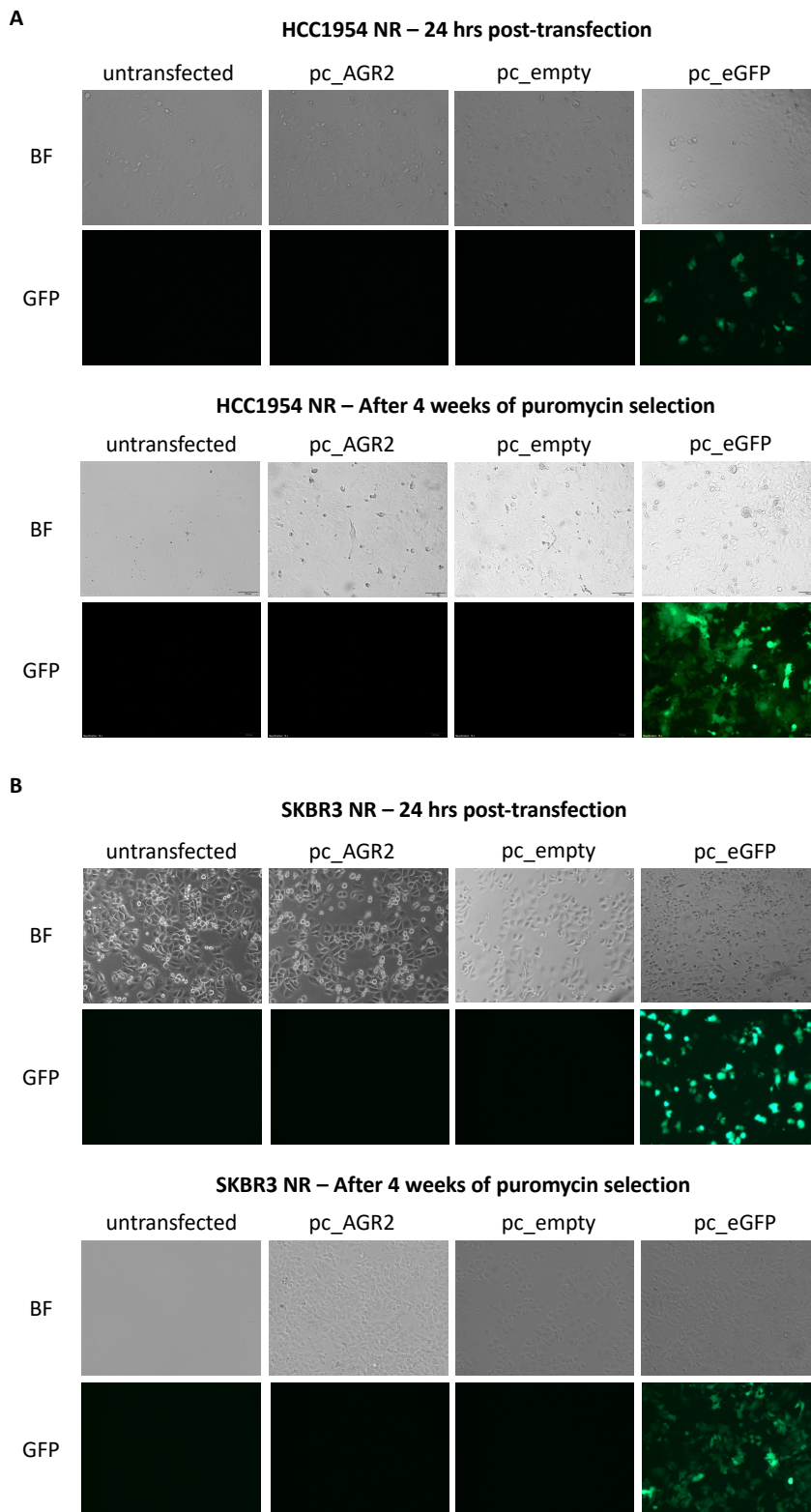
Figure II-14. Representative images of the successful stable transfection after 4 weeks puromycin selection.

(**A**) HCC1954 NR and (**B**) SKBR3 NR cells were selected under puromycin presence for 4 weeks. Non-transfected cells were dead by the end of the puromycin selection. Images were taken at 10x magnification. BF=Brightfield; GFP = Green Fluorescent Protein (GFP) filter.
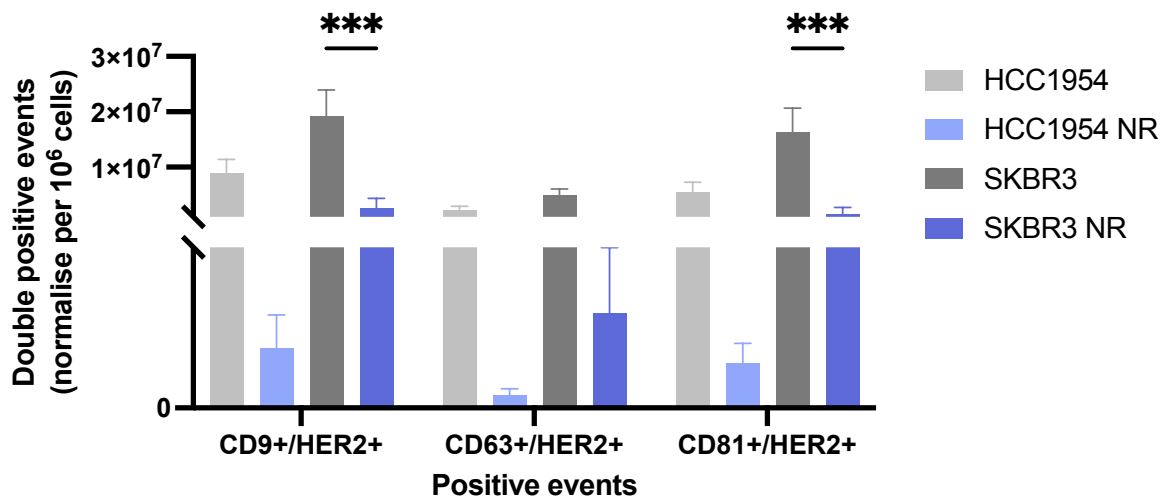
Appendix III

Chapter 4 – IFCM Supplementary Data

Figure III-1. Imaging Flow Cytometry analysis of the surface of the EVs.
Amnis ImageStreamX was used to measure double positive events for EVs markers and HER2 on HCC1954 variants-derived isolates and SKBR3 variants-derived isolates. Neratinib-resistant (NR) cell variants released fewer CD9+HER2+, CD63+/HER2+, and CD81+/HER2+ particles compare to their neratinib-sensitive counterparts. Graphs are representative of n = 3 experiments ± SEM. Unpaired t test used to calculate significance: *p<0.05.

Appendix IV

Chapter 5 – Effect of hypoxia on EVs' release and EVs' cargo
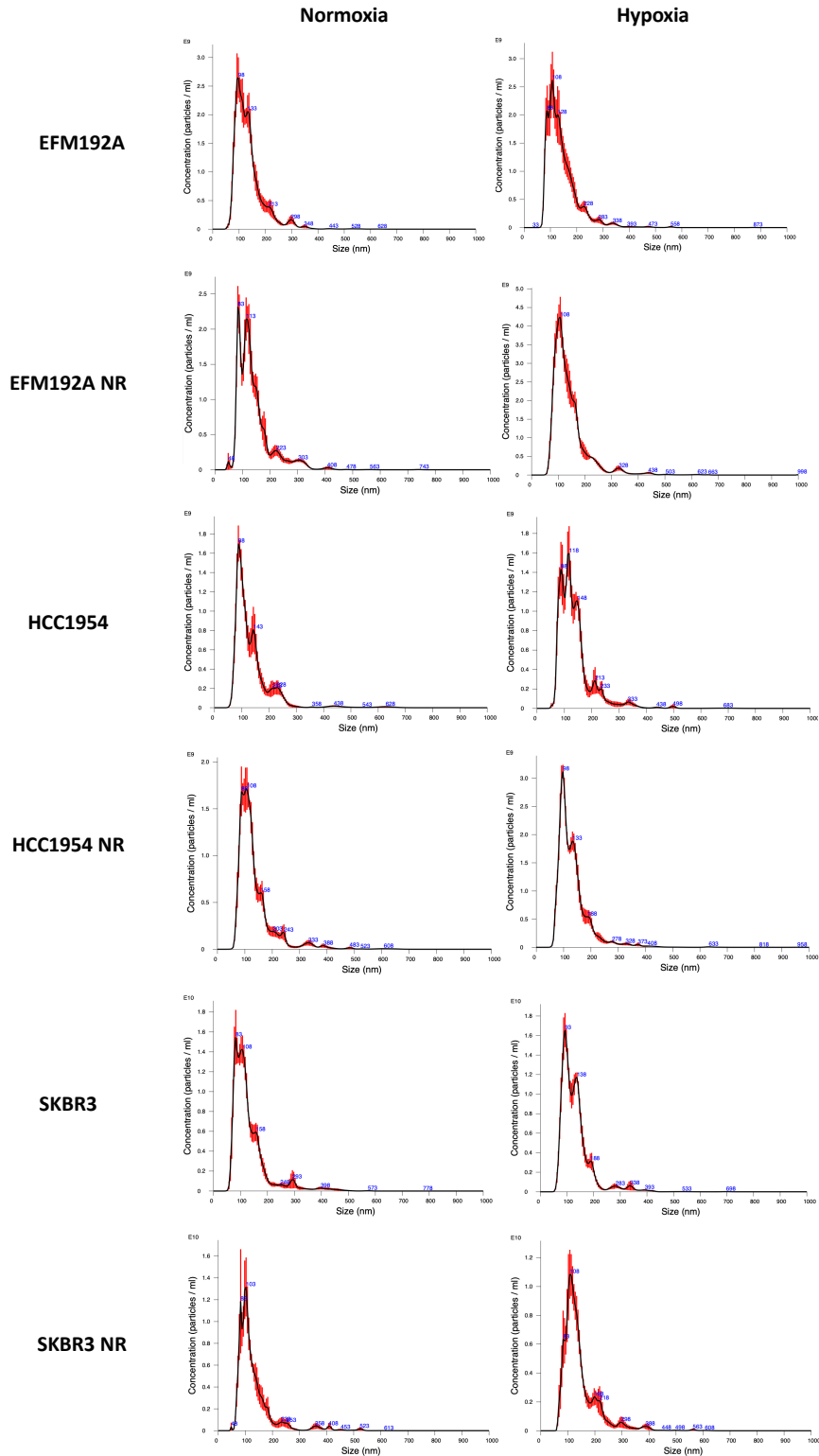

Figure IV-1. Representative nanoparticle tracking analysis (NTA) images.

EVs obtained by dUC from HER+ breast cancer cells under normoxic and hypoxic conditions.
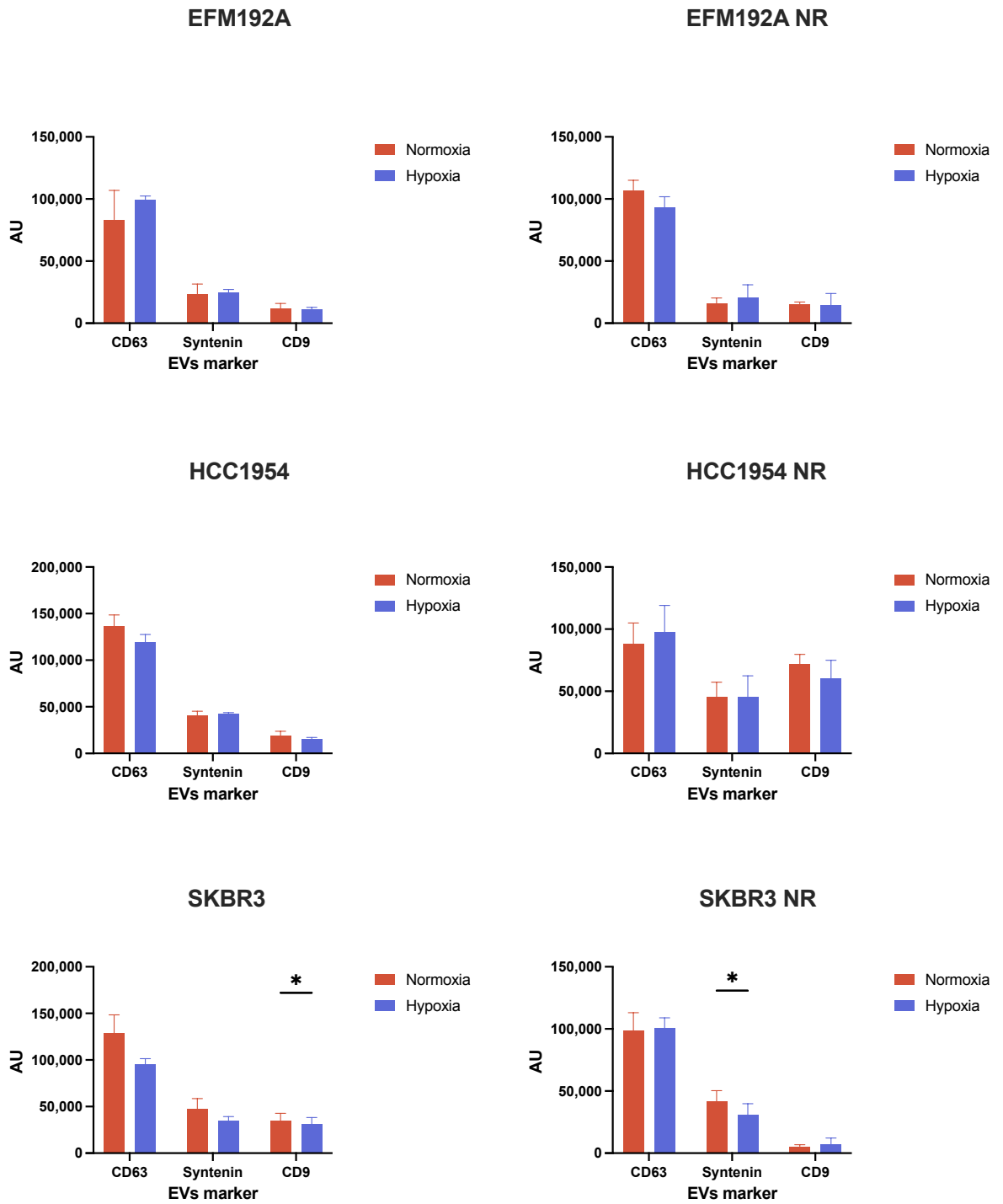
120K

Figure IV-2. The relative intensity (AU) of the EVs marker signal on the 120K samples. Enrichment of EVs positive markers in 120K EVs samples released from HER2-positive cells under normoxic and hypoxic conditions. The densitometric analysis of three independent experiments are presented as the mean ± SEM (*p<0.05).

Table IV-1. RNA yields (ng/µl) and RNA purities (A260/A230; A260/280) of RNA-EVs samples.

| Sample	Replicate	Condition	RNA yield (ng/µl)	A260/280	A260/230
EFM192A	N1	Normoxia	0.502	1.93	0.24
		Hypoxia	0.59	1.11	0.14
	N2	Normoxia	0.784	1.43	0.02
		Hypoxia	0.642	1.14	0.1
	N3	Normoxia	0.532	2.02	0.09
		Hypoxia	0.5	1.24	0.08
EFM192A NR	N1	Normoxia	0.618	1.4	0.06
		Hypoxia	0.934	1.16	0.04
	N2	Normoxia	0.834	1.38	0.26
		Hypoxia	0.686	1.65	0.04
	N3	Normoxia	0.726	1.32	0.13
		Hypoxia	0.812	1.15	0.11
HCC1954	N1	Normoxia	1.64	1.45	0.14
		Hypoxia	1.63	1.12	0.07
	N2	Normoxia	1.48	1.21	0.16
		Hypoxia	1.44	1.19	0.02
	N3	Normoxia	3.76	1.96	0.03
		Hypoxia	6.34	1.27	0.29
HCC1954 NR	N1	Normoxia	1.57	1.48	0.01
		Hypoxia	1.71	1.43	0.11
	N2	Normoxia	1.45	1.66	0.14
		Hypoxia	1.1	1.26	0.12
	N3	Normoxia	1.54	2.05	0.18
		Hypoxia	2.22	1.46	0.22
SKBR3	N1	Normoxia	1.12	0.98	0.08
		Hypoxia	2.1	1.01	0.06
	N2	Normoxia	0.966	1.41	0.3
		Hypoxia	1.31	1.4	0.26
	N3	Normoxia	1.2	2.09	0.02
		Hypoxia	1.86	1.18	0.09
SKBR3 NR	N1	Normoxia	1.07	1.21	0.18
		Hypoxia	1.21	1.59	0.1
	N2	Normoxia	1.12	1.34	0.09
		Hypoxia	1.62	1.81	0.15
	N3	Normoxia	1.79	1.8	0.16
		Hypoxia	2.56	1.57	0.22
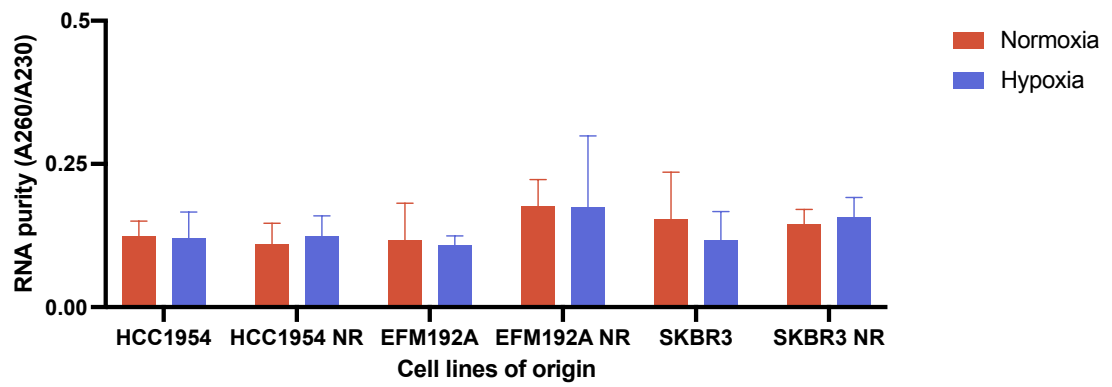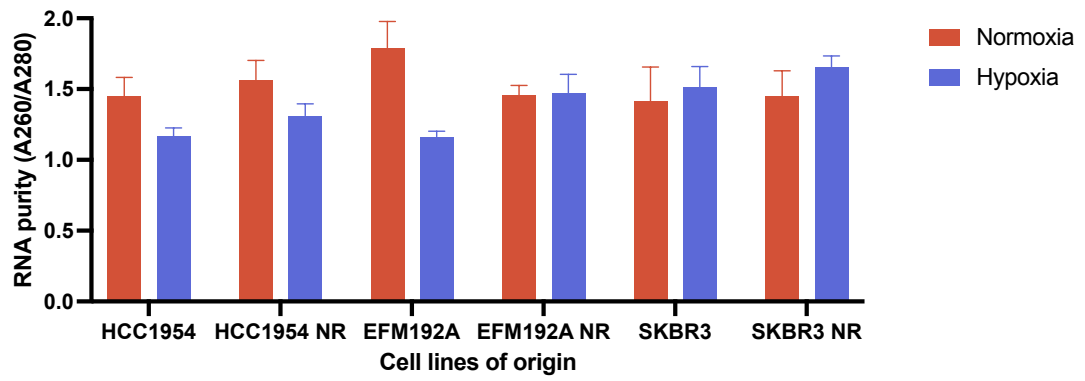
Figure IV-3. RNA purities (A260/A230; A260/280) of RNA-EVs samples.

Graphs are representative of n = 3 experiments ± SEM.

Appendix V

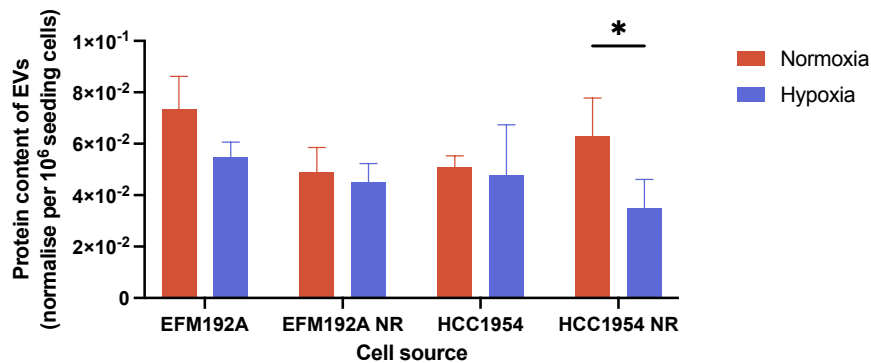## Chapter 6 – Additional normalisation based on seeding density

Figure V-1. Protein content of EVs derived from 3D cultured cells was measured by BCA.
The amount of protein was normalised to millions of seeding cells. Paired t-test used to calculate significance: *$p<0.05$ ($n = 3 \pm$ SEM).
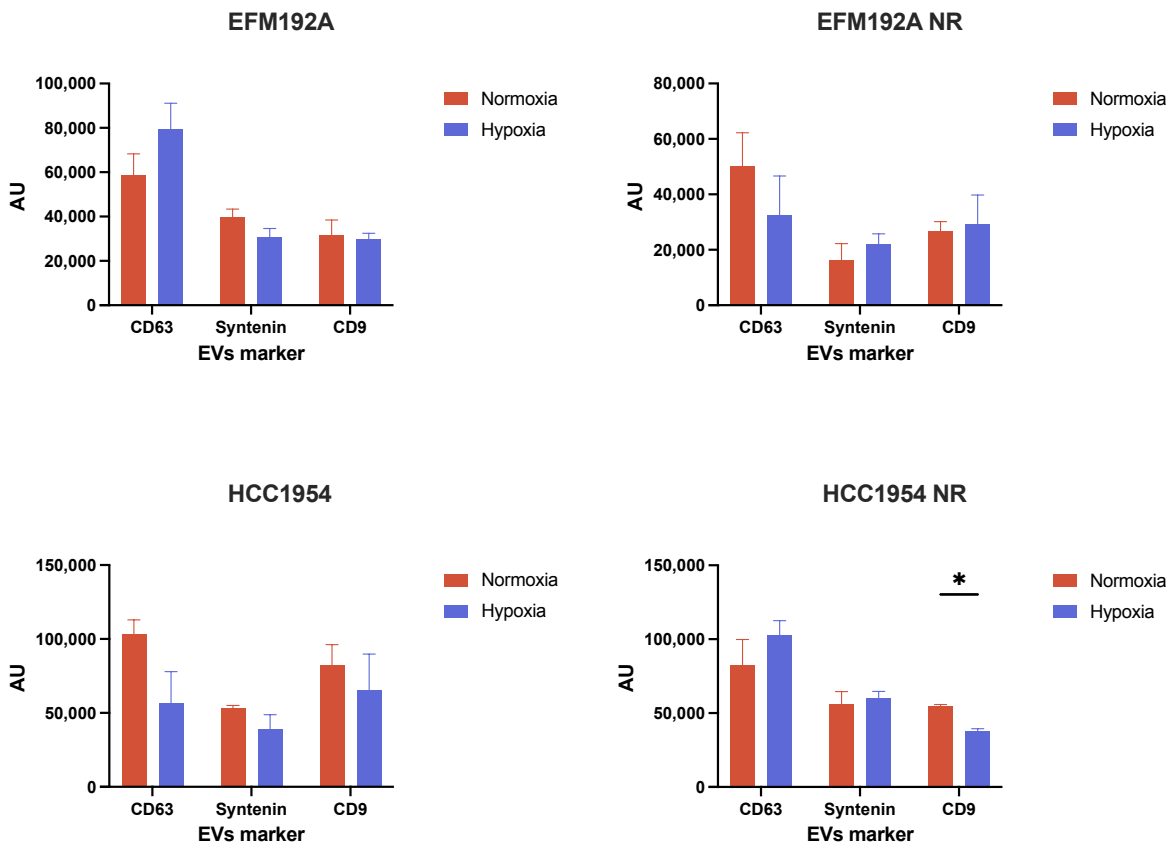

Figure V-2. The relative intensity (AU) of the EVs marker signal on the EVs samples.
Enrichment of EVs positive markers in the EVs samples released from HER2-positive cells grown in 3D culture under normoxic and hypoxic conditions. The densitometric analysis of three independent experiments are presented as the mean $\pm$ SEM (*$p<0.05$)
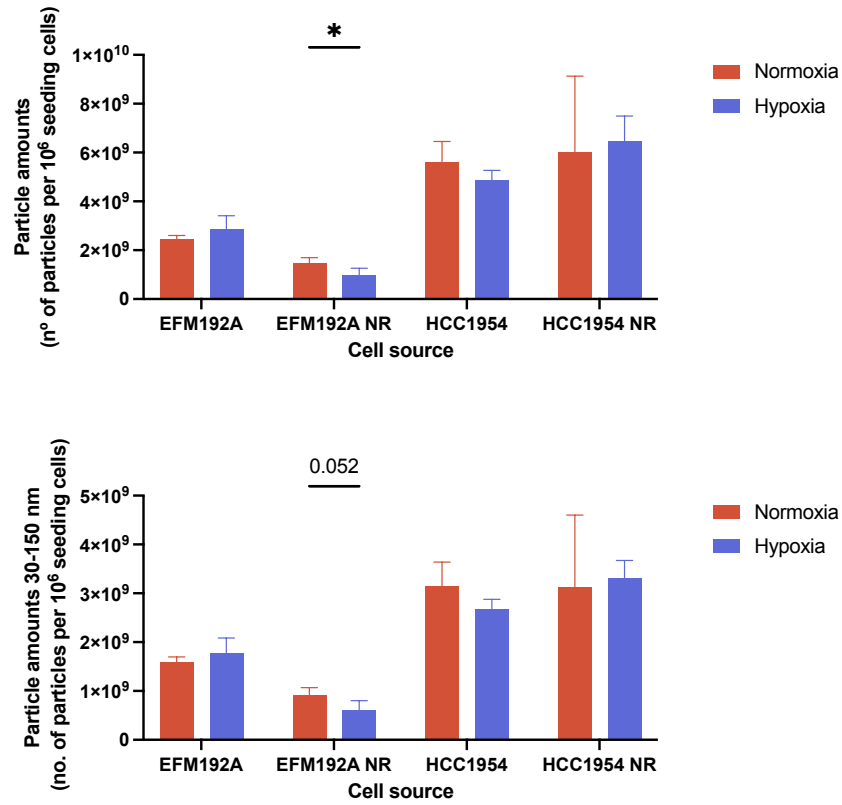
Figure V-3. Particle numbers measured by NTA.

Quantification of EVs particle numbers estimated by NTA and normalise per seeding cells. Error bars represent SEM (*n* = 3). Multiple paired t-test was used to calculate the significance: *p<0.05.
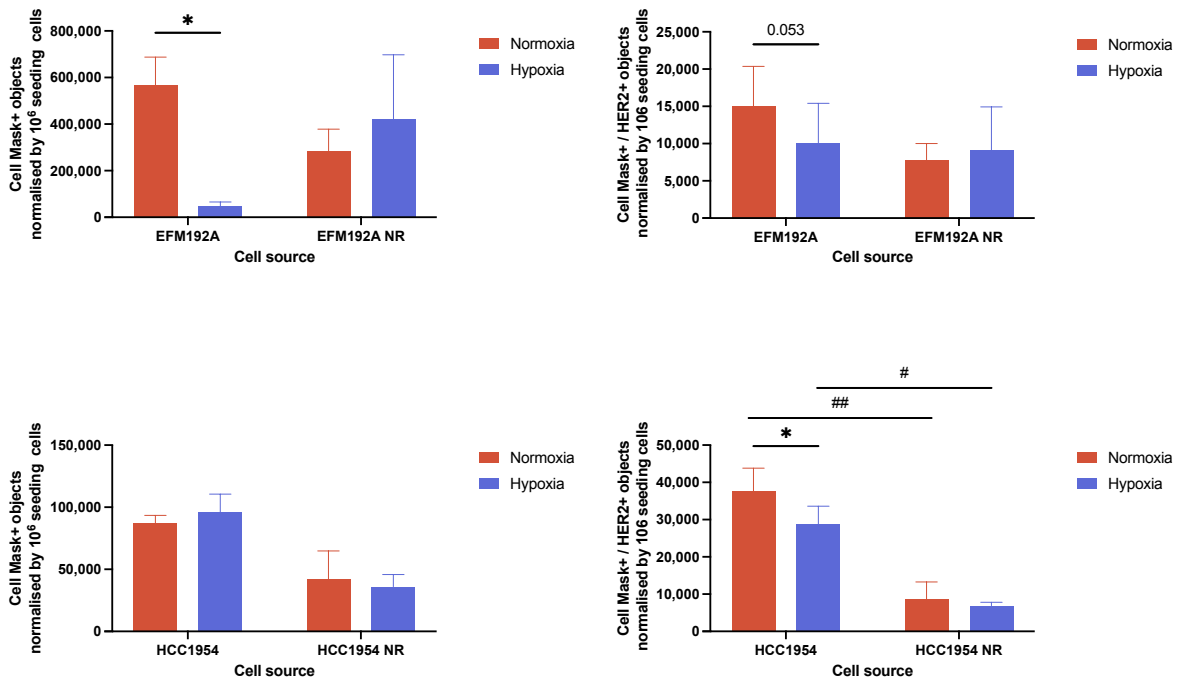
Figure V-4. IFCM analysis of EVs derived from 3D cell cultured cells.

Imaging flow cytometry (IFCM) analysis of EVs samples obtained from 3D cultured cells under normoxic and hypoxic conditions. Data was collected by measuring the CellMask cell membrane signal (**Top**) and CellMask together with HER2 signal (**Bottom**) on the EVs samples obtained from two HER2+ cell lines and their neratinib-resistant counterparts. Positive objects were normalise per million of seeding cells. Two-way *ANOVA* was used to calculate significance: *$p < 0.05$ ($n = 3 \pm$ SEM).
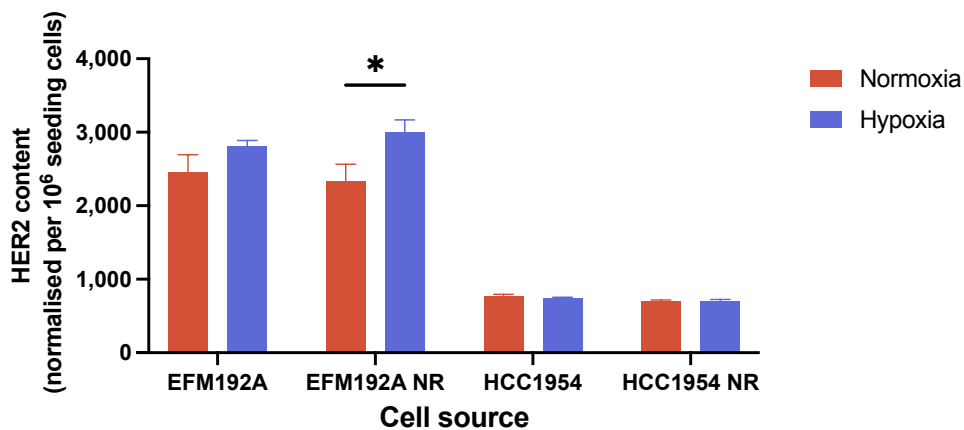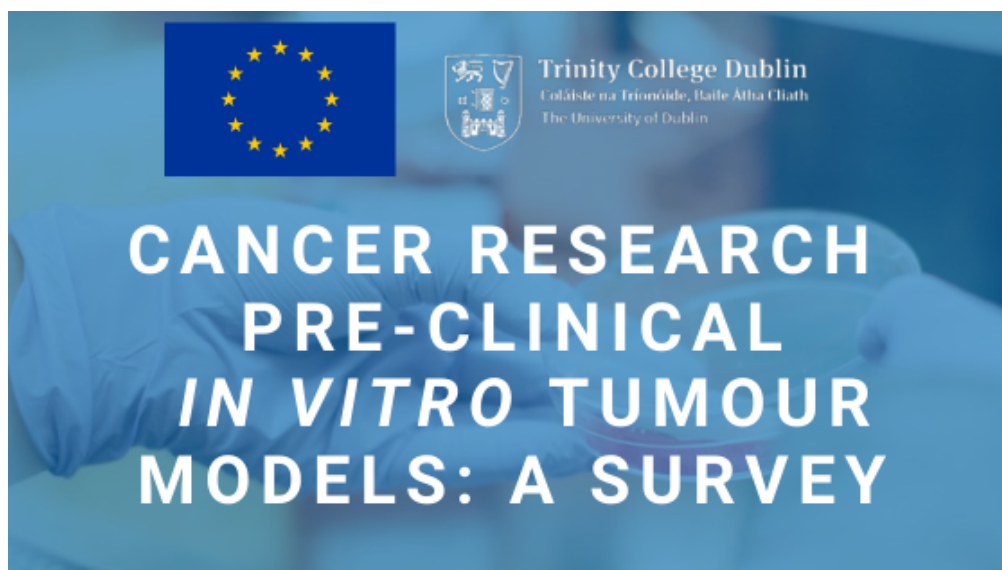

Figure V-4. HER2 ELISA analysis.

Investigating the HER2 presence on non-lysed EVs isolates under normoxic and hypoxic conditions (**Bottom**). Data are represented as mean ± SEM ($n = 3$). Multiple paired t-test was used to calculate the significance: *$p < 0.05$.

Appendix VI

Chapter 7 – Survey questionnaire

Participant Information and Consent

Substantial efforts have been made over recent years to develop *in vitro* tumour models with increased complexity to better represent tumours in the body and to reduce animal testing. However, there are still challenges in developing realistic *in vitro* models that reproduce the complexity of tumour tissue and stromal architecture, as it exists in the body. And, although several types of 3D culture models are being developed, monolayer (2D) cell-based assays remain an important pillar in cancer research. The goal of our research is to collate information on the uses of pre-clinical *in vitro* models and the reasons for the choices made.

We invite individuals, who are 18 years or older and who have knowledge working with pre-clinical cancer research models, to please complete this survey, which should take only 15 minutes of your time. Participation in this research survey is voluntary. This survey is anonymous, so if you decide to take part, responses cannot be withdrawn after submission, as respondents cannot be traced.
The Survey was designed by me, Sarai Martinez Pacheco (a H2020-MSCA-TRAIN-EV PhD student working with Prof. Lorraine O'Driscoll at Trinity College Dublin, Ireland). When the Survey is completed, the results will be analysed and disseminated so that we can all learn from this.

This study has been approved by the School of Pharmacy & Pharmaceutical Sciences (SoPPS) Level 1 Research Ethics Committee (REC), Trinity College Dublin on 25 May 2019.
If you have any questions about the survey or need technical support, please contact at me
smartin6@tcd.ie

We really appreciate your input

Survey questions (* mandatory questions)

1. By submitting this form, I am indicating that: *
    - I am 18 years of age or older.
    - I have knowledge of working with pre-clinical cancer research models.
    - I have read and understand the participant information above and voluntarily agree to participate in this research study.
    - *I consent* ➡ *Start Survey*
    - *I do not consent* ➡ *End*

2. In which **country** do you work? *
    - Dropdown Question
    - Options: List of countries

3. Optional: Please provide the name of the **institution** where your work is located
    - Comment box

4. Select your **sector***
    - Checkboxes question
    - Options:
        - Academia
        - Industry
        - Clinic

5. Which of the following best describes your **career stage/ institution role**? *
    - Dropdown question
    - Options:
        - Undergraduate Researcher
        - MSc Student
        - PhD Student
        - Research Assistant
        - Clinical Researcher
        - Laboratory Technician
        - Post-doctoral Researcher
        - Associate Researcher
        - Senior Researcher
        - Principal Investigator
        - Other (specify)

6. Which of the following best describes your **field** of **cancer research**? *
    - Multiple Choice question
    - Options:
        - Cancer Biology
        - Cancer Genomics
        - Cancer Biomarkers
        - Drug Screening
        - Cancer Drug Sensitivity/Resistance
        - Cancer Immunology
        - Extracellular Vesicles Research
        - Other (specify)

7. What **cancer type(s)** are you studying? *
    - Multiple choice question
    - Options:
        - Lung cancer
        - Brain cancer
        - Skin cancer
        - Liver cancer
        - Bone cancer
        - Colorectal cancer
        - Lymphoma
        - Breast cancer
        - Bladder cancer
        - Stomach cancer
        - Pancreatic cancer
        - Prostate cancer
        - Childhood cancer
        - Endometrial cancer
        - Uterine cervical cancer
        - Thyroid cancer
        - Ovarian cancer
        - Other (please specify)

8. What is your **main cell source**? *
    - Multiple choice question
    - Options:
        - Primary cells
        - Commercially available cell lines

- Other (specify)

9. What type(s) of cells is your **main cell source**? *
  - ▪ Multiple choice
  - ▪ Options:
    - Cancer cells
    - Stem cells
    - Immune cells
    - Stromal cells
    - Other: (specify)

If the answer in Q8 is Primary cells and the answer in Q9 is cancer cells ➡ Go to Q10

All other cases ➡ jump to Q11.

10. Which of the following characteristics best describe your cancer cells? *
  - ▪ Multiple choice
  - ▪ Options:
    - Primary tumor cells
    - Secondary tumor cells
    - Cells obtained from pre-metastatic niche
    - Cells obtained from metastatic niche
    - Other (specify)

11. Do you use **co-culture** model(s)? *
  - ▪ Yes
  - ▪ No

  If Yes ➡ Q12

  If No ➡ Q13

12. What type(s) of **cells** do you **co-culture** with your main cell source? *
  - ▪ Multiple choice
  - ▪ Options:
    - Cancer cells
    - Stem cells
    - Immune cells
    - Stromal cells
    - Other: (specify)

13. What **type(s)** of *in vitro* tumor model(s) do you use **mostly**? *
    - **Checkboxes question (at least 1)**
    - Options:
        - 2D Culture
        - 2.5D Culture
        - 3D Culture
        - Other (specify)

If the answer is:

If the answer is:	Go to:
2D	Q28
2.5D	Q27
3D	Q14
Other	Q28
2D+2.5D	Q27
2D+3D	Q14
2D+Other	Q28
2.5D+3D	Q14-Q27-Q29
2.5D+Other	Q27
3D+Other	Q14
2D+2.5+3D	Q14-Q27-Q29
2D+2.5D+Other	Q27-Q29
2D+3D+Other	Q14-Q29
2.5+3D+other	Q14-Q27-Q29
2D+2.5D+3D+Other	Q14-Q27-29

14. The purpose here is to collect the **main characteristics** of the 3D culture that you use **the most**. <u>If you use more than one</u>, indicate it later in the survey.
    - **Multiple choice question**
    - Options:
        - (A) Scaffold-based
        - (B) scaffold-free culture
        - (C) "Specialised" 3D Culture Platforms (Microfluidic cell culture platforms / organ-on-a-chip)
        - (D) Hybrid System
        - (E) Other (specify)

    If the answer contains (A) ➡ *Q15*

    If not ➡ *Q16*

15. Scaffold-based related questions

a. Which of the following types of **scaffold-based models** do you use to develop your model?

- **Multiple choice question**
- Options:
    - Natural Scaffold
    - Synthetic Scaffold
    - Semi-synthetic Scaffold (biohybrid)
    - Other (specify)
    - Not applicable

b. Which of the following **natural materials** do you use in your principal 3D model?

- **Multiple choice question**
- Options:
    - Not applicable
    - Matrigel™
    - Cultrex™ BME, PathClear
    - ECM Gel™
    - ECL Cell Attachment Matrix™
    - Geltrex™
    - HuBiogel™
    - Collagen
    - Gelatin
    - Fibronectin
    - Fibrin
    - Glucan
    - Hyalouronic Acid
    - Chitosan
    - Alginate
    - Agarose
    - Self-assembling peptides
    - Nanofibrillar cellulose scaffolds (NFC)
    - Other (specify)

c. Which of the following **synthetic materials** do you use in your principal 3D model?

- **Multiple choice question**
- Options:
    - Not applicable
    - Polyethylene glycol (PEG)
    - Poly(ethylene oxide) (PEO)
    - Poly(acrylic acid) (PAA)

xxx

- Poly(vinyl alcohol) (PVA)
- Polyglycolic acid (PGA)
- Poly-L-lactic acid (PLA)
- Poly(hydroxyethyl methacrylate) (p-HEMA)
- Poly(methacrylic acid) (PMMA)
- TrueGel3D™
- Other (specify)

d. Which of the following **semi-synthetic materials** you use?
- Multiple choice question
- Options:
    - Not applicable
    - PEGylated protein scaffolds
    - Gelatine methacrylamide (GelMA)-based scaffolds
    - HyStem™
    - Other (specify)

e. Is your scaffold **functionalised**?
- Options:
    - Yes ➡ *Go to Q15f*
    - No ➡ *Go to Q16*
    - Not applicable ➡ *Go to Q16*

f. If yes, please give more **details** on the **functionalization**:
- Comment

16. What technique do you use for the **spheroid formation**?
- **Multiple choice question**
- Options:
    - Not applicable
    - Hanging drop
    - Low attachment plate
    - Magnetic levitation
    - Pellet culture
    - Microgravity bioreactors
    - 3D Bio-printing
    - Matrix-on-top
    - Matrix-embedded
    - Matrix-encapsulation

- Spinner flask
- Micropatterned plates
- Other (specify)

If the answer in Q14 was:

If the answer was	Go to
Hybrid system	**Q17**
Not Hybrid system	**Q18**
Not Hybrid system, not other, but was Specialised platform	**Q19**
All other cases	**Q20**

17. If you select Hybrid System, please briefly **describe** the hybrid system used:
   - Comment

If the Q14 was Other ➡ Q18

If the Q14 was not Other and was Specialised platform ➡ Q19

All other cases jump ➡ Q20

18. If you select Other, please briefly **describe** the system used:
   - Comment

If the Q14 was Specialised platform ➡ Q19

All other cases jump ➡ Q20

19. "Specialised" 3D Culture platforms related questions.
   a. Which of the following **"Specialised" 3D Culture platforms** do you use?
      - Multiple choice question
      - Options:
         - CellASIC® ONIX Microfluidic Plates
         - Quasi Vivo®
         - Organovo (ONVO)
         - 2-OC and 4-OC (TissUse)
         - OrganoPlate®
         - Other (specify)

20. Do you use **co-culture** in your main **3D model**?
      - Yes ➡ *Go to Q23*
      - No ➡ *Go to Q24*

21. What type of **cells** do you culture **in combination** with your cancer cells **in this model**?
   - Options:
     - Other cancer cells
     - Stem cells
     - Immune cells
     - Stromal cells
     - Other: (specify)

22. How many **weeks** are required for successful establishment of model *de novo*?
   - Comment (Insert number)

23. How many **weeks** are required before using the model for a set of experiments?
   - Comment (Insert number)

Additional 3D Models

If you develop/use more than one different 3D culture model, we would appreciate if you could complete this part of the survey too

24. Do you use more than one 3D Culture model?
   - Options:
     - Yes. ➡ *Go to question 25*
     - No ➡ *Go to question 26*

25. Please choose which of the following options best describe your additional 3D models (Tick all that apply)
   - Multiple choice question
   - Options:
     - 3D natural scaffold
     - 3D natural scaffold Co-Culture
     - 3D synthetic scaffold
     - 3D synthetic scaffold Co-Culture
     - 3D semi-synthetic scaffold
     - 3D semi-synthetic scaffold Co-Culture
     - 3D scaffold-free culture
     - 3D scaffold-free culture Co-Culture
     - Microfluidic cell culture platforms / organ-on-a-chip
     - Hybrid System
     - Other (specify)

26. Please use this space for additional comments related to 3D-culture (commercial kits used to develop the models, biochemical signals, etc.) **(not mandatory)**
    - Comment

27. Which of the following strategies do you use for your **2.5D Culture**?
    - Multiple choice question
    - Options:
        - Microwells
        - Topographic patterning
        - Other (specify)

28. What are the **main reasons** why you **do not use** 3D Culture models?
    - Multiple choice question
    - Options:
        - Lack of availability/access
        - Lack of infrastructure
        - Additional cost
        - Lack of experience in appropriate skill
        - Lower throughput
        - Complex, difficult-to-replicate systems
        - Time-limitation
        - Other: (specify)

29. What technique(s) do you **use** for the **<u>analysis of the cells</u>** in the model(s)? *
    Please, select the technique(s) carried out for each type of *in vitro* model.

    a. What technique(s) do you **use** for the **analysis of the cells** in the **2D model(s)**?
    - Multiple choice
    - Options:
        - I do not use 2D models
        - Cell viability assays
        - Optical microscopy
        - Electron microscopy
        - Flow cytometry
        - Immunoblot
        - RT-qPCR
        - Cryosectioning
        - Oxygen measurement
        - Other (specify)

b. What technique(s) do you **use** for the **analysis of the cells** in the **2.5D model(s)**?
   - Multiple choice
   - Options:
     - I do not use 2.5D models
     - Cell viability assays
     - Optical microscopy
     - Electron microscopy
     - Flow cytometry
     - Immunoblot
     - RT-qPCR
     - Cryosectioning
     - Oxygen measurement
     - Other (specify)

c. What technique(s) do you **use** for the **analysis of the cells** in the **3D model(s)**?
   - Multiple choice
   - Options:
     - I do not use 3D models
     - Cell viability assays
     - Optical microscopy
     - Electron microscopy
     - Flow cytometry
     - Immunoblot
     - RT-qPCR
     - Cryosectioning
     - Oxygen measurement
     - Other (specify)

d. What technique(s) do you **use** for the **analysis of the cells** in the **other model(s)**?
   - Multiple choice
   - Options:
     - I do not use 2D models
     - Cell viability assays
     - Optical microscopy
     - Electron microscopy
     - Flow cytometry
     - Immunoblot
     - RT-qPCR
     - Cryosectioning
     - Oxygen measurement

- Other (specify)

30. What are the **experimental outputs** / **downstream applications** for your *in vitro* culture assays? * Please, select what type of *in vitro model* you use for the following experiments:

- ▪ Multiple choice questions

a. Proliferation/Migration/Invasion assays

- ▪ Options:
  - I do not do proliferation/migration/invasion assays
  - 2D Culture
  - 2D Co-Culture
  - 2.5D Culture
  - 2.5D Co-culture
  - 3D natural scaffold
  - 3D natural scaffold Co-Culture
  - 3D synthetic scaffold
  - 3D synthetic scaffold Co-Culture
  - 3D semi-synthetic scaffold
  - 3D semi-synthetic scaffold Co-Culture
  - 3D scaffold-free culture
  - 3D scaffold-free culture Co-Culture
  - Microfluidic cell culture platforms / organ-on-a-chip
  - Hybrid System

b. Drug screening assays

- ▪ Options:
  - I do not do drug screening assays
  - 2D Culture
  - 2D Co-Culture
  - 2.5D Culture
  - 2.5D Co-culture
  - 3D natural scaffold
  - 3D natural scaffold Co-Culture
  - 3D synthetic scaffold
  - 3D synthetic scaffold Co-Culture
  - 3D semi-synthetic scaffold
  - 3D semi-synthetic scaffold Co-Culture
  - 3D scaffold-free culture
  - 3D scaffold-free culture Co-Culture
  - Microfluidic cell culture platforms / organ-on-a-chip
  - Hybrid System

c. Angiogenesis assays
  - Options:
    - I do not do angiogenesis assays
    - 2D Culture
    - 2D Co-Culture
    - 2.5D Culture
    - 2.5D Co-culture
    - 3D natural scaffold
    - 3D natural scaffold Co-Culture
    - 3D synthetic scaffold
    - 3D synthetic scaffold Co-Culture
    - 3D semi-synthetic scaffold
    - 3D semi-synthetic scaffold Co-Culture
    - 3D scaffold-free culture
    - 3D scaffold-free culture Co-Culture
    - Microfluidic cell culture platforms / organ-on-a-chip
    - Hybrid System

d. Cellular uptake & cellular release assays
  - Options:
    - I do not do cellular uptake & cellular release assays
    - 2D Culture
    - 2D Co-Culture
    - 2.5D Culture
    - 2.5D Co-culture
    - 3D natural scaffold
    - 3D natural scaffold Co-Culture
    - 3D synthetic scaffold
    - 3D synthetic scaffold Co-Culture
    - 3D semi-synthetic scaffold
    - 3D semi-synthetic scaffold Co-Culture
    - 3D scaffold-free culture
    - 3D scaffold-free culture Co-Culture
    - Microfluidic cell culture platforms / organ-on-a-chip
    - Hybrid System

e. Immune cell response assays
  - Options:
    - I do not do immune cell response assays

- 2D Culture
- 2D Co-Culture
- 2.5D Culture
- 2.5D Co-culture
- 3D natural scaffold
- 3D natural scaffold Co-Culture
- 3D synthetic scaffold
- 3D synthetic scaffold Co-Culture
- 3D semi-synthetic scaffold
- 3D semi-synthetic scaffold Co-Culture
- 3D scaffold-free culture
- 3D scaffold-free culture Co-Culture
- Microfluidic cell culture platforms / organ-on-a-chip
- Hybrid System

f. Extracellular vesicles´ *in vitro* function assays
  - Options:
    - I do not do extracellular vesicle assays
    - 2D Culture
    - 2D Co-Culture
    - 2.5D Culture
    - 2.5D Co-culture
    - 3D natural scaffold
    - 3D natural scaffold Co-Culture
    - 3D synthetic scaffold
    - 3D synthetic scaffold Co-Culture
    - 3D semi-synthetic scaffold
    - 3D semi-synthetic scaffold Co-Culture
    - 3D scaffold-free culture
    - 3D scaffold-free culture Co-Culture
    - Microfluidic cell culture platforms / organ-on-a-chip
    - Hybrid System

g. Gene manipulation assays
  - Options:
    - I do not do gene manipulation assays
    - 2D Culture
    - 2D Co-Culture
    - 2.5D Culture

- 2.5D Co-culture
- 3D natural scaffold
- 3D natural scaffold Co-Culture
- 3D synthetic scaffold
- 3D synthetic scaffold Co-Culture
- 3D semi-synthetic scaffold
- 3D semi-synthetic scaffold Co-Culture
- 3D scaffold-free culture
- 3D scaffold-free culture Co-Culture
- Microfluidic cell culture platforms / organ-on-a-chip
- Hybrid System

h. Other: Please specify the application and what type of *in vitro* model you use **(not mandatory)**

31. Have you published on any kind of novel *in vitro* model?
- Yes ➡ *Go to Question 32*
- No ➡ *Go to Question 33*

32. Optional: Please, include DOI/PMID for the publications.
- Comment

33. Do you perform additional *in vivo* studies in your laboratory?
- Yes ➡ *Go to Question 34*
- No ➡ *Go to Question 36*

34. If you use in vivo models, please indicate which *in vivo* model you use
- Comment ➡ *After this question, go to question 35*

35. Is your research based predominantly *on in vitro* or *in vivo* studies? ➡ *After this question, go to Question 37*
- *In vitro*
- *In vivo*

36. If you do not use *in vivo* models, what are the main reasons for that?
- Multiple choice question
- Options:
  - Lack of availability
  - The 3Rs (replacement, reduction, refinement)
  - Lack of resources

- Personal choice
- Other: (specify)

37. How much do you agree or disagree with the following statements?
   - Rating scale question
   - Affirmations:
      - If both techniques (*in vitro/ in vivo*) could achieve the same result, I prefer to use an *in vitro* approach.
      - I am interested using 3D culture models
      - I am reluctant to invest a lot of time and resources into developing a 3D model culture as I am not confident of its success.
      - I think that it is still not feasible to completely replace *in vivo* with *in vitro* models.
      - 2D cell culture models should be completely replaced by 3D cell culture models.
      - My main concern with the use 3D culture models is that many assays are not adapted for them.

38. From your experience, list the 3 main benefits and 3 main limitations of using 3D *in vitro* culture system
   a. Main benefits (Comment box)
   b. Main limitations (Comment box)

39. If you would like to suggest how the use of 3D models could be improved to enhance cancer research, please do so below (Comment box)

40. If you would like to add any other comments/suggestions/remarks, please do so below (Comment box)

Thanks Page

Thank you for your time and effort in completing this survey.

Your input is important to us. When the Survey is completed, we will analyze the information and share the outcome.

Please forward this Survey to anyone who you fell might be interested in participating. You can also share using the social media sharing buttons that appeared below:
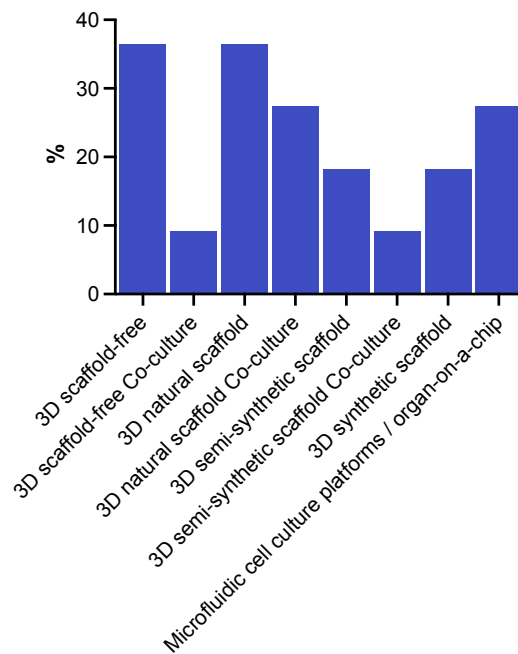

Figure VI-1. Types of additional 3D models most used by respondents (%).
Note: some respondents indicated to use more than one additional 3D models.

Appendix VII

Experimental controls for CM screening by IFCM

Experimental controls used for IFCM analysis of HER2+ breast cancer cell lines CM after tucatinib treatment for CD9 positivity are shown. Unstained control and non-conditioned media control (RPMI-1640 media used cells that were set up the same but was not conditioned by cells) were included in the analysis to determine background of CD9 positivity (**Figure VII-1**) or HER2 positivity (**Figure VII-2**) in the media for EFM192A, HCC1954, and SKBR3 cells. NP-40 controls were included to determine if the CD9 positivity detected was derived from EVs in the CM. There was a decrease in CD9 in the CM when comparing untreated CM and NP-40 control of EFM192A, HCC1954, and SKBR3 cells.
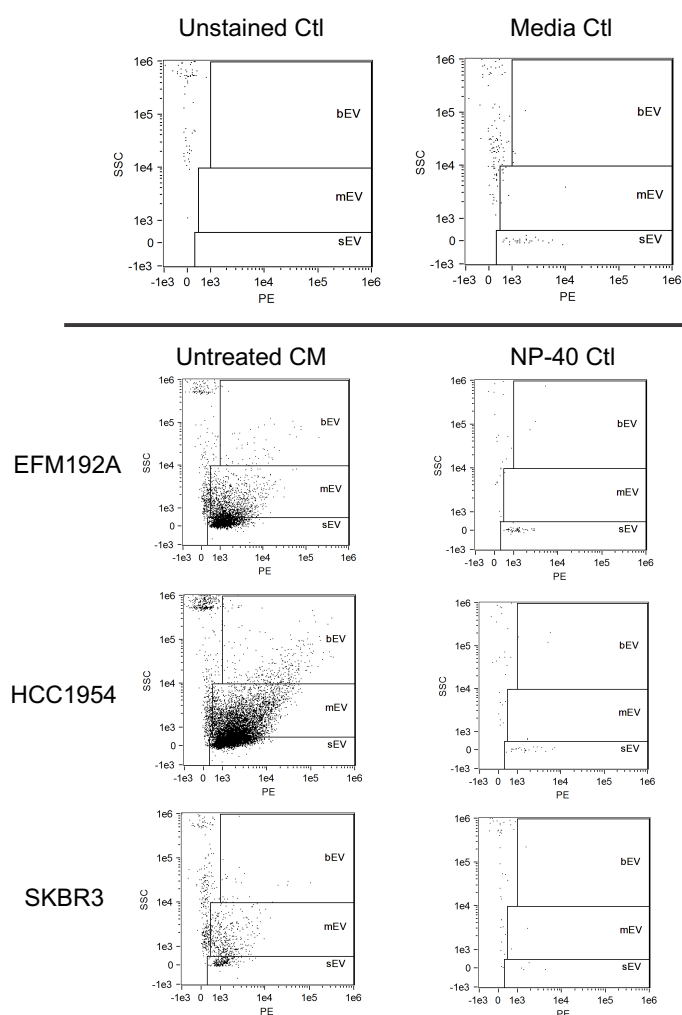

Figure VII-1. Experimental controls for CM screening assay by IFCM.
Representative dot plots from IFCM experimental controls for CD9 positivity, including (**Top**) unstained control and non-conditioned media control; (**Bottom**) untreated CM media was compared with their respective NP-40 controls for each cell line. A final concentration of 2% NP-40 was used.

Figure VII-2. Experimental controls for CM screening assay by IFCM.

Representative dot plots from IFCM experimental controls for HER2 positivity, including (**Top**) unstained control and non-conditioned media control; (**Bottom**) untreated CM media was compared with their respective NP-40 controls for each cell line. A final concentration of 2% NP-40 was used.
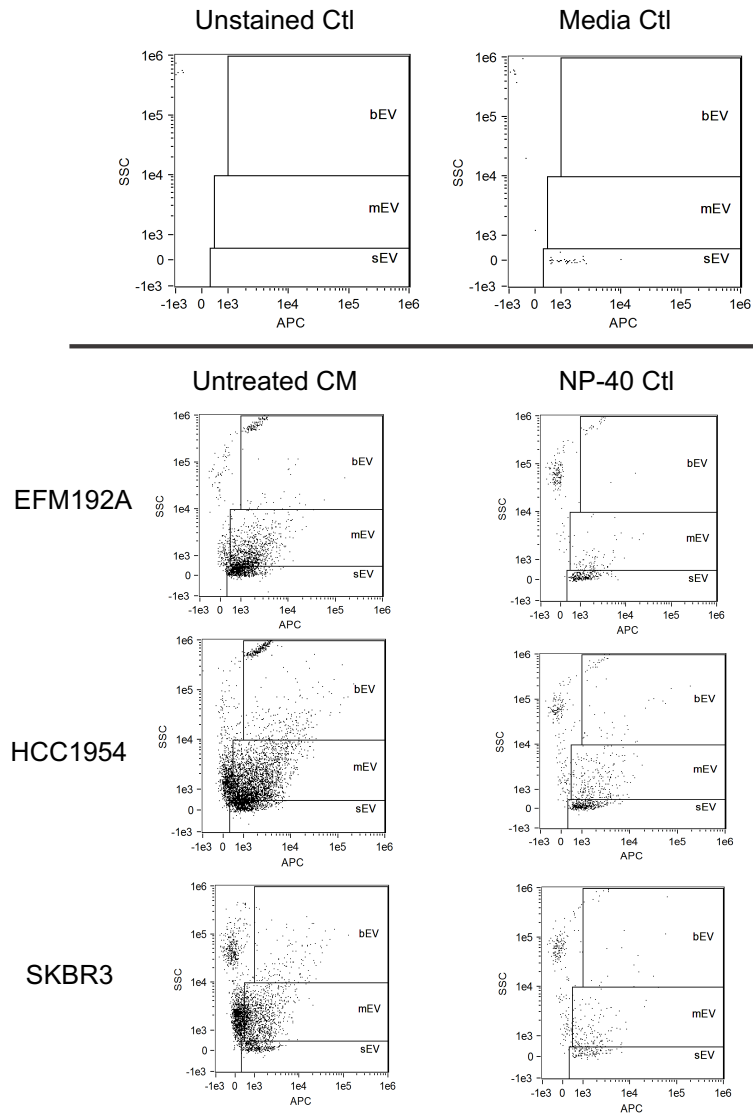
Appendix VIII

Publications, achievements, and presentations

A. PUBLICATIONS

Research articles:
- **Martinez-Pacheco, S.**, & O'Driscoll, L. (2021). Evidence for the Need to Evaluate More Than One Source of Extracellular Vesicles, Rather Than Single or Pooled Samples Only, When Comparing Extracellular Vesicles Separation Methods. Cancers, 13(16), 4021. https://doi.org/10.3390/cancers13164021
- **Martinez-Pacheco, S.**, & O'Driscoll, L. (2021). Pre-Clinical In Vitro Models Used in Cancer Research: Results of a Worldwide Survey. Cancers, 13(23), 6033. https://doi.org/10.3390/cancers13236033

Published abstracts:
- **Martinez-Pacheco, S.**, & O'Driscoll, L. (2020). Analysing Extracellular Vesicles from Drug-Resistant and Drug-Sensitive Cancer Cells As Potential Predictive Biomarkers in the Liquid Biopsy. ISEV2020 Abstract Book, Journal of Extracellular Vesicles, 9:sup1, DOI: 10.1080/20013078.2020.1784511
- **Martinez-Pacheco, S.**, & O'Driscoll, L. (2021). Currently use of pre-clinical in vitro models in cancer research: the first global survey. JRC Summer School on Non-animal Approaches in Science, May 2021. *Alternatives to Laboratory Animals: ATLA*, *49*(6), 235–300. https://doi.org/10.1177/02611929211065919
- **Martinez-Pacheco, S.**, & O'Driscoll, L. (2021). The importance of including multiple cell lines when comparing Extracellular Vesicles separation methods: A Differential Ultracentrifugation and Polyethylene glycol-based precipitation comparison. ISEV2021 Abstract Book, Journal of Extracellular Vesicles, 10(Suppl 1), e12083. https://doi.org/10.1002/jev2.12083

B. INTERNATIONAL AND NATIONAL CONFERENCES

- **Martinez-Pacheco, S.**, & O'Driscoll, L. Analysing extracellular vesicles from drug-resistant and drug-Sensitive cancer cells as potential predictive biomarkers in the liquid biopsy. International Society for Extracellular Vesicles (ISEV) Conference 2020, Virtual (August 2020).
- **Martinez-Pacheco, S.**, & O'Driscoll, L. Evaluating extracellular vesicles from neratinib-resistant and neratinib-sensitive breast cancer cells as potential predictive biomarkers. Biomedical Sciences Section of the Royal Academy of Medicine in Ireland (RAMI) meeting 2021, Virtual (February 2021).

- **Martinez-Pacheco, S.**, & O'Driscoll, L. The use of preclinical *in vitro* models in cancer research: results of a worldwide survey. Biomedical Sciences Section of the Royal Academy of Medicine in Ireland (RAMI) meeting 2021, Virtual (February 2021).
- **Martinez-Pacheco, S.**, & O'Driscoll, L. Potential use of extracellular vesicles from neratinib-resistant and neratinib-sensitive breast cancer cells as predictive biomarkers. Irish Association for Cancer Research (IACR) meeting, Virtual (March 2021).
- **Martinez-Pacheco, S.**, & O'Driscoll, L. Pre-clinical *in vitro* models used in cancer research: results of a worldwide survey. Irish Association for Cancer Research (IACR) meeting 2021, Virtual (March 2021).
- **Martinez-Pacheco, S.**, & O'Driscoll, L. Pre-clinical *in vitro* models used in cancer research: results of a worldwide survey. Irish Association for Cancer Research (IACR) meeting 2021, Virtual (March 2021).
- **Martinez-Pacheco, S.**, & O'Driscoll, L. Currently use of pre-clinical *in vitro* models in cancer research: the first global survey. Joint Research Centre (JRC) Summer School on "Non- animal Approaches in Science", Virtual (May 2021).
- **Martinez-Pacheco, S.**, & O'Driscoll, L. Comparation of differential ultracentrifugation and polyethylene glycol-based precipitation method as method to isolate EVs in breast cancer cells. International Society for Extracellular Vesicles (ISEV) Conference 2021, Virtual (May 2021).
- **Martinez-Pacheco, S.**, & O'Driscoll, L. Low levels of anti-cancer drugs may contribute to drug resistance and cancer aggressiveness by increasing HER2 expression and release of extracellular vesicles. The European Association for Cancer Research (EACR) Conference 2022, Seville (June 2022).
- **Martinez-Pacheco, S.**, Jurado-Maqueda, J., Oliveira, C., & O'Driscoll, L. Global proteomics profiling to understand potential mechanisms of neratinib-resistance in HER2-positive breast cancer. The European Association for Cancer Research (EACR) Conference 2022, Seville (June 2022).
- **Martinez-Pacheco, S.**, & O'Driscoll, L. Investigating how exposure to low dose of tucatinib may contribute to cancer aggressiveness and drug resistance in HER2-positive breast cancer. Trinity St James' Cancer Institute (TSJCI) 12th International Cancer Conference, Dublin (October 2022).
- **Martinez-Pacheco, S.**, Jurado-Maqueda, J., Oliveira, C., & O'Driscoll, L. The proteomic landscape of neratinib-resistance and neratinib-sensitive HER2-positive breast cancer. Trinity St James' Cancer Institute (TSJCI) 12th International Cancer Conference, Dublin (October 2022).
- **Martinez-Pacheco, S.**, & O'Driscoll, L. Unravelling the effect of hypoxia on the release of extracellular vesicles from drug resistance and drug-sensitive HER2+ breast cancer. Irish Association for Cancer Research (IACR) meeting 2023, Athlone (February 2023).
- **Martinez-Pacheco, S.**, Jurado-Maqueda, J., Oliveira, C., & O'Driscoll, L. Comparative proteomic profiling suggests a potential role of AGR2 on neratinib-resistance in HER2-

positive breast cancer. Irish Association for Cancer Research (IACR) meeting 2023, Athlone (February 2023).

C. AWARDS AND OTHER

- **TBSI Early Career Researcher Collaboration Grant (2023).** Dr Fiona Henkel (Department of Biochemistry and Immunology) Sarai Martinez Pacheco (Department of Pharmacy and Pharmaceutical Sciences) "Investigating Mitochondrial RNA as intercellular messengers in inflammatory diseases".

- **Senior Sophister Capstone Research Project 2022.** Co-supervisor of SS Project 2022 titled "Differences in the proteome between drug-resistant and drug- sensitive".

D. FUNDING